UNIVERSITY OF Southampton

University of Southampton Research Repository
ePrints Soton

Copyright © and Moral Rights for this thesis are retained by the author and/or other copyright owners. A copy can be downloaded for personal non-commercial research or study, without prior permission or charge. This thesis cannot be reproduced or quoted extensively from without first obtaining permission in writing from the copyright holder/s. The content must not be changed in any way or sold commercially in any format or medium without the formal permission of the copyright holders.

When referring to this work, full bibliographic details including the author, title, awarding institution and date of the thesis must be given e.g.

AUTHOR (year of submission) "Full thesis title", University of Southampton, name of the University School or Department, PhD Thesis, pagination

http://eprints.soton.ac.uk

UNIVERSITY OF SOUTHAMPTON

FACULTY OF NATURAL AND ENVIRONMENTAL SCIENCES

School of Ocean and Earth Science

The natural variability and climate change response in phytoplankton phenology

by

Harriet Stephanie Cole

Thesis for the degree of Doctor of Philosophy

October 2013

UNIVERSITY OF SOUTHAMPTON

ABSTRACT

FACAULTY OF NATURAL AND ENVIRONMENTAL SCIENCES

Ocean and Earth Sciences

Doctor of Philosophy

THE NATURAL VARIABILITY AND CLIMATE CHANGE RESPONSE IN PHYOTPLANKTON PHENOLOGY

By Harriet Stephanie Cole

Large areas of the world's oceans experience a significant seasonal cycle in phytoplankton biomass. Variability in the phenology of these phytoplankton blooms affect ecosystem dynamics with implications for carbon export production and food availability at higher trophic levels. Climate change is expected to alter phytoplankton seasonality through changes to the underlying physical drivers controlling bloom timing. This thesis focusses on the drivers of contemporary variability and climate change-driven trends in phytoplankton phenology. Satellite-derived chlorophyll data (GlobColour) are used to examine phenological characteristics on a global scale. This dataset is complimented by remotely sensed photosynthetically active radiation (PAR; MODIS), net heat flux (remotely sensed and reanalysis products) and Argo float-derived mixed layer depth datasets in addition to global biogeochemical model output.

Four bloom timing metrics are developed to quantify the timing of bloom initiation and termination in a consistent manner. The advantages and limitations of each metric are discussed in the context of the required criteria for a suitable metric definition. The choice of metric definition is based on the performance of the metrics against these criteria.

The impact of missing data in the time series on the accuracy of the bloom timing metrics is investigated using the global biogeochemical model NOBM. It is found that missing data cause errors of approximately 30, 15 and 50 days in the date of bloom initiation, peak and termination respectively. The exact cause and implications for phenological studies of these errors is discussed.

The physical drivers of interannual variability are examined using global datasets of mixed layer depth, net heat flux and mean mixed layer PAR. The date the net heat flux becomes positive is seen to be a strong predictor for the onset of the subpolar spring bloom, especially in the North Atlantic. This finding is the first to support the critical turbulence hypothesis over Sverdrup's critical depth theory using satellite observations on a global scale. Physical drivers are only weakly related to interannual variability in bloom timing in the subtropics. The reasons for these relationships and other potential drivers of bloom timing are discussed.

Finally, the climate change-driven trends in phytoplankton phenology are investigated using a suite of global biogeochemical models. The ability of the models to capture contemporary seasonality is discussed. The climate change response is found to be strongest at higher latitudes and the phenological changes are consistent with longer periods of strong stratification and earlier onset of ocean warming. Furthermore, it is found that using higher temporal resolution may enable the earlier detection of climate change-driven trends but only at high latitudes.

Contents

ABSTRACT i

Contents iii

List of Figures v

List of Tables xiii

DECLARATION OF AUTHORSHIP xv

Acknowledgements xvii

Definitions and Abbreviations xix

1 Introduction 1

1.1 Why Phytoplankton Seasonality Matters 1

1.2 Aims and Objectives 2

1.3 The Classic North Atlantic Spring Bloom 3

1.4 Controls on Bloom Timing 8

1.5 Variability in Phytoplankton Seasonality 21

1.6 Impact of Climate Change 36

1.7 Thesis Outline 44

1.8 Summary 44

2 Data 47

2.1 Chlorophyll-a 48

2.2 Mixed Layer Depth 60

2.3 Net Heat Flux 67

2.4 Mixed Layer Irradiance 69

2.5 Summary 73

3 Seasonality Metric Development 75

3.1 Detecting Seasonality 75

3.2 Bloom Timing Metrics 86

3.3 Summary 120

4 Impact of Data Gaps on the Accuracy of Bloom Timing Metrics 123

4.1 Introduction 123

4.2 Seasonality in Missing Data 124
4.3 Data, Model and Methods 128
4.4 Results 132
4.5 Discussion 146
4.6 Summary 152
5 Physical Drivers of Interannual Variability in Phytoplankton Phenology 123
5.1 Introduction 153
5.2 Data and Methods 156
5.3 Results 166
5.4 Discussion 194
5.5 Summary 212
6 Climate Change-driven Trends in Bloom Timing 213
6.1 Models and Methods 213
6.2 Assessment of Modelled Contemporary Seasonality 217
6.3 Trends in Bloom Timing 226
6.4 Temporal Resolution and Detectability 252
6.5 Summary 266
7 Summary 269
7.1 Summary of Conclusions 269
7.2 Evaluation of Data and Methods 273
7.3 Future Directions 276
8 Appendix A 279
9 Appendix B 289
10 Appendix C 291
11 Appendix D 293
12 Appendix E 293
13 References 75

List of Figures

Figure number	Title	Page number
1.1	Sketches of typical seasonal cycles from the North Atlantic for light, nutrient concentrations, mixed layer depth (MLD) and phytoplankton and zooplankton abundances.	5
1.2	Schematic of the critical depth hypothesis.	6
1.3	Schematic of nutrient limitation in the surface mixed layer through formation of the thermocline.	7
1.4	Hovmöller plots showing relationship between (a) latitude and day length (hours) calculated using the Brock model (Brock, 1981) and (b) the relationship between latitude and mean SeaWiFS photosynthetically active radiation (PAR).	10
1.5	Example climatological (2002-2010) chlorophyll concentration time series from subpolar, subtropical and oligotrophic gyre regions from the GlobColour dataset.	14
1.6	Schematic showing the match-mismatch hypothesis.	20
1.7	The correlation of chlorophyll-a anomalies (Chl-a, %) and wind speed anomalies (U, m/s) from the western Equatorial Pacific.	23
1.8	Net primary production (NPP) anomalies for the permanently stratified ocean plotted against (a) the Multivariate ENSO Index (MEI), and (b) stratification.	23
1.9	The timing of the spring bloom in the North Atlantic.	26
1.10	Interannual variability in bloom timing and climate oscillations.	33
1.11	Example time series showing phenological changes in the Arctic.	39
1.12	Relationships between temperature and phytoplankton size class.	39
2.1	Seasonal maps of GlobColour chlorophyll concentration.	51
2.2	Seasonal maps of NOBM chlorophyll concentration.	56
2.3	Time series from locations shown in Figures 2.1 and 2.2 comparing the chlorophyll time series from GlobColour (blue) and NOBM (black).	59
2.4	Scatter plots comparing a visual estimate of MLD to MLD calculated from commonly used methods.	63
2.5	Seasonal maps of MLD (m) using the Holte and Talley (2009) density threshold method.	64
2.6	Global maps of the annual mean objective analysis error statistics on temperature and salinity measurements for 2002 and 2006.	65

2.7	Example MLD time series using the Holte and Talley (2009) density threshold method.	65
2.8	Seasonal maps of net heat flux (W m^{-2}) for December, January, February (DJF), March, April May (MAM), June, July, August (JJA), September, October, November (SON).	68
2.9	Seasonal maps of mean mixed layer irradiance (W m^{-2}) for December, January, February (DJF), March, April May (MAM), June, July, August (JJA), September, October, November (SON).	72
3.1	Cartoon of an idealised phytoplankton bloom showing the seasonality metrics that can be calculated: bloom initiation, peak, termination and duration.	76
3.2	The cumulative sum for two climatological time series.	79
3.3	The number of pixels with a coefficient of determination value (R^2) below a set threshold R^2 value.	79
3.4	Low frequency part of the periodograms calculated from the time series in Table 3.1.	81
3.5	Global map showing the normalised amplitude of the annual frequency from the Lomb-Scargle Periodogram.	81
3.6	Results from X-11 decomposition: the original time series (blue), trend component (black), seasonal component (red) and residual component (green).	83
3.7	Global map showing the fraction of total time series variance explained by the seasonal component from the X11 decomposition.	83
3.8	Global map of the coefficient of variation.	85
3.9	The number of pixels that fall below a coefficient of variation (CV) value.	85
3.10	Time series from the Atlantic section of the Southern Ocean where the bloom peak occurs in December/January.	89
3.11	Example time series to illustrate the estimation of the bloom peak date.	89
3.12	Example time series (2004-2008) to show the annual mean threshold metric definition.	93
3.13	Time series (2004-2008) to show the cumulative sum metric definition.	93
3.14	Time series (2004-2008) showing the percentage of maximum chlorophyll metric definition.	96
3.15	Time series (2004-2008) showing the largest gradient metric definition.	96
3.16	Diagram to illustrate how mean bloom peak timing dates are calculated in regions where the metric dates occur at the turn of the year.	100
3.17	Global maps showing the mean bloom initiation date over 2002-2010.	103
3.18	Latitudinal mean bloom initiation date.	103

3.19	Time series from subpolar regions with the dates of bloom initiation from the different metrics.	104
3.20	Time series from subtropical regions with the dates of bloom initiation from the different metrics.	105
3.21	Scatter plots comparing the bloom initiation dates from each of the metric definitions in selected time series.	106
3.22	Global maps showing the mean bloom termination date over 2002-2010.	109
3.23	Latitudinal mean bloom termination date.	110
3.24	Time series from subpolar regions with the dates of bloom termination from the different metrics.	111
3.25	Time series from subtropical regions with the dates of bloom termination from the different metrics.	112
3.26	Scatter plots comparing the bloom termination dates.	113
3.27	Global maps showing the mean bloom duration over 2002-2010, for the annual median based metric.	115
3.28	Latitudinal mean bloom duration.	116
3.29	Scatter plots comparing the bloom durations from each of the metric definitions from selected locations.	117
4.1	The percentage of missing data annually calculated from GlobColour dataset from 2002 to 2009.	125
4.2	Latitudinal variations in the percentage of missing data.	125
4.3	Spatial variations in the percentage of missing data.	127
4.4	Taylor diagram comparing the bloom initiation (cross), bloom peak (plus) and bloom termination (star) metric results from the full NOBM dataset to those from GlobColour satellite observations (circle).	131
4.5	Scatter plots showing the linear relationship between bloom metric GlobColour dates and metric dates from the subsampled NOBM.	131
4.6	Regression results for polynomials of order 1 to 6 applied to bloom initiation date error versus the total annual percentage of missing data.	133
4.7	Regression results for polynomials of order 1 to 6 applied to bloom peak date error versus the total annual percentage of missing data.	134
4.8	Regression results for polynomials of order 1 to 6 applied to bloom termination date error versus the total annual percentage of missing data.	139
4.9	Relationship between percentage of missing data and the error in (a) bloom initiation date, (b) peak date and (c) bloom termination date.	139
4.10	Maps of (a) mean bloom initiation date (2002–2006), (b) uncertainty in bloom initiation date calculated from equation (4.1) (days).	142
4.11	Maps of (a) mean bloom peak date (2002–2006), (b) uncertainty in bloom peak date calculated from equation	143

(4.2) (days).

4.12 Maps of (a) mean bloom termination date (2002–2006), (b) uncertainty in bloom termination date calculated from equation (4.3) (days). 144

4.13 Maps of the probability that an error resulting from missing data termination is towards a date later than the true date. 145

4.14 Difference between the threshold values calculated from the full NOBM chlorophyll time series and the subsampled NOBM time series. 148

4.15 Maps showing the sign of the difference in the metric dates using the full NOBM dataset and an altered NOBM dataset for bloom initiation (a, c) and bloom termination (b, d). 148

5.1 Map showing the regions where correlations in interannual variability were calculated. 160

5.2 Cartoon of the annual cycle in mixed layer depth (MLD). 160

5.3 Cartoon of the annual cycle in net heat flux (NHF). 161

5.4 Cartoon of the annual cycle in mixed layer mean PAR. 161

5.5 Maps showing the mean date of bloom initiation from (a) GlobColour (2002-2009), (c) NOBM (2002-2007) and the standard deviation. 163

5.6 Maps showing the mean date of bloom peak from (a) GlobColour (2002-2009), (c) NOBM (2002-2007) and the standard deviation 164

5.7 Maps showing the mean date of bloom termination from (a) GlobColour (2002-2009), (c) NOBM (2002-2007) and the standard deviation. 165

5.8 Mean time series (2002-2009) across the North Atlantic. 167

5.9 Mean time series (2002-2009) across the North Pacific. 167

5.10 Mean time series (2002-2009) across the Southern Ocean. 168

5.11 Latitudinal mean date for bloom initiation (red) and associated physical timing metrics (blue) for (a) North Atlantic, (b) North Pacific and (c) Southern Ocean. 173

5.12 Latitudinal mean date for bloom peak (red) and associated physical timing metrics (blue) for (a) North Atlantic, (b) North Pacific and (c) Southern Ocean. 174

5.13 Latitudinal mean date for bloom peak termination timing metrics (blue) for (a) North Atlantic, (b) North Pacific and (c) Southern Ocean. 175

5.14 Scatter plots of interannual anomalies in bloom initiation date and associated physical metric for subpolar regions. 177

5.15 Scatter plots of interannual anomalies in bloom peak date and associated physical metric for subpolar regions. 178

5.16 Scatter plots of interannual anomalies in bloom termination date and associated physical metric for 179

subpolar regions.

5.17 Mean time series (2002-2009) across the subtropical North Atlantic. 181

5.18 Mean time series (2002-2009) across the subtropical South Pacific. 181

5.19 Latitudinal mean date for bloom initiation (red) and associated physical timing metrics (blue) for the subtropical (a) Atlantic, (b) Pacific and (c) Indian Oceans. 189

5.20 Latitudinal mean date for bloom peak (red) and associated physical timing metrics (blue) for the subtropical (a) Atlantic, (b) Pacific and (c) Indian Oceans. 190

5.21 Latitudinal mean date for bloom termination (red) and associated physical timing metrics (blue) for the subtropical (a) Atlantic, (b) Pacific and (c) Indian Oceans. 191

5.22 Scatter plots of interannual anomalies in bloom initiation date and associated physical metric for the subtropical basins. 195

5.23 Scatter plots of interannual anomalies in bloom peak date and associated physical metric for the subtropical basins. 196

5.24 Scatter plots of interannual anomalies in bloom termination date and associated physical metric for the subtropical basins. 197

5.25 Conditions at bloom initiation for all pixels in the subpolar North Atlantic. 206

5.26 Conditions at bloom initiation for all pixels in the subpolar North Pacific. 207

5.27 Conditions at bloom initiation for all pixels in the subpolar Southern Ocean. 208

5.28 Global maps showing the pixel-by-pixel correlation between bloom initiation and (a) the date that NHF turns positive and (b) MLD shoals. 209

6.1 Global maps of mean bloom initiation date for observations and models. 219

6.2 Global maps of mean bloom peak date for observations and models. 219

6.3 Global maps of mean bloom termination date for observations and models. 220

6.4 Global maps of standard deviation in bloom initiation date for observations and models. 220

6.5 Global maps of standard deviation in bloom peak date for observations and models. 221

6.6 Global maps of standard deviation in bloom termination date for observations and models. 221

6.7 Taylor diagrams showing the agreement between GlobColour metric dates of (a, d) bloom initiation (b, e) peak and (c, f) termination. 224

6.8	Peak date estimation using different calendar configurations.	228
6.9	Example bloom timing time series to show correction for trend estimation.	228
6.10	Geographical distribution of the oceanographic biomes in MEDUSA (a), TOPAZ (b) and CESM1 (c).	229
6.11	Time series showing the change in area of the oceanographic biomes over time.	231
6.12	Time series showing the change in mean latitude of the oceanographic biomes over time in the northern hemisphere (blue) and southern hemisphere (red).	231
6.13	Difference in the mean bloom initiation date between 2007-2026 and 2079-2098 for MEDUSA (a), TOPAZ (b) and CESM1 (c) in days	234
6.14	Difference in the mean bloom peak date between 2007-2026 and 2079-2098 for MEDUSA (a), TOPAZ (b) and CESM1 (c) in days.	235
6.15	Difference in the mean bloom termination date between 2007-2026 and 2079-2098 for MEDUSA (a), TOPAZ (b) and CESM1 (c) in days.	236
6.16	Difference in the mean bloom duration between 2007-2026 and 2079-2098 for MEDUSA (a), TOPAZ (b) and CESM1 (c) in days.	237
6.17	Difference in the length of the mean bloom initiation-peak interval between 2007-2026 and 2079-2098 for MEDUSA (a), TOPAZ (b) and CESM1 (c) in days.	238
6.18	Difference in the length of the mean bloom peak-termination interval between 2007-2026 and 2079-2098 for MEDUSA (a), TOPAZ (b) and CESM1 (c) in days.	239
6.19	Difference in the mean bloom initiation (a), peak (b) and termination (c) dates between 2007-2026 and 2079-2098 for each ocean basin and each oceanographic biome	241
6.20	Difference in the mean length of the bloom duration (a), initiation-peak interval (b) and peak-termination interval (c) between 2007-2026 and 2079-2098 for each ocean basin and each oceanographic biome.	242
6.21	Difference in the annual mean mixed layer depth (MLD) (a), MLD amplitude (b) net heat flux (c) and dissolved inorganic nitrogen (d) between 2007-2026 and 2079-2098 for each ocean basin and each oceanographic biome.	243
6.22	Difference in the mean date of maximum MLD (a), MLD shoaling (b) and NHF turning positive (c) between 2007-2026 and 2079-2098 for each ocean basin and each oceanographic biome.	244
6.23	The difference in (a) bloom initiation, (b) bloom peak (c) bloom termination and (d) bloom duration when using 5 day and 30 day temporal resolution.	256
6.24	Maps showing the value of n* (the number of years required to detect a trend).	257

6.25	Median percentage change in n* with temporal resolution for bloom initiation (a), bloom peak (b), bloom termination (c) and bloom duration (d) for different ocean basins.	258
6.26	Median change from 5 day temporal resolution values in the residual variability (a), trend magnitude (b) and autocorrelation (c) for bloom initiation n* calculation.	260
6.27	Median change from 5 day temporal resolution values in the residual variability (a), trend magnitude (b) and autocorrelation (c) for bloom peak n* calculation.	261
6.28	Median change from 5 day temporal resolution values in the residual variability (a), trend magnitude (b) and autocorrelation (c) for bloom termination n* calculation.	262
6.29	Median change from 5 day temporal resolution values in the residual variability (a), trend magnitude (b) and autocorrelation (c) for bloom duration n* calculation.	263

List of Tables

Table number	Title	Page number
1.1	Table of selected climate oscillations and characteristics.	30
2.1	Ocean colour sensor characteristics.	49
3.1	Results from different approaches for detecting strong seasonality.	77
3.2	Summary of bloom timing metric definitions.	87
3.3	Root mean square difference in days between bloom timing metrics.	118
4.1	Goodness-of-fit parameters for regression of bloom initiation error on percentage of missing data.	137
4.2	Goodness-of-fit parameters for regression of bloom peak error on percentage of missing data.	137
4.3	Goodness-of-fit parameters for regression of bloom termination error on percentage of missing data.	138
5.1	Correlation coefficients and latitudinal speeds for bloom initiation and associated physical timing metrics in the subpolar basins.	170
5.2	Correlation coefficients and latitudinal speeds for bloom peak and associated physical timing metrics in the subpolar basins.	171
5.3	Correlation coefficients and latitudinal speeds for bloom termination and associated physical timing metrics in the subpolar basins.	172
5.4	Correlation coefficients between interannual variability in bloom initiation and physical timing metrics in the subpolar basins.	180
5.5	Correlation coefficients between interannual variability in bloom peak and physical timing metrics in the subpolar basins.	180
5.6	Correlation coefficients between interannual variability in bloom termination and physical timing metrics in the subpolar basins.	180

5.7	Correlations coefficients and latitudinal speeds for bloom initiation and associated physical timing metrics in the subtropical basins.	183
5.8	Correlation coefficients and latitudinal speeds for bloom peak and associated physical timing metrics in the subtropical basins.	185
5.9	Correlation coefficients and latitudinal speeds for bloom termination and associated physical timing metrics in the subtropical basins.	187
5.10	Correlation coefficients between interannual variability in bloom initiation and physical timing metrics in the subtropical basins.	193
5.11	Correlation coefficients between interannual variability in bloom peak and physical timing metrics in the subtropical basins.	193
5.12	Correlation coefficients between interannual variability in bloom termination and physical timing metrics in the subtropical basins.	194
5.13	Conditions at bloom initiation for the North Atlantic, North Pacific and Southern Oceans.	203
6.1	Statistics for comparison of seasonality metric between GlobColour and global biogeochemical models.	225
6.2	Oceanographic biome definitions.	232
6.3	Mean number of years required to detect a trend (n*) per ocean basin and globally for each of the bloom timing metrics.	259

DECLARATION OF AUTHORSHIP

I, HARRIET STEPHANIE COLE declare that the thesis entitled

THE NATURAL VARIABILITY AND CLIMATE CHANGE RESPONSE IN PHYTOPLANKTON PHENOLOGY

and the work presented in the thesis are both my own, and have been generated by me as the result of my own original research. I confirm that:

- this work was done wholly or mainly while in candidature for a research degree at this University;
- where any part of this thesis has previously been submitted for a degree or any other qualification at this University or any other institution, this has been clearly stated;
- where I have consulted the published work of others, this is always clearly attributed;
- where I have quoted from the work of others, the source is always given. With the exception of such quotations, this thesis is entirely my own work;
- I have acknowledged all main sources of help;
- where the thesis is based on work done by myself jointly with others, I have made clear exactly what was done by others and what I have contributed myself;
- parts of this work have been published as:
- Cole, H., S. Henson, A. Martin and A. Yool (2012), Mind the gap: The impact of missing data on the calculation of phytoplankton phenology metrics, *Journal of Geophysical Research*, **117**(C8), C08030, doi:10.1029/2012jc008249. – attached as Appendix A

Signed: …….

Date:…….

Acknowledgements

Firstly I would like to thank my fantastic supervisory team, Steph, Adrian and Andrew for all their help and support over the last three years. Thank you for giving me this opportunity and for all that you have taught me. I would also like to thank my Panel Chairs, Meric and Eleanor for all their useful input, support and encouragement at our meetings. Additionally, I would like to thank John Dunne, Erik Buitenhaus and Ivan Lima who gave me access to output from their models.

There are many other people I would like to thank who have made the last three years so much fun and much less stressful. In particular, thanks to Jason Hopkins, Simon Van Gennip, Sam Lew, Charlotte Marcinko and Sian Harrington for all the help and advice. A special thanks goes to Hayley Evers-King for teaching me more than I ever wanted to know about satellite algorithms. A huge thank you goes to my brilliant office mates, Helen and Dave for all the laughs during the good times, support in moments of despair and also for answering my numerous questions on basic marine biology. A special thanks goes to Liz for being so motivated, enthusiastic and knowledgeable. You have given me great ideas and advice as well as being a great friend. I will miss our early morning coffees! Thanks for making me a better scientist.

I would like to give a huge thank you to my family for their kind words, encouragement and enthusiasm for my PhD. I love you all very much. Thanks to Nick and Hugh for your proof reading feedback, Emily for her continued support and Mum for your outstanding knowledge of Microsoft Word. Thanks also to Dad for all the lively science discussions and enthusiasm over the last three years. Thank you for believing in me.

Finally, my biggest thanks goes to my partner and best friend, Tom, to whom I dedicate my thesis. Thank you for all the support and advice you have given me over the last three years. Thanks also for putting up with me when I got frustrated and for taking time to talk through ideas and problems with me. Thanks for always believing I could do it!

Definitions and Abbreviations

ALOHA	A Long-term Oligotrophic Habitat Assessment
AIC	Akaike Information Criterion
AMO	Atlantic Meridional Oscillation
ANOVA	Analysis of Variance
BATS	Bermuda Atlantic Time-series Study
BEC	Biogeochemical Elemental Cycling Model
BIC	Bayesian Information Criterion
CCSM	Community Climate System Model
CDOM	Coloured Dissolved Organic Matter
CESM	Community Earth System Model
CPR	Continuous Plankton Recorder
CV	Coefficient of Variation
CZCS	Coastal Zone Color Scanner
DCM	Deep Chlorophyll Maximum
DOM	Dissolved Organic Matter
ECMWF	European Centre for Medium-range Weather Forecasts
ENSO	El Niño-Southern Oscillation
ESA	European Space Agency
EUC	Equatorial Under Current
GBM	Global Biogeochemical Model
GES DISC	Goddard Earth Sciences Data and Information Services Center
GFDL	Geophysical Fluid Dynamics Laboratory
GISS	Goddard Institute for Space Studies
GLM	Generalised Linear Model
HNLC	High Nutrient Low Chlorophyll
HOTS	Hawaii Ocean Time Series
ISCCP	International Satellite Cloud Climatology Project
ISIN	Integerized SINusoidal
MAD	Median Absolute Difference
MEDUSA	Model of Ecosystem Dynamics, nutrient Utilisation, Sequestration and Acidification
MEI	Multivariate ENSO index
MERIS	MEdium Resolution Imaging Spectrometer
MIZ	Marginal Ice Zone
MLD	Mixed Layer Depth
MODIS	Moderate Resolution Imaging Spectroradiometer
NaN	Not a Number
NAO	North Atlantic Oscillation
NASA	National Aeronautics Space Administration
NCAR	National Center for Atmospheric Research
NCEP	National Centers for Environmental Prediction
NEMO	Nucleus for European Modelling of the Ocean

NHF	Net Heat Flux
NOAA	National Oceanic and Atmospheric Administration
NOBM	NASA Ocean Biogeochemical Model
NOC	National Oceanography Centre
NODC	National Ocean Data Center
NPGO	North Pacific Gyre Oscillation
NPP	Net Primary Production
OASIM	Ocean Atmosphere Spectral Irradiance Model
OBC	Online Bias Correction
PAR	Photosynthetically Active Radiation
PAR_{ML}	Mean Mixed Layer Photosynthetically Active Radiation
PDO	Pacific Decadal Oscillation
PFT	Plankton Functional Types
POP	Parallel Ocean Program
R^2	Coefficient of Determination
RMS	Root Mean Square
RMSD	Root Mean Square Difference
SAT	Surface Air Temperature
SeaWiFS	Sea-viewing Wide Field-of-view Sensor
SEIK	Singular Evolutive Interpolated Kalman
SLP	Sea Level Pressure
SOI	Southern Oscillation Index
SST	Sea Surface Temperature
TAO	Tropical Atmosphere Ocean
TEOS-10	Thermodynamic Equation of Seawater 2010
TOPAZ	Tracers for Ocean Phytoplankton with Allometric Zooplankton
TRITON	Triangle Trans-Ocean Buoy Network
WHOI	Woods Hole Oceanographic Institution
WOA	World Ocean Atlas
XBT	eXpendable BathyThermograph
XCTD	eXpendable Conductivity Temperature and Depth

1 Introduction

1.1 Why Phytoplankton Seasonality Matters

Phytoplankton are microscopic plant-like organisms that obtain energy from sunlight using photosynthesis. They are found throughout the world's oceans and given the right environmental conditions, phytoplankton populations can increase dramatically over large areas of the ocean. This substantial increase in biomass is called a phytoplankton bloom and they are seen to occur annually over much of the world's oceans (e.g. Heinrich (1962)). In the North Atlantic Ocean this blooming is seen on a yearly basis in the springtime though an additional bloom may sometimes occur in the autumn (Raymont, 1980). Although the blooms occur annually, the size of the bloom, the date on which it occurs and how long it lasts varies from year to year. Because of its role in driving ocean food webs, the annual bloom has been a focus of research for decades e.g. (Gran and Braarud, 1935, Riley, 1942, Sverdrup, 1953, Holmes, 1956, Hulburt *et al.*, 1960, Pingree *et al.*, 1975, Dagg and Turner, 1982). However, the exact mechanisms that cause these microscopic plants to reach such high abundances are still not entirely understood.

Phytoplankton are vital to life on Earth as they produce half of all the oxygen we breathe (Field *et al.*, 1998) as well as forming the base of the marine food web. Phytoplankton are primarily grazed by zooplankton, a collective term encompassing small marine animals such as fish larvae and microscopic crustaceans, which in turn are the food source for larger organisms. The bloom is a time of high productivity and variability in its seasonality can change the timing of maximum food abundance for zooplankton. The impact of this can echo up the food chain and affect the abundance of organisms at higher trophic levels, some of which may be commercially important. Consequently, phytoplankton seasonality has global implications for the fishing industry and ultimately for human food supplies.

Phytoplankton also play an important role in biogeochemical cycles as they are an integral part of the global carbon cycle. When phytoplankton photosynthesise they take up carbon dioxide and assimilate it into their cell structures. Sinking phytoplankton detritus exports the carbon assimilated in their cells out of the ocean's surface layer. The depth to which the cells sink before being wholly remineralised determines the timescale on which the carbon is released back into the atmosphere. Potentially, if the cells are buried at the sea floor the carbon would be locked away for millennia. However, they are more likely

to be remineralised further up in the water column, keeping the carbon in that water mass for tens to thousands of years until it recirculates back to the surface. Thus, phytoplankton provide a pathway for carbon in the atmosphere to be stored in the deep ocean. This is a key part of the global carbon cycle and is often referred to as the biological carbon pump. The quantity of carbon exported is related to productivity, which is highest during blooms though export efficiency has been inversely related to production (Francois *et al.*, 2002). Additionally, it has been noted that variability in bloom timing can influence carbon export (Townsend *et al.*, 1994). Therefore, variability in phytoplankton seasonality potentially has implications for the efficiency of the biological pump.

The processes that control the timing, magnitude and composition of the bloom are still not fully understood. Consequently, there is a need to examine the influence of the ocean environment on phytoplankton in the contemporary ocean, as this will allow us to better predict the future impacts of climate change. Phytoplankton seasonality and bloom timing (phenology) are the focus of this thesis as variability in bloom timing is just as important ecologically and biogeochemically as bloom magnitude. Studying the variability in bloom timing is paramount to the detection of long-term trends in phytoplankton phenology above the natural seasonal and interannual variability. Due to the uncertainty in the response of the Earth system to anthropogenic climate change, detecting these trends in phenology is especially important.

1.2 Aims and Objectives

The main aims of this thesis are to quantify seasonal variability in the contemporary ocean and to assess trends in bloom timing due to climate change. The project aims to use satellite-derived ocean colour data and *in situ* observations to examine biophysical interactions that give rise to variability in bloom timing. This knowledge is then used with output from global biogeochemical models to examine the drivers of future trends in bloom timing. More specifically, the main objectives of this project are:

- To develop a range of seasonality metrics that are suitable for application to a wide range of annual cycles (i.e. single vs. double peak, subpolar bloom vs. subtropical bloom) and are relatively insensitive to incomplete time series.
- To develop a suitable method to identify regions where a seasonal cycle cannot be distinguished.

- To estimate the uncertainty in the seasonality metrics associated with missing data in the time series and explain how the gaps directly affect the bloom timing calculations.
- To quantify interannual variability in the bloom timing metrics and investigate the physical drivers of the variability.
- To verify that the suite of biogeochemical models used in this work simulate contemporary seasonality adequately.
- To calculate the magnitude of climate change-driven trends in bloom timing and link this to changes in the physical drivers of variability.
- To investigate the effect of model temporal resolution on the number of years of continuous data needed to detect a trend over natural variability.

1.3 The Classic North Atlantic Spring Bloom

The growth of a phytoplankton population is controlled by both top-down and bottom-up processes. Light and nutrient availability are the bottom-up processes while grazing by herbivorous zooplankton act as a top-down control. To understand why phytoplankton blooms occur it is useful to examine the annual cycle of the factors that influence phytoplankton growth. Typical cycles for the subpolar North Atlantic are shown in Figure 1.1. The spring bloom in phytoplankton is seen to coincide with increasing surface irradiance, shoaling mixed layer depth (MLD), low number of grazers and high nutrient concentrations.

The interplay of the bottom-up controls was examined by Sverdrup (1953) to form the critical depth hypothesis. Based on observations from the North Atlantic Ocean the critical depth hypothesis states that a bloom will occur when the MLD is shallower than the critical depth (see Figure 1.2). The critical depth is defined as the depth at which integrated photosynthesis (the production of organic carbon) is balanced by integrated respiration (the consumption of organic carbon). This balance is dependent on the integrated light levels, which determine the rates of photosynthesis. Net growth occurs when integrated photosynthesis is larger than integrated respiration in the mixed layer. If the MLD is deeper than the critical depth then respiration will outweigh photosynthesis and there will be no net growth.

During winter in the North Atlantic, light levels are low and the MLD is at its deepest. Vertical stratification is weak due to strong wind mixing and heat loss from the ocean to the atmosphere. As winter progresses to spring, light levels start

to increase. However, the phytoplankton are dispersed throughout the mixed layer, which at this time is still deeper than the critical depth. This means that on average, the light levels are inadequate for net growth as the phytoplankton spend time below the critical depth as well as above it. During spring, the ocean surface begins to warm and at the same time a drop in wind stress reduces mixing. This leads to the formation of a more buoyant surface layer that is warmer relative to deep waters creating a sharp gradient in temperature. This feature is called the seasonal thermocline and its presence marks the base of the mixed layer. As the heating at the surface continues and mixing remains low the thermocline sharpens and shallows, shoaling the MLD. As a result, thermal stratification brings the MLD above the critical depth. Phytoplankton are then in the presence of sufficient light levels for net growth and a bloom may occur. However, this is not a smooth transition from winter to spring as high mixing rates associated with synoptic weather events can interrupt the start of the bloom (Waniek, 2003).

The availability of nutrients (primarily nitrogen, phosphorous, silicon and iron) is also essential for phytoplankton growth as they are needed to build both cells and cellular machinery. It is useful to examine the seasonal cycle of nutrient availability to understand its role in controlling phytoplankton growth (Figure 1.3). In the North Atlantic, surface nutrient concentrations are highest in late winter when the MLD is deepest and the water column is well mixed. Come the spring, when the water column is stratified, the phytoplankton begin to utilize and deplete the nutrients in the mixed layer as the bloom starts. When the nutrient concentrations become depleted and/or grazing pressure increases, the bloom peaks and starts to decline. Nutrient concentrations are only elevated if mixing from wind and waves is strong enough to overcome the stratification and entrain them from deeper in the water column where concentrations are generally higher. The seasonal thermocline effectively acts as a barrier to mixing, as significant mixing is needed to overcome strong stratification. Some locations in the North Atlantic experience an additional bloom in the autumn when light levels are still high enough for photosynthesis and the erosion of the stratification introduces nutrients from below the thermocline (Raymont, 1980). The occurrence of an autumn bloom has been shown to be dependent on the rate of deepening (Findlay *et al.*, 2006). If the rate of deepening is too slow then the increase in nutrient concentrations in the mixed layer will result in a perturbation that is too small to result in a bloom. Additionally, if the rate of deepening is too rapid then the phytoplankton population will be exposed to lower average levels of light in the deeper mixed layer and will not be able to take advantage of the elevated nutrient concentrations (Findlay *et al.*, 2006).

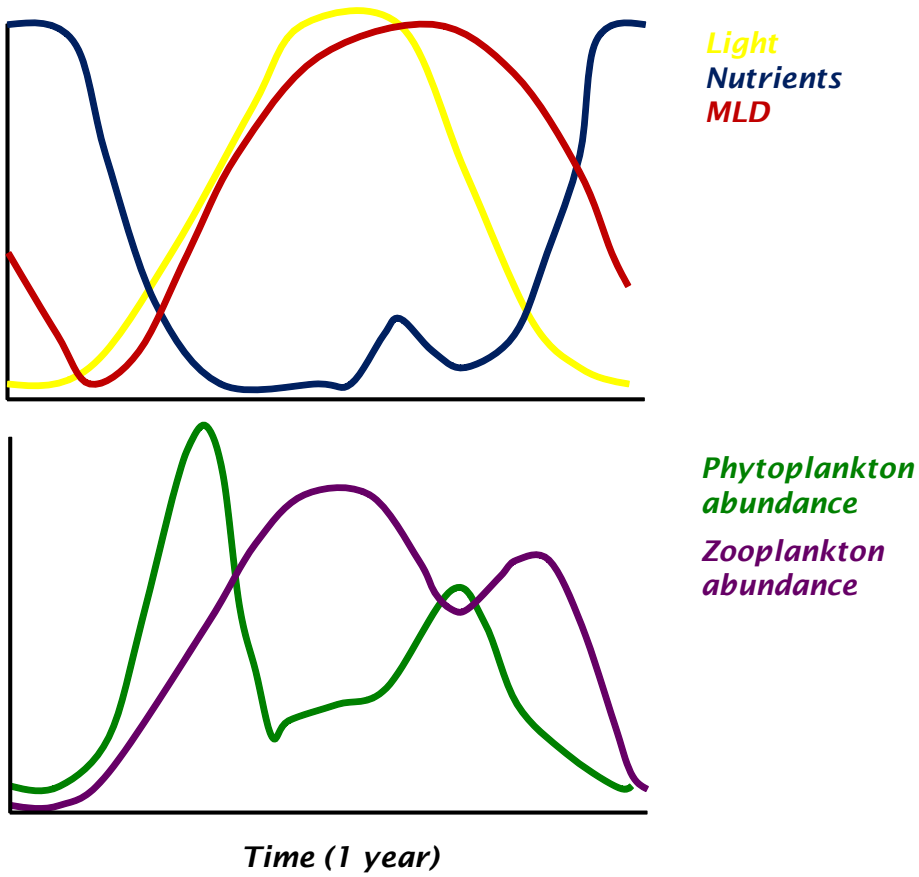

Figure 1.1: Sketches of typical seasonal cycles from the North Atlantic for light, nutrient concentrations, mixed layer depth (MLD) and phytoplankton and zooplankton abundances.

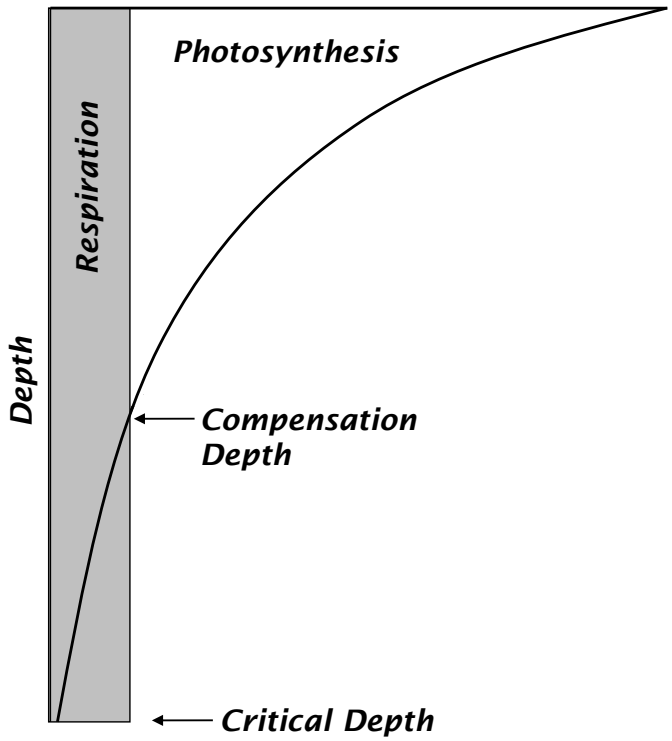

Figure 1.2: Schematic of the critical depth hypothesis. Respiration is assumed constant with depth but photosynthesis decreases exponentially with depth and declining light. The compensation depth occurs where respiration and photosynthesis are equal. At the critical depth, integrated respiration is equal to integrated photosynthesis for the water column. For net growth to occur the mixed layer depth must be shallower than the critical depth. Redrawn from Sverdrup (1953).

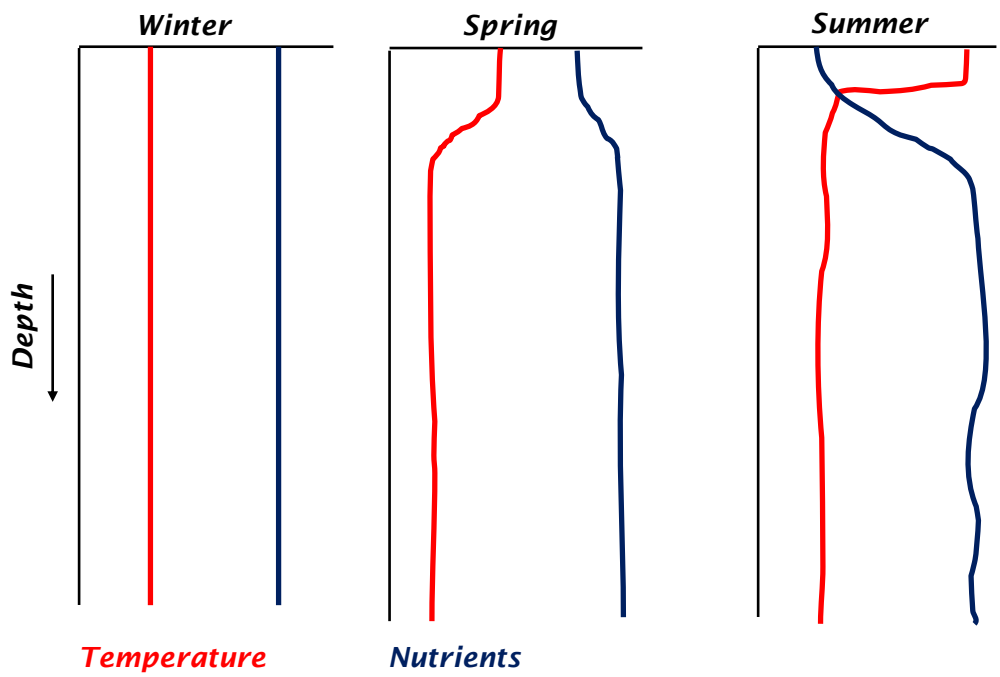

Figure 1.3: Schematic of nutrient limitation in the surface mixed layer through formation of the thermocline. In winter, temperature and nutrient concentrations are constant with depth. During spring, the sun heats the surface to form a thermocline, reducing the depth of the mixed layer and creating a barrier to mixing. As nutrients are not replenished through mixing the nutrient concentrations in the surface layer decrease as phytoplankton utilize them. In summer, this situation is more pronounced as the thermocline is sharper and the nutrients have been depleted over the growing season. During autumn and winter, reduced heating from the sun and increased mixing from wind and waves break down the thermocline and temperature and nutrients become constant with depth again.

Sverdrup's critical depth hypothesis identifies MLD shoaling as the trigger for bloom initiation as it increases the average amount of light in the water column. However, other studies of the North Atlantic have suggested that the onset of stratification is not a requirement for a bloom (Townsend *et al.*, 1992, Behrenfeld, 2010, Boss and Behrenfeld, 2010). Blooms have been observed at times when the mixed layer was very deep (Townsend *et al.*, 1992, Huisman *et al.*, 1999). In the case of Townsend (1992), although the mixed layer was deep, periods of calm weather reduced mixing sufficiently to allow a bloom to develop. This was possible because phytoplankton were not being mixed throughout the whole mixed layer but kept at the surface by their neutral buoyancy (high turbulence is a key assumption of the critical depth hypothesis). Boss and Behrenfeld (2010) explain their own observations by proposing a dilution-recoupling hypothesis in which, when the mixed layer is deep, phytoplankton and zooplankton are diluted sufficiently that the encounter rate of their populations becomes low and grazing rates decrease. This results in an accumulation of phytoplankton cells when the MLD stops deepening, starting the bloom. This implies that the bloom occurs due to deep mixed layers allowing phytoplankton to escape from grazing pressure. This highlights that grazers may be an important aspect of bloom timing in addition to the physical processes.

Exceptions to the critical depth hypothesis have also been seen in subtropical regions (Obata *et al.*, 1996, Dutkiewicz *et al.*, 2001, Siegel *et al.*, 2002). The critical depth hypothesis explains the role of light availability in initiating a bloom but subtropical regions are not limited by light and so other processes must be responsible. Further controls on bloom timing are discussed in the next section.

1.4 Controls on Bloom Timing

The availability of light and nutrients, together with grazing pressure control the amount of phytoplankton growth and thus bloom phenology. The start of the annual bloom represents a transition into ideal growth conditions that are brought about through seasonal changes to the physical environment. For the seasonal cycle in the North Atlantic, thermal stratification is identified as the main physical control on bloom initiation in light-limited regions. In both the North Atlantic and other regions, chemical or biological processes may also control bloom timing and often it is not clear if one single factor dominates population growth. Light levels and nutrient concentrations were seen to account for only 50% of the chlorophyll variance through the year in the North Atlantic between 1999 and 2006 (Irwin and Finkel, 2008) . Despite this complexity, the world's oceans can be broadly split into light-limited and nutrient-limited regions. Identifying the physical processes that

affect light and nutrient availability allow us to understand how the seasonal changes in the ocean environment influence phytoplankton phenology.

1.4.1 Light-limited Regions

Based on the biogeochemical provinces defined and described by Longhurst (1995), light-limited regions stretch from the poles to approximately 40°N or 40°S encompassing the North Atlantic, North Pacific and Southern Oceans. In light-limited regions stratification is often needed to increase the amount of light phytoplankton receive. Thus, changes in the balance of stratifying and mixing processes will dictate if conditions are suitable for a bloom to start (Henson, 2007). Stratification occurs when heating or freshwater input at the ocean's surface forms layers of water with different densities. Mixing acts to smooth out these differences and homogenise the water column, and so high rates of mixing may inhibit or delay phytoplankton growth. In the winter, especially in the North Atlantic, cooling of the surface ocean (and in some cases an additional increase in salinity) leads to deep convection as surface water becomes denser than deeper water and sinks, and is subsequently replaced by subsurface water (Marshall and Schott, 1999). Wind is also a key input of mixing with the number and intensity of storms over subpolar regions being highest in winter. This combined with convective mixing results in deep winter mixed layers (Cronin and Sprintall, 2001).

The meteorological conditions over winter are thought to influence bloom timing, not just the short time scale weather events occurring around the start of the bloom (Waniek, 2003, Henson *et al.*, 2006). The timing of spring bloom initiation in the Irminger Basin was seen to be dependent on the previous winter's heat flux and wind speed (Henson *et al.*, 2006). The bloom started later than average in years when winter cooling and wind speeds were high as these conditions result in deeper than average mixed layers and delayed MLD shoaling. Similar relationships have been recorded in the Southern Ocean where from the 1980s to 2000s an increase in wind stress resulted in a 10.4% reduction in primary productivity (Gregg *et al.*, 2003a).

However, though intense winter mixing can delay the bloom the occurrence of a deep mixed layer in the winter months benefits phytoplankton growth by elevating nutrients to deep-water concentrations every winter. Nutrient concentrations in the surface layer are depleted by phytoplankton growth over spring and summer. Winter mixing replenishes the nutrient supply and is thus essential for the growth of next year's bloom.

Polar seas represent the regions most limited by light as there is permanent darkness throughout the winter months and the annual mean irradiance is lowest at

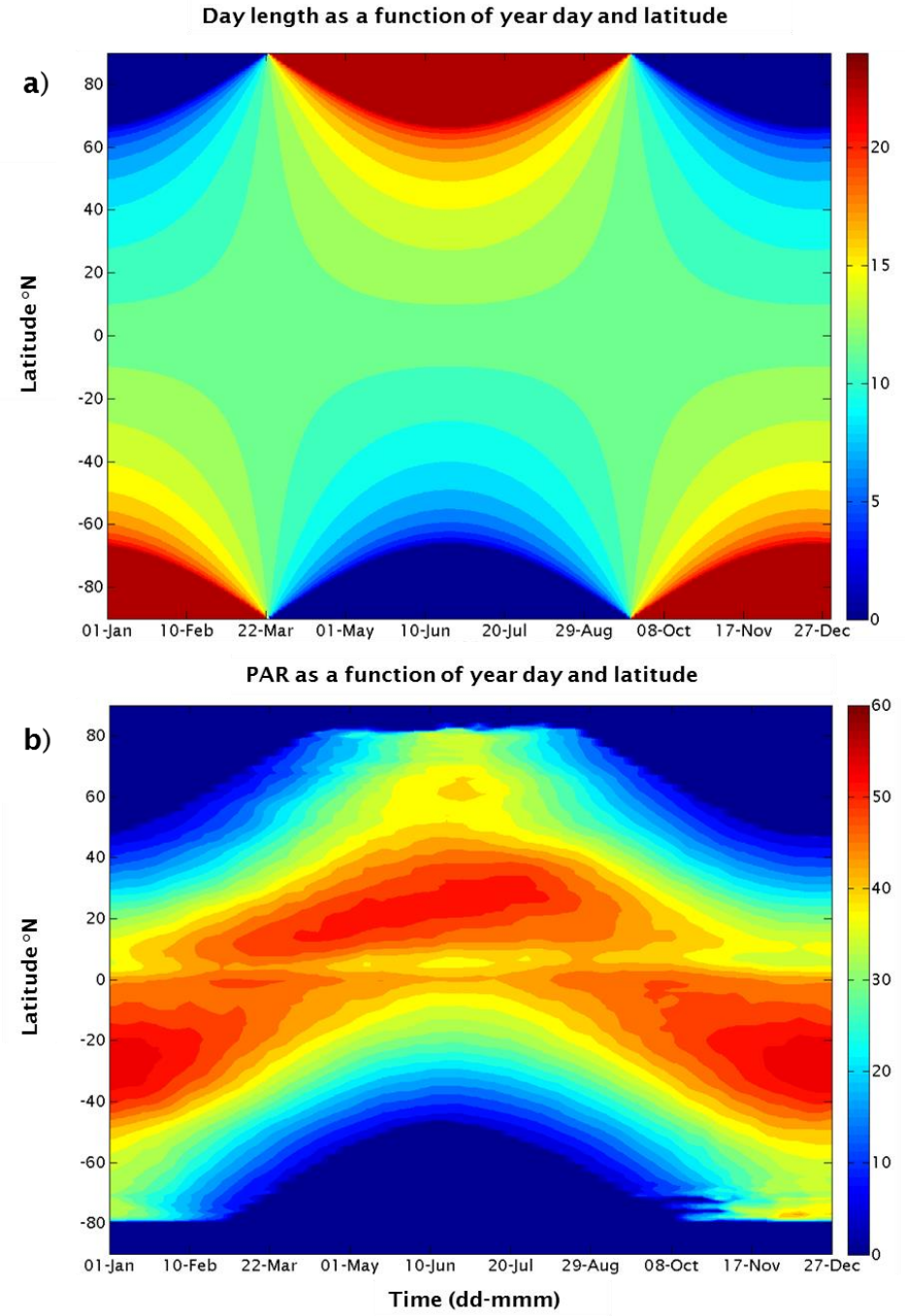

Figure 1.4: Hovmöller plots showing relationship between (a) latitude and day length (hours) calculated using the Brock model (Brock, 1981) and (b) the relationship between latitude and mean SeaWiFS photosynthetically active radiation (PAR) (W m^{-2})

these latitudes (Longhurst, 1995), (Figure 1.4). However, blooms do occur, and contrary to the expected latitudinal progression of bloom start date, are often seen to occur earlier in the year than at latitudes located further from the poles (Waniek *et al.*, 2005, Wu *et al.*, 2007). This occurs due to early stratification, not from the heating of the surface ocean, but from the input of freshwater as the seasonal sea ice melts. The fresher water is less dense than the existing surface water and forms a halocline which acts in the same way as the seasonal thermocline to shoal the MLD and increase the depth-averaged irradiance that phytoplankton experience (Wu *et al.*, 2008, Frajka-Williams *et al.*, 2009).

Despite all the evidence for stratification being necessary for reducing light limitation there are many studies that report the presence of blooms in unstratified waters. These have led to the development of an alternative to Sverdrup's critical depth model based on a reduction in near surface turbulence (Huisman *et al.*, 1999). If wind-driven vertical mixing is low then phytoplankton are not mixed throughout the entire mixed layer (i.e. low turbulence conditions). The low mixing rates combined with the neutral buoyancy of phytoplankton means that phytoplankton cells can maintain their position in the water column. These cells are then not limited by light as they are not being rapidly mixed down out of the euphotic zone. Thus, though the MLD is below the critical depth a bloom may develop. One study argues that the critical depth hypothesis is only valid when mixing rates are high and phytoplankton are being mixed throughout the whole mixed layer (Huisman *et al.*, 1999). When mixing rates are low, such as during periods of weak physical forcing, the formation of a bloom is dependent on a critical turbulence, below which phytoplankton growth rates exceed those of vertical mixing rates (Huisman *et al.*, 1999, Taylor and Ferrari, 2011).

Light limitation is primarily of consequence in the subpolar and polar regions since light becomes plentiful nearer the equator due to both increased solar irradiation and shallow MLDs. As high levels of phytoplankton are not observed throughout the year in these regions there must be other factors limiting their growth. These regions are limited by nutrients.

1.4.2 Nutrient-limited Regions

The nutrients needed by phytoplankton for growth can be split into two groups; macronutrients and micronutrients. Macronutrients include nitrogen, phosphorous and, in the case of phytoplankton that form siliceous tests, silicon. Nitrogen is usually available in the form of nitrate, nitrite, ammonia or urea, and phosphorous as phosphate (Raymont, 1980). Micronutrients include metals such as

copper, iron, cobalt, zinc and manganese with iron being the most important (Raymont, 1980).

Regions that are perennially limited by macronutrients typically have a shallow thermocline due to low mixing and strong heating. As the thermocline is present at shallow depths even in the winter, surface nutrient levels are not elevated to deep ocean concentrations as mixing is not strong enough to fully erode the thermocline. This leads to nutrient levels that are generally low throughout the whole year, and results in a different seasonal cycle than seen in subpolar regions (see Figure 1.5). Nutrient-limited regions in the general sense cover the area from the poleward edge of the subtropical gyres (approximately 40˚N/40˚S) to the equator. Subtropical areas have an annual bloom that is seen to start in the autumn or winter months rather than in the spring (Henson *et al.*, 2009). These blooms are driven by an increase in wind stress, which promotes the entrainment of water from below the thermocline. Whereas mixing in subpolar regions lowers productivity by reducing the amount of light that is available, in the subtropics mixing increases productivity by increasing the nutrient concentrations in the surface mixed layer (Dutkiewicz *et al.*, 2001, Chiba *et al.*, 2008). As in subpolar regions it is the balance of stratifying and mixing processes that control the timing of the start of the bloom except that for the subtropics it is the alleviation of nutrient limitation with increased mixing that starts the bloom. However, the timing of the peak and end of the bloom are both still associated with exhaustion of nutrients and/or an increase in grazing pressure outweighing growth.

Oligotrophic gyres are regions where nutrient concentrations and productivity are very low. These regions are generally found at the heart of the subtropical gyres where stratification is very strong and the thermocline very shallow. These are the regions most limited by nutrient availability, as the hydrological conditions do not vary much over the year. As a result, phytoplankton do not display a strong seasonal cycle (see Figure 1.5). Any peaks in algal biomass are a result of sporadic mixing events that bring nutrient-rich water up from below the thermocline (Sournia, 1969, Shevyrnogov and Vysotskaya, 2006). Nitrogen (in the form of ammonium and dissolved organic nitrogen) can also be added by nitrogen fixing organisms (e.g. *Trichodesnium*) (Mulholland and Bernhardt, 2005, Mulholland *et al.*, 2006). For example, the summertime blooms regularly seen at Station ALOHA in the oligotrophic North Pacific are supported by nitrogen added through this biological process (Dore *et al.*, 2008). Additionally, sporadic blooms seen south east of Madagascar are thought to be dependent on diazotrophs as a source of nitrogen (Uz, 2007).

The oligotrophic regions are often seen to have a deep chlorophyll maximum (DCM) that is well below the depth that satellites can detect. This DCM has been seen to have a seasonal cycle that is dependent on light and nutrient availability at Station ALOHA in the North Pacific subtropical gyre. The DCM is found deeper in the water column in summer and also has larger chlorophyll values than in winter (Letelier *et al.*, 2004). This corresponds to a deepening of the nitracline and increases in irradiance. However, the DCM is a maximum in chlorophyll concentrations and not necessarily a maximum in biomass or primary production because the chlorophyll to carbon ratio is higher in the DCM than at the surface (Perez *et al.*, 2006). This is likely a response to lower light levels. The DCM is an interesting feature and its seasonal cycle is similar to that of a surface bloom. However, due to its depth in the water column it cannot be monitored on a global scale by satellites.

Equatorial regions (20°N – 20°S) have complex physical-biological interactions and nutrient supply depends on a wide range of factors. Some equatorial regions have the same conditions that characterise much of the subtropical and oligotrophic gyres with the thermocline being shallower than the nutricline. Nutrient limitation is alleviated when the MLD deepens towards the nutricline and nutrients are entrained from below (Wilson and Coles, 2005). Processes that act to deepen the MLD will increase productivity. This occurs in the western Pacific Ocean where periods of higher wind speed are associated with increased chlorophyll values (Kahru *et al.*, 2010). In upwelling regions in the tropics the relationship between chlorophyll and MLD is reversed with shallow MLD being associated with high chlorophyll values (Wilson and Coles, 2005). In upwelling systems the MLD and nutricline track each other so a shallow MLD gives phytoplankton near the surface access to nutrients. Equatorial regions are very complex and variable but not likely to follow a distinct seasonal cycle. In these regions phytoplankton population growth is modulated by equatorial upwelling, migration of the Intertropical Convergence Zone, passing eddies and tropical instability waves which drive variability at sub-seasonal timescales (Strutton *et al.*, 2001, Perez *et al.*, 2006).

1.4.2.1 Iron Limitation

In contrast to the nutrient-limited regions described above, some regions have abundant macronutrients but still have low phytoplankton abundance. These so-called High Nutrient Low Chlorophyll (HNLC) areas include the Southern Ocean, the north-east Pacific and the equatorial Pacific Ocean (Martin *et al.*, 1991). These regions are now generally considered to be limited by iron, which is the most important micronutrient for phytoplankton. Iron is readily oxidised to Fe(III) in the

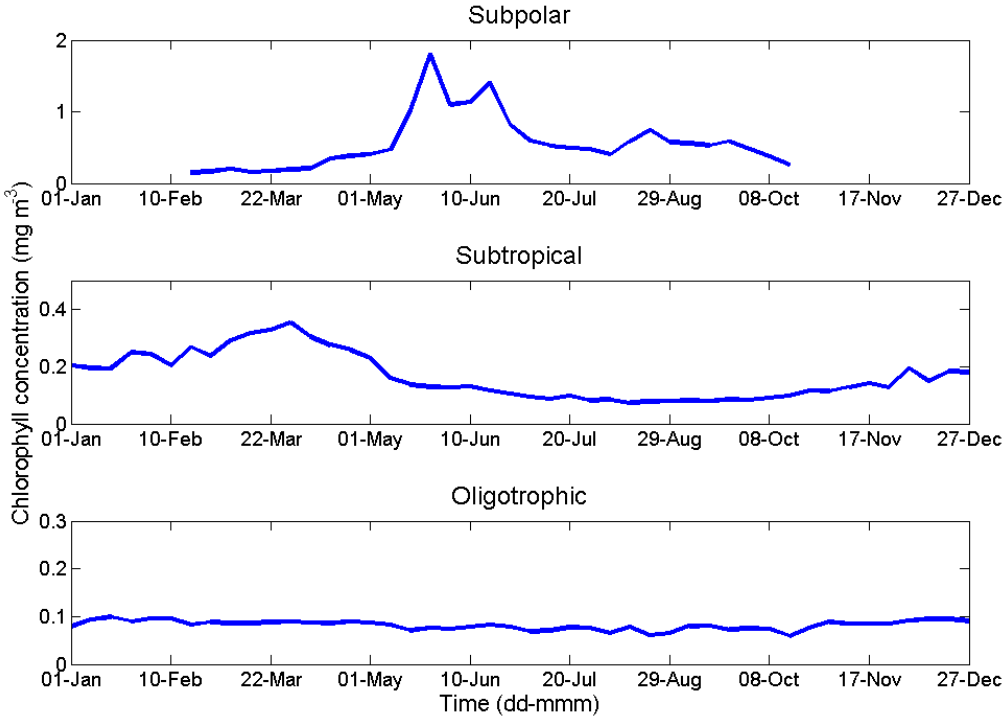

Figure 1.5: Example climatological (2002-2010) chlorophyll concentration time series from subpolar, subtropical and oligotrophic gyre regions from the GlobColour dataset. The subpolar region is heavily affected by missing data due to cloud cover plus low sun angle in the winter but the spring and autumn blooms are clearly seen. In the subtropics where the bloom starts in the autumn months, the bloom evolves more slowly than in subpolar regions. In the oligotrophic gyre a seasonal cycle is absent and chlorophyll concentrations are low year round. Note that the y-axes of the three panels cover significantly different chlorophyll concentration ranges.

ocean which is insoluble and cannot be taken up by phytoplankton. Only certain forms of iron are useful to phytoplankton such as dissolved inorganic iron (Hudson and Morel, 1990) or iron complexes (Hutchins *et al.*, 1999). The input of iron into the ocean originates either from the land, from benthic sediments or deposition of atmospheric dust. As such, it is typically areas that are far from the influence of land that are limited by iron. Several iron addition experiments have shown that phytoplankton doubling rates increased by a factor of 2-3 in the presence of increased iron concentrations (Martin *et al.*, 1991).

When iron concentrations are low the phytoplankton may adapt to reduce their iron requirements. The iron demand of a cell is mostly determined by its size and so large phytoplankton need more iron than small phytoplankton thus small phytoplankton typically dominate the community structure in HNLC regions (Chavez, 1989, Morel *et al.*, 1991). Another adaptation is using ammonia as a source of nitrogen rather than nitrate. Generally, phytoplankton take up nitrate, which then needs to be reduced before it can be used by the cell. This is done through the enzyme nitrate reductase and iron is needed for its synthesis (Timmermans *et al.*, 1994). If phytoplankton take up ammonia the nitrogen is already in its reduced form thus the cells iron demand is lower. These adaptations will give some phytoplankton functional types an advantage.

There is additionally some evidence that iron limitation has an impact on the phytoplankton community structure, as some phytoplankton functional types are more adapted to cope with living in an iron-limited region. In the north-east Pacific large phytoplankton cells were found to be abundant in the iron-rich coastal waters whereas the iron-limited oceanic waters were populated by small algal cells (Boyd and Harrison, 1999). A change in community structure and the type of nutrients used was observed in an iron addition experiment in the equatorial Pacific (Price *et al.*, 1991). When iron was added all phytoplankton increased in abundance but the largest increase was seen in large diatoms. The addition of iron also resulted in an increase in the rate of nitrate uptake whereas the uptake of ammonia was unaffected. This indicates that adding iron may either allow phytoplankton that use nitrate to be more efficient or increase the nitrate use for all phytoplankton present.

The Southern Ocean is a HNLC region but despite the low concentrations of iron Demidov *et al.* (2010) found a clear spatial trend in the timing of the bloom maximum. The chlorophyll peak occurred in November north of the Antarctic polar front, in December south of the front in Antarctic waters and then in January near the continent. Demidov *et al.* (2010) analysed the major factors affecting phytoplankton growth and concluded that light availability, determined by the depth of the mixed layer, was more important than iron availability.

1.4.3 Grazing

Grazing by zooplankton has been observed to be an important top-down control on phytoplankton populations (Dagg and Turner, 1982, Frost, 1991, Landry *et al.*, 1993, Gifford *et al.*, 1995). Zooplankton graze on phytoplankton and their seasonal cycle is driven by the seasonal cycle of phytoplankton. How efficient zooplankton are at grazing down the phytoplankton population depends on how closely their respective seasonal cycles are coupled. If they are closely coupled then zooplankton will respond immediately to rapid increases in phytoplankton and graze down the population. This may result in the absence of a bloom from the chlorophyll time series even though growth rates may be high (Heinrich, 1962, Parsons and Lalli, 1988). Alternatively, if they are described as loosely coupled, sometimes referred to as decoupled, then a bloom can occur as the slow zooplankton response means phytoplankton biomass can increase rapidly. The response of zooplankton to phytoplankton growth may depend on the hydrological regime of a region as well as the life history of the dominant grazer. In the North Atlantic the dominant grazer, *Calanus finmarchius,* has low overwintering stocks and long generation times so they are unable to increase quickly in response to the spring increase in phytoplankton (Colebrook, 1979). This is especially noteworthy west of Greenland where very cold water temperature restricts copepod development and reduces the grazing pressure resulting in a massive bloom (Colebrook, 1979). Additionally the timing and speed of onset of a bloom can influence grazing rates. From modelling North Atlantic blooms Waniek (2003) noticed that short, intensive blooms were rarely intensely grazed because the zooplankton abundance increased at a slower rate compared to the bloom; essentially they could not keep up. When the bloom was delayed with a slow onset, the bloom developed at a similar rate to zooplankton growth rates which resulted in higher grazing rates.

The subpolar North Pacific is characterised by the absence of a spring bloom and low constant chlorophyll values throughout the year (Banse and English, 1999, Goes *et al.*, 2004). Both Banse and English (1999) and Goes *et al.* (2004) report an absence of a spring bloom in the subpolar North Pacific though spring blooms are observed in coastal regions. The eastern subpolar gyre has low constant chlorophyll values throughout the year whereas some areas in the western subpolar gyre display only an autumn bloom. The first hypothesis to explain this pattern was that zooplankton grazed down the spring bloom (Heinrich, 1962). Due to the life history of copepods, the dominant zooplankton type in the subpolar North Pacific, their larvae are in copepodite form and ready to feed when phytoplankton growth rate increases in spring, resulting in the absence of a bloom. The adults emerge

from their winter hibernation and immediately lay their eggs, using up their lipid reserves. In contrast copepods in the North Atlantic emerge from hibernation and then need to feed in order to produce and lay eggs (Parsons and Lalli, 1988). This hypothesis also explains the autumnal bloom in the North Pacific as a result of relaxation in grazing pressure as the zooplankton start to migrate down deeper into the water column to overwinter (Banse and English, 1999).

However, an alternative hypothesis was postulated by Miller (1993) and Banse and English (1999) stating that it was microzooplankton not the large copepods that represent the main grazing control. The local hydrography may also play a role as the shallow and permanent halocline results in favourable light conditions and allows for low, but continuous, levels of production over the winter, which sustains the microzooplankton population until the spring when primary production rates increase (Evans and Parslow, 1985, Boyd and Harrison, 1999).

As previously mentioned the North Pacific is a HNLC region, and so an alternative hypothesis is that iron limitation suppresses the spring bloom in the chlorophyll time series. An explanation for the autumn bloom was discussed in Banse and English (1999) in which phytoplankton growth is limited by iron in the spring but an addition of iron in the autumn months allows for an autumn bloom to occur. The source of this iron may be from the advection of coastal water, enhanced mid ocean upwelling, dust deposition from inner Asia or volcanic eruptions (Hamme *et al.*, 2010) though not all of these processes have a seasonal cycle. Overall, the absence of a spring bloom and the sporadic presence of an autumn bloom may be the result of the combination of grazing control and iron limitation (Landry *et al.*, 1993).

Grazing is seen to be a major control in oligotrophic regions where zooplankton abundance is tightly coupled with that of phytoplankton (Sournia, 1969, Blackburn *et al.*, 1970, Shevyrnogov and Vysotskaya, 2006). As nutrient concentrations are low all year round small perturbations that increase nutrients result in only a small increase in phytoplankton abundance to which grazers respond quickly. As a result phytoplankton and zooplankton populations remain closely coupled throughout the year (Longhurst, 1995). Additionally, as the mixed layer depth varies little throughout the year zooplankton do not overwinter and encounter rates stay fairly constant. Any increase in phytoplankton growth such as that due to mixing by a passing storm is grazed immediately resulting in low, constant surface chlorophyll concentrations throughout the year.

1.4.3.1 Match-mismatch Hypothesis

As phytoplankton form the base of the marine food web, changes in their seasonality will have implications for higher trophic levels. One implication is the degree of match or mismatch between the abundance of phytoplankton and fish larvae, which form part of the zooplankton population. Ideally, the timing of phytoplankton blooms and timing of spawning will coincide so that larvae have a plentiful food supply (Figure 1.6). Indeed, zooplankton abundance has been reported to be more dependent on the length of time food is available rather than the magnitude or timing of phytoplankton abundance (Colebrook, 1979, Mackas *et al.*, 2012). On George's Bank, North-western Atlantic, warmer years are associated with earlier bloom onset and a longer growing season. This gives a large overlap in the coexistence of phytoplankton and cod larvae resulting in higher cod survival rates (Kristiansen *et al.*, 2011). Additionally, Platt *et al.* (2003) found a link between the timing of the peak of the bloom and the survival of haddock larvae with larger year-classes in years when the bloom peak occurs earlier. This indicates that the degree of overlap may be more important than a match in peak timing between phytoplankton and grazers.

The match-mismatch hypothesis also tells us about the reproductive strategy of different types of grazers. Fish typically release their eggs before the bloom has occurred and are "predicting" that the timing of the bloom will coincide with the eggs hatching (Mackas *et al.*, 2012). As fish are relatively long-lived organisms they will have more than one chance to reproduce so by aiming for the mean date of bloom timing, over an organism's lifetime, they are likely to be successful in reproduction. In contrast, many smaller zooplankton species get only one chance to reproduce and so they need to be able to "sense" when the bloom is happening. This is probably done through a currently unknown environmental cue as many zooplankton phenology studies show strong correlations with temperature (Beaugrand, 2004, Chiba *et al.*, 2006, Mackas *et al.*, 2012).

The shrimp, *Pandalus borealis*, is an example of a species that has evolved to time their egg hatching to the mean bloom timing. The length of the egg development period and the timing of hatching for *Pandalus borealis* is determined by the bottom water temperature (~200-500m) (Koeller *et al.*, 2009). Colder bottom water temperatures cause a long egg development time and later hatching. Although the processes controlling bottom temperature are separate from surface processes that control bloom timing, a strong relationship between bloom timing and the timing at which 50% of the eggs had hatched was reported (Koeller *et al.*, 2009). It is hypothesised that spawning times evolved according to the long-term mean in local bottom temperatures so that spawning coincided with the bloom.

The consequence of this is that some years will be a perfect timing match resulting in very large year-classes.

In the Arctic the timing of ice melt determines whether boreal or Arctic zooplankton species dominate which has implications that echo up the food chain (Leu *et al.*, 2011). Before the ice melts, Arctic zooplankton species feed on ice algae and then lay their eggs. These eggs hatch when the post-ice breakup pelagic bloom occurs which they then feed on. In years when the ice breaks up earlier than usual the ice algae bloom is shortened and the pelagic bloom occurs earlier (Leu *et al.*, 2011). Though overall production is increased, there are lower abundances of Arctic zooplankton species and less recruitment, while boreal zooplankton species dominate the community. At the other extreme, in years when the ice breaks up later than normal then the Arctic species thrive. This has repercussion for predators of zooplankton as Arctic species are a higher quality food source (i.e. they have higher concentrations of lipids) than boreal species. Potentially, this could transfer up the food chain and affect foraging times of larger species.

The implications of the match-mismatch hypothesis become even more pertinent when a trend towards either earlier or later blooms is considered, a situation that is probable under climate change. A decline in the recruitment of fish larvae may occur if the timing of the phytoplankton bloom shifts either earlier or later but the timing of larval spawning continues to target the mean bloom timing. This may in turn result in the decline of many economically important fish species. Climate change may also result in zooplankton changing their phenology or evolving to have feed and spawn life strategies where the adults spawn when they are well fed rather than spawning at a time of year when food is expected to be plentiful (Cushing, 1990). Many studies find that zooplankton phenology follow an "earlier when warmer" response to environmental conditions though the exact trigger for zooplankton population growth is not known *(Mackas et al., 2012)*. While it might be suspected that this is a simple function of warm temperatures accelerating zooplankton development, the observed variability in zooplankton phenology is greater than that predicted by the relationship between developmental rates and temperature (Mackas *et al.*, 2012). Furthermore, zooplankton species which peak in the autumn show a "delayed when warmer" response (Conversi *et al.*, 2009). Regardless of whether zooplankton are responding to temperature or to a variable that co-varies with temperature it is likely that in a future warmer world there will be significant changes to both phytoplankton and zooplankton phenology.

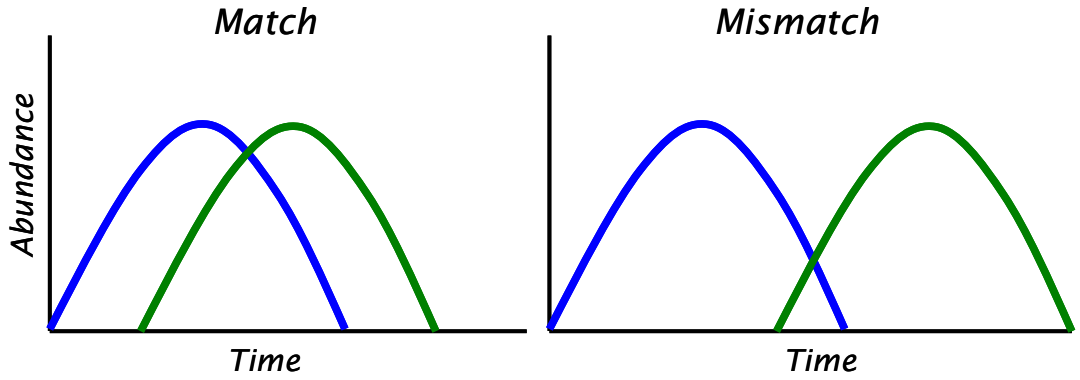

Figure 1.6: A cartoon of the match-mismatch hypothesis. The diagram shows the timing of larvae hatching (blue) and phytoplankton bloom (green) (larval food). The timing of the phytoplankton bloom is shown to be very variable. Where high phytoplankton abundance coincides with the larvae bloom there is a "match" in the respective timings. When the bloom occurs later there is a shorter amount of time where larvae and their food are both present (i.e. a "mismatch"). Adapted from Cushing (1990).

1.5 Variability in Phytoplankton Seasonality

As has just been discussed, phytoplankton growth is dependent on sufficient light, nutrient concentrations and grazing pressure and many physical processes affect their availability. The interplay and variability of these processes in turn gives rise to variability in the magnitude and phenology of phytoplankton seasonal cycles. This variability may be seen on a variety of temporal and spatial scales and the dominant control of that variability may differ between scales. For temporal variability we can quantify annual, interannual and decadal variability and for spatial variability we can examine the effect of mesoscale features such as eddies up to basin scale circulation processes on phytoplankton. Additionally, many long-term, large-scale modes of variability can be described by climate oscillations and these are often used to explain interannual and decadal variability in phytoplankton abundance.

Investigating the drivers of phytoplankton variability has two main applications. The first is to extend and deepen our understanding of phytoplankton dynamics and the causes and effects of variable seasonality. The second is to use our knowledge of contemporary variability to predict future trends. By understanding relationships based on historical variability we may be able to make predictions for changed conditions. In this way, we may also be able to detect climate change-driven trends because we will have quantified what is "normal". This section summarises our current understanding of variability in phytoplankton seasonality and the drivers behind it.

1.5.1 Characterising Seasonality

Phytoplankton seasonality is a way of describing the seasonal cycle of phytoplankton growth and can be split into two themes, timing and magnitude. The variability in the magnitude of the seasonal cycle (either chlorophyll or primary production) has received much attention in the literature (e.g. Edwards *et al.* (2001), Follows and Dutkiewicz (2002), Gregg and Conkright (2002), Behrenfeld *et al.* (2006), Kahru *et al.* (2010), Lozier *et al.* (2011)) but timing is a relatively new aspect of blooms that has recently become better studied (Ji *et al.*, 2010). In the case of phytoplankton blooms we can calculate the events that are of interest to us, mainly the timing or date of the beginning, peak and end of the bloom. These characteristics are given the term phenology (i.e. the study of the timing of annually occurring events).

The variability in magnitude has been well examined and there are several global studies that identify physical parameters that are important drivers of variability in phytoplankton production (e.g. wind speed (Kahru *et al.*, 2010), stratification (Behrenfeld *et al.*, 2006) and SST (Martinez *et al.*, 2009, Boyce *et al.*, 2010)). Correlations of chlorophyll concentration with physical parameters are often used to determine the dominant physical processes. Some parameters such as SST and wind speed or wind stress are relatively straightforward to measure from remote sensing platforms. These are useful indicators of the degree of stratification as warmer SST is associated with higher stratification whereas wind increases mixing, cools the surface and erodes stratification. Other measurements could also be used for correlations such as nutrient concentrations, thermocline depth and current speeds although these require *in situ* monitoring.

Wind strength was seen to be well correlated with surface chlorophyll concentrations in a global study of wind speed and chlorophyll-a concentration anomalies ((Kahru *et al.*, 2010) see Figure 1.7). The sign of the correlation also followed the expected spatial pattern. Subpolar regions were negatively correlated as stronger winds deepen the mixed layer, reduce light availability and therefore inhibit growth. Meanwhile, the subtropics were positively correlated as stronger winds deepen the mixed layer, entraining nutrients and boosting productivity.

SST is a good indicator of the depth of the mixed layer with high SST being associated with shallow MLD. This negatively correlated relationship was reported to occur over 87% of the world's oceans by (Wilson and Coles, 2005). SST is used as an indicator as it is easy to measure from space whereas a direct measurement of the MLD requires *in situ* information on density variations with depth. Many studies have reported a strong relationship between SST and phytoplankton growth on interannual timescales (Behrenfeld *et al.*, 2006, Grodsky *et al.*, 2008, Martinez *et al.*, 2009). An inverse relationship between SST and net primary production is seen for 74% of the permanently stratified ocean, where a strong and relatively shallow thermocline is present all year, by Behrenfeld *et al.* (2006) (Figure 1.8). Higher SST is indicative of higher stratification which in the permanently stratified oceans results in greater nutrient limitation and lower primary production. In the subpolar North Atlantic, the opposite relationship was observed with high SST being indicative of high chlorophyll concentrations (Edwards *et al.*, 2001).

The first steps towards characterising seasonality through bloom timing have been to define seasonality metrics such as the timing of bloom initiation, peak and end (Platt *et al.*, 2010), although there are several ways in which these phenological events can be defined (see Ji *et al.* (2010) for a summary). A couple of recent

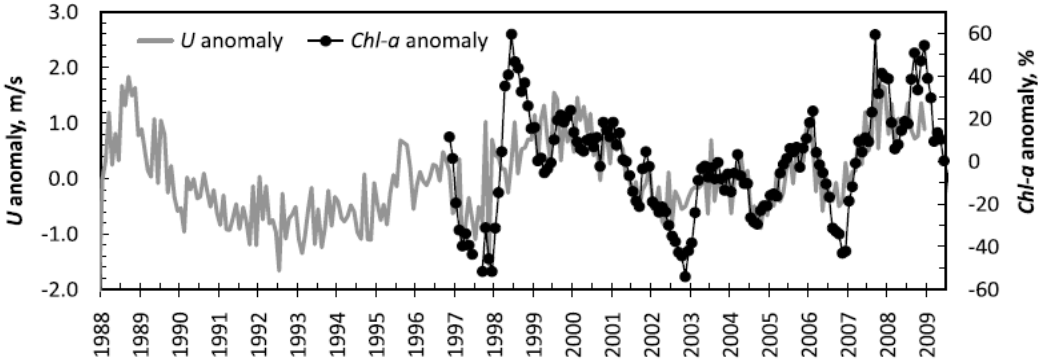

Figure 1.7: The correlation of chlorophyll-a anomalies (Chl-a, %) and wind speed anomalies (U, ms^{-1}) from the western Equatorial Pacific. From Kahru *et al.* (2010).

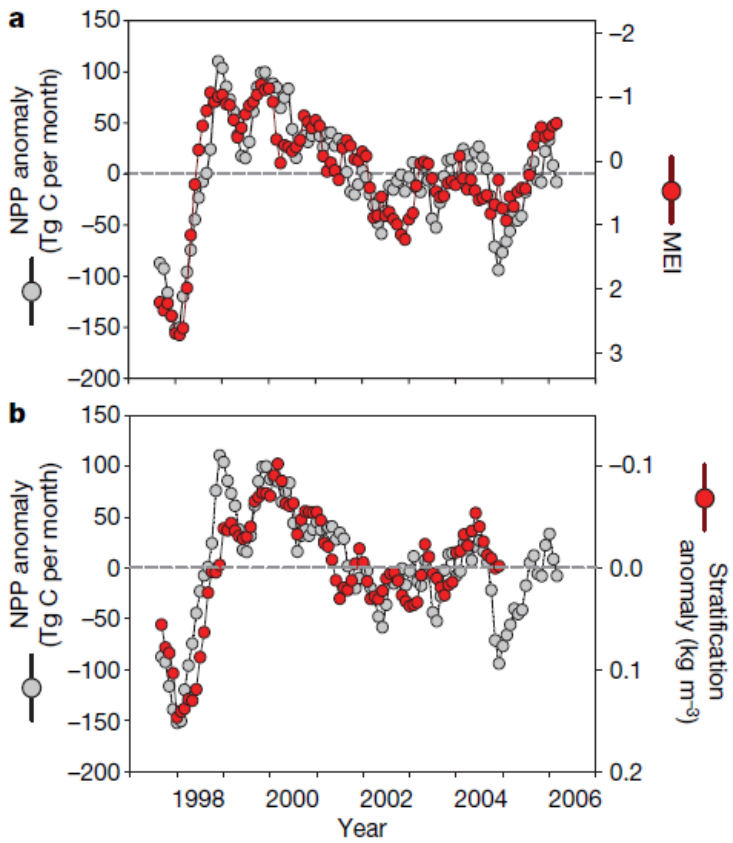

Figure 1.8: Net primary production (NPP) anomalies for the permanently stratified ocean plotted against (a) the Multivariate ENSO Index (MEI), and (b) stratification. Note that the y-axis for both MEI and stratification is in an opposite sense to NPP. Both MEI and stratification are seen to be negatively correlated with NPP. From Behrenfeld *et al.* (2006).

studies have built a climatology of bloom characteristics to attempt to quantify phytoplankton phenology and form a baseline for future studies.

Sapiano *et al.* (2012) formed a global climatology of bloom characteristics by fitting Generalized Linear Models (GLM) to Sea-viewing Wide Field-of-view Sensor (SeaWiFS) chlorophyll time series. From this climatology the date of phenological events was seen to occur later with increasing latitude, following the seasonal increase in light gradient. This spatial pattern in dates was fairly constant zonally with subpolar blooms starting in spring and ending in autumn and subtropical regions starting in autumn and ending in spring. Similar latitudinal gradients in bloom timing were found by Racault *et al.* (2012). Additionally, Racault *et al.* (2012) found strong positive correlations between SST and subpolar bloom duration and negative correlations with subtropical bloom duration. These relationships indicate that earlier stratification (and thus warmer than usual surface waters) result in an extension to the subpolar growing season and a contraction of the subtropical growing season. These results support the existing evidence for subpolar blooms driven by the alleviation of light limitation and subtropical blooms driven by increased nutrient concentrations.

An additional aspect of quantifying seasonality is defining those areas where a seasonal cycle dominates the annual variability and those areas where variability is concentrated at shorter time scales. Doney *et al.* (2003) used satellite-derived chlorophyll time series to determine the spatial structure of processes that occur on time scales of less than one month. This was done by measuring the ratio of the variance of submonthly processes to the variance of the whole time series. These submonthly processes were found to be the dominant influence on the variability in the oligotrophic gyres whereas processes with longer time scales dominated the variability at higher latitudes. This type of analysis can add to our understanding of interactions between phytoplankton and their environment on different temporal scales.

1.5.2 Variability in Bloom Timing

Recently there have been many studies on the variability in bloom timing. Many of these studies are regional and a variety of methods are used to quantify phenological events. Despite these differences, a consistent picture emerges detailing the variability in different regions and the controls on the timing of events.

1.5.2.1 Polar and Sea Ice Regions

Over the majority of the ocean the depth of the mixed layer is controlled by the balance between thermal stratification and mixing. Salinity variations become important in regions where large amounts of freshwater enter the ocean such as the

marginal ice zones in the polar seas. The melt water is fresher and less dense and so forms a density gradient which stratifies the water column. Additionally, riverine input is an important source of freshwater input and has been reported to establish haline stratification especially over shelf regions (Carmack *et al.*, 2006, Popova *et al.*, 2010). The effect on phytoplankton is exactly the same as thermal stratification (i.e. the shallower the MLD the more light phytoplankton receive).

The effect of melting sea ice on the timing of the spring bloom creates variability both spatially and temporally. Satellite observations from the northwest Atlantic analysed by Platt *et al.* (2010) found that the spring bloom at 61.5°N occurred on average 33 days earlier than the spring bloom further south at 59.5°N. This is contrary to the expected latitudinal gradient, indicating that blooms happen later further north as these regions stratify later due to the spring warming occurring later in the year. From the same region, Wu *et al.* (2007) correlated the date on which the spring bloom started with the date on which the ice began to retreat and found that, on an interannual scale, they were strongly correlated. Similar results were obtained by Ji *et al.* (2012) with the timing of the pelagic bloom being strongly linked to the timing of sea ice melt in the Arctic Ocean. Together these studies identify haline stratification as a major control on bloom initiation in marginal sea ice zones.

1.5.2.2 Subpolar Regions

The timing of the subpolar North Atlantic bloom has been relatively well studied. However, Follows and Dutkiewicz (2002) showed that interannual variability in the bloom magnitude has weak links to meteorological forcing. The variability in bloom initiation dates has been reported to vary by 2-3 weeks over the whole basin (Henson *et al.*, 2009), (Figure 1.9) and by up to 1 month in the Irminger Basin (Henson *et al.*, 2006). This variability has been linked to meteorological conditions, namely wind speed and net heat flux (Henson *et al.*, 2006). Furthermore, the annual mean MLD showed a strong negative correlation with the bloom initiation date (Henson *et al.*, 2009).

Wind was also identified as a key factor in bloom timing variability by Ueyama and Monger (2005). They examined the spatial variability in bloom timing and found that it could be explained by the pattern of variability in wind mixing over the bloom period. They also concluded that convection was important for the seasonal development of blooms but wind-induced mixing during the bloom period appeared to affect the timing of bloom onset. Both Henson *et al.* (2009) and Ueyama and Monger (2005) saw links between the bloom timing and the dominant atmospheric mode of interannual variability in the North Atlantic, the North Atlantic Oscillation (NAO) (see section 1.4.3).

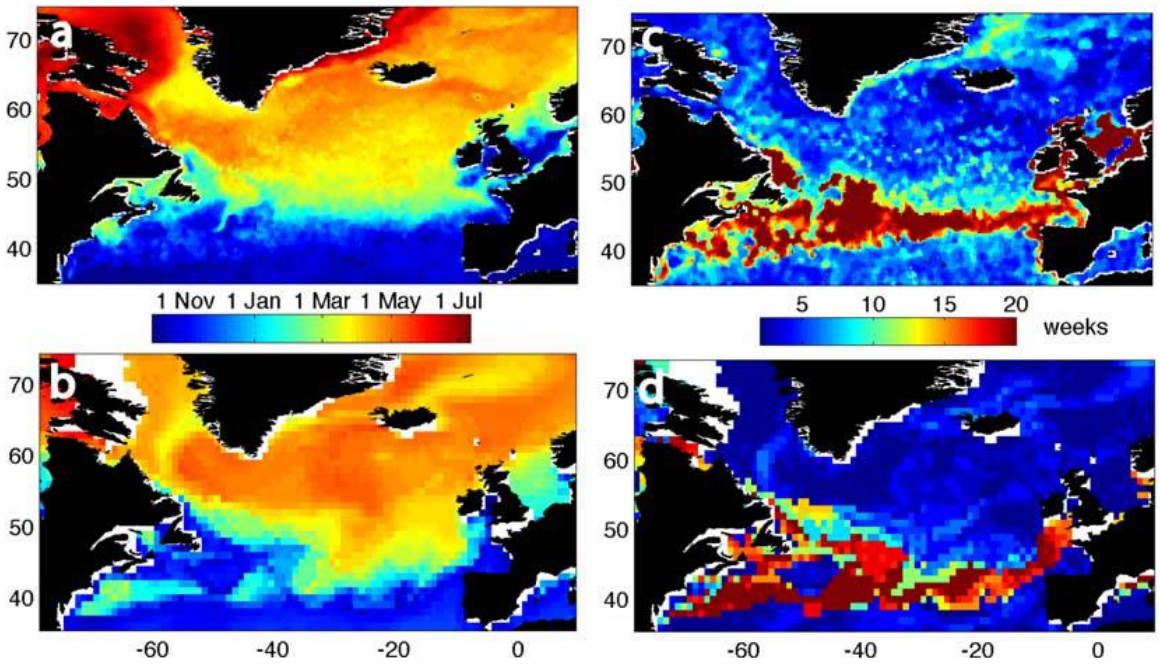

Figure 1.9: The timing of the spring bloom in the North Atlantic as assessed from (a) SeaWiFS chlorophyll data and (b) Geophysical Fluid Dynamics Laboratory (GFDL) model output. On the right hand side of the plot are shown (c) the range in the bloom start date from SeaWiFS chlorophyll data and (d) from the GFDL model output. The transition zone (see text) is clearly seen as a band of red in plots c and d. From Henson *et al.* (2009).

The North Pacific also offers opportunities to highlight differences between various regimes. The California Current System is situated on the eastern side of the North Pacific and is a coastal upwelling system. The bloom onset date varies between 1-3 months interannually and coincides with the onset of upwelling favourable winds (Henson and Thomas, 2007). This event usually occurs in spring and as the water upwells it drags nutrient-rich water up to the surface at the coast fuelling the bloom. The variability in the timing of upwelling winds was reported to be controlled by the North Pacific Gyre Oscillation (NPGO) index (Chenillat *et al.*, 2012) another atmospheric mode of variability. On the western side of the Pacific Ocean in the Japan Sea the peak timing was seen to vary by 40 days and was earlier in years when the thermal stratification was stronger than average (Yamada and Ishizaka, 2006). The date of bloom initiation varied by up to a month between years and was earlier when the bloom period wind speed was weaker than average.

The controls on phytoplankton growth in the Southern Ocean are very complex; the region is iron-limited as well as light-limited, ocean fronts are ubiquitous and the seasonal melt of sea ice produces haline effects. Thomalla *et al.* (2011) classified different regions in the Southern Ocean according to the seasonal characteristics of chlorophyll magnitude and seasonal reproducibility (high reproducibility means low interannual variability in the shape and size of the seasonal cycle) and linked these regions to certain physical and chemical settings. Four major regions were defined based on whether annual chlorophyll and seasonal reproducibility were high or low. High chlorophyll and high reproducibility regions represented the characteristic subpolar cycle and were found at ocean fronts, continental margins and shallow bathymetry. These regions are not iron-limited and the seasonal cycle is driven by the seasonal cycle in light, MLD and heat fluxes. Regions of low chlorophyll but high reproducibility were nutrient-limited but this limitation was seasonally alleviated to give its high reproducibility. Regions with low chlorophyll and low reproducibility were perennially iron-limited. High chlorophyll regions with low reproducibility were regions where there was high interannual and intraseasonal variability in the MLD and thus nutrients and light. This shows how iron limitation can alter the seasonal cycle and introduce substantial variability in the timing of blooms (as in the regions of low reproducibility).

Over the whole basin the bloom initiation date varied by 24-48 days in the subpolar regions (Thomalla *et al.*, 2011). Centred at 40°S a transition zone representing the boundary between subpolar and subtropical regions where interannual variability in bloom timing is high (up to 80 days standard deviation) was identified. This agrees with observations by Henson *et al.* (2009) which saw a

similar transition zone in the North Atlantic where bloom initiation ranged by up to 20 weeks.

1.5.2.3 Subtropical Regions

In subtropical regions, the increase in mixing and entrainment of nutrients in autumn starts the bloom and the strengthening of stratification in early summer causes the bloom to decline. In the North Atlantic the date of bloom initiation was seen to vary by 2-3 weeks (Henson *et al.*, 2009). Spatially, the timing of subtropical blooms becomes later further poleward (Dandonneau *et al.*, 2004, Vargas *et al.*, 2009) However, Dandonneau *et al.* (2004) observed some anomalous regions where blooms started in subtropical regions which were not in keeping with the poleward progression of bloom timing. These bloom start dates occurred during the period of low nutrient concentrations so another source of nutrients must be present to fuel the bloom. One such source could be strong mesoscale activity which drives nutrient entrainment (Longhurst, 2001). On the other hand, blooms of *Trichodesdium* may be responsible for the anomalous bloom initiation dates as they fix atmospheric nitrogen and are able to be a nutrient supply for other phytoplankton when stratification is high and growth is expected to be low (Mulholland *et al.*, 2006).

Interannual variability in bloom magnitude in the subtropics has not been very strongly linked to environmental factors, though on seasonal timescales there can be very strong relationships. For example, at the Bermuda Atlantic Time-series Study (BATS) site located in the subtropical North Atlantic, primary productivity is strongly related to the strength of stratification (Menzel and Ryther, 1961). In contrast, at Station ALOHA (A Long-term Oligotrophic Habitat Assessment part of the Hawaii Ocean Time Series (HOTS) project) in the subtropical North Pacific Ocean, Dave and Lozier (2010) found that on seasonal timescales primary production was highest when stratification was highest because of the presence of nitrogen fixing phytoplankton. These organisms thrive in highly stratified waters, and while they are also present at BATS they only contribute significantly in summer when stratification is highest. In winter, BATS experiences a substantial deepening of the mixed layer and so conditions are not ideal for nitrogen fixers whereas high stratification and shallow mixed layer conditions persist throughout the whole year at Station ALOHA. Despite the strong seasonal relationships, on interannual time scales primary production was not seen to be related to stratification at Station ALOHA (Dave and Lozier, 2010) and a similar result was obtained in a basin scale analysis of the subtropical North Atlantic (Lozier *et al.*, 2011). In light of this, although no obvious driver of interannual variability in primary production has been identified, this may not be true for variability in bloom timing. Investigating the

interannual drivers of bloom timing in subtropical regions may shed light on the complex interplay of processes that affect phytoplankton growth in these locations.

1.5.2.4 Coastal Regions and Shelf Seas

Though the focus here is on blooms in the open ocean, variability in bloom timing may also be seen in coastal regions. It is useful to discuss these briefly as, although the response to physical changes may be different, the underlying concept of environmental conditions affecting seasonality is the same.

In the North Sea, Edwards and Richardson (2004) assessed the phenological changes in the seasonal peak over several decades in five functional groups and linked the variability in timing of phytoplankton and zooplankton to NAO. Nearly all the species that reach their peak abundance when the water column is stratified are seen to have a trend towards earlier peak dates with a positive NAO index. A positive NAO index is indicative of warmer SST and weaker westerly winds resulting in potentially earlier stratification. Temperature changes were important for other functional types especially those where their development is either controlled by temperature or only bloom once stratification occurs. One such example is the date of benthic larval release, which was seen to become earlier from 1992-2002 over which time the NAO index was predominantly positive. In addition to this study, two species of diatoms from the North Sea studied by Schlüter *et al.* (2012) were seen to bloom earlier in warmer years. Interestingly, they also observed the impact of grazing pressure on bloom timing as one of the species had earlier blooms when grazing pressure was lower.

In coastal locations where the tides are strong, the spring-neap tidal cycle may also play a role in causing variability in bloom timing. Using a 1-D numerical model, Sharples *et al.* (2006) found that the strong mixing during spring tides broke down the stratification in the water column built up over the neap tides, which resulted in a range of 13 days in the bloom initiation date. In some years a double pulse bloom was reported when stratification was broken down and then built up again as the tides changed from neap to spring and back to neap again.

There are many other processes associated with coastal systems that have been related to variability in bloom timing. In Narragansett Bay bloom timing is correlated with the position of the Gulf Stream North Wall (Borkman and Smayda, 2009). Conversely, wind speed was the most significant driver of bloom initiation date which varied up to 6 weeks in the Strait of Georgia (Collins *et al.*, 2009). Furthermore, in two different studies on the Scotian shelf, Song *et al.* (2010) found that surface salinity was the most strongly correlated variable with the date of spring bloom onset, and Zhai *et al.* (2011) found the position of the shelf break

front marked two different bloom start date regions. These coastal examples may not be wholly applicable to the open ocean but they do give further insight into the many ways the physical environment can influence phenology. All these coastal studies are complicated by the additional processes found in coastal systems such as fronts, river discharge, shallow bathymetry and tides but in summary, there is still a sense that stratification, light, nutrient and grazing are important for bloom timing variability.

1.5.3 Climate Oscillations

Climate oscillations encapsulate how large-scale patterns in environmental conditions change over time and can explain much of the variance in the magnitude of blooms as well as timing. They are often based on physical parameters such as SST, wind stress and sea level pressure differences (Table 1.1). The strength of an oscillation is described by its index, which represents the deviation of physical parameters (e.g. SST) away from the long-term mean. The sign of the index shows if the oscillation is in a positive or negative phase and this indicates the impacts seen on the environment.

Table 1.1: Table of selected climate oscillations and characteristics.

Name	Periodicity	Region	Positive phase	Negative phase
ENSO[a] (Rasmusson and Wallace, 1983)	Inter-annual	Equatorial Pacific (but also has global impacts)	Warm phase is known as El Niño. Positive SST anomalies in eastern Pacific. Deepening of thermocline in eastern Pacific and shoaling in the west. Weakening or reversal of easterly winds.	Cold phase known as La Niña. Negative SST anomalies in eastern Pacific. Shoaling of thermocline in eastern Pacific and deepening in the west. Strong easterly winds.
NAO[b] (Hurrell, 1995)	Decadal	North Atlantic	Large difference in pressure between Azores high and Icelandic low. Stronger westerly winds. Negative (positive) SST anomalies in eastern (western) Atlantic.	Small difference in pressure between Azores high and Icelandic low. Weaker westerly winds. Positive (negative) SST anomalies in eastern (western) Atlantic.
PDO[c] (Mantua *et al.*, 1997)	Decadal	North Pacific	Cool SST in central N. Pacific but warmer along west coast of USA. SLP[d] is low over central N. Pacific but higher over west coast USA. Anticlockwise wind stress over N. Pacific.	Warm SST in central N. Pacific and cooler SST along the west coast of North America. SLP[d] is higher over central Pacific and lower over west coast of North America. Wind stress direction is reversed (i.e. clockwise).

[a] ENSO stands for El Niño-Southern Oscillation and is often represented by the multivariate ENSO index based on SLP[d] surface wind components, SST, surface air temperature and total cloudiness fraction of the sky (Wolter, 1987).

[b] NAO is the North Atlantic Oscillation and is based on the difference in SLP between the Azores high and Icelandic low pressure systems.

[c] PDO is the Pacific Decadal Oscillation and is based on the leading principal component of SST anomalies in the North Pacific.

[d] SLP stands for sea level pressure.

For example, the NAO index is based on differences in sea level pressure between the Icelandic low and the Azores high pressure systems. Though the index does not provide a mechanistic explanation of why the oscillation occurs or what causes it, it does give a numerical index which describes variability in environmental conditions. These may be increases or decreases in wind speed, SST, or stratification and this in turn determines light and nutrient availability and thus affects the response of phytoplankton to changes in the phase of the oscillation.

These large-scale climate indices have been linked to variability in chlorophyll concentrations in many regions. Since they are based on physical parameters, they can help to identify the physical processes that may be important for bloom variability on interannual and decadal time scales. There are many climate indices so only a few specific examples are given below.

1.5.3.1 Interannual variability

The El Niño-Southern Oscillation (ENSO) is a climate oscillation that acts over interannual time scales. It is classed as interannual because positive or negative phases will last approximately one year giving rise to variability between years. Decadal oscillations remain in one phase for several years and so results in variability between decades. Therefore there may be modes of variability acting in the same region on both interannual and decadal timescales. Long time series are needed to fully capture these long-term oscillations. This prevents several years of an increase or decrease in a variable (i.e. phytoplankton abundance) being mistaken for a long-term trend.

1.5.3.1.1 El Niño-Southern Oscillation

The El Niño-Southern Oscillation is comprised of two parts; the first is El Niño which described anomalously warm waters in the equatorial Pacific and the second is the Southern Oscillation which describes the corresponding changes in the atmosphere (Trenberth, 2001). El Niño events are often reported as having an impact on chlorophyll or primary production (Dandonneau *et al.*, 2004, Behrenfeld *et al.*, 2006, Strutton *et al.*, 2008, Boyce *et al.*, 2010). The normal conditions in the equatorial Pacific are that winds blow east to west piling up warm water in the western Pacific and causing cold, nutrient-rich water to be upwelled in the eastern Pacific. The thermocline is deepest in the west and shallow in the east. During an El Niño event, the easterly winds weaken which weakens the upwelling and deepens the thermocline. It also allows the warm water in the west to spread eastwards which also inhibits upwelling. La Niña is an extreme of normal conditions and is characterised by a very shallow thermocline in the eastern Pacific and strong

upwelling. ENSO primarily describes variability in phytoplankton abundance in the equatorial Pacific Ocean.

The multivariate ENSO index (MEI) is often used to describe the oscillation between El Niño and La Niña events. It combines information on sea-level pressure, SST, surface air temperature, surface winds and cloudiness. Net primary productivity anomalies over the permanently stratified regions of the global ocean were seen to be negatively correlated with the MEI (Behrenfeld *et al.*, 2006). When the MEI is in a positive phase (an El Niño event) SST is higher, stratification increases and the nutricline is deeper which inhibits phytoplankton growth.

However, when focusing on just the equatorial Pacific to study local effects of ENSO, Strutton *et al.* (2008) found that though chlorophyll concentrations decreased during El Niño events they did not increase during La Niña events. Strutton *et al.* (2008) argue that the increase in primary production reported by Behrenfeld *et al.* (2006) was due to the increase in the spatial extent of the upwelling tongue. To examine why La Niña events did not increase primary production Strutton *et al.* (2008) looked at the dominant processes correlated with phytoplankton variability. In the eastern basin, El Niño suppresses the thermocline and thus the availability of macronutrients, which are normally entrained from below the thermocline resulting in lower abundance. During La Niña conditions strong upwelling favourable winds raise the concentration of macronutrients. However, Strutton *et al.* (2008) does not report a response in phytoplankton abundance. Over large spatial scales La Niña events increase primary productivity because the extent of the tongue increases but locally there is not necessarily an increase in production. This suggests that there must be another limiting factor. Strutton *et al.* (2008) suggest iron limitation as the reason for this lack of response. Nutrient concentrations increased due to stronger upwelling but the source of iron to this region is from the equatorial undercurrent (EUC) (Landry *et al.*, 1997). Iron concentrations will only increase with wind mixing that is strong enough to reach the EUC, which is located deeper in the water column than the nutricline. As a result, while macronutrient concentrations are elevated during La Niña events, the availability of the micronutrient iron is responsible for the seemingly anomalous non-response by phytoplankton.

The effects of ENSO are also felt in phytoplankton communities in the subpolar North Pacific. Sasaoka *et al.* (2011) linked timing variability of the blooms to the mean winter Southern Oscillation Index (SOI) index which described the atmospheric changes associated with ENSO. Sasaoka *et al.* (2011) clustered together similar regions based on the chlorophyll time series across the subpolar

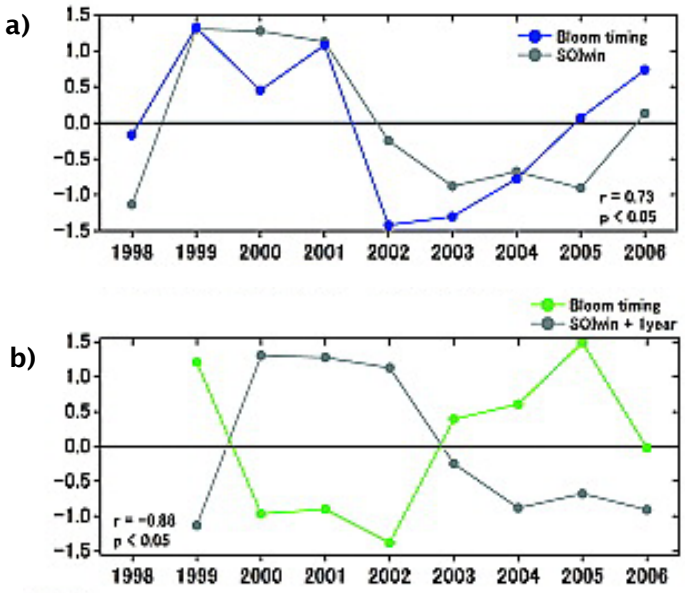

Figure 1.10: Interannual variability in bloom timing and climate oscillations. Panels show the interannual variability of (a) Group A (marginal sea/coastal) bloom timing and the winter mean Southern Oscillation Index and (b) Group B bloom timing and the mean Southern Oscillation Index with a 1 year lag. Group A bloom timing is earlier in El Niño years and Group B (open ocean) bloom timing is earlier in La Niña years. Bloom timing was calculated from SeaWiFS chlorophyll data. From Sasaoka *et al.* (2011).

North Pacific and found two groups which responded to ENSO. The marginal sea/coastal group (group A) had earlier blooms in El Niño years, which are associated with warmer SST and thus earlier stratification that alleviates light limitation (see Figure 1.10a). Meanwhile, the open ocean group had the opposite response with earlier blooms occurring in La Niña years (see Figure 1.10b). Group B are regions of the Pacific know to be limited by iron so in La Niña years when SST is cooler, this indicates there is more vertical mixing and more entrainment of iron from below the thermocline to alleviate nutrient limitation.

Phenological changes associated with ENSO have also been reported in the western North Atlantic. D'Ortenzio *et al.* (2012) clustered chlorophyll time series from SeaWiFS data and found that the "Transitional Bloom" group expanded during La Niña years at the expense of "Bloom" and "Subtropical" groups. Closer analysis revealed that this change was characterised by a muted seasonal cycle and an earlier bloom peak. Concurrently, in this region, the annual maximum MLD became shallower in La Niña years. The phenological response to the MLD changes is consistent with a reduced nutrient flux to the surface because of stronger stratification. This example also highlights that ENSO influences bloom variability in ocean basins outside of the Pacific.

1.5.3.2 Decadal Variability

1.5.3.2.1 North Atlantic Oscillation

In the Atlantic Ocean the North Atlantic Oscillation (NAO) influences phytoplankton abundance on interannual timescales (Irigoien *et al.*, 2000, Edwards *et al.*, 2001, Gladan *et al.*, 2010). The NAO Index is expressed as the difference in sea level pressure between the Azores high and the Icelandic low pressure systems. When in its positive phase the difference in pressure is large which results in stronger westerly winds. This in turn will negatively affect phytoplankton growth in subpolar regions as stronger winds mean deeper MLD and therefore increased light limitation. Thus, as expected, Boyce *et al.* (2010) found that the NAO index was negatively correlated with annual chlorophyll anomalies in the North Atlantic (~20˚N to 60˚N).

The NAO has also been related to changes in phenology in addition to chlorophyll concentrations. In the subpolar North Atlantic the relationship between NAO and the timing of the bloom was assessed using both satellite-derived data and model output (Henson *et al.*, 2009). A correlation coefficient of 0.61 between the NAO index in subpolar regions and bloom timing was reported indicating that blooms occur later when the NAO index is positive (indicating stronger westerly winds and a deeper mixed layer). In addition, the mean latitude and spatial extent

of the transition zone between the subpolar and subtropical gyres was seen to vary with the NAO index. In positive NAO years the transition zone curved southwards in the middle of the Atlantic and northwards at the edges of the ocean basin. In negative NAO years the spatial pattern was reversed with the transition zone curving northwards in the middle of the Atlantic and southwards at the edges. This movement means that areas located in or near the mean position of the transition zone can show strong interannual variability in their seasonal cycles as they switch back and forth between transition, subpolar and subtropical conditions. Ultimately, this explains the high interannual variability in the timing of the bloom in the regions around the transition zone.

1.5.3.2.2 Pacific Decadal Oscillation

The Pacific Decadal Oscillation (PDO) is a mode of variability that affects the Pacific Ocean, over longer timescales than ENSO, changing from one phase to another on decadal timescales (Mantua *et al.*, 1997). Most recently, this happened in 1976/77 when the PDO changed from a warm to a cold phase and again in 1988/89 when it changed back to a warm phase. When in a warm (cool) phase the SST is warmer (cooler) and sea level pressure is higher (lower) in the central North Pacific but lower (higher) over the west coast of North America.

In the western North Pacific Ocean, Chiba *et al.* (2008) observed differences in the way phytoplankton in the subpolar Oyashio region and the subtropical region reacted to shifts in the PDO from *in situ* data. In 1976/77 when the PDO switched to a cold phase, the winter MLD became deeper resulting in increased spring phytoplankton biomass in the nutrient-limited subtropical region as nutrient concentrations were increased over the winter enabling more growth in the spring. Simultaneously, the deeper MLD decreased winter-time phytoplankton biomass in the light-limited subpolar region as it decreased the average amount of light phytoplankton received in the mixed layer. The opposite was seen in 1988/89 when the PDO shifted back to a warm phase.

Additionally, Chiba *et al.* (2008) propose that the PDO can affect zooplankton seasonal cycles. Chiba *et al.* (2008) ran a hindcast model for the subarctic western North Pacific. They found that after 1976-77, when the PDO index became positive, the start date of the spring bloom was delayed, on average, by 5 days. After the mid-1990s, when the PDO index became negative again, the mean start date of the spring bloom reverted to similar values as those seen before the mid-1970s. Chiba *et al.* (2008) suggest that this phenological change may decouple the cycle of phytoplankton and zooplankton, and is related to observed ecological changes in higher trophic levels. For instance, the change in the PDO index in 1976-77 was associated with a change in the abundance of salmon off the coasts of Alaska and

mainland USA (Mantua *et al.*, 1997). When the PDO index became positive (cool phase), the sea level pressure became low over the central North Pacific inhibiting upwelling favourable winds off the coast of north-west USA. Biological productivity decreased off the coast of North-west USA and increased off the coast of Alaska, as did the abundance of salmon. When the PDO index is negative (warm phase) the situation is reversed, with lower biological productivity and salmon abundance off the coast of Alaska (Mantua *et al.*, 1997).

Overall, there are many processes that cause variability in phytoplankton blooms on interannual to decadal time scales and much of this can be explained through climate oscillations that describe the physical environment (e.g. Henson *et al.* (2009), Sasaoka *et al.* (2011), Chiba *et al.* (2012), D'Ortenzio *et al.* (2012), Racault *et al.* (2012)). The interplay of climate oscillations with different time scales leads to very complex time series. The years when the phases of the climate oscillations perfectly coincide may experience the largest or the earliest blooms. If they are completely out of phase there may be only the smallest of expressions in phytoplankton abundance. The phenological variability is complicated further by the issue of time lags and preconditioning of the water column (i.e. conditions during the last year or season affect this season). The North Pacific study by Sasaoka *et al.* (2011) is an example of both of these as they address both ENSO and PDO and find a 1 year lag in some correlations. All of this complexity makes it difficult to attribute any changes in phytoplankton seasonality to long-term trends related to climate change. However, if it is known how physical processes will respond to climate change then it may be possible to predict how the phytoplankton will respond, possibly by using the response to climate oscillations as an analogue.

1.6 Impact of Climate Change

After the beginning of the industrial revolution in the 18th century, the burning of fossil fuels by humans for energy has significantly increased the concentration of carbon dioxide (CO_2) in the Earth's atmosphere above its long-term Holocene value 278 ppm. Carbon dioxide is a so-called greenhouse gas that permits passage of short-wave radiation (visible) from the sun, but "traps" long-wave radiation (infra-red) emitted by the Earth's surface. Without it, the planet would be significantly cooler, but as anthropogenic activities continue to increase the amount of CO_2 in the atmosphere - to more than 400 ppm in 2013 - the climate is expected to warm and it is believed that this will have significant consequences for life in the oceans. However, there are still many questions about how much the

Earth will warm, what the exact impacts will be and when the influence of higher temperatures will be detectable above the natural variability of the system.

1.6.1 Expected Changes in the Pelagic Environment

SST is expected to rise as a result of climate change and this has two important impacts on phytoplankton. Firstly, a rise in temperature increases the community growth rate. Different phytoplankton species thrive at different temperatures depending on their optimum temperature range for growth. But as temperature increases there will be a switch to species that have a higher optimum growth temperature resulting in an overall increase in the growth rate of the community (Eppley, 1972). The second is that higher SST is indicative of increased stratification, which influences the availability of light and nutrients in the euphotic zone. Several studies (Barnett *et al.*, 2001, Levitus *et al.*, 2001) have linked SST trends with climate change. From this, it follows that primary production may alter as climate change increases SST.

Variability in phytoplankton abundance between past years and decades provides information on their response to warmer or cooler temperatures. A decadal comparison of variability in chlorophyll and SST revealed spatial patterns dominated by two climate oscillations; PDO in the Pacific and the Atlantic Meridional Oscillation (AMO) in the Atlantic (Martinez *et al.*, 2009). Martinez *et al.* (2009) demonstrated that warmer SST in the Pacific and Atlantic Oceans broadly resulted in reduced chlorophyll concentrations. Biophysical relationships such as these may be used to infer future changes in chlorophyll concentration that may occur as global temperatures increase.

However, this approach assumes that the spatial pattern of global warming is the same as the modes of variability (e.g. PDO) (Sarmiento *et al.*, 2004). An example of this would be using the phytoplankton response to the warm phase of PDO as a prediction for the phytoplankton response to climate change. This prediction would be based on the spatial extent of the PDO signal as well as assuming the magnitude of the phytoplankton response remains similar to the relative temperature change. Essentially, this would be a shift in the mean SST and phytoplankton abundance but variability around the mean would remain similar. If the spatial patterns are different then climate oscillations cannot be used to predict the biological response as the climate oscillation would be impacted in a non-linear way. A linear change adds on a trend component to the climate oscillation whereas a non-linear change alters the shape of the oscillation. Stone *et al.* (2001) investigated the impact of climate change on the dominant modes of variability in sea level pressure (SLP) and surface air temperatures (SAT) using an atmosphere

and ocean coupled model. Though the climate change signal was seen to project onto the dominant modes of variability for SLP and SAT, only some changes were linear. For example, if SAT were dependent on the presence of ice then the effect of climate change was non-linear as the situation switched from ice to ice-free conditions. These relationships are currently an active area of research that aims to clarify just how climate change will influence modes of variability in many physical parameters.

Another indicator of climate change is modifications in the spatial distribution of species. There are several examples where warm water species have been found further poleward than expected. The dinoflagellate *Ceratium trichoceros* was only seen south of the UK before 1970 but is now found off the coast of Scotland (Hays *et al.*, 2005). Atlantic phytoplankton species have been observed blooming in regions of the Arctic Ocean where ice free conditions enable their survival (Hegseth and Sundfjord, 2008). Additionally, the calanoid copepod species moved poleward in the North Atlantic at a mean speed of 23.16 km yr^{-1} over the period 1960-1999 as observed using Continuous Plankton Recorder (CPR) data (Beaugrand *et al.*, 2009).

As well as moving spatially phytoplankton abundance may also shift in time through changes to their annual cycle (Edwards and Richardson, 2004, Sommer and Lengfellner, 2008). A specific example is the timing of the annual chlorophyll peak in the Arctic Ocean which occurred up to 50 days earlier in 2009 than 1997 (Kahru *et al.*, 2011) (see Figure 1.11). This trend is driven by earlier retreat of seasonal ice cover as SST in the Arctic continues to rise. Another interesting situation was discussed by Ji *et al.* (2010) in the Mediterranean Sea. Species found here will be unable to move spatially as SST rises as the Mediterranean Sea is bounded by land to the north. They propose that the outcome will be either phenological changes, evolution to cope with higher temperatures, or extinction of certain species. In accordance with this theory, Conversi *et al.* (2009) observed large changes in the phenology of *Pseudocalanus elongates* in this region with spring and autumn abundance peaks in 2005 occurring 1 month earlier and 2 months later respectively compared to 1970.

In attempting to analyse such change, it is possible to split the global oceans into biomes or provinces based on ecological parameters such as irradiance, nutrient availability, biomass and SST. Many studies looking at ecological responses to climate change found the size of these biomes has changed over time. Using satellite chlorophyll data, Irwin and Oliver (2009) found that most oligotrophic gyres shifted to a more extreme oligotrophic regime between 2003 and 2007 as a result of several years of warming in the subtropics increasing stratification. Additionally, expansion of the oligotrophic gyres have been recorded

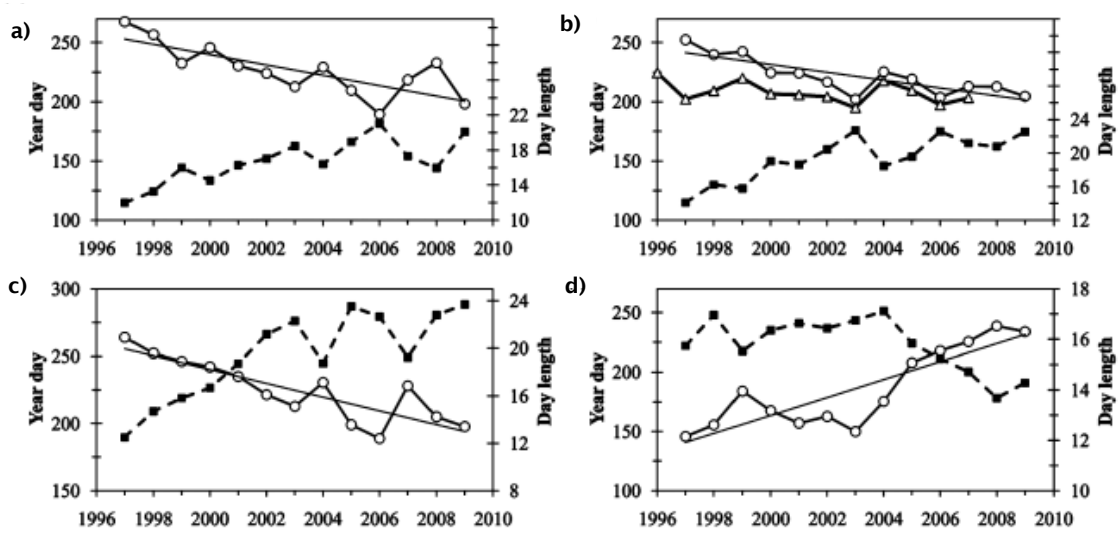

Figure 1.11: Example time series of changes in the year day on which the bloom peak occurs (solid line) and day length on the bloom peak date (dashed line) for Foxe Basin (a), Baffin Sea (b) Kara Sea (c) and the central North Atlantic (d). The open triangles in plot d show the year day on which the ice concentration in the Baffin Sea becomes less than 15%. An increase in day length indicates an earlier bloom initiation date as the year day becomes closer to the summer solstice. From Kahru *et al.* (2011)

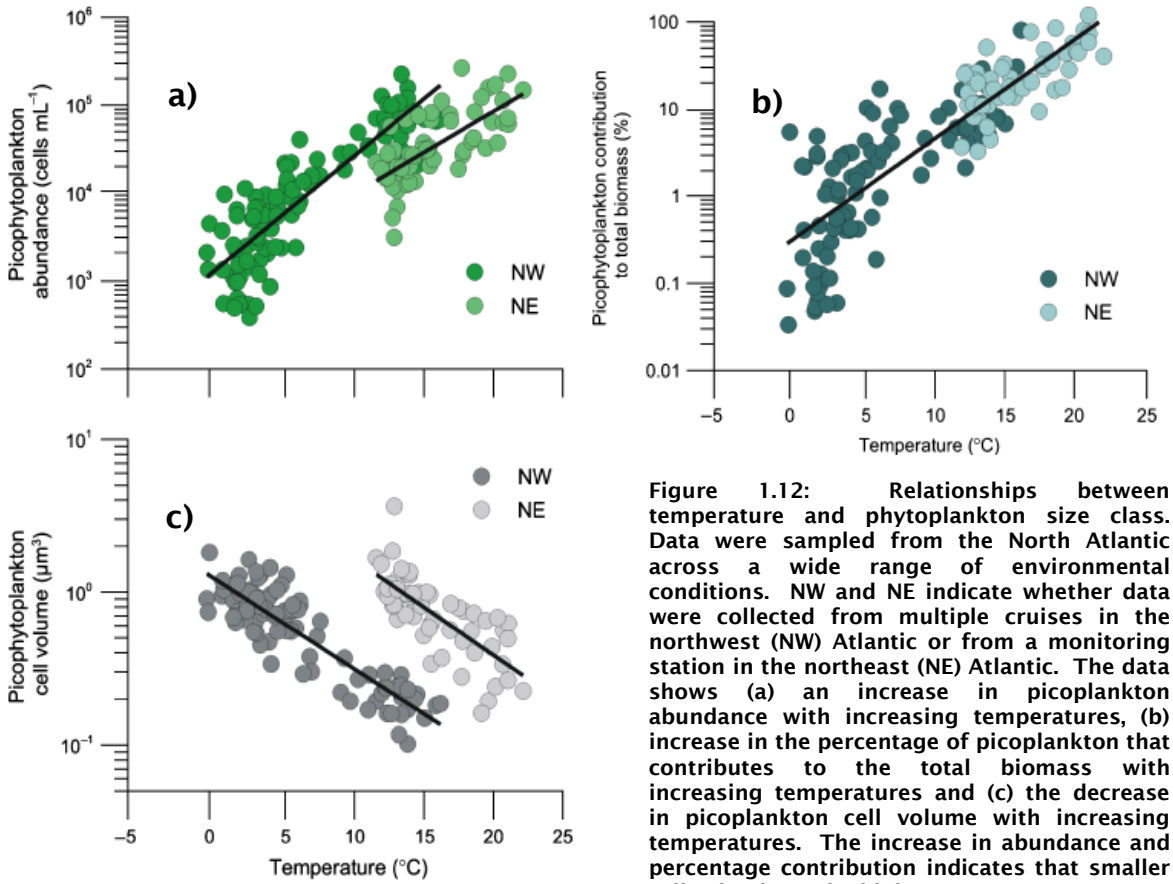

Figure 1.12: Relationships between temperature and phytoplankton size class. Data were sampled from the North Atlantic across a wide range of environmental conditions. NW and NE indicate whether data were collected from multiple cruises in the northwest (NW) Atlantic or from a monitoring station in the northeast (NE) Atlantic. The data shows (a) an increase in picoplankton abundance with increasing temperatures, (b) increase in the percentage of picoplankton that contributes to the total biomass with increasing temperatures and (c) the decrease in picoplankton cell volume with increasing temperatures. The increase in abundance and percentage contribution indicates that smaller cells dominate in higher temperature waters. From Moran *et al.* (2010)

by McClain *et al.* (2004) and Polovina *et al.* (2008) with Polovina *et al.* (2008) also noting that the rate of expansion is fastest for winter months. A modelling study by Sarmiento *et al.* (2004) compared the simulation output of 6 different models which use biogeochemical changes predicted from using empirical equations derived from satellite data. Oceanographic biomes were determined using physical parameters and the extent of the biomes was tracked over time. The results show the oligotrophic gyre biome expanding into the seasonally stratified biome due to climate change over approximately 200 years (late 1800 to 2100). Additionally, the subpolar biome expanded at the expense of the marginal ice zone. Overall, these changes resulted in an increase in primary productivity ranging from 0.7% to 8.1% for all the models.

1.6.2 Implications of Changes in Seasonality

As the studies above show, it is difficult to predict how phytoplankton seasonality may be affected both globally and regionally due to climate change. However, it is still possible to identify the implications of phenological changes. It is expected that these changes will be greatest at the boundaries between oceanographic biomes as one biome expands into another. Eppley curves predict that as the temperature increases the community will change as conditions suit phytoplankton with a different optimal range, which can then outcompete others (Eppley, 1972). If a Lagrangian point of view is taken this indicates that the optimal range for a particular species will change location (i.e. biogeographical shift). However, from an Eulerian point of view the community structure becomes dominated by phytoplankton suited to higher temperatures. Thus the seasonal timing and succession of phytoplankton species may also be different. Furthermore, it is easy to see how climate change-driven trends in bloom timing will impact on the temporal overlap with grazers and thus larval survival and fish stocks. From this, we can predict the changes that may manifest in phytoplankton community structure and carbon export.

1.6.2.1 Community Structure

Phytoplankton species have an optimal range in which they thrive and as conditions in a specific location change, some species will be outcompeted by others that are more suited to higher temperatures. This changes the community structure and as different functional types of phytoplankton have different ecological and biogeochemical roles this can have knock on effects and feedbacks.

Changes in stratification are expected to alter nutrient supply which has been seen to be an important predictor for phytoplankton size. Marinov *et al.* (2010) hypothesised that a nutrient threshold (a certain nutrient concentration that also

marks the boundary between 2 regimes) present at approximately ±45° N was responsible for the response of different size classes of phytoplankton to changes in nutrient concentrations. Above the (poleward of the) threshold diatoms dominate the community whereas (equatorward) below it smaller phytoplankton functional types dominate. Using model output to test this hypothesis, Marinov *et al.* (2010) showed that small phytoplankton were affected more by increases in nutrient concentrations below the threshold than above it (i.e. if nutrient concentrations are above the threshold then increasing it more does not make them grow anymore) with the opposite being true for diatoms. An increase in stratification due to climate change may result in this nutrient threshold expanding poleward which the authors state may result in a shift from diatom dominated to small phytoplankton dominated communities. In agreement with this, an observational study by Moran *et al.* (2010) found that smaller phytoplankton species were seen to dominate over larger phytoplankton species at higher ambient temperatures. Moran *et al.* (2010) went on to propose a future shift towards smaller phytoplankton species dominating larger areas of the ocean with global warming (see Figure 1.12).

1.6.2.2 Export

Changes in community structure may have implications for primary production as it influences the efficiency of carbon export. Large phytoplankton such as diatoms are associated with large carbon export events (Buesseler, 1998). They can form extensive blooms and when the cells die they sink relatively rapidly exporting carbon from the surface layer to deeper waters. This represents a transport of carbon dioxide from the atmosphere to deep waters, where carbon is sequestered for long timescales (100s to 1000s years). Smaller phytoplankton are associated more with intense recycling of nutrients by bacteria and so there is minimal carbon export as most of their detrital material is recycled (Eppley and Peterson, 1979).

Microplankton such as diatoms dominate in subpolar regions whereas picoplankton dominate in nutrient-limited subtropical regions (Uitz *et al.*, 2010). Export production is related to the primary production at the surface with oligotrophic regions exporting less (Eppley and Peterson, 1979). If the permanently stratified waters expand as a result of climate change then the dominance of picoplankton will be extended over a larger area potentially reducing carbon export. In agreement with this prediction, results from a range of biogeochemical models found that on average a 6% global reduction in carbon export over the next century as a result of climate change (Bopp *et al.*, 2001). However, the situation is more complex than it first appears as the type of material that is exported, not just the

quantity, is important for modulating the climate. Material exported from highly seasonal regions is more labile (easily degraded) whereas less seasonal regions export more refractory (less easily degraded) material (Lutz *et al.*, 2007). Easily degraded material will remineralise (dissolve back into the water column) at a shallower depth than refractory material and thus be circulated back to the surface more rapidly. Therefore an expansion of the low seasonality, permanently-stratified waters may result in a reduction in the global carbon flux but also a deepening of remineralisation depths. This in turn will modulate the levels of CO_2 in the atmosphere as a deeper remineralisation depth means that exported carbon is more likely to take longer to be ventilated back to the atmosphere (Kwon *et al.*, 2009).

Furthermore, temperature may also have a direct effect through metabolic processes. Both observational (Wohlers *et al.*, 2009) and modelling (Taucher and Oschlies, 2011) studies have seen a reduction in carbon export and higher respiration rates at higher temperatures.

Although future predictions about the response of phytoplankton to higher SST remain uncertain, changes in bloom magnitude, timing, spatial extent and species composition are expected. Current datasets rarely extend into the past far enough to adequately quantify decadal variability and on a global scale consistent remote sensing time series currently only span 16 years. To determine a global warming trend we need a much longer time series to establish background natural variability.

1.6.3 Detecting Trends

A major obstacle in studying long-term trends is the availability of long time series with consistent coverage in time and space. This can be overcome by using a proxy for chlorophyll concentration to extend the dataset back in time. One such method was attempted by Boyce *et al.* (2010) using historical ocean transparency measurements to estimate *in situ* chlorophyll concentrations back to 1899. However, using light penetration as a proxy introduces uncertainty as the relationship between light and chlorophyll is different for the open ocean and for regions affected by coastal processes (e.g. sediment from rivers). Additionally, the spatial sampling of light penetration since 1899 has not been uniform with a heavy bias towards the northern hemisphere. The study reported a 1% per year reduction in chlorophyll over the last century which contradicts the findings of other long-term datasets (Continuous Plankton Recorder, HOTS, BATS, CalCOFI) which show an increase in phytoplankton biomass over the last 20-50 years (McQuatters-Gollop *et al.*, 2011).

Another popular method for examining long-term changes in chlorophyll is comparing data from two different decades to determine decadal scale changes. There are several studies that compare satellite ocean colour data from the Coastal Zone Color Scanner (CZCS operational from 1979 to 1986) to data from SeaWiFS (operational from 1997-2010) (Gregg and Conkright, 2002, Antoine *et al.*, 2005). Surprisingly, this seemingly simple approach has obtained very different results dependent on differences in the satellite algorithms applied. Comparisons of these two datasets blended with *in situ* data by Gregg and Conkright (2002) and Gregg *et al.* (2003a) found a global decrease in chlorophyll concentrations of ~6% with the majority of change being seen at high latitudes. However, the results of a similar study by Antoine *et al.* (2005) were contradictory with a global increase in chlorophyll concentrations of 22%. Consequently, it is important to bear in mind that the data collected from these two sensors do not overlap in time thus, observed differences in chlorophyll concentrations may simply originate from differences between the sensors. This places doubt on whether a direct comparison of CZCS and SeaWiFS data can produce meaningful results. Overall, it is clear that consistently measured global datasets spanning many years are needed to obtain a baseline of natural variability to assess climate change-driven trends.

Assessing the extent and impact of climate change in the Earth system is a difficult task as there is no control dataset for comparison with observations. However, although highly simplified, biogeochemical models may function in place of a control dataset. For example, they may be run in two modes in which one represents the natural variability where greenhouse gas concentrations are kept at pre-industrial levels, and the second represents the situation where the system is anthropogenically forced by higher concentrations of greenhouse gases. By using the natural variability run as a control dataset it is possible to identify climate change-driven trends in the global warming run. In one such study, Henson *et al.* (2010) used model simulations with and without future CO_2 emissions to determine when it may be possible to distinguish a climate change signal in global primary production. The results indicated that on average it would take around 40 years for the trend associated with climate change to become larger than the natural variability in primary production. This varied between regions and suggests that different parts of the oceans will respond to climate change at different rates. At the present time, using biogeochemical models is the only feasible method for predicting future changes though caution is needed with interpreting the results since models are a highly simplified representation of the Earth system.

1.7 Thesis Outline

This chapter gave an overview of the main topics of the thesis by examining the processes that govern when and if a bloom may occur, variability that has already been documented and by discussing the implications of climate change in terms of altered seasonality.

Chapter 2 describes the observational datasets and the methods used to calculate related variables such as mixed layer depth. A discussion of the limitations and errors associated with the data is included.

An objective method to quantify seasonality is developed in Chapter 3 in addition to a method to identify regions that do not display a seasonal cycle (objectives 1 and 2).

Chapter 4 examines the impact gaps in the time series have on the accuracy of the seasonality metrics and derives an equation to estimate the likely uncertainty from the amount of data missing from a time series (objective 3).

The physical drivers of interannual variability in bloom timing are investigated in Chapter 5. The dominant drivers, the strength of their relationship with the bloom timing metrics and the differences between ocean basins are discussed (objective 4).

Chapter 6 addresses future trends in bloom timing by first assessing how well biogeochemical models simulate contemporary bloom timing, investigating the climate change-driven trends and assessing the influence of temporal resolution of trend detectability (objectives 5, 6 and 7).

A summary of the project, a discussion of future direction and the further implications of the study are presented in Chapter 7.

1.8 Summary

- Variability in phytoplankton seasonality is an important aspect of the marine food web and the Earth's carbon cycle. Additionally, since seasonality is closely linked to meteorological and physical ocean forcing, seasonality metrics can be used as indicators for monitoring pelagic ecosystems and detecting natural and anthropogenically-driven trends.
- This thesis aims to objectively measure phenological events, quantify phenological variability, investigate the physical drivers and examine the climate change-driven trends in bloom timing.

- The studies reviewed above indicate that light and nutrient availability are important controls on bloom timing. What is also clear is that current observations do not necessarily fit current theories on bloom initiation and that processes that are strong drivers of interannual variability in bloom magnitude may not be expressed in the interannual variability of bloom timing and vice versa.
- In the future, climate change will alter phytoplankton seasonality but how fast and by how much are still unknown. However, we do expect changes to community structure, carbon export and the marine food web because of altered seasonality.
- Ultimately, since we do not have consistently measured multi-decadal datasets we will need to utilize global biogeochemical models to investigate future trends in phytoplankton phenology.

2 Data

This thesis aims to globally assess phytoplankton seasonality on interannual and decadal time scales. Therefore the datasets used will need to provide consistent measurements over the whole globe and cover many years (preferably at least a decade) to properly quantify interannual variability. Phytoplankton respond to changes in their environment quickly and blooms can last from a few days to weeks and multiple blooms can occur sequentially at a particular location. Blooms can cover hundreds of square kilometres and mesoscale activity can cause significant spatial variability and patchiness. This project is interested in the broad patterns in bloom timing over basin scales (100-1000 km) and so spatial resolutions fine enough to resolve eddies and other mesoscale features (1-100km) are not required. Conversely, high temporal resolutions are preferred due to the rapid development of blooms and for the ability to detect small differences in bloom timing between years. However, a compromise is often needed between the data requirements, the data that are available, data storage space and computation time.

Satellite-derived datasets are the best option for consistent measurements that are available globally and covering consecutive years. Satellite-derived data are usually available at daily, 8 day or monthly frequency and at spatial resolutions of 1/12° to 1° or greater. Since basin scales are suitable for this project for the reasons given above, spatial resolutions of 1°x1° are adequate. Though satellite data are available with daily frequency, the data are also incomplete as the ocean colour satellites obtain global coverage only every 2-3 days. This is because the paths of the satellite swaths do not fully overlap after 24 hours with inter-orbit gaps occurring at low latitudes. Complete coverage within 24 hours would be achievable if the swath was wider but this would also degrade the spatial resolution of the data. Additionally, gaps in the data will occur due to cloud cover, sea ice, sun glint and atmospheric aerosols which obscure the sea surface or contaminate the reflected radiances. Therefore, daily data increases computation time and data storage requirements without providing global coverage. Using the 8 day composites represents an acceptable compromise between coverage and temporal resolution. Therefore, the target data requirements are datasets covering multiple years with spatial resolutions of at least 1°x1° and temporal resolutions of 8 days or weekly.

Furthermore, in all the datasets used here, the changes observed over time at a pixel are a combination of temporal and spatial processes. For example, an observed increase in chlorophyll between two time steps could result from increased growth at that location or the advection of a water mass that is high in chlorophyll into an area that previously had low chlorophyll concentrations. However, since separating temporal from spatial changes is difficult without high resolution in both space and time, in this thesis the spatial changes are ignored and changes at a particular pixel are assumed to be a local change in the parameter.

This chapter discusses the various datasets used in this study by detailing the processing steps and discussing the limitations. The parameters used are chlorophyll, mixed layer depth, net heat flux and mean mixed layer irradiance.

2.1 Chlorophyll-a

Light entering the ocean is absorbed and scattered by suspended particles (e.g. particulate inorganic carbon), coloured dissolved organic matter (CDOM) and pigments found within phytoplankton such as chlorophyll. The way in which pure seawater absorbs and scatters light produces the characteristic deep blue colour. Increasing concentrations of pigments, particles and CDOM will alter this blue colour. CDOM and particulates give the water a brown/yellow colour. This is characteristic of “case 2” waters which typically include coastal regions where effluent from the land adds sediments and CDOM to the water. In contrast, “case 1” waters, which typically include open ocean regions, are dominated by chlorophyll-a, which primarily absorbs blue light. As the concentration of chlorophyll-a increases the seawater becomes increasingly green. By looking at the ratio of blue to green light in water-leaving radiances we can estimate the concentration of chlorophyll-a. This is then used as a proxy for phytoplankton biomass as chlorophyll-a is present in all phytoplankton, though they may also have other pigments.

Over the last decade there have been 3 ocean colour sensors that provide high quality data (see Table 2.1 for the sensor characteristics). The Sea-viewing Wide Field-of-view Sensor (SeaWiFS) on GeoEye’s SeaStar spacecraft was fully operational from September 1997 through to December 2010 when the sensor failed. The MEdium Resolution Imaging Spectrometer (MERIS) on the European Space Agency’s (ESA) Envisat mission was fully operational from April 2002 to March 2012 when it too failed. The Moderate Resolution Imaging Spectroradiometer (MODIS) on National Aeronautics and Space Agency’s(NASA) Aqua mission has been operational since July 2002. From these three missions we currently have global chlorophyll data that spans 15 years. The dataset used here combines data from all

three of these sensors. Previously, the Coastal Zone Color Scanner (CZCS) on the Nimbus 7 spacecraft was in operation from 1979 to 1986 but did not overlap with the SeaWiFS era. Thus no cross-calibration could take place to extend the ocean colour time series back to 1979.

Table 2.1: Ocean colour sensor characteristics

	SeaWiFS[a]	MODIS[b]	MERIS[c]
Operational dates	2002-2010	2002-present	2002-2012
Number of bands	8	36	15
Spectral coverage (nm)	402 – 885	40 – 14385	412 - 1050
Orbital period (minutes)	99	99	100
Swath (km)	2801	2330	1150
Resolution (km)	1.1	1.0	1.2
Global coverage	2 days	1-2 days	3 days

[a] Details obtained from SeaWiFS mission home webpage: oceancolor.gsfc.nasa.gov/SeaWiFS.

[b] Details obtained from MODIS mission home webpage: modis.gsfc.nasa.gov.

[c] Details obtained from MERIS mission home webpage: earth.esa.int/web/guest/missions/esa-operational-eo-missions/envisat/instruments/meris

2.1.1 GlobColour Chlorophyll Dataset

GlobColour is an ESA project that produces global ocean colour products by merging together data from multiple sensors, namely SeaWiFS, MODIS and MERIS. The output is available as a simple or weighted average of the three sensors. The dataset used here spans Jan 1st 2002 – 31st Dec 2010 and was downloaded from http://www.globcolour.info. The data has a spatial resolution of 1/4°x1/4° and a temporal resolution of 8 days, thus each calendar year has 46 time steps. This consists of 45 time steps which are 8 day mean values and a 46th time step which is an average of the last 5 days (or last 6 days in leap years). Combining the data from different sensors increases the daily coverage of the oceans to ~30% whereas individual sensors cover 8-16% of the globe (Durand, 2007).

2.1.1.1 GlobColour Processing

Satellite retrievals go through several processing steps. The merging method uses products that have been processed to L3 (Barrot, 2010). The L1 and L2 processing steps are applied to each individual sensor (including atmospheric correction, cloud detection, converting water-leaving radiance to chlorophyll-a measurement). From the L2 data, L3 products are produced in which the data is mapped to a uniform grid. Since the processing and chlorophyll formulae are different for each sensor the L3 data are different. At the beginning of the averaging process an inter-calibration correction is applied to the MODIS and SeaWiFS daily L3 products to give compatible chlorophyll concentrations with respect to MERIS. The merged chlorophyll data are then calculated as an average of

all 3 sensors. This is either a simple or a weighted mean depending on the method chosen by the user. Care needs to be taken when merging the three datasets as each individual sensor will have sampled at different times of day, different locations and at different spatial resolutions within the same 24 hour period (Barrot, 2010). Additionally, the satellite data are first recorded onto the ISIN (Integerized SINusoidal) swath grid which is a map projection where each grid cell is of equal area. This is then remapped onto the regular geographical grid used in the mapped products where the pixels are not of equal area. Since the ISIN pixels may overlap several pixels in the regular geographic grid care must also be taken when merging the three sensor datasets at this stage. The merging is performed on the L3 daily data at 1/24˚ resolution and lower resolution products (e.g.1/4˚, 8 days) are calculated from the high resolution daily data (Barrot, 2010). The weighted mean chlorophyll dataset is used here (Figure 2.1) though the match up statistics for the simple and weighted mean were similar (Durand, 2007). Error statistics from the original 3 datasets are incorporated in the merging process and propagated through to give error estimates on the merged output product.

As this study focuses on the open ocean it is desirable to exclude coastal regions. A bathymetry mask was created from the National Oceanic and Atmospheric Administration (NOAA) National Geophysical Data Centre ETOPO1 Global Relief model downloaded from http://www.ngdc.noaa.gov/mgg/global/. This dataset was regridded from 1 arc minute to 1/4˚x1/4˚ to match the chlorophyll data and any region with bathymetry (or topography) above 200m depth was excluded. The threshold of 200m depth is often used to delineate the edge of the continental shelf and marks the assumed extent of the influence of coastal processes. This dataset was used to mask out coastal regions in all datasets.

2.1.1.2 GlobColour Limitations

Remote sensing is an extremely useful tool for Earth Observation on global scales and at high frequency. However, the remote sensing of chlorophyll is limited in several ways. Most obviously, when the satellite cannot "see" the sea surface a gap occurs in the data record. As noted above, for chlorophyll measurements, gaps occur when there is cloud cover, sea ice, atmospheric aerosol (i.e. dust), low sun angle and where the satellite swathes do not overlap. Additionally, as each pixel is an average of the radiances over a certain area there will always be a discrepancy between satellite-derived chlorophyll and *in situ* measurements which are point measurements. SeaWiFS had a target global error of 35% root mean square (RMS) log error and the satellite values are often compared against the SeaBASS database of *in situ* measurements (McClain *et al.*, 1998). Gregg and Casey (2004) reported a global RMS log error of 31% with a coefficient of determination of 0.76 for SeaWiFS.

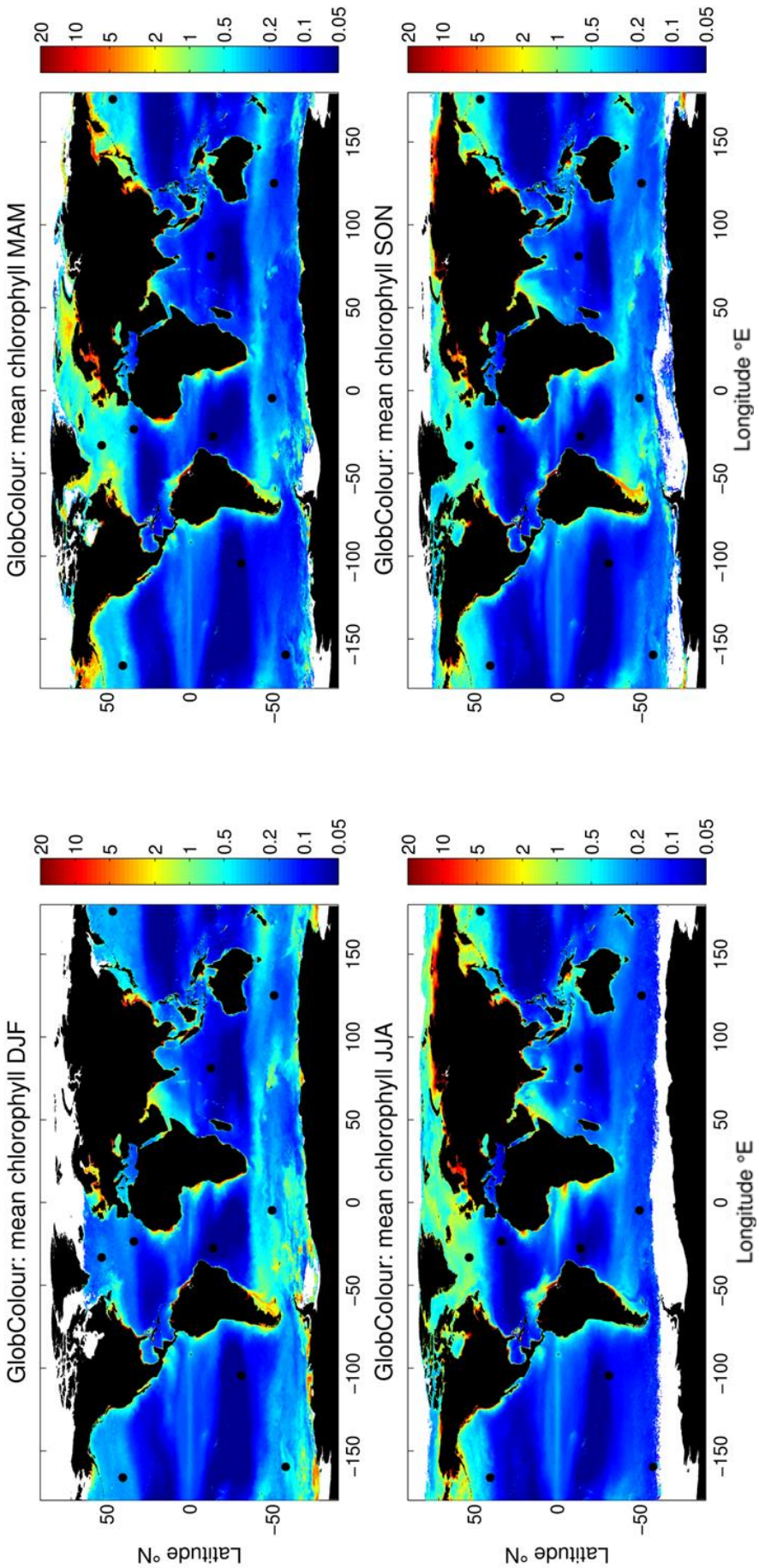

Figure 2.1: Seasonal maps of GlobColour chlorophyll concentration (mg m^{-3}) for December, January, February (DJF), March, April May (MAM), June, July, August (JJA), September, October, November (SON). Black spots mark location of time series in Figure 2.3. Note that the colour bar uses a log scale.

The GlobColour dataset is reported to perform better against the SeaBASS database than the individual sensors across many variables. For chlorophyll the match-up statistics of GlobColour were better than 2 sensors (MODIS and MERIS) and similar to the third (SeaWiFS) with a RMS log error of 30% and a coefficient of determination of 0.73 (Durand, 2007). Overall, GlobColour has smaller errors as well as improved coverage than the SeaWiFS dataset.

Another limitation of averaging over a pixel is that fine scale detail is lost. Though the aims of this research do not need fine spatial resolution it still has an impact on the accuracy of the chlorophyll values. Features such as sub-pixel clouds or aerosols will escape detection but may artificially raise the chlorophyll concentration. The large discrepancies in the Gregg and Casey (2004) comparison of SeaWiFS to *in situ* chlorophyll data were seen in the Equatorial and North Atlantic and the Equatorial Indian Oceans where dust blown from land over the ocean and CDOM from tropical rivers increased the absorbance. These errors will also be present in the other 2 sensor datasets and therefore also in GlobColour.

Extracting a chlorophyll concentration from the water-leaving radiances received by the satellite also introduces uncertainty. The signal is corrected for foam reflectance, sun glint, and atmospheric scattering, then an algorithm is used to convert the radiances to a chlorophyll concentration (O'Reilly *et al.*, 1998). However these algorithms may fail, for example, if cyanobacteria or coccolithophores dominate the population as they bring other pigments into the equation (O'Reilly *et al.*, 1998). Additionally, though the water-leaving radiances represent light coming out of the water it is difficult to know the depth to which the upwelling light is representative. Typically, the water-leaving radiances represent all the light interactions occurring in the top 50m (Platt and Sathyendranath, 1988). Because light is attenuated as it travels through the water the water-leaving radiance is heavily biased towards contributions from nearer the surface. Thus, the satellite can only measure the near-surface region whereas the entire euphotic zone is generally much deeper. For example, deep chlorophyll maxima (DCM) are common in nutrient-limited waters and this chlorophyll may not be seen by the satellite.

Though all phytoplankton cells contain chlorophyll-a there are several reasons why chlorophyll concentration may not be a reliable proxy for phytoplankton biomass. Marra (1997) summarised that changes in chlorophyll in a cell over diel timescales were related to changes to the chlorophyll:carbon ratio as well as changes in phytoplankton carbon. If chlorophyll and carbon change together then these changes are due to changes in abundance representing a shift in the balance of growth and loss terms. However, changes in temperature, nutrients and

irradiance can change the ratio. In low production regions (classified as chlorophyll<0.14 mg m^{-3}) these processes dominate the seasonal variability in the chlorophyll:carbon ratio (Behrenfeld *et al.*, 2005). Carbon concentrations remain constant but chlorophyll changes in response to seasonal cycles in light and nutrient availability. Moderate to highly productive regions have a chlorophyll:carbon ratio that is dominated by changes in abundance and exhibit a pronounced seasonal cycle. Some of these regions (subtropical) show a rise in chlorophyll before a rise in carbon (Behrenfeld *et al.*, 2005). This occurs in autumn and indicates that cells increase their chlorophyll in response to decreased light levels (photoacclimation) and then the population starts to grow after a delay when nutrient concentrations increase. In highly productive regions (i.e. subpolar) the chlorophyll:carbon ratio is dominated by the seasonal bloom which represents large changes in biomass. In these regions chlorophyll and carbon covary together and chlorophyll is a good indicator for biomass. Additionally, the chlorophyll:carbon ratio changes not just in time and space but also between species. This is referred to as photoadaptation rather than acclimation as these species have evolved to have a range of chlorophyll:carbon ratios that are adapted to exploit a certain irradiance levels (Platt *et al.*, 1982).

Despite these limitations, satellite-derived ocean colour data are the only feasible way of studying phytoplankton on a global scale at high temporal frequency. Though the accuracy of the chlorophyll measurements is less than *in situ* measurements relative changes in chlorophyll are accurately captured by the satellites and this is more important when studying the seasonal cycle than absolute values of chlorophyll. The most significant limitation to seasonality studies is the suitability of using chlorophyll as a proxy for phytoplankton biomass. As carbon and chlorophyll are closely coupled in moderate to highly productive regions this is a safe assumption to make for the most seasonally variable regions of the ocean. Care must be taken when interpreting the seasonal cycle in chlorophyll in oligotrophic regions as this mostly reflects photoacclimation.

2.1.2 NASA Ocean Biogeochemical Model

The NASA Ocean Biogeochemical Model (NOBM) is a fully coupled global model made up of 3 submodels: a radiative model, a general circulation model and a biogeochemical model. The Ocean Atmosphere Spectral Irradiance Model (OASIM) explicitly models subsurface light fields and adjusts the irradiance in the presence of clouds as well as spectral and directional properties of light in the water (Gregg, 2002). The OASIM is forced by datasets of winds, ozone, relative humidity, pressure, precipitation, clouds and aerosols. The general circulation model is modelled by the Poseidon ocean model (Schopf and Loughe, 1995). The

biogeochemical model has 4 phytoplankton groups (diatoms, coccolithophores, chlorophytes and cyanobacteria), 1 grazing group, 3 detrital (nitrogen/carbon detritus, silica detritus, iron detritus) and 4 nutrient pools (silica, nitrate, ammonia and iron) (Gregg *et al.*, 2003b). The biogeochemical model additionally models carbon flow between phytoplankton, grazers and detritus and models the exchange of carbon dioxide with the atmosphere. The forcing fields include atmospheric iron deposition, sea ice and pCO_2. The phytoplankton chlorophyll:carbon ratio is allowed to vary and is related to the photoacclimation state but the ratio of carbon to nutrients remains constant at the Redfield ratio throughout the model (Gregg *et al.*, 2003b). Most forcing fields in the model are NCEP reanalysis products (winds, shortwave radiation, sea surface temperature (SST), relative humidity, pressure, precipitation, aerosols) using monthly fields. Observational datasets for ozone, soil dust, cloud and carbon dioxide were obtained from other sources detailed in Nerger and Gregg (2007).

The chlorophyll output from NOBM was downloaded as daily fields using the Oceans Portal of the Giovanni application run by NASA's Goddard Earth Sciences Data and Information Services Center (http://disc.sci.gsfc.nasa.gov/giovanni). The available output covered the time span 2002-2007. The time series were averaged to 8 day composites to match the satellite chlorophyll data. To do this every 8 day period after 1st January was averaged until the last few days of the year (a 5 day period or 6 day in leap years) which were averaged together to form the last time step in the same way the NASA satellite 8 day composites are calculated. Consequently, each calendar year has 46 time steps. The resolution of the model is constant at 2/3° latitude by 5/4° longitude.

2.1.2.1 Assimilation of SeaWiFS Chlorophyll Data

The NOBM chlorophyll output used here is not from the free run model but has assimilated SeaWiFS chlorophyll data to improve the accuracy of the surface chlorophyll fields. The free run model broadly matches the expected spatial and seasonal patterns in SeaWiFS chlorophyll data and has a global mean value that is only 3.9% higher than the SeaWiFS global mean (Gregg *et al.*, 2003b) By assimilating SeaWiFS data the match of NOBM output with SeaWiFS chlorophyll and *in situ* measurements is improved (Nerger and Gregg, 2007). The benefit of assimilating satellite chlorophyll data is that it improves the models representation of reality by correcting for problems caused by finite spatial and temporal discretisation, minor processes that are missing from the model or crude parameterisations which would make the model drift away from reality. For the assimilation, model parameters remain fixed while the model fields (i.e. chlorophyll) were improved by being constrained by the observations (Nerger and Gregg, 2007)

The assimilation of SeaWiFS chlorophyll data is performed using a singular evolutive interpolated Kalman (SEIK) filter with an online bias correction (Nerger and Gregg, 2008). The filter does not force the model to reproduce the observations but rather takes errors in the model field and SeaWiFS data to give a "best answer" somewhere within the range of model and SeaWiFS uncertainties. Only the state variable, chlorophyll, is changed directly by the assimilation. Other equation and parameter values remain the same. However, other variables that are derived from chlorophyll such as primary production, will also be altered by the assimilation (Nerger and Gregg, 2007).

The assimilation is limited by missing data in the SeaWiFS record (from clouds, ice cover, sun glint, inter-orbital gaps and aerosols). On a daily basis between 13000 and 18000 grid points out of a potential 40697 have corresponding SeaWiFS data. Furthermore, some of these gaps can be persistent in which case the model is unconstrained by the data for long periods (Nerger and Gregg, 2007). In this case the assimilation of SeaWiFS data would be relaxed (i.e. relatively larger uncertainty in the model state). Conversely, some regions are known to have larger uncertainties in the SeaWiFS chlorophyll concentration due to the prevalence of atmospheric aerosols or CDOM. Again, in this situation the assimilation would be relaxed through large error estimates on the SeaWiFS data.

The filter is applied locally meaning that the observations used to adjust the model value at a grid point are all within an influence radius (5 grid points horizontally weighted by e-folding distance) (Nerger and Gregg, 2007). When gaps in the SeaWiFS dataset occur, the resulting assimilation output is a combination of chlorophyll values calculated from the model integration and from some extrapolation of surrounding SeaWiFS data into the gap (within an influence radius). The assimilation updates are done daily and so even with incomplete daily SeaWiFS data most regions are updated frequently. However, where gaps do occur the results are determined by the free run model dynamics driven by other model variables, which are only indirectly affected by the assimilation (Nerger and Gregg, 2007).

The result of the assimilation depends on the error estimation of the model and SeaWiFS dataset. The model errors were derived from a 6 year free model run by calculating monthly deviations from a 3 month running mean (Nerger and Gregg, 2008). The SeaWiFS errors were derived from regional error estimates reported by Gregg and Casey (2004) but modified by Nerger and Gregg (2007) to be compatible with the assimilation. An example would be increasing the error in the North and Equatorial Indian Ocean where atmospheric dust reduces the accuracy of chlorophyll measurements. The larger errors allow for a less constrained

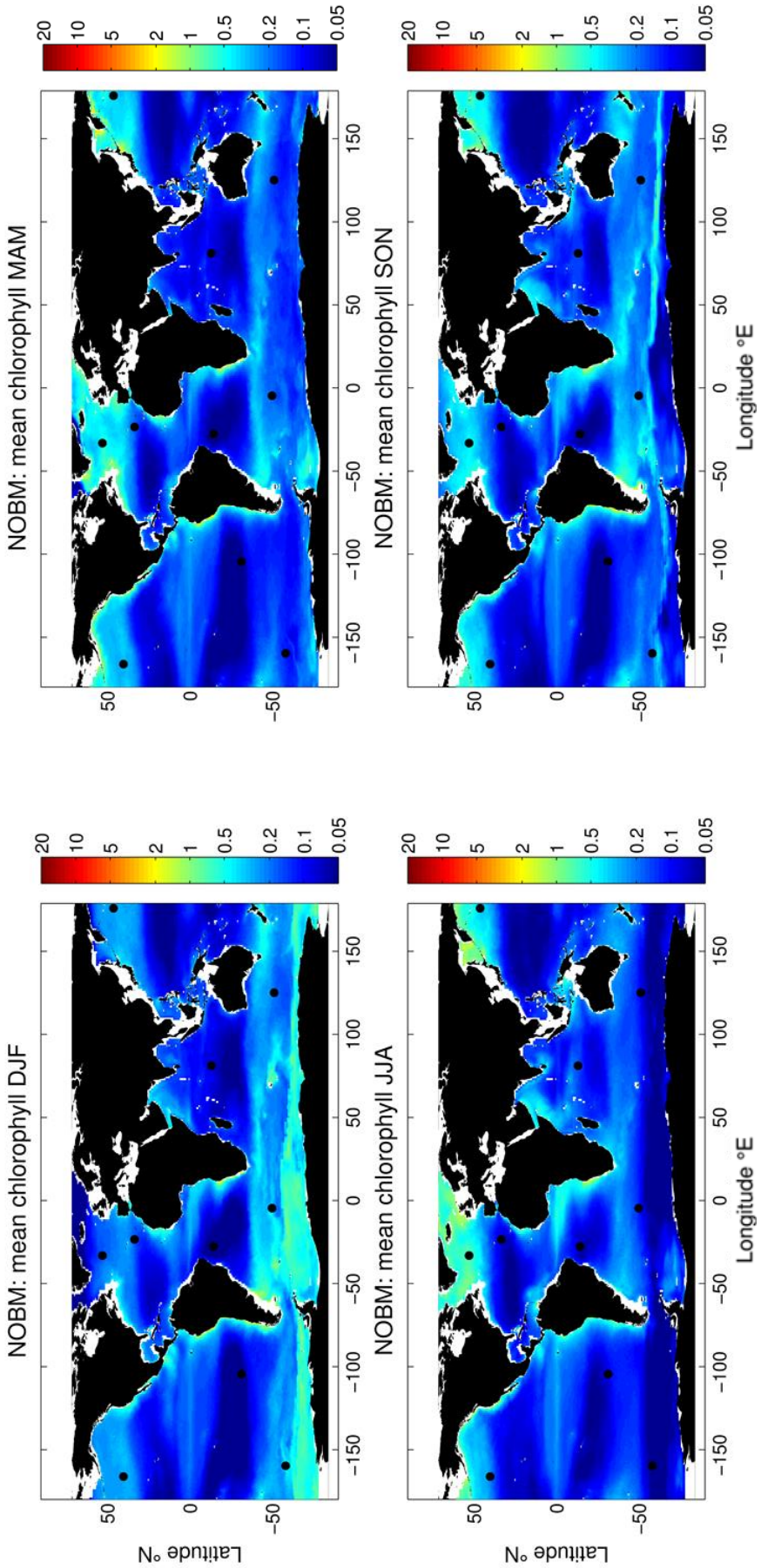

Figure 2.2: Seasonal maps of NOBM chlorophyll concentration (mg m^{-3}) for December, January, February (DJF), March, April May (MAM), June, July, August (JJA), September, October, November (SON). Black spots mark location of time series in Figure 2.3. Not that the colour bar is on a log scale.

assimilation, which is beneficial when large differences in chlorophyll might occur. This could be when SeaWiFS chlorophyll is over estimated (by contamination such as aerosols or CDOM) or when a persistent gap in the SeaWiFS record ends and the model estimate has deviated substantially from observational values. The relaxed assimilation prevents negative nutrient concentrations which could occur when the nutrient field subsequently reacts to a large change in chlorophyll (Nerger and Gregg, 2007).

The daily SeaWiFS dataset used was version 5.1 at 9km resolution, which was remapped to match the model grid. Outliers were defined as being greater than twice the monthly mean and were removed. In particular regions (North and Equatorial Indian Ocean, Amazon and Congo outflow regions) chlorophyll values over 1mg m^{-3} were also removed because these regions are known to be affected by atmospheric aerosols or high concentrations of CDOM, which give artificially high SeaWiFS chlorophyll values (Nerger and Gregg, 2007). These were the regions given larger error estimates to prevent the model being forced to conform to an erroneous value.

The model error is split into random error and a systematic bias with the bias being accounted for before the assimilation adjustment to the model chlorophyll is done in an online bias correction (OBC) scheme (Nerger and Gregg, 2008). This is particularly relevant for regions and time periods where the model consistently over or underestimates the chlorophyll values. This improves the efficiency of the SEIK filter as at each time step the bias is removed so the filter does not have to correct for the bias at every time step (Nerger and Gregg, 2008). This reduces the size of the model error estimation and enables a tighter assimilation because the systematic error has been accounted for. Additionally, the fields that will react to the changes in chlorophyll will not be adversely altered. For example, if the North Atlantic bloom was consistently underestimated then without a bias correction, each time step in the assimilation would have to correct for the systematic error. Subsequently this would also result in a reduction in nutrients at each time interval as the field reacted to the change in chlorophyll. The OBC prevents this from happening by correcting for the bias before performing the assimilation update and creates a more stable model integration (Nerger and Gregg, 2008). The systematic bias was not always in the same direction and was seen to underestimate the bloom chlorophyll concentrations and overestimate end of bloom concentrations in the North Atlantic and Pacific and Southern Ocean (Nerger and Gregg, 2008).

The assimilation results were compared to the *in situ* database SeaBASS and the NOAA/National Ocean Data Center (NODC)/Ocean Climate Laboratory (OCL) archives. The free run model had a global RMS log error of 0.441, which was

reduced to 0.266 by the assimilation of SeaWiFS data. This is 3.3% lower than SeaWiFS global RMS log error of 0.275 (Nerger and Gregg, 2008). The global correlation coefficient increased from 0.52 for the free run model to 0.83 for the assimilation result compared to a correlation coefficient of 0.81 for SeaWiFS. Thus on a global basis the NOBM assimilation output is in higher agreement with *in situ* data. However, on a regional basis the agreement is highest in subtropical and equatorial regions but reduces at higher latitudes due to the amount of missing data in the SeaWiFS dataset.

The assimilation was performed for the surface chlorophyll fields only, therefore the vertical profile of modelled chlorophyll was not changed. Nerger and Gregg (2007) state that improving the surface chlorophyll will inevitably improve the accuracy of variables derived from it such as primary production and export. The free run model shows a moderate degree of fidelity to the chlorophyll seasonal cycle but the assimilation improves the surface chlorophyll values as well. The result of this is that the timing of seasonal cycles agrees well with satellite-derived chlorophyll datasets (e.g. GlobColour) though absolute concentrations of chlorophyll may not be exactly the same as shown in Figure 2.3. The great advantage the NOBM output has over the satellite data is that it is free of gaps. These gaps are filled by extrapolation of SeaWiFS data within the influence radius as well as the model chlorophyll value propagated from the previous time step. Because seasonal timing is captured adequately due to the assimilation, it suggests that the NOBM output may be used to obtain accurate bloom timing estimates that will not be as adversely affected by data gaps at satellite chlorophyll datasets. For this reason, although the NOBM chlorophyll dataset involves an ecosystem model, it is included in this data section because it can be viewed as a "gap free satellite-derived record".

2.1.2.2 NOBM Limitations

The output from NOBM matches well with the SeaWiFS chlorophyll but there are still some regions that have large discrepancies. Nerger and Gregg (2008) state that when compared to *in situ* databases RMS log errors in the Equatorial Pacific, Southern and North Indian Oceans are up to 9% larger than SeaWiFS RMS log error. Overall, the seasonal cycle is represented well with respect to timing but absolute values of chlorophyll can be erroneous. Additionally, as only surface chlorophyll is updated analysis of the NOBM output is restricted here to the surface and is not extended to incorporate integrated chlorophyll.

The Poseidon model range only extends to 72°N and so seasonal cycles in the Arctic are not included in this dataset. This is a significant disadvantage as an

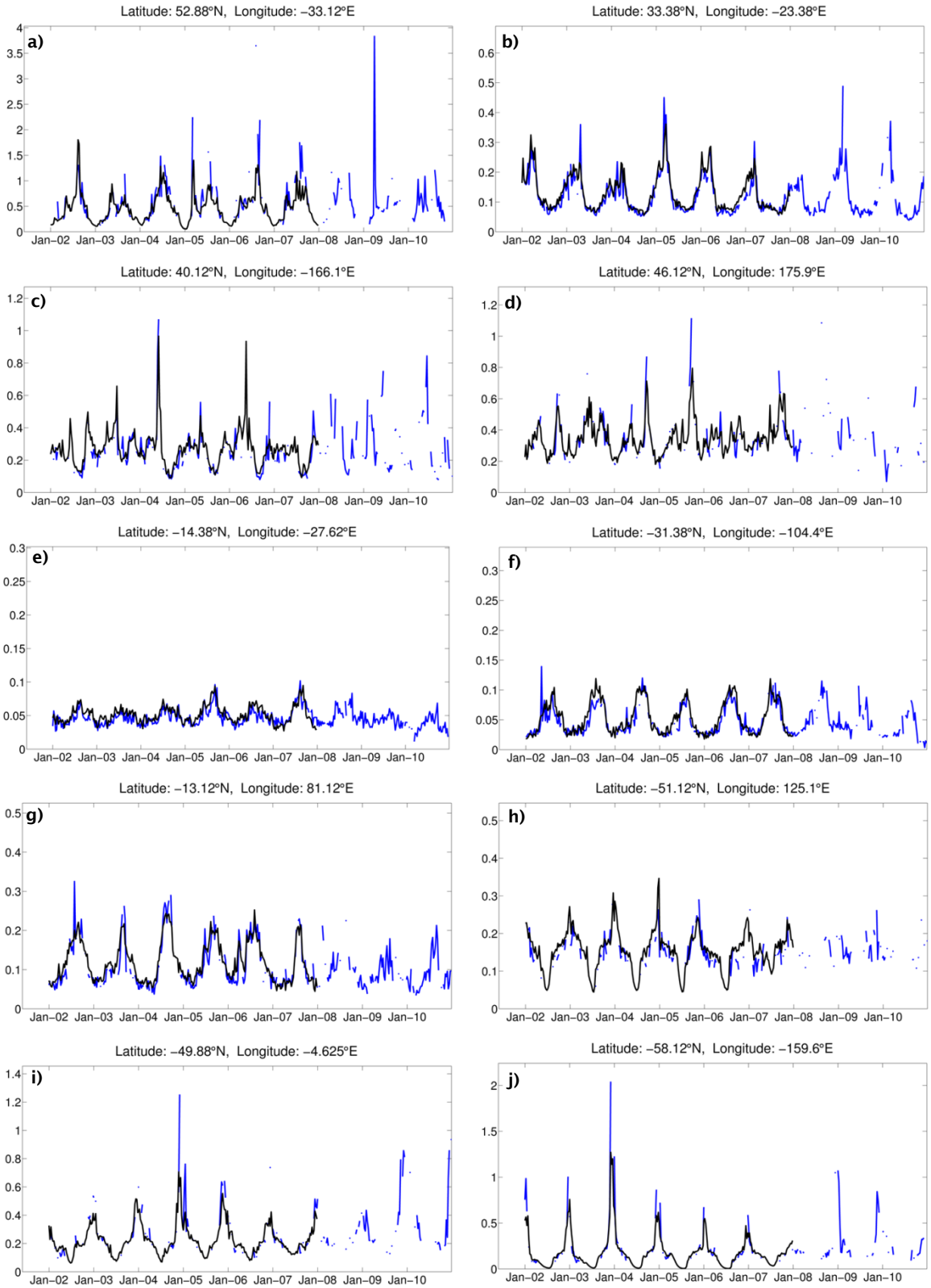

Figure 2.3: Time series from locations shown in Figures 2.1 and 2.2 comparing the chlorophyll time series from GlobColour (blue) and NOBM (black). GlobColour data were available from 2002-2009 whereas NOBM covers 2002-2007. Fidelity to seasonal timing by NOBM is higher than for absolute magnitudes of chlorophyll. Panels (a) and (b) are from the North Atlantic, (c) and (d) are from the North Pacific, (e), (f) and (g) are from the South Atlantic, South Pacific and Indian Oceans respectively and (h), (i) and (j) are located in the Southern Ocean.

estimate of natural variability in the Arctic will not be available from this dataset and thus cannot be used to assess the fidelity of global biogeochemical models.

The SEIK filter method also has its limitations as the way the covariance matrices for the errors are formed affect how well the assimilation performs. Firstly, the covariance matrices are calculated for the free run model and so assume that the free run model is a perfect representation of reality. Using multiple runs of the same model with slight variations in model parameters (such as atmospheric forcing) would lead to improved estimates of the model uncertainty (Nerger and Gregg, 2007). Additionally, the way the model covariance matrix is formed (monthly deviations from 3 monthly running mean) limits how realistic the variances and correlations between different model variables are and how they vary as the seasonal cycle progresses for example, surface and subsurface chlorophyll (Nerger and Gregg, 2007). By using higher temporal resolutions when calculating the error covariance matrix the error estimates would be improved. However, the assimilation improves the surface chlorophyll fields sufficiently so that the seasonal cycle is reproduced accurately in most regions.

2.2 Mixed Layer Depth

A ubiquitous feature in the physical structure of the upper ocean is the mixed layer where variables such as temperature, salinity, density and turbulence are generally constant with depth (Brainerd and Gregg, 1995). Its depth reflects the balance of mixing (i.e. wind, waves, convection) and stratification forces (density changes through heating or freshening) and can be very deep in winter (>500m) when mixing dominates and very shallow in summer when strong stratification is present. The depth of the mixed layer is an important driver in variability in bloom dynamics as it affects changes in light and nutrient availability. However, regular subsurface sampling of temperature and salinity in both space and time has only recently becoming widespread. The ARGO float program has been responsible for radically increasing the number of coincident temperature and salinity profiles since 2000. The ARGO array plus other sources of temperature and salinity data can be combined to give a comprehensive mixed layer depth dataset covering the majority of the globe at relatively high frequency though coverage is less synoptic than for surface, satellite-observed properties.

2.2.1 Data Sources and Processing

Mixed layer depths were calculated from density profiles using global gridded fields of temperature and salinity. The temperature and salinity data were collected

and made freely available by the Coriolis project and programmes that contribute to it (http://www.coriolis.eu.org). The gridded fields use temperature and salinity profiles collected by ARGO floats, XBTs (eXpendable BathyThermograph), CTD/XCTDs (eXpendable Conductivity Temperature and Depth) and moorings. They are available as delayed mode products meaning that detailed quality control checking has taken place (Gaillard *et al.*, 2009). The Coriolis project gridded the individual profiles onto a regular grid using the statistical estimation method for objective analysis. This method takes irregularly sampled data and maps it onto a regularly spaced grid in space and time. Objective analysis also provides an estimation of the error on the data at each grid point which is dependent on the data coverage (i.e. regions of the ocean that are infrequently sampled by floats have a lower confidence). The North Atlantic is the most frequently sampled region and has good coverage in both time and space (Gaillard *et al.*, 2009). The fields were available at weekly temporal resolution from 2002-2009 with each year having 52 time steps (i.e. the temperature and salinity fields were available as 7 day means). The gridded temperature and salinity data were downloaded with a spatial resolution of 1˚ longitude by 1/10˚ latitude and regridded to 1˚x1˚ resolution to reduce further processing time. This regridding was performed with the temperature and salinity values being weighted by pixel area.

The regridded fields were then used to calculate density profiles using the recently updated standard for seawater properties (the new standard, Thermodynamic Equation of Seawater 2010 (TEOS-10) (www.teos-10.org) replaces the old EOS80 standard for seawater thermodynamics and equation of state). The depth of the mixed layer was then calculated using the definition described below for each density profile.

2.2.2 Mixed Layer Depth Definition

When deciding on a definition for the depth of the mixed layer it is important to consider the differences between mixed layers and mixing layers. The mixed layer is considered to be a time integrated view of the depth of mixing over a specified time scale (Brainerd and Gregg, 1995). In other words, the mixing layer is the depth of turbulent mixing at any given point in time and the mixed layer represents the depth range over which mixing has happened recently, but may have subsequently ceased. A density difference of 0.01 kg m^{-3} has been used to define the base of the daily mixed layer and represents diurnal processes of daily heating and cooling (Brainerd and Gregg, 1995). However, temperature differences of 0.5-0.8˚C often overestimated the seasonal mixed layer (Montégut *et al.*, 2004) and a density difference of 0.125 kg m^{-3} is often used for monthly mean data where the MLD is averaged over a month or longer (Thomson and Fine, 2003). A mixed layer

definition that represents the mixing over at least one day to the order of a few days is believed to be adequate to track the seasonal mixed layer depth (Brainerd and Gregg, 1995). Thomson and Fine (2003) found that a density difference of 0.03 kg m^{-3} was equal to their own "split and merge" method at defining the base of the mixed layer. Kara *et al.* (2000) choose a temperature change of 0.8˚C and Montégut *et al.* (2004) choose a density difference of 0.03 kg m^{-3} for their definition. A more recent study used an algorithm to calculate mixed layer depths based on a variety of definitions (differences and gradients in temperature, salinity and density) and used clustering to decide on the final MLD (Holte and Talley, 2009). Density differences are considered to be more consistent than gradient definitions as sharp gradients are often needed for the MLD to be correctly identified (Brainerd and Gregg, 1995). Similarly, Thomson and Fine (2003) found that the density difference method produced more consistent results than integral or regression methods.

Before deciding on a MLD definition an inter-comparison of many definitions commonly used in the literature was conducted. The definitions were based on density differences and gradients, variable density changes (density differences derived from a set temperature change), (Kara *et al.*, 2000, Thomson and Fine, 2003, Montégut *et al.*, 2004) as well as the various outputs from the Holte and Talley (2009) algorithm. A randomly chosen (but still excluding low seasonality regions) subset of the global density profiles calculated from the gridded temperature and salinity fields was used to compare the different methods. The depth of the mixed layer was estimated through visual inspection of over 3000 individual density profiles (following a similar approach used by Fiedler (2010) and Montégut *et al.* (2004)). The Holte and Talley (2009) density difference algorithm gave the closest match with the visually estimated MLD (RMSD 29.38 m) (Figure 2.4). Holte and Talley (2009) define the mixed layer depth by a density difference of 0.03 kg m^{-3} from the density at a reference depth, in this case 10 m to avoid diurnal changes in temperature and salinity at the surface (Figure 2.5). This algorithm incorporates linear interpolation to estimate the exact depth at which the density difference is crossed. Using a density difference over a temperature difference is preferred as a global study needs to consider the effects of freshwater input from large rivers and sea ice melt.

2.2.3 Limitations

The global objective analysis gives a dataset that is easy to work with as it is available on a regularly spaced grid whereas in reality the ocean is irregularly sampled by the ARGO floats. However, the objective analysis method works by propagating sampled data into data gaps or filling with a climatological value. The

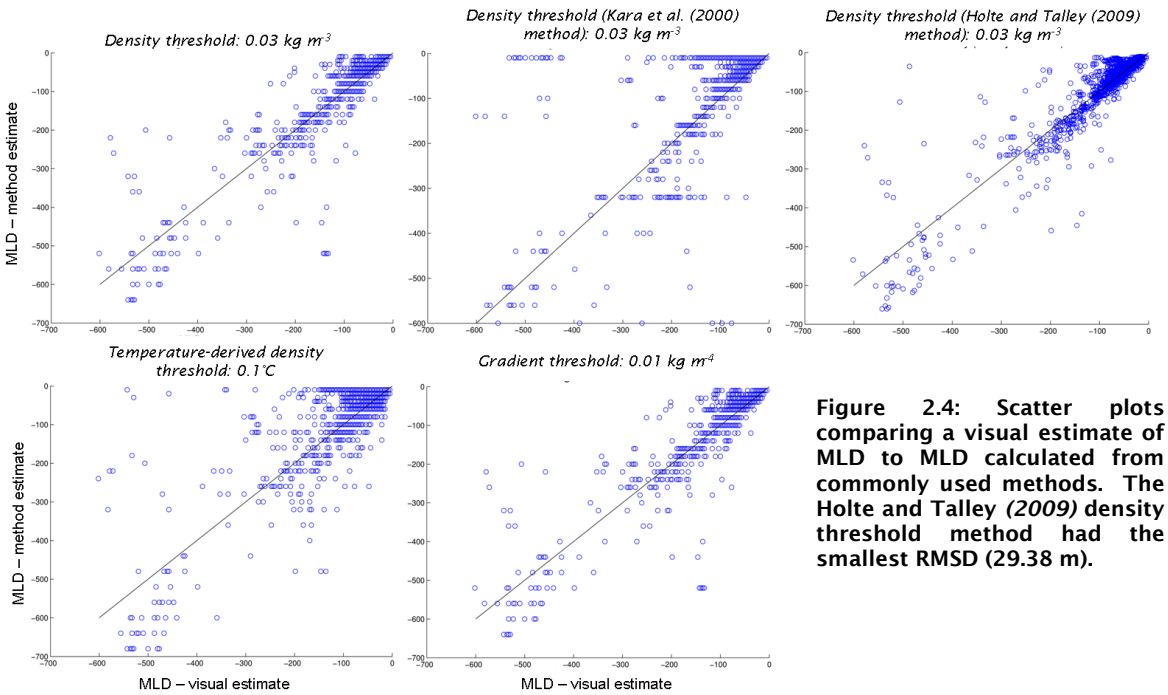

Figure 2.4: Scatter plots comparing a visual estimate of MLD to MLD calculated from commonly used methods. The Holte and Talley *(2009)* density threshold method had the smallest RMSD (29.38 m).

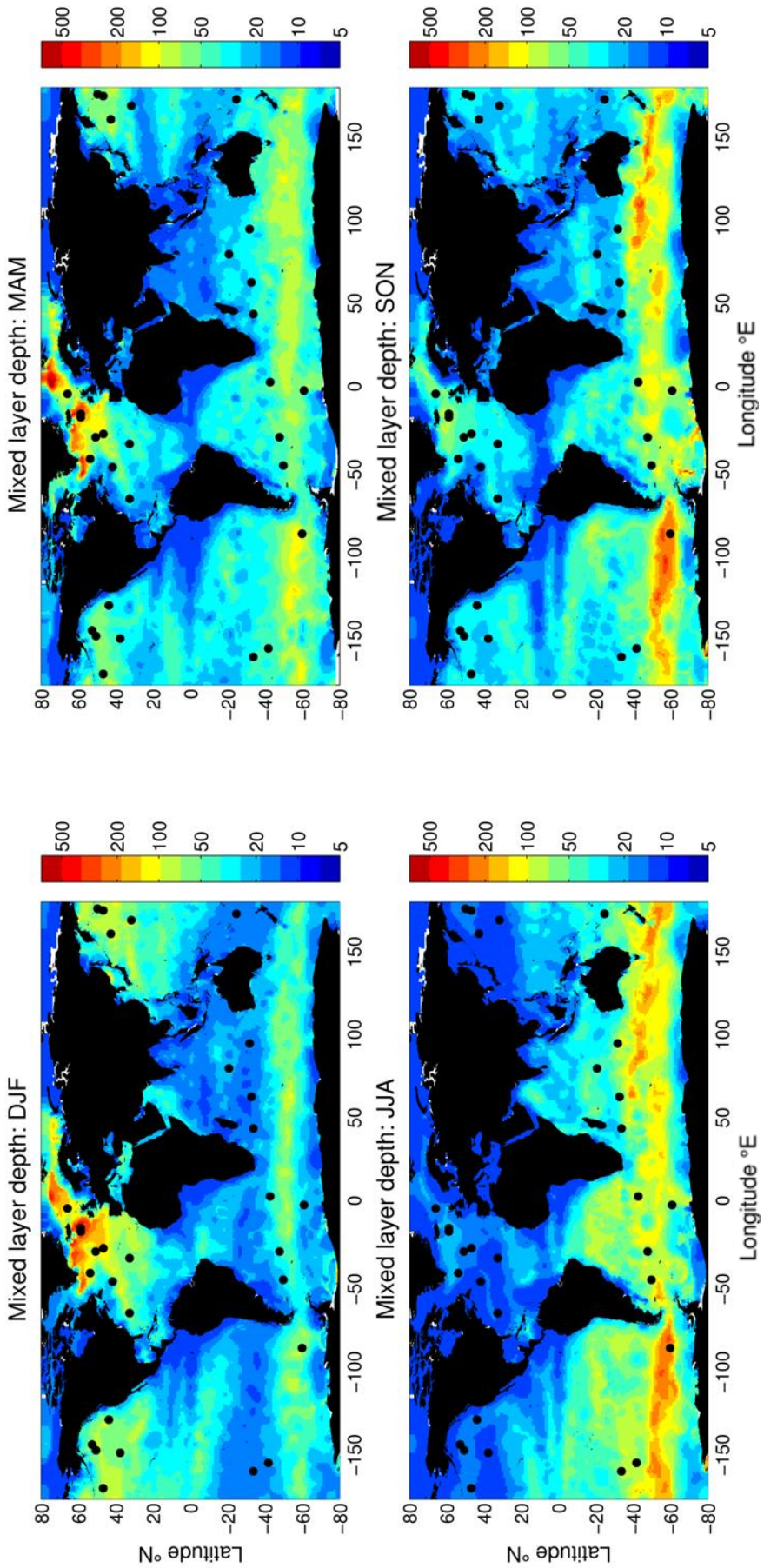

Figure 2.5: Seasonal maps of MLD (m) using the Holte and Talley (2009) density threshold method with a threshold value of 0.03 kg m^{-3}. Seasons are defined as December, January, February (DJF), March, April May (MAM), June, July, August (JJA), September, October, November (SON). Black spots mark location of the time series (2 years of data were used at each location) used for MLD definition comparisons in Figure 2.4. Note that the colour bar is on a log scale.

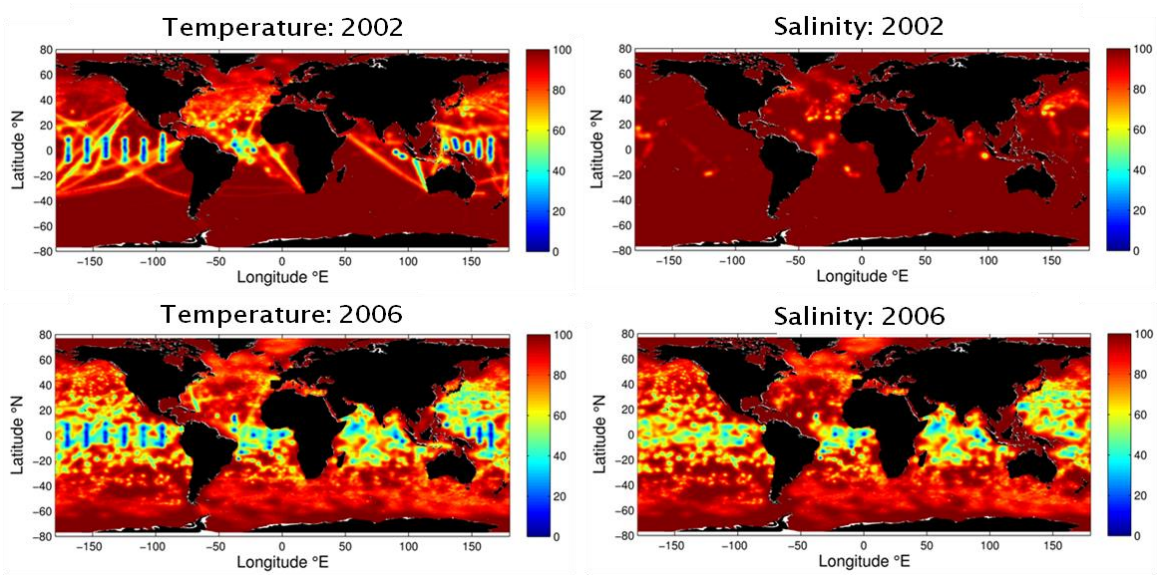

Figure 2.6: Global maps of the annual mean objective analysis error statistics on temperature and salinity measurements for 2002 and 2006. Errors are expressed as a percentage of the *a priori* variance, with 100% indicating that no data were available to modify the climatological value and 0 indicating that data were available at all time steps at that pixel. The coverage of temperature data is greater than salinity and coverage improves for both variables over time.

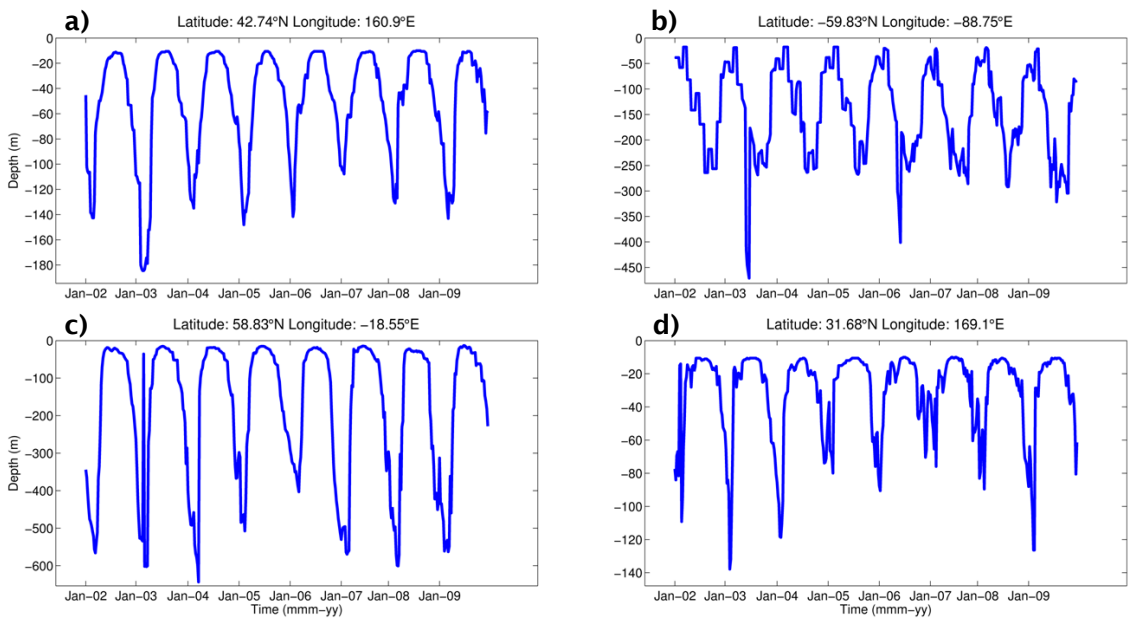

Figure 2.7: Example MLD time series using the Holte and Talley (2009) density threshold method with a threshold value of 0.03 kg m^{-3} from the North Pacific (a, c), Southern Ocean (b) and the North Atlantic (d). Variability increases over time as temperature and salinity data coverage improves.

objective analysis uses all available data to produce a climatology and from that produces *a priori* estimates of the expected variance (Gaillard *et al.*, 2009). From the *a priori* statistics the objective analysis gives an estimate of the uncertainty at each grid point which is expressed as a percentage of the *a priori* variance (see Appendix B for more details on how the errors are calculated). Figure 2.6 shows how the errors for temperature and salinity vary globally and through time. Values of 100% indicate that there are no data available to update the climatology whereas lower values indicate that data has been incorporated. For example, the vertical lines of very low error in Figure 2.6 are caused by the Tropical Atmosphere Ocean/ Triangle Trans-Ocean Buoy Network (TAO/TRITON) array where data are available and incorporated on a regular basis (i.e. all points in time have a corresponding data point). This is important to bear in mind because error values of 100% indicate an absence of interannual variability in the temperature and salinity datasets (i.e. gaps are filled with climatological values).

From Figure 2.6 it can be seen that the coverage improves over time and the errors become smaller. This is also reflected in individual time series where the variability is clearly seen to be greater in later years (Figure 2.7). Large portions of the Southern Ocean are relatively under-sampled, whereas the North Atlantic has the best coverage. However, the majority of the world is adequately sampled after 2004 (Gaillard *et al.*, 2009). Error statistics of less than 50% are considered to be adequately sampled as the error statistics include other sources of missing variability: measurement error and representivity error. Measurement errors are associated with the accuracy of the instrument used while representivity errors include variability on scales smaller than those which the floats can capture (i.e. unresolved variability). These are derived from the target resolution of 300km of the ARGO array.

The situation is additionally complicated as temperature and salinity have different data coverage. Any attempt to try and exclude certain regions based on the error statistics would most likely be done using a subjectively chosen threshold. Furthermore, for the majority of the ocean, temperature is more important for driving MLD changes than salinity. Because of this it is arguably preferable to keep the salinity climatological values than to remove temperature data where salinity data is absent. Instead, these maps of error statistics can be used to assess the quality of the data in regions of interest.

2.3 Net Heat Flux

The net heat flux (Qnet) is a measure of how much the ocean is heating or cooling relative to the overlying air. It is calculated as the sum of 4 terms (equation 2.1): shortwave radiation (SW), longwave radiation (LW), sensible (SH) and latent (LH) heat flux.

The units of net heat flux used here are W m^{-2} and the convention is that a positive value indicates heat gain by the ocean. Shortwave and longwave radiation are the incoming solar radiation and the emitted heat from the sea surface respectively. The sensible heat flux quantifies the transfer of heat across the air-sea interface (i.e. heat conducted from the surface to the air). The latent heat flux is a measure of the exchange of heat during evaporation. Broadly, stronger winds increase surface cooling and evaporation resulting in more negative sensible and latent heat fluxes and a reduction in the net heat flux. This is because as air molecules come into contact with the water they pick up heat (sensible) and moisture (latent). Faster winds mean that this happens at a faster rate. Large negative net heat flux values indicate strong cooling and are associated with winter convection. The sensible and latent heat fluxes have their greatest variability over western boundary currents because of the cool, dry air blown over them from the continents (Yu *et al.*, 2008). The magnitude of these fluxes is therefore smaller in the Southern Ocean compared to the subpolar northern hemisphere as the overlying air is relatively warmer and moister.

$$Q_{net} = SW + LW + SH + LH \tag{2.1}$$

2.3.1 Data Sources and Processing

The net heat flux dataset used here was downloaded from the Woods Hole Oceanographic Institute (WHOI) OAflux project webpage (http://oaflux.whoi.edu). The net heat flux is obtained by the OAflux project by combining an objective analysis of sensible and latent heat fluxes with shortwave and longwave radiation output from the International Satellite Cloud Climatology Project (ISCCP). The ISCCP use the Goddard Institute for Space Studies (GISS) radiative model to calculate the shortwave and longwave radiation fluxes (Rossow and Zhang, 1995, Zhang *et al.*, 2004). The latent and sensible heat fluxes were estimated using remotely sensed meteorological data and numerical weather prediction reanalysis products from National Centers for Environmental Prediction (NCEP) and European Centre for Medium-range Weather Forecasts (ECMWF) (Yu *et al.*, 2008). The input data used

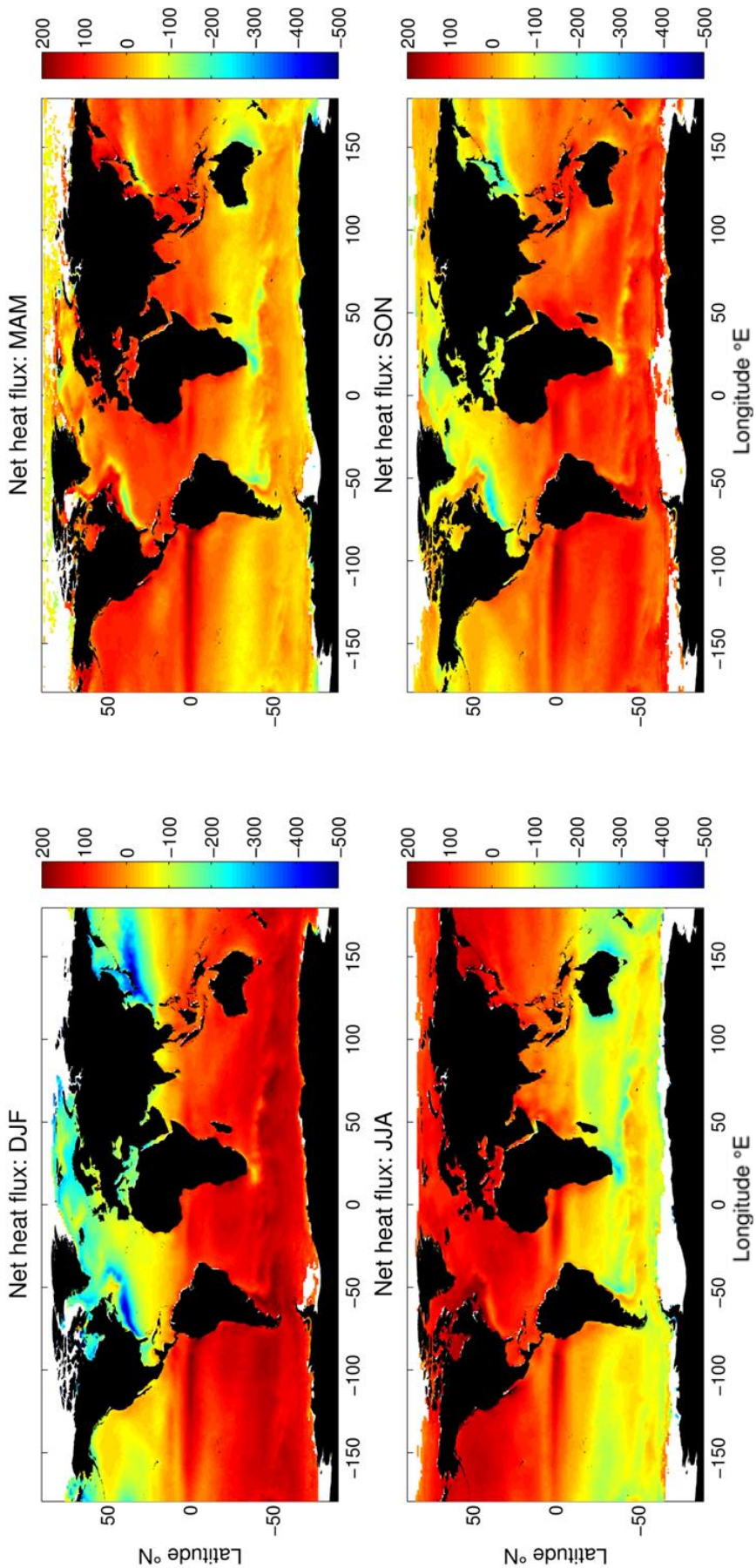

Figure 2.8: Seasonal maps of net heat flux (W m^{-2}) for December, January, February (DJF), March, April May (MAM), June, July, August (JJA), September, October, November (SON). Positive values indicate heat gain by the ocean.

are SST, wind speed, surface air temperature and humidity. The GISS radiative model uses data from weather satellites for top-of-atmosphere visible and infrared radiation, snow and ice cover, ozone concentration, air temperature, humidity and surface temperature as well as the ISCCP cloud property data (Rossow and Zhang, 1995, Zhang *et al.*, 2004).

The data were available on a 1˚x1˚ grid at daily temporal resolution. The dataset spans from 1958 to the present but only the years 2002-2009 were used here to match the chlorophyll dataset availability. This was averaged down to 8 day composites to match the chlorophyll data and so each year has 46 time steps (Figure 2.8).

2.3.2 Limitations

The dataset's largest limitation is that the net heat flux is not directly measured but is reliant on the accuracy of the numerous input datasets and reanalysis products as well as the performance of the GISS model. Indeed, the error estimations in sensible and latent heat fluxes are mostly determined by the data coverage of the satellite data inputs. Additionally, the satellite data are a snapshot of the conditions at the time when the satellites pass over head which is converted into a daily flux. However, this is the only feasible method of obtaining a global dataset of net heat flux. Furthermore, it provides complete coverage over the whole study period.

2.4 Mixed Layer Irradiance

Photosynthetically active radiation (PAR) is the portion of visible section of the electromagnetic spectrum in visible wavelengths that is used for photosynthesis. It is the part of total solar irradiance that covers the spectral range 400-700nm. The mean irradiance in the mixed layer represents the average amount of light phytoplankton are exposed to. To calculate the mean mixed layer irradiance the following equation 2.2 is used.

$$I_D = \left(\frac{I_0}{kD}\right)\left(1 - e^{-kD}\right) \qquad (2.2)$$

Where I_D is the mean mixed layer irradiance (Figure 2.9), I_0 is the surface irradiance, D is the mixed layer depth and k is the attenuation coefficient for PAR wavelengths. To calculate the mean mixed layer irradiance, values of daily mean

surface PAR, the depth of the mixed layer and the attenuation coefficient for PAR wavelengths are needed.

2.4.1 PAR

The amount of PAR reaching the sea surface is estimated from the top-of-atmosphere solar irradiance from which the reflected and absorbed solar energy is subtracted (Frouin *et al.*, 2001). The solar irradiance that is reflected is a satellite-derived quantity calculated by integrating the radiance measurements across the satellite wavelength channels within the PAR part of the spectrum. A model is used to estimate the atmospheric absorption. A daily average is then calculated for every observed pixel. No data are available in the spaces in between swaths and the poles are observed more than once in a day increasing the accuracy of the PAR calculations in those regions (Frouin *et al.*, 2001).

The output is available on the NASA ocean colour website (http://oceancolor.gsfc.nasa.gov) as a standard MODIS-Aqua product. This was downloaded as 8 day composites at 9km resolution for the years 2002 - 2009. This was regridded to 1˚x1˚ resolution weighting the values by pixel area. The original data units were Einstein m^{-2} day^{-1} and were converted to W m^{-2} using the conversion factors: 86400 seconds in a day and one Einstein (defined as 1 mole of photons) m^{-2} s^{-1} equal to 0.2174×10^6 W m^{-2} (equation 2.3).

$$PAR\ W\ m^{-2} = \frac{PAR\ Einsteins\ m^{-2} day^{-1}}{86400 \times 0.2174 \times 10^6} \qquad (2.3)$$

2.4.2 Attenuation Coefficient

The attenuation coefficient (Kd(λ)) indicates the rate at which light is attenuated in the water column for a given wavelength (λ). It has units of m^{-1} and so $Kd(\lambda)^{-1}$ represents the first optical depth, which is the bottom of the layer in which 90% of the surface signal of upwelling irradiance originates (Gordon and McCluney, 1975). Higher values represent more attenuation which is driven by substances that absorb and scatter light (i.e. chlorophyll, CDOM, particulates, water itself). One of the standard ocean colour products is Kd(490), the attenuation coefficient at 490nm since the contribution of all optical components in seawater to absorption and scattering are significant at this wavelength (Doron *et al.*, 2007). From Kd(490) we can estimate Kd(PAR) which is the attenuation of all the PAR wavelengths.

There are several ways to calculate Kd(490). Kd(490) is the sum of the attenuation of pure water and biological attenuation (scattering and absorption by phytoplankton) for open ocean (case 1) waters (Morel *et al.*, 2007). Previously, the ratio of normalised water-leaving radiance at 490 and 555 nm was used to estimate the biological attenuation. However, recently Morel *et al.* (2007) has proposed that a new equation that derives Kd(490) from chlorophyll concentration should be adopted as it matched *in situ* measurements better at the extremes of possible Kd(490) values. It is this derivation that is used by the GlobColour project for their Kd(490) values (equation 2.4)

$$Kd(\lambda) = Kw(\lambda) + \chi(\lambda) \cdot chl^{a(\lambda)} \qquad (2.4)$$

where Kw(490) is 0.0166 m^{-1}, $\chi(490)$ is 0.08349 and a(490) is 0.63303 (Barrot, 2010). The differences in wavelength bands between ocean colour sensors are already taken into account through the chlorophyll algorithms. Additionally, Kd(490) from GlobColour will have improved coverage due to the merging of the three ocean colour sensors. However, since it is derived from chlorophyll measurements it will have the same gaps as the chlorophyll time series.

Kd(490) data were download from the GlobColour website (http://www.globcolour.info/) as 8 day composites at 1/4˚x1/4˚ resolution from 2002 – 2009. These data were regridded to 1˚x1˚ weighting each value by pixel area before being converted to Kd(PAR). The equation used to convert Kd(490) to Kd(PAR) depends on the thickness of the layer of water considered because the attenuation of PAR wavelengths decreases with depth as the wavelengths that attenuate quickest are depleted near the surface. The layer of interest is the mixed layer which in general will be deeper than the first optical depth (first optical depth is ~35-40 metres in subtropical and 10-25 metres in subpolar regions). Therefore, equation 2.5 is used to convert Kd(490) to Kd(PAR) though this equation assumes the mixed layer is equal to twice the first optical depth (Morel *et al.*, 2007) (i.e. it is the mean attenuation over the first two optical depths).

$$Kd(PAR) = 0.0665 + 0.874 \cdot Kd(490) - 0.00121 \cdot Kd(490)^{-1} \qquad (2.5)$$

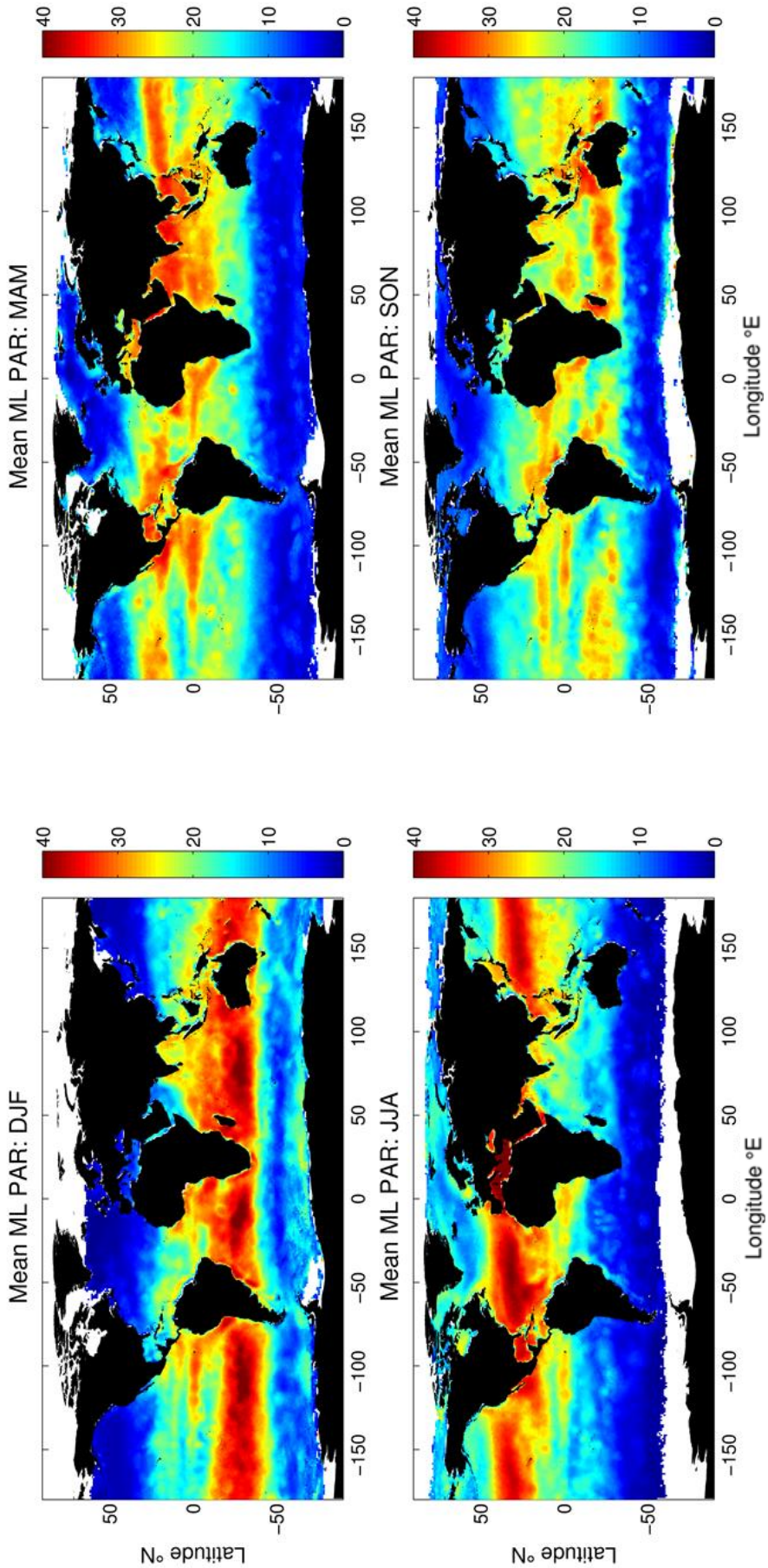

Figure 2.9: Seasonal maps of mean mixed layer irradiance (W m^{-2}) for December, January, February (DJF), March, April May (MAM), June, July, August (JJA), September, October, November (SON).

2.4.3 Limitations

For PAR values, clear sky estimates of surface irradiance are very accurate when compared to *in situ* measurements with the greatest errors occurring because the effect of clouds (Frouin *et al.*, 2001) This effect is largest in regions of strong diurnal variability in cloud cover as it is assumed that the cloud cover stays constant over the day. However, these errors will be reduced by averaging over larger time and space scales as is done here.

Attenuation coefficient data are only available when chlorophyll data are available so while this dataset is incomplete it is no more so than the GlobColour chlorophyll dataset. The derivation of Kd(490) from chlorophyll has been shown to be more accurate than previous methods (Morel *et al.*, 2007). Additionally, the conversion to Kd(PAR) will introduce some uncertainty as it is dependent on the depth of the mixed layer of water being considered. Thus, an assumption about the depth of the mixed layer being twice the first optical depth of Kd(490) is needed. This assumption is approximately satisfied in the subtropics where the second optical depths are mostly less than 80m and MLDs are generally less than 100m. However, the MLD is much deeper than the second optical depth in subpolar regions in winter but approximately equal in summer.

2.5 Summary

- The requirements for the datasets used here were spatial resolutions of 1˚x1˚, temporal resolutions of approximately 1 week and a time span covering the same period of several years. The variables used were chlorophyll concentration, mixed layer depth, net heat flux and mean mixed layer irradiance and all satisfy these requirements.
- Chlorophyll data comes from two sources: a satellite-derived dataset, GlobColour, and a global biogeochemical model, NOBM, which assimilates satellite chlorophyll data.
- The mixed layer depth dataset was calculated from temperature and salinity profiles, predominantly from ARGO floats, and available from the Coriolis Project website. The depth of the mixed layer was defined by using the Holte and Talley (2009) algorithm with a density difference threshold of 0.03 kg m^{-3}.
- The net heat flux dataset was obtained from the WHOI OAflux project website. To calculate the mean mixed layer irradiance data, surface

irradiance and the attenuation coefficient were needed in addition to mixed layer depths.

- The surface irradiance data were obtained from the NASA Ocean Color website, and the attenuation coefficient data were downloaded from the GlobColour Project website.
- Each of these datasets has their limitations with the most common arising from using objective analysis. The temperature, salinity and net heat flux datasets were formed using objective analysis to propagate data into data-free regions. The SEIK filter used in the assimilation of SeaWiFS data into NOBM is another method that is part of the optimal estimation family.
- A major limitation affecting both the GlobColour chlorophyll and attenuation coefficient datasets is the presence of gaps in the time series, and this provides the subject of the fourth chapter.
- Notwithstanding the preceding limitations, each dataset described here displays a realistic seasonal cycle which is a greater priority than the accuracy of the actual data values.

3 Seasonality Metric Development

Phytoplankton seasonality can be quantified in two ways: magnitude and timing. Variability in the magnitude of blooms is relatively well studied and so this thesis will focus on the timing of bloom events or bloom phenology. Phenology is the study of the timing of periodic biological events. In the case of a phytoplankton bloom we can look at the timing of bloom initiation, peak and termination (Figure 3.1). In addition, the duration of the bloom can be calculated using the bloom initiation and termination dates. The first half of this chapter explores methods for identifying regions with significant seasonality. The second half deals with developing and comparing a suite of seasonality metrics that will identify bloom timing accurately and consistently.

3.1 Detecting Seasonality

A strong, recognisable seasonal cycle in phytoplankton biomass is not observed everywhere in the ocean. As will be discussed in section 3.2, seasonality metrics assume that a significant increase in chlorophyll concentrations delineates the bloom, thus the metrics will be unreliable in regions with low seasonal variability. As a result, a reliable method for identifying regions with weak seasonal cycles is needed so that these regions can be removed from further analysis.

Below is a brief description of the various methods tested as a suitable way to identify weak seasonality. Each method was initially tested on a subset of 12 GlobColour chlorophyll time series, each 9 years long. These were located in the North Atlantic at 32°W and approximately every 2° of latitude between 47°N and 20°N to capture the transition from regions of high to low seasonal variability (Table 3.1). If the method being tested seemed suitable based on the time series subset then it was applied globally and additional longitudinal transects in the other ocean basins were checked to ensure the method was consistent. The most suitable method was chosen based on the performance of the method on both the time series and the global spatial pattern.

3.1.1 Measures of Shape

The shape of a distribution can be determined using measures of shape such as kurtosis and skewness. Kurtosis is a measure of peakedness with a normal

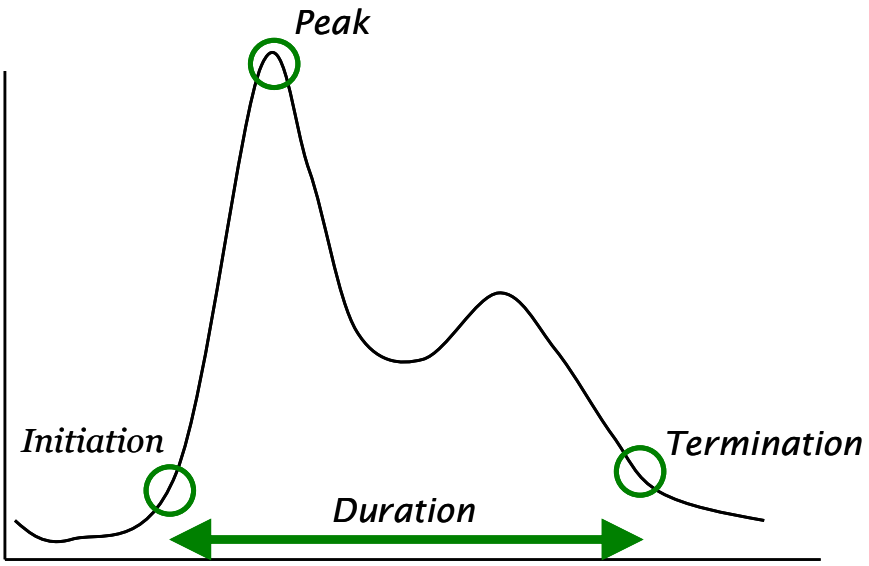

Figure 3.1: Cartoon of an idealised phytoplankton bloom showing the seasonality metrics that can be calculated: bloom initiation, peak, termination and duration.

Table 3.1: Results from different approaches for detecting strong seasonality

Climatology[a]	Latitude	Kurtosis[b]	Skew-ness[b]	Cumula-tive sum[b]	Ann. ampli-tude[b]	Seasonal fraction[b]	Coeff. of variation[b]
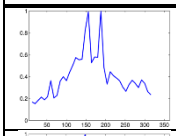	47.67°N	3.346	0.650	0.977	0.090	0.493	0.742
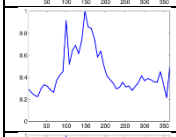	45.12°N	4.056	0.680	0.986	0.099	0.485	0.677
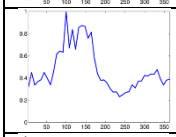	42.62°N	3.520	0.818	0.979	0.150	0.583	0.590
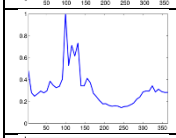	40.12°N	5.997	1.194	0.969	0.091	0.194	0.850
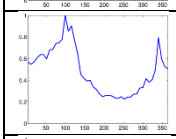	37.62°N	2.584	0.391	0.962	0.236	0.604	0.572
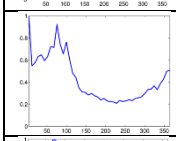	35.12°N	3.881	0.872	0.956	0.195	0.569	0.698
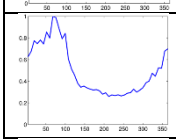	32.62°N	2.249	0.496	0.957	0.320	0.764	0.527
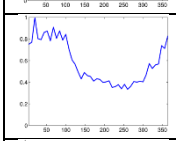	30.12°N	2.381	0.467	0.977	0.293	0.802	0.417
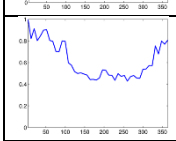	27.62°N	2.812	0.562	0.990	0.213	0.793	0.369
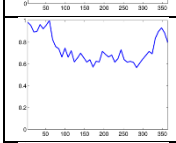	25.12°N	2.498	0.274	0.997	0.136	0.452	0.274
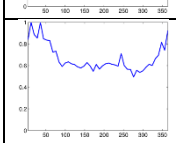	22.62°N	3.842	0.261	0.997	0.137	0.490	0.268
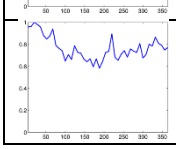	20.12°N	3.478	0.416	0.999	0.080	0.343	0.260

[a] Climatological annual cycles were calculated from GlobColour chlorophyll time series (2002-2009) along a transect at 32°W. Values were normalised to the maximum chlorophyll value in each time series. X-axis is time in days (1 to 365).

[b] The values are the results from various methods tested for identifying strong seasonality. More details can be found in section 3.1.1 (Kurtosis and Skewness), section 3.1.2 (Cumulative sum), section 3.1.3 (Annual amplitude (Ann. Amplitude)), section 3.1.4 (Seasonal fraction) and section 3.1.5 (Coefficient of variation (Coeff. of variation)).

distribution having a kurtosis of 3. The symmetry of a distribution is measured through skewness with a normal distribution being symmetrical and having a skewness of 0. If a distribution is more peaked then it will have a larger kurtosis value whereas a smaller kurtosis indicates a lack of peakedness. If a distribution is less symmetrical then it will have a larger magnitude of skewness (though this can be positive or negative). Histograms of the log-transformed chlorophyll time series in low seasonality regions were seen to be approximately normally distributed whereas the distributions in regions with a strong seasonal cycle were heavily skewed and more peaked. This observation led to testing measures of shape as a method for identifying regions of significant seasonality.

Based on this observation the kurtosis and skewness for the time series subset were calculated using the corresponding Matlab functions and are shown in Table 3.1. The expected result was a gradual decline in kurtosis with latitude from high peakedness toward a value of ~3 and a decline in skewness with latitude towards a value of 0 for low seasonality time series. However, though Table 3.1 shows a general decline in skewness a similar trend was not seen for kurtosis. Additionally, for both measures it would be difficult to pick a threshold value indicative of a seasonal cycle. This was also observed in longitudinal transects in the North Pacific and Southern Oceans. As a result this method was not developed any further as it was not possible to distinguish high and low seasonality regions from these measures of shape.

3.1.2 Cumulative Sum Regression

Another observation made from the time series was differences in the shape of the cumulative sum of the time series. Figure 3.2 shows the cumulative sum for two climatological time series, one with high and one with low seasonality. The cumulative sum for the low seasonality time series is very linear whereas the high seasonality time series is curved and more variable. This observation showed that high and low seasonality regions could potentially be separated based on how close to a straight line the cumulative sum was.

The cumulative sums for the subset were calculated using the log transformed climatological time series to reduce the impact that gaps had on the shape of the cumulative sum. The Matlab function regress was used to find the linear equation ($y=mx+c$) that best fit the cumulative sum. The coefficient of determination (R^2) is one of the outputs of this function and describes how much of the cumulative sum variability is explained by the linear fit. The expected result was that this would be much higher for the low seasonality cumulative sums.

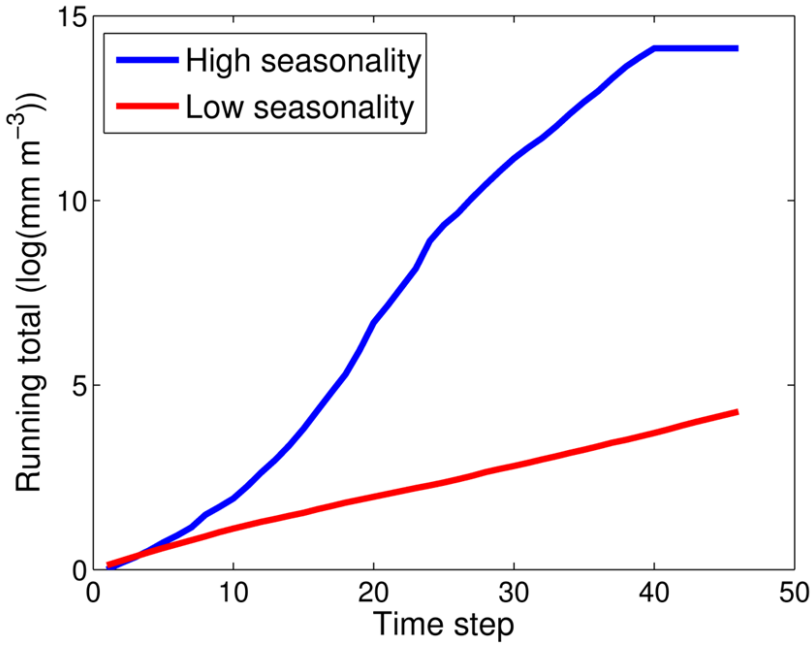

Figure 3.2: The cumulative sum for two climatological time series (first and last time series in Table 3.1, one with high seasonality (blue) and one with low seasonality (red).

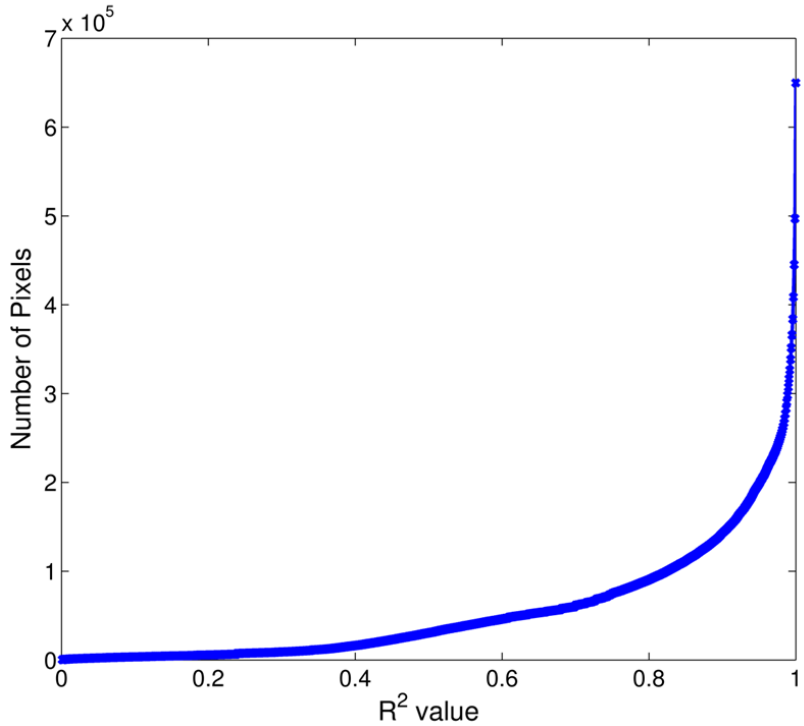

Figure 3.3: The number of pixels with a coefficient of determination value (R^2) below a set threshold R^2 value

The results for the transect subset are shown in Table 3.1 and the R^2 value were observed to increase with lower seasonality. However, all the values were very similar especially for subtropical-like (~35°N onwards) and oligotrophic-like (~30°N onwards) time series and only varied at 1/1000ths level. This makes it difficult to choose a threshold value as the number of pixels enclosed varied greatly with small changes in the threshold value (Figure 3.3). Additionally, this method cannot be applied to each year individually as gaps in the time series would cause apparent high seasonality. Though on a global scale the linearity of the cumulative sum captures the expected spatial pattern quite well, the sensitivity to the chosen threshold value is a major disadvantage.

3.1.3 Spectral Analysis

Spectral analysis is a useful tool for identifying dominant frequencies in a time series. If the seasonal cycle is assumed to be contributing most strongly to the variability in a time series then the annual time scale will be identified by spectral analysis as being the dominant frequency. Many spectral analysis methods require a complete time series to fully resolve the variability in each frequency and are therefore usually unsuitable for use with satellite chlorophyll time series which are incomplete. However, the Lomb-Scargle Periodogram has been developed to perform spectral analysis on incomplete time series and has previously been used on chlorophyll data (Lomb, 1976, Scargle, 1982, Yoo *et al.*, 2008). The amplitude of a frequency of interest can be extracted from the Periodogram output and used to identify regions with weak seasonal cycles (low amplitude). This amplitude is normalized by the variance of the time series to quantify how much of the total variability is caused by the seasonal cycle. Additionally, each frequency has an associated p-value to distinguish it from noise within a defined confidence interval. Here the commonly used p-value of 0.05 for the 95% confidence interval is used as the threshold for very low seasonality regions.

From the time series subset, unexpectedly, the highly seasonal time series (top row of Figure 3.4) were seen to have low normalised amplitudes. The maximum normalised amplitudes were seen in the subtropical time series (second row of Figure 3.4) though there was a reduction in amplitude towards the low seasonality time series (bottom row of Figure 3.4). This was also seen in the global pattern of normalised amplitude for the annual frequency (Figure 3.5). High latitude regions which have strong seasonal cycles were observed to have low relative amplitudes which in some cases were indistinguishable from noise. The largest normalised amplitudes were seen in the subtropics. The oligotrophic gyres, much like the high latitudes had low normalised amplitudes.

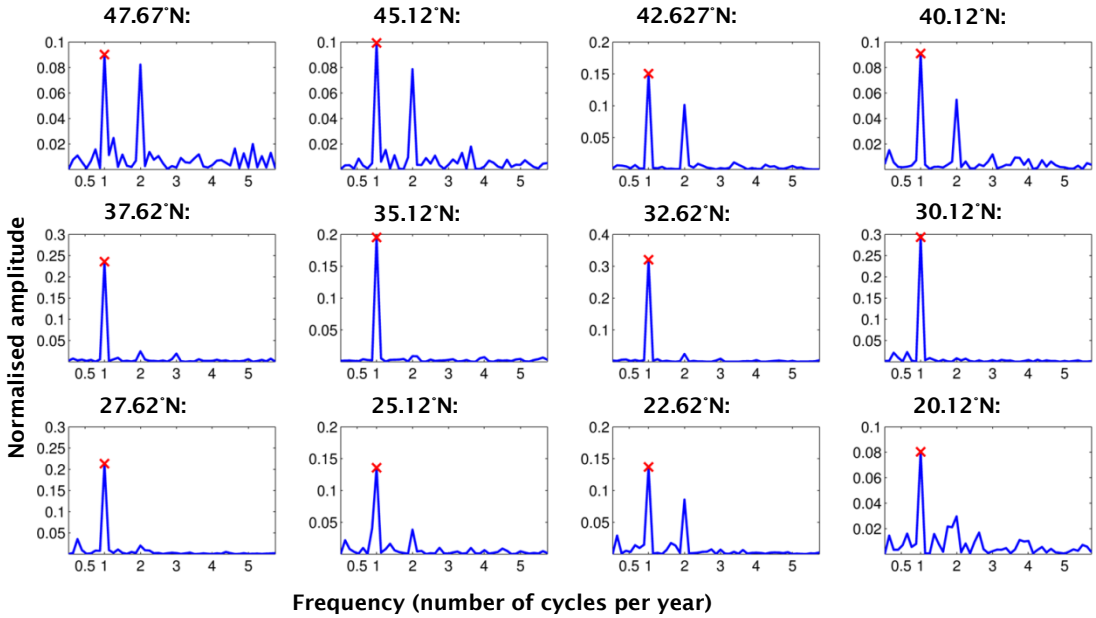

Figure 3.4: Low frequency part of the periodograms calculated from the time series in Table 3.1. The red cross indicates the normalised amplitude of the annual cycle. Location of the time series and amplitude of the annual frequency is displayed above each subplot.

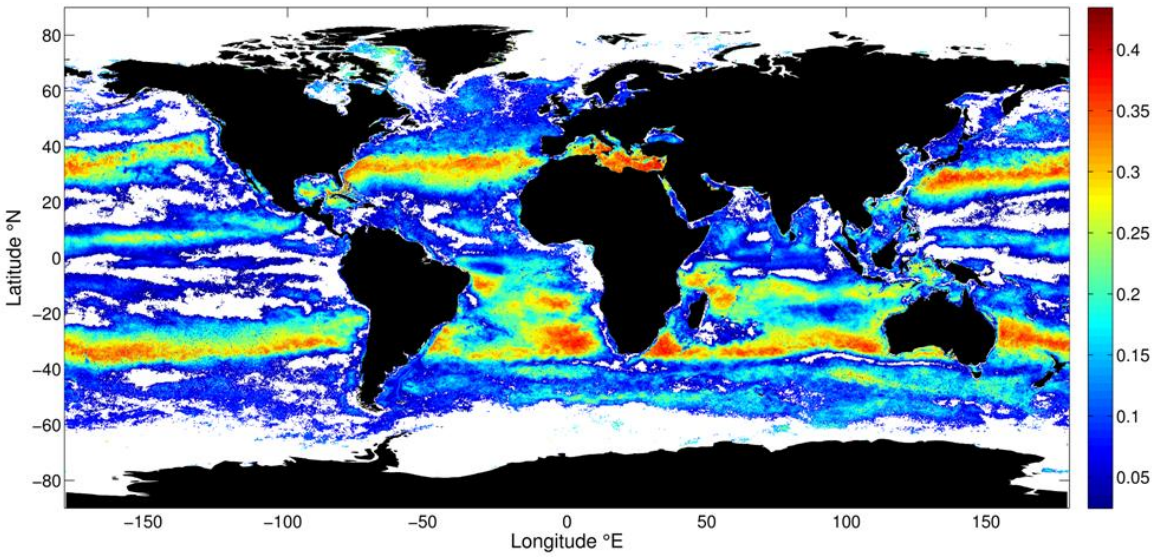

Figure 3.5: Global map showing the normalised amplitude of the annual frequency from the Lomb-Scargle Periodogram. Values are normalised to the total variance of the time series. Areas in white are regions where the amplitude was not statistically significant (i.e. not significantly different from zero at the 95% confidence interval (p>0.05)).

These results suggest that much of the total variability is contained within the seasonal cycle in subtropical regions. Oligotrophic and subpolar regions have relatively small amounts of variability at this frequency indicating that other time scales are major components of the total variability. In oligotrophic regions this is due to variability at shorter time scales dominating the time series. In subpolar regions the seasonal cycle signal is weakened because of spurious frequencies arising from the long gaps in the dataset over winter. The Lomb-Scargle Periodogram was designed to cope with small gaps and so using it on regions with large gaps leads to erroneous results. Another assumption of the Periodogram is that the frequencies are periodic meaning that there is no interannual variability in the timing or duration of the seasonal cycle. As the interannual variability in the timing and duration of the seasonal cycle is typically strong, especially in subpolar regions, the resulting normalised amplitudes for the annual frequency in these regions will be smaller. To reduce the effect of these limitations a climatology could be used to reduce the number of gaps and reduce interannual variability. However, this gave similar results as using the full time series with the subtropical climatological time series having the largest amplitudes. Moreover, using a climatology would prevent this approach being applied to each individual year. Because of the limitations of this method and the impact this has on the apparent amplitude of the annual frequency in subpolar regions, this method was not pursued any further.

3.1.4 Seasonal Adjustment: X-11

The X-11 seasonal adjustment method was first developed to assess seasonal and long-term trends in economics data and has recently been applied to geophysical datasets (Vantrepotte and Melin, 2009). The X-11 applies running means of different window lengths to decompose a time series into three components. In this case the three components are a trend, seasonal and residual component. This method allows for interannual variability in the timing and length of the seasonal cycle.

The X-11 method was applied to the original full chlorophyll time series and follows the seasonal adjustment method described in Pezzulli *et al.* (2005). The running mean window lengths were one year for estimating the trend component and one month for the seasonal component. Therefore, the residual component represents time scales of less than one month. After decomposing the time series into the three components the variance of the seasonal component was calculated and expressed as a fraction of the total variance of the time series. This indicated how much of the total variance in the time series was captured at different time

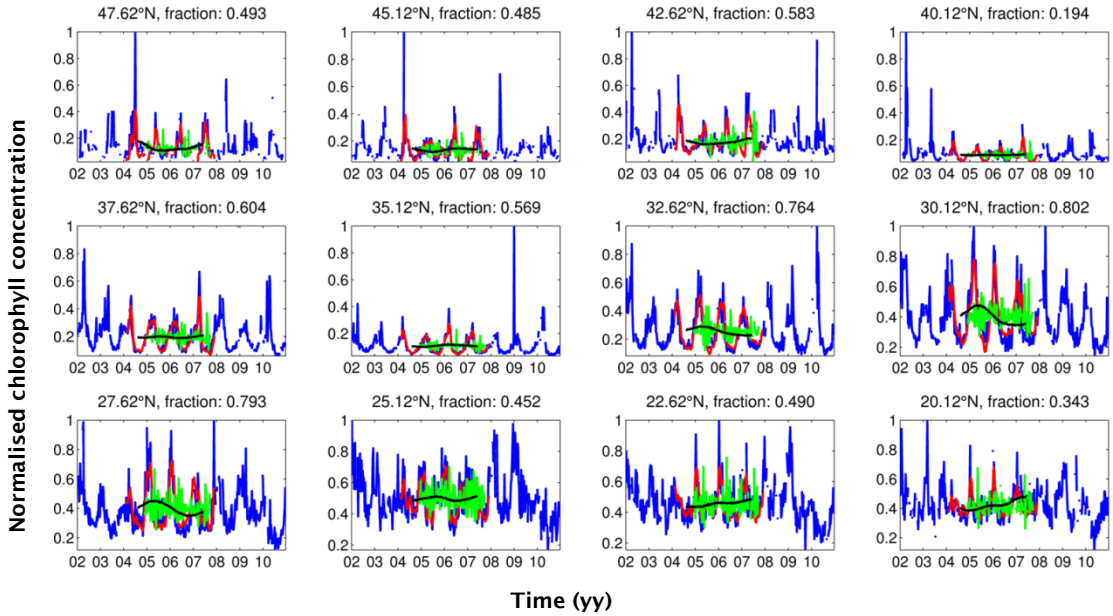

Figure 3.6: Results from X-11 decomposition: the original time series (blue), trend component (black), seasonal component (red) and residual component (green). The application of running means in the decomposition results in a reduction in the length of the time series. Time series and components are normalised by the maximum chlorophyll value.

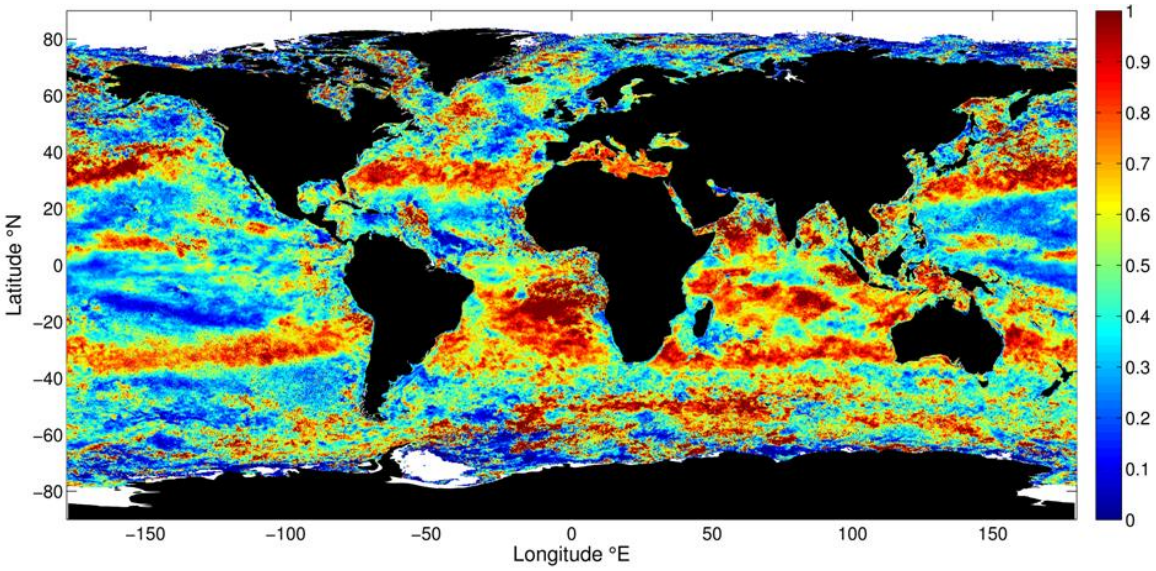

Figure 3.7: Global map showing the fraction of total time series variance explained by the seasonal component from the X11 decomposition. White areas are regions of permanent ice cover.

scales signifying the types of processes that dominate the time series variability (i.e. annual cycle versus submonthly processes).

The fraction of the total variance contained in the seasonal component is shown for the time series subset in Figure 3.6 and globally in Figure 3.7. In the time series subset the trend with latitude was similar to that of the Lomb-Scargle Periodogram results with the highest fractions seen in subtropical regions and lower values in both oligotrophic and subpolar regions. This pattern was replicated globally with larger fractions dominating in subtropical regions.

At high latitudes the variance within the residual component, representing processes with periods of less than one month, was a significant component contributing to the total variance. This arises either from the presence of gaps in the time series or from the genuine noisy nature of the time series at these latitudes. This approach performed slightly better than the Lomb Scargle Periodogram at recognizing strong seasonal variability at high latitudes. However, large portions of subpolar regions were still classed as having low seasonal variability. As the X-11 method fails in this respect it was deemed unsuitable.

3.1.5 Coefficient of Variation

The coefficient of variation was calculated by normalising the standard deviation by the mean. This enables the comparison of the variability of different regions with respect to their mean values. Higher values indicated time series which were more variable, which was assumed to be due to a stronger seasonal cycle. The coefficient of variation is also known as the seasonal variation index (Lutz *et al.*, 2007).

The standard deviation and mean of the multi-year time series were computed to calculate the coefficient of variation. Though the entire time series was used the coefficient of variation could also be applied to each year individually to capture the interannual variability in seasonality. This is an advantage over the Lomb-Scargle Periodogram, X-11 and cumulative sum regression methods as they require multiple annual cycles to be computed. However, the Periodogram and X-11methods try to isolate and quantify the seasonal cycle whereas higher coefficient of variation values are assumed to indicate high variability resulting from the presence of a strong seasonal cycle.

A clear decline was seen in the coefficient of variation with latitude, with low values seen in the oligotrophic gyres and larger values at higher latitudes (Table 3.1). This was replicated globally with much of the subpolar regions being highly seasonal and the oligotrophic gyres being weakly seasonal (Figure 3.8). Another

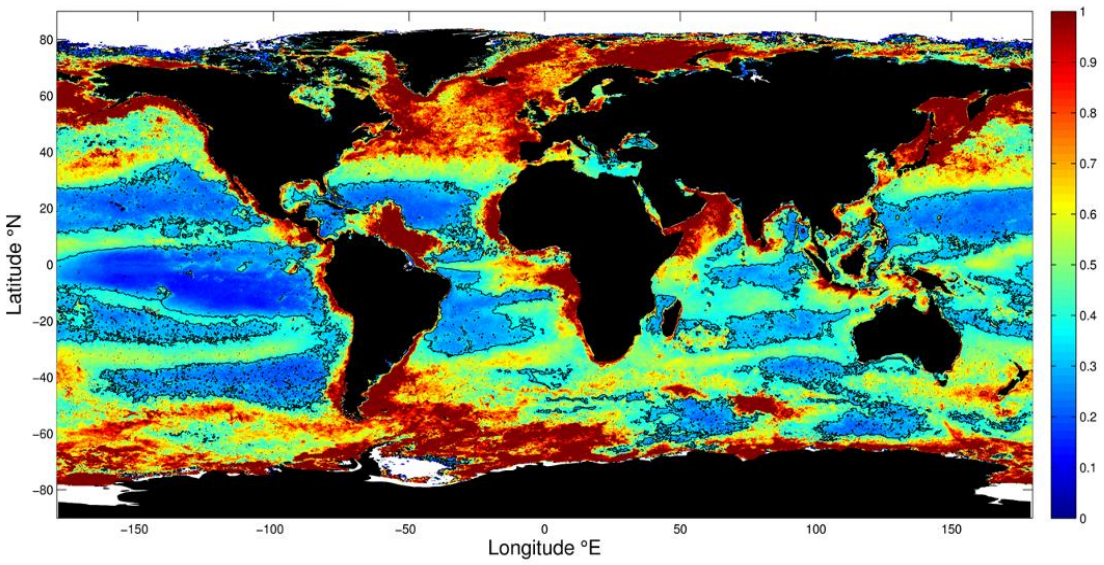

Figure 3.8: Global map of the coefficient of variation. The black contour line represents a coefficient of variation value of 0.35. Regions bounded inside of this contour line are deemed to have a weak seasonal cycle. White areas are regions of permanent ice cover.

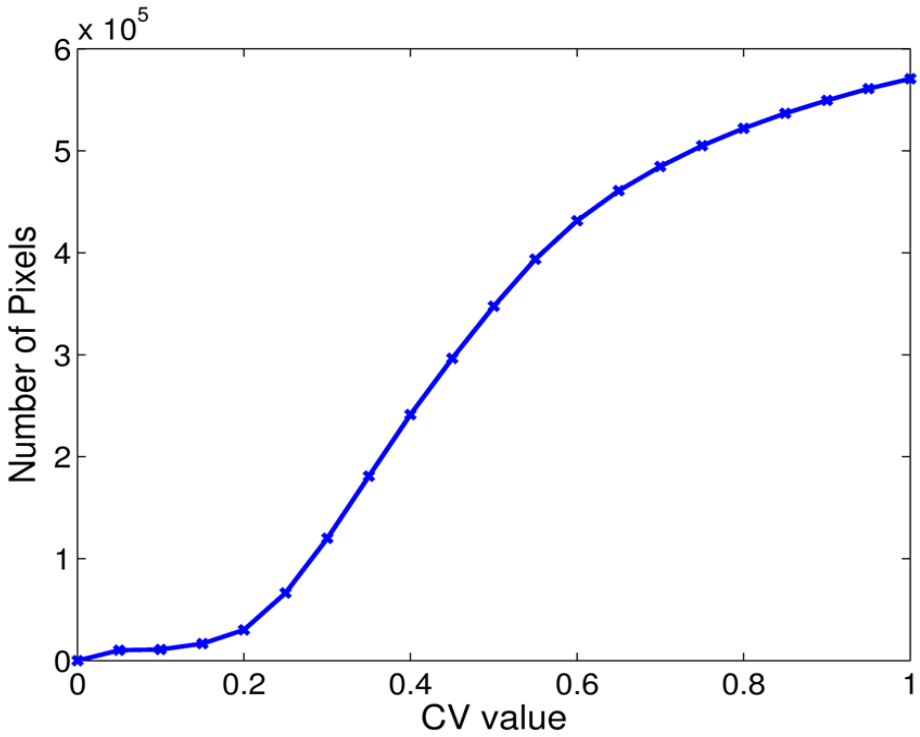

Figure 3.9: The number of pixels that fall below a coefficient of variation (CV) value.

interesting point is that the North Atlantic has a higher coefficient of variation than much of the North Pacific perhaps reflecting that the North Atlantic has larger blooms and so more variability (Parsons and Lalli, 1988). Additionally, parts of the Southern Ocean have low coefficient of variation values which is congruent with regions of low seasonality observed by Thomalla *et al.* (2011). Furthermore, the increased variability was seen around islands in the Southern Ocean suggesting that the increased iron concentrations there increase the variability (Blain *et al.*, 2001). Therefore it is likely that the coefficient of variation in the Southern Ocean is reflecting actual variability and not data coverage which can be poor in this region.

A value of 0.35 was chosen as the threshold for weak seasonality. This value was chosen based on the spatial pattern of the coefficient of variation (Figure 3.8) and on the visual estimation of time series from numerous transects running from low seasonality to high seasonality regions. All pixels with a coefficient of variation above 0.35 were deemed to be strongly seasonal. Though this is a subjectively chosen threshold it does agree well with the spatial pattern of high and low seasonality from the results of the Lomb-Scargle Periodogram and the X-11 decomposition.

Furthermore, this method is relatively insensitive to gaps and noisy time series and it is quick and simple to calculate and can be done on a year-by-year basis. Moreover, the number of pixels (i.e. the fraction of weakly seasonal locations) excluded is less sensitive to the threshold chosen than the cumulative sum regression method (Figure 3.9). However, high variability compared to the mean is assumed to be due to a strong seasonal cycle which may not always be true. Despite this limitation this method was chosen to exclude regions with a weak seasonal cycle from further analysis.

3.2 Bloom Timing Metrics

The bloom timing metrics of interest here are the dates of bloom initiation, peak and termination, as well as bloom duration (initiation to termination). The metric definition must be applicable to a wide range of different seasonal cycle shapes for it to be used globally. In addition, it must be able to capture interannual variability in bloom timing. Ultimately, the performance of a bloom timing metric will have to be assessed through the visual validation of multiple time series. Several different methods have been used to define blooms in the past (see Ji *et al.* (2010) for a comprehensive review). In many cases the most suitable approach to define a bloom is dependent on the question being asked. For example, an absolute biomass value may be best if the user is interested in grazing behaviour as

that is more likely to be dependent on actual phytoplankton abundance rather than a relative change (Ji *et al.*, 2010). The start of the bloom can also be defined by positive growth rates rather than changes in biomass or chlorophyll (Behrenfeld, 2010, Boss and Behrenfeld, 2010). However, this definition indicates that the bloom initiates in mid-winter when the MLD is deepest and biomass is low. If phytoplankton losses (i.e. grazing) increase with the growth rate then an accumulation of biomass may not occur. Basing the definition on a biomass change identifies bloom initiation as the beginning of a rise in biomass. The subsequent increase in biomass indicates surplus food for higher tropic levels and the potential for carbon export events which are the primary motivation for quantifying variability in bloom timing. In this thesis a bloom will be defined in accordance with this as a substantial rise in chlorophyll from a prolonged period of low concentrations. Relative changes in chlorophyll are best for defining the bloom in this study as the range of chlorophyll values changes both spatially and interannually. This makes the metrics suitable for use globally as it accounts for regional variations in the annual range in chlorophyll concentration.

There are four commonly used bloom timing metric definitions based on relative changes in chlorophyll, which are summarised in Table 3.2. By looking at relative changes in chlorophyll these metrics can be used on any time series no matter the range in chlorophyll values. Furthermore, using relative changes mean that the bloom timing dates are not dependent on the accuracy of the chlorophyll values.

Table 3.2: Summary of bloom timing metric definitions

Metric	Definition	References
Initiation	Date on which the chlorophyll concentration rises by a defined percentage above the annual median	(Siegel *et al.*, 2002, Henson *et al.*, 2009, Racault *et al.*, 2012)
	Date on which the cumulative sum of chlorophyll reaches a defined percentage of the annual total	(Greve *et al.*, 2005)
	Date on which the chlorophyll concentration rises above a define percentage of the annual maximum	(Fuentes-Yaco *et al.*, 2007, Vargas *et al.*, 2009)
	Date of maximum positive growth rate	(Sharples *et al.*, 2006)
Peak	The date that the maximum chlorophyll concentration occurs	(Kahru *et al.*, 2011)
Termination	Date on which the chlorophyll concentration falls below a defined percentage above the annual median	(Racault *et al.*, 2012)
	Date on which the cumulative sum of chlorophyll reaches a defined percentage of the annual total	(Greve *et al.*, 2005)
	Date on which the chlorophyll concentration falls below a defined percentage of the annual maximum	(Fuentes-Yaco *et al.*, 2007, Vargas *et al.*, 2009)
	Date of maximum negative growth rate	(Sharples *et al.*, 2006)
Duration	Potential for 4 definitions using the corresponding pairs of bloom initiation and termination definitions.	

In the following subsections each metric will be described fully, the specifics of it detailed and examples given. Following that, the performance of the different definitions will be compared.

The largest issue for accurately and consistently estimating bloom timing is gaps in the time series. Usually methods employed to fill or reduce gaps include averaging over large scales and/or interpolation. However, averaging results in a smoother time series and thus degrades finer scale detail in the interannual variability. Interpolation works best on small gaps because there is less error in the interpolated data when there is plenty of real data to constrain it. However, gaps lasting several months occur over winter in subpolar regions and interpolation schemes did not perform well in filling these gaps. In this case it is preferable to develop a metric that is relatively unaffected by gaps in the time series. The effects of missing data on the accuracy of estimates of bloom timing are discussed extensively in Chapter 4.

3.2.1 Bloom Peak Timing

The timing of the bloom peak is defined here as the date on which the maximum chlorophyll value occurs. Though this may seem rather simple to implement it is complicated by interannual variability in the magnitude of the blooms. In regions such as the Southern Ocean the bloom peak timing can be misidentified if it occurs around the turn of the year as illustrated in Figure 3.10. For example, the basic approach is to find the peak timing each year by splitting the time series into calendar years running January to December and finding the maximum value in each year. However, imagine that in year B the peak occurs in the first few weeks of January and that this bloom is larger than the one that occurred in January of year A. By essentially splitting the bloom in half by using a January to December calendar, the bloom that peaks at the beginning of year B starts at the end of year A. As bloom B is larger than bloom A the maximum value in year A is found in December and is actually part of bloom B. Thus the peak timing is misidentified. This is illustrated in Figure 3.10 by the red crosses. To properly separate the individual blooms it would be better to split the time series so that years ran from June to May. Therefore the blooms in the example given here would occur in the middle of the “year” (peaks from this approach are represented by the blue circles in Figure 3.10).

The decision on how to split up the time series must be able to automatically calculate the peak timing globally. Latitude would seem an obvious choice since, meteorologically speaking, northern hemisphere summers occur in June whereas southern hemisphere summers occur in December. However, latitude cannot be

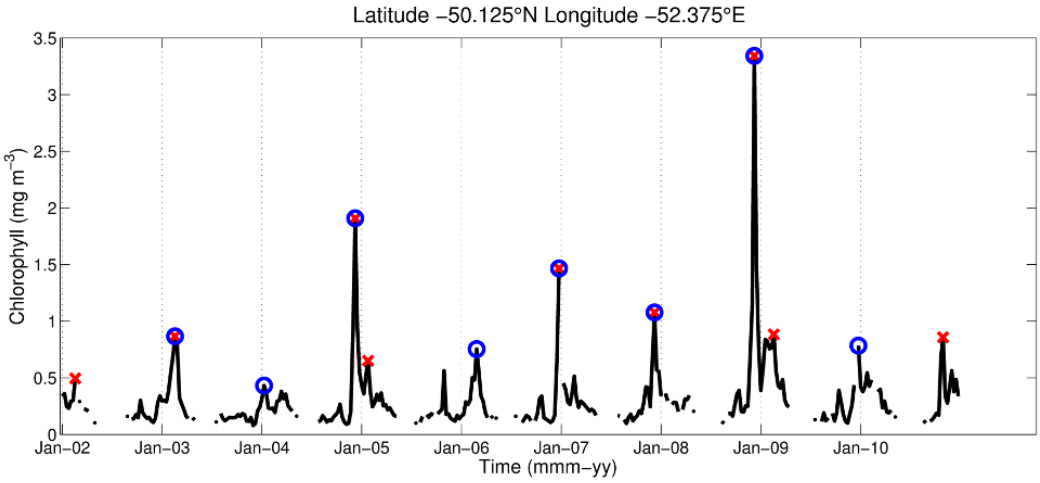

Figure 3.10: Time series from the Atlantic section of the Southern Ocean where the bloom peak occurs in December/January. Red crosses indicate the annual maximum chlorophyll concentrations when the years run from January to December. Blue circles indicate the annual maximum chlorophyll concentrations when the years run from June to May. The bloom in 2002 does not have a peak date when using a June to July calendar (blue circle) since the bloom is halfway through during June and so an estimate for the peak is likely to be erroneous. Similarly, the January to December calendar (red cross) results in an absent peak date in 2004, 2006 and 2010 because the calendar divides the bloom and so either the peak of the previous or subsequent year is identified as the maximum value instead.

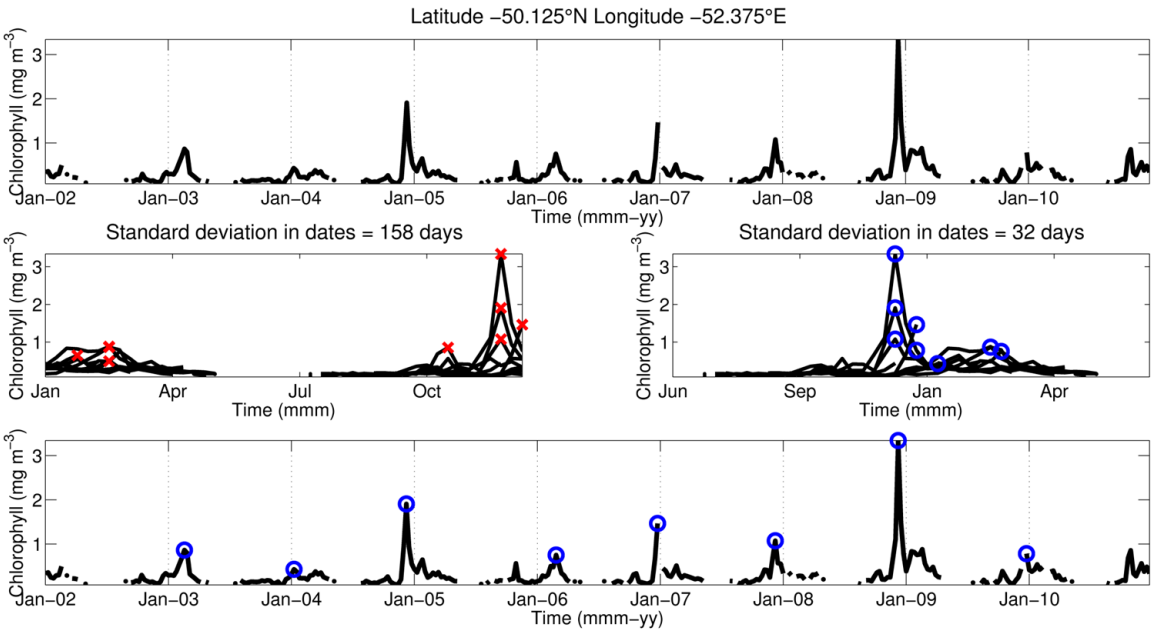

Figure 3.11: Example time series to illustrate the estimation of the bloom peak date. The original time series (a) is split into individual years running from January to December (b) and June to May (c). The maximum chlorophyll value in each year is then identified, indicated by the red cross for January-December years and blue circles for June-May years. The June-May years capture the peak timing more accurately since the time series is centred on the peak. This is evident in the smaller standard deviation of the peak dates indicated in the title of (b) and (c). The original time series with the correct peak dates (blue circles) are plotted in (d).

used as a simple proxy because the subpolar and subtropical regions in both hemispheres are approximately 6 months out of phase with each other. Instead, the decision was made based on the standard deviations of the peak timing dates returned by each year split approach (i.e. January to December split or June to May split). In the example in Figure 3.10 the standard deviation in peak timing for a January to December year split was ~158 days whereas it was ~32 days for a June to May year split. Thus, the year split with the smallest standard deviation was subsequently used to accurately calculate the peak timing. Further details on calculating the peak timing are described below.

To calculate the peak timing (Figure 3.11):

- On a pixel-by-pixel basis, the chlorophyll time series was extracted, running from January 2002- December 2010.
- The time series was rearranged into individual years running from January to December and June to May and the date of maximum chlorophyll in each year was found. It is important to note that for the years running June to May there will be only 8 complete years.
- The standard deviations in the timing of the peak for each set of dates (January-December set and June-May set) were compared and the set with the smallest standard deviation was used as the peak dates. The dates calculated from June to May time series were adjusted to account for the shift in the calendar year.

3.2.2 Bloom Initiation and Termination Timing

Four definitions for the timing of bloom initiation and termination (see Table 3.2) were chosen for comparison. To make these metrics adaptable to the global ocean some small changes in the way they are implemented were needed. These are described below for each of the metric definitions. Before refining the metric implementation it is useful to define which feature in the chlorophyll time series is of interest. In this thesis the primary focus when defining bloom initiation and termination is to bookend the productive season. Thus, the primary increase in biomass toward the annual maximum after an extended period of low productivity is the feature defined as bloom initiation. Bloom termination is defined here as the end of the productive season characterised by a reduction in biomass back towards low productivity values. It is these features which are of interest to food supply at higher trophic levels and to carbon export. By identifying these features we are able to examine the associated drivers of variability and the potential susceptibility to climate change. Thus, the definitions above exclude a summer minimum in

chlorophyll being identified as the bloom termination as a subsequent secondary bloom is still of significance to overall production.

3.2.2.1 Annual Median Based Threshold

This method uses a threshold value based on the annual median to define the start and end of the bloom. This has previously been used in other studies mostly in the North Atlantic (Siegel *et al.*, 2002, Henson *et al.*, 2009) but also globally (Racault *et al.*, 2012). Siegel *et al.* (2002) decided on a threshold value of 5% above the annual median after finding that the bloom initiation dates were relatively insensitive to the choice of percentage above the annual median (tried 1-30%).

This metric requires a date from which to start looking for the bloom initiation and termination. For blooms peaking in boreal (northern hemisphere) spring, the 1st January is a reasonable start date for the annual time series since this is when chlorophyll values are lowest. Alternatively, for blooms starting in autumn or winter the 1st September is an appropriate start date (Henson *et al.*, 2009). The first approach tried was to find the minimum value (or least 4 consecutive gaps which were taken to indicate winter) and use that date as the calendar start point. However, for some regions in the North Atlantic the minimum value occurs in mid-summer rather than winter. This was most evident in some subtropical regions where the spring and autumn blooms were separated by a large reduction in chlorophyll due to nutrient-limited conditions. These mid-summer values were much lower than winter chlorophyll concentrations. Therefore, this approach did not capture the main bloom very well in places where there is a strong reduction in surface chlorophyll during the highly stratified summer period.

Thus, something more reliable than the minimum value had to be used to define the start of the annual time series. Therefore, the timing of the bloom peak was used as a reference point from which to find the bloom initiation date. Rather than search for a rise above the threshold value from the start of the growing season the bloom initiation was found by searching backwards through time from the peak for a fall below the threshold. The end of the bloom proved more problematic as a similar search forwards in time for a fall below the threshold identified the mid-summer minimum in chlorophyll as the bloom termination if the mid-summer values were low enough to fall below the threshold value. This is not ideal as it would exclude autumn blooms and it is variability in the end of the productive season which is of primary interest here. Because of this, the end of the bloom is defined as the last of two consecutive points that are greater than the threshold value.

In each case the rise or fall below the threshold value had to be sustained for 16 days (i.e. two time steps) to be considered an actual sustained increase or decrease in chlorophyll and not a spike in the chlorophyll data (due to the overestimation of chlorophyll due to the presence of contaminants such as sub-pixel clouds or atmospheric aerosols). This criterion was a compromise between using 8 days (1 time step) which was sensitive to spikes in the chlorophyll data or 24 days (3 time steps) which increased the likelihood of encountering a gap in the time series and therefore a failure to identify an initiation date for that year (see Chapter 4 for more details on the impact of data gaps).

To calculate bloom initiation and termination (Figure 3.12):

- Having defined the peak dates, the annual time series was delineated as the period starting at the peak date minus 6 months and running to the peak date plus 6 months.
- The annual median values were calculated from the data within the period of +/- 6 months of the peak. If the start and end dates of this period fell outside the limits of the total 9 year time series (i.e. earlier than January 1st 2002 or later than December 31st 2010) then the threshold was deemed unreliable and bloom initiation and termination dates were not calculated. Calculating the annual median from the 6 month before and 6 months after the peak makes the annual median representative of the bloom in question. Using a median value calculated from individual years (i.e. January – December) would not be representative especially if the bloom was not centred on boreal summer. In this case the median value would be calculated from the last and first half of two successive blooms. Because of the high interannual variability in bloom magnitudes, the resulting median could be substantially over or underestimated and resulting in erroneous initiation and termination dates.
- The threshold value was calculated as 105% of the median value.
- To calculate the bloom initiation date all the time steps in the first half of the annual time series that had chlorophyll values of less than the threshold value were found. The second of the last two consecutive time steps occurring in that period that were below the threshold was defined as the bloom initiation date. If no consecutive points were found then the initiation date was set as NaN. This is a special Matlab value described as Not a Number which is easily excluded from further analysis. It is a useful alternative to zero, which has a numerical value.

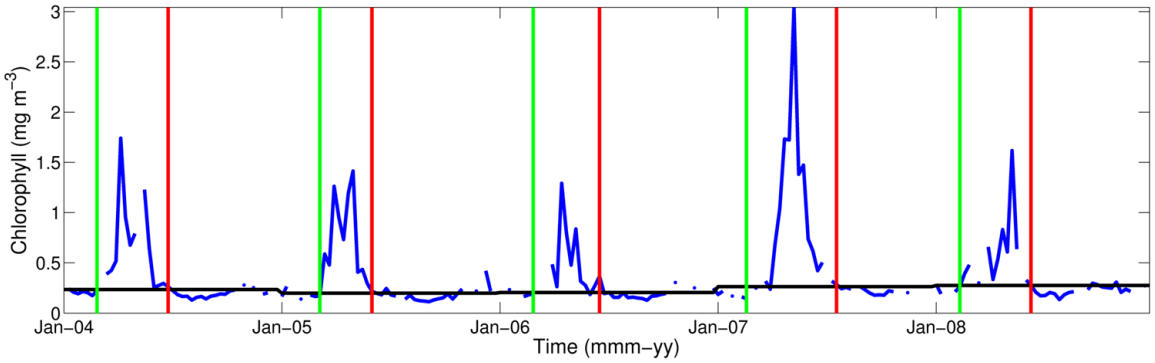

Figure 3.12: Example time series (2004-2008) to show the annual mean threshold metric definition. Time series is from the subpolar North Atlantic (~45N, ~12W). Black horizontal bars show the threshold value for each year (5% above the annual median). Green vertical bars indicate the timing of bloom initiation. Red vertical bars indicate the timing of bloom termination.

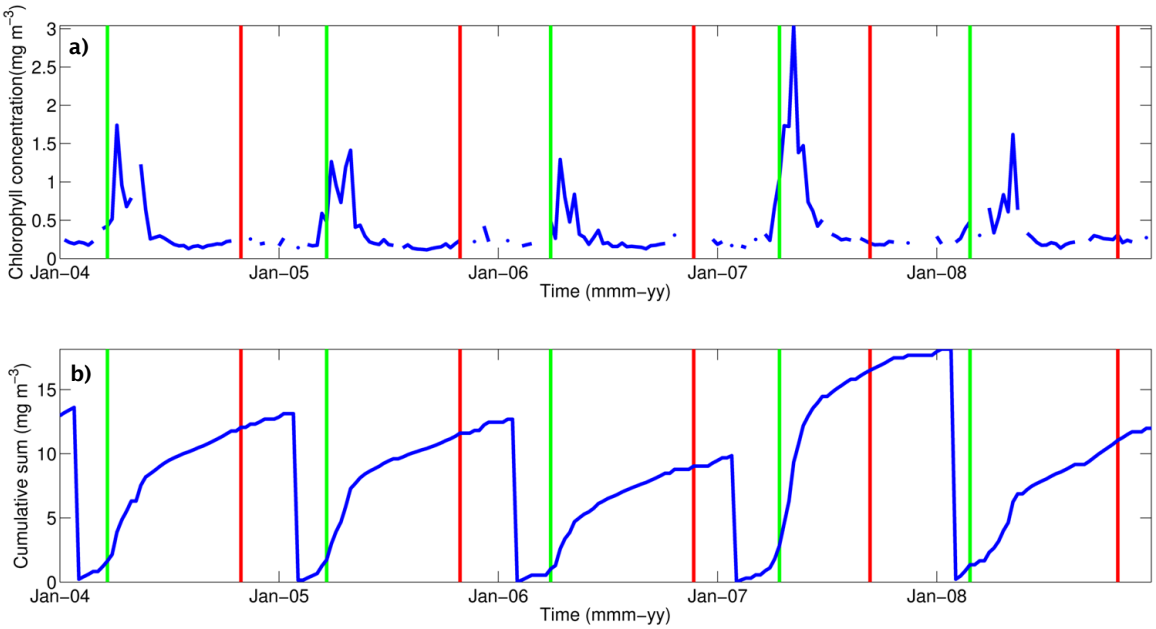

Figure 3.13: Time series (2004-2008) to show the cumulative sum metric definition. Time series is from the subpolar North Atlantic (~45N, ~12W) (a) and the annual cumulative sum time series (b). Green bars indicate the timing of bloom initiation (10% of annual total chlorophyll). Red bars indicate the timing of bloom termination (90% of annual total chlorophyll).

- To estimate the timing of bloom termination, the minimum value in the second half of the annual time series was first found. The section of the time series between the peak and the minimum value was isolated to be used to find the bloom termination date. This prevented the rise into next year's bloom being included in the estimate of bloom timing.
- From this subset, the time steps with values greater than the threshold were found and the second of the last two consecutive points above it was defined as the end date of the bloom.

3.2.2.2 Cumulative Sum Threshold

The cumulative sum of the annual time series has been used to examine zooplankton phenology (Greve *et al.*, 2005) but is applied to phytoplankton phenology here. This method defines the start and end of the bloom using thresholds associated with surpassing a percentage of the total sum of chlorophyll over the year. Greve *et al.* (2005) applied this method to time series of zooplankton abundance using 15% and 85% of the annual total abundance to determine the start and end of the season. When applied to the chlorophyll data here, a range of values were tried and10% and 90% were decided on to determine the dates of bloom initiation and termination based on a visual analysis of multiple time series.

This metric was easily adapted to chlorophyll time series though some considerations needed to be made. It is particularly influenced by the choice of start date for the calendar year as the thresholds are based on knowledge of what has happened previously. This assumes that the beginning of the time series is during low chlorophyll values which build up to a peak and then decline again. Thus the start of the time series must be around the time of the minimum values. This is in contrast to centring the time series on the bloom peak as in the annual median threshold method. This was defined using the climatology as individual years are heavily influenced by data gaps. Furthermore, this indicates that the accuracy of the bloom timing dates may be influenced by missing data as gaps will result in large jumps in the cumulative sum of the time series as incremental values are missing.

To calculate the bloom initiation and termination (Figure 3.13):

- The climatological year was formed and the date of the minimum value was defined as the start of the year. Each individual year was then formed using this date as the start and ending 46 time steps later.
- For each individual year the cumulative sum was calculated.

- The first time step over 10% and 90% were defined as the initiation and termination dates, respectively.
- The bloom initiation and termination dates were set to NaN in years where the first time step exceeded 10% of the total as these were deemed to be pixels where the start of season date was ill-defined.

3.2.2.3 Percentage of Maximum Threshold

Another variation of threshold based metrics is basing the threshold on a percentage of the maximum value. Consequently, many of the considerations raised in section 3.2.2.1 are also valid here. Again, the beginning and end of the bloom are found using the peak as a reference point. Additionally, the chlorophyll concentration must exceed or fall below the threshold value for at least 16 days (two time steps).

The threshold is based on a percentage of the peak chlorophyll value in each year as described in Ji *et al.* (2010). Fuentes-Fuentes-Yaco *et al.* (2007) used 20% to define the bloom initiation on the raw chlorophyll time series and Vargas *et al.* (2009) used 10% to define the bloom initiation and termination on the results of fitting a Generalised Linear Model to the chlorophyll time series (i.e. a smoothed version of the chlorophyll data). A value of 20% of the maximum was chosen here as this value gave the most consistent bloom timing results based on a visual examination of multiple time series. A lower value such as 10% did not perform well with the noisy nature of the data and often identified a date too early or too late to be considered the bloom initiation or termination date. Using larger values than 20% gave consistent initiation and termination timing results but the identified dates were considered to be either too late or too early for the bloom initiation or termination, respectively. Additionally, a threshold based on the maximum value is more susceptible to the size of the spike than a median based threshold is (see Figure 3.12 and 3.14). Anomalous spikes overestimated chlorophyll values will increase the 20% threshold more than it will raise the annual median. Thus, this metric definition will be more susceptible to anomalous chlorophyll concentrations than the annual median based metric.

To calculate bloom initiation and termination (Figure 3.14):

- Bloom peaks were defined as described above and the bloom initiation was found in the 6 months prior to the peak and bloom termination in the 6 months after the peak. Again, if the peak minus 6 months or plus 6 months was outside of the limits of the time series the initiation or termination dates were set to NaN for that year.

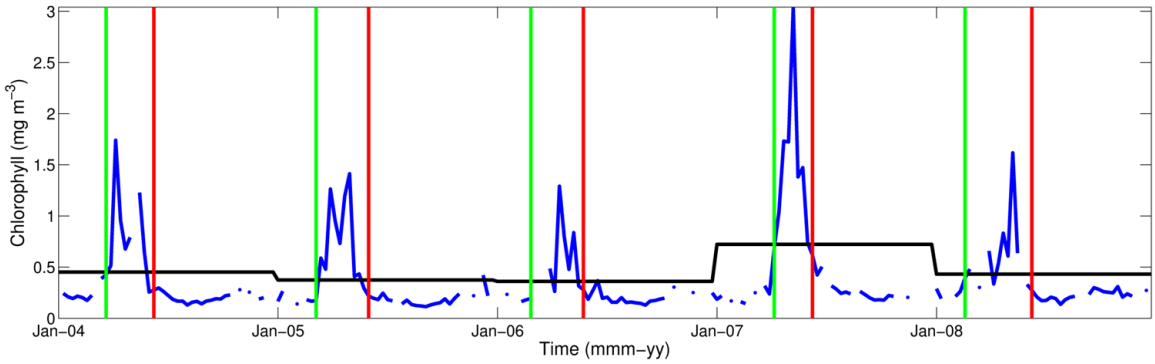

Figure 3.14: Time series (2004-2008) showing the percentage of maximum chlorophyll metric definition. Time series is from the subpolar North Atlantic (~45N, ~12W). Black bars indicate the threshold value in each year (20% of maximum chlorophyll concentration). Green bars indicate the timing of bloom initiation and red bars indicate the timing of bloom termination.

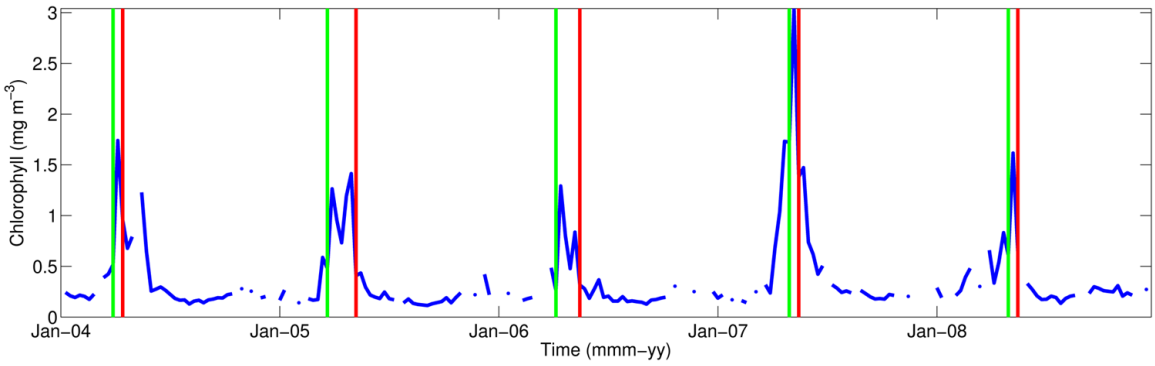

Figure 3.15: Time series (2004-2008) showing the largest gradient metric definition. Time series is from the subpolar North Atlantic (~45N, ~12W). Green bars indicate the timing of bloom initiation based on the largest positive gradient in chlorophyll. Red bars indicate the timing of bloom termination based on the largest negative gradient.

- The threshold value was set as 20% of the annual maximum chlorophyll value.
- The annual time series centred on the peak timing was normalised by subtracting the minimum value and then dividing by the range of values in the time series. This prevented occurrences of no initiation or termination being found because the chlorophyll values did not become lower than 20% of the annual maximum value. This is different to the way this metric is described by Fuentes-Yaco et al. (2007), (Vargas et al., 2009) and (Ji et al., 2010) as they did not normalise the annual time series. The approach used here would be better described as the percentage of annual amplitude threshold method.
- In the 6 months prior to the peak the time steps with values below the threshold value were found. The bloom initiation date was defined as the second of the last two consecutive time steps that were below the threshold.
- The termination of the bloom was defined in a similar manner but for the 6 months after the peak. The first of the first two consecutive points below the threshold was taken as the bloom termination date.

3.2.2.4 Growth Rate

This method defines the bloom initiation and termination dates as the dates of greatest positive or negative change in chlorophyll concentration. This method was used by Sharples *et al.* (2006) and also by Brody *et al.* (2013). Sharples *et al.* (2006) used output from a 1D model whereas Brody *et al.* (2013) reconstructed the time series from a Fourier decomposition to give a smooth time series.

The advantage of this metric is that it is based on the maximum gradients and there is thus no subjective choice of threshold value. On the other hand, gaps will be a problem as a gradient cannot be calculated. Also the noisy nature of the data means that spikes are likely to be picked up as the initiation and termination dates. This could be overcome with smoothing techniques but with the potential loss of temporal resolution.

To calculate the bloom initiation and termination (Figure 3.15):

- The peaks defined above are used to focus the search for an initiation date in the 6 months before the peak and the termination in the 6 months after. Again, any years where the periods extend further than the limits of the 9 year time series were not used.

- The gradient in chlorophyll was calculated as the difference in chlorophyll across one time step. If there was a gap in the time series then a gradient was not calculated.
- The bloom initiation was defined as the time step with the largest positive gradient.
- The bloom termination date was defined as the time step with the largest negative gradient.
- In some very small cases no consecutive data points could be found anywhere in the annual time series and so a gradient could not be calculated. In this case the metric dates were set to NaN.

3.2.3 Additional Processing

3.2.3.1 Date Format

As the metrics were calculated from a time series the raw dates are actually time step number (ranging from 1 to 414; 9 years of 46 time steps). However, it is more useful to think of the dates as a "year week" (or year 8 day composites) as this makes further analysis easier. For example, if the bloom started on the 3rd 8 day composite in 2002, the 3rd 8 day composite in 2003 and 3rd 8 day composite in 2004 then each year would have a year week value of 3. But the time step numbers would be 3, 49, 95 etc. To convert the time step numbers to year week numbers, modulus mathematics has to be implemented. This is a way of resetting the counter every x number of counts. An everyday example is a clock, where the counter gets reset every 12 or 24 hours.

The equation used is:

$$W = floor\left(a - \left(floor\left(\frac{a}{nt}\right) \times nt\right)\right) \tag{3.1}$$

Where *W* is the year week number, *a* is the time step number and *nt* is the number of time steps in a year. The floor function rounds the number down to the nearest whole number. If the time step number input is a multiple of the number of time steps in a year then *W* would be equal to 0. In this case it was converted to equal *nt*. For the chlorophyll datasets *nt* was 46.

3.2.3.2 Bloom Duration

The satellite data provides a time vector that contains the dates associated with each time step. Using this the bloom duration was calculated as the difference

between the bloom start and end dates using the time vectors. In Matlab any date can be converted to the total number of days that have passed since 1st Jan 0000. By using the actual dates from the satellite data and the datenum function the correct duration can be calculated. Otherwise, if week numbers were used, it is possible to have negative bloom durations where the bloom starts in November and ends in March the next year as the bloom termination week number would be lower than the bloom initiation week number.

3.2.3.3 Calculating Means and Anomalies

Additionally, the wrap-around nature of the calendar created problems for calculating means. This is most obvious when you consider the Southern Ocean or subtropical regions in the northern hemisphere where blooms peak at the turn of the year (i.e. either December (week number 46) or January (week number 1)). A straight mean of these two numbers would be ~23 giving an average date occurring at the beginning of July. To account for this the means were calculated using trigonometry (Figure 3.16).

To calculate the mean date:

- First the time step number was converted to degrees (e.g. Date_deg=(360/nt)*year_week).
- The x coordinates were equal to cos(date_deg) and the y coordinates equal to sin(date_deg) (plotted as blue crosses in Figure 3.16).
- Then points occurring in either quadrant 1 and 4 were identified. The value of date_deg indicates which quadrant the date falls in.
- If there were dates in both quadrants 1 and 4 then the angles falling in quadrant 4 were converted to negative angles. So instead of falling in the range 270˚ - 360˚ they would now be in the range -90˚ - 0˚.
- The mean of the resulting angles was then found and converted back to year week numbers (red cross in Figure 3.16).
- The example given in the text above would now have a mean date of 0.5 weeks.

Additionally the same concept can be used to calculate differences in dates or anomalies from the mean. Following the same procedure as above, week numbers

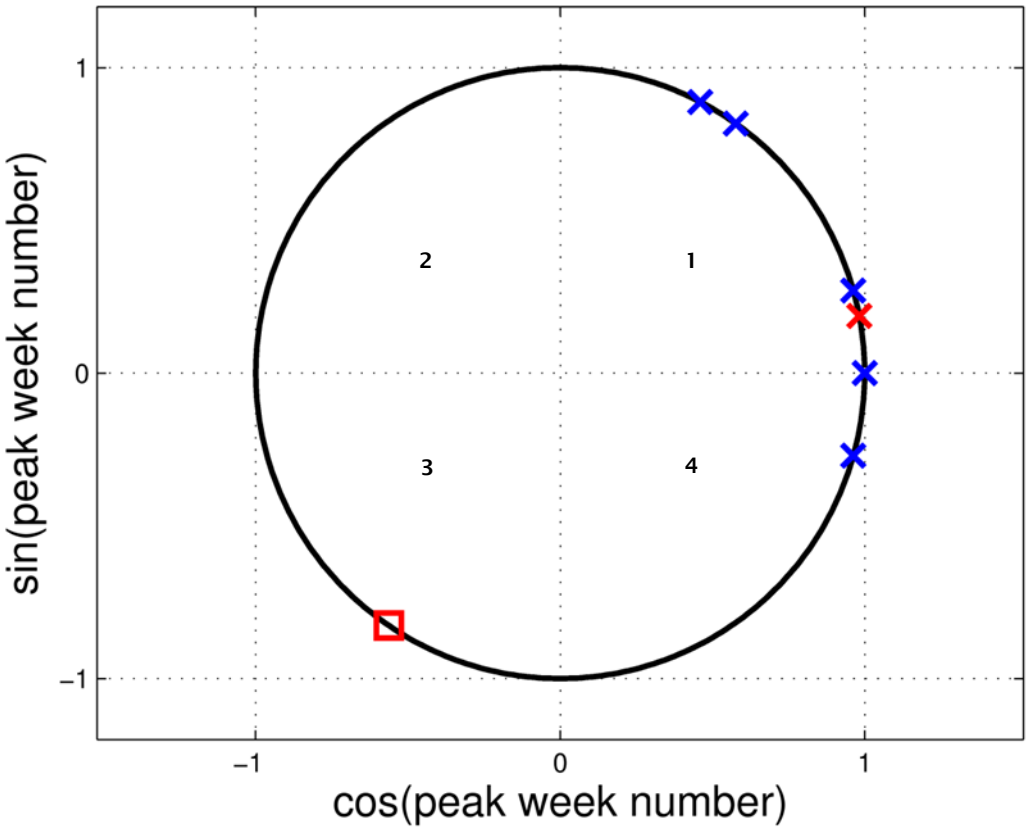

Figure 3.16: Diagram to illustrate how mean bloom peak timing dates are calculated in regions where the metric dates occur at the turn of the year (December/January). Numbers indicate the quadrant numbers. Blue crosses indicate the date of peak timing from the time series in Figure 3.14. The red square indicates the mean of these dates. The red cross indicates the mean date if the cyclic nature of the calendar is taken into account. This is also valid for bloom initiation and termination dates.

were converted to degrees, the x and y coordinates found and data points in quadrant 4 were converted to a negative angle. Both angles were then converted back to week numbers and were simply subtracted from each other to find the difference. Anomalies from a mean date were found in this way.

3.2.4 Comparison of Metric Definitions

Each metric described above was calculated using the GlobColour chlorophyll dataset globally, over the whole time span (2002-2010) at a spatial resolution of 1/4˚x1/4˚. Below is a discussion of the performance of each metric using spatial means and individual time series.

3.2.4.1 Bloom Initiation

Broadly, the global, spatial pattern in mean bloom initiation date was similar for all four metric definitions (Figure 3.17 and Figure 3.18), especially the annual median and chlorophyll maximum based metrics. The metric based on the largest gradient was the least similar to the others except in the Southern Ocean. Moreover, the gradient-based metric dates were slightly later compared to the other metrics especially in the subtropics (note that in the context of the northern hemisphere January is actually later in the growing season than December). The cumulative sum had slightly earlier dates compared to the other metrics especially in the subtropics. Furthermore, there was a discontinuity in the cumulative sum metric dates between the subtropical and subpolar regions whereas the transition was more gradual in the other metrics (note that the colour scale means a change from December to January is a change from red to blue). Overall the cumulative sum had the least spatial variability. In the Southern Ocean, large amounts of missing data mean that, even over 9 years, the metrics based on the annual median and chlorophyll maximum failed to estimate a bloom timing date (indicated by white patches unbounded by a black contour line)

From a set of individual time series it is easier to see how the different metric dates perform in relation to the time series (Figure 3.19 and 3.20). In both subpolar and subtropical regions any of the metric dates identified could be argued to be the bloom initiation date as they all broadly identify the primary increase in chlorophyll towards the annual maximum. However, the metrics need to also be applicable to different shapes of seasonal cycle, capture interannual variability and be relatively insensitive to noise and gaps in the time series,

The gradient metric was often seen to be slightly later than the other metric dates generally capturing the end of the seasonal increase in chlorophyll. This was especially apparent in the subtropical time series where the metric does not capture

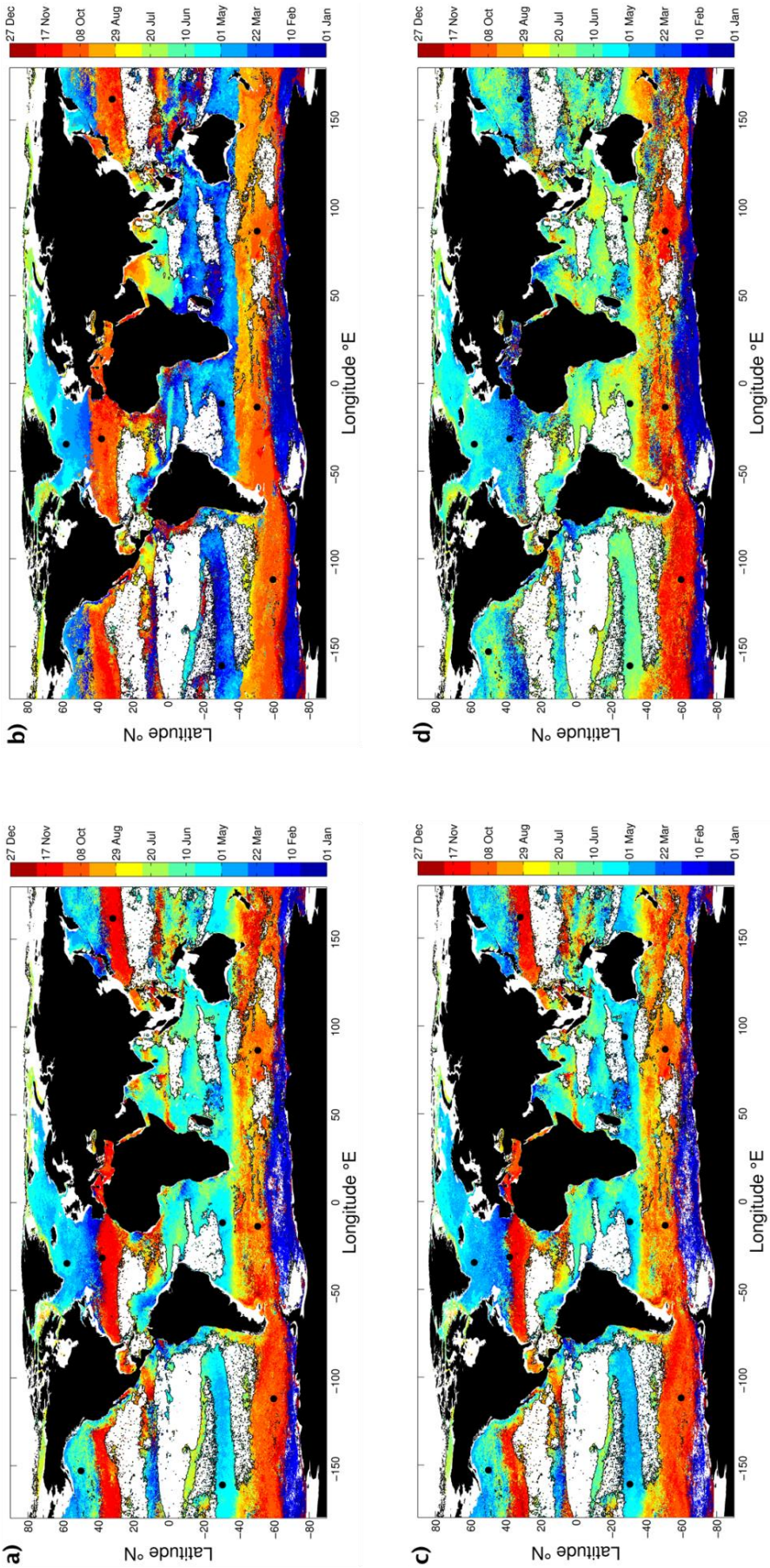

Figure 3.17: Global maps showing the mean bloom initiation date over 2002-2010, for the annual median based metric (a), cumulative sum based metric (b), chlorophyll maximum based metric (c) and the gradient based metric (d). Regions in white bounded by a black line are considered to have a weak seasonal cycle and are excluded. Black circles indicate locations of time series used in Figures 3.18 and 3.19.

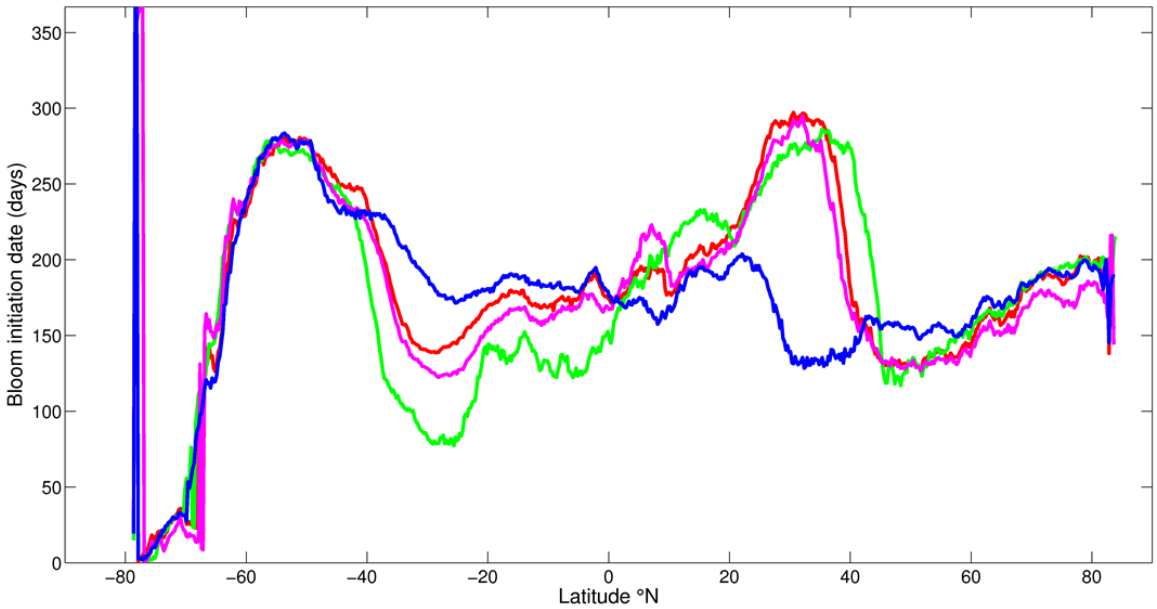

Figure 3.18: Latitudinal mean bloom initiation date calculated from 5% above annual median metric (red), cumulative sum (green), 20% of chlorophyll maximum (pink) and largest gradient (blue). In the Southern Ocean bloom initiation date occur during December and January, crossing over the turn of the year.

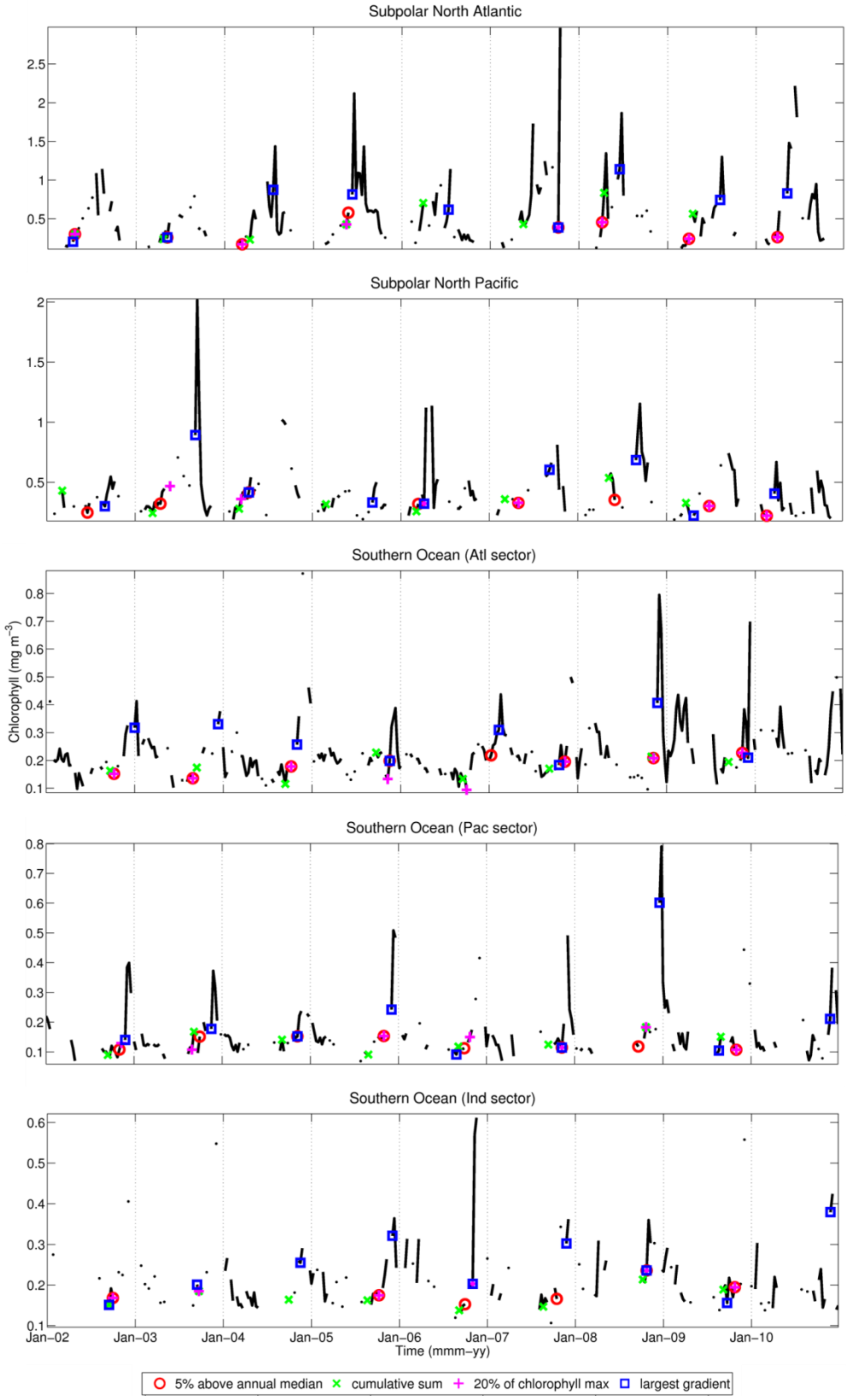

Figure 3.19: Time series from subpolar regions with the dates of bloom initiation from the different metrics indicated with different symbols. Note that some symbols overlap where different metrics indicate the same date. Locations are indicated by black circles in Figure 3.17.

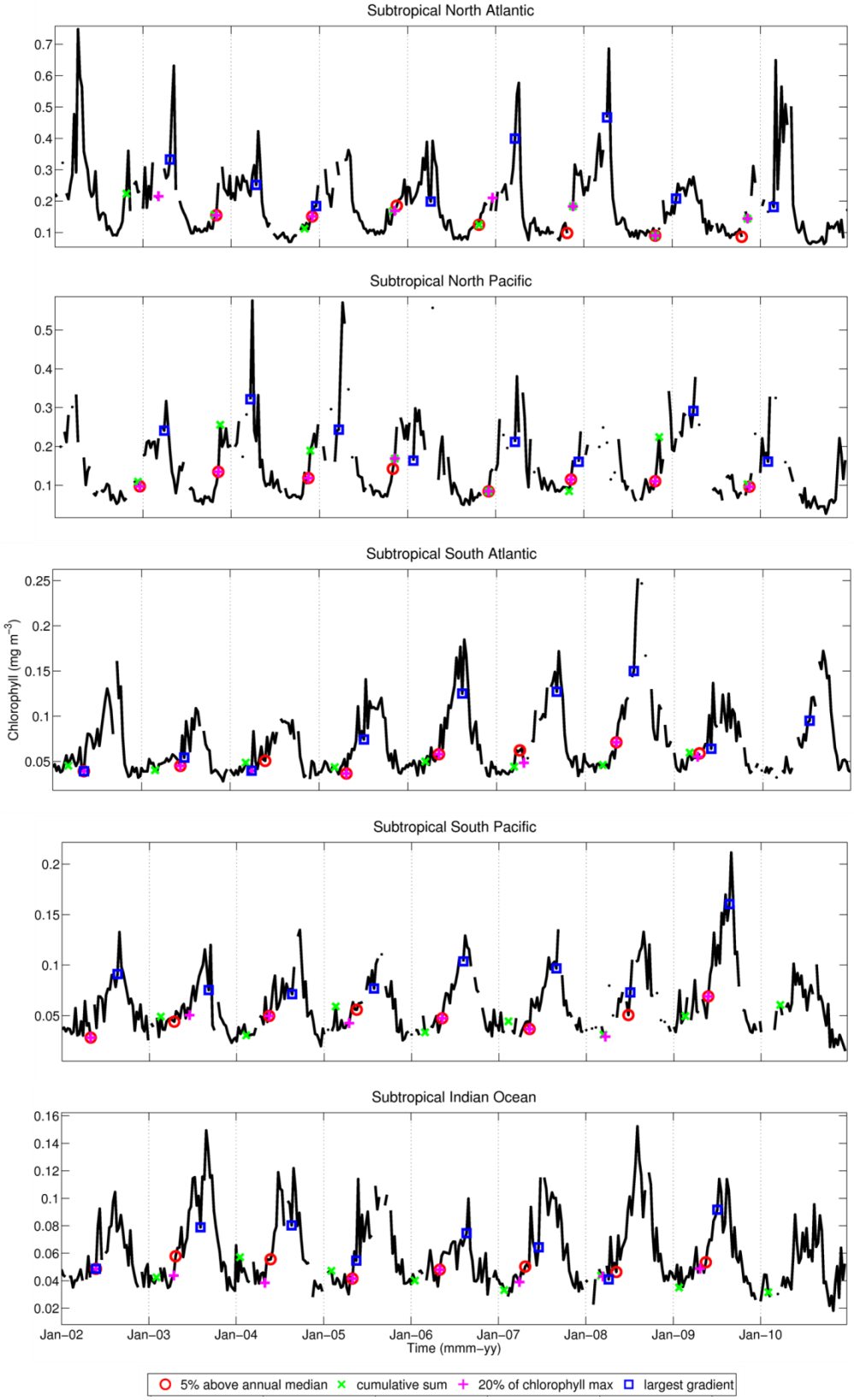

Figure 3.20: Time series from subtropical regions with the dates of bloom initiation from the different metrics indicated with different symbols. Note that some symbols overlap where different metrics indicate the same date. Locations are indicated by black circles in Figure 3.17.

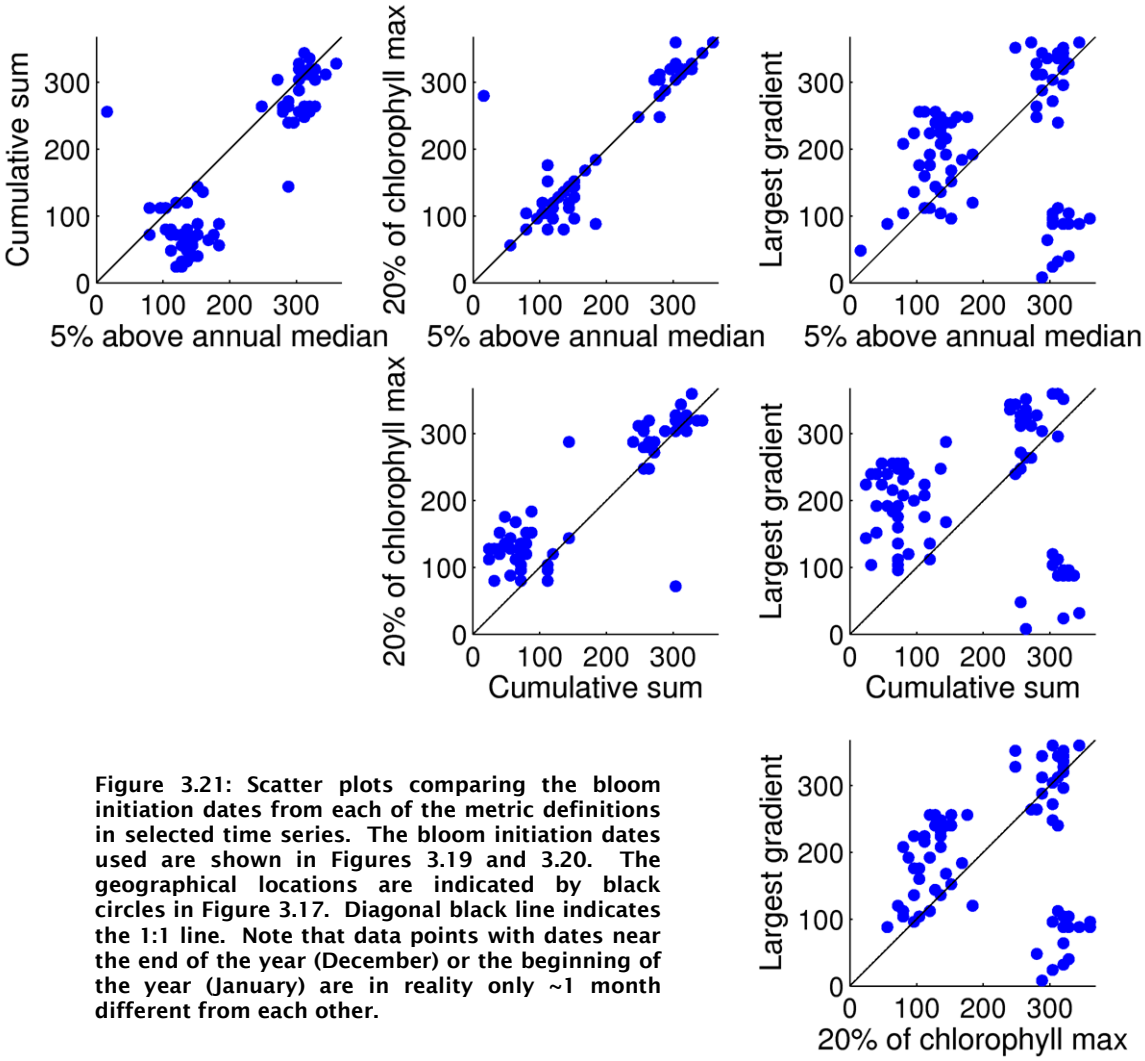

Figure 3.21: Scatter plots comparing the bloom initiation dates from each of the metric definitions in selected time series. The bloom initiation dates used are shown in Figures 3.19 and 3.20. The geographical locations are indicated by black circles in Figure 3.17. Diagonal black line indicates the 1:1 line. Note that data points with dates near the end of the year (December) or the beginning of the year (January) are in reality only ~1 month different from each other.

the slow, gradual increase in chlorophyll as the onset of the bloom. This suggests that this metric may not be suitable for seasonal cycles of this shape (Figure 3.20). Furthermore, in subpolar time series which are heavily affected by missing data the gradient metric dates are seen to be earlier than in other years.

The cumulative sum estimate was seen to consistently identify the same stage of the bloom in the subtropical time series (Figure 3.20). However, the bloom stage identified as bloom initiation was seen to vary with different shapes of seasonal cycle. Furthermore, this metric was seen to be sensitive to small, short-lived peaks in chlorophyll that occur before the primary seasonal chlorophyll increase (Figure 3.20, Indian: 2003, 2004, South Pacific: 2007, 2009). This suggests that the best choice of threshold is different for various types of seasonal cycle. Furthermore, in subpolar regions (Figure 3.19) the consistency in the stage of the bloom identified by this metric was seen to become more variable in time series affected by large amounts of missing data at the beginning of the time series.

The bloom initiation dates from both the annual median and chlorophyll maximum metrics were very similar. Both metrics consistently identified the same stage of bloom development as the bloom initiation between years in both subpolar and subtropical time series. However, for both metrics, bloom initiation dates are missing in some years because the condition of two consecutive data points was not met.

A comparison of the dates from each metric shows the degree of agreement between them (Figure 3.21). The annual median and chlorophyll maximum based metrics show the greatest agreement whereas the gradient metric is the most different to the others having quite a large scatter in the dates. Furthermore, the gradient metric dates are typically later than the annual median and chlorophyll maximum metric dates and much later than the cumulative sum metric dates. The lack of variability in the cumulative sum metric is also seen here as the dates are clustered in two groups whereas the other metrics tend to have a more continuous range of dates. In addition, the cumulative sum metric dates are consistently earlier than the other metric dates.

3.2.4.2 Bloom Termination

The basic spatial pattern in the bloom termination metric dates was similar to that of bloom initiation (Figure 3.22 and Figure 3.23). All four metrics show similar spatial patterns and also broadly similar dates. The greatest agreement was seen between the annual median and chlorophyll maximum metrics although large differences occur in the North Pacific and some regions of the Southern Ocean. Similar to the bloom initiation, the cumulative sum metric dates for the end of the

bloom again show less spatial variability, were relatively later than the other metrics and had a discontinuity at the subpolar-subtropical boundary. Conversely, the gradient metric had slightly earlier dates in most regions relative to the other metric dates.

Looking at individual time series, in most cases there was a good agreement in the bloom termination date between the metrics and the part of the time series that could be considered the end of the bloom (Figure 3.24 and 3.25). However, in subpolar time series, the gradient metric identifies the end of the peak rather than the end of the growing season as the bloom termination though it consistently identifies the same stage of bloom decline between years. In subtropical time series (Figure 3.25) the gradient metric again identified the sharp decline in chlorophyll after the peak as bloom termination but in these regions this signifies the end of the productive season. The South Pacific and Indian Ocean time series in Figure 3.25 are exceptions to this as the seasonal cycle is more symmetrical.

The cumulative sum metric was seen to be affected by missing data which resulted in the bloom termination date being identified when chlorophyll values have reached their minimum rather than during the seasonal decrease in chlorophyll. Furthermore, if blooms were of short duration then the bloom termination occurred during the winter minimum values as seen earlier in Figure 3.13. In the subtropical time series, the stage of the bloom decline that is identified as the bloom termination was again seen to be dependent on the shape of the seasonal cycle as it was for the bloom initiation dates (Figure 3.25).

Once again, the annual median and chlorophyll maximum threshold metrics identified similar dates for the bloom termination. Both were consistent in identifying the same stage of the seasonal decrease in chlorophyll as the bloom termination date. In subpolar regions, the annual median threshold metric occurred earlier in the time series if the amount of missing data during the seasonal decrease in chlorophyll was relatively high (Figure 3.24). In some cases in the subpolar time series, the chlorophyll maximum metric identified the summer minimum as the bloom termination. However, in the subtropical time series the date often identified by the chlorophyll maximum metric occurred later in the annual cycle and missed the decline in chlorophyll especially in the South Atlantic, South Pacific and Indian Ocean time series. The annual median metric was consistent in identifying the same stage of bloom decline as bloom termination in the subtropical time series. However, in years when the amount of missing data during the bloom decline was relatively high the annual median metric identified a relatively earlier date as the date of bloom termination (e.g. Figure 3.25: South Pacific, 2006).

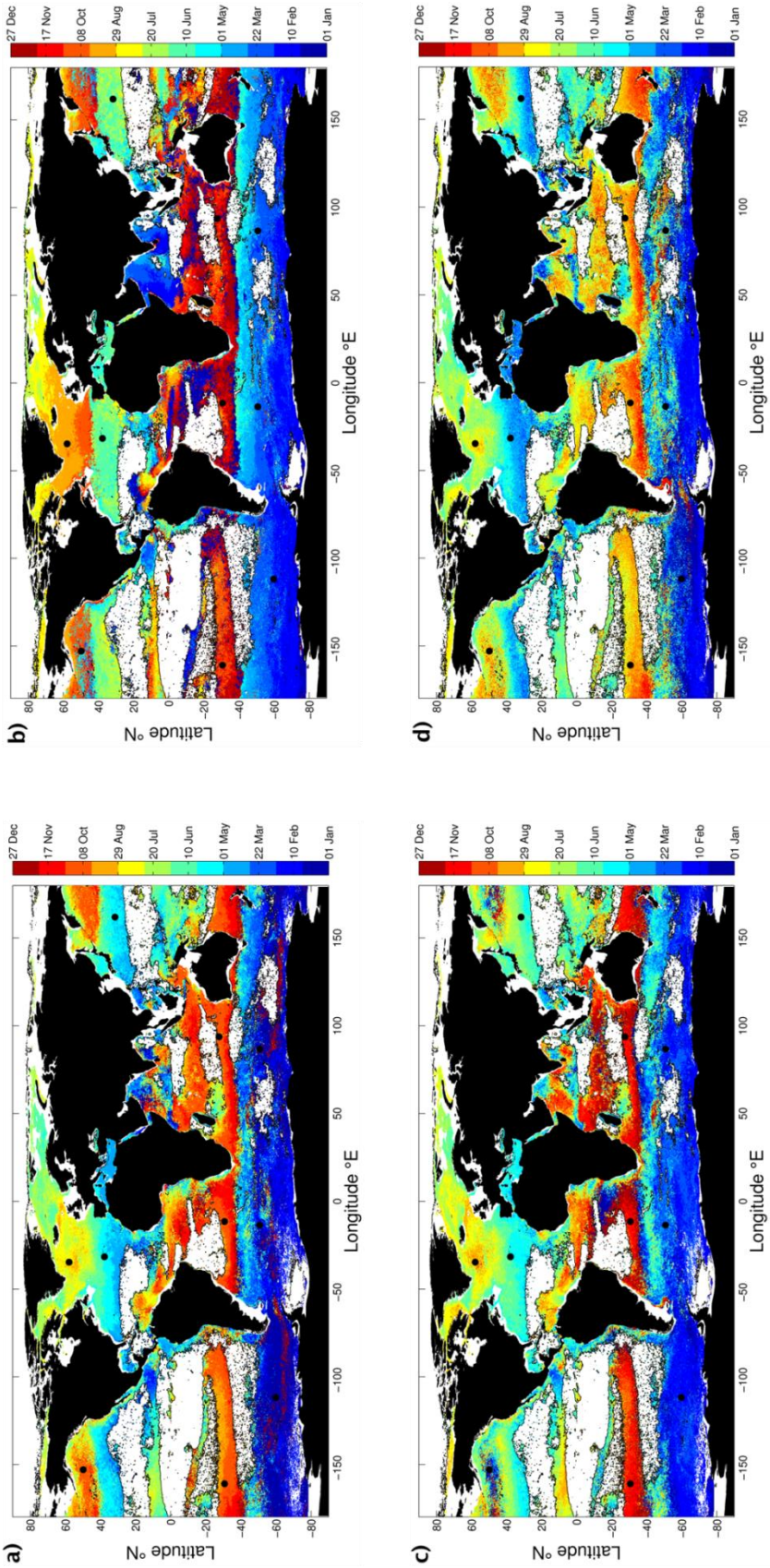

Figure 3.22: Global maps showing the mean bloom termination date over 2002-2010, for the annual median based metric (a), cumulative sum based metric (b), chlorophyll maximum based metric (c) and the gradient based metric (d). Regions in white bounded by a black line are considered to have a weak seasonal cycle and are excluded. Black circles indicate locations of time series used in Figures 3.24 and 3.25.

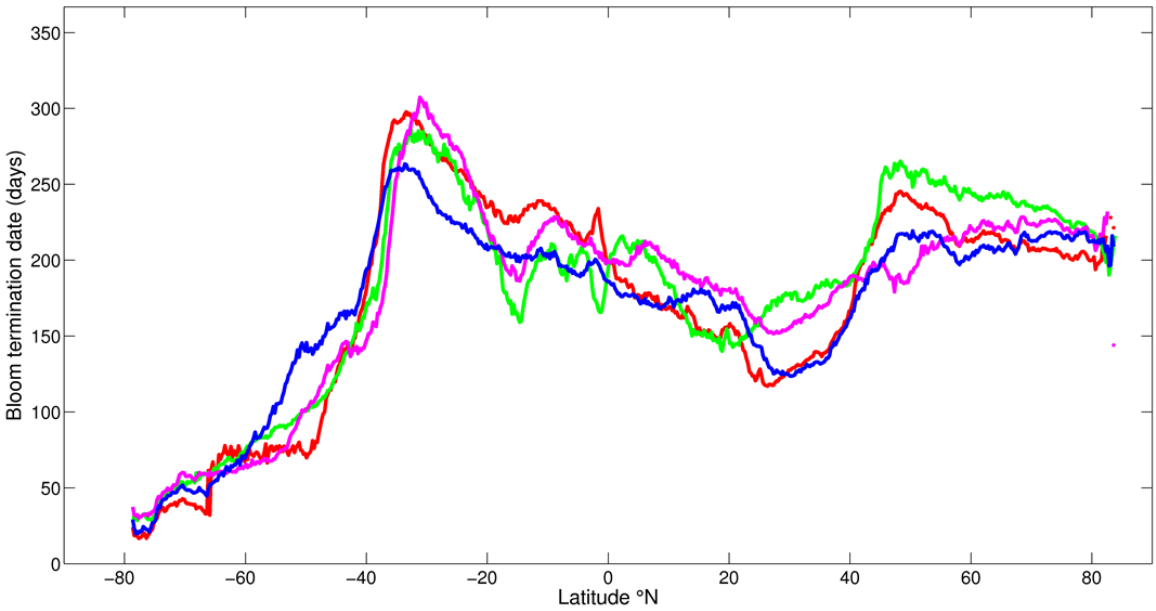

Figure 3.23: Latitudinal mean bloom termination date calculated from 5% above annual median metric (red), cumulative sum (green), 20% of chlorophyll maximum (pink) and largest gradient (blue).

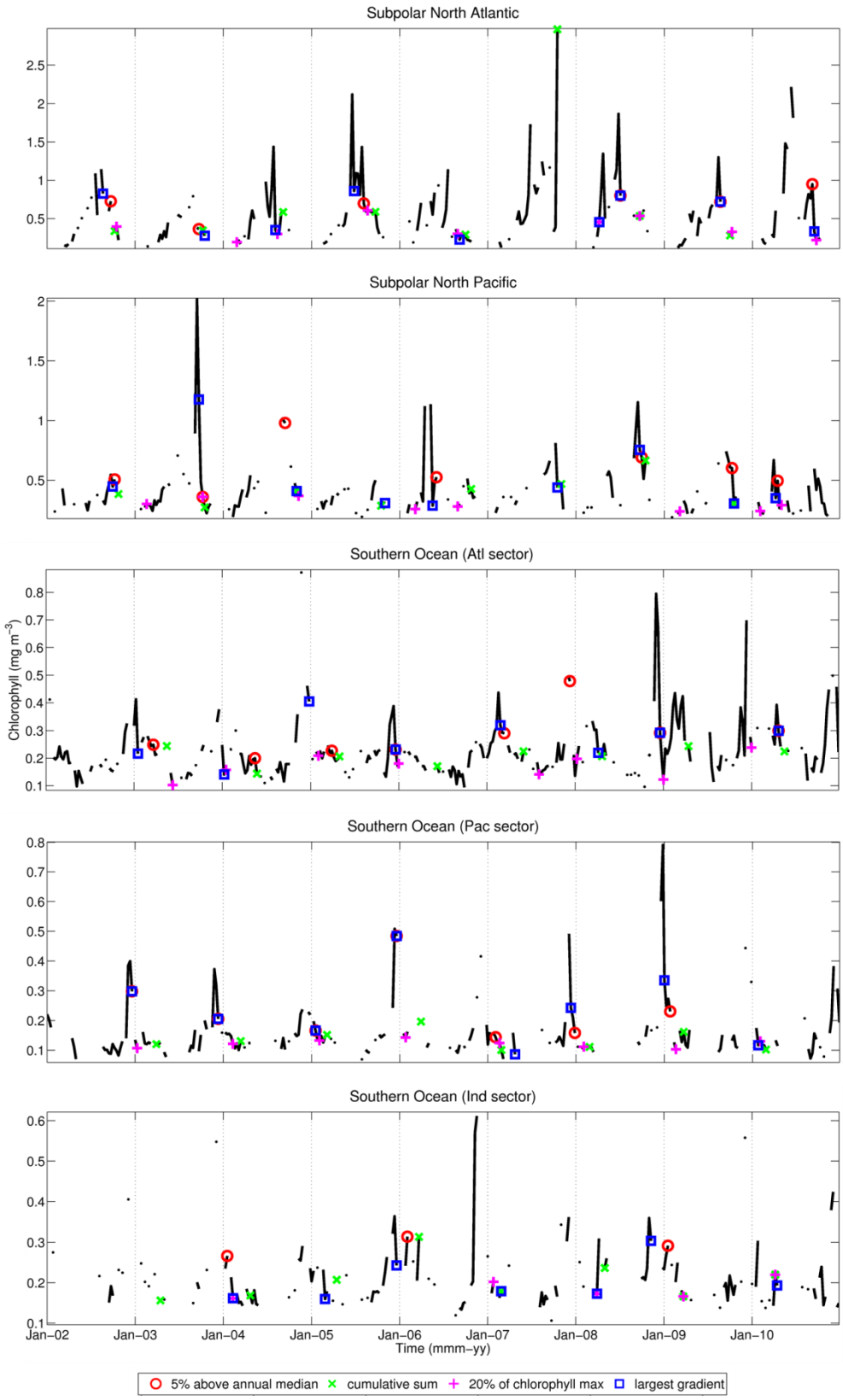

Figure 3.24: Time series from subpolar regions with the dates of bloom termination from the different metrics indicated with different symbols. Note that some symbols overlap where different metrics indicate the same date. The largest gradient metric refers to the largest negative gradient for bloom termination. Locations are indicated by black circles in Figure 3.22.

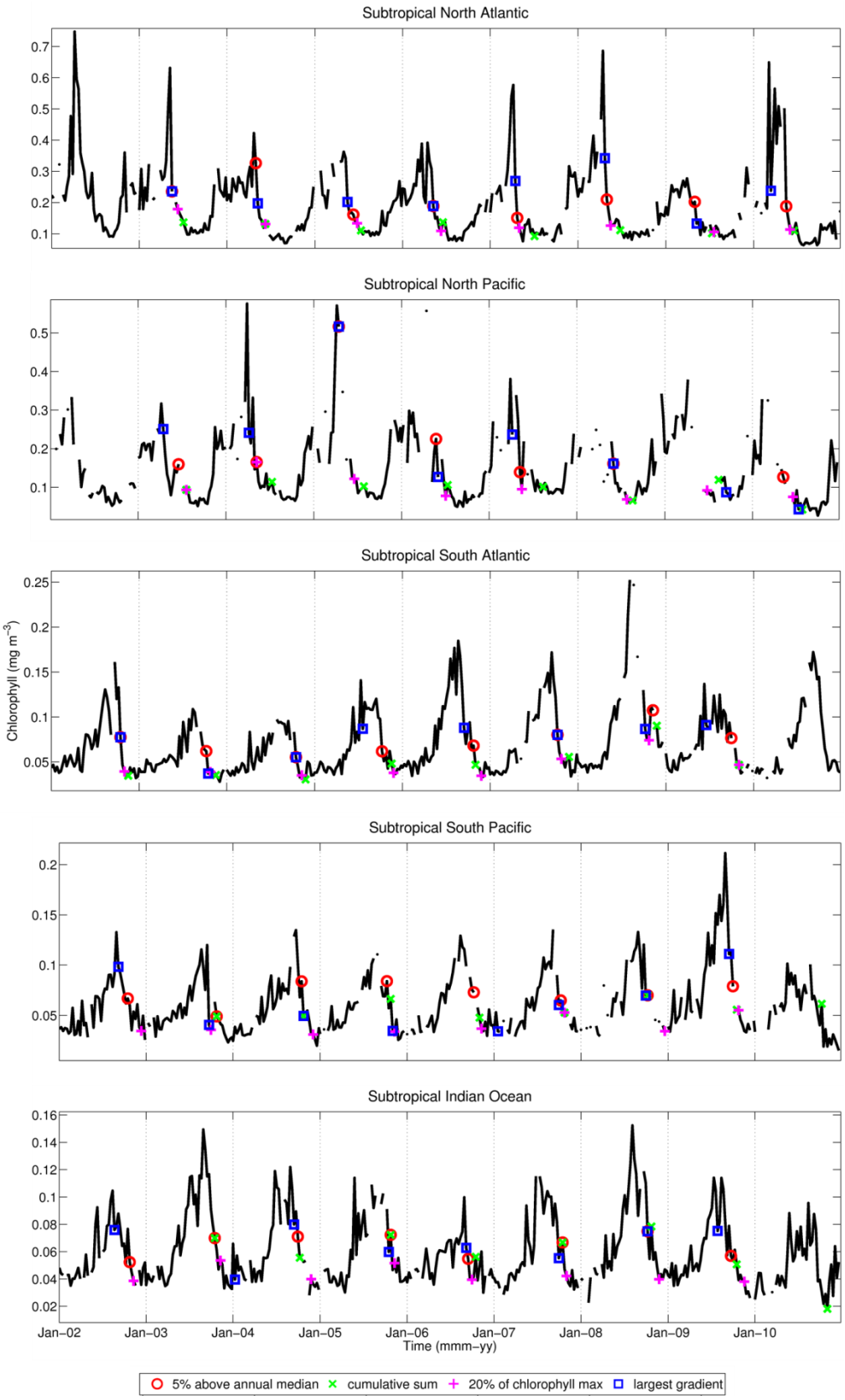

Figure 3.25: Time series from subtropical regions with the dates of bloom termination from the different metrics indicated with different symbols. Note that some symbols overlap where different metrics indicate the same date. The largest gradient metric refers to the largest negative gradient for bloom termination. Locations are indicated by black circles in Figure 3.22.

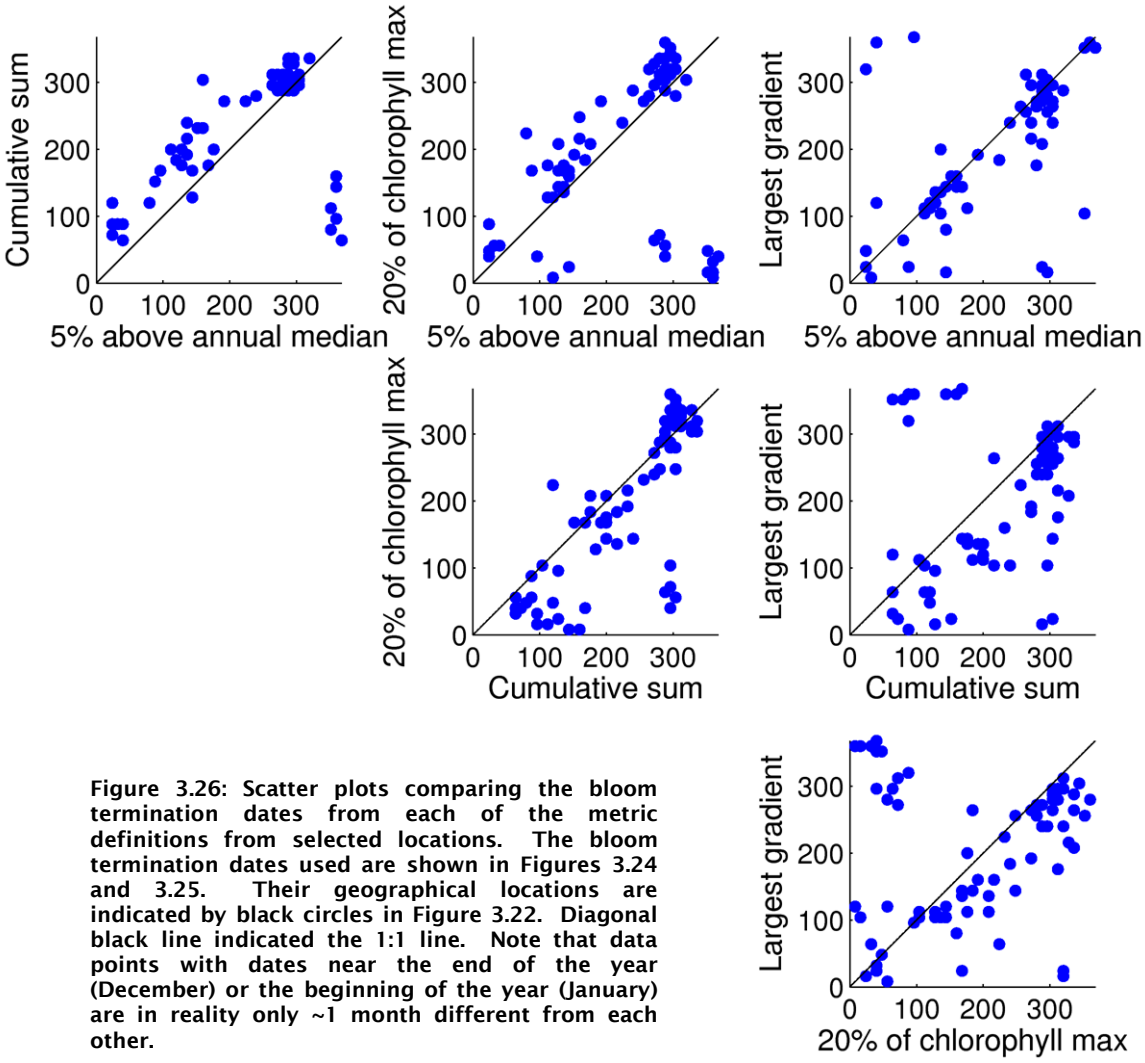

Figure 3.26: Scatter plots comparing the bloom termination dates from each of the metric definitions from selected locations. The bloom termination dates used are shown in Figures 3.24 and 3.25. Their geographical locations are indicated by black circles in Figure 3.22. Diagonal black line indicated the 1:1 line. Note that data points with dates near the end of the year (December) or the beginning of the year (January) are in reality only ~1 month different from each other.

There was better agreement between the bloom termination metrics than bloom initiation metrics (Figure 3.26). Unlike the bloom initiation dates, the bloom termination dates for the cumulative sum metric are more variable and not clustered into two groups. The cumulative sum and chlorophyll maximum metric dates were consistently later than the annual median and gradient based metrics. This was a similar result as seen in the global mean metric date maps and latitudinal variability (Figure 3.22 and 3.23).

3.2.4.3 Bloom Duration

The duration is simply the difference between the start and end of the bloom for each of the metrics. The spatial pattern varies greatly with the metric used (Figure 3.27 and 3.28). Broadly the duration was seen to be longer in subtropical regions compared to subpolar regions with three of the metrics (all except the gradient metric). The cumulative sum gave the longest durations of 216-280 days (7 to 9 months) in subtropical regions and less than 216 days in subpolar regions. This metric was expected to give the longest durations since the bloom initiation dates were generally earlier than the other metrics and the bloom termination dates a little later (Figure 3.21 and 3.26). The gradient metric gave the shortest durations with most being less than 152 days (5 months) and the longest being seen in the North Pacific of ~184 days (6 months). This reflects the relatively later bloom initiation and earlier bloom termination dates associated with this metric definition. The annual median and chlorophyll maximum metrics displayed very similar spatial variability but slightly different values with durations from the annual median metric being slightly shorter. These differences in duration between the metrics are summarised in Figure 3.29. The cumulative sum metric gives the longest, and the gradient metric gave the shortest durations while the chlorophyll maximum gave longer durations than the annual median metric. Overall, the pattern seen across the metrics was for longer duration blooms in the subtropics and shorter duration blooms in subpolar regions.

3.2.5 Bloom Metrics Summary

In summary, each of the metrics gave broadly similar bloom timing dates and had similar spatial patterns. Furthermore, there is a sound argument for using each of the metrics in preference to the others. However, it is difficult to argue that one is “better” than another as each metrics has different advantages and limitations. In agreement with this, a recent study in the North Atlantic compared three of the bloom initiation metric definitions and found that though each definition gave broadly similar results, though each had examples of where the metric implementation was not appropriate to the data (Brody *et al.*, 2013).

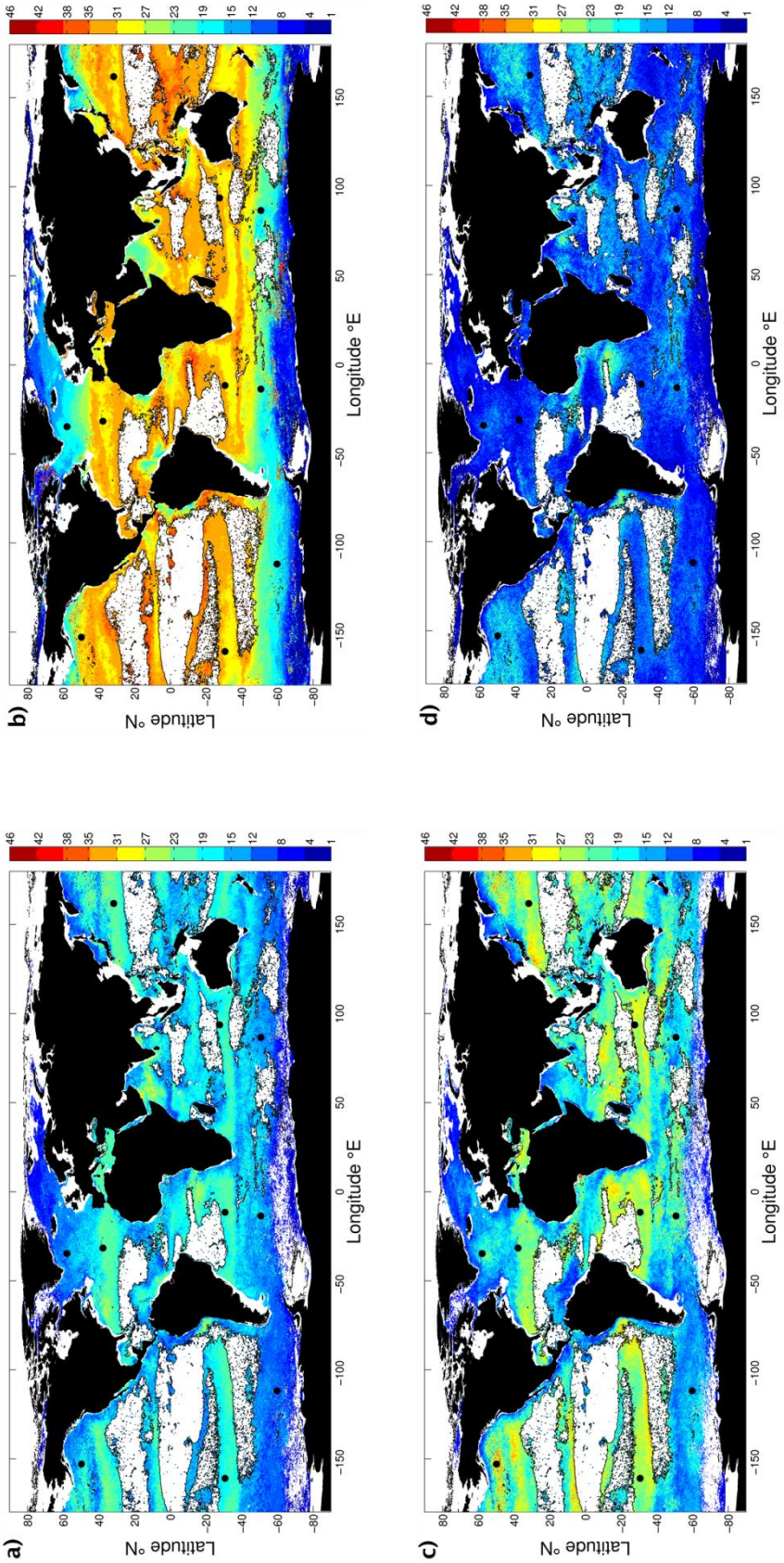

Figure 3.27: Global maps showing the mean bloom duration over 2002-2010, for the annual median based metric (a), cumulative sum based metric (b), chlorophyll maximum based metric (c) and the gradient based metric (d). Regions in white bounded by a black line are considered to have a weak seasonal cycle and are excluded. Black circles indicate locations of duration data points used in Figure 3.29.

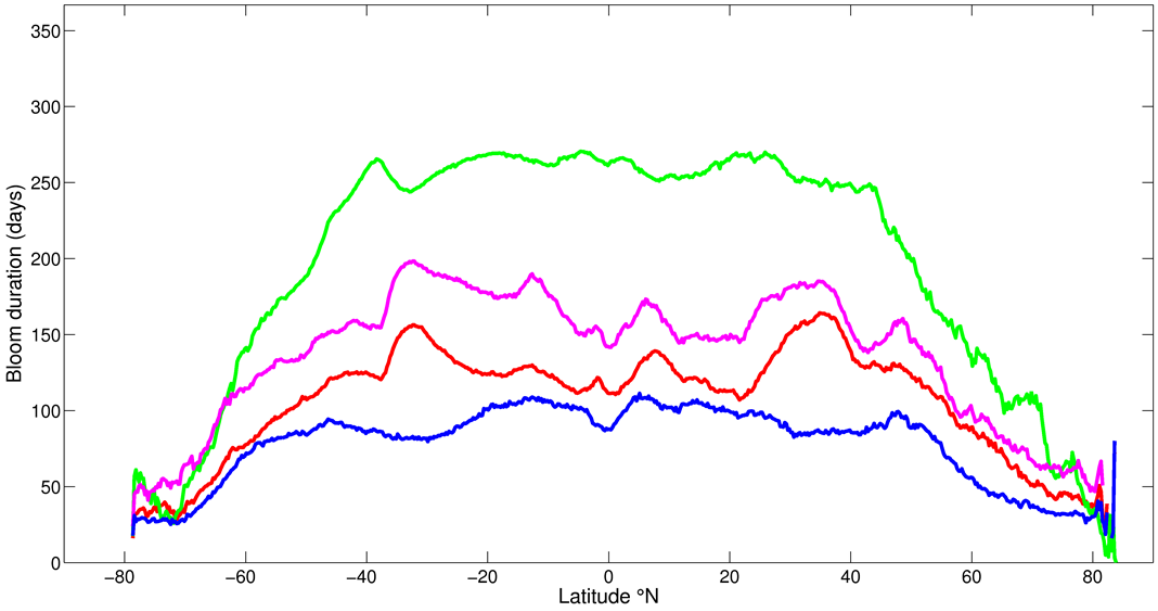

Figure 3.28: Latitudinal mean bloom duration calculated from 5% above annual median metric (red), cumulative sum (green), 20% of chlorophyll maximum (pink) and largest gradient (blue).

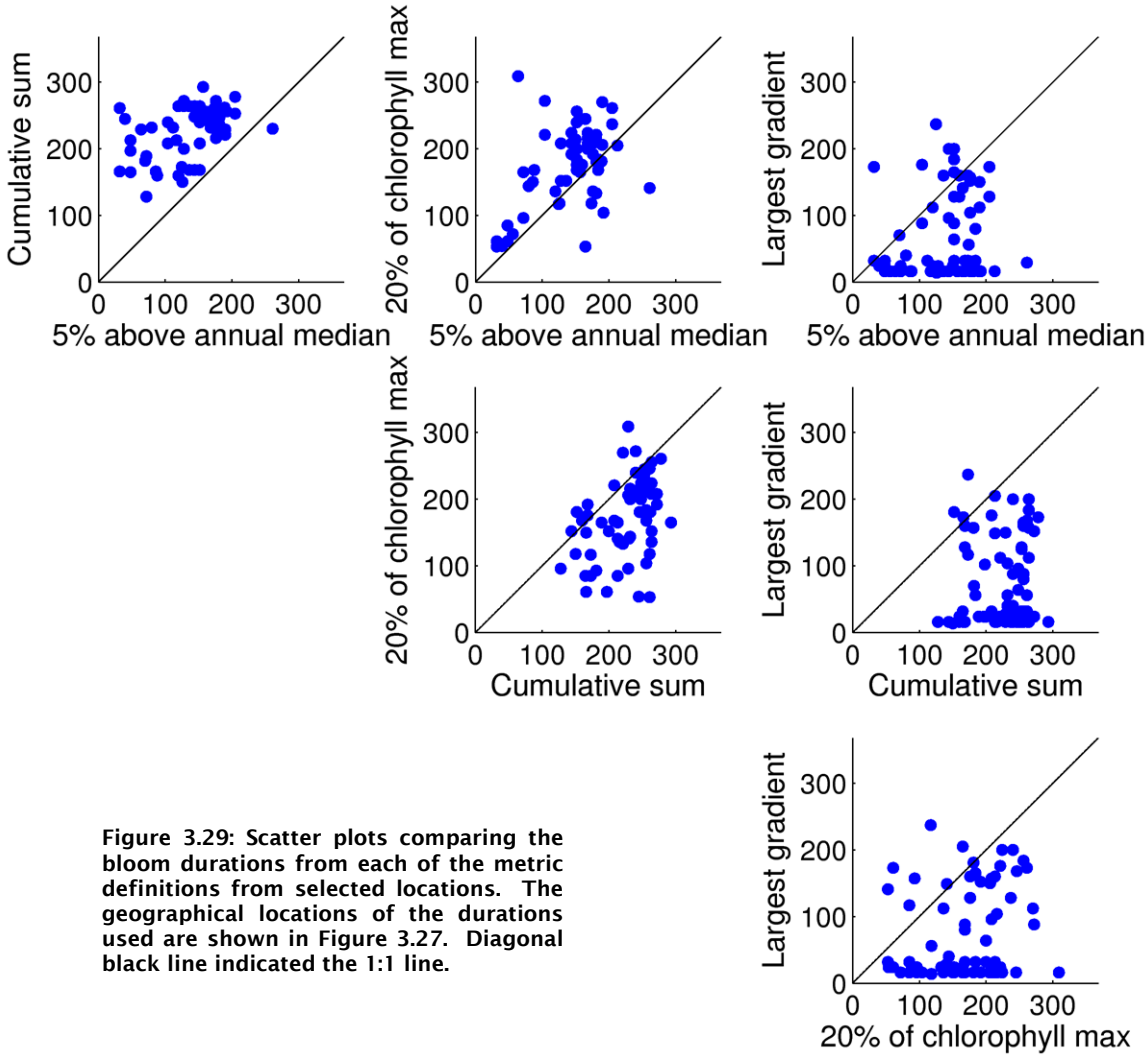

Figure 3.29: Scatter plots comparing the bloom durations from each of the metric definitions from selected locations. The geographical locations of the durations used are shown in Figure 3.27. Diagonal black line indicated the 1:1 line.

The gradient metric is the most different to the others in both its spatial pattern and the dates that it identifies as the start and end of the bloom. This is because it is calculated in an objective manner whereas the other metrics have all had their threshold values chosen to match a visual analysis of bloom timing dates. Though this objectivity is an advantage, this metric consistently overestimates the bloom initiation and underestimates the bloom termination dates relative the stages of bloom development considered to be the start and end of the productive season. Additionally, it is susceptible to erroneous spikes in the data which have large gradients but are not associated with the main annual bloom event. Furthermore, its sensitivity to missing data may result in an overestimation of the interannual variability. Brody *et al.* (2013) examined this metric and found it to be quite robust. However, their approach employed a Fourier decomposition to smooth and fill gaps in the time series. This indicates that this metric may performed more consistently with a smooth and complete time series.

Table 3.3: Root mean squared difference in days between bloom timing metrics[a]

	Bloom initiation				Bloom termination			
	Annual median	Cumulative sum	Chlorophyll maximum	Largest gradient	Annual median	Cumulative sum	Chlorophyll maximum	Largest gradient
Annual median		83	38	68		84	57	61
Cumulative sum			83	105			79	100
Chlorophyll maximum				71				72
Largest gradient								

[a] The root mean square difference between the metric was calculated globally using all individual years.

The cumulative sum metric is less sensitive to gaps in the data as it always returns a bloom timing date for each complete year. However, this metric showed the least amount of variability. Moreover, in subtropical regions this metric was sensitive to small, short-lived peaks in chlorophyll which were not associated with the main annual bloom. The stages of bloom development or decline that is identified by this metric varied with the shape of the seasonal cycle suggesting that the threshold value could be adjusted for particular types of seasonal cycle. A similar observation was made by (Brody *et al.*, 2013) where the most suitable threshold value was seen to differ between subpolar and subtropical time series. Furthermore, missing data not only delays the crossing of the thresholds but also affects the annual total chlorophyll from which the thresholds are calculated. Thus,

this metric would be more suitable for complete time series as it requires full knowledge of the seasonal cycle to perform consistently.

The annual median and chlorophyll maximum metrics both identified very similar dates. The global root mean square difference (RMSD) between the two metrics for individual years was relatively small at 38 days for bloom initiation and 57 days for bloom (Table 3.3). Both these metrics were more consistent in identifying the primary increase and seasonal decline in chlorophyll because of the need for two consecutive data points above or below the threshold. However, these criteria can result in years where a bloom timing date cannot be found because of missing data. Thus, a trade-off of having a full set of bloom timing dates for greater consistency can be made. Despite this, the chlorophyll maximum metric was less consistent in its termination dates. In subtropical regions the chlorophyll maximum metric termination date was sometime seen to occur after the chlorophyll values had already declined whereas in the subpolar time series the summer minimum was occasionally identified as the termination date. The performance of the annual median metric for identifying bloom initiation dates was examined by Brody *et al.* (2013). From their results Brody *et al.* (2013) concluded that this metric would be most suitable for studies that focussed on the primary seasonal increase in chlorophyll since it was not affected by small, short-lived pulses in chlorophyll occurring before the sustained, seasonal increase.

One assumption that is made for all of the metrics is that the highest chlorophyll value is associated with the spring bloom. This may cause errors in regions where the autumn blooms are larger than spring blooms. Further work would be needed to identify the occurrence of autumn blooms and calculate their metrics separately. This would be particularly important in regional studies such as in the North Indian Ocean which is strongly influenced by the monsoons which give rise to a distinct 6 monthly cycle. Despite this assumption, all the metrics give reasonable bloom peak timing dates so the presence of large autumn blooms will likely only affect individual years.

Overall, any of these metrics could be used to define bloom timing though the metric definitions are optimal for different research questions. The research aims here focus on the variability in the timing of the main, annual bloom event. Therefore, the bloom timing metrics must consistently (both year to year and spatially) pick out the main seasonal increase and decrease in chlorophyll concentrations with enough accuracy that interannual variability can be properly captured. Furthermore, the consistency of the metric must be relatively insensitive to missing data and noisy time series. From these criteria the annual median and chlorophyll maximum based metrics would be most suitable. The maximum

gradient metric is unsuitable as it does not identify the correct part of the time series and is sensitive to data spikes. The cumulative sum metric is unsuitable as it shows limited variability and the derivation of the annual total is sensitive to gaps. However, the annual median is considered here to satisfy the criteria more fully than the chlorophyll maximum metric. This is because the identification of bloom termination is more consistent and the chlorophyll maximum threshold value is adversely affected by the overestimation of chlorophyll peak concentrations. The altered threshold value would result in erroneous initiation and termination dates. Despite this, the two metric give very similar bloom timing results and have relatively small RMSD values. Analysis in further chapters will focus on the annual median metric as this is most often used in the literature and so provides a broader context for the results and makes comparisons to previous studies easier.

3.3 Summary

- Seasonality metrics are used to measure bloom timing in a consistent manner. The bloom events that are of interest here are bloom initiation, peak, termination and duration. The metrics must be applicable globally and be adaptable to the different types of seasonal cycles that occur. They must also be able to cope with gaps and noise in the time series. Additionally, it is prudent to remove regions that do not display a strong seasonal cycle from further analysis.
- Several methods were tried to distinguish high and low seasonality regions from each other, mostly based on the variance of the time series.
- The coefficient of variation was chosen as the best method as it's calculation is insensitive to gaps, allows for interannual variability in the size and duration of the bloom and properly captured the large seasonal variability at high latitudes.
- A value of 0.35 was chosen as the coefficient of variation threshold. All pixels with a value less than this were deemed to have a weak seasonal cycle and were excluded from further analysis. This choice was based on examination of individual time series and its spatial pattern.
- The timing of the bloom peak was defined as the date on which the maximum chlorophyll value occurred. The timing of bloom initiation and termination were defined using four metrics based on relative changes in chlorophyll concentration. The duration of the bloom was calculated as the difference between the start and end.

- Based on a visual analysis of multiple time series and global maps, each of the metrics identified the timing of bloom initiation and termination well. The annual median and chlorophyll maximum metrics both identified consistently the same stage of seasonal chlorophyll increase and decrease as the bloom initiation and termination. Additionally, these two metric definitions were relatively insensitive to missing data and noise in the time series compared to the other metric definitions.
- The annual median and chlorophyll maximum metrics both gave similar dates for bloom initiation and termination. This was evident in the relatively small global RMSD of 38 days for bloom initiation and 57 days for bloom termination.
- Though two metric definitions satisfy the original criteria, the timing of bloom initiation, termination and duration will be defined using the annual median threshold based metric in subsequent chapters. This defines the start and end of the bloom using a threshold value of 105% of the annual median. This definition has been used regularly in the literature and so provides context for subsequent results.

4 Impact of Data Gaps on the Accuracy of Bloom Timing Metrics

During the development of the bloom timing metrics described in the previous chapter it was apparent that missing data represented the largest disadvantage to using satellite data. However, as satellites provide the only means with which to measure bloom timing globally it is useful to be able to quantify the likely uncertainty on the bloom timing dates caused by missing data. The NASA Ocean Biogeochemical Model (NOBM) was introduced in Chapter 2 where the similarity between NOBM seasonal cycles and GlobColour seasonal cycles was discussed. Using NOBM as a gap free satellite dataset this chapter aims to quantify the impact missing data has on the accuracy of seasonality metrics and to present a method for estimating the likely uncertainty in the metric based on the proportion of missing data. Part of this work has previously been published and is included in Appendix A (Cole *et al.*, 2012).

4.1 Introduction

Several methods have been employed to reduce the impact of gaps in satellite data time series. Although averaging over time and space reduces the number of gaps it also smoothens high-frequency variability (Winder and Cloern, 2010). This means that higher frequency processes cannot be resolved and so trade-offs often need to be made between resolution and data coverage (i.e. datasets with monthly resolution have better data coverage but processes acting on daily and weekly timescales cannot be resolved). This is an important consideration for bloom timing studies since finer temporal resolutions will be more sensitive to smaller interannual variability in bloom timing. Interpolation is also an unsatisfactory method for filling the long persistent gaps in winter. Interpolation can work well over small gaps but produces unrealistic annual cycles and often underestimates variability when filling long gaps in the data as trends may not be linear. This was especially apparent at mid to high latitudes where linear interpolation of the time series was attempted and resulted in the long period of missing data over winter being estimated by an unrealistic straight line. Other studies exclude high-latitude regions from analysis in order to remove the most gap affected regions (Dandonneau *et al.*, 2004). However, high-latitude areas are very productive and

display some of the strongest and most seasonally variable cycles and furthermore, can be relatively cloud-free in the summer months.

4.2 Seasonality in Missing Data

Remote sensing of ocean colour is an invaluable tool for studying phytoplankton phenology at large spatial scales and at high temporal resolution over annual cycles (Platt *et al.*, 2010). However, many regions that display a strong seasonal cycle, such as high latitudes, also experience frequent cloud cover which may persist for long periods (Figure 4.1). Long gaps in satellite ocean colour data also occur due to low sun angle in winter, sea ice and atmospheric aerosols. The loss of data coverage in the North Pacific was recognised as a potential problem in bloom timing studies by Sasaoka *et al.* (2011). They found that ocean colour data was present between 3 and 15 days per month at individual pixels over their spring and summer study period. Missing data may affect the accuracy of seasonality metrics in two ways. The date of interest might occur during a period of missing data or the calculation method of the metric may be biased by missing data.

The seasonality of the amount of missing data may also be important for the accuracy of bloom timing estimates. Cloud cover displays strong seasonality at high latitudes with greater cloud cover occurring in winter. Additionally, the sun angle is lowest and sea ice most extensive in winter, severely affecting the amount of satellite chlorophyll data retrieved. Furthermore, different sources of missing data will cause data gaps of varying size through time. For instance, gaps occurring in winter due to a low sun angle will last for months and will occur at the same time each year whereas missing data during the summer from passing weather systems will be relatively short and show large interannual variability in their timing. Before assessing the impact of missing data on the bloom timing metrics, it will be useful to become familiar with the seasonality of missing data.

A 9 year global dataset representing missing data was calculated using the GlobColour chlorophyll time series where a time step with a gap present was given a value of 1 and those with a chlorophyll value given a value of 0. From these time series a climatology was created to quantify the total amount of missing data (expressed as a percentage) at each pixel both annually and for each of the seasons. Additionally, the number of gaps and their mean length was also calculated. The number of gaps is not the same as the percentage of missing data if some of the time steps of missing data are consecutive (i.e. if 10% of data is missing but are missing in consecutive time steps then this counts as 1 gap).

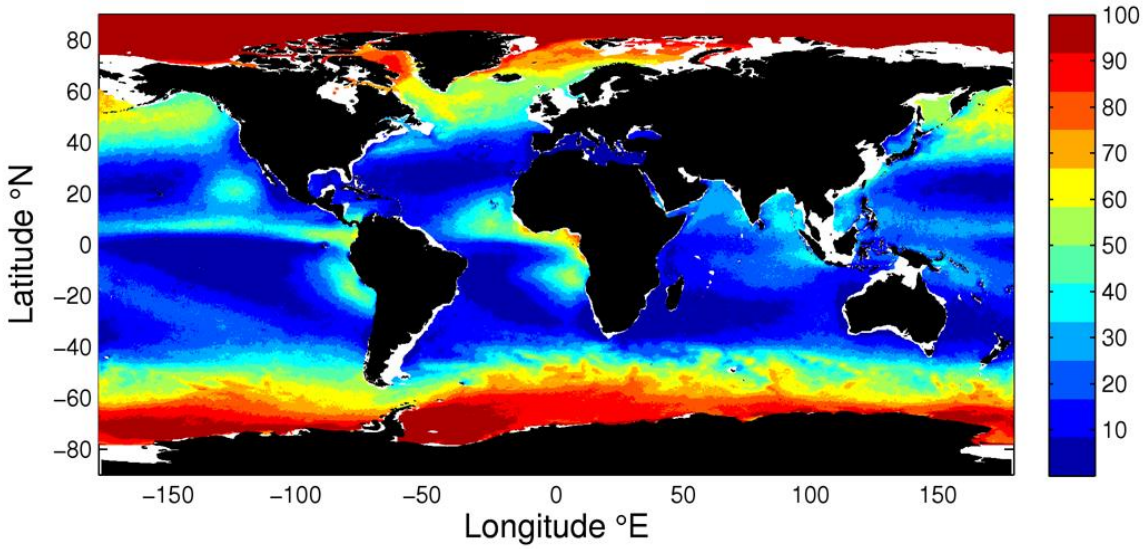

Figure 4.1: The percentage of missing data annually calculated from GlobColour dataset from 2002 to 2009.

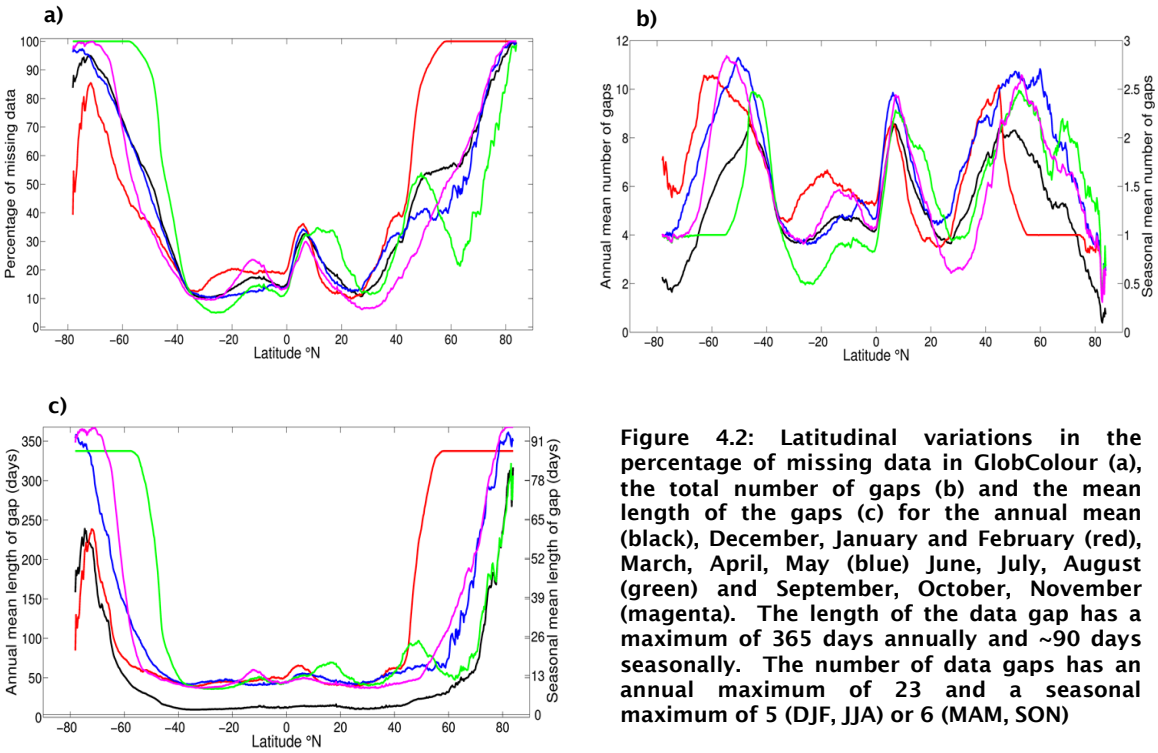

Figure 4.2: Latitudinal variations in the percentage of missing data in GlobColour (a), the total number of gaps (b) and the mean length of the gaps (c) for the annual mean (black), December, January and February (red), March, April, May (blue) June, July, August (green) and September, October, November (magenta). The length of the data gap has a maximum of 365 days annually and ~90 days seasonally. The number of data gaps has an annual maximum of 23 and a seasonal maximum of 5 (DJF, JJA) or 6 (MAM, SON)

On an annual basis, the total percentage of missing data was highest at the poles (>90%) and in subpolar regions (~50-60%) and lowest in the subtropical gyres (10-20%) with slightly higher amounts of missing data in equatorial regions where cloud cover is more common (30-40%), (Figure 4.1 and 4.2). A similar pattern was seen seasonally with higher latitudes showing greater intraseasonal variability, (Figure 4.2 and 4.3). In the Southern Ocean the percentage of missing data was reduced in austral spring and summer, with the greatest reductions seen between 60˚S and 40˚S. Seasonal differences in missing data at high latitudes were larger in the northern hemisphere with the percentage of missing data reducing to ~20-30% in boreal spring and summer from ~80% in boreal winter at ~60-70˚N (where the largest change occurs) (Figure 4.2). At ~50˚N the North Pacific has a greater amount of missing data during boreal spring and summer compared to the North Atlantic (Figure 4.3). In contrast, the subtropical regions have small seasonal differences in the percentage of missing data. However, the northern and southern subtropical gyres show differences in their seasonality. In the northern hemisphere subtropical gyres, the largest amounts of missing data occurred during boreal winter and the least in boreal summer. However, in the southern hemisphere the subtropical gyres experienced more missing data during austral summer though the intraseasonal differences in missing data across the southern subtropical gyres were small (Figure 4.3).

Seasonal variation was also seen in the number and length of gaps in the time series (Figure 4.2). Each year in the time series is comprised on 46 time steps, each time step being an 8-day mean chlorophyll value. The maximum number of gaps in a year is 23 time steps and 6 time steps seasonally, representing missing data at every other time step. Peaks in the number of gaps on an annual basis occur at ~50˚S and ~10˚N and ~40˚-50˚N with minima occurring in the subtropical gyres and towards the poles. Seasonal variations were most apparent in the latitude of the maximum and minimum points. In the Southern Ocean the maximum number of gaps moves from 45˚S in austral winter to 65˚S in austral summer. To the north, in boreal winter the maximum is at 45˚N but moves to two maxima in the number of gaps at 50˚N and 70˚N in boreal summer. There is also large seasonal variation between -45˚S and 0˚N in the subtropical gyres with more gaps present during austral spring and summer. These latitudinal variations in the number of gaps are complemented by latitudinal variations in the mean length of the gaps (Figure 4.2c). From this, the difference between high-latitude and subtropical regions, which both have low numbers of gaps can be seen. In the subtropics there is a relatively low mean number of gaps which are also short in length both annually (<16 days) and seasonally (<24 days). Conversely, the low number of gaps at high latitudes are

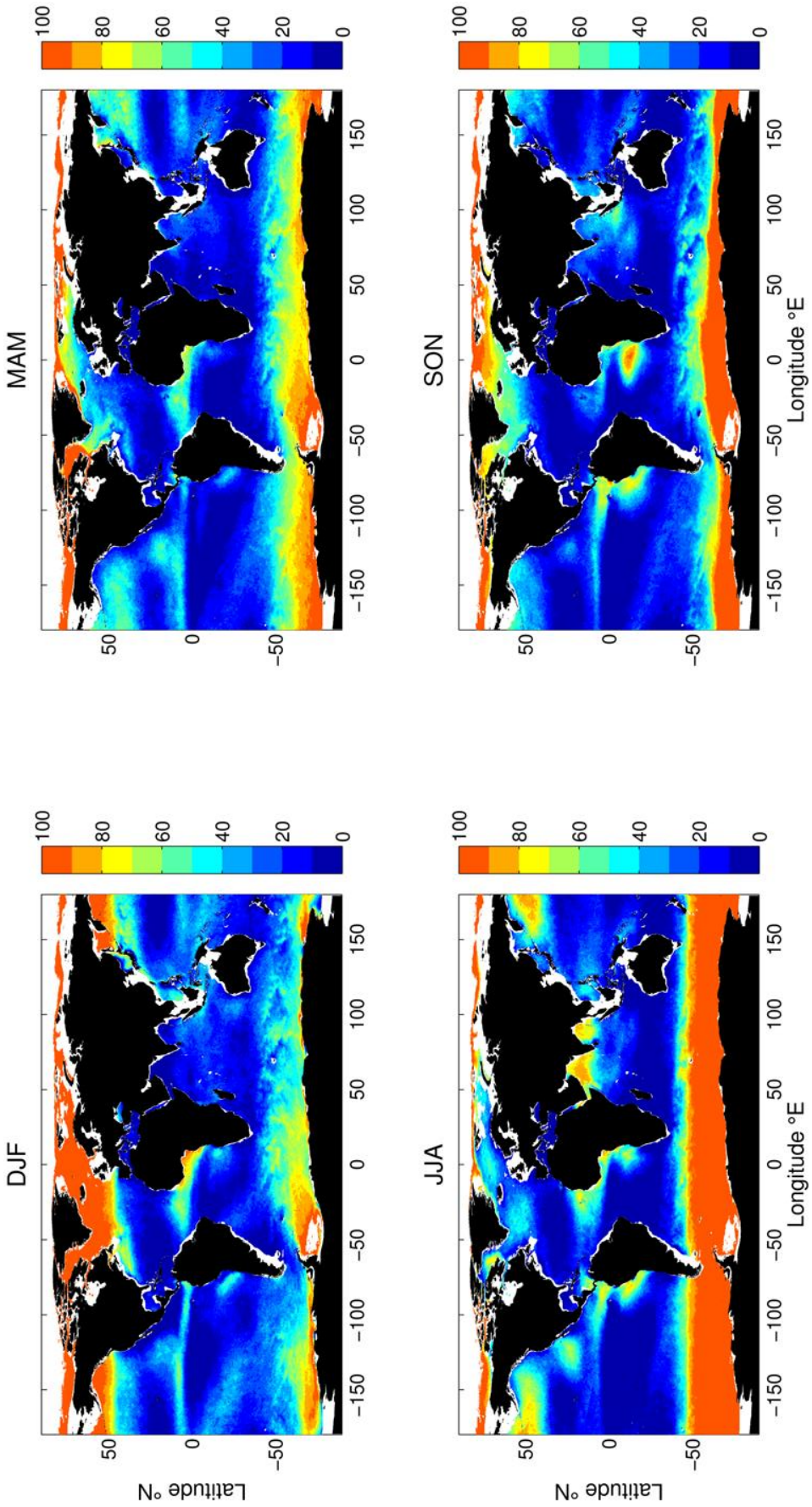

Figure 4.3: Spatial variations in the percentage of missing data in December, January, February (DJF), March, April, May (MAM), June, July, August (JJA), September, October, November (SON). Seasonal means were calculated from GlobColour dataset 2002 -2010.

relatively long in length (~160 days). The largest seasonal variation in the mean length of the gaps was seen at mid to high latitudes where longer gaps occur closer to the equator in winter months compared to summer months. The subtropics and equatorial regions are characterised by short gaps with very small seasonal variation.

To summarise, missing data varies strongly both seasonally and geographically. Subpolar regions are characterised by long gaps in winter and shorter, but more frequent gaps in summer. This results in a higher percentage of missing data in winter. Subtropical regions generally have smaller and less frequent gaps and a lower percentage of missing data when compared to subpolar regions. Interestingly, the southern hemisphere subtropical gyres have larger amounts of missing data in austral summer with more gaps relative to winter but still of very short length. The northern hemisphere subtropical gyre (especially between 20˚N and 40˚N) follows the expected pattern of lower amounts of missing data, and less gaps in boreal summer.

4.3 Data, Model and Methods

4.3.1 Satellite Data and Model Output

To estimate errors in the metrics a completely gap free dataset was needed to calculate the true metric date for comparison to those estimated from intermittent time series. The NASA Ocean Biogeochemical Model (NOBM) is a fully coupled radiative, general circulation and biogeochemical model that assimilates Sea-viewing Wide Field-of-view Sensor (SeaWiFS) chlorophyll data on a daily basis (Nerger and Gregg, 2008). As a result the phases of the annual cycles in NOBM and satellite observations from the GlobColour dataset are very similar (see section 2.1.2 in Chapter 2). For this phenological study it is important that the start, peak and end of the bloom occur at the same point in time in NOBM and satellite observations. The NOBM output was obtained from the Giovanni application developed by the NASA Goddard Earth Sciences Data and Information Services Center (GES DISC) available from http://giovanni.gsfc.nasa.gov. Daily fields of 2/3˚ latitude and 5/4˚ longitude resolution were averaged to 8 day composites to match the satellite dataset.

GlobColour is a level 4 merged product that incorporates data from the SeaWiFS, MODIS and MERIS instruments and uses a weighted average to generate a global chlorophyll dataset (see section 2.1.1 for further details on the GlobColour dataset). Combining the 3 sensors increases the data coverage in both time and space. Eight day composites with a spatial resolution of 0.25˚ were obtained from

the GlobColour website http://www.globcolour.info. The satellite dataset was regridded using area weighted means onto the coarser resolution grid of the NOBM. GlobColour and NOBM overlap for the years 2002 to 2006.

Regions that did not display a seasonal cycle in chlorophyll were removed before further analysis. The coefficient of variation (standard deviation/mean) was calculated from the climatological year. Low coefficient of variation values characterise oligotrophic regions where production is relatively constant all year round with no pronounced annual cycle (Doney *et al.*, 2003, Lutz *et al.*, 2007). Any pixel with a coefficient of variation value below 0.35 was classified as having a weak, indistinct seasonal cycle. This value was chosen based on the spatial pattern of the coefficient of variation and a visual inspection of individual time series (see section 3.1.5 in Chapter 3 for more details). These regions are masked out in the figures presented here.

4.3.2 Metrics

Three metrics, the dates of the bloom initiation, peak and termination, were chosen for this thesis. Many phenological metrics have been defined in previous studies and several different methods to calculate the same metric have been described e.g. (Siegel *et al.*, 2002, Platt and Sathyendranath, 2008, Henson *et al.*, 2009, Kahru *et al.*, 2011). As the timing of bloom events varies with location using 1st January as the starting point for each annual cycle of chlorophyll was not appropriate. For example, in the Southern Ocean and northern hemisphere subtropical gyres the chlorophyll peak occurs at the turn of the year (December and January) and so dividing the year from January to December result in these chlorophyll peaks being divided in half. To work around this, the bloom peak dates (date of maximum chlorophyll concentration) were found using both a January to December calendar and a June to May calendar. If the calendar configuration divided the peak in half then the standard deviation in the peaks would be relatively high. Thus, the calendar configuration with the smallest standard deviation in peak dates was used to define the peak timing. Then the timing of the bloom peak was used to determine the centre point of the annual cycle for each grid location. To form the annual time series the bloom peak in each year of the GlobColour dataset was found; then the 6 months of data before and after this date were used to form the "year" around the peak of the bloom (see Section 3.2.1 for more details).

Using a fixed chlorophyll concentration to define a bloom would only be valid for short-term regional applications since the seasonal amplitude of phytoplankton blooms is highly variable both spatially and interannually. This is why a relative threshold was used to define the start of a bloom. Siegel *et al.* (2002) tested

threshold values ranging from 1% to 30% above the annual median and found little difference in the resultant bloom initiation date. We use 5% here to remain consistent with Siegel *et al.* (2002) and calculated the annual median from the peak-centred annual time series so that the each year's median value is representative of each year's bloom. This metric definition was chosen as it identified the stages of bloom development and decline that were deemed to be indicative of bloom initiation and termination consistently between different regions and different years. Furthermore, it has been used extensively in other studies and is suitable to apply on a global scale encompassing areas that incorporate many different types of annual cycle (Siegel *et al.*, 2002, Henson *et al.*, 2006, Henson *et al.*, 2009, Platt *et al.*, 2009, Thomalla *et al.*, 2011, Racault *et al.*, 2012).

More specifically, the bloom peak date is used as a reference point and the first time step moving backward in time from before the peak that fell below the threshold was estimated to be the start of the bloom. This condition had to be met for two consecutive time steps (i.e. 16 days) to be valid and the second of the two consecutive points was the date of bloom initiation. The date of bloom termination was defined as the last of two consecutive time steps that were above the threshold in the 6 months following the peak (see section 3.2 in Chapter 3 for more details on metric definition).

4.3.3 Error Estimation

The NOBM provides a gap free chlorophyll time series with high fidelity to the seasonal characteristics of the satellite data while the satellite observations supply a record of when missing data occurred. The seasonality metrics were calculated using the NOBM output twice: once with the complete chlorophyll time series and again when NOBM was sub-sampled only on the dates when GlobColour data were present. The error in bloom timing at each location was found by calculating the difference between the two metric estimates. The satellite observations and NOBM output overlapped in time by 5 years and so only 5 error estimates could be calculated initially at each pixel. To increase the number of error estimates at each pixel, each of the 5 years in NOBM was sub-sampled 5 times. This was done by shuffling around the 5 years in the GlobColour gap dataset so that every year in NOBM was sub-sampled using gaps from every year in GlobColour. In other words, each year in NOBM was sub-sampled using dates when GlobColour data were present in 2002, then the dates when data were present in 2003, then the dates when data were present in 2004, etc. This gives a total of 25 error estimates at each pixel. While this creates a larger pool to draw estimates from, it does assume

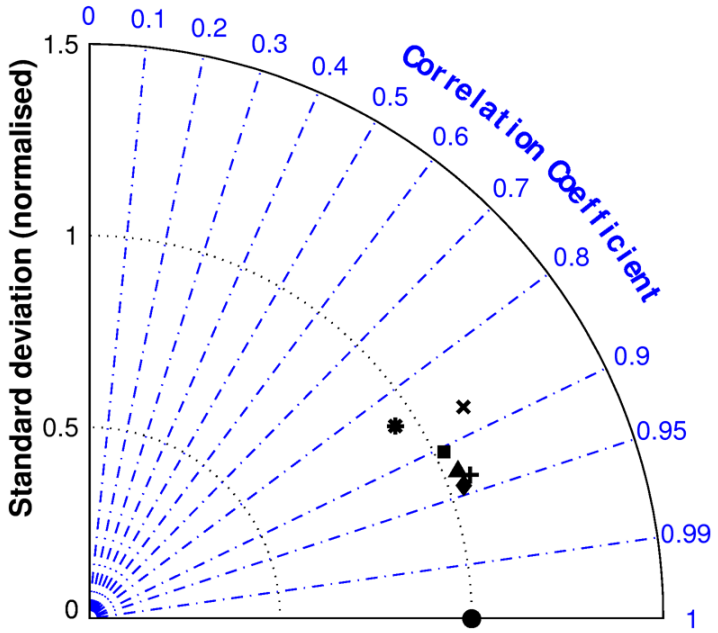

Figure 4.4: Taylor diagram comparing the bloom initiation (cross), bloom peak (plus) and bloom termination (star) metric results from the full NOBM dataset to those from GlobColour satellite observations (circle). The NOBM dataset was then subsampled where GlobColour data was present (i.e. added the same data gaps as those present in GlobColour). The agreement between the metric dates from the subsampled NOBM dataset and the GlobColour dates are indicated for bloom initiation (square), peak (diamond) and termination (triangle).

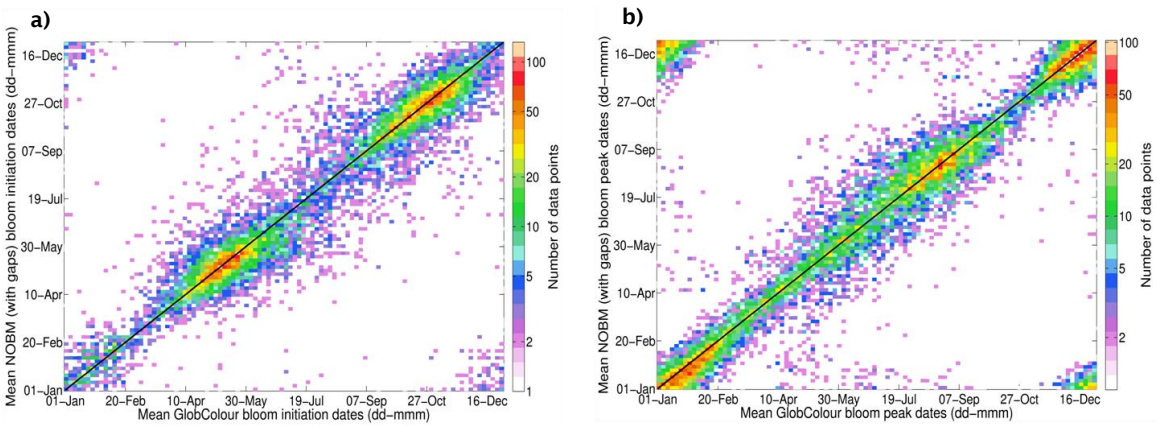

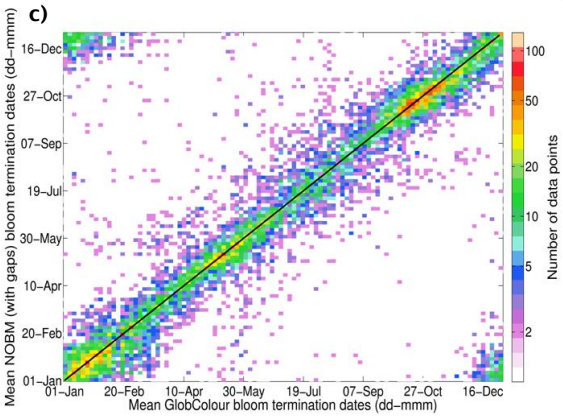

Figure 4.5: Scatter plots showing the linear relationship between bloom metric GlobColour dates and metric dates from the subsampled NOBM dataset for bloom initiation (a), bloom peak (b), bloom termination (c). The colour bar represents data density. Data in the top left and bottom right hand corners represent data where one bloom timing estimate gives a January date and the other a December date or vice versa. Though this looks erroneous it is just a plotting artifact due to the cyclic nature of the annual calendar. In reality these satellite and NOBM data points have very small differences. Note that the colour bar is on a log scale.

that the temporal distribution of missing data is broadly similar each year and that it does not strongly regulate underlying chlorophyll concentrations. The mean error magnitude and percentage of missing data at each pixel was calculated and ln(y+1) transformation applied to make the data more Gaussian (since the distribution of bloom timing error dates were approximately log-normal) for regression analysis which was performed on the global dataset.

4.3.4 Regression Analysis

A range of polynomials were fitted to the full dataset to obtain a relationship between the percentage of missing data and the error in metric date. As the error should be zero when all data are present the regressions were forced to go through zero. Overfitting is something to be avoided when fitting curves in the interest of parsimony. The simplest curve that explains the shape of the data reasonably well is the preferred one. Measures of goodness-of-fit for each polynomial fitted to the data are reported in Table 4.1 (for bloom initiation), Table 4.2 (for peak timing) and Table 4.3 (for bloom termination). Goodness-of-fit parameters and a visual inspection of the model fit and residual distribution were used to define which polynomials fit the data reasonably well.

4.4 Results

4.4.1 Comparison of NOBM and GlobColour

To use NOBM as a gap free dataset to estimate bloom timing we must first ensure that bloom timing in NOBM matches that in GlobColour for the error estimates to have any meaning. Co-located time series from NOBM and GlobColour (see Figure 2.3, Chapter 2) show that bloom timing characteristics are very similar. This is summarized globally in a Taylor diagram (Figure 4.4) and in scatter plots (Figure 4.5). There is high agreement between satellite observations and NOBM output for bloom initiation (correlation coefficient of 0.87), bloom peak (0.94) and bloom termination (0.85). The metrics have a normalized standard deviation of 1.12 for bloom initiation, 1.06 for bloom peak and 0.95 for bloom termination. As these values are close to 1 it indicates that the metric spatial variability is approximately equal in both the satellite observations and NOBM output. The correlation may be reduced due to gaps present in the GlobColour dataset which may change the bloom timing dates. This means that NOBM bloom timing dates will not agree with GlobColour dates even if their seasonal cycle matches perfectly. When NOBM is sub-sampled on dates when GlobColour data is present the agreement between NOBM and GlobColour for all metrics improves with the

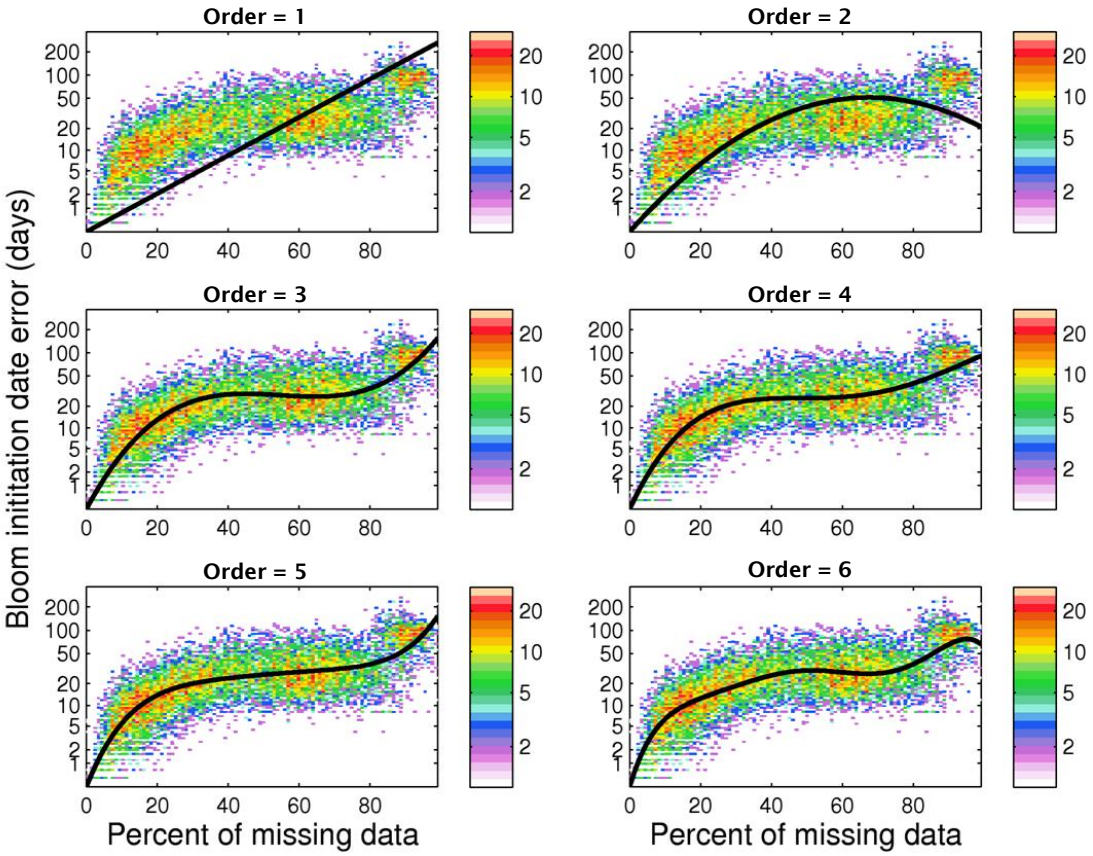

Figure 4.6: Regression results for polynomials of order 1 to 6 applied to bloom initiation date error versus the total annual percentage of missing data. The colour bar represents the density of data. The regression was applied to the full dataset though it is binned for plotting purposes. Note that the colour bar is on a log scale.

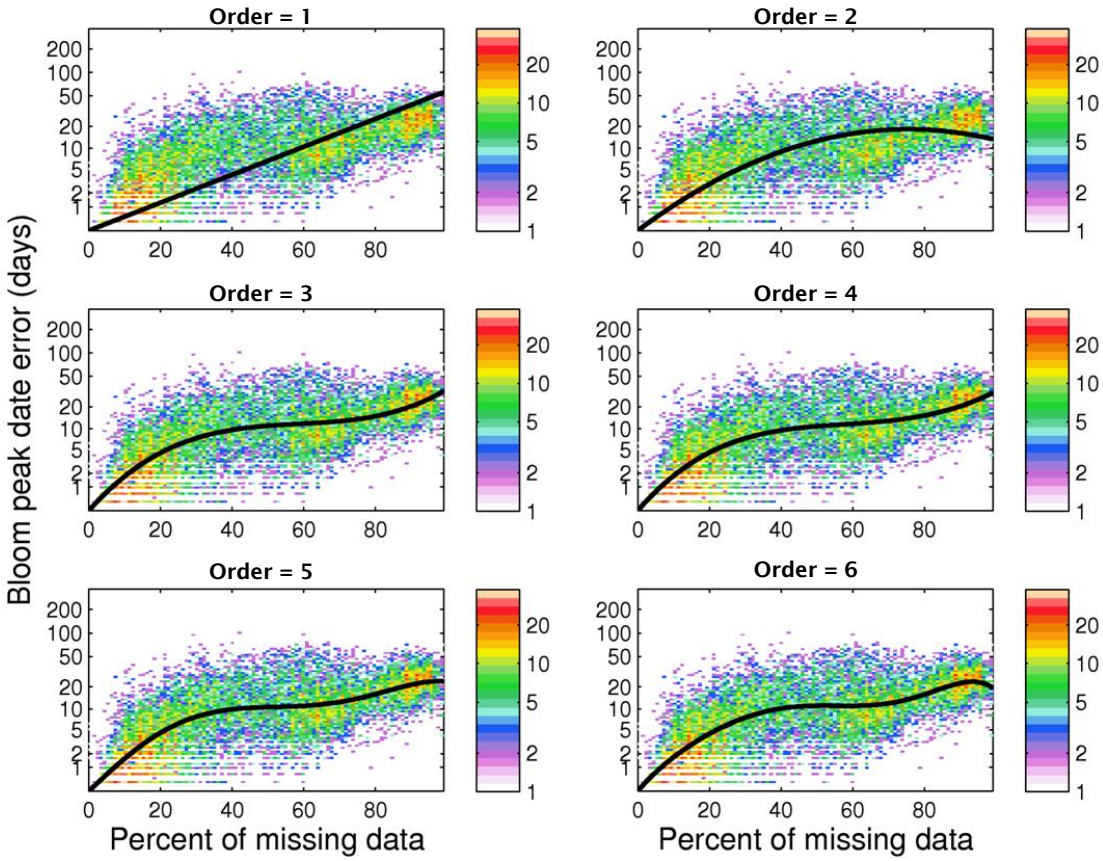

Figure 4.7: Regression results for polynomials of order 1 to 6 applied to bloom peak date error versus the total annual percentage of missing data. The colour bar represents the density of data. The regression was applied to the full dataset though it is binned for plotting purposes. Note that the colour bar is on a log scale.

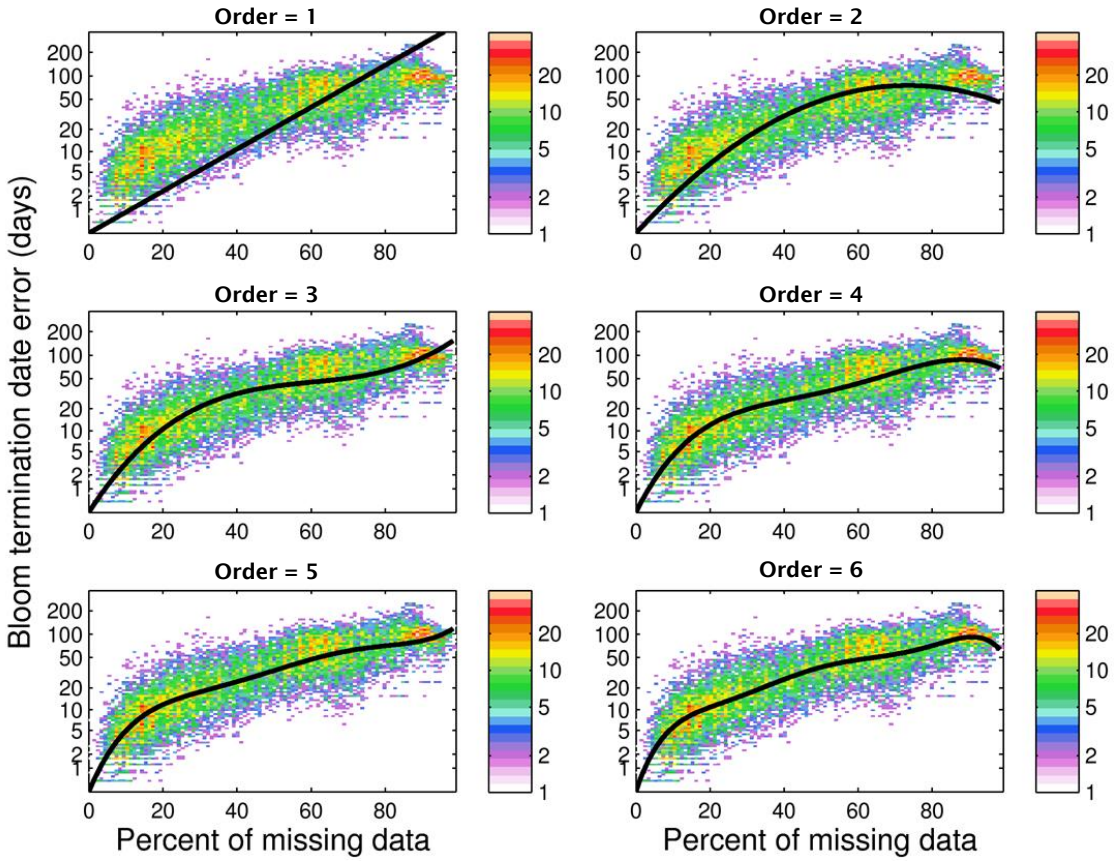

Figure 4.8: Regression results for polynomials of order 1 to 6 applied to bloom termination date error versus the total annual percentage of missing data. The colour bar represents the density of data. The regression was applied to the full dataset though it is binned for plotting purposes. Note that the colour bar is on a log scale.

standard deviation moving closer to 1 (1.02 for initiation, 1.04 for peak and 1.04 for termination) and the correlation coefficient rising to 0.92 for bloom initiation, 0.94 for bloom peak and 0.93 for the bloom termination. This suggests that the introduction of missing data to the NOBM time series affects the bloom timing metrics in the same way as missing data in the satellite observations since the agreement between these two datasets is high. Regions without a strong seasonal cycle were removed from the datasets before comparison. Using different coefficient of variation values had little effect on the correlations and normalised standard deviations (see Appendix C).

The relationship between the metric dates from the GlobColour and the NOBM dataset with matching gaps is linear (Figure 4.5). Additionally, the highest number of data points occurs along the 1:1 line (74% for initiation, 72% for peak and 73% for termination) indicating that the majority of metric dates from GlobColour are almost identical to the subsampled NOBM metric dates. This strongly supports the use of NOBM chlorophyll as a gap free dataset for estimating bloom timing and quantifying the error in metric dates from intermittent time series.

4.4.2 Picking the Best Regression Model

Several polynomials were fitted to describe the regression of bloom metric error against the percentage of missing data (Figure 4.6-4.8). It was clear that the first and second-order polynomials were unsuitable as they do not fit the data well; the data clearly do not fall along a straight line and the second order polynomial decreases in value at high percentages of missing data. The residuals for the first and second-order polynomials were not normally distributed indicating a poor fit whereas, residuals for the higher order polynomials were all approximately normally distributed. The higher order polynomials all exhibit approximately the same shape with more polynomial terms resulting in small refinements to the fitted curve. The goodness-of-fit parameters (Table 4.1-4.3) all indicate that the 6th-order polynomial is the "best" fit (smallest RMSD, largest R^2, smallest ΔAIC and ΔBIC) for all metrics. The third-order polynomial was chosen as the simplest model that fits the data reasonably well for the bloom initiation and peak. Increasing the polynomial order any further resulted in only a slight improvement in the goodness-of-fit (relative to the improvements when increasing from order 2 to 3) and almost no change in the shape of the fitted curve (Table 4.1 and 4.2). The bloom termination is a similar situation though the flattening out of the goodness-of-fit parameters is less defined than for the initiation and peak. The goodness-of-fit parameters and residuals indicate that 3rd and 4th order polynomials are the best fit. In the interest of parsimony and because the 4th order polynomial decreases in value at high percentages of missing data, the 3rd polynomial is used.

Table 4.1: Goodness-of-fit parameters for regression of bloom initiation error on percentage of missing data

Polynomial order	RMSD[a]	R^2 [b]	ΔAIC[c]	ΔBIC[c]
1	1.23	0.45	32967	32926
2	0.84	0.42	14687	14654
3	0.64	0.52	1716	1692
4	0.63	0.52	1044	1028
5	0.63	0.52	669	661
6	0.62	0.53	0	0

[a] RMSD stands for Root Mean Square Difference with smaller values signify a better fit.

[b] R^2 is the reported value from the regression of actual metric error values against fitted metric error values; all have a p-value of less than 0.01. The R^2 value indicates the proportion of variance in the metric error data that is explained by the fitted values. However, care must be taken over its interpretation as the regressions were forced through the origin.

[c] ΔAIC (Akaike Information Criterion) and ΔBIC (Bayesian Information Criterion) are model selection parameters that penalise for the number of terms used in the model. A value of zero represents the model with the best compromise between goodness-of-fit and model complexity. Large ΔAIC and ΔBIC values indicate models that are least likely to be the best compromise between goodness-of-fit and model complexity.

Table 4.2: Goodness-of-fit parameters for regression of bloom peak error on percentage of missing data

Polynomial order	RMSD[a]	R^2 [b]	ΔAIC[c]	ΔBIC[c]
1	0.99	0.37	12661	12620
2	0.82	0.39	3103	3071
3	0.77	0.43	147	123
4	0.77	0.43	142	126
5	0.77	0.43	43	35
6	0.77	0.43	0	0

[a] Here RMSD stands for Root Mean Square Difference with smaller values signify a better fit.

[b] R^2 is the reported value from the regression of actual metric error values against fitted metric error values; all have a p-value below 0.01. The R^2 value indicates the proportion of variance in the metric error data that is explained by the fitted values. However, care must be taken over its interpretation as the regressions were forced through the origin.

[c] ΔAIC (Akaike Information Criterion) and ΔBIC (Bayesian Information Criterion) are model selection parameters that penalise for the number of terms used in the model. A value of zero represents the model with the best compromise between goodness-of-fit and model complexity. Large ΔAIC and ΔBIC values indicate models that are least likely to be the best compromise between goodness-of-fit and model complexity.

Table 4.3: Goodness-of-fit parameters for regression of bloom termination error on percentage of missing data

Polynomial order	RMSD[a]	R^2 [b]	ΔAIC[c]	ΔBIC[c]
1	1.11	0.64	27638	27598
2	0.74	0.63	8288	8256
3	0.66	0.65	2534	2509
4	0.64	0.66	889	873
5	0.63	0.67	430	422
6	0.62	0.67	0	0

[a] Here RMSD stands for Root Mean Square Difference with smaller values signify a better fit.

[b] R^2 is the reported value from the regression of actual metric error values against fitted metric error values; all have a p-value below 0.01. The R^2 value indicates the proportion of variance in the metric error data that is explained by the fitted values. However, care must be taken over its interpretation as the regressions were forced through the origin.

[c] ΔAIC (Akaike Information Criterion) and ΔBIC (Bayesian Information Criterion) are model selection parameters that penalise for the number of terms used in the model. A value of zero represents the model with the best compromise between goodness-of-fit and model complexity. Large ΔAIC and ΔBIC values indicate models that are least likely to be the best compromise between goodness-of-fit and model complexity.

4.4.3 Empirical Relationship between Error and Missing Data

The spatial variability of missing data from satellite ocean colour data is shown in Figure 4.1 where the highest proportion of missing data is found at high latitudes and in equatorial regions. This pattern varies seasonally with the majority of gaps occurring during the winter and persisting for months at high to mid-latitudes. Though a relatively large proportion of gaps occur in equatorial regions these gaps are smaller, lasting for days to weeks.

Figure 4.9 shows the relationship between the percentage of missing data and the ln(y+1) transform of the absolute magnitudes of the bloom initiation, peak and termination metric errors. Every pixel was included in the regression though data has been binned for plotting purposes. The cubic polynomials fitted to the transformed data for all three metrics gives the relationship with the percentage of missing data, x:

$$Err_{BI} = e^{\left(2.27(\pm 0.03)\times 10^{-5}x^3 - 3.72(\pm 0.04)\times 10^{-3}x^2 + 0.20\left(\pm 1.34\times 10^{-3}\right)x\right)} - 1 \qquad (4.1)$$

RMSD = 0.64, R^2 = 0.515 (p-value <0.05)

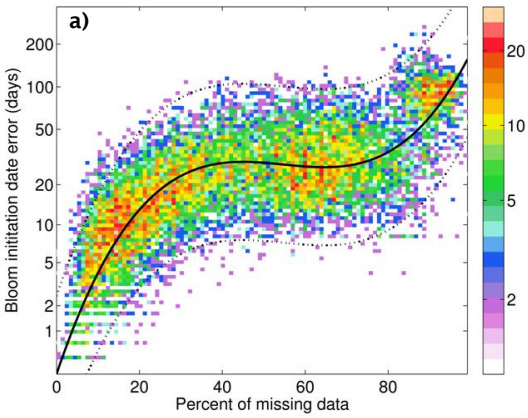

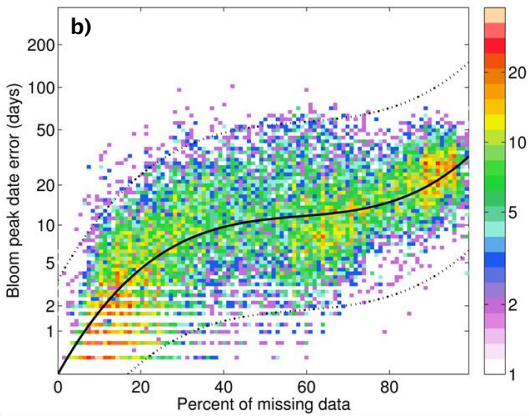

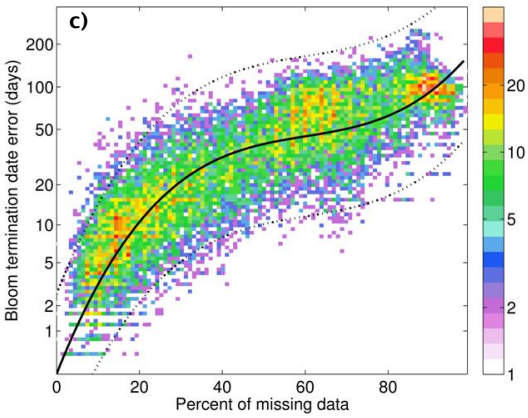

Figure 4.9: Relationship between percentage of missing data and the error in (a) bloom initiation date, (b) peak date and (c) bloom termination date. Regression lines for all three metrics are cubic polynomial fits (these plots are the same as the 3rd order polynomials in Figures 4.6, 4.7 and 4.8). Dotted lines represent the 95% confidence intervals. Data has been binned for plotting purposes and the colour bar denotes the number of data points in a particular bin and is on a log scale.

$$Err_P = e^{\left(1.10(\pm 0.04)\times 10^{-5}x^3 - 1.94(\pm 0.05)\times 10^{-3}x^2 + 0.21\left(\pm 1.62\times 10^{-3}\right)x\right)} - 1 \qquad (4.2)$$

RMSD = 0.77, R^2 = 0.428 (p-value<0.05)

$$Err_T = e^{\left(1.45(\pm 0.04)\times 10^{-5}x^3 - 2.62(\pm 0.05)\times 10^{-3}x^2 + 0.17\left(\pm 1.40\times 10^{-3}\right)x\right)} - 1 \qquad (4.3)$$

RMSD = 0.66, R^2 = 0.6485 (p-value<0.05)

where Err_{BI} is the error in bloom initiation date, Err_P is the error in bloom peak date and Err_T is the error in bloom termination date. The values in brackets indicate the 95% confidence intervals on the regression coefficients and were obtained through bootstrapping the regression by repeatedly sub-sampling 100% of the data. Though coefficient of determination values are reported (R^2) they are not an exact representation of the variability explained by the fitted line since the regression was forced through the origin. Thus, RMSD values are also reported to give further indication of the goodness-of-fit. Pixels that did not show a strong seasonal cycle (coefficient of variation value of less than 0.35) were removed from the dataset before deriving the coefficients. Using other values of the coefficient of variation had little impact on the regression coefficient values (see Appendix C).

4.4.4 Application to Determining Uncertainty in Metric Dates

Error prediction maps for the bloom initiation, peak and termination metrics using equations 4.1, 4.2 and 4.3 respectively, are displayed alongside the seasonality metrics calculated from the satellite observations in Figures 4.10, 4.11 and 4.12. In the northern hemisphere there is a clear gradient in bloom initiation date from subtropical regions where it starts in November/December through to June/July at high latitudes (Figure 4.10a). A similar pattern is seen in the Southern Hemisphere with blooms starting during May/June in subtropical regions through to October/January at higher latitudes. The error uncertainty on the bloom initiation date varies spatially, but the majority of mid to high-latitude regions (excluding the Southern Ocean) have a predicted error of less than 35 days, decreasing to close to zero toward subtropical regions (Figure 4.10b). In the Southern Ocean the predicted errors are much higher and can be as large as 120 days. However, on average, the predicted error in subpolar regions is approximately 30 days, 14 days in subtropical/oligotrophic regions and 19 days in equatorial regions. The mean error in the high-latitude Southern Ocean (60-80°S) is 74 days.

A clear latitudinal gradient is also seen in the peak metric date (Figure 4.11a). In the Northern Hemisphere the bloom peak transitions from February in subtropical regions through to August at high latitudes. These timings are 6

months out of phase in the Southern Hemisphere with the peak occurring in August/September in subtropical regions and in December/January at high latitudes. The uncertainty in peak date shows more spatial variability than the bloom initiation metric (Figure 4.11b). The largest uncertainty is approximately 30 days and is again seen in the high-latitude Southern Ocean. Outside of the Southern Ocean the predicted error is typically less than 15 days, again highest at high latitudes and decreasing towards the subtropical gyres. The majority of the mid to high latitudes have a predicted error of approximately 10 days. Mean values are relatively small compared to the other metrics with a mean predicted error in subpolar regions of ~12 days, ~9 days in subtropical/oligotrophic regions and 7 days in equatorial regions. The high-latitude Southern Ocean (60-80˚S) mean error is 22 days.

Bloom termination dates also show similar latitudinal gradient (Figure 4.12a). In subtropical regions, blooms end in boreal (April/May) or austral (October/November) late spring progressing to boreal (August/September) or austral (January-March) late summer/autumn dates nearer the poles. The uncertainty in the date of bloom termination is more spatially variable than the uncertainty of the other two metrics with the subtropics having uncertainties of less than 20 days and subpolar regions generally less than 60 days (Figure 4.12b). The largest errors are again seen in the Southern Ocean and were typically greater than 90 days. In the majority of regions the mean error in bloom termination timing is relatively large compared to the other metrics. Mean predicted errors in subpolar regions are ~50 days, ~15 days in subtropical/oligotrophic regions and ~21 days in equatorial regions. The mean error in the high-latitude Southern Ocean (60-80˚S) is 100 days.

Broadly speaking, the largest errors in bloom initiation, peak and termination timing metrics were seen in the subpolar regions, whilst the smallest errors occurred at lower latitudes. The regions with large errors unsurprisingly coincide with regions that have a high percentage of missing data. More specifically, large errors in the bloom initiation date (~50-60 days) were seen in the North Pacific (between 35˚N and 50˚N) and the western North Atlantic (north of 40˚N). The largest bloom initiation errors of ~100-120 days occurred in the Weddell Sea region of the Southern Ocean. Substantial errors in the peak date (~35-49 days) occur in the North Pacific, equatorial Atlantic and subpolar North Atlantic. Errors in the bloom termination date were generally higher in the North Atlantic (40-60 days north of 50˚N) than in the central subpolar North Pacific (10-30 days). The largest errors occurred in the Southern Ocean, south of 60˚S where the errors in bloom

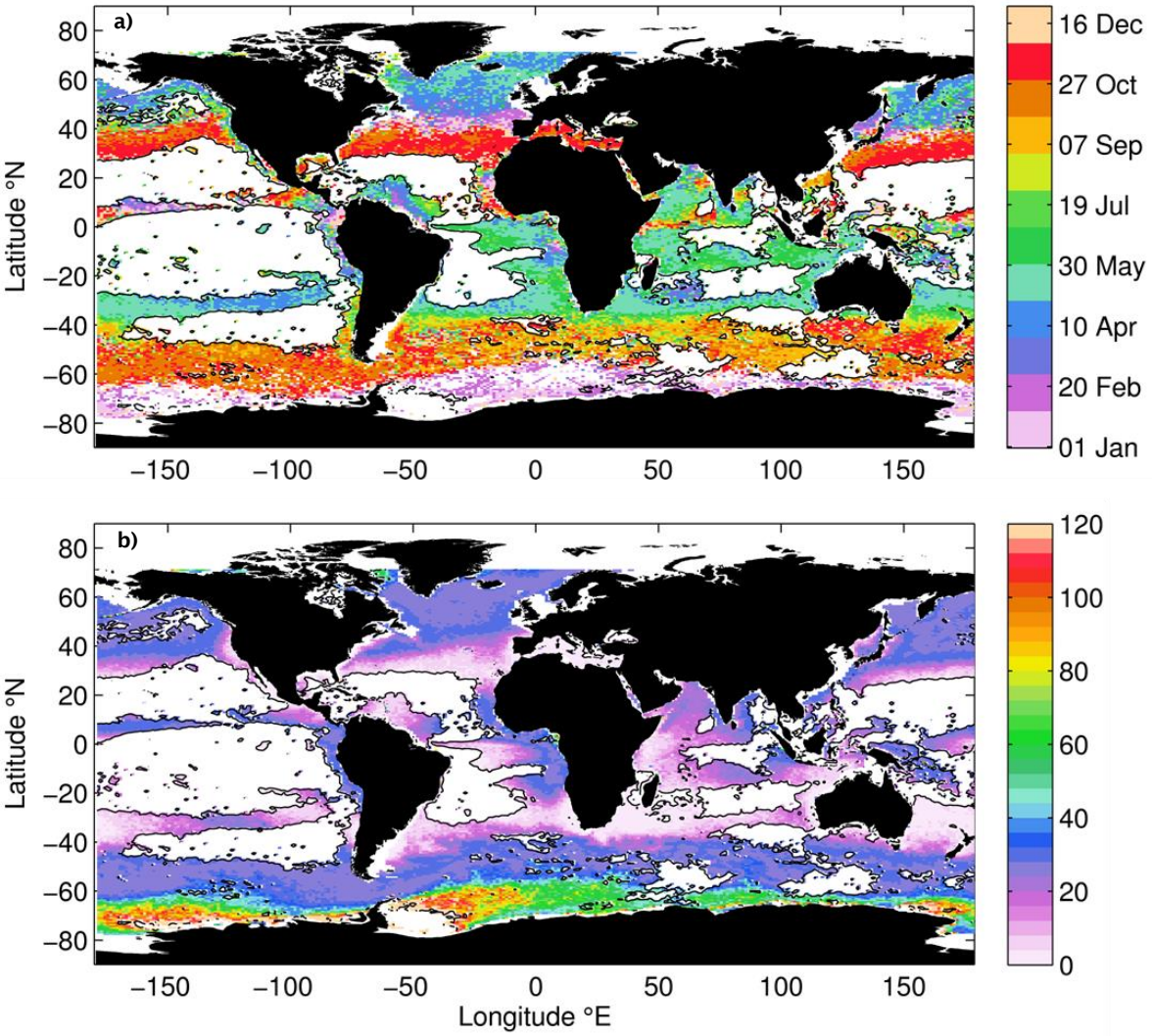

Figure 4.10: Maps of (a) mean bloom initiation date (2002–2006), (b) uncertainty in bloom initiation date calculated from equation (4.1) (days). White areas within the black contour do not display a distinct seasonal cycle whereas other white areas are regions of permanent ice cover.

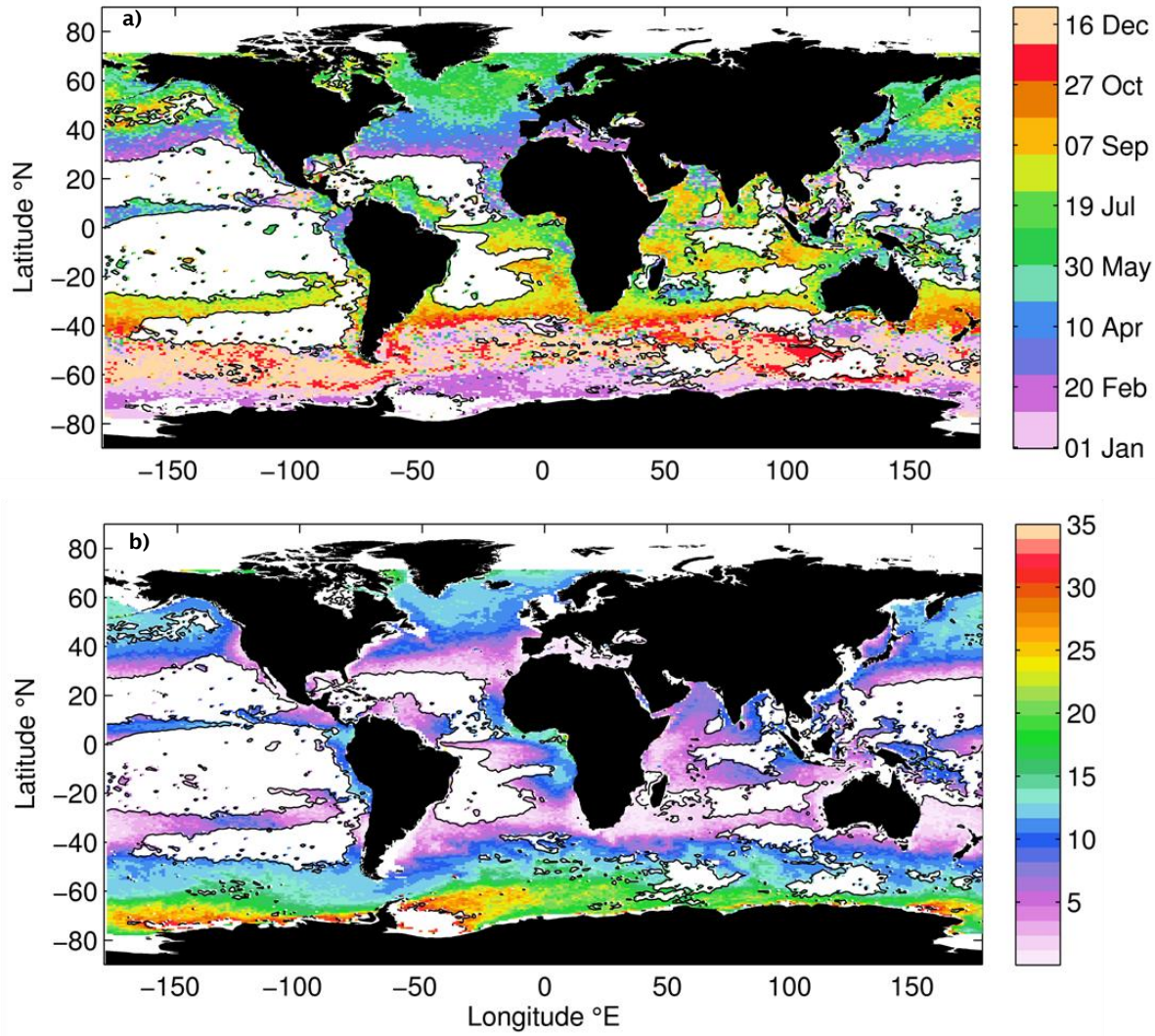

Figure 4.11: Maps of (a) mean bloom peak date (2002–2006), (b) uncertainty in bloom peak date calculated from equation (4.2) (days). White areas within the black contour do not display a distinct seasonal cycle whereas other white areas are regions of permanent ice cover.

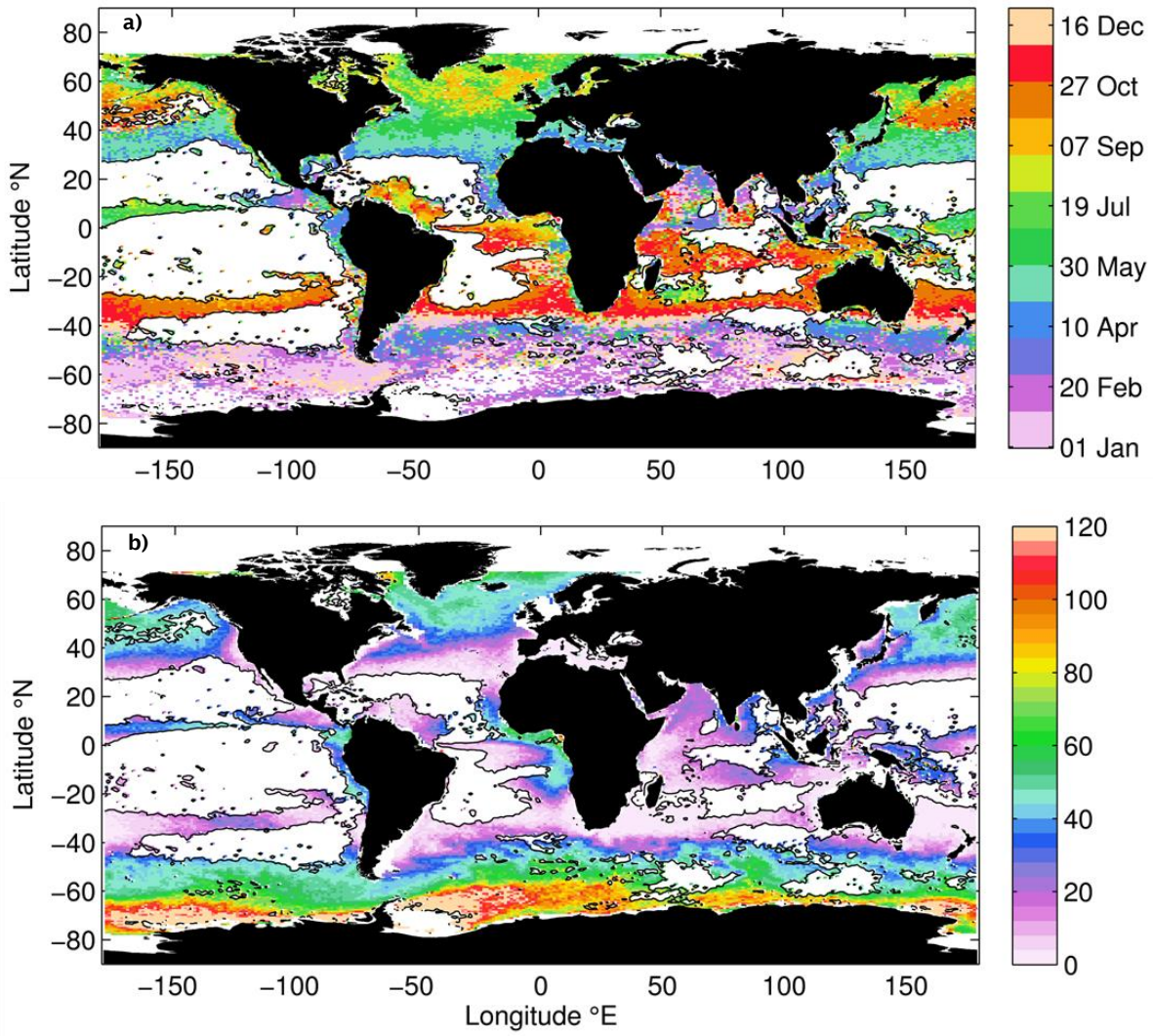

Figure 4.12: Maps of (a) mean bloom termination date (2002–2006), (b) uncertainty in bloom termination date calculated from equation (4.3) (days). White areas within the black contour do not display a distinct seasonal cycle whereas other white areas are regions of permanent ice cover.

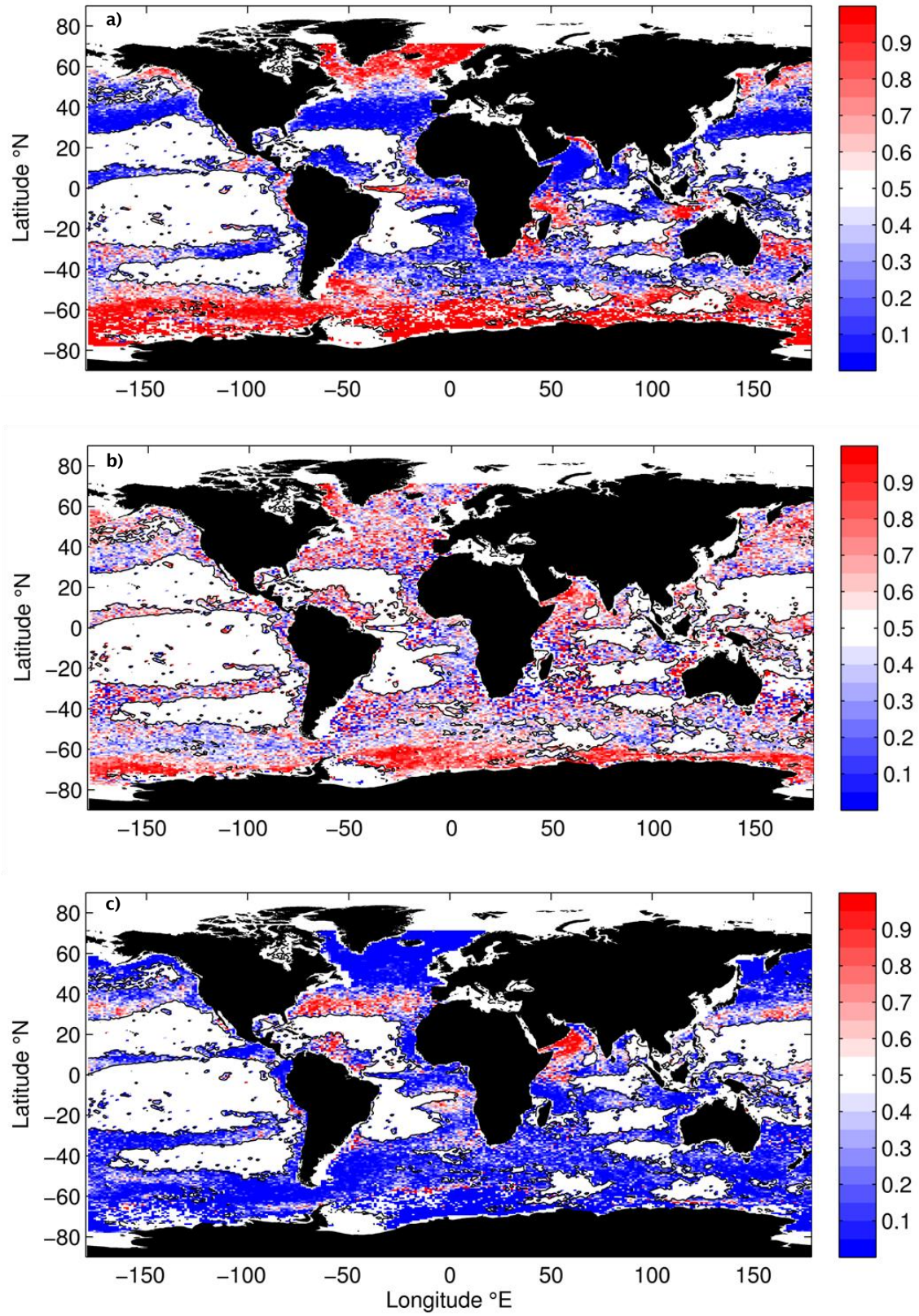

Figure 4.13: Maps of the probability that an error resulting from missing data is towards a date later than the true date for (a) bloom initiation, (b) bloom peak and (c) bloom termination. If probability is greater than 0.5 then the error is more likely to be toward a date later than the true date. If probability is less than 0.5 then the error is more likely to be toward a date earlier than the true date. White areas within the black contour do not display a distinct seasonal cycle whereas other white areas are regions of permanent ice cover.

initiation and termination dates were 3-4 months. Overall, the peak metric had smaller errors (~15 days) than the bloom initiation metric (~30 days) and bloom termination metric (~50 days).

Errors in estimating bloom metrics can be earlier or later than the true metric date. Given that an error has occurred the probability that an error is later is plotted in Figure 4.13. The direction of the error in bloom initiation date depends on latitude. Missing data in the subpolar regions (north of 50°N and south of 50°S) are more likely to result in the bloom start date identified from intermittent data being later than the true start date. At subtropical latitudes, this is reversed with the bloom initiation identified from intermittent data likely to be earlier than the true date.

The majority of ocean regions display a random pattern with no coherent patches where the errors in peak date are consistently earlier or later than the true date. Only the Southern Ocean stands out as a region where the peak date identified from intermittent data is consistently later than the actual date (Figure 4.13b).

For the majority of regions, missing data is more likely to result in a bloom termination date identified from intermittent data being earlier than the true termination date. Bloom termination dates are only more likely to be later in the Northern Hemisphere subtropical regions (Figure 4.13c). However, these regions are less coherent than the corresponding regions of "too early" errors for the bloom initiation dates (Figure 4.13a).

4.5 Discussion

4.5.1 Impact on Seasonality Metrics

The mean dates of bloom initiation, peak and termination (Figure 4.10a, 4.11a and 4.12a) are consistent with those reported by previous studies and exhibit a similar spatial pattern (Vargas *et al.*, 2009, Racault *et al.*, 2012, Sapiano *et al.*, 2012). However, missing data in chlorophyll time series are shown here to have a significant impact on the accuracy of seasonality metrics. The majority of heavily affected regions display uncertainty of approximately 30 days for the bloom initiation date, 12 days for the peak date and 50 days for the bloom termination. The reason for these differences lies in how the metrics are calculated.

The peak date is defined as the date of maximum chlorophyll concentration, and its accuracy depends on the presence of a data point on the date in question. If data are missing on that particular date then the next highest concentration is likely

to occur on a date very near the actual date. This is evident in Figure 4.13b which shows the error in bloom peak date is equally likely to be either earlier or later.

Conversely, the accuracy of the bloom initiation and termination metrics depends both on the presence of data on the date in question and on the accuracy of the threshold value used. The threshold value used here is 105% of the annual median and missing data in the time series results in the annual median being incorrectly estimated (Figure 4.14). This arises from the seasonality of missing data for example; if more data are missing during the winter months then the median-based threshold value will be biased toward the higher summer values. In the case of the subpolar bloom initiation date this means that the chlorophyll concentration exceeds the threshold later in the growing season. Conversely, for the subpolar bloom termination, a higher threshold value means that the chlorophyll concentration falls back below the threshold earlier in the growing season. This is highlighted in Figure 4.13 which shows that the errors in subpolar regions are more likely to be later than the true date for bloom initiation and earlier than the true date for the bloom termination. For this particular method of calculating the bloom initiation and termination date, the timing of missing data has a significant effect on the accuracy of the metric with further implications for the estimation of bloom duration.

Subtropical regions characterised as displaying a seasonal cycle are subject to either very small or zero errors for all metrics. Unlike subpolar regions these regions do not experience long gaps in the time series from low sun angle and persistent cloud cover though intermittent gaps do occur through short-term cloud cover and atmospheric aerosols. Consequently, errors are small as the small amount of missing data has a minor impact on the calculation of the seasonality metrics. In the Northern Hemisphere, just like subpolar regions missing data are most common during the local winter months. However, in subtropical regions this is when chlorophyll values are highest. This results in the threshold value being biased toward lower values (Figure 4.14). A reduction in the threshold value causes the threshold to be exceeded earlier, bringing bloom initiation earlier, and moving bloom termination later as chlorophyll concentration remain above the threshold for longer. As shown in Figure 4.13a, errors in the bloom initiation date in northern hemisphere subtropical regions are more likely to be toward an earlier date and towards a later date for bloom termination.

In the Southern Hemisphere subtropics, missing data are more common in the local summer months though the seasonal difference in missing data is smaller than in the Northern Hemisphere (Figures 4.2 and 4.3). However, the resulting change in the threshold value is small in these regions (Figure 4.14). From Figure

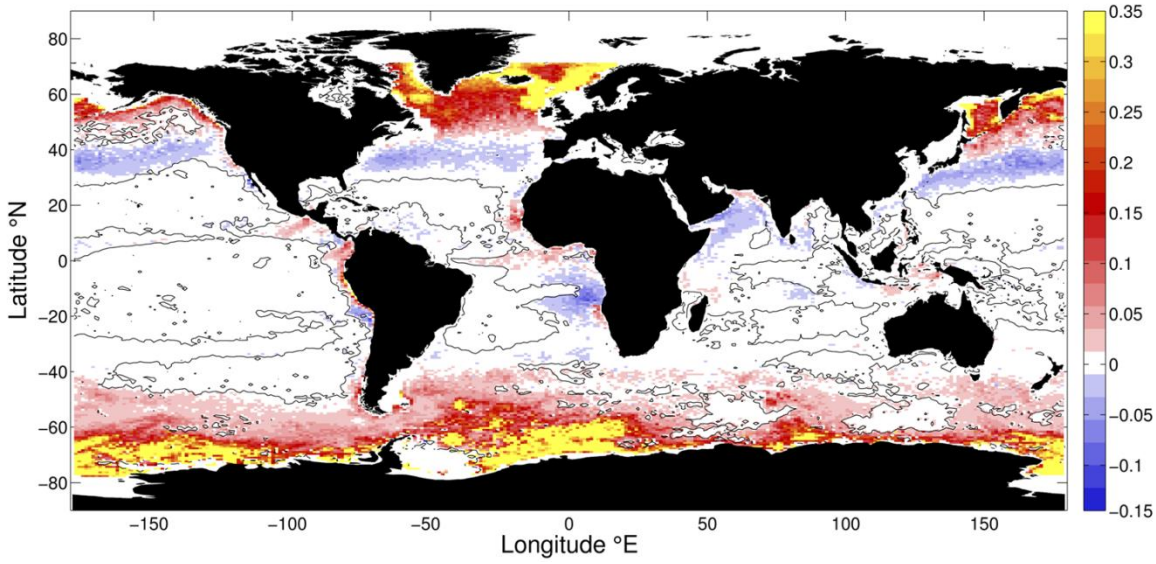

Figure 4.14: Difference between the threshold values calculated from the full NOBM chlorophyll time series and the subsampled NOBM time series (i.e. NOBM with the same quantity and timing of missing data as GlobColour). Positive values indicate that missing data increases the threshold value. The threshold value is used for defining bloom initiation and termination. White areas within the black contour do not display a distinct seasonal cycle whereas other white areas are regions of permanent ice cover.

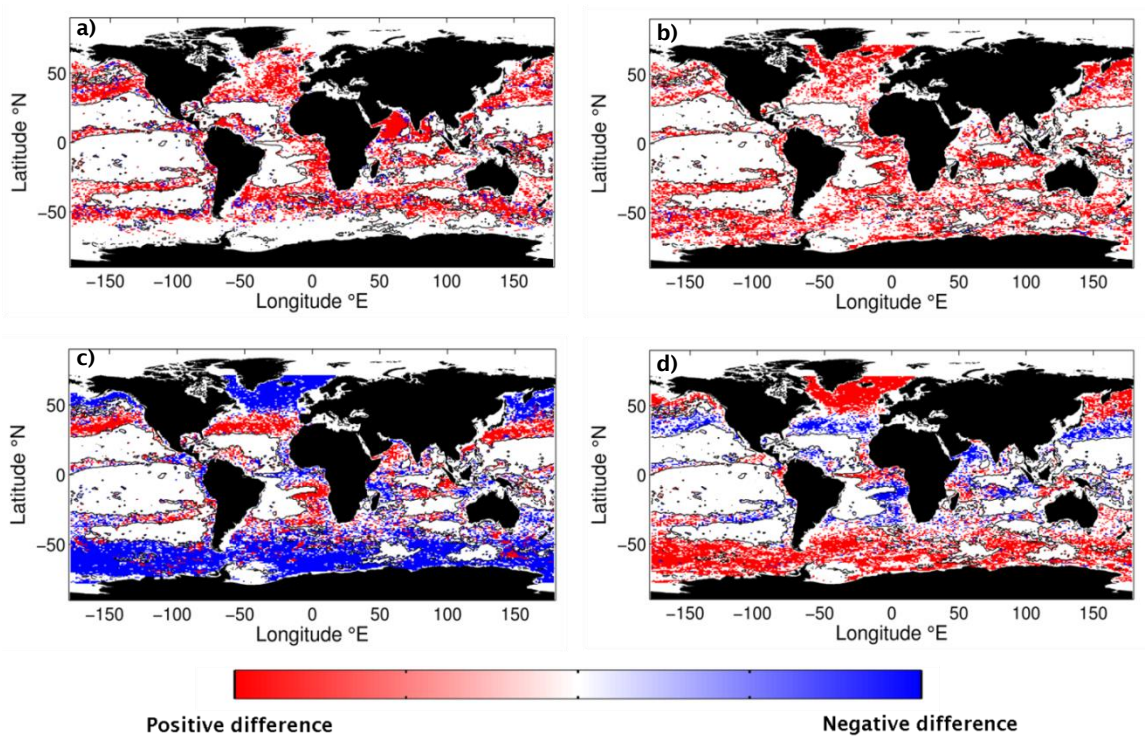

Figure 4.15: Maps showing the sign of the difference in the metric dates using the full NOBM dataset and an altered NOBM dataset for bloom initiation (a, c) and bloom termination (b, d). The altered NOBM datasets are altered by using the subsampled NOBM time series with the full NOBM dataset threshold values (a, b) or by using the full NOBM time series with the subsampled NOBM dataset threshold values (c, d). A positive value indicates the metric date became earlier whereas a negative value indicates the metric date became later. White areas within the black contour do not display a distinct seasonal cycle whereas other white areas are regions of permanent ice cover.

4.13, despite the small change in the threshold value, it can be seen that bloom initiation errors in the Southern Hemisphere subtropics are more likely to be towards an earlier date than the true date. However, unlike its Northern Hemisphere counterpart, the error in bloom termination is more likely to be towards an earlier date in the Southern Hemisphere subtropics. Thus, the same effect on the date of bloom initiation from missing data is seen in all subtropical regions though the exact mechanism seems to be different whereas, the effect on the termination dates is seen to differ between the Northern and Southern Hemisphere. This then calls into question the exact cause of the bloom initiation and termination date errors in subtropical regions and this is discussed next.

To investigate why the northern and southern subtropics behave differently, the bloom initiation and termination dates were calculated again using the original threshold value (i.e. the threshold value calculated from the full NOBM time series without gaps) but using the subsampled NOBM time series to find the metric dates. This tests the impact of the presence of gaps in the time series without the complication of an altered threshold value. A further set of metric dates were calculated using the altered threshold value (i.e. the threshold value calculated from the subsampled NOBM time series) and using the full NOBM time series without gaps. This tests the impact of an altered threshold value without the added complication of the presence of gaps in the time series.

The results of this show that the presence of gaps (without a change in the threshold value) made the bloom initiation date earlier than the true date over the majority of the global ocean (Figure 4.15a). The same is true for the bloom termination date (Figure 4.15b). However, a change in the threshold value (without gaps in the time series) resulted in later bloom initiation and earlier termination dates in subpolar regions and earlier initiation and later termination dates in the subtropics (Figure 4.15c and 4.15d). This confirms the earlier suggestion that in subpolar regions the pattern in the likelihood of a “too late” error in bloom initiation and a “too early” error in termination dates are driven by a change in the threshold value.

In subtropical regions, the bloom initiation date error is more likely to be a “too early” error and the results here suggest this arises from a combination of a change in the threshold and the presence of gaps (Figure 4.15a and 4.15c). For the bloom termination errors this explanation is also valid in the Northern Hemisphere subtropical regions where the high probability of “too late” errors results primarily from an altered threshold. However, in the southern hemisphere where the termination date errors are more likely to be “too early”, the change in the threshold

value appears to be small enough that the error from the presence of gaps dominates.

4.5.2 Implications

These results have implications for any studies using intermittent data to determine the timing of seasonal events. In the case of phytoplankton phenology, the missing data adds uncertainty to the estimation of seasonality metrics that may be mistaken for real interannual variability in bloom timing. Current research uses seasonality metrics as ecological indicators for assessing interannual variability and detecting trends through either natural or anthropogenic influences (Chiba *et al.*, 2008, Martinez *et al.*, 2011, Thomalla *et al.*, 2011, Racault *et al.*, 2012). However, trends may go undetected due to the noise that missing data add to the interannual variability of bloom timing. Furthermore, drivers of observed trends in bloom timing can only be attributed once trends in the quantity of missing data have been verified. The metrics are designed to enable quantitative comparison between different bloom regimes, but the uncertainty in the metrics varies spatially, making intercomparison of different regions difficult. The results here are particularly relevant to ongoing research into the relationship between bloom timing and the survival and recruitment of fish and invertebrates, specifically with regards to the match-mismatch hypothesis (Cushing, 1990, Platt *et al.*, 2003, Fuentes-Yaco *et al.*, 2007).

The uncertainty in bloom timing estimates must be smaller than the interannual variability for the interannual variability to be calculated with any certainty. Bloom timing studies so far have found that the bloom initiation and peak date are highly variable interannually relative to the errors calculated here. Reported variability can be compared to the mean errors presented here by calculating the mean difference in the NOBM and GlobColour dates across approximately the same study area. For example, in the California Current region the range in bloom initiation date varied from 1 to 3 months interannually (Henson and Thomas, 2007) with a mean error calculated here of ~21 days due to missing data. In the North Atlantic the range in bloom initiation date varied from 2-3 weeks up to 10 weeks in most subpolar regions (mean error of ~26 days), 5-6 weeks in the Irminger Basin (mean error of ~27 days) and up to 20 weeks in the subpolar-subtropical boundary region (mean error of ~24 days) (Henson *et al.*, 2006, Henson *et al.*, 2009). Similar spatial patterns have been described in the Southern Ocean with a typical standard deviation in bloom initiation timing of 24 days in subpolar regions (mean error of ~51 days) and 64-80 days in the subpolar-subtropical boundary region (mean error of ~19 days) (Thomalla *et al.*, 2011). The date of peak timing varied by 40 days in the Japan Sea (mean error of 7 days) (Yamada and

Ishizaka, 2006) and an advancement of 50 days in peak timing over 1997-2009 was reported in some regions of the Arctic Ocean (mean error of 16 days in Baffin Bay, the only region that overlapped spatially with this study where an advancement was reported) (Kahru *et al.*, 2011). Many studies have examined links between interannual variability in physical ocean processes and bloom timing to deepen our understanding of bloom dynamics (Edwards and Richardson, 2004, Chiba *et al.*, 2008, Sasaoka *et al.*, 2011, Racault *et al.*, 2012). This may not be possible in regions where the uncertainty in bloom timing is too great. At the time of writing, estimates of interannual variability in the date of bloom termination have not been reported.

Satellite observations are an ideal tool to expand the studies cited above over larger areas and the results shown here will enable researchers to calculate the uncertainty in bloom timing metrics. It also provides a useful tool for making objective decisions about the accuracy of interannual variability estimates. Furthermore, there is the potential to apply these results to *in situ* time series, where regular sampling is interrupted through poor weather or equipment failure. This is pertinent to any seasonal study that uses satellite or *in situ* data of any variable with gaps in the time series where the timing of an event is important. There are several other seasonality metrics that define the onset and decline of the bloom differently, in addition to metrics that quantify other phenological characteristics of phytoplankton blooms. The methodology used here provides a useful way to identify those metrics which are most insensitive to gaps and for developing methods to reduce the uncertainty in bloom timing. The results presented here suggest that one approach to compensate for the influence of missing data is to improve the estimate of the threshold value. Fundamentally, the method of metric calculation must be considered carefully to understand the influence that missing data may have on the accuracy of the results.

The results presented here have specific implications for the aims and objectives of the thesis. Firstly, the added uncertainty in the metric dates must be carefully considered when assessing interannual variability in bloom timing. This is especially relevant when investigating the physical drivers of variability as the required accuracy in bloom timing may not be met with the GlobColour dataset, especially where missing data is extensive. Secondly, when assessing climate change-driven trends a useful parameter to calculate is the number of years of continuous data needed to distinguish the trend over natural variability. Added noise in the bloom timing estimates implies that longer time series of data will be needed to detect a climate change-driven trend. As remote sensing of chlorophyll looks set to continue to be a primary tool for globally monitoring phytoplankton

dynamics this has significant implications for the timely detection of changes in pelagic ecosystems.

4.6 Summary

- Significant portions of the ocean colour record are heavily affected by missing data through cloud cover, sea ice, aerosols and low sun angle in winter. These missing data have a pronounced seasonality and the timing of missing data is found to be important for accurately estimating bloom timing.
- NOBM is used as a gap free dataset since the agreement in bloom timing between GlobColour and NOBM time series is high. When NOBM is subsampled on the dates when GlobColour values are missing the agreement between the bloom timing estimates improves.
- Substantial errors in bloom timing metrics can occur as a result of missing data. Errors in the metrics dates were regressed against the total annual percentage of missing data to derive equations giving the expected uncertainty on the bloom metric dates. Several polynomials were tested but a 3rd order polynomial gave the most acceptable fit for all three metrics.
- The expected uncertainty in the bloom metric dates was smaller in subtropical regions and larger in subpolar regions with the Southern Ocean having the largest errors. The error was generally less than 30 days for bloom initiation, 15 days for the peak and 50 days for bloom termination in most regions.
- The likelihood of these errors being either a “too late” error (i.e. missing data means a date later than the true date is identified as the metric date) or a “too early” error varied geographically and between metrics. The error in peak date showed no bias in direction.
- In subpolar regions, missing data in the time series were more likely to identify a bloom initiation date later than the true date. Conversely, missing data in the time series were more likely to identify a date earlier than the true date as the bloom termination date. The source of this error is the change in threshold value that defines the date of bloom initiation and termination. Missing data occur mostly in the winter causing the threshold value to be biased toward higher summer chlorophyll values.

5 Physical Drivers of Interannual Variability in Phytoplankton Phenology

Having developed a consistent method for estimating bloom timing, the metrics will now be used to investigate the physical drivers that may be responsible for interannual variability in bloom timing, for both subpolar and subtropical regions. Firstly, a range of likely physical drivers will be identified and the environmental conditions during bloom initiation, peak and termination will be examined. Then, relationships between the physical drivers and bloom timing metrics will be investigated through comparing latitudinal gradients and anomalies in timing. The conditions during bloom initiation are examined more closely to determine what process starts the subpolar spring bloom. This chapter concludes by considering what the results mean for bloom timing under climate change.

5.1 Introduction

The seasonal cycle in phytoplankton biomass is driven by variations in light and nutrient availability. Thus, it is believed that phytoplankton population growth is primarily driven by changes in the physical environment which, cause variations in the availability of these two resources through changes in mixing and stratification.

Several studies have investigated the link between variability in environmental conditions and phytoplankton blooms. Spatially, strong relationships were seen between the mean bloom period chlorophyll concentration and vertical mixing in the subpolar North Atlantic (Follows and Dutkiewicz, 2002). The variability in chlorophyll was closely related to variability in the buoyancy forcing driven by the net heat flux with regions of lower net heat flux also being regions of smaller blooms. In the subtropics this relationship was reversed with regions of stronger mixing having larger blooms since nutrient availability was increased. On an interannual basis, the subtropical variations in bloom period chlorophyll, and mixing had the same strong relationship, with years of higher mixing also having larger blooms. Conversely, there was no interannual relationship between mixing and bloom chlorophyll in the subpolar North Atlantic. Thus, on interannual timescales, while mixing is a good indicator for bloom magnitude in the subtropics, in subpolar regions other processes such as mesoscale variability or grazing may be

important for interannual variations in bloom chlorophyll (Follows and Dutkiewicz, 2002).

Further to this, a study of interannual variability in the subtropical North Atlantic concluded that annual mean stratification was a poor predictor for interannual variability in annual mean chlorophyll and integrated primary production (Lozier *et al.*, 2011). Similar results were found in a previous study in the subtropical North Pacific (Dave and Lozier, 2010). Extending the analysis to all permanently stratified regions revealed an absence of strong local correlations between stratification and chlorophyll in all regions except the western Equatorial Pacific (Dave and Lozier, 2013). In this region productivity and stratification are strongly driven by the El Niño-Southern Oscillation (ENSO). From this Dave and Lozier (2013) argue that the results of Behrenfeld *et al.* (2006), which found strong correlations between primary productivity and stratification across all permanently stratified regions, were dominated by the strong ENSO-driven relationship in the western equatorial Pacific. The conclusions of these studies suggest that the absence of a strong relationship may be because the variations in stratification on interannual timescales are not large enough to influence annual mean chlorophyll variability. Additionally, though stratification is a measure of resistance to overturning, wind or buoyancy forcing is still needed to actually overturn the water column. As a result the interannual variability in wind and buoyancy forcing may contribute more to chlorophyll variability as observed in the subtropical North Atlantic by Follows and Dutkiewicz (2002). Lozier *et al.* (2011) conclude by indicating that since changes in these variables all converge when the bloom starts and ends, it may be that stronger relationships are seen in the interannual variability in bloom timing. Thus, drivers of variability in bloom timing may reveal more about bloom dynamics and their relationship to variability in physical forcing than has currently been found from bloom magnitude.

Knowing the drivers of variability in bloom timing may improve predictions of primary production changes under global warming, and the potential impacts on food availability at higher trophic levels and on carbon export. The ocean response to climate change is expected to include stronger stratification of the water column which will occur earlier in the year and break down later (Sarmiento *et al.*, 2004). Based on this supposition, primary production in subpolar regions is expected to increase as the longer period of stratification extends the growing season with blooms starting earlier and ending later. In contrast, productivity in the subtropics is expected to decrease as nutrient limitation will be more severe and longer lasting. However, considering the results of Dave and Lozier (2010), Lozier *et al.* (2011) and Dave and Lozier (2013), changes in the timing of subtropical blooms may be more apparent than changes in the magnitude of primary production.

Thus, bloom timing metrics can be used as additional monitoring indicators to detect changes in the pelagic ecosystem (Platt *et al.*, 2009).

Previous studies have found the timing of the spring bloom to have relatively small variability with reported standard deviations in initiation date of ~10 days in the coastal western North Pacific (Chiba *et al.*, 2012), ~5 weeks in the subpolar western and eastern North Pacific (Sasaoka *et al.*, 2011), 2-4 weeks in the Southern Ocean (Thomalla *et al.*, 2011) and ranges of 2-3 weeks in the subpolar and subtropical North Atlantic gyres (Henson *et al.*, 2006, Henson *et al.*, 2009). Other regions were seen to be highly variable, especially boundary regions between subpolar and subtropical gyres. In these boundary regions, bloom initiation dates varied by ~20 weeks in the North Atlantic (Henson *et al.*, 2009) and had standard deviations of ~10 weeks in the Southern Ocean (Thomalla *et al.*, 2011). Large standard deviations (~10 weeks) in bloom timing were also associated with Southern Ocean fronts (Thomalla *et al.*, 2011). With respect to the drivers of bloom timing variability, several studies have identified various physical drivers. Most studies have found relationships between bloom timing variability and an annual, seasonal or bloom period mean in a physical parameter. The parameters identified include the winter mean net heat flux and wind speed (Henson *et al.*, 2006), bloom period wind speed (Ueyama and Monger, 2005) and the timing of sea ice melt (Kahru *et al.*, 2011). Additionally, bloom timing variability has been linked to large-scale climate indices such as the Pacific Decadal Oscillation (Sasaoka *et al.*, 2011, Chiba *et al.*, 2012) and the North Atlantic Oscillation (Henson *et al.*, 2009, Zhai *et al.*, 2013).

Naturally, studying the drivers of bloom timing variability may also lead to greater insight into the mechanisms that lead to the onset of the spring bloom. Currently, there are several theories as to what conditions cause the bloom to start in subpolar regions (see section 1.3 and 1.4.1 in Chapter 1 for further details on these theories). Briefly, the critical depth hypothesis states that the bloom starts when the mixed layer depth shoals to a point where the average irradiance in the mixed layer is high enough to alleviate light limitation (Sverdrup, 1953). The critical turbulence hypothesis is an extension of this and states that blooms may start when mixed layers are still very deep. Blooms can occur providing the rate of vertical mixing has reduced sufficiently that phytoplankton are no longer rapidly mixed out of the euphotic zone, and are able to accumulate in the near surface (Huisman *et al.*, 1999, Taylor and Ferrari, 2011). Another theory is the dilution-recoupling hypothesis which states that the bloom starts when the mixed layer is at its maximum depth, when phytoplankton and grazers are sufficiently diluted so encounter rates are minimal and growth can overcome losses (Behrenfeld, 2010, Boss and Behrenfeld, 2010). However, this hypothesis bases bloom initiation on the

specific growth rate of phytoplankton whereas a bloom is defined here as a significant rise in chlorophyll above background levels. On smaller spatial scales, mesoscale eddies have been observed to play a role in starting the spring bloom by restratifying the water column in spring, earlier and more quickly than by solar heating alone (Mahadevan *et al.*, 2012). The conditions needed for this mechanism are weak cooling (i.e. weakly negative net heat flux) and a drop in wind speed and/or change in wind direction which cause eddy-driven slumping of a north-south density gradient. However, the spatial resolution of the data used in this thesis is too coarse to fully resolve mesoscale eddies so this theory cannot be examined.

This chapter aims to quantify contemporary variability in bloom timing, both spatially and interannually, and to explore the drivers of interannual variability in bloom timing. Many of the studies discussed above focus on seasonal or annual means in parameters such as mixed layer depth, net heat flux or wind speed. Here, the focus will be on the relationships between variability in bloom timing and variability in the timing of a change in the physical environment (i.e. timing of MLD shoaling), to see if they lead to greater insight on the mechanisms that control bloom timing. Nevertheless, seasonal means in some physical parameters will be used to investigate the role of water column preconditioning on bloom development. Additional aims of this chapter are to ascertain if all aspects of bloom timing are driven by changes in the physical environment alone as well as identifying dominant drivers of bloom timing variability on basin scales.

5.2 Data and Methods

5.2.1 Bloom Timing Metrics

Bloom timing metrics (initiation, peak and termination) were calculated as described in Chapter 3 from both the GlobColour and NOBM chlorophyll datasets. Briefly, the initiation and termination date were defined as the dates on which the chlorophyll concentration exceeded or fell below a threshold value of 105% of the annual median. The peak date was defined as the date of maximum chlorophyll value. Analysis was performed on both datasets as the GlobColour dataset extends further towards the poles giving wider global coverage and spans more years (2002-2009) than NOBM (2002-2007). However, as seen from the results of Chapter 4 the accuracy of the metric dates from GlobColour are significantly affected by missing data in the chlorophyll time series. The largest differences between the results from the two datasets were seen in gap-driven interannual variability whereas spatial means were similar. Both bloom metric datasets were regridded to 1˚x1˚ grid to match the physical datasets. Interannual variability was

quantified by calculating the standard deviation in bloom metric dates. Anomalies in the metric dates were calculated at each pixel as a deviation from the long-term mean date (2002-2009 for GlobColour, 2002-2007 for NOBM). Both these measurements were made by taking into account the cyclic nature of the calendar (see section 3.2.3.3). Pixels without a strong seasonal cycle were excluded using a coefficient of variation (CV) value of 0.35 (this approach was also used in Chapter 4; see section 3.1.5 in Chapter 3 for more details on its development). The results reported were not seen to be sensitive to the choice of CV value (see Appendix D).

5.2.2 Physical Timing Metrics

The physical parameters used to calculate physical timing metrics were mixed layer depth (MLD), net heat flux (NHF) and mean mixed layer photosynthetically active radiation (PAR_{ML}). These datasets were available on a 1˚x1˚ grid with a temporal resolution of 8 days for NHF and PAR_{ML} and 7 days for the MLD. The differences in the way these datasets were calculated have implications for the results. The MLD dataset was derived non-synoptically from *in situ* profiles and thus are point measurements, whereas the NHF and surface PAR datasets are satellite-derived products, thus each data point is an areal average. Thus, the datasets are not "equal" in their relationship to the bloom timing metrics and so resulting correlations cannot be easily ranked against each other between datasets. These implications are also valid for the PAR_{ML} dataset as it incorporates the MLD data.

A suite of physical timing metrics were devised based on those used in previous studies (i.e. MLD shoaling or NHF becoming positive) or which an extant theory predicts should coincide with bloom initiation, peak and termination. The seasonal cycles of the physical parameters generally run from January to December in the Northern Hemisphere and July to June in the Southern Hemisphere. As a result the timing metrics were calculated from time series running either January to December or July to June depending on the hemisphere. This sometimes resulted in a discontinuity at the equator where there is strong 6-monthly variability rather than an annual cycle.

Since the drivers of bloom timing variability will be different in subpolar and subtropical regions, for the analysis it is necessary to separate the two regions. To do this the correlation between the chlorophyll and MLD climatological annual cycle at each pixel was used. Subpolar regions were negatively correlated (shallower MLD associated with higher chlorophyll) whereas subtropical regions were positively correlated (shallower MLD associated with lower chlorophyll). Regions poleward of the boundary line between positive and negative correlations were defined as

subpolar; regions equatorward of the boundary line were defined as subtropical. This does not account for interannual variability in the position of the boundary and so pixels in this region may actually have a subpolar-like response in chlorophyll one year and a subtropical-like response the next.

The resulting anomalies in physical timing metric dates were correlated with anomalies in bloom timing metric dates. Each ocean basin was split into a number of 30˚ longitude by 10˚ latitude boxes, for which interannual anomalies in the metric dates were calculated (Figure 5.1). These boxes were distributed centrally over each basin and situated to encompass areas that were expected to be homogenous in their bloom timing response to changes in the physical environment. The size of the boxes were chosen to be large enough to reduce variability on small scales but small enough to obtain a sufficient number of data points to reach statistical significance when calculating correlation coefficients (each box has 6 data points). For all basins the anomalies in bloom and physical metric dates were approximately normally distributed. Additionally, pixel-by-pixel correlations were made to investigate the spatial coherency of the relationships between the bloom timing and physical timing metrics. To do this, at each pixel, the surrounding pixels were included (i.e. a 3x3 pixel box) in the correlation to have enough data points to reach statistical significance. It is important to note that geophysical time series are usually subject to a high degree of autocorrelation which can result in inflated correlation coefficients (Racault *et al.*, 2012). However, the results can still be used qualitatively to distinguish relationships in interannual variability.

In addition to the metric date anomalies, basin mean time series were calculated for each parameter in each ocean basin. Furthermore, latitudinal means of the physical and bloom timing metrics were calculated between 45˚N/45˚S and the poles for subpolar basins and between 45˚S and 45˚N for subtropical basins.

5.2.2.1 Mixed Layer Depth

The MLD dataset was formed from using gridded temperature and salinity profiles obtained from the Coriolis project (http://www.coriolis.eu.org) (see Chapter 2 for more details). From the annual cycle of MLD there were four timing metrics of interest. These were the timing of maximum MLD, minimum MLD, MLD shoaling and MLD deepening (Figure 5.2). The maximum and minimum MLD dates were defined simply as the dates in each calendar year when the MLD reached its maximum (deepest) and minimum (shallowest) value. When the maximum or minimum MLD occurred for more than one time step the last date of MLD maximum and first date of MLD minimum was used. The maximum MLD date represents the transition from MLD deepening to MLD shoaling and the restratification of the water

column. The date on which the minimum MLD is first reached signifies the start of the sustained stratified summer period where the MLD remains relatively shallow for several weeks. The timing of MLD shoaling was defined as the date of greatest negative change in MLD (i.e. becoming shallower) which occurred between the maximum and minimum MLD dates. This metric represents the rapid restratification of the water column, associated with increases in mean mixed layer irradiance as well as the formation of a barrier to the deep water nutrient supply. Conversely, the timing of MLD deepening was defined as the date of greatest positive change in MLD (i.e. becoming deeper) which occurred after the minimum MLD date and before next year's maximum MLD date. This signifies the transition from highly stratified conditions to more turbulent conditions with greater mixing, entrainment of nutrients and decreasing light levels. Additionally, the mean winter MLD was calculated as the mean MLD during the months preceding the spring bloom. These months were January, February and March for the Northern Hemisphere and July, August and September for the Southern Hemisphere. These months also represent the period preceding subtropical bloom termination. This metric was used to investigate the effect of water column preconditioning on bloom timing as it is expected that years when the mixed layer reaches greater depths will be years when the bloom is delayed as the water column takes longer to restratify. Conversely, in the subtropics, greater winter MLD are expected to prolong the growing season by delaying bloom termination. With all of these MLD metrics it is expected that positive correlations will be seen with the bloom timing metrics. The expected result is that the later the MLD timing (or greater the mean winter MLD) the later the bloom initiation, peak and end timing will be in both subpolar and subtropical regions.

5.2.2.2 Net Heat Flux

The NHF dataset used here was obtained from the Wood Hole Oceanographic Institute OAflux project (http://oaflux.whoi.edu) (see Chapter 2 for more details). From the annual cycle of the NHF, three timing metrics were calculated (Figure 5.3). These were the date the NHF became positive, date of maximum NHF and the date the NHF became negative. The date on which the NHF became positive was defined as the date it first exceeds zero for at least 16 days (2 consecutive time steps) since the transition from negative to positive NHF is rarely smooth. This metric is a proxy for a change to less turbulent conditions with weak buoyancy forcing, reduced mixing rates and net warming of the ocean (Taylor and Ferrari, 2011). Similarly, the date the NHF becomes negative was defined by the NHF falling below zero for at least 16 days (two consecutive time steps). This signifies a return to net cooling of

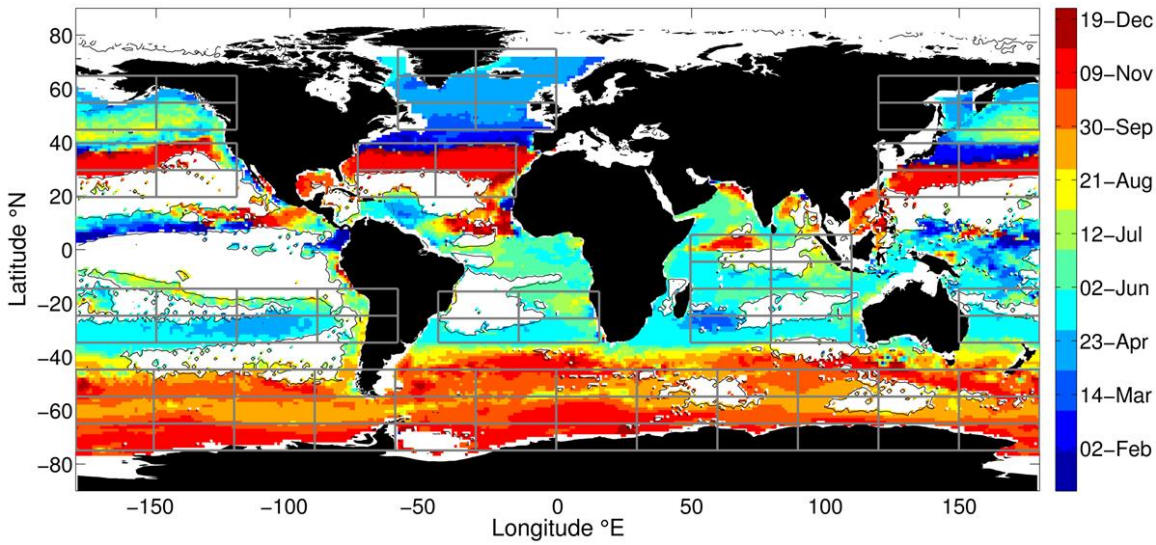

Figure 5.1: Map showing the regions where correlations in interannual variability were calculated. Each basin was split into boxes from which annual anomalies in bloom timing dates were calculated. Each box is 30˚ longitude by 10˚ latitude. Map is of mean bloom initiation date from GlobColour dataset (2002-2009). White regions bounded by the black contour are regions of low seasonality. Other white regions are areas of permanent sea ice cover.

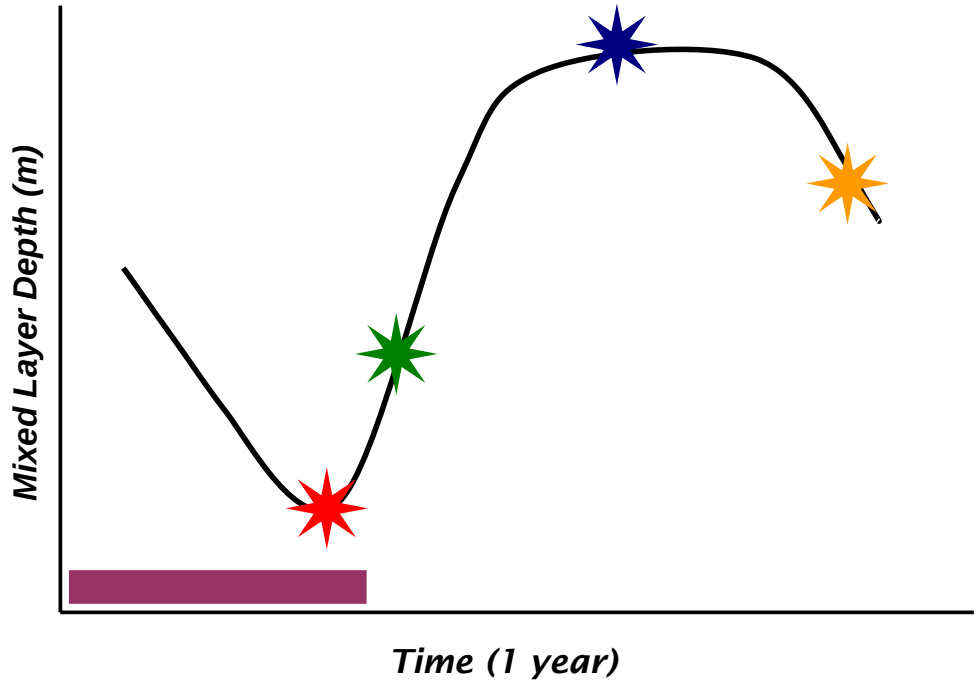

Figure 5.2: Cartoon of the annual cycle in mixed layer depth (MLD) to show the mixed layer depth timing metrics: maximum MLD (red), MLD shoaling (green), minimum MLD (blue), MLD deepening (yellow) and mean winter MLD (purple).

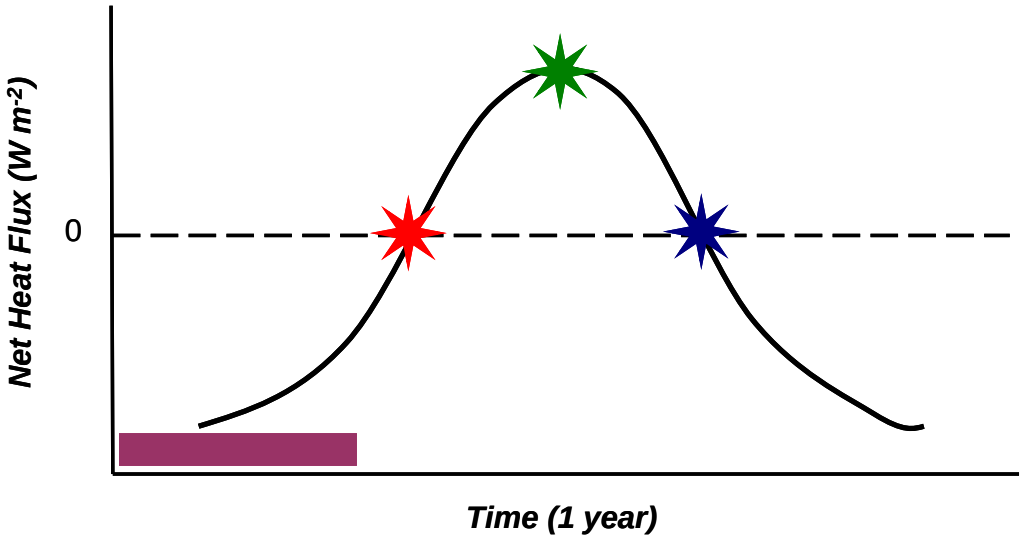

Figure 5.3: Cartoon of the annual cycle in net heat flux (NHF) to show the net heat flux timing metrics: NHF becomes positive (red), maximum NHF (green), NHF becomes negative (blue) and mean winter NHF (purple). Dotted line indicates zero line.

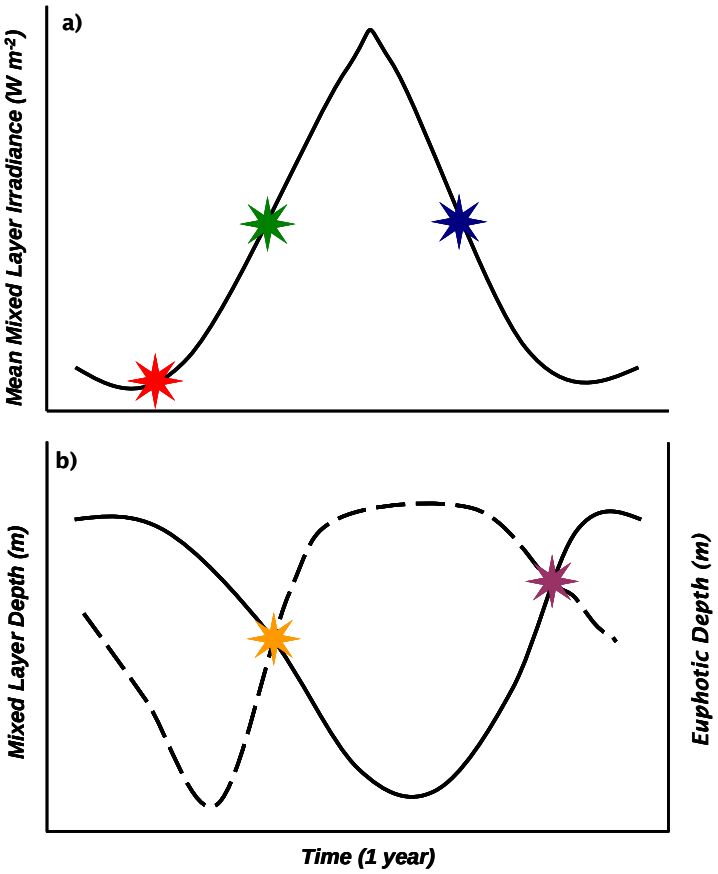

Figure 5.4: (a) Cartoon of the annual cycle in mixed layer mean PAR (PAR_{ML}) to show the PAR_{ML} timing metrics: PAR_{ML} starts to increase (red), fastest rise in PAR_{ML} (green) and fastest fall in PAR_{ML} (blue). (b) Cartoon of annual cycle in mixed layer depth (MLD) (dotted line) and euphotic depth (solid line) to show the timing metrics: MLD becoming shallower than (yellow) and deeper than (purple) the euphotic depth.

the ocean and is a proxy for an increase in turbulence and mixing rates. The date of maximum NHF was simply defined as the date the NHF first reached its cycle and the maximum PAR_{ML} maximum value signifying the period when warming was greatest. As with the MLD, the mean winter NHF was also calculated to quantify the amount of cooling occurring over the winter. This was identified as a good predictor of bloom initiation date when combined with the mean winter wind speed through preconditioning of the water column (Henson *et al.*, 2006) . The three NHF timing metrics are expected to be positively correlated with the bloom timing metrics such that a later NHF metric date results in a later bloom metric date in both subpolar and subtropical regions. However, the mean winter NHF is expected to be negatively correlated with bloom timing as winters with greater cooling (more negative) are expected to result in later subpolar bloom initiation dates and later subtropical termination dates.

5.2.2.3 Mixed Layer Mean PAR

The PAR_{ML} was calculated using datasets of MLD, attenuation coefficient (http://www.globcolour.info) and surface PAR (http://oceancolor.gsfc.nasa.gov) (see Chapter 2 for further details) The dates of interest from the annual cycle of PAR_{ML} include the date PAR_{ML} starts to increase, the date of fastest rise and the date of fastest fall in PAR_{ML} (Figure 5.4). The date on which the PAR_{ML} started to increase was defined as the date the gradient in PAR_{ML} between the beginning of the annual cycle and the maximum PAR_{ML} value became positive. This metric indicates the period when light conditions are beginning to become more favourable for growth. This coincided closely with the timing of maximum MLD indicating that the shoaling of the MLD is the dominant factor that influences PAR_{ML} at this time rather than changes in surface irradiance. The date of fastest rise in PAR_{ML} was calculated by finding the date of greatest increase in PAR_{ML} between the beginning of the annual cycle and the maximum PAR_{ML} value. Equally, the date of fastest fall in PAR_{ML} was estimated by finding the date of greatest PAR_{ML} decrease between the PAR_{ML} maximum and the end of the annual cycle. These two metrics represent the period when PAR_{ML} is rapidly increasing and becoming less limiting or rapidly decreasing and becoming more limiting. Additionally, the depth of the euphotic zone, defined as the depth at which 1% of the surface PAR still remained, was calculated. From this the date the MLD becomes shallower than the euphotic zone (abbreviated as MLD<Zeu) and then deeper again (abbreviated as MLD>Zeu) were also calculated to serve as a proxy for the MLD crossing the critical depth and light levels ceasing to be limiting. These two metrics again stipulated that the MLD had to surpass the euphotic depth for at least 16 days. As with the NHF and MLD metrics, positive

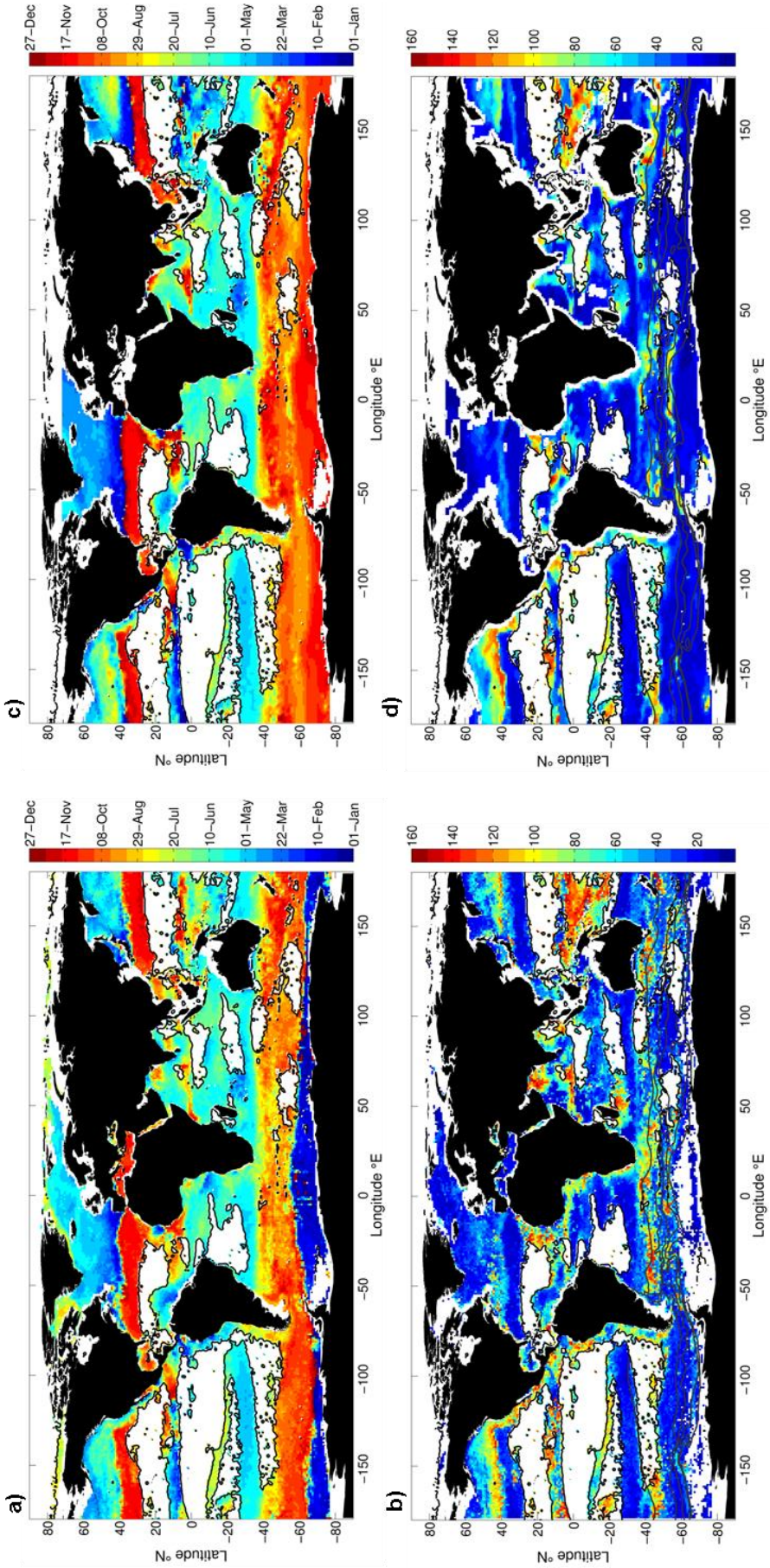

Figure 5.5: Maps showing the mean date of bloom initiation from (a) GlobColour (2002-2009), (c) NOBM (2002-2007) and the standard deviation (in days) from (b) GlobColour and (d) NOBM. White areas bounded by a black contour line are regions that do not display a strong seasonal cycle. Other white regions are either regions of permanent sea ice or are classed as the continental shelf (<200m deep). Grey lines in the Southern Ocean mark the mean position of the subtropical front, subantarctic front, polar front, southern Antarctic Circumpolar Current (ACC) front and the southern ACC boundary front. Mean frontal positions were obtained from http://woceatlas.tamu.edu.

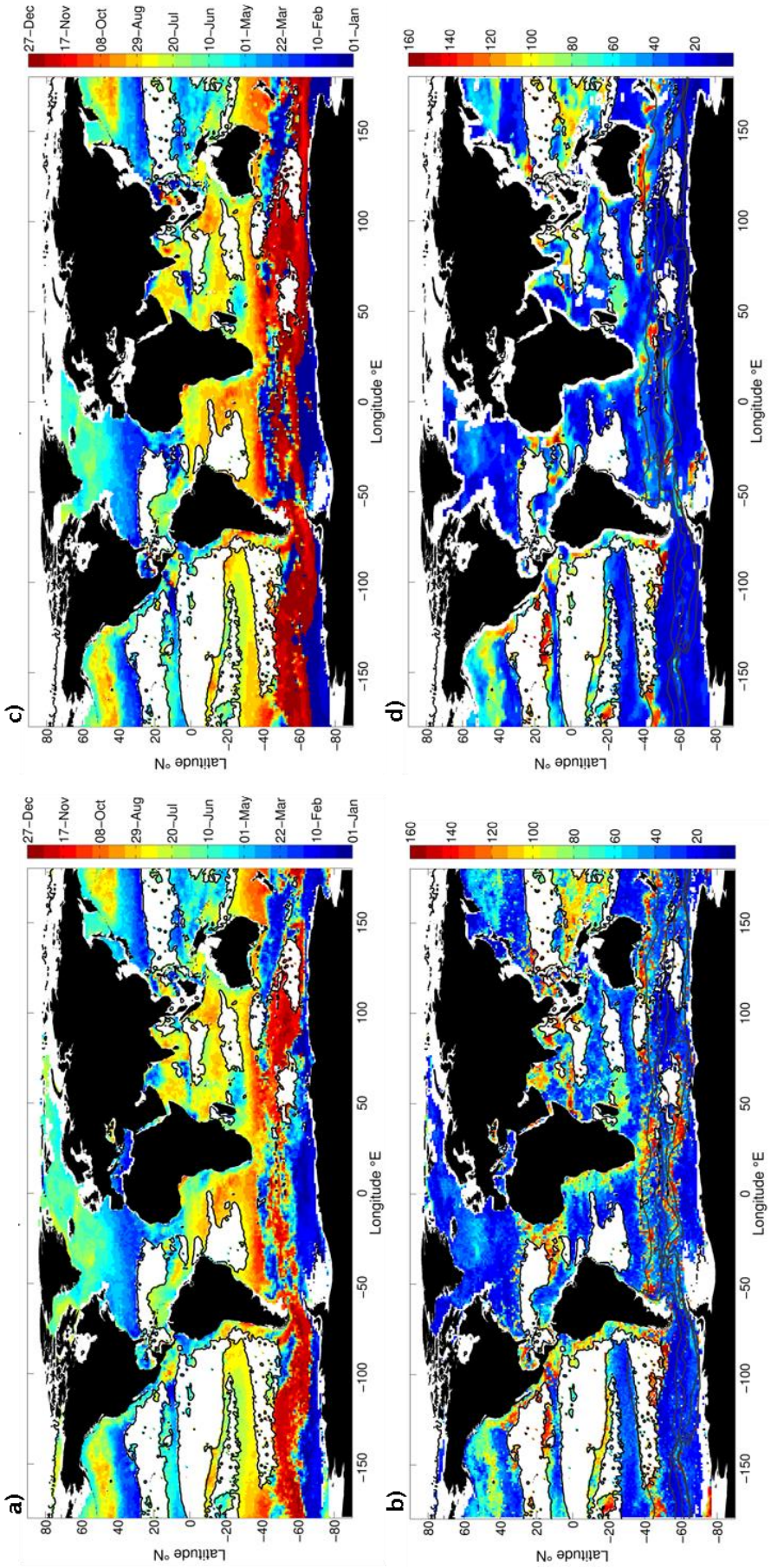

Figure 5.6: Maps showing the mean date of bloom peak from (a) GlobColour (2002-2009), (c) NOBM (2002-2007) and the standard deviation (in days) from (b) GlobColour and (d) NOBM. White areas bounded by a black contour line are regions that do not display a strong seasonal cycle. Other white regions are either regions of permanent sea ice or are classed as the continental shelf (<200m deep). Grey lines in the Southern Ocean mark the mean position of the subtropical front, subantarctic front, polar front, southern Antarctic Circumpolar Current (ACC) front and the southern ACC boundary front. Mean frontal positions were obtained from http://woceatlas.tamu.edu.

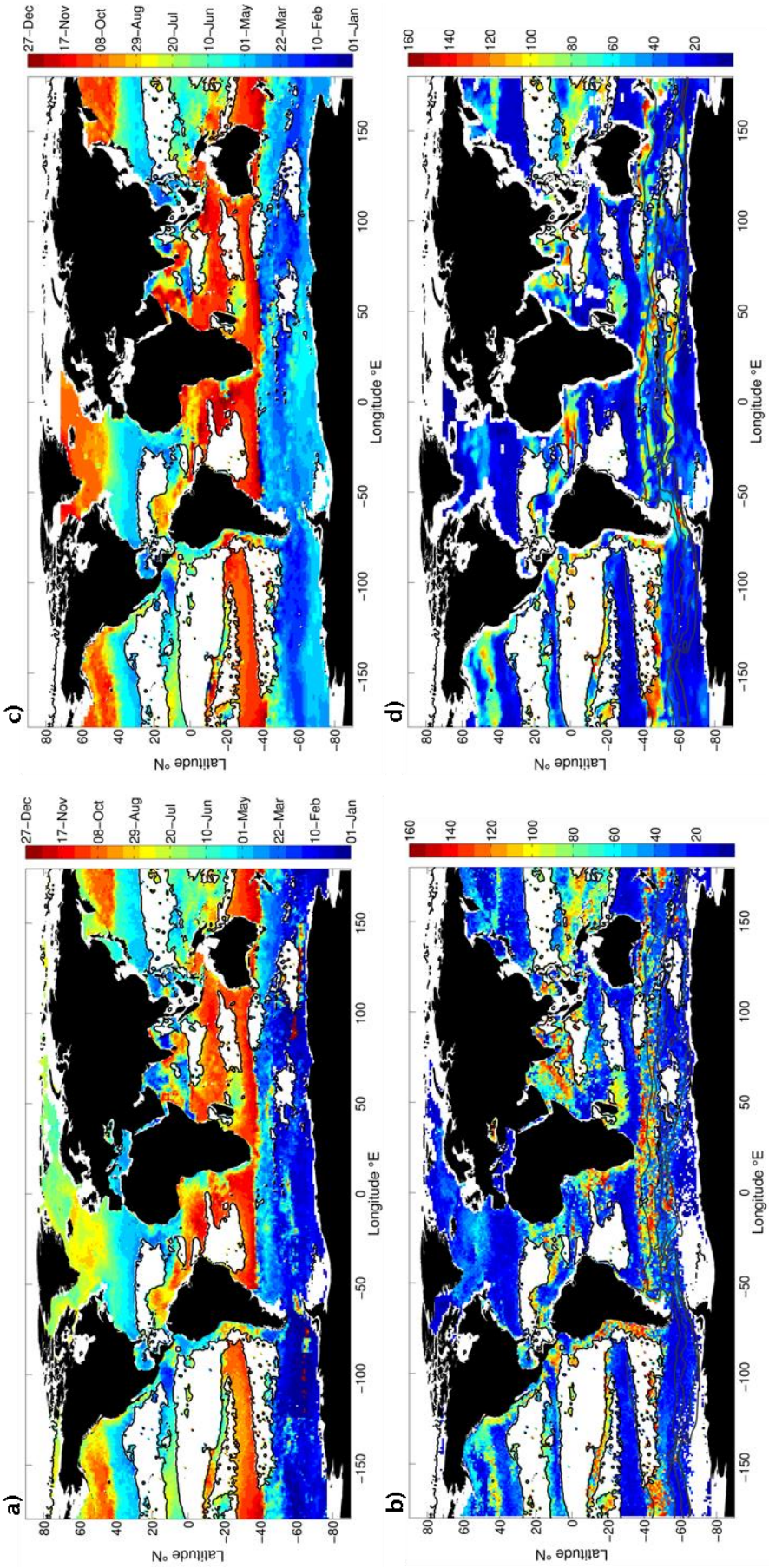

Figure 5.7: Maps showing the mean date of bloom termination from (a) GlobColour (2002-2009), (c) NOBM (2002-2007) and the standard deviation (in days) from (b) GlobColour and (d) NOBM. White areas bounded by a black contour line are regions that do not display a strong seasonal cycle. Other white regions are either regions of permanent sea ice or are classed as the continental shelf (<200m deep). Grey lines in the Southern Ocean mark the mean position of the subtropical front, subantarctic front, polar front, southern Antarctic Circumpolar Current (ACC) front and the southern ACC boundary front. Mean frontal positions were obtained from http://woceatlas.tamu.edu.

correlations are expected between the PAR_{ML} timing metrics and the bloom timing metrics.

5.3 Results

5.3.1 Interannual Variability in Phenology

A similar spatial pattern in the interannual variability was seen in all the bloom timing metrics for both GlobColour and NOBM (Figures 5.5, 5.6 and 5.7). The highest interannual variability (bloom initiation ~60-140 days, peak ~80-140 days, bloom termination ~80-140 days) was generally found at the subpolar-subtropical boundaries, in association with fronts in the Southern Ocean as well as upwelling and equatorial regions. This relatively high variability is congruent with previous studies in the North Atlantic and Southern Ocean (Henson *et al.*, 2009, Thomalla *et al.*, 2011). The interannual variability was much smaller in the centre of subpolar and subtropical gyres for all metrics (standard deviation of ~16-48 days). Furthermore, regions of low and high interannual variability were broadly similar in location in all three metrics.

5.3.2 Subpolar Regions

5.3.2.1 Spatial Relationships

Average time series from the North Atlantic (45:80˚N, -60-0˚E), North Pacific (50:70˚N, -120-120˚E) and Southern Ocean (-80:-50˚N, -180:180˚E) show the degree to which the timing of bloom and physical metrics coincide (Figures 5.8, 5.9 and 5.10). The timing of bloom initiation occurred when the NHF was ~zero, the MLD was shoaling and the PAR_{ML} was increasing in all three basins except for the Southern Ocean, where the MLD was at its maximum rather than shoaling. The timing of the peak was associated with the NHF and PAR_{ML} approaching or being at its maximum and the MLD reaching its minimum in all three basins. The conditions at bloom termination varied more between the three basins than for bloom initiation and peak timing. In the North Atlantic, the end of the bloom was seen to be concurrent with decreases in NHF, minimum MLD and maximum PAR_{ML}. In the North Pacific, it was associated with deepening MLD and falling PAR_{ML} values and with maximum NHF values in the Southern Ocean.

Similar results were seen when using bloom timing results from NOBM. However, some differences did occur when using NOBM dates, mostly with the timing of bloom termination which was slightly later when using NOBM (Figure 5.7). From the NOBM bloom timing metrics, in the North Atlantic, the peak coincided

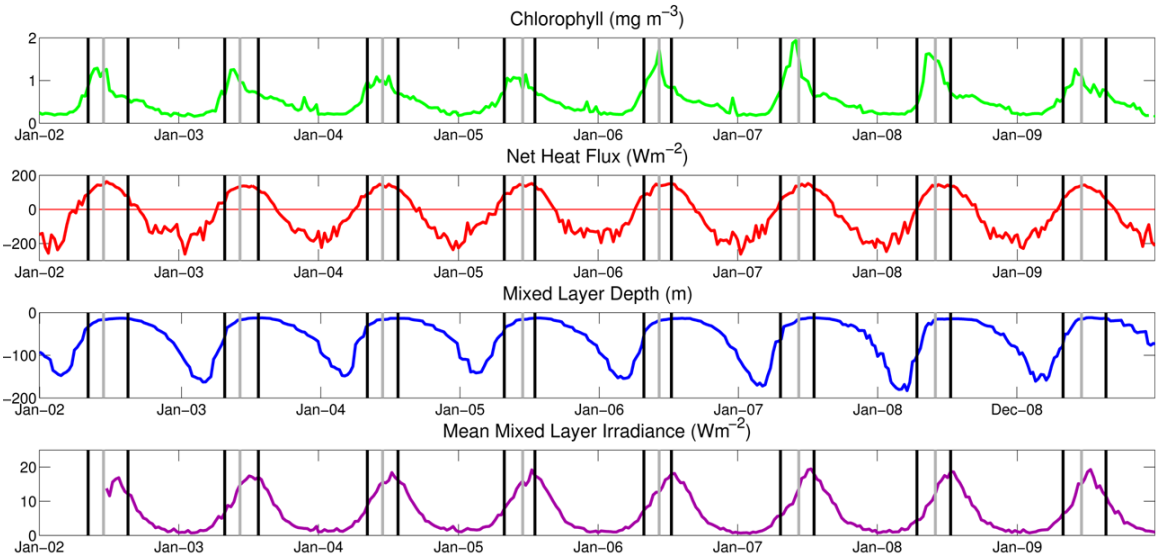

Figure 5.8: Mean time series (2002-2009) across the North Atlantic for GlobColour chlorophyll (mg m^{-3}), net heat flux (W m^{-2}), mixed layer depth (m) and mean mixed layer irradiance (W m^{-2}). The grey vertical line represents the mean bloom peak date in that year, the black vertical line preceding it is the mean bloom initiation date and the black vertical line following the peak is the mean bloom termination date. The mean bloom timing dates are calculated from averaging the metric dates in each year across the basin (i.e. they are not calculated from the chlorophyll time series above). The grey peak lines do not always line up with the maximum chlorophyll concentration in the time series due to variability in the magnitude of the peak concentrations. Thus, the timing of the maximum concentrations in the chlorophyll time series above is biased towards the largest blooms whereas the grey lines are not.

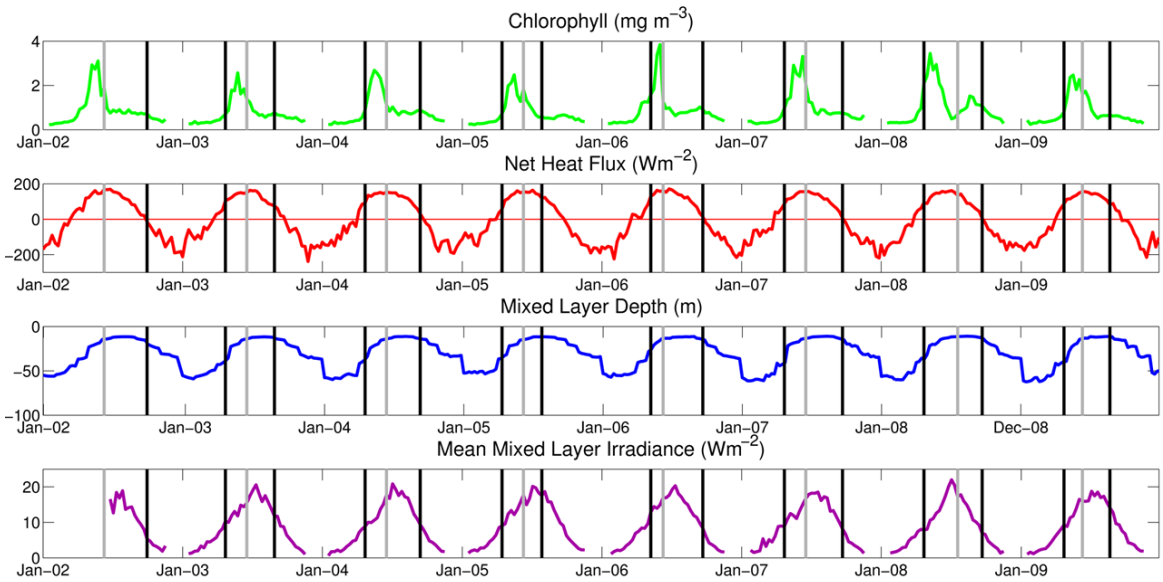

Figure 5.9: Mean time series (2002-2009) across the North Pacific for GlobColour chlorophyll (mg m^{-3}), net heat flux (W m^{-2}), mixed layer depth (m) and mean mixed layer irradiance (W m^{-2}). The grey vertical line represents the mean bloom peak date in that year, the black vertical line preceding it is the mean bloom initiation date and the black vertical line following the peak is the mean bloom termination date. The mean bloom timing dates are calculated from averaging the metric dates in each year across the basin (i.e. they are not calculated from the chlorophyll time series above). The grey peak lines do not always line up with the maximum chlorophyll concentration in the time series due to variability in the magnitude of the peak concentrations. Thus, the timing of the maximum concentrations in the chlorophyll time series above is biased towards the largest blooms whereas the grey lines are not.

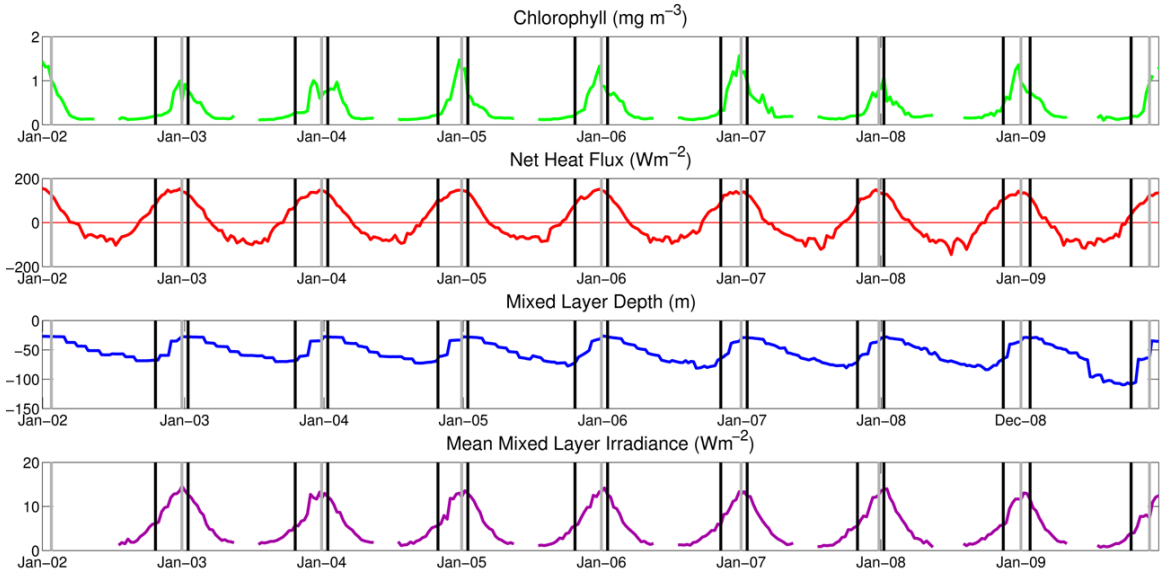

Figure 5.10: Mean time series (2002-2009) across the Southern Ocean for GlobColour chlorophyll (mg m^{-3}), net heat flux (W m^{-2}), mixed layer depth (m) and mean mixed layer irradiance (W m^{-2}). The grey vertical line represents the mean bloom peak date in that year, the black vertical line preceding it is the mean bloom initiation date and the black vertical line following the peak is the mean bloom termination date. The mean bloom timing dates are calculated from averaging the metric dates in each year across the basin (i.e. they are not calculated from the chlorophyll time series above). The grey peak lines do not always line up with the maximum chlorophyll concentration in the time series due to variability in the magnitude of the peak concentrations. Thus, the timing of the maximum concentrations in the chlorophyll time series above is biased towards the largest blooms whereas the grey lines are not.

with the rising limb of PAR_{ML} rather than the maximum in PAR_{ML}. Moreover, in the North Atlantic and Southern Oceans the bloom terminated when NHF became negative, the MLD was deepening and PAR_{ML} values were falling when using NOBM bloom timing dates.

Turning to the variability in the time series of the physical parameters (NHF, MLD and PAR_{ML}) there were obvious differences between the three basins. The NHF was fairly similar between the three basins ranging from -200 W m^{-2} to 200 W m^{-2}. The largest differences were seen in the maximum depth the mixed layer reached. In the North Atlantic the maximum MLD varied between 150 and 200 m (though the standard deviation was 276 m), was ~50 m (standard deviation = 17 m) at its deepest in the North Pacific and ~110 m (standard deviation = 147 m) in the Southern Ocean. The PAR_{ML} was highest in the North Pacific (~23 W m^{-2}) though this was reasonably similar to values in the North Atlantic (~20 W m^{-2}) and Southern Ocean (~15 W m^{-2}).

If a physical timing event is a driver of variability in bloom timing then it is expected that the two metrics will occur at similar times and have similar latitudinal gradients. The coincident timing of the physical and bloom timing metrics was demonstrated in Figure 5.11, 5.12 and 5.13. From this, the bloom initiation was seen to have a similar timing and latitudinal gradient to most of the physical timing metrics (NHF turning positive, MLD shoaling, MLD becoming shallower than the euphotic depth, fastest rise in PAR_{ML} and PAR_{ML} starting to rise) though not consistently between basins. Most of these physical metrics were strongly correlated over latitude with the bloom initiation date and travelled poleward at similar speeds (Table 5.1). In particular, the NHF turning positive in the North Atlantic, North Pacific and Southern Ocean was strongly correlated (0.95, 0.90 and 0.99) and had similar latitudinal speeds to bloom initiation (North Atlantic: bloom initiation = 5.72 km day^{-1}, NHF turning positive = 6.72 km day^{-1}, North Pacific: bloom initiation = 2.76 km day^{-1}, NHF turning positive = 2.29 km day^{-1}, Southern Ocean: bloom initiation = 2.83 km day^{-1}, NHF turning positive = 2.58 km day^{-1}). Additionally, the date that PAR_{ML} started to rise covaried strongly with the bloom initiation date in all basins (correlation coefficients: 0.87, 0.83 and 0.97 and latitudinal speeds: 7.29, 3.63 and 2.93 km day^{-1} for North Atlantic, Pacific and Southern Ocean respectively). Strong relationships were also seen between the date of bloom initiation and the date the MLD became shallower than the euphotic depth and the date of fastest rise in PAR_{ML} in both the North Pacific and Southern Ocean, and the date of maximum MLD in the Southern Ocean.

Latitudinal relationships between the physical timing metrics and bloom peak timing were much weaker and generally were not statistically significant at the 95%

Table 5.1: Correlation coefficients and latitudinal speeds for bloom initiation and associated physical timing metrics in the subpolar basins for both GlobColour and NOBM chlorophyll datasets

			Bloom initiation	NHF positive	MLD max	MLD shoaling	MLD<Zeu[a]	Fastest rise in PAR_{ML}	PAR_{ML} starts to increase
North Atlantic	GlobColour	Correlation coefficient[b]		0.95*	0.72*	0.77*	0.67*	0.59*	0.87*
		Latitudinal speed (km day^{-1})[c]	5.72	6.72	13.37	11.88	3.99	5.05	7.29
	NOBM	Correlation coefficient[b]		0.51*	0.19	0.44*	0.73*	-0.45*	0.65*
		Latitudinal speed (km day^{-1})[c]	7.54	8.03	13.24	11.97	3.96	4.37	6.89
North Pacific	GlobColour	Correlation coefficient[b]		0.90*	0.93*	0.69*	0.88*	0.89*	0.83*
		Latitudinal speed (km day^{-1})[c]	2.76	2.29	4.67	2.95	2.07	4.24	3.63
	NOBM	Correlation coefficient[b]		-0.76*	0.65*	0.80*	0.97*	-0.88*	-0.94*
		Latitudinal speed (km day^{-1})[c]	-2.30	2.26	4.93	3.01	1.87	3.93	3.26
Southern Ocean	GlobColour	Correlation coefficient[b]		0.99*	0.89*	0.72*	0.90*	0.97*	0.97*
		Latitudinal speed (km day^{-1})[c]	2.83	2.58	2.45	8.02	4.16	5.92	2.93
	NOBM	Correlation coefficient[b]		0.73*	0.48*	0.55*	0.42*	0.77*	0.66*
		Latitudinal speed (km day^{-1})[c]	6.92	2.60	2.46	8.41	3.77	5.75	2.81

[a] MLD<Zeu stands for the date the MLD becomes shallower than the euphotic depth.

[b] A * indicates correlation coefficients which are statistically significant at the 95% confidence interval. Correlations were calculated between the bloom initiation latitudinal mean date and the physical metric latitudinal mean date. Mean dates were calculated over the years 2002-2009 for GlobColour data and 2002-2007 for NOBM data.

[c] Latitudinal speeds were calculated by regressing the metric dates on latitude (latitude = a+ b*date) and then multiplying the linear coefficient (b) by 111.19493 km/°latitude.

Table 5.2: Correlation coefficients and latitudinal speeds for bloom peak and associated physical timing metrics in the subpolar basins for both GlobColour and NOBM chlorophyll datasets

			Bloom peak	NHF positive	MLD min	NHF max
North Atlantic	GlobColour	Correlation coefficient[a]		0.10	-0.01	-0.25
		Latitudinal speed (km day^{-1})[b]	4.56	6.72	3.80	7.98
	NOBM	Correlation coefficient[a]		0.26	-0.11	-0.59*
		Latitudinal speed (km day^{-1})[b]	3.99	8.03	-12.17	8.98
North Pacific	GlobColour	Correlation coefficient[a]		0.10	0.33	0.25
		Latitudinal speed (km day^{-1})[b]	-0.65	2.29	-12.11	6.46
	NOBM	Correlation coefficient[a]		-0.81*	0.90*	-0.25
		Latitudinal speed (km day^{-1})[b]	-2.16	2.26	-11.06	6.09
Southern Ocean	GlobColour	Correlation coefficient[a]		0.95*	0.46*	0.90*
		Latitudinal speed (km day^{-1})[b]	4.08	2.58	9.81	10.28
	NOBM	Correlation coefficient[a]		0.81*	0.59*	0.91*
		Latitudinal speed (km day^{-1})[b]	6.42	2.60	10.30	10.62

[a] A * indicates correlation coefficients which are statistically significant at the 95% confidence interval. Correlations were calculated between the bloom peak latitudinal mean date and the physical metric latitudinal mean date. Mean dates were calculated over the years 2002-2009 for GlobColour data and 2002-2007 for NOBM data.

[b] Latitudinal speeds were calculated by regressing the metric dates on latitude (latitude = a+ b*date) and then multiplying the linear coefficient (b) by 111.19493 km/°latitude.

Table 5.3: Correlation coefficients and latitudinal speeds for bloom termination and associated physical timing metrics in the subpolar basins for both GlobColour and NOBM chlorophyll datasets

			Bloom termination	NHF negative	MLD min	MLD deepening	NHF max	MLD>Zeu[a]	Fastest fall in PAR_{ML}
North Atlantic	GlobColour	Correlation coefficient[b]		0.35*	-0.42*	0.49*	-0.03	0.32	0.16
		Latitudinal speed (km day^{-1})[c]	-6.35	-20.38	3.80	-8.58	7.98	-6.01	-13.51
	NOBM	Correlation coefficient[b]		-0.69*	-0.59*	-0.71*	-0.03	-0.89*	-0.73*
		Latitudinal speed (km day^{-1})[c]	4.24	-18.27	-12.17	-7.88	8.98	-5.86	-12.94
North Pacific	GlobColour	Correlation coefficient[b]		0.83*	0.71*	0.42*	-0.42*	0.67*	0.90*
		Latitudinal speed (km day^{-1})[c]	-4.65	-13.25	-12.11	-5.96	6.46	-5.69	-5.26
	NOBM	Correlation coefficient[b]		-0.51	-0.47	-0.49	0.54	-0.39	-0.47
		Latitudinal speed (km day^{-1})[c]	6.50	-13.97	-11.06	-5.49	6.09	-5.76	-4.98
Southern Ocean	GlobColour	Correlation coefficient[b]		0.36*	0.06	0.07	-0.11	0.74*	0.35*
		Latitudinal speed (km day^{-1})[c]	-7.35	-6.11	9.81	-4.98	10.28	-7.80	-9.89
	NOBM	Correlation coefficient[b]		-0.73*	0.19	0.03	0.86*	-0.61*	0.01
		Latitudinal speed (km day^{-1})[c]	6.12	-5.96	10.30	-5.69	10.62	-6.30	-9.05

[a] MLD>Zeu stands for the date the MLD becomes deeper than the euphotic depth.

[b] A * indicates correlation coefficients which are statistically significant at the 95% confidence interval. Correlations were calculated between the bloom termination latitudinal mean date and the physical metric latitudinal mean date. Mean dates were calculated over the years 2002-2009 for GlobColour data and 2002-2007 for NOBM data.

[c] Latitudinal speeds were calculated by regressing the metric dates on latitude (latitude = a+ b*date) and then multiplying the linear coefficient (b) by 111.19493 km/°latitude.

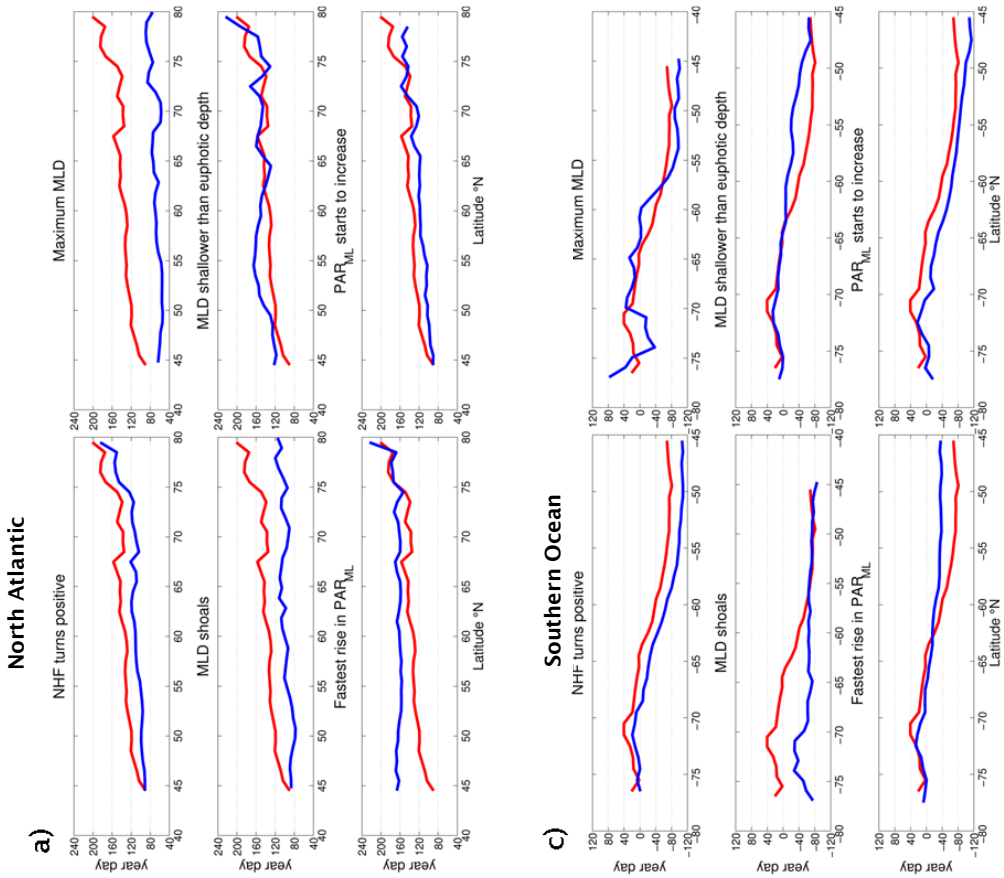

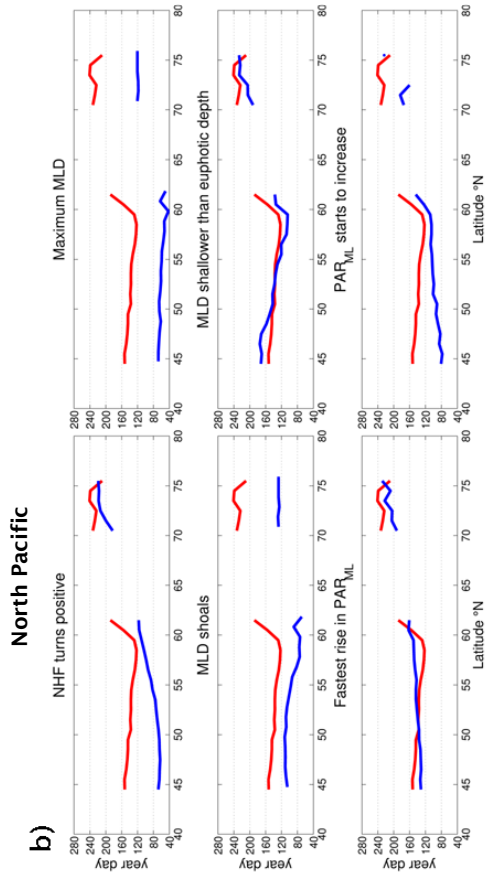

Figure 5.11: Latitudinal mean date for bloom initiation (red) and associated physical timing metrics (blue) for (a) North Atlantic, (b) North Pacific and (c) Southern Ocean. Pixels with shallow bathymetry (<200m) or without a significant seasonal cycle (coefficient of variation <0.35) were removed before longitudinal averaging.

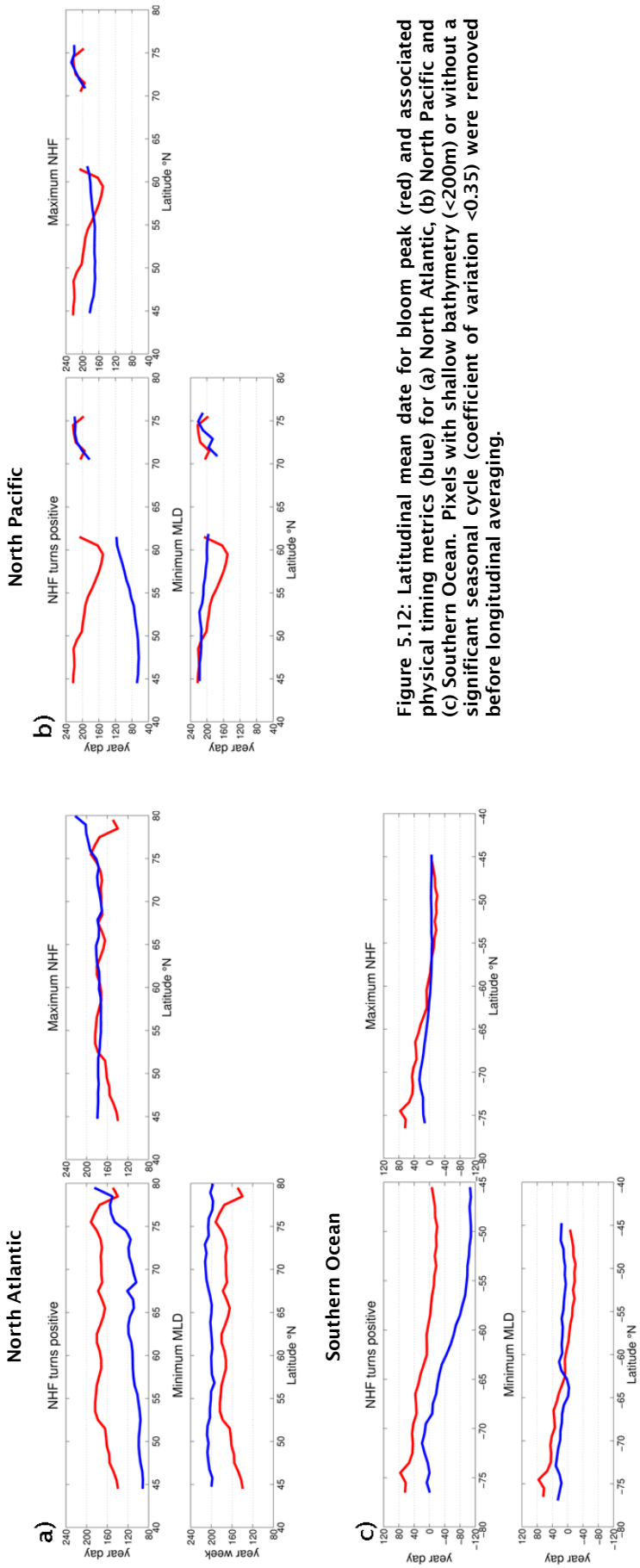

Figure 5.12: Latitudinal mean date for bloom peak (red) and associated physical timing metrics (blue) for (a) North Atlantic, (b) North Pacific and (c) Southern Ocean. Pixels with shallow bathymetry (<200m) or without a significant seasonal cycle (coefficient of variation <0.35) were removed before longitudinal averaging.

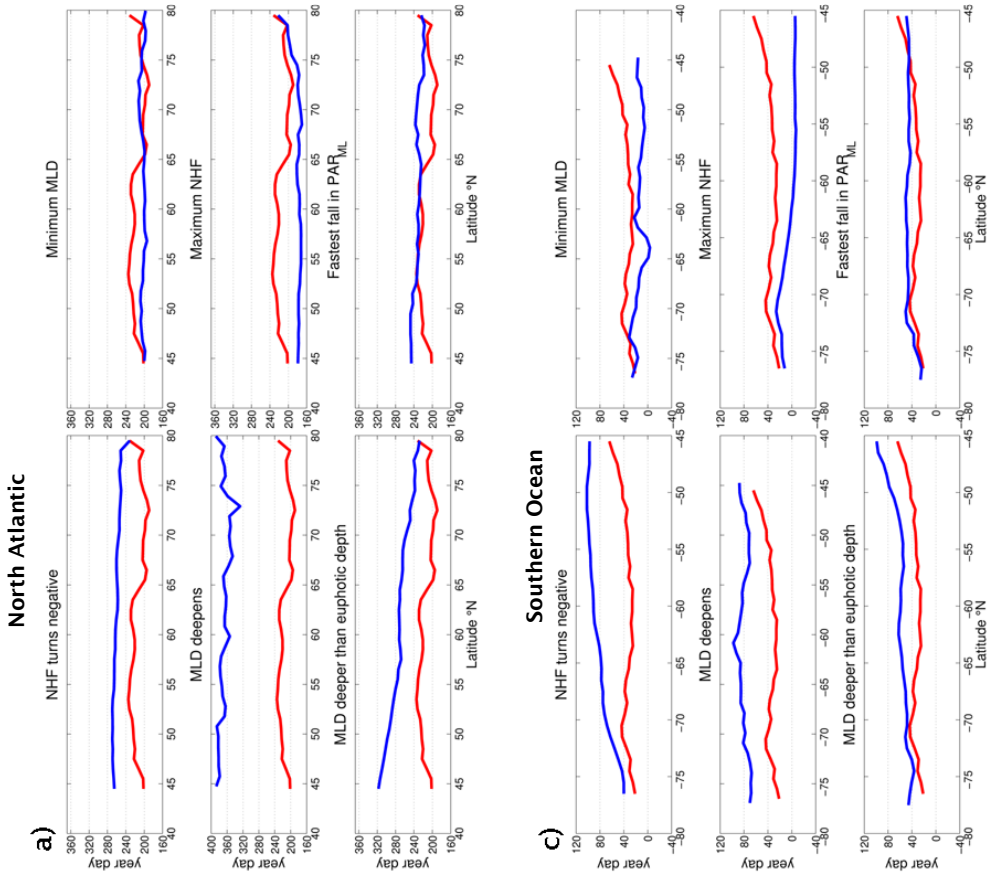

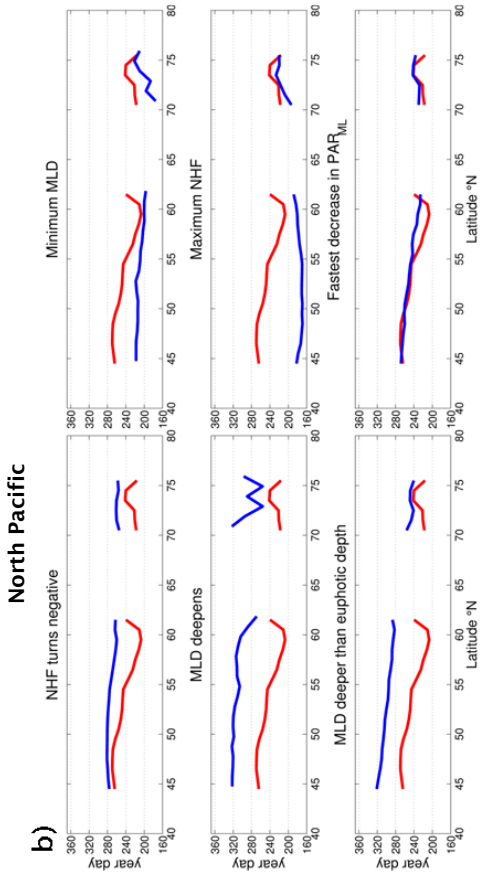

Figure 5.13: Latitudinal mean date for bloom termination timing metrics (blue) for (a) North Atlantic, (b) North Pacific and (c) Southern Ocean. Pixels with shallow bathymetry (<200m) or without a significant seasonal cycle (coefficient of variation <0.35) were removed before longitudinal averaging.

confidence interval (Figure 5.12 and Table 5.1). Broadly, peak timing coincided with the date of maximum NHF in the North Atlantic and with the minimum MLD in the North Pacific. However, statistically significant correlations were seen in the Southern Ocean where the peak timing covaried strongly with the date of maximum NHF (0.90) and NHF turning positive (0.95).

Some stronger relationships were seen with the timing of bloom termination than for the bloom peak (Figure 5.12 and 5.13, Table 5.2 and 5.3). Broadly in the North Atlantic, the bloom termination timing was seen to be most coincident with the timing of minimum MLD and fastest fall in PAR_{ML} though correlations were weak or negative (-0.42 and 0.16 respectively). However, in the North Pacific the fastest fall in PAR_{ML} was strongly correlated (0.90) with similar latitudinal speeds (bloom termination, -4.65 km day^{-1}; fastest decrease in PAR_{ML} -5.26 km day^{-1}). A strong correlation in this basin was also seen with the date the NHF turns negative (0.83). However, in the Southern Ocean bloom termination timing was weakly correlated with the date of fastest fall in PAR_{ML} (0.35), while being strongly related to the date on which the MLD becomes deeper than the euphotic depth (0.74). Additionally, they possessed very similar latitudinal speeds (bloom termination: -7.35 km day^{-1}, MLD>Zeu: -7.80 km day^{-1}).

Overall, the physical metrics that covaried most strongly with bloom initiation in all three basins were the date the NHF turns positive and the PAR_{ML} starts to increase. The peak timing was not strongly associated with any of the metrics but significant relationships were seen with the date of maximum NHF and NHF turning positive in the Southern Ocean. The date of fastest fall in PAR_{ML} coincided with the bloom termination timing in all three basins though strong correlations only occurred in the North Pacific. NOBM bloom timing dates were similar to those calculated from GlobColour however, it is important to note that the spatial extent of NOBM in the northern hemisphere is less than that of GlobColour. This has resulted in differences in the correlation coefficient and latitudinal speeds between GlobColour and NOBM.

5.3.2.2 Interannual Variability

Turning now to interannual variability, strong correlations were found between the bloom and physical timing metrics (Figures 5.14, 5.15 and 5.16 and Tables 5.4, 5.5 and 5.6). In all cases except for the mean winter NHF, bloom timing is expected to be positively correlated with the physical metrics. In the North Atlantic interannual variability in bloom initiation was seen to be strongly correlated with variability in the date the NHF turns positive (0.73) with anomalies of similar magnitude (approximately -20 to 20 days) (Figure 5.14). Additionally, weak but significant correlations were also seen with the timing of MLD maximum (0.38) and

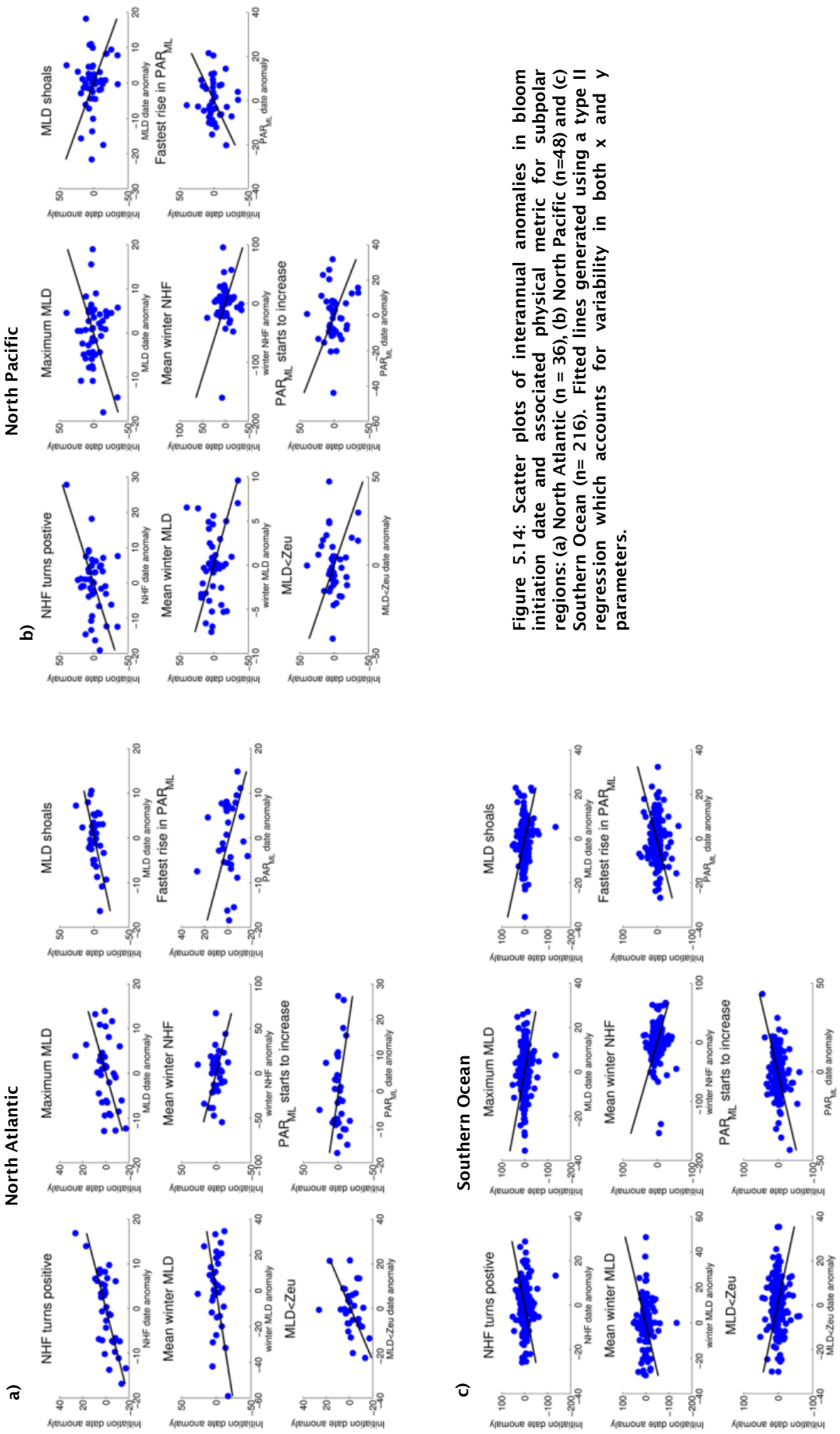

Figure 5.14: Scatter plots of interannual anomalies in bloom initiation date and associated physical metric for subpolar regions: (a) North Atlantic (n = 36), (b) North Pacific (n=48) and (c) Southern Ocean (n= 216). Fitted lines generated using a type II regression which accounts for variability in both x and y parameters.

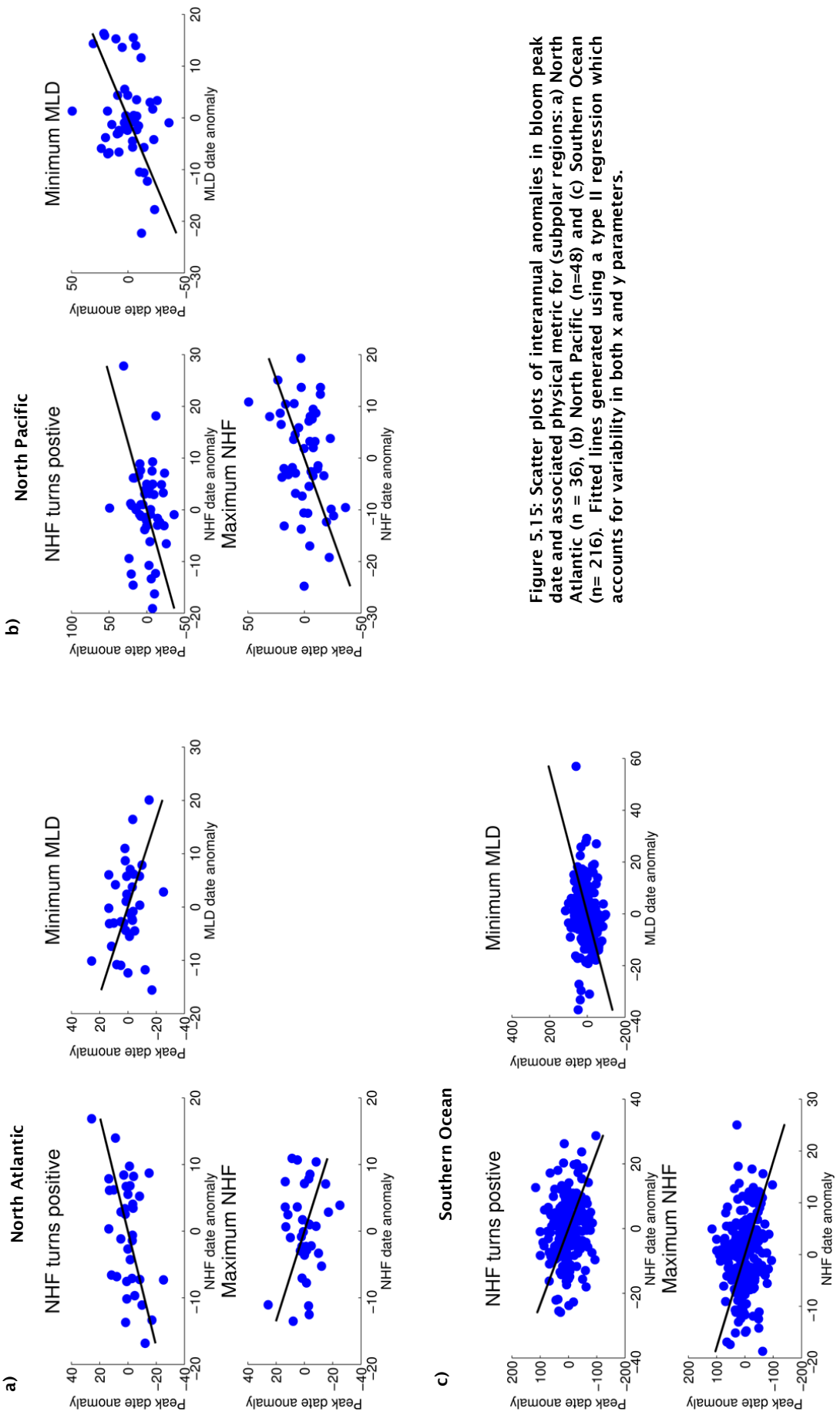

Figure 5.15: Scatter plots of interannual anomalies in bloom peak date and associated physical metric for (subpolar regions: a) North Atlantic (n = 36), (b) North Pacific (n=48) and (c) Southern Ocean (n= 216). Fitted lines generated using a type II regression which accounts for variability in both x and y parameters.

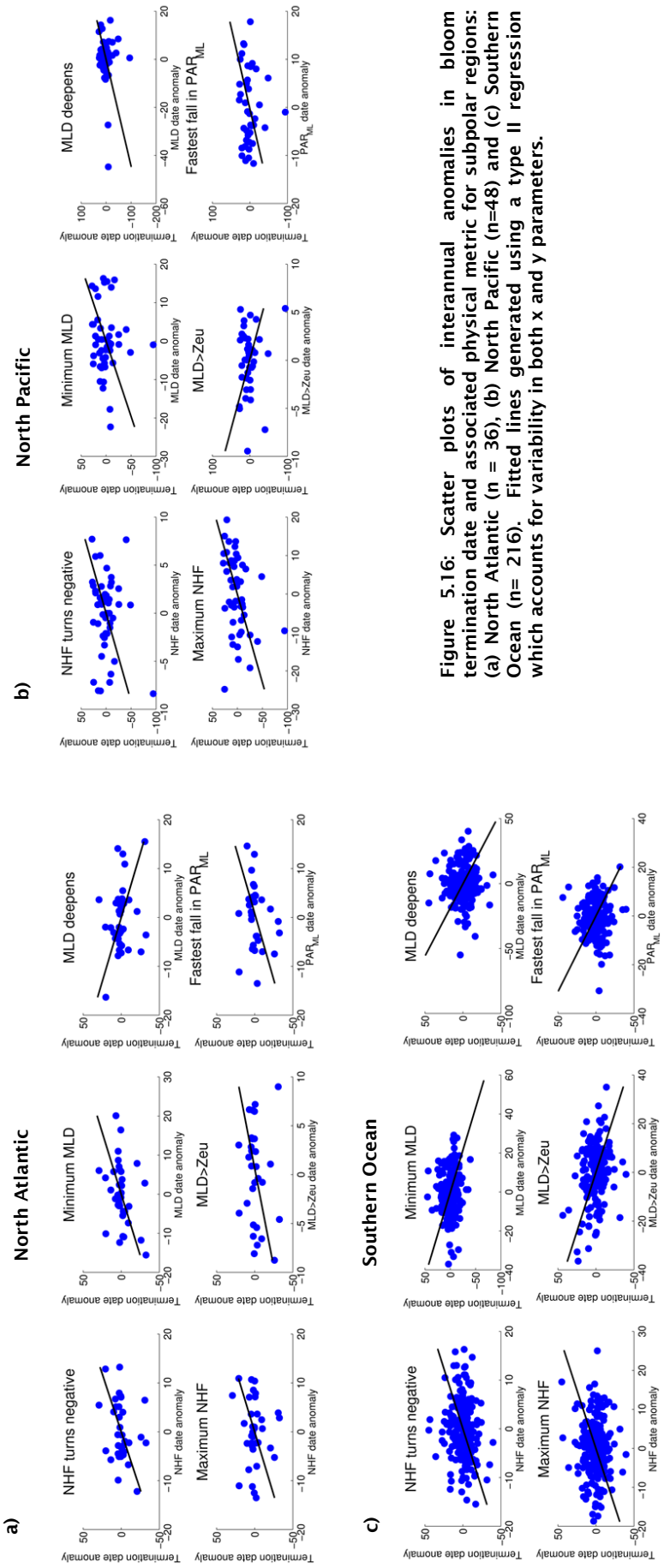

Figure 5.16: Scatter plots of interannual anomalies in bloom termination date and associated physical metric for subpolar regions: (a) North Atlantic (n = 36), (b) North Pacific (n=48) and (c) Southern Ocean (n= 216). Fitted lines generated using a type II regression which accounts for variability in both x and y parameters.

MLD shoaling (0.45). Furthermore, the timing of bloom initiation was weakly correlated with NHF turning positive in the North Pacific (0.32) and with the date PAR_{ML} begins to increase in the Southern Ocean (0.23) (Figure 5.14 and Table 5.4).

Table 5.4: Correlation coefficients between interannual variability in bloom initiation and physical timing metrics in the subpolar basins[a]

	NHF positive	MLD max	MLD shoaling	Mean winter MLD	Mean winter NHF	Fastest rise in PAR_{ML}	MLD<Zeu[b]	PAR_{ML} starts to increase
North Atlantic	0.73*	0.38*	0.45*	0.19	-0.20	-0.12	0.36	-0.01
North Pacific	0.32*	0.03	-0.11	-0.14	-0.04	0.06	-0.04	-0.07
Southern Ocean	0.02	-0.11	-0.08	0.03	-0.06	0.09	-0.03	0.23*

[a] A * indicates correlation coefficients which are statistically significant at the 95% confidence interval.
[b] MLD<Zeu stands for the date the MLD becomes shallower than the euphotic depth.

Table 5.5: Correlation coefficients between interannual variability in bloom peak and physical timing metrics in the subpolar basins[a]

	NHF positive	MLD min	NHF max
North Atlantic	0.46*	-0.21	-0.13
North Pacific	0.12	0.28	0.32*
Southern Ocean	-0.17*	0.08	-0.10

[a] A * indicates correlation coefficients which are statistically significant at the 95% confidence interval.

Table 5.6: Correlation coefficients between interannual variability in bloom termination and physical timing metrics in the subpolar basins[a]

	MLD min	NHF max	NHF negative	MLD deepening	MLD>Zeu[b]	Fastest fall in PAR
North Atlantic	0.31	0.07	0.24	-0.20	0.13	0.17
North Pacific	0.08	0.34*	0.18	0.04	-0.14	0.06
Southern Ocean	-0.06	0.05	0.14*	-0.01	-0.25*	0.02

[a] A * indicates correlation coefficients which are statistically significant at the 95% confidence interval.
[b] MLD>Zeu stands for the date the MLD becomes deeper than the euphotic depth

Significant but weak relationships were observed between the bloom peak timing and the NHF turning positive in the North Atlantic (0.46) and with the maximum NHF timing in the North Pacific (Figure 5.15 and Table 5.5). Similarly, relationships with the interannual variability in bloom termination date were also weak, being correlated with the NHF turning negative in the Southern Ocean (0.14) and with the timing of maximum NHF in the North Pacific (0.34) (Figure 5.16, and Table 5.6). Overall, the strongest relationships were apparent in the North Atlantic with bloom initiation.

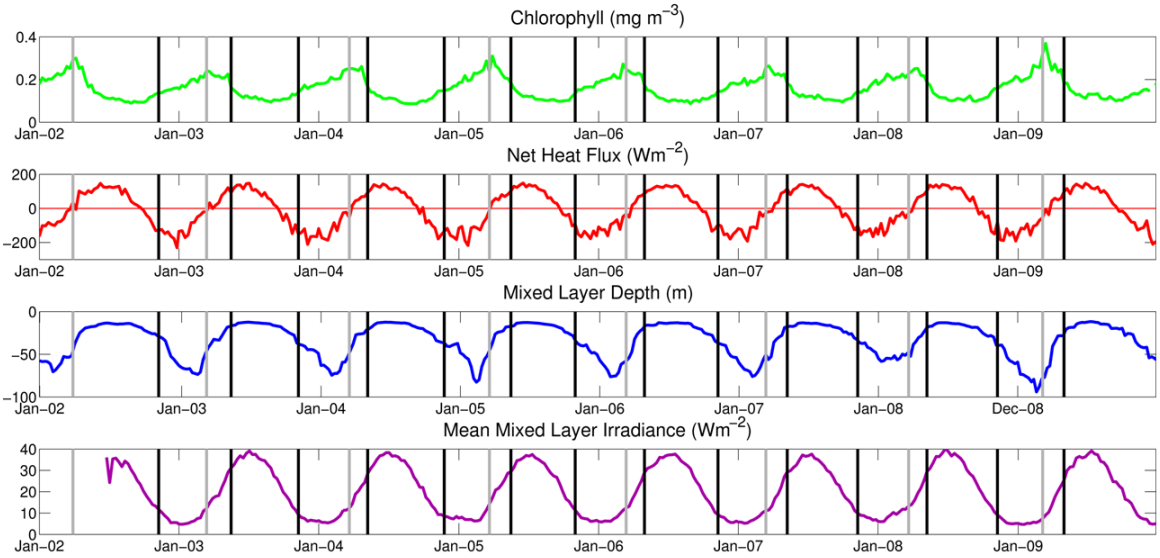

Figure 5.17: Mean time series (2002-2009) across the subtropical North Atlantic for GlobColour chlorophyll (mg m^{-3}), net heat flux (W m^{-2}), mixed layer depth (m) and mean mixed layer irradiance (W m^{-2}). The grey vertical line represents the mean bloom peak date in that year, the black vertical line preceding it is the mean bloom initiation date and the black vertical line following the peak is the mean bloom termination date. The mean bloom timing dates are calculated from averaging the metric dates in each year across the basin (i.e. they are not calculated from the chlorophyll time series above). The grey peak lines do not always line up with the maximum chlorophyll concentration in the time series due to variability in the magnitude of the peak concentrations. Thus, the timing of the maximum concentrations in the chlorophyll time series above is biased towards the largest blooms whereas the grey lines are not.

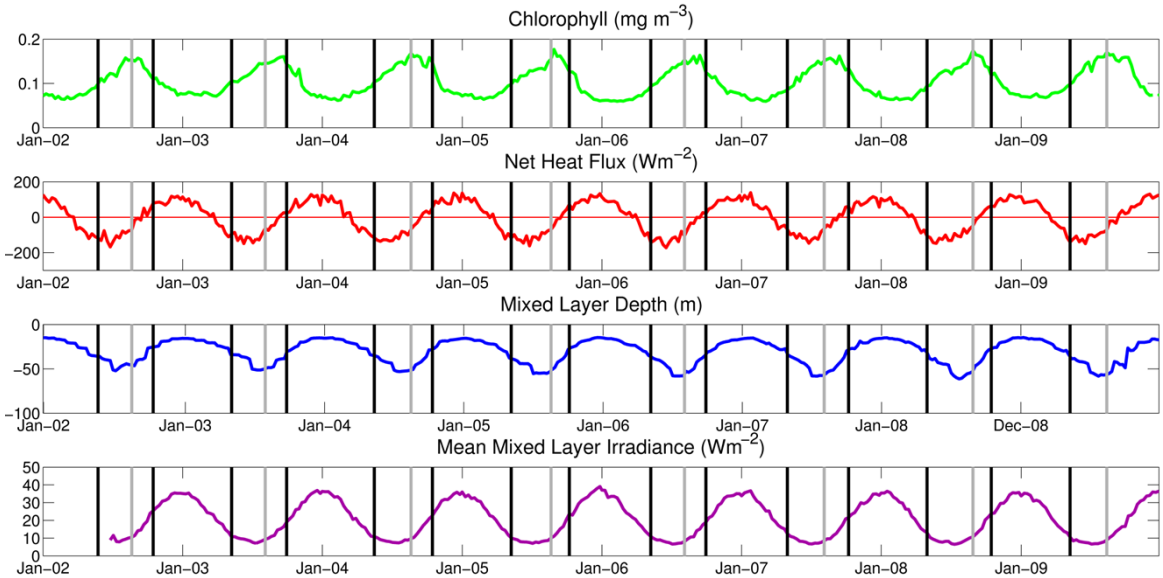

Figure 5.18: Mean time series (2002-2009) across the subtropical South Pacific for GlobColour chlorophyll (mg m^{-3}), net heat flux (W m^{-2}), mixed layer depth (m) and mean mixed layer irradiance (W m^{-2}). The grey vertical line represents the mean bloom peak date in that year, the black vertical line preceding it is the mean bloom initiation date and the black vertical line following the peak is the mean bloom termination date. The mean bloom timing dates are calculated from averaging the metric dates in each year across the basin (i.e. they are not calculated from the chlorophyll time series above). The grey peak lines do not always line up with the maximum chlorophyll concentration in the time series due to variability in the magnitude of the peak concentrations. Thus, the timing of the maximum concentrations in the chlorophyll time series above is biased towards the largest blooms whereas the grey lines are not.

5.3.3 Subtropical Regions

5.3.3.1 Spatial Relationships

The physical setting when the bloom initiation, peak and termination occur in the subtropics was more consistent between the basins than for the subpolar regions (examples are shown in Figure 5.17 and 5.18). In all five basins the bloom initiation occurred when the NHF and PAR_{ML} were decreasing and MLD was deepening. The peak occurred when the NHF was ~zero, MLD was shoaling and PAR_{ML} rising. However, in the South Pacific and Indian Oceans the peak occurred slightly earlier compared to the other basins and so at this time the NHF was negative but rising, MLD was at its maximum and PAR_{ML} was just starting to increase (Figure 5.18). The bloom terminated concurrently with the NHF reaching its maximum, the MLD reaching its minimum and PAR_{ML} was near its maximum value. However, again the bloom termination happened slightly earlier in the South Pacific and Indian Oceans just preceding the NHF maximum with the MLD still shoaling and the PAR_{ML} still rising. Similar results were seen when using the NOBM dates for bloom timing rather than GlobColour dates including the slightly earlier peak and termination dates in the South Pacific and Indian Oceans.

The seasonal cycles of NHF, MLD and PAR_{ML} were fairly consistent between the basins (Figures 5.17 and 5.18). The NHF was the most consistent and varied between -200 and 200 W m^{-2} in all basins. The maximum MLD was ~70m each year in the North Atlantic, South Atlantic and North Pacific but was <60m in the South Pacific and <50m in the Indian Ocean. The maximum PAR_{ML} in all basins was values ~40 W m^{-2}.

Great similarity was observed between the latitudinal gradients in bloom initiation, peak and termination dates and those of the physical timing metrics and some were significantly correlated (Figures 5.22, 5.23 and 5.24 and Tables 5.7, 5.8 and 5.9). The bloom initiation coincided closely with the date of MLD deepening, MLD becoming deeper than the euphotic depth and the fastest fall in PAR_{ML}. However, significant positive correlations were only seen with the date the MLD becomes deeper than the euphotic depth in both the North Atlantic (0.54) and the North Pacific (0.53) (Table 5.7, Figure 5.22). In the Indian basin, the match in timing was strongest south of the equator. However, latitudinal speeds varied between the metrics and were relatively small for the bloom initiation. Overall, the latitudinal variability in some of the physical metrics was relatively low compared to that of bloom initiation.

The timing of the peak of the bloom was seen to coincide closely with all of the metrics tried (NHF turning positive, MLD maximum, MLD shoaling, fastest rise

Table 5.7: Correlations coefficients and latitudinal speeds for bloom initiation and associated physical timing metrics in the subtropical basins for both GlobColour and NOBM chlorophyll datasets

			Bloom Initiation	NHF negative	MLD min	MLD deepening	NHF max	MLD>Zeu[a]	Fastest fall in PAR_{ML}
North Atlantic	GlobColour	Correlation coefficient[b]		-0.11	-0.32	0.01	-0.07	0.54*	-0.12
		Latitudinal speed (km day^{-1})[c]	-0.03	-5.07	-5.88	6.95	2.50	-9.25	-5.83
	NOBM	Correlation coefficient[b]		0.40*	-0.01	-0.18	-0.17	0.66*	0.33*
		Latitudinal speed (km day^{-1})[c]	-0.76	-5.31	-6.53	6.63	3.71	-6.78	-5.29
South Atlantic	GlobColour	Correlation coefficient[b]		-0.49*	0.48*	0.20	-0.09	-0.81*	-0.03
		Latitudinal speed (km day^{-1})[c]	-2.44	5.01	0.82	-1.99	-0.70	10.79	5.48
	NOBM	Correlation coefficient[b]		0.56*	-0.36	0.27	-0.01	0.37	0.36
		Latitudinal speed (km day^{-1})[c]	2.19	4.36	0.12	-0.99	-0.60	17.70	4.76
North Pacific	GlobColour	Correlation coefficient[b]		-0.37*	-0.72*	-0.13	-0.45*	0.53*	-0.36*
		Latitudinal speed (km day^{-1})[c]	-0.88	-4.93	-0.86	9.73	1.22	-9.24	-8.35
	NOBM	Correlation coefficient[b]		0.02	-0.61*	-0.54*	0.07	0.82*	-0.07
		Latitudinal speed (km day^{-1})[c]	-1.49	-4.76	-0.55	12.84	-0.21	-9.21	-7.78
South Pacific	GlobColour	Correlation coefficient[b]		0.09	-0.54*	0.00	-0.07	-0.75*	-0.24
		Latitudinal speed (km day^{-1})[c]	-1.64	5.56	0.43	5.03	-0.92	12.39	4.78
	NOBM	Correlation coefficient[b]		0.17	-0.42*	-0.20	0.08	-0.84*	-0.40*
		Latitudinal speed (km day^{-1})[c]	-1.85	5.76	0.46	8.07	-0.92	10.69	5.67
North Indian	GlobColour	Correlation coefficient[b]		-0.69*	-0.62*	0.10	0.04	0.23	0.34
		Latitudinal speed (km day^{-1})[c]	0.84	-4.03	-1.97	3.03	-2.54	-2.30	-3.00
	NOBM	Correlation coefficient[b]		0.22	0.26	-0.06	-0.52	-0.40	0.10
		Latitudinal speed (km day^{-1})[c]	0.95	-4.24	-2.00	2.21	-2.19	-14.05	3.03

			Bloom Initiation	NHF negative	MLD min	MLD deepening	NHF max	MLD>Zeu[a]	Fastest fall in PAR_{ML}
South Indian	GlobColour	Correlation coefficient[b]		-0.02	-0.43*	0.21	0.04	-0.90*	-0.28
		Latitudinal speed (km day^{-1})[c]	-1.94	7.60	-0.54	4.96	2.39	10.10	5.90
	NOBM	Correlation coefficient[b]		-0.01	-0.24	0.01	0.10	-0.89*	-0.27
		Latitudinal speed (km day^{-1})[c]	-1.51	7.99	-0.57	4.61	2.03	9.22	6.37

[a] MLD>Zeu stands for the date the MLD becomes deeper than the euphotic depth.

[b] A * indicates correlation coefficients which are statistically significant at the 95% confidence interval. Correlations were calculated between the bloom initiation latitudinal mean date and the physical metric latitudinal mean date. Mean dates were calculated over the years 2002-2009 for GlobColour data and 2002-2007 for NOBM data. Correlations were calculated separately for the North (11˚N to 45˚N) and South (45˚S to 11˚S) basins using data shown in Figure 5.22.

[c] Latitudinal speeds were calculated by regressing the metric dates on latitude (latitude = a+ b*date) and then multiplying the linear coefficient (b) by 111.19493 km/˚latitude. Speeds were calculated separately for the North (11˚N to 45˚N) and South (45˚S to 11˚S) basins using data shown in Figure 5.22.

Table 5.8: Correlation coefficients and latitudinal speeds for bloom peak and associated physical timing metrics in the subtropical basins for both GlobColour and NOBM chlorophyll datasets

			Bloom Peak	NHF positive	MLD max	MLD shoaling	Fastest rise in PAR_{ML}	PAR_{ML} starts to rise
North Atlantic	GlobColour	Correlation coefficient[a]		-0.64*	0.35*	0.61*	0.14	0.38*
		Latitudinal speed (km day^{-1})[b]	-3.33	6.48	-2.31	-5.78	6.46	1.19
	NOBM	Correlation coefficient[a]		-0.07	0.36*	0.42*	0.56*	0.56*
		Latitudinal speed (km day^{-1})[b]	0.19	6.97	-0.29	-5.84	6.39	4.31
South Atlantic	GlobColour	Correlation coefficient[a]		0.32	-0.28	-0.23	-0.11	-0.14
		Latitudinal speed (km day^{-1})[b]	-2.32	-5.89	6.78	6.92	-2.26	0.14
	NOBM	Correlation coefficient[a]		-0.19	-0.1	0.05	-0.16	-0.03
		Latitudinal speed (km day^{-1})[b]	9.2	-5.81	9.78	8.44	-2.93	-0.12
North Pacific	GlobColour	Correlation coefficient[a]		0.77*	0.54*	0.51*	-0.38*	-0.17
		Latitudinal speed (km day^{-1})[b]	-1.65	3.9	-2.99	-1.97	4.77	7.58
	NOBM	Correlation coefficient[a]		-0.75*	0.63*	0.65*	0.16	0.34*
		Latitudinal speed (km day^{-1})[b]	-0.32	4.02	-2.88	-2.08	4.64	7.98
South Pacific	GlobColour	Correlation coefficient[a]		0.57*	0.38*	0.1	0.64*	-0.80*
		Latitudinal speed (km day^{-1})[b]	-4.82	-7.2	-9.18	-5.24	-5.21	10.4-
	NOBM	Correlation coefficient[a]		0.38*	0.18	0.32*	0.69*	-0.44*
		Latitudinal speed (km day^{-1})[b]	-4.85	-7.71	-0.24	-5.25	-4.92	13.77
North Indian	GlobColour	Correlation coefficient[a]		-0.63*	0.78*	0.76*	-0.81*	0.12
		Latitudinal speed (km day^{-1})[b]	-1.14	4.3	-1.37	-1.35	5.67	10.28
	NOBM	Correlation coefficient[a]		-0.68*	0.86*	0.87*	0.32*	-0.79*
		Latitudinal speed (km day^{-1})[b]	-0.75	4.32	-1.40	-1.33	5.64	9.69

			Bloom Peak	NHF positive	MLD max	MLD shoaling	Fastest rise in PAR_{ML}	PAR_{ML} starts to rise
South Indian	GlobColour	Correlation coefficient[b]		-0.06	0.77*	0.54*	0.33	0.44*
		Latitudinal speed (km day^{-1})[c]	-1.73	-3.76	0.86	7.18	-4.96	-4.27
	NOBM	Correlation coefficient[b]		-0.07	0.77*	0.52*	0.31	0.39*
		Latitudinal speed (km day^{-1})[c]	-2.11	-3.25	0.59	7.18	-4.91	6.89

[a] A * indicates correlation coefficients which are statistically significant at the 95% confidence interval. Correlations were calculated between the bloom peak latitudinal mean date and the physical metric latitudinal mean date. Mean dates were calculated over the years 2002-2009 for GlobColour data and 2002-2007 for NOBM data. Correlations were calculated separately for the North (11˚N to 45˚N) and South (45˚S to 11˚S) basins using data shown in Figure 5.23.

[b] Latitudinal speeds were calculated by regressing the metric dates on latitude (latitude = a+ b*date) and then multiplying the linear coefficient (b) by 111.19493 km/˚latitude. Speeds were calculated separately for the North (11˚N to 45˚N) and South (45˚S to 11˚S) basins using data shown in Figure 5.23.

Table 5.9: Correlation coefficients and latitudinal speeds for bloom termination and associated physical timing metrics in the subtropical basins for both GlobColour and NOBM chlorophyll datasets

			Bloom termination	NHF positive	MLD max	MLD shoaling	Fastest rise in PAR_{ML}	MLD<Zeu[a]	PAR_{ML} starts to increase
North Atlantic	GlobColour	Correlation coefficient[b]		0.14	0.27	0.28	0.62*	0.22	0.58*
		Latitudinal speed (km day^{-1})[c]	2.13	6.48	-2.31	-5.78	6.46	6.16	1.19
	NOBM	Correlation coefficient[b]		0.16	0.44*	0.40*	0.65*	0.30	0.64*
		Latitudinal speed (km day^{-1})[c]	2.72	6.97	-0.29	-5.84	6.39	5.73	4.31
South Atlantic	GlobColour	Correlation coefficient[b]		-0.17	-0.53*	-0.61*	-0.18	-0.19	-0.44*
		Latitudinal speed (km day^{-1})[c]	0.88	-5.89	6.78	6.92	-2.26	-2.51	0.14
	NOBM	Correlation coefficient[b]		0.29	-0.05	-0.19	0.11	-0.52*	-0.41*
		Latitudinal speed (km day^{-1})[c]	0.06	-5.81	9.78	8.44	-2.93	-2.61	-0.12
North Pacific	GlobColour	Correlation coefficient[b]		-0.32	0.21	0.36*	0.72*	0.73*	0.69*
		Latitudinal speed (km day^{-1})[c]	4.71	3.90	-2.99	-1.97	4.77	3.05	7.58
	NOBM	Correlation coefficient[b]		-0.04	0.03	0.15	0.76*	0.81*	0.81*
		Latitudinal speed (km day^{-1})[c]	5.45	4.02	-2.88	-2.08	4.64	3.09	7.98
South Pacific	GlobColour	Correlation coefficient[b]		0.73*	0.09	-0.15	0.39*	0.08	-0.77*
		Latitudinal speed (km day^{-1})[c]	-3.41	-7.20	-9.18	-5.24	-5.21	-3.72	10.40
	NOBM	Correlation coefficient[b]		0.64*	0.06	-0.12	0.16	-0.10	-0.46*
		Latitudinal speed (km day^{-1})[c]	-2.89	-7.71	-0.24	-5.25	-4.92	-3.63	3.77
North Indian	GlobColour	Correlation coefficient[b]		-0.53*	0.77*	0.75*	-0.75*	-0.21	0.09
		Latitudinal speed (km day^{-1})[c]	-2.20	4.30	-1.37	-1.35	5.67	7.64	10.28
	NOBM	Correlation coefficient[b]		-0.48	0.70*	0.70*	-0.62*	-0.39	-0.70*
		Latitudinal speed (km day^{-1})[c]	-0.72	4.32	-1.40	-1.33	5.64	7.46	9.69

			Bloom termination	NHF positive	MLD max	MLD shoaling	Fastest rise in PAR_{ML}	MLD<Zeu[a]	PAR_{ML} starts to increase
South Indian	GlobColour	Correlation coefficient[b]		0.10	0.52*	0.46*	0.03	0.30	0.46*
		Latitudinal speed (km day^{-1})[c]	0.93	-3.76	0.86	7.18	-4.96	-4.27	6.02
	NOBM	Correlation coefficient[b]		0.09	0.56*	0.30	-0.18	0.09	0.56*
		Latitudinal speed (km day^{-1})[c]	0.82	-3.25	0.59	7.18	-4.91	-4.13	6.89

[a] MLD<Zeu stands for the date the MLD becomes shallower than the euphotic depth.

[b] A * indicates correlation coefficients which are statistically significant at the 95% confidence interval. Correlations were calculated between the bloom termination latitudinal mean date and the physical metric latitudinal mean date. Mean dates were calculated over the years 2002-2009 for GlobColour data and 2002-2007 for NOBM data. Correlations were calculated separately for the North (11˚N to 45˚N) and South (45˚S to 11˚S) basins using data shown in Figure 5.24.

[c] Latitudinal speeds were calculated by regressing the metric dates on latitude (latitude = a+ b*date) and then multiplying the linear coefficient (b) by 111.19493 km/˚latitude. Speeds were calculated separately for the North (11˚N to 45˚N) and South (45˚S to 11˚S) basins using data shown in Figure 5.24.

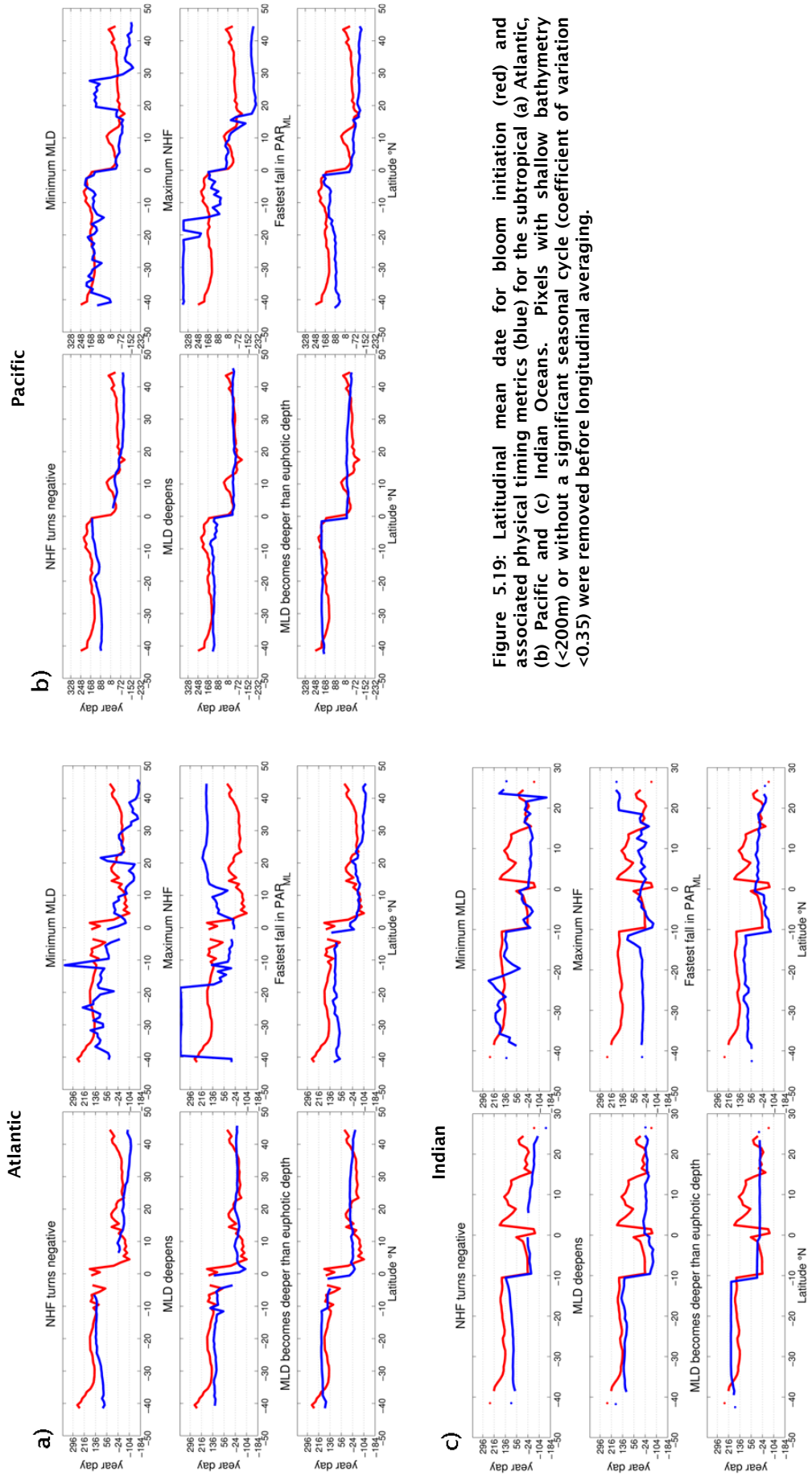

Figure 5.19: Latitudinal mean date for bloom initiation (red) and associated physical timing metrics (blue) for the subtropical (a) Atlantic, (b) Pacific and (c) Indian Oceans. Pixels with shallow bathymetry (<200m) or without a significant seasonal cycle (coefficient of variation <0.35) were removed before longitudinal averaging.

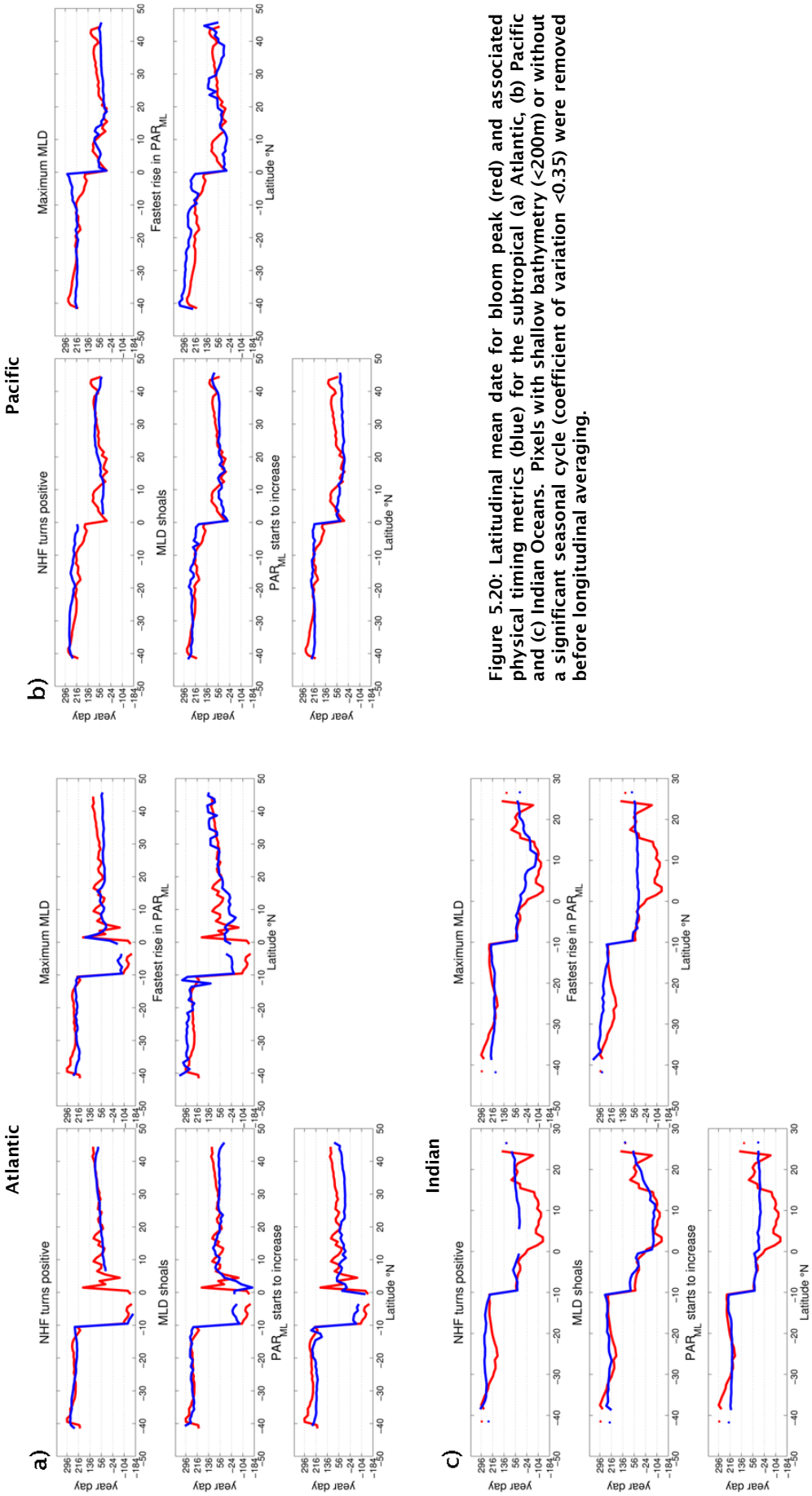

Figure 5.20: Latitudinal mean date for bloom peak (red) and associated physical timing metrics (blue) for the subtropical (a) Atlantic, (b) Pacific and (c) Indian Oceans. Pixels with shallow bathymetry (<200m) or without a significant seasonal cycle (coefficient of variation <0.35) were removed before longitudinal averaging.

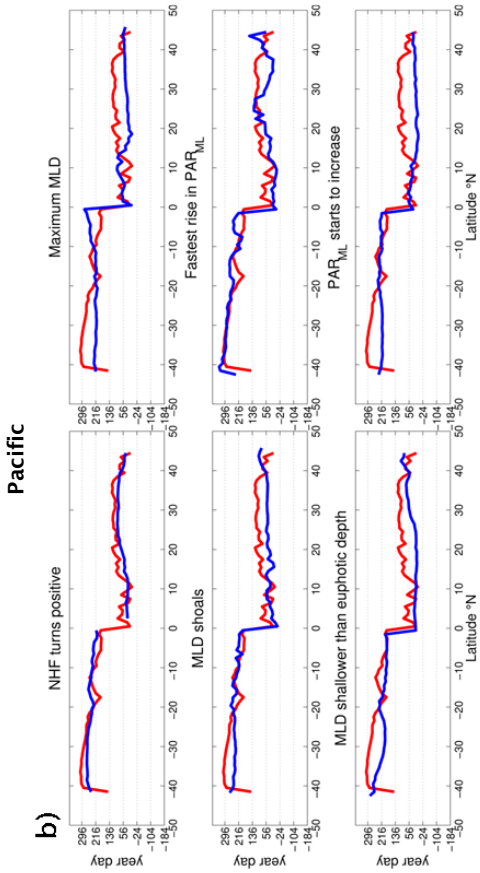

Figure 5.21: Latitudinal mean date for bloom termination (red) and associated physical timing metrics (blue) for the subtropical (a) Atlantic, (b) Pacific and (c) Indian Oceans. Pixels with shallow bathymetry (<200m) or without a significant seasonal cycle (coefficient of variation <0.35) were removed before longitudinal averaging.

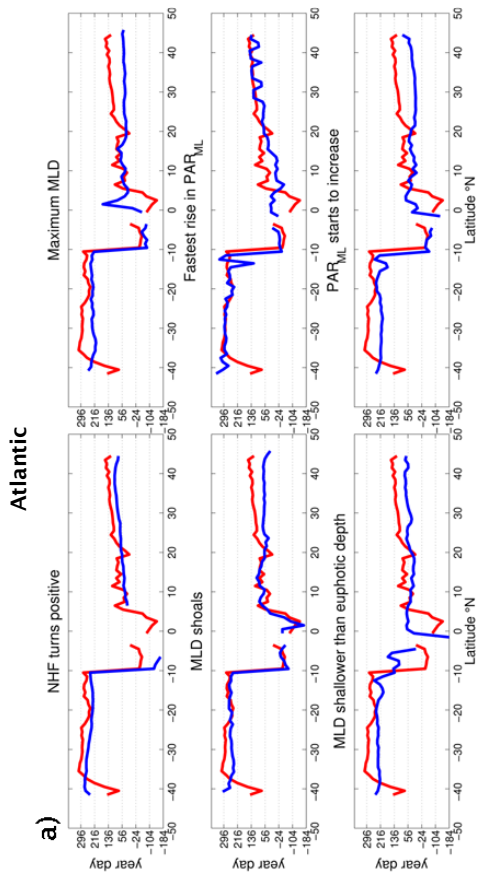

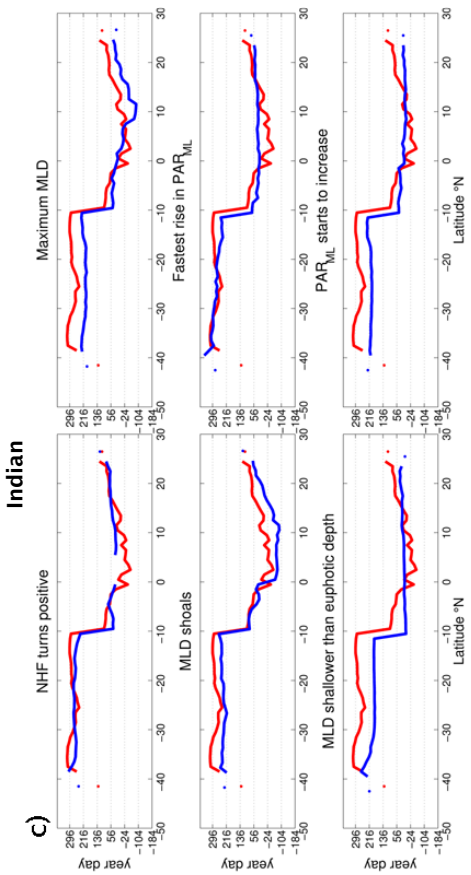

in PAR_{ML}, and PAR_{ML} starting to increase) (Figure 5.23, Table 5.8). Significant correlations were observed in most basins for the date of maximum MLD (North Pacific (0.54), North Indian (0.78) and South Indian (0.77)) and the date of MLD shoaling (North Atlantic (0.61), North Pacific (0.51), North Indian (0.76) and South Indian (0.54)). Additionally, the date the NHF becomes positive was significantly positively correlated in the North Pacific (0.77) and South Pacific (0.57). Positive correlations were only seen with the date the MLD becomes deeper than the euphotic depth in the North Atlantic (0.54) and the North Pacific (0.53) (Table 5.7, Figure 5.22). In the Indian basin, the match in timing was strongest south of the equator. However, much like bloom initiation, the latitudinal variability in some of the physical metrics was relatively low compared to that of bloom peak timing.

The agreement between bloom initiation and peak and the physical timing metrics broke down north of the equator in the Indian Ocean, although the timing of bloom termination had strong relationships across the whole of the basin (Figure 5.24). Strong positive correlations were seen in both the North and South Indian Ocean with the date of maximum MLD (0.70 and 0.52 respectively) and MLD shoaling (0.70 and 0.46 respectively). In the other basins strong positive correlations were seen in the North Atlantic and North Pacific with the date of fastest rise in PAR_{ML} (0.62 and 0.72 respectively) and the date PAR_{ML} starts to increase (0.58 and 0.69 respectively). Additionally, in the North Atlantic the date the MLD becomes shallower than the euphotic depth was strongly correlated (0.73), as was the date of NHF turning positive (0.73) in the South Pacific.

Overall, the physical timing metrics of significance are consistently identified across the subtropical basins. The bloom initiation date across all subtropical latitudes was closely associated with the date of MLD deepening, MLD becoming deeper than the euphotic depth and the fastest fall in PAR_{ML}. Moreover, the timing of the bloom peak and termination were both closely associated with the date of NHF turning positive, maximum MLD, MLD shoaling and fastest rise in PAR_{ML}. However, in some basins strong negative correlations were seen between the bloom timing and physical timing metrics and some physical metrics exhibited relatively low latitudinal variability.

5.3.3.2 Interannual Variability

On an interannual basis the correlations between bloom initiation and the physical timing metrics were generally weak (Figure 5.25, Table 5.10). Of those correlations which were statistically significant, most were also negative despite positive correlations being expected since a later change in the physical environment is expected to delay bloom initiation, peak and termination. Those that were statistically significant for the bloom initiation were the date of MLD

deepening in the North Pacific (-0.40), and NHF turning negative (-0.27), MLD minimum (-0.30) and MLD deepening (-0.43) in the South Pacific. However, a positive, statistically significant correlation was seen in the North Atlantic with the timing of maximum NHF (0.35).

Positive correlations (as well as some negative ones) were seen between the interannual variability in bloom peak timing and the associated physical timing metrics (Figure 5.26, Table 5.11). The most consistent relationships were found in the North Atlantic, Pacific and Indian Oceans with the date the NHF turns positive (0.44, 0.45 and 0.33 respectively). Additionally, positive correlations were found with the timing of maximum MLD in the North Atlantic (0.56) and North Pacific (0.35) and with MLD shoaling in the North Atlantic (0.35).

Table 5.10: Correlation coefficients between interannual variability in bloom initiation and physical timing metrics in the subtropical basins[a]

	NHF negative	MLD min	MLD deepening	NHF max	MLD>Zeu[b]	Fastest fall in PAR_{ML}
North Atlantic	0.30	0.23	0.26	0.35*	-0.10	-0.10
South Atlantic	-0.12	-0.36	-0.19	-0.01	0.40	0.05
North Pacific	-0.07	0.14	-0.40*	0.08	0.02	-0.07
South Pacific	-0.27*	-0.30*	-0.43*	-0.16	0.28	-0.20
Indian	0.12	-0.06	0.00	-0.27	0.12	-0.28

[a] A* indicates correlation coefficients which are statistically significant at the 95% confidence interval.
[b] MLD>Zeu stands for the date the MLD becomes deeper than the euphotic depth.

Table 5.11: Correlation coefficients between interannual variability in bloom peak and physical timing metrics in the subtropical basins[a]

	NHF positive	MLD max	MLD shoaling	Fastest rise in PAR_{ML}	PAR_{ML} starts to rise
North Atlantic	0.44*	0.56*	0.35*	-0.05	0.21
South Atlantic	-0.12	0.35*	-0.02	-0.19	-0.64*
North Pacific	-0.40*	0.35*	-0.16	-0.02	0.03
South Pacific	0.45*	0.24	-0.00	0.22	-0.35*
Indian	0.33*	0.08	-0.07	-0.15	0.03

[a] A * indicates correlation coefficients which are statistically significant at the 95% confidence interval.

Table 5.12: Correlation coefficients between interannual variability in bloom termination and physical timing metrics in the subtropical basins[a]

	NHF positive	MLD max	MLD shoaling	MLD winter mean	NHF winter mean	Fastest rise in PAR_{ML}	MLD<Zeu[b]	PAR_{ML} starts to increase
North Atlantic	0.25	0.32	0.04	0.24	-0.44*	-0.10	-0.24	0.37
South Atlantic	-0.59*	-0.25	-0.22	-0.32	0.36	-0.12	-0.44*	0.34
North Pacific	-0.25	-0.02	0.09	0.08	-0.04	0.43*	-0.25	-0.30
South Pacific	0.09	0.04	-0.05	0.14	-0.29*	0.06	0.06	-0.25
Indian	-0.00	-0.08	0.09	-0.09	-0.13	0.02	-0.01	0.12

[a] A * indicates correlation coefficients which are statistically significant at the 95% confidence interval.
[b] MLD<Zeu stands for the date the MLD becomes shallower than the euphotic depth.

Some negative correlations were also seen with interannual variability in bloom termination (Figure 5.27, Table 5.12). However, the bloom termination was, as expected, negatively correlated with the mean winter NHF (-0.44) in the North Atlantic and South Pacific (-0.29). Furthermore, a positive correlation was seen with the fastest rise in PAR_{ML} in the North Pacific (0.43)

5.4 Discussion

On the large spatial scales explored here, interannual variability in bloom timing was relatively low (~1-2 months) in both the subpolar and subtropical gyres (Figures 5.14-5.16 and Figures 5.25-5.27). The low variability suggests that variability in the forcing of bloom timing is also low and consistent between years. This is shown in the small phenological variability in the seasonal cycles of MLD, NHF and PAR_{ML} (Figures 5.14-5.16 and Figures 5.25-5.27). In agreement with this, Thomalla *et al.* (2011) hypothesised that regions of the Southern Ocean with low interannual variability and high seasonal reproducibility (similar magnitude and phasing of seasonal cycles between years) were primarily driven by the low variability seasonal cycle in light, MLD and NHF rather than higher frequency, sub-seasonal processes. On the other hand, regions of high interannual variability in bloom timing were indicative of regions where the interannual variation in the mechanisms driving the supply of light and nutrients was also high (Thomalla *et al.*, 2011). High interannual variability was seen at the boundaries between subpolar and subtropical gyres in all three metrics. These so-called “transition zones” have previously been highlighted by Henson *et al.* (2009) and Thomalla *et al.* (2011). The high interannual variability is the result of the subpolar and subtropical gyres expanding

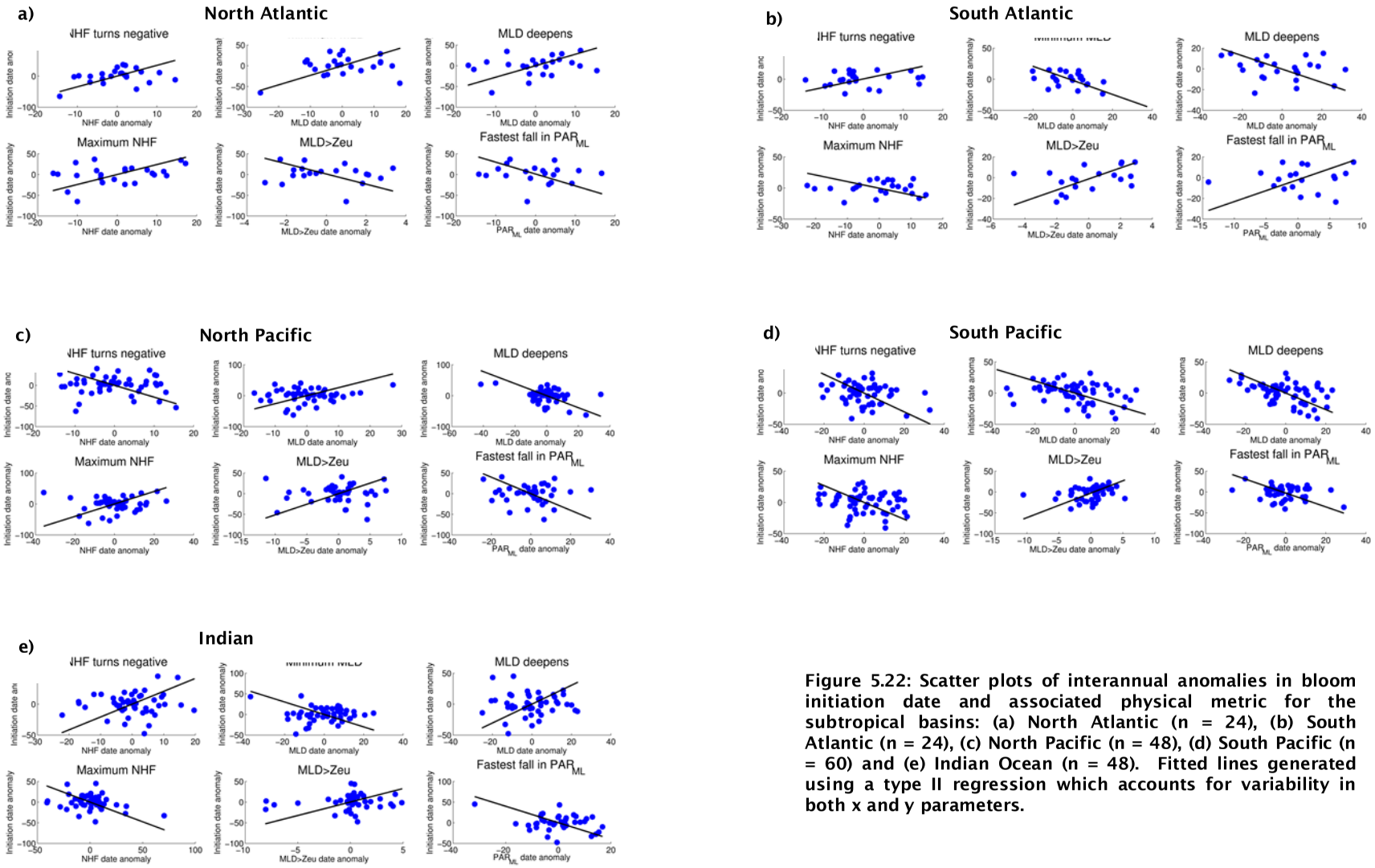

Figure 5.22: Scatter plots of interannual anomalies in bloom initiation date and associated physical metric for the subtropical basins: (a) North Atlantic (n = 24), (b) South Atlantic (n = 24), (c) North Pacific (n = 48), (d) South Pacific (n = 60) and (e) Indian Ocean (n = 48). Fitted lines generated using a type II regression which accounts for variability in both x and y parameters.

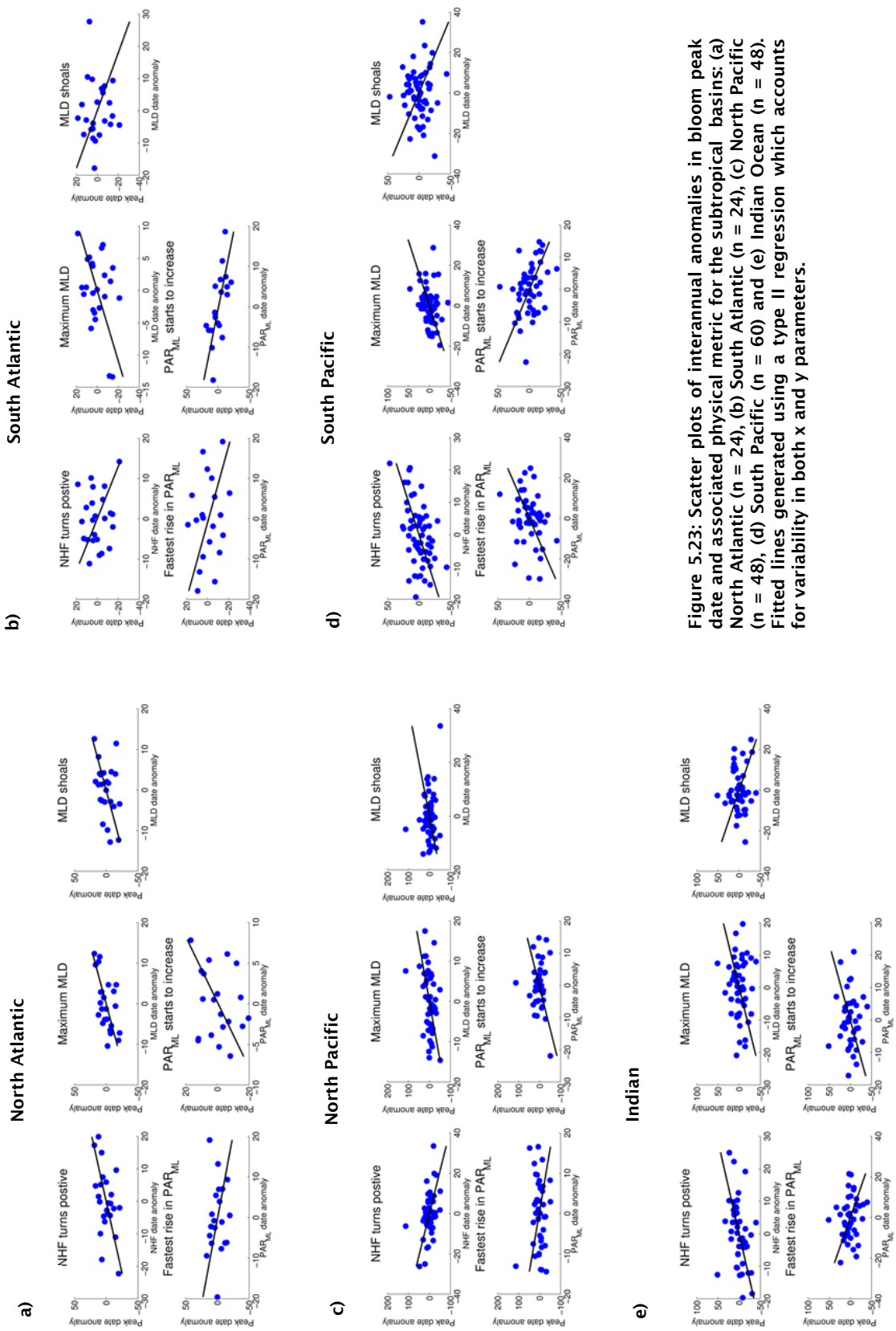

Figure 5.23: Scatter plots of interannual anomalies in bloom peak date and associated physical metric for the subtropical basins: (a) North Atlantic (n = 24), (b) South Atlantic (n = 24), (c) North Pacific (n = 48), (d) South Pacific (n = 60) and (e) Indian Ocean (n = 48). Fitted lines generated using a type II regression which accounts for variability in both x and y parameters.

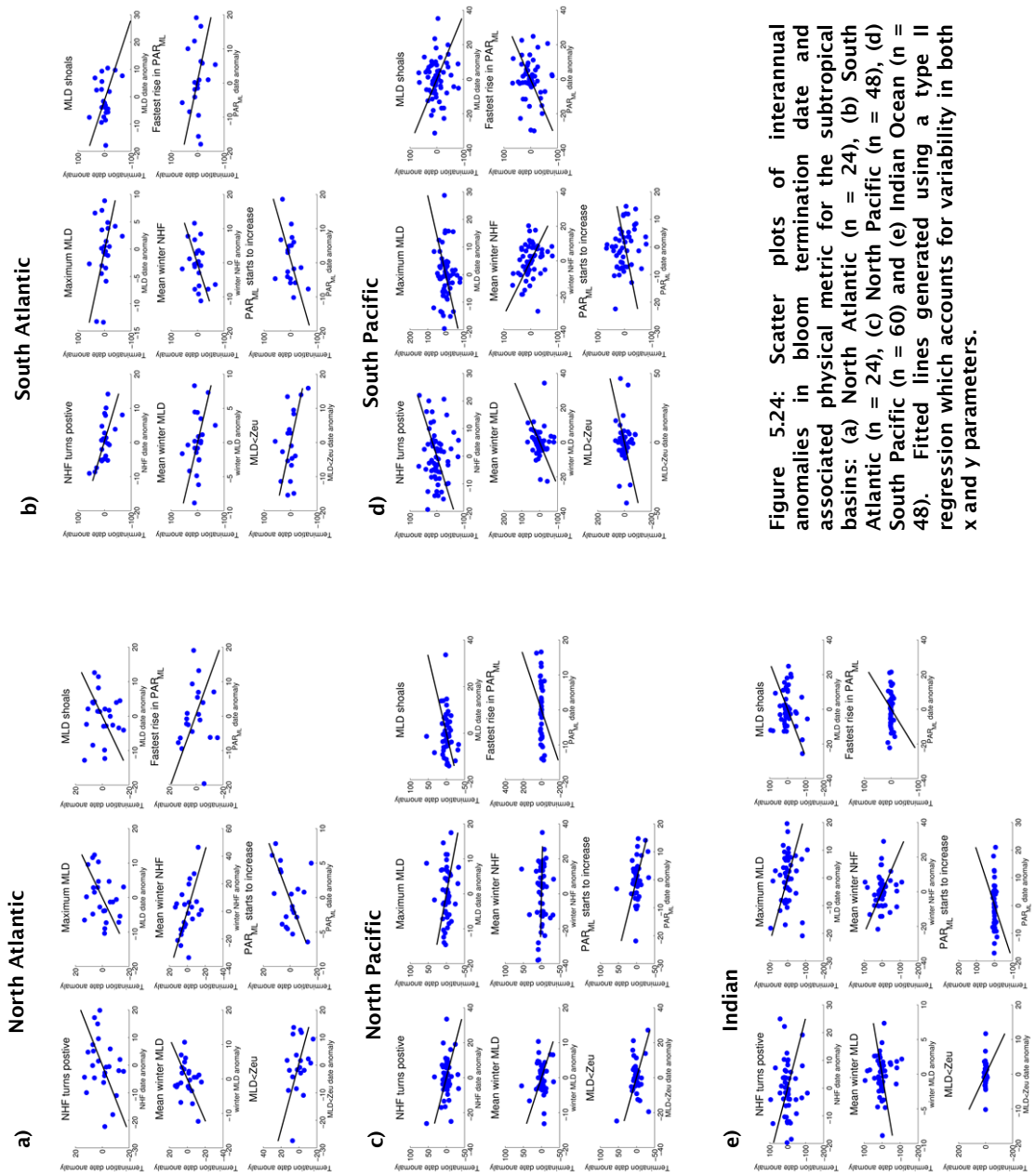

Figure 5.24: Scatter plots of interannual anomalies in bloom termination date and associated physical metric for the subtropical basins: (a) North Atlantic (n = 24), (b) South Atlantic (n = 24), (c) North Pacific (n = 48), (d) South Pacific (n = 60) and (e) Indian Ocean (n = 48). Fitted lines generated using a type II regression which accounts for variability in both x and y parameters.

and contracting between years resulting in this transition zone to experience subpolar-like forcing in some years and subtropical-like forcing in others (Henson *et al.*, 2009). Additionally, high interannual variability is associated with ocean fronts, equatorial and upwelling regions which all experience strong intraseasonal variability in forcing. However, low (<1.5 months) interannual variability dominates the majority of the globe and this discussion will focus on the drivers of bloom timing variability in these regions though, locally, variability can be high (>4 months).

5.4.1 Drivers of Subpolar Variability

From the basin mean time series across the three subpolar basins, the bloom timing metrics are associated consistently with certain environmental conditions. Bloom initiation occurs during a period of increasing stratification and reduction in mixing as the NHF becomes positive, the MLD shoals and PAR_{ML} increases (Figures 5.8-5.10). The peak occurs during the time of maximum warming and stratification with the maximum NHF, minimum MLD and high levels of PAR_{ML}. The bloom termination happens as the stratification breaks down with a reduction in NHF, MLD deepening and falling PAR_{ML}. This consistent coincident timing suggests that the occurrence of these conditions may potentially be prominent drivers for interannual variability in bloom timing.

To confirm this, the timing of bloom metrics and physical metrics should be similar and well correlated across the basin. In all three subpolar basins the poleward latitudinal progression of bloom initiation coincided closely and was highly correlated with the timing of NHF turning positive (Figure 5.11). This relationship was especially strong in the North Atlantic. Additionally, the date the PAR_{ML} starts to increase was also highly correlated with timing across the basins. This suggests that these metrics may be important drivers of latitudinal variability in the date of bloom initiation. The NHF turning positive indicates a reduction in mixing rates that, through the critical turbulence hypothesis (Taylor and Ferrari, 2011), alleviates light imitation as phytoplankton are not rapidly mixed out of the euphotic zone. High correlations with the date PAR_{ML} starts to increase are congruent with this scenario as this metric indicates that the MLD is still deep and mean irradiance levels in the mixed layer are still low, but that irradiance levels at the surface may be sufficient for growth.

Further metrics associated with MLD driven changes to light (MLD becoming shallower than the euphotic depth and fastest rise in PAR_{ML}) were strongly related to bloom initiation in the North Pacific and Southern Oceans where, on average, the MLD was shallower than in the Atlantic. This indicates that the shoaling of the

mixed layer raises mean irradiance levels and alleviates light limitation allowing the bloom to start.

A consistent driver for latitudinal variability in bloom peak timing was not apparent since the physical timing metrics were only weakly correlated with the peak timing in all three basins (Figure 5.12). However, concurrent timing was seen with the bloom termination date and the date of fastest fall in PAR_{ML} across the three basins, though a strong correlation was only present in the North Pacific (Figure 5.13). In addition, the date that the MLD becomes deeper than the euphotic depth is strongly correlated with bloom termination variability in the Southern Ocean. Both these metrics are indicative of decreasing light availability suggesting that in the North Pacific and Southern Ocean the latitudinal variability in termination date is driven by light availability.

However, on an interannual basis not all of the metrics identified as strong drivers of spatial variability were strong drivers of interannual variability. The majority of the physical timing metrics were only weakly correlated, if at all. The strongest relationships were seen in the North Atlantic where the date the NHF turns positive was seen to be a strong predictor for the bloom initiation date (Figure 5.14). The date the NHF turns positive explain ~53% of the variability in bloom initiation date and has approximately equal sized anomalies. This means that if the NHF turning positive was 7 days later than average then the bloom initiation would also be 7 days later than average. The relationship between NHF turning positive and bloom initiation was much weaker in the North Pacific where it explained only ~10% of the variability. The other metric identified as a consistent spatial driver was the date PAR_{ML} starts to rise. However, it is only weakly related to bloom initiation variability in the Southern Ocean (~5% of variability explained). Interannual variability in the date of MLD shoaling was also a moderately good predictor for bloom initiation (~21% variance explained) though only in the North Atlantic.

Much like the latitudinal variability the interannual variability in bloom peak and termination timing was not strongly related to any of the physical timing metrics (Figure 5.15 and 5.16). Weak correlations were seen in the North Atlantic with the date the NHF turns positive. However, this most likely results from the strong dependence of peak timing on bloom initiation, which reflects the rapid transition from bloom onset to bloom peak in subpolar regions.

Interestingly, many of the dominant drivers of latitudinal variability were not found to be drivers of interannual variability and even then not consistently across the basins. A similar result was also obtained by Follows and Dutkiewicz (2002) in the subpolar North Atlantic for physical drivers of bloom magnitude. Spatially, the

relationship between proxies for mixing (e.g. bloom period net heat flux and wind speed) were strongly correlated with bloom period chlorophyll concentration but were not on an interannual basis. Follows and Dutkiewicz (2002) proposed that this lack of correlation was due to a number of factors being jointly responsible for variability in bloom magnitude. Thus, the lack of an obviously dominant driver in bloom peak and termination interannual variability may be because it is a combination of variables that are all responsible but that each only has a small influence on the date. There are many variables not included in this set of timing metrics, especially those representing non-physical processes. In the subpolar regions it is expected that peak and termination timing may be greatly influenced by biological processes such as grazing pressure, nutrient limitation and seasonal succession. It is interesting that the broad latitudinal gradients suggest that light limitation is an important driver for the timing of bloom termination but that on interannual scales there is no relationship. Though the broad spatial variability follows the gradient in light the smaller interannual variability in timing is clearly driven by a different, unknown factor.

5.4.2 Drivers of Subtropical Variability

The mean time series for all five subtropical basins indicate that the conditions at bloom initiation, peak and termination are relatively consistent (Figures 5.17-5.19). The bloom was seen to initiate during the breakdown of stratification (NHF decreasing, MLD deepening and PAR_{ML} falling) when nutrients were being entrained into the mixed layer from below the thermocline, fuelling the bloom. The bloom peak occurred during the spring transition from winter to summer conditions when there was net heating of the ocean (NHF becomes positive), shoaling of the MLD and rising PAR_{ML}. Conditions were indicative of high stratification (NHF high, MLD shallow, PAR_{ML} high) and thus low nutrient concentrations when the bloom terminated. The mean time series in the physical parameters were very similar between the basins. However, the South Pacific and Indian basins had slightly shallower maximum MLD depths and slightly earlier peak and termination dates compared to the other basins.

The latitudinal variability in bloom initiation date had a consistent set of drivers with which coincident timing was seen across the basins (Figure 5.20). Coincident timing was seen with the timing of MLD deepening, MLD becoming deeper than the euphotic depth and the fastest fall in PAR_{ML}. Despite the coincident timing, strong, positive, basin-wide correlations were only seen with the date that the MLD becoming deeper than the euphotic depth in the North Atlantic and North Pacific. These metrics are all related to the deepening of the mixed layer and this result is consistent with the entrainment of nutrients as a trigger for the bloom. It

should be noted that in the Indian Ocean these relationships break down north of the equator, probably as a result of the intraseasonal variability arising from the monsoons.

The timing of the peak was strongly correlated with all of the associated physics metrics, with the strongest relationships being with the date that NHF becomes positive, maximum MLD and MLD shoaling (Figure 5.21). This signifies a change from mixing to stratified conditions suggesting that the peak occurs when stratification reduces the nutrient supply.

In contrast to the bloom initiation and peak, the relationships in the Indian Ocean with the timing of bloom termination continued north of the equator (Figure 5.22). In all basins the latitudinal variability in termination was seen to covary strongly with the MLD maximum, MLD shoaling and fastest rise in PAR_{ML}. These conditions are very similar to the timing of the peak and are congruent with nutrient limitation causing the bloom to end.

On an interannual basis the relationships were weak between most of the bloom timing and physical metrics. Unlike the latitudinal variability, the interannual variability in bloom initiation did not have a strong, positive correlation with any of the metrics (Figure 5.22). Moderate to weak correlations were seen with the timing of the peak on an interannual basis though not consistently in all basins (Figure 5.23). Later peak timing was associated with later timing of NHF becoming positive (North Atlantic, South Pacific and Indian Ocean), the maximum MLD (North Atlantic, South Atlantic and North Pacific) and MLD shoaling (North Atlantic). In agreement with the latitudinal results, this indicates that variability in the peak timing is dictated by the reduction in nutrient supply which occurs when there is net warming of the ocean and MLD begins to shoal.

A dominant driver of bloom termination variability was not apparent since most metrics were very weakly correlated (Figure 5.24). However, the mean NHF over winter did covary with bloom termination dates in the North Atlantic and South Pacific, though not strongly. This would suggest that the timing of bloom termination was influenced by how much mixing occurred over the winter period. If more mixing than average occurred then the bloom end also occurred later. This indicates a greater amount of mixing and greater entrainment of nutrients from below the thermocline resulting in a prolonged bloom.

In the North Pacific, interannual variability in the timing of bloom termination covaried weakly with the date of fastest rise in PAR_{ML} (Figure 5.24). Careful interpretation needs to be used here as it was not correlated with any other indicator of MLD shoaling (indicating the reduction in nutrient supply). Instead, this could be a result of photoacclimation where phytoplankton reduce the amount of

chlorophyll in their cells in response to increased irradiance rather than an actual reduction in biomass (Behrenfeld *et al.*, 2005) though this response was not seen in other basins.

The weak or absent relationships between the physical and bloom timing metrics in the subtropics suggest that the physical changes are not wholly responsible for driving interannual variability and other factors may play a significant role. The interannual variability was very small, much like interannual variability in subtropical primary production previously reported (Dave and Lozier, 2010, Lozier *et al.*, 2011, Dave and Lozier, 2013). Using datasets with higher temporal frequency may reveal stronger associations if the interannual variability is smaller than 8 days. Additionally, biological factors may influence bloom timing such as through grazing control which is tighter in the subtropics compared to the subpolar regions (Longhurst, 1995). Furthermore, changes in phytoplankton community structure may be important, such as in the subtropical Pacific where positive correlations between stratification and chlorophyll correlations have been explained by nitrogen fixing phytoplankton (diazotrophs) which thrive in highly stratified waters (Dave and Lozier, 2010). Another factor to take into account is that using satellite-derived chlorophyll means only the surface expression of the seasonal cycle is captured. Thus, subsurface changes in chlorophyll will not be included in the comparison with physical changes. However, this could be achieved with *in situ* monitoring.

5.4.3 Mechanisms for Subpolar Bloom Initiation

Identifying strong relationships between changes in the physical environment and interannual variability in bloom initiation may reveal the mechanisms responsible for starting the subpolar spring bloom. Phytoplankton in subpolar regions are primarily light-limited and their blooms will start when that limitation is overcome. Two of the main theories on the conditions needed for bloom initiation are the critical depth hypothesis, for which MLD shoaling is a proxy and the critical turbulence hypothesis, for which NHF turning positive is a proxy. The date of NHF turning positive was more strongly and more consistently related to bloom initiation both latitudinally and interannually than the shoaling of the MLD. This suggests that the critical turbulence hypothesis is a better description of the processes that lead to a bloom than the critical depth hypothesis. Though, it is important to note that the NHF and MLD datasets are not “equal” in their relationship to the bloom timing metrics. They cannot be easily ranked against each other because the way the datasets are derived may result in a limit on the variability that one dataset can show.

To investigate this further the conditions in the North Atlantic at the time of bloom initiation were examined (Figure 5.25). In the North Atlantic the majority of blooms started when the median NHF was positive but low (~31 W m^{-2}), median MLD was relatively shallow (~80 m) and median PAR_{ML} was low (~3 W m^{-2}). In accordance with the critical turbulence hypothesis a number of blooms were seen to start in deep mixed layers but when the NHF was low and positive (~25 W m^{-2}) (Figure 5.25a). Conversely, blooms were also seen to start when MLDs were shallow with NHF mostly ranging from 0 to 100 W m^{-2}. Additionally, the PAR_{ML} was seen to range from very low values, indicating deep MLD, when the bloom started to very high values when the MLD was very shallow. Based on these results it would seem there is evidence to support both hypotheses.

Table 5.13: Conditions at bloom initiation for the North Atlantic, North Pacific and Southern Oceans[a]

		North Atlantic	North Pacific	Southern Ocean
Net heat flux	Min	-406.54	-237.16	-421.80
	Max	219.84	237.22	284.09
	Median	31.41	122.33	47.40
	MAD	44.94	33.16	57.18
Mixed layer depth	Min	10.09	10.01	10.59
	Max	1011.81	172.03	690.88
	Median	80.04	20.67	58.42
	MAD	50.38	8.08	32.73
Mean mixed layer PAR	Min	0.17	0.78	0.19
	Max	37.52	38.67	39.77
	Median	2.74	10.68	4.61
	MAD	1.61	4.91	2.79

[a] Minimum, maximum, median and median absolute difference (MAD) for the net heat flux, mixed layer depth and mean mixed layer PAR in the three subpolar basins. Median and MAD values were calculated from pixel values weighted by area.

The distribution in PAR_{ML} values allows further examination of the critical depth hypothesis. One key parameter for the critical depth hypothesis is the compensation irradiance which is the irradiance level at which photosynthesis is equal to respiration. Assuming that at bloom initiation the MLD is equal to the critical depth, the mean mixed layer irradiance (PAR_{ML}) will be equal to the community compensation irradiance (includes all community losses not just phytoplankton respiration). The median PAR_{ML} for the North Atlantic at bloom initiation was 2.74 W m^{-2} (1.09 mol photon m^{-2} day^{-1}, see section 2.3.1 in Chapter 2

for conversion). This compares favourably to values found by Siegel *et al.* (2002) across the North Atlantic (1.3 mol photon m^{-2} day^{-1} = 3.27 W m^{-2}) and Henson *et al.* (2006) in the Irminger basin (2.5 mol photon m^{-2} day^{-1} = 6.29 W m^{-2}). Other estimates of the compensation irradiance (but including only phytoplankton respiration) range from 0.1 to 0.8 mol photon m^{-2} day^{-1} (0.25 – 2.01 W m^{-2}) (Sverdrup, 1953, Riley, 1957, Langdon, 1988, Marra, 2004). Nevertheless, the large variability in PAR_{ML} at bloom initiation suggests that the critical turbulence hypothesis is a valid mechanism for initiating a bloom. This is because bloom initiation does not seem to be dependent on the mean mixed layer irradiance reaching a certain threshold level that is sufficient for net population growth. Blooms starting in low PAR_{ML} suggest that phytoplankton were not being mixed throughout the whole mixed layer because of low turbulence meaning that their exposure to sufficient irradiance levels for net growth was lengthened. Conversely, some blooms initiated when PAR_{ML} was higher than average. This suggests that another limiting factor delayed the start of the bloom since the mean mixed layer irradiance would not be expected to be limiting at these levels.

Since many of the physical metrics are interdependent it is difficult to separate out the effects of just one on bloom timing. As the NHF starts to increase from its winter minimum the MLD begins to shoal as well because the switch from net cooling to net heating encourages restratification of the water column (Huisman *et al.*, 1999). Thus, on the weekly timescales used it is difficult to definitively say which mechanism, MLD shoaling or a reduction in mixing, starts the bloom. However, the results here indicate that on basin scales, the critical turbulence hypothesis dominates at these spatial scales. Furthermore, in a comparison study of three different bloom timing metric definitions (threshold method, cumulative sum method and rate of change method) Brody *et al.* (2013) demonstrated that all three gave bloom initiation dates that were approximately synchronous with the NHF turning positive. This suggests that this result is robust to some extent to the choice of bloom metric definition.

In the North Pacific there is also evidence supporting the critical turbulence hypothesis. Though interannual relationships between NHF turning positive and bloom initiation are weak (correlation = 0.32), bloom initiation does occur when NHF is low and positive (~75 W m^{-2}) and the MLD still relatively deep (Figure 5.26). However, the median value at bloom initiation for NHF is much higher than in the Atlantic (~122 W m^{-2}), MLD much shallower (~21 m) and PAR_{ML} much higher (~11 W m^{-2}). This suggests that for the majority of the basin the initiation of the bloom is delayed compared to the North Atlantic, occurring later in the season when ocean warming is larger, the MLD shallower and as a result the PAR_{ML} higher. This is reflected in the map of mean bloom initiation dates in Figure 5.5. The delayed

bloom in the North Pacific has been previously reported and several hypotheses proposed (Heinrich, 1962, Miller, 1993, Fasham, 1995, Banse and English, 1999, Boyd and Harrison, 1999). These hypotheses have focussed on the role of grazing on bloom development. The life history of the dominant copepod species in the Pacific means that adults emerge from winter hibernation and immediately lay their eggs, ensuring that their larvae are ready to feed once the bloom starts (Parsons and Lalli, 1988). In the North Atlantic the adult copepods need to feed on the bloom before being able to lay eggs. Alternatively, the elevated light levels resulting from the relatively shallow winter MLD in the North Pacific may sustain production over the winter. This allows microzooplankton populations to be maintained at levels high enough to graze down the bloom once it starts (Evans and Parslow, 1985, Fasham, 1995, Boyd and Harrison, 1999). In addition, iron limitation may also play a role in limiting phytoplankton growth in the spring (Landry *et al.*, 1993, Banse and English, 1999).

In the Southern Ocean the median values for NHF (~47 W m^{-2}), MLD (~58 m) and PAR_{ML} (~5 W m^{-2}) were more similar to the North Atlantic values than the North Pacific. This similarity was seen again in Figure 5.27 with evidence of blooms initiating in deep mixed layers when the NHF is low and positive (25-30 W m^{-2}). Again, much like the Atlantic this is not the end of the story since there are many pixels where the bloom started when the MLD was shallow and NHF ranged from 0 to 200 W m^{-2} (Figure 5.27). Though this implies that the critical depth and critical turbulence hypotheses may be applicable in different areas neither the MLD shoaling or NHF turning positive were strongly correlated with interannual variability in the bloom initiation date.

The strength of the relationship between NHF turning positive and bloom initiation in the North Atlantic is again obvious in its spatial pattern (Figure 5.28a). A positive correlation is seen over the majority of the North Atlantic (covers 62.32% of basins, mean patch size, 3.81×10^5 km^2) whereas relatively smaller but coherent patches occur in the North Pacific (covers 28.24% of basin, mean patch size, 2.29×10^5 km^2) and Southern Oceans (covers 28.02% of basin, mean patch size, 1.69×10^5 km^2). This detail becomes lost when averaging over the boxes shown in Figure 5.1 and the correlations become statistically insignificant. Despite this, the spatial extent of the positive correlation indicates that the critical turbulence hypothesis is a valid mechanism for initiation the spring bloom over large regions in all three basins (Figure 5.28). It is interesting to note that many of the patches of positive correlation with MLD shoaling are in the same areas as NHF turning positive indicating that these two metrics are strongly inter-dependent.

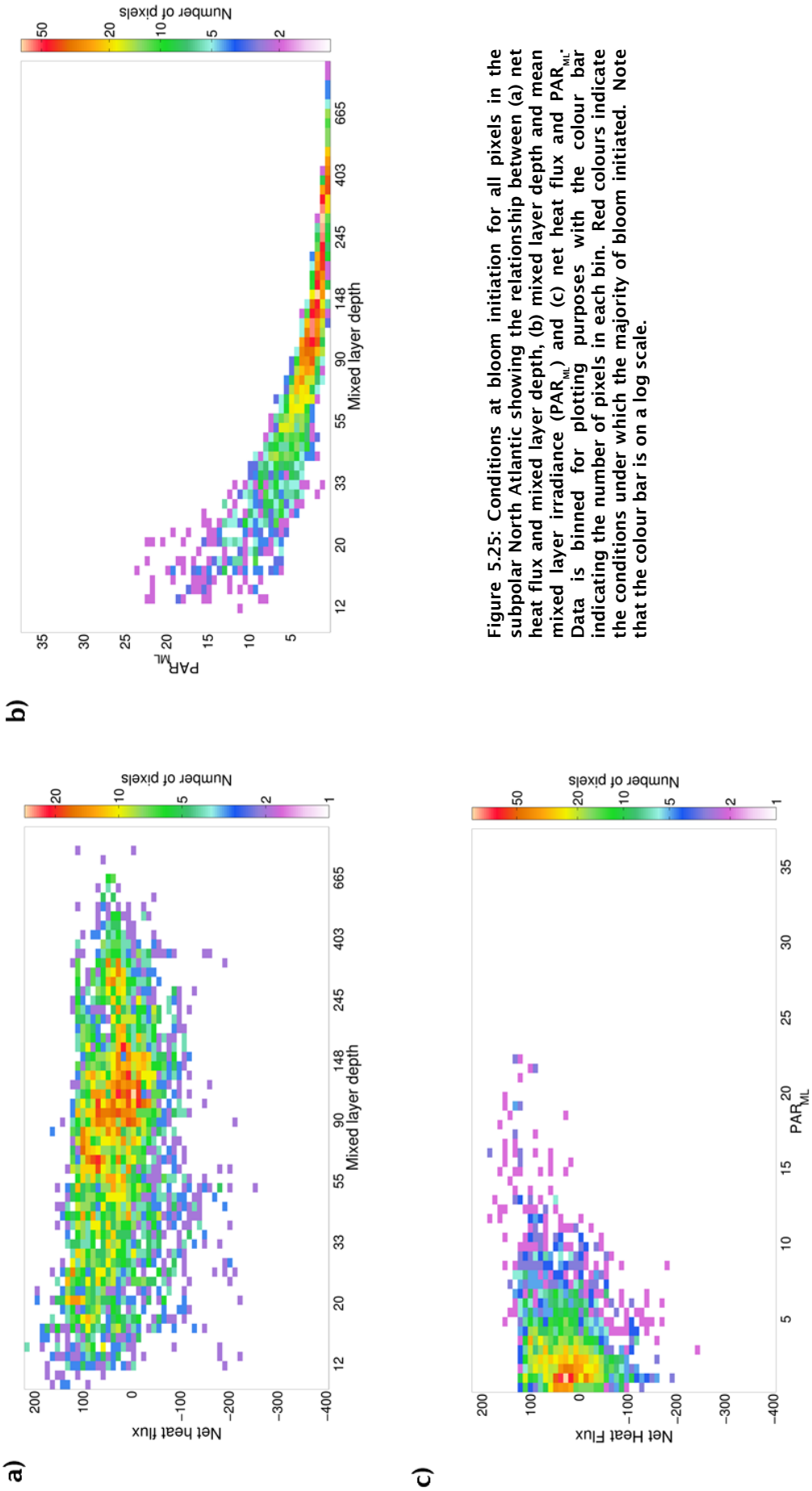

Figure 5.25: Conditions at bloom initiation for all pixels in the subpolar North Atlantic showing the relationship between (a) net heat flux and mixed layer depth, (b) mixed layer depth and mean mixed layer irradiance (PAR_{ML}) and (c) net heat flux and PAR_{ML}. Data is binned for plotting purposes with the colour bar indicating the number of pixels in each bin. Red colours indicate the conditions under which the majority of bloom initiated. Note that the colour bar is on a log scale.

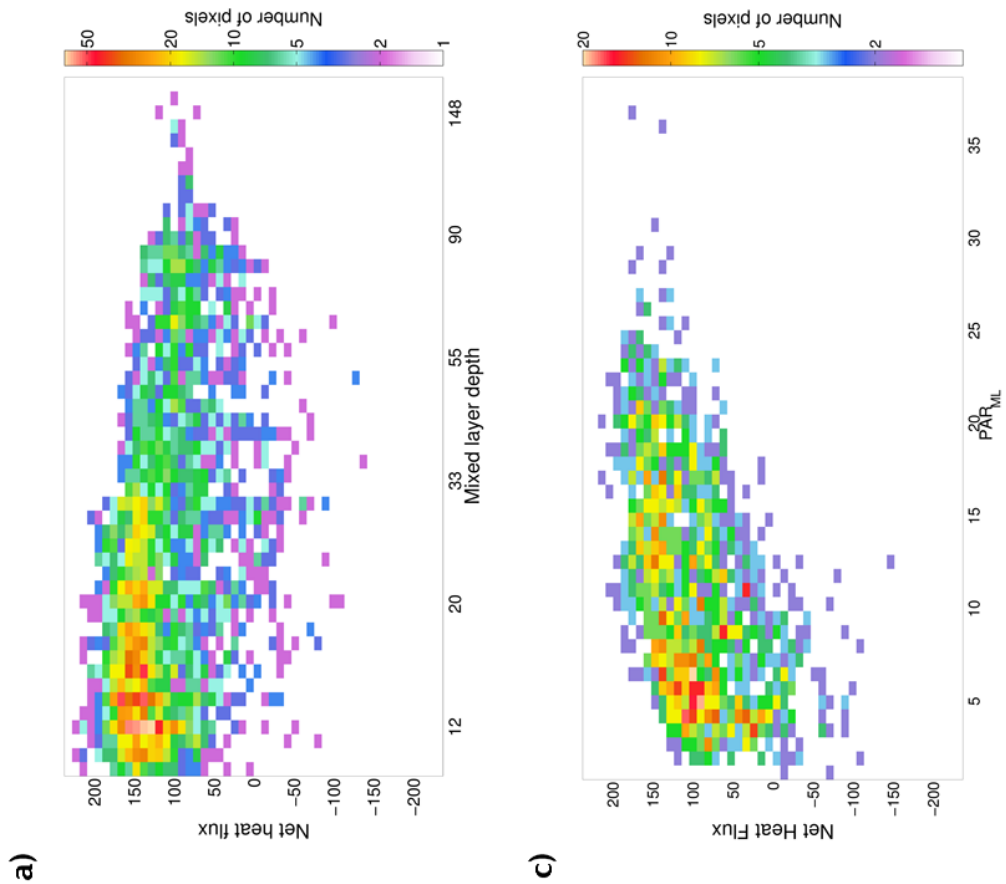

Figure 5.26: Conditions at bloom initiation for all pixels in the subpolar North Pacific showing the relationship between (a) net heat flux and mixed layer depth, (b) mixed layer depth and mean mixed layer irradiance (PAR_{ML}) and (c) net heat flux and PAR_{ML}. Data is binned for plotting purposes with the colour bar indicating the number of pixels in each bin. Red colours indicate the conditions under which the majority of bloom initiated. Note that the colour bar is on a log scale.

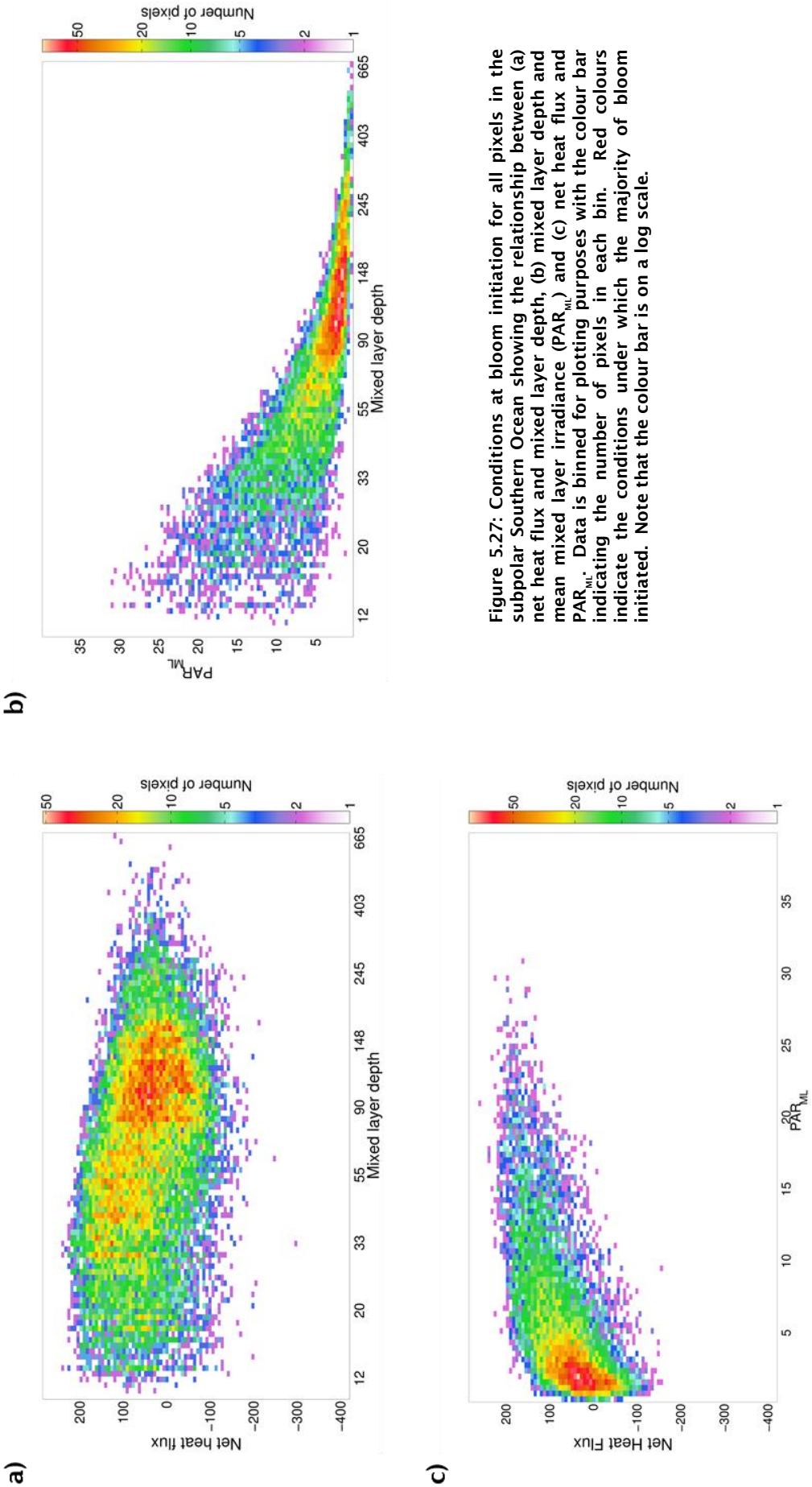

Figure 5.27: Conditions at bloom initiation for all pixels in the subpolar Southern Ocean showing the relationship between (a) net heat flux and mixed layer depth, (b) mixed layer depth and mean mixed layer irradiance (PAR_{ML}) and (c) net heat flux and PAR_{ML}. Data is binned for plotting purposes with the colour bar indicating the number of pixels in each bin. Red colours indicate the conditions under which the majority of bloom initiated. Note that the colour bar is on a log scale.

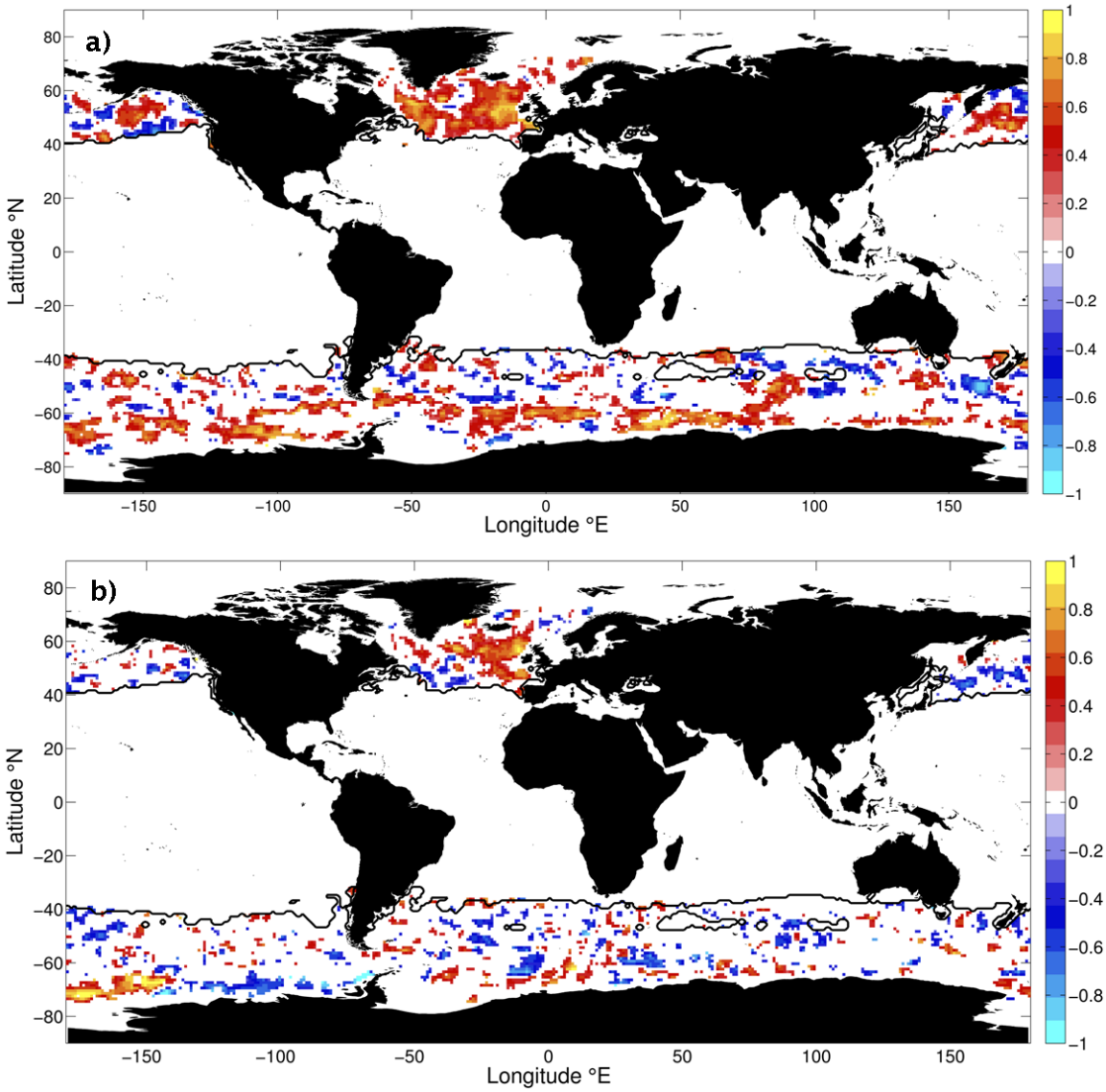

Figure 5.28: Global maps showing the pixel-by-pixel correlation between bloom initiation and (a) the date that NHF turns positive and (b) MLD shoals. The black contour line indicates the boundary of subtropical regions which are removed. Other white regions are areas where correlations were not statically significant at the 95th confidence interval.

This raises the question: why does the North Atlantic behave differently? Perhaps as already discussed above for the North Pacific, grazing pressure plays a significant role in the timing of bloom initiation. The North Pacific and Southern Ocean are both HNLC regions and so processes that deliver iron to these regions may dictate the start date of the bloom. Additionally, the role of wind mixing has not been assessed here but it is another parameter that modulates turbulence and mixed layer depth and may also be a significant driver of bloom timing. Alternatively, large difference in the physical environments in the three basins have been observed here namely, the larger MLD in the North Atlantic, even though the NHF annual cycle is broadly the same across the basin. The North Atlantic is saltier than the North Pacific due to the northward advection of warm and salty water from the subtropics by the Atlantic Meridional Overturning Circulation (AMOC) (Schmittner *et al.*, 2005). Thus, the same degree of cooling would result in denser surface waters, a more easily overturned water column and deeper MLD in the Atlantic. It is interesting that the North Atlantic seems to be different from the other subpolar basins given that many theories in oceanography have been based on Atlantic observations and are still widely accepted today. The North Atlantic may in fact be a poor base for theoretical understanding.

In accordance with the critical depth hypothesis the water column is preconditioned through winter cooling and mixing resulting in deep mixed layers. Greater preconditioning is indicative of prolonged winter conditions and thus a delayed spring. The mean winter NHF and MLD were used as proxies for preconditioning. However, neither metric gave significant correlations across all three basins indicating these are not basin scale drivers of variability in bloom initiation date. However, on regional scales, the mean winter NHF and wind speed were seen to be good predictors of the bloom initiation date in the Irminger Basin (Henson *et al.*, 2006). On basin scales, the weak relationship with winter mean values supports the conclusion that weak atmospheric forcing (NHF turning positive) is the dominant driver for variability in bloom initiation. This is because the conditions required for bloom onset are independent of the depth of the mixed layer but are associated instead with a reduction in turbulent mixing.

In conclusion, there is strong evidence that the critical turbulence hypothesis is a valid mechanism for bloom initiation, especially in the North Atlantic where it dominates across the basin. The NHF turning positive has been used as a proxy for weak atmospheric forcing following the example of Taylor and Ferrari (2011). The strong correlations in the North Atlantic with this proxy indicates that the reduction in turbulent mixing caused by the decline in surface ocean cooling allows the bloom to start as phytoplankton cease to be rapidly mixed out of the euphotic zone. The influence of this mechanism was patchier in the North Pacific and Southern Ocean

though large areas of these basins did show strong relationships. This indicates that other drivers, not considered here, are likely also responsible for variability in bloom initiation date and the drivers which dominated in particular years or regions will prescribe the interannual variability.

To definitively identify the mechanisms that initiate the spring bloom *in situ* measurements of additional parameters (e.g. turbulence, nutrients, grazing rates) would be needed. However, these results identify key drivers of variability on the basin scale though smaller scale processes may introduce variability at smaller spatial scales. For example, the results of Mahadevan *et al.* (2012) demonstrate the role of frontal slumping as a mechanism for restratifying the water column and initiating the bloom on mesoscales. Interestingly, one trigger for this process is weak surface cooling (i.e. small NHF) as well as a weakening in down front surface winds. Furthermore, the exact mechanisms for the survival of phytoplankton over winter are still not known in great detail. One such theory is that although phytoplankton are convectively mixed down to great depths they are also returned to the surface euphotic zone with sufficient frequency that production can be sustained over winter (Backhaus *et al.*, 1999, Backhaus *et al.*, 2003). Alternatively, the mixed layer eddies observed by Mahadevan *et al.* (2012) may sustain production in winter by intermittently stratifying some of the water column. Nevertheless, greater understanding of the processes that allow phytoplankton to survive in winter may give greater insights into the mechanism for bloom initiation.

5.4.4 Climate Change Implications

With anticipated future climate change, thermal stratification is expected to increase in strength and occur for longer periods (Sarmiento *et al.*, 2004). The predicted response in primary production in the subpolar regions is earlier bloom initiation, longer growing seasons and increased production (Doney, 2006, Henson *et al.*, 2009, Jang *et al.*, 2011). The subtropical gyres are expected to become more nutrient-limited with shorter growing seasons as well as expanding geographically (Sarmiento *et al.*, 2004, Irwin and Oliver, 2009).

However, though strong relationships have been seen in the equatorial Pacific between interannual variability in primary production and stratification, none were observed in other subtropical locations (Dave and Lozier, 2010, Lozier *et al.*, 2011). The explanation put forward was that the interannual variability was too small or that a combination of factors drives the variability. Similarly, weak associations have also been found here with interannual variability in physical timing and bloom timing metrics. Furthermore, recent evidence suggests that fast subsurface warming is actually decreasing the amount of stratification in the subtropics,

though the exact mechanism remains unexplained (Dave and Lozier, 2013). This introduces doubt over the expectation that future climate change will automatically result in stronger stratification. Furthermore, other potential drivers such as grazing pressure, nutrient limitation and seasonal succession, need to be examined to assess their effect on bloom timing and reaction to future climate change.

The next chapter focuses on calculating climate change-driven trends in bloom timing. The physical timing metrics with the strongest relationships with bloom timing may also be important drivers of interannual variability in the future. Thus, the results found here may help with understanding the processes driving future trends in bloom timing.

5.5 Summary

- Interannual variability in bloom timing was relatively low (16-48 days) in the subtropical and subpolar gyres but higher at the gyre boundaries, upwelling regions and at fronts in the Southern Ocean (60-140 days).
- Mean time series across subpolar and subtropical basins showed consistent matches in timing between bloom events (initiation, peak and termination) and physical events (e.g. MLD shoaling, PAR_{ML} falling).
- In subpolar regions the NHF turning positive was a strong predictor for the bloom initiation date, especially in the North Atlantic. Weaker relationships were seen in the North Pacific and Southern Ocean though strong correlations did occur in large coherent patches.
- Further evidence that the critical turbulence hypothesis is a valid mechanism for bloom onset was found in all three subpolar basins.
- Variability in the timing of the peak and termination of the bloom were not seen to be strongly related to the physical drivers.
- Latitudinally, all aspects of bloom timing were strongly related to multiple drivers in subtropical regions. However, relationships between drivers and bloom timing were weak on interannual timescales.

6 Climate Change-driven Trends in Bloom Timing

The results from the previous chapters can now be brought together to investigate the impact of climate change on phytoplankton phenology. The bloom metrics developed in Chapter 3 provide an objective way to quantify bloom timing. This gives us a tool to monitor phenology over time and detect both anthropogenically-forced and natural changes. Furthermore, results from the previous chapter identified the potential drivers of natural variability in bloom timing. Thus, future changes may be explained by trends in the drivers or reveal which other processes, not examine previously here, may be responsible.

Global biogeochemical models (GBM) provide a means by which to predict the impact of climate change on phytoplankton phenology and primary production. This chapter uses a suite of GBMs to investigate climate change-driven trends in bloom timing. First, the skill of the models in capturing contemporary seasonality and bloom timing variability will be assessed. Then, the magnitude of bloom timing trends will be quantified to identify regions and biomes where changes are predicted to be greatest, and hence the environmental changes driving the trends. Finally, the impact of temporal resolution on the detectability of the trends will be examined.

6.1 Models and Methods

6.1.1 Global Biogeochemical Models

Global biogeochemical models are a useful tool to estimate the impact of climate change on phytoplankton ecology. They provide global coverage at relatively high temporal resolution and are thus useful for providing further insights when used in tandem with *in situ* and remotely sensed datasets. Furthermore, they provide output for a multitude of variables that are currently unobtainable on the same spatial and temporal scales in the real world such as nutrient concentrations. However, they represent a highly simplified version of the real ocean and are limited by the availability of observational data for validation, current understanding of processes and parameterisation sensitivity (Anderson, 2005). Another factor is that of resolution, which drives up computational time and costs as it becomes finer. The resolution used will dictate the type of processes that can be studied. The

models used here are all of a medium spatial resolution (~1°x1°) and are not eddy permitting, meaning that mesoscale eddies cannot be resolved. Thus, the focus here will be on basin scale changes. The models used in this chapter are all based on nutrients-phytoplankton-zooplankton-detritus (NPZD) type models. These have been further developed to expand the 4 basic state variables to include additional processes such as limitation of specific nutrients. The plankton groups have been split into differing numbers of Plankton Functional Types (PFT), which are broad groups of plankton types that are ecologically or biogeochemically important and typically have specific environmental, physiological and/or nutrient requirements (Quéré *et al.*, 2005). These groups may include diatoms, coccolithophores, diazotrophs and a small/mixed phytoplankton group. Diatoms need silica to form frustules and are important for carbon export since they form large blooms and have fast sinking speeds due to the ballasting effect of their frustules. Coccolithophores form coccoliths from calcium carbonate which has a significant effect on surface ocean carbonate chemistry and also provides ballast. Diazotrophs thrive in high sea surface temperature environments and fix atmospheric nitrogen, providing a nitrogen source for other phytoplankton (Mulholland *et al.*, 2006). Zooplankton are typically split into different size classes and graze on different phytoplankton size classes. Each group has its own individual physiology (light and nutrient requirements, growth rates etc.).

Different simulations for each model were used. Firstly, for comparing contemporary variability, a hindcast simulation at approximately weekly resolution was used. These hindcasts should simulate observed variability because they are forced with real data. For assessing future trends, a climate change forecast simulation was needed. The next section (6.1.2) provides a brief overview of the models used. More details on the models runs are provided in sections 6.2 (Contemporary Seasonality) and 6.3 (Trends in Bloom Timing).

6.1.2 Model Descriptions

6.1.2.1 MEDUSA

MEDUSA (Model of Ecosystem Dynamics, nutrient Utilisation, Sequestration and Acidification) is the National Oceanography Centre (NOC) intermediate complexity model of plankton ecosystems (Yool *et al.*, 2013). The underlying physical model is the Nucleus for European Modelling of the Ocean (NEMO) (Madec, 2008). There are 64 vertical levels with a nominal horizontal resolution of 1°x1° that becomes finer towards the equator.

MEDUSA was forced by output fields from HadGEM2-ES, the Earth System model developed at the UK Meteorological Office from 1860 to 2005. The forcing

fields include precipitation (monthly frequency) shortwave and long wave radiation (daily frequency), winds at 10m, air temperature at 2m and humidity at 2m above sea level (all 6 hourly frequency). Temperature and salinity fields were both initialised using the corresponding HadGEM2-ES output to remain consistent with the surface forcing. In 2005 the simulation followed the Representative Carbon Pathway 8.5 (RCP8.5) to the end of 2099. The biogeochemical initialisation fields for nitrogen and silicic acid also came from the World Ocean Atlas (WOA) whereas the iron fields came from a long duration model simulation (Dutkiewicz *et al.*, 2005, Parekh *et al.*, 2005).

The MEDUSA ecosystem model simulates the biogeochemical cycles of iron, nitrogen and silicon. Four groups of plankton based on size classes are present: small phytoplankton (prokaryotic nanophytoplankton), small zooplankton (microzooplankton), large phytoplankton (diatoms) and large zooplankton (mesozooplankton). Zooplankton primarily feed on the phytoplankton in their size class though mesozooplankton also eat mesozooplankton and detritus. Detritus is split into large, fast sinking and small, slow sinking particles and a sub model simulates carbon export. Phytoplankton chlorophyll is explicitly modelled and phytoplankton are able to photoacclimate. Details of the model parameterisation can be found in Yool *et al.* (2013).

6.1.2.2 TOPAZ

The Tracers for Ocean Phytoplankton with Allometric Zooplankton (TOPAZ) model (version 2) was developed by National Ocean and Atmospheric Administration's (NOAA) Geophysical Fluid Dynamics Laboratory (GFDL) (Dunne *et al.*, 2010). It is integrated within the MOM4 model (Griffies *et al.*, 2004) which is forced with the CORE forcing dataset when run in hindcast mode. The model has 50 vertical levels and a nominal resolution of 1°x1° but with higher resolution at the equator (1/3°).

TOPAZ is a biogeochemical and ecology model and includes three phytoplankton groups, two forms of organic matter and models the cycling of carbon, nitrogen, phosphorous, silicon, iron, calcium carbonate and oxygen. The first of three phytoplankton groups are small phytoplankton (termed cyanobacteria) including picoplankton and nanoplankton forming part of the microbial loop. Large phytoplankton (termed diatoms) are nano and microplankton which are characterised as being bloom forming, able to escape grazing pressure easily and are involved with particulate carbon export. The third group are diazotrophs which fix atmospheric nitrogen.

Zooplankton are not included but grazing of the phytoplankton groups is proportional to their concentration, with cyanobacteria and diazotrophs being more tightly coupled (2nd power of concentration) than the diatoms (4/3rd power concentration). The model explicitly simulates light, macro nutrient and iron limitation, and growth rates are calculated as a function of the chlorophyll to carbon ratio. The phytoplankton are assumed to be photoacclimated to the mean irradiance in the mixing layer. Further details can be found in Dunne *et al.* (2013).

6.1.2.3 CCSM3 and CCSM4/CESM1

The Community Earth System Model (CESM) is a fully coupled ocean, atmosphere, land and sea ice model (Gent *et al.*, 2011), developed at the National Center for Atmospheric Research (NCAR). Different versions of the model were used here for the comparison with contemporary seasonality and for the climate change trends assessment but, the biogeochemistry and ecosystem components are the same in each case (Moore *et al.*, 2013). The CCSM3 (Community Climate System Model version 3) was used for the contemporary seasonality comparison. The ocean component of the CCSM3 model is the POP version 1.4.3 (Los Alamos National Laboratory) which has a nominal resolution of 3˚x3˚ decreasing to 0.9° at the equator and has 25 vertical levels (Yeager *et al.*, 2006).

The CCSM4/CESM1 (Community Earth System Model version 1; CCSM4 is a subset of the CESM1 output) was used for the climate change run which is part of the Coupled Model Intercomparison Project Phase 5 (CMIP5) multi-model archive (available from http://cmpi-pcmdi.llnl.gov/cmip5/data_portal.html). The ocean component of the CCSM4/CESM1 model is POP version 2 (Smith *et al.*, 2010). This version has 60 vertical levels and 1.11° zonal resolution and latitudinal resolution ranging from 0.27° at the equator to 0.54° poleward of 33°N/S. The ocean component is forced using the CORE forcing dataset and initialised with the Polar Science Center Hydrographic Climatology datasets for potential temperature and salinity (Danabasoglu *et al.*, 2011).

The biogeochemical elemental cycling (BEC) model is embedded in the POP model to simulate ecosystem and biogeochemical dynamics (Moore *et al.*, 2013). Four phytoplankton groups are included: diatoms, diazotrophs, small phytoplankton and coccolithophores. Nutrient pools present include nitrate, ammonium, phosphate, silicate and iron. There is one zooplankton group, one DOM pool and one sinking particulate pool. Photoacclimation is achieved by allowing variable chlorophyll to nitrogen ratios following Geider *et al.* (1998). In addition, when concentrations of iron, and in the case of diatoms silica, get too low the phytoplankton cells are able to adapt their cellular quotas (Lindsay, 2012). Full details are available in Lindsay (2012).

6.1.2.4 PlankTOM5

The Plankton Type Ocean Model (PlankTOM5) was developed by the Dynamic Green Seas Group from the PICES-T biogeochemical model (Buitenhuis *et al.*, 2010). It focuses on defining a range of PFTs of which 5 are used in this version of the model. It is coupled to the NEMO physical model and has longitudinal resolution of 2˚ and an average latitudinal resolution of 1.1˚ decreasing to 0.5˚ at the equator. The World Ocean Atlas provides the temperature, salinity and biogeochemical fields used to initialise the model. The NCEP analysis dataset is used to force the model with wind speed and stress, air temperature, humidity, total cloud cover, precipitation and freshwater input (Enright *et al.*, 2009). The temperature and salinity fields are initialised using WOA fields.

As the version name of the model suggests there are five PFTs in this model. These are diatoms, coccolithophores, mixed phytoplankton, microzooplankton and mesozooplankton (Enright *et al.*, 2009). Cycles of carbon, phosphorus, silicon, oxygen and iron are explicitly modelled (Enright *et al.*, 2009). The phytoplankton can be limited by phosphate, nitrate and ammonium, silicon and iron. Water column nitrogen fixation and denitrification are modelled and the concentrations of phosphate and nitrogen are kept at the Redfield ratio. There are two size classes of detrital particles (small and large) and particles sink according to Stokes Law. Calcium carbonate and biogenic opal provide ballast and sink at the same speed as large particles. Further details can be found in Enright *et al.* (2009) and Buitenhuis *et al.* (2010).

6.2 Assessment of Modelled Contemporary Seasonality

Comparing the seasonality in the models to satellite data ensures that similarities and discrepancies between the models and contemporary observations are identified. This validates the model results and raises confidence in future trends predicted in the models. Thus bloom timing represents another validation metric for modellers, as agreement with chlorophyll concentration can be low in models. For example, chlorophyll fields from MEDUSA were only weakly correlated to satellite chlorophyll datasets (correlation coefficient between 0.2 and 0.4) (Yool *et al.*, 2011), though seasonality and bloom timing may be captured better. This section aims to quantify the agreement between the model and satellite bloom timing by comparing mean bloom dates and interannual variability globally.

6.2.1 Methods

To accurately compare the contemporary seasonality to the model, output had to be available at approximately weekly resolution to match the 8-day satellite composites. MEDUSA was available as 5 day means, and CCSM3 as 7 day means. TOPAZ and PlankTOM5 were both available as daily means and so were averaged to 8 day composites. The satellite data spanned the period 2002-2010, as did the available output from MEDUSA and PlankTOM5. However, TOPAZ was only available for the years 2002-2007 and CCSM3 for 2002-2006. For the comparison, since the models use real observational forcing, only the corresponding years from the satellite data were used.

The dates of bloom initiation, peak and termination were calculated for each pixel and each year in the model output as described in Chapter 3. Total chlorophyll was calculated as the sum of chlorophyll contribution in each PFT before calculating the timing metric. The metrics were converted to a year day (e.g. day 220) to make them comparable across the models as they used different "weekly" averages. The mean over the total time span for each model was calculated, as was the standard deviation in order to quantify the interannual variability. Since most of the models were mapped onto irregularly spaced grids the results were remapped to a regular grid for comparison with the satellite data. The satellite data mean dates and standard deviations for the corresponding years were then remapped onto the same regular grid using an area weighted mean scheme. The satellite data was mapped to the model grids because the model grids had coarser resolution. Finer resolution is not needed here since the focus is on basin scales. Additionally, regridding coarser resolution data onto a finer resolution grid introduces uncertainty as it is not known how the coarser resolution average should be split between the finer resolution grid cells. Thus, the decision was made to regrid onto the coarser resolution model grids. Statistics were calculated for each model, with its comparison to the satellite data and used to create Taylor diagrams. These were the root mean square difference (RMSD) and correlation coefficient between the satellite and model bloom timing dates and the model standard deviation normalised by the satellite data standard deviation.

Regions of low seasonality were excluded using the coefficient of variation (CV) as described in Chapter 3. As chlorophyll in the models was less variable than the satellite data a lower CV value was needed as a threshold point. This was determined by finding the CV value that would exclude an area of the oceans a similar size as for the satellite data (CV values were: MEDUSA 0.23, TOPAZ 0.25, CCSM 0.20, PlankTOM5 0.47). Though this excluded slightly different regions in each model and in the GlobColour dataset, it ensured that the low seasonality

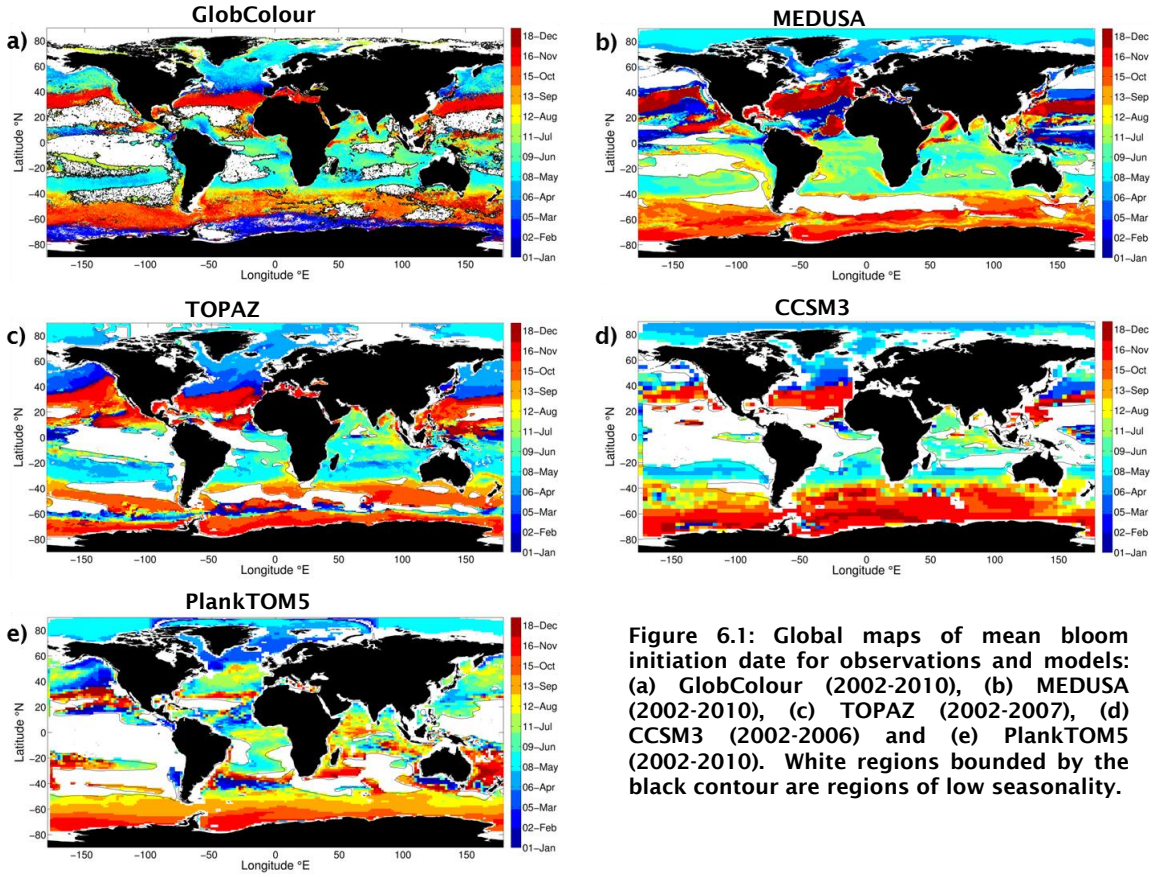

Figure 6.1: Global maps of mean bloom initiation date for observations and models: (a) GlobColour (2002-2010), (b) MEDUSA (2002-2010), (c) TOPAZ (2002-2007), (d) CCSM3 (2002-2006) and (e) PlankTOM5 (2002-2010). White regions bounded by the black contour are regions of low seasonality.

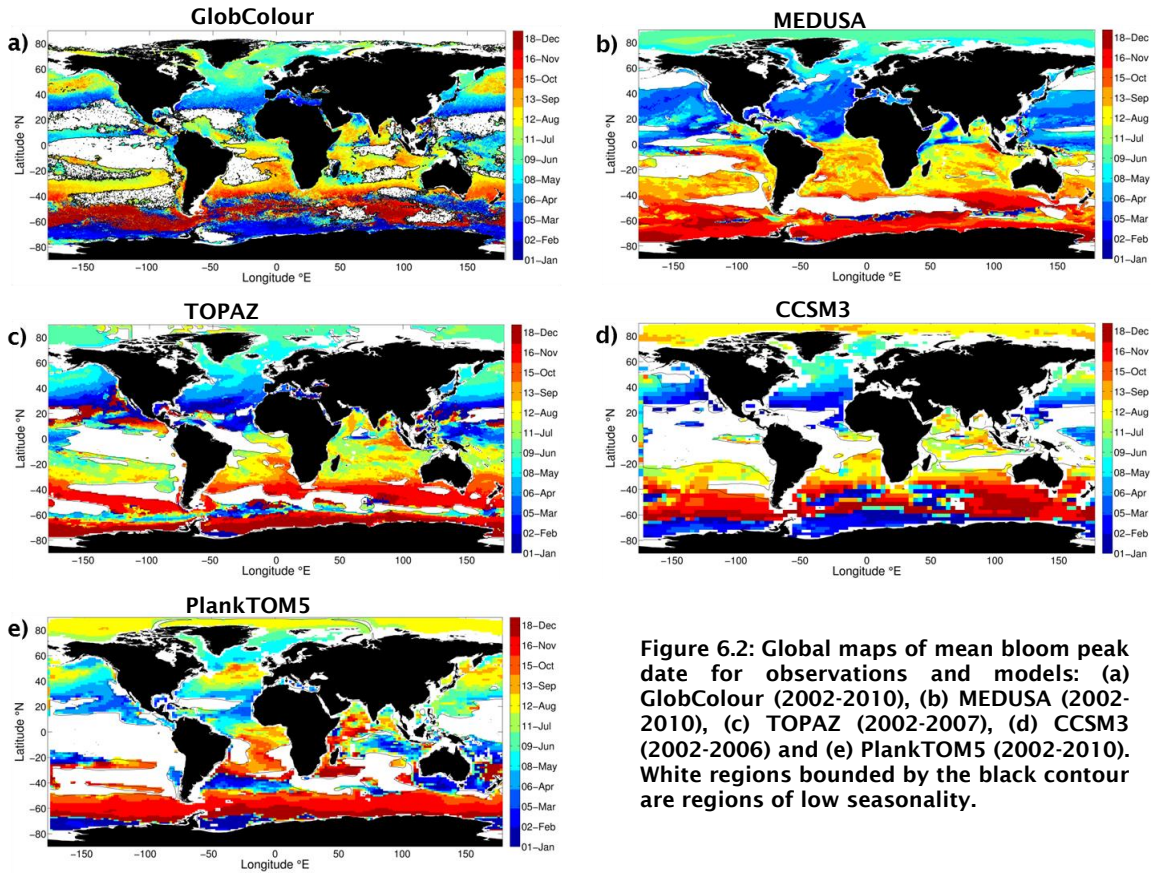

Figure 6.2: Global maps of mean bloom peak date for observations and models: (a) GlobColour (2002-2010), (b) MEDUSA (2002-2010), (c) TOPAZ (2002-2007), (d) CCSM3 (2002-2006) and (e) PlankTOM5 (2002-2010). White regions bounded by the black contour are regions of low seasonality.

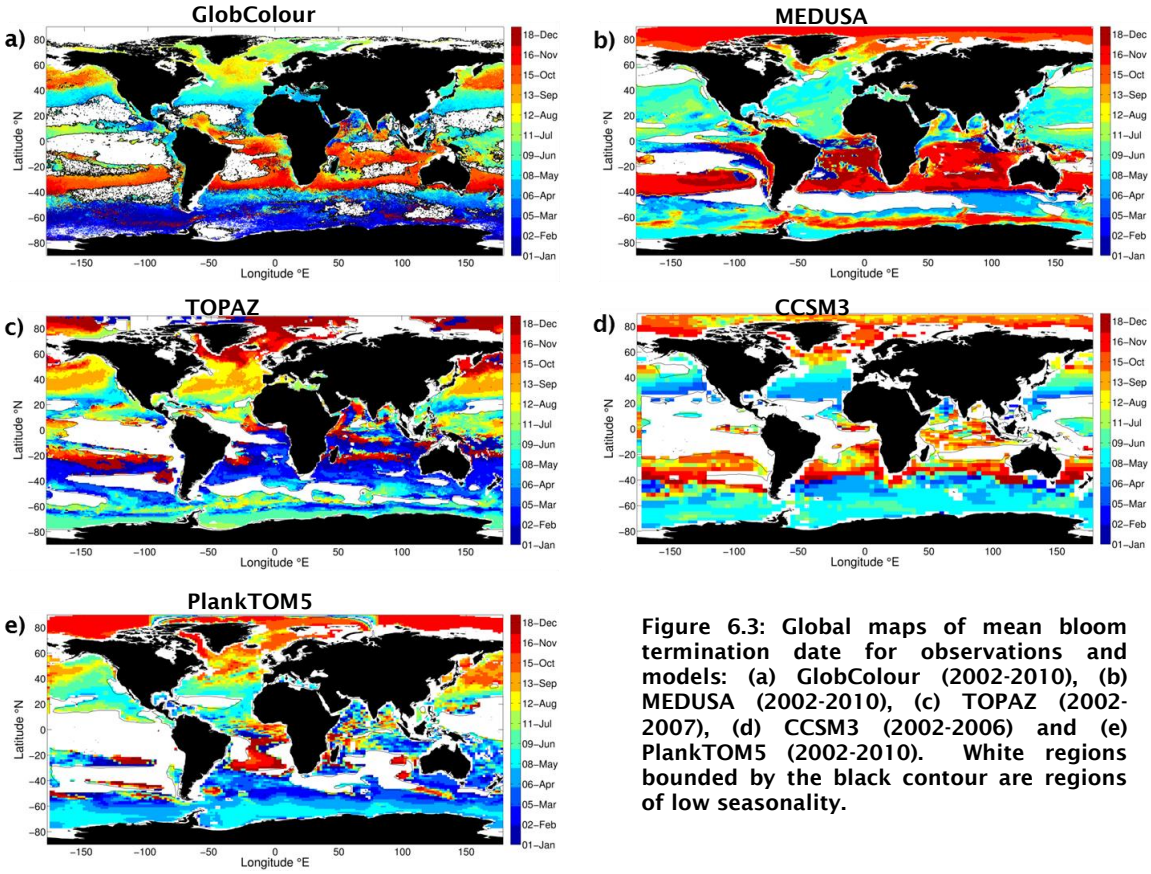

Figure 6.3: Global maps of mean bloom termination date for observations and models: (a) GlobColour (2002-2010), (b) MEDUSA (2002-2010), (c) TOPAZ (2002-2007), (d) CCSM3 (2002-2006) and (e) PlankTOM5 (2002-2010). White regions bounded by the black contour are regions of low seasonality.

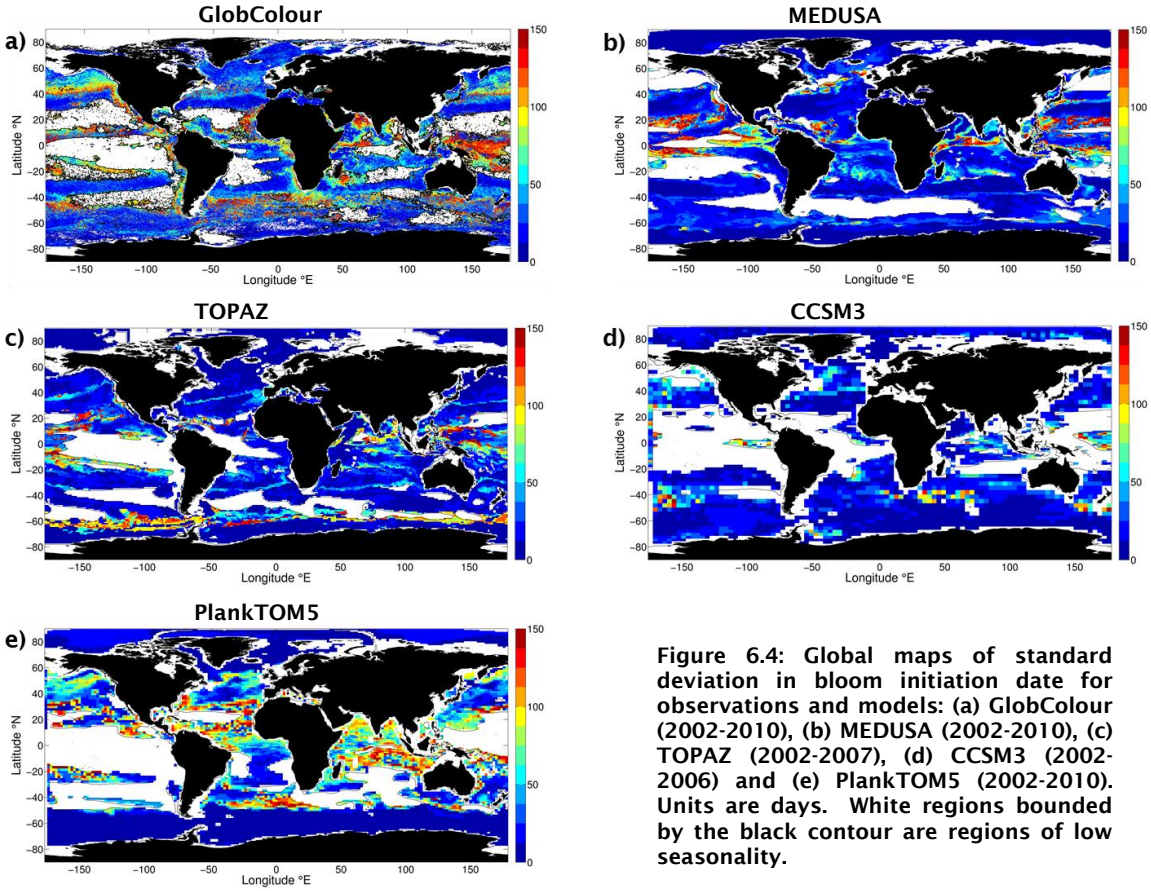

Figure 6.4: Global maps of standard deviation in bloom initiation date for observations and models: (a) GlobColour (2002-2010), (b) MEDUSA (2002-2010), (c) TOPAZ (2002-2007), (d) CCSM3 (2002-2006) and (e) PlankTOM5 (2002-2010). Units are days. White regions bounded by the black contour are regions of low seasonality.

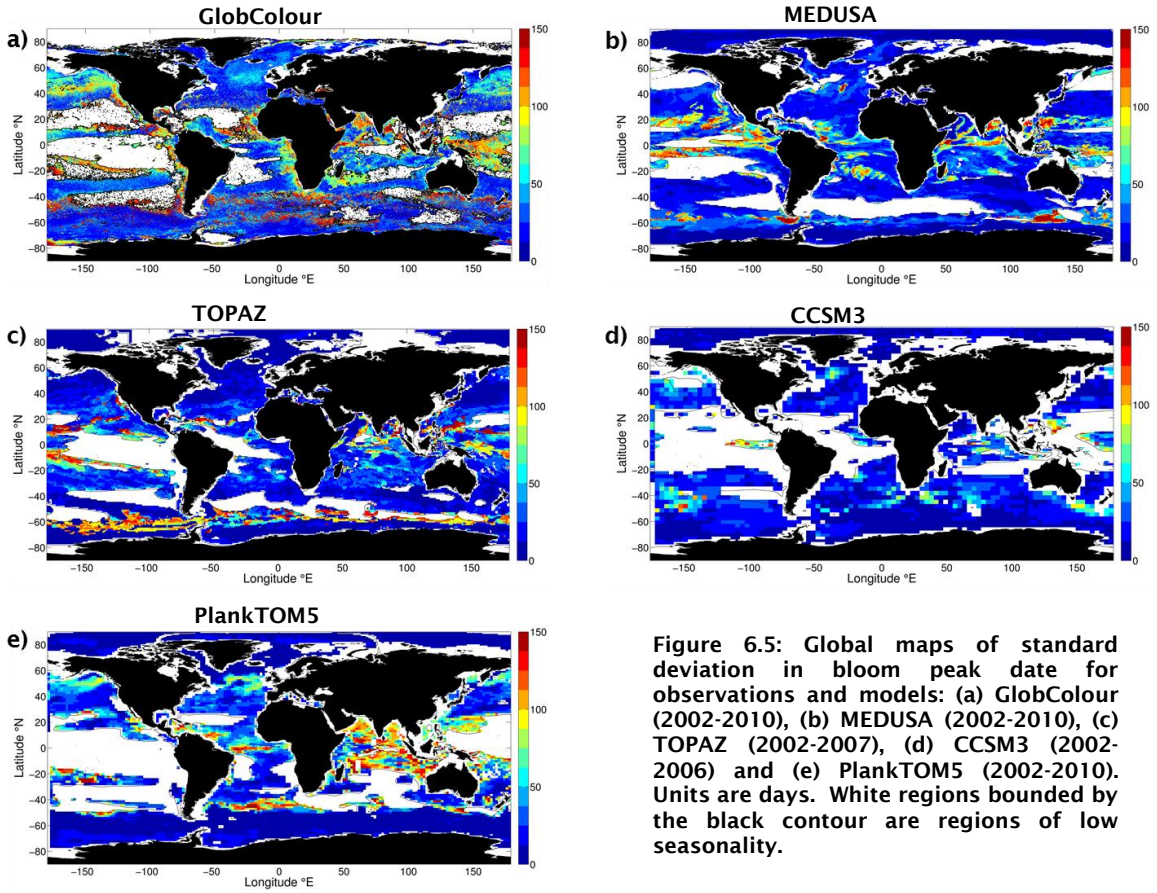

Figure 6.5: Global maps of standard deviation in bloom peak date for observations and models: (a) GlobColour (2002-2010), (b) MEDUSA (2002-2010), (c) TOPAZ (2002-2007), (d) CCSM3 (2002-2006) and (e) PlankTOM5 (2002-2010). Units are days. White regions bounded by the black contour are regions of low seasonality.

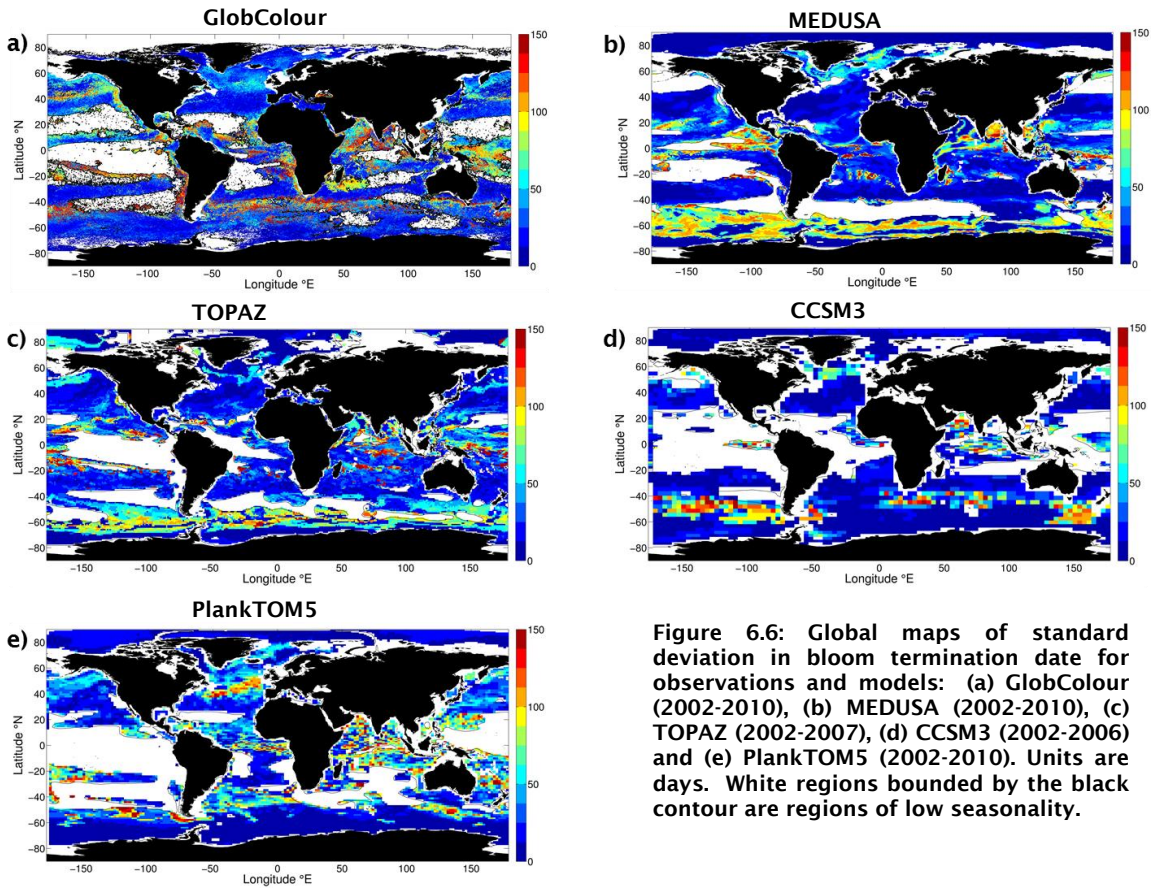

Figure 6.6: Global maps of standard deviation in bloom termination date for observations and models: (a) GlobColour (2002-2010), (b) MEDUSA (2002-2010), (c) TOPAZ (2002-2007), (d) CCSM3 (2002-2006) and (e) PlankTOM5 (2002-2010). Units are days. White regions bounded by the black contour are regions of low seasonality.

regions in all the models were removed. Removing the same regions from the models as from the GlobColour dataset would introduce errors as model regions which have low seasonality would remain. The comparison statistics were seen to vary little with changes in the CV threshold value (see Appendix E).

6.2.2 Model Comparison

The mean and standard deviation of metric dates in each model were compared to the dates from GlobColour for the years that overlapped (Figures 6.1 - 6.7). Broadly, the models capture the spatial pattern seen in the observations well. The bloom initiation date is earlier in the models than the satellite data in the North Atlantic and North Pacific (~1-2 months). Additionally the spatial variability in the TOPAZ bloom initiation date in the Southern Ocean is strongly influenced by fronts resulting in a banded pattern. The initiation dates in subtropical regions were very similar in the models and the observations in the northern hemisphere. The subtropical southern hemisphere gyres had slightly later bloom initiation than the observations (~1 month) in MEDUSA and PlankTOM5, but were similar to observations in TOPAZ and CCSM3. Overall, the models perform comparable, although PlankTOM5 showed the largest discrepancies with the GlobColour dates.

The bloom peak dates in the Southern Ocean in the models were similar to the GlobColour dates, occurring mostly in December and January (Figure 6.2). In the southern subtropical basins the bloom peak dates in MEDUSA and PlankTOM5 were slightly later (<1 month) than the GlobColour dates, though TOPAZ and CCSM3 dates were slightly earlier (~1 month). In the northern subtropical basins the TOPAZ and CCSM3 dates were earlier (~ 1 month) whereas PlankTOM5 was later (~1-2 months) than the observations. All models had similar dates to GlobColour in the North Atlantic and Pacific.

The bloom termination dates in the Southern Ocean were generally all 2-3 months later than the satellite data (Figure 6.3). The PlankTOM5 model does not compare very well in the southern subtropical basins especially the South Pacific and Indian Oceans. CCSM3 had very similar dates, while MEDUSA and TOPAZ both had later dates, than the satellite data. In the northern subtropical basins, MEDUSA and TOPAZ dates were again later (1-2 months) than observations whereas, CCSM3 and PlankTOM5 matched more closely. Most of the models had later bloom termination dates than GlobColour in the subpolar North Atlantic and North Pacific.

The agreement between interannual variability in the bloom dates from GlobColour and the models is reduced compared to the mean dates (Figures 6.4 – 6.6). For all the metrics the GlobColour dates are more variable (standard deviation 20 to 140 days) than the model dates and this high variability extends over a larger

area of the oceans. However, for the bloom initiation, the high interannual variability in PlankTOM5 extends over a larger area compared to the other models and matches the spatial pattern in the GlobColour data well (Figure 6.4). All the models capture the raised variability at the gyre boundaries and in equatorial regions although mostly with smaller values than in GlobColour. The largest variability in the peak date was found in the Southern Ocean in all the models as well as GlobColour (Figure 6.5). PlankTOM5 again is the model that shows the largest variability over extended areas. This is also true in the variability of bloom termination dates (Figure 6.6). The other models had higher variability in the bloom termination dates compared to the other metrics though the variability in the Southern Ocean was generally overestimated.

The comparison of each model and metric with the GlobColour metric dates can be illustrated using Taylor diagrams (Figure 6.7). Three statistics are needed to construct a Taylor diagram. The normalised standard deviation of the model results, the normalised root mean square difference (RMSD) between GlobColour and model dates and the Pearson's linear correlation coefficient. The standard deviation and RMSD were normalised using the standard deviation of the GlobColour metric results. A perfect match between GlobColour and model would have a normalised standard deviation of 1, RMSD of 0 and correlation coefficient of 1. The results for each model are detailed in Table 6.1. The comparison was done on a pixel-by-pixel basis and thus the statistics represent the spatial agreement in mean bloom date or bloom date interannual variability.

Overall, the mean dates from the models agree more favourably with the GlobColour dates than the interannual variability (Figure 6.7). The highest correlation coefficients (~0.82) and lowest normalized RMSD (~0.76) were seen in bloom initiation mean dates in CCSM3. PlankTOM5 performs the least well and has the lowest correlation coefficients (0.61) and highest normalised RMSD (1.05). However, all the model results for the bloom initiation dates were more spatially variable than the GlobColour dates (normalised standard deviations greater than 1). This result was also true for the mean bloom peak dates. For this metric MEDUSA was in greatest agreement with GlobColour with the highest correlation coefficient (0.74) though TOPAZ had the lowest RMSD (0.88). The bloom termination dates were more weakly correlated than the initiation and peak metrics (0.60 - 0.68). PlankTOM5 matched closely in its spatial variability (normalised standard deviation of 1.04) though CCSM3 had the strongest correlation (0.68).

Moving on to interannual variability, the majority of the models had low correlation coefficients (<0.5) though the agreement in spatial variability varied

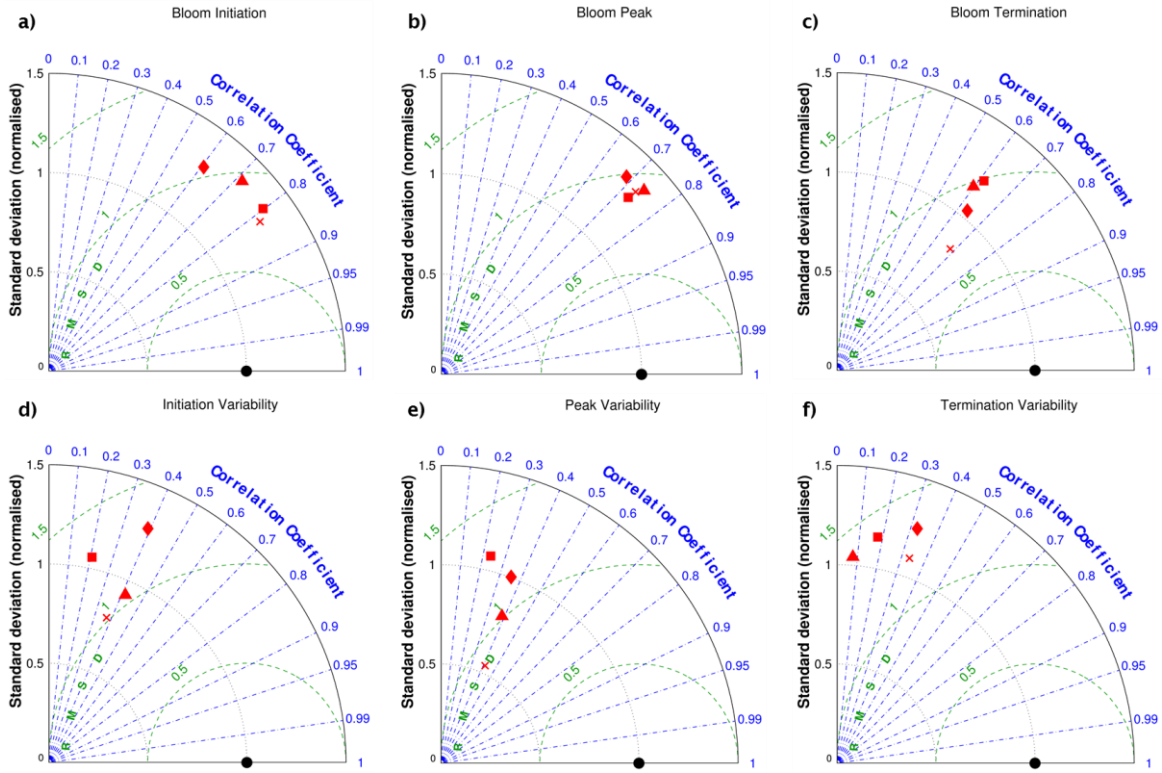

Figure 6.7: Taylor diagrams showing the agreement between GlobColour metric dates of (a, d) bloom initiation (b, e) peak and (c, f) termination and those from the ocean biogeochemical models MEDUSA (triangle, 2002-2010), TOPAZ (square, 2002-2007), CCSM3 (cross, 2002-2006) and PlankTOM5 (diamond, 2002-2010). The radial axis indicates the standard deviation of the model results normalised by the GlobColour standard deviation and the circumference axis indicates the strength of the correlation. The green lines represent the normalised root mean squared difference between the model and satellite metric dates. The black circle represents a perfect match between observations and the models and the closer to this point the better the match between GlobColour and the model results.

Table 6.1: Statistics for comparison of seasonality metric between GlobColour and global biogeochemical models[a]

		MEDUSA	TOPAZ	CCSM3	PlankTOM5
Initiation mean date	Standard deviation[b]	1.37	1.36	1.31	1.29
	RMSD[c]	0.96	0.82	0.76	1.05
	Correlation[d]	0.72	0.80	0.82	0.61
Peak mean date	Standard deviation[b]	1.37	1.28	1.33	1.35
	RMSD[c]	0.92	0.88	0.91	0.99
	Correlation[d]	0.74	0.73	0.73	0.68
Termination mean date	Standard deviation[b]	1.15	1.21	0.84	1.04
	RMSD[c]	0.98	0.99	0.75	0.87
	Correlation[d]	0.60	0.61	0.68	0.63
Initiation interannual variability	Standard deviation[b]	0.93	1.06	0.79	1.28
	RMSD[c]	1.04	1.30	1.02	1.28
	Correlation[d]	0.42	0.21	0.37	0.39
Peak interannual variability	Standard deviation[b]	0.80	1.07	0.54	1.00
	RMSD[b]	1.01	1.28	0.92	1.14
	Correlation[c]	0.39	0.24	0.42	0.35
Termination interannual variability	Standard deviation[b]	1.04	1.16	1.10	1.25
	RMSD[c]	1.39	1.39	1.21	1.32
	Correlation[d]	0.08	0.18	0.33	0.33

[a] Metric mean dates were calculated from the years in which GlobColour and the models overlapped.

[b] Model metric standard deviation is normalised by the satellite metric standard deviation.

[c] RMSD is the root mean square difference between the satellite and model metric dates. RMSD is normalised by the satellite metrics standard deviation.

[d] Correlation values are Pearson's linear correlation coefficient and all were statistically significant at the 95% confidence interval ($p<0.05$).

between models. The strongest correlations were seen in MEDUSA for bloom initiation variability (0.42), CCSM3 for peak variability (0.42) and termination variability (0.33). As a group there was not one bloom timing metric that was simulated better, nor one model that performed better, than any other.

Overall, the models perform well in simulating mean bloom timing dates, each having moderately high correlation coefficients though the spatial variability is typically overestimated (normalised standard deviation >1). The agreement with the GlobColour results for the mean dates was higher than the interannual variability which had lower correlation coefficients. However, this is expected as models are inherently less variable than observations due to the coarse spatial resolution, low frequency temporal forcing and reduced biogeochemical complexity. Discrepancies may also arise from mismatches in the geographical location of major ocean currents and biome boundaries as well as inaccuracies in the modelled chlorophyll seasonal cycle.

6.3 Trends in Bloom Timing

Having established that the models simulate contemporary bloom timing fairly well, we can move on to calculate climate change-driven trends in bloom timing. Multiple models are used here as averaging the results from a suite of models raises confidence in the results and minimises the impact of model bias. As well as quantifying changes in bloom timing over the next century, models can also inform us of the drivers of this change. As a result, in addition to the bloom timing metrics, this section will also assess trends in the physical environment (such as mixed layer depth (MLD), net heat flux (NHF), etc.) and parameters not available from remote sensing platforms, such as nutrient availability and mixed layer depth, that are believed will change into the future.

6.3.1 Methods

Monthly resolution model output was downloaded from the CMIP5 archive database for TOPAZ and CCSM4/CESM1, MEDUSA output was available from A. Yool at NOC. The RCP8.5 run was selected which is the Representative Carbon Pathway resulting in a global warming of 8.5W by 2100. The years covered are 2006-2099. PlankTOM5 was not available on the CMIP5 database and so was excluded here however; its inclusion in the previous section gives a wider context for the performance of the other models.

The bloom metrics were calculated at each pixel in each year for all three models as described in Chapter 3. The only alteration made was the way the

calendar year was divided up. In Chapter 3 the peak dates were found in a time series running January-December and again in a time series running June to May at each pixel. The time series configuration that gave the lowest standard deviation in dates was used to calculate the bloom initiation and termination dates. This prevented blooms that peaked in December/January being split in half by a January-December calendar (see section 3.2.1 in Chapter 3 for further details). When calculating the bloom trends this procedure was repeated but with the addition of two more configurations: March to February and September to August. When using just the original two configurations the peak dates were observed to be incorrectly identified when individual time series were examined. This was because many bloom timing dates were seen to transition over a whole season during the century (i.e. the date of bloom peak moved from summer to spring between 2000s and 2090s). Thus, more accurate results were obtained if the option of these extra configurations were available.

Annual means of MLD, NHF and dissolved inorganic nitrogen (DIN) were also calculated. Physical timing metrics, seen to be important across both subpolar and subtropical regions in Chapter 5, were also calculated (date of maximum MLD, MLD shoaling and NHF turns positive). In some regions the time series of bloom metric date over the century saw the bloom dates shift over the turn of the year (i.e. move from a January date to a December date) (Figure 6.8). These time series had to be corrected for their cyclic nature before fitting a linear trend. This was done by reconstructing the time series of bloom metric dates from the anomalies in timing from the 20-year mean date (Figure 6.9). To do this, first the mean bloom timing date for the first 20 years was calculated. Then, this mean date was replicated to form a bloom date time series spanning the century. This time series has the same bloom date in each year (i.e. there is no interannual variability). Then the difference between this mean date time series and the original bloom date time series was found. The difference was then added to the mean date to form the reconstructed bloom date time series. The effect of this was to adjust dates that were transitioning from January to December (Figure 6.9a) to become negative year day numbers (Figure 6.9c) so that the sign of a fitted linear trend would reflect the actual direction of the movement in bloom timing.

To make comparisons between regions with similar characteristics, ocean biomes were defined. These were based on the biome definitions of Sarmiento *et al.* (2004) using vertical velocity, MLD, sea ice presence and latitude. The definitions used here were adapted, however, to include surface irradiance as this gave more coherent and homogenous biome regions than the definitions of Sarmiento *et al.* (2004), especially for the subpolar biome (see Table 6.2). An

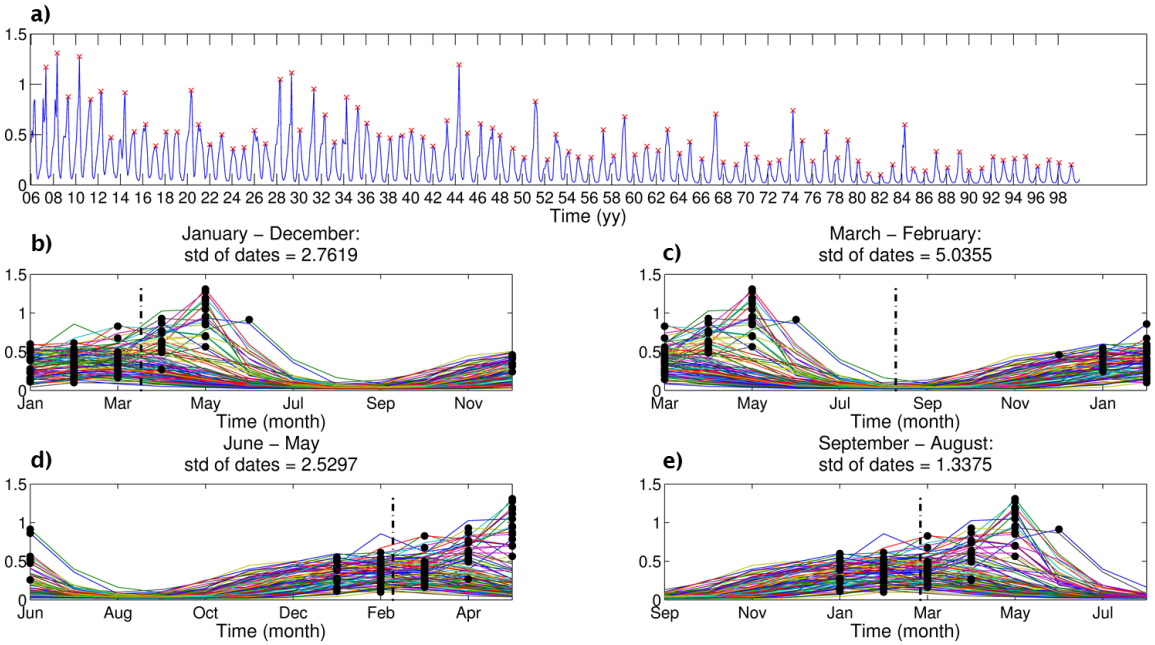

Figure 6.8: Peak date estimation using different calendar configurations. The chlorophyll time series (a) (located in the subpolar North Atlantic) can be split up January to December (b), March to February (c), June to May (d) and September to August (e). Red crosses in (a) indicate the timing of bloom peak in each year. The coloured lines in (b-e) are the chlorophyll time series for each individual year running from and to the months indicated in the title. Black circles indicate the month in which the peak occurs in each year. The black dashed vertical line shows the mean on these dates which is not always representative of the actual average peak month. The calendar configuration which gives the lowest standard deviation in peak dates is used for calculating the bloom timing metrics since the mean is a true representation of the average month and is not affected by the cyclic nature of the calendar.

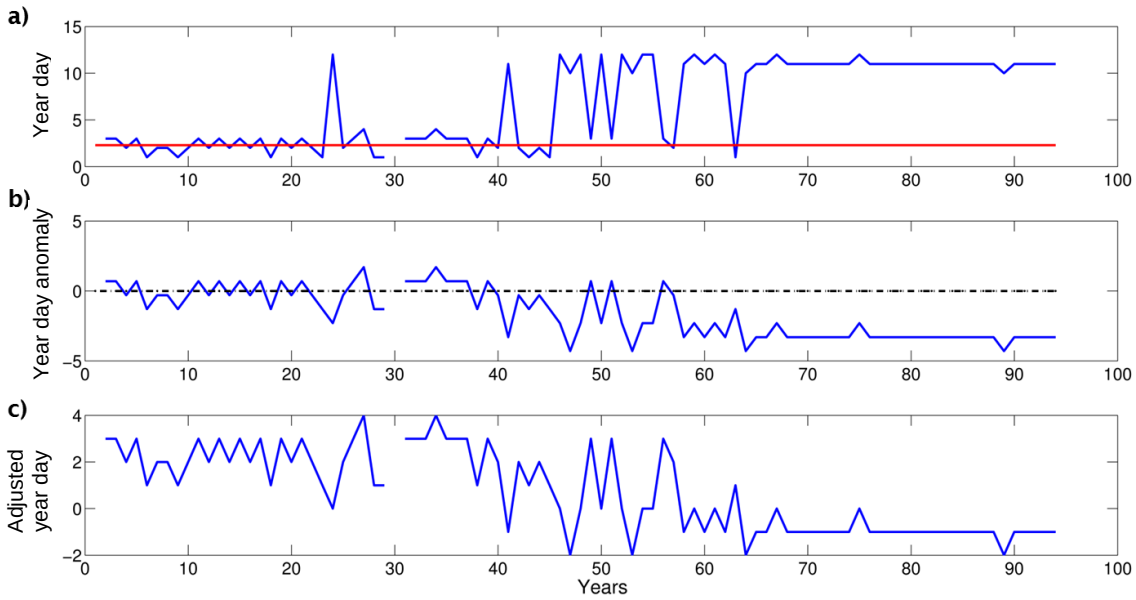

Figure 6.9: Example bloom timing time series to show correction for trend estimation. An adjustment in the bloom timing metric is needed when the date transitions over the turn of the year (i.e. January to December). The original time series (blue) and first 20 year mean (red) is plotted in (a). The mean date is repeated to form a time series without any variability. The difference between this time series and the actual time series (a) is plotted in (b). The mean date is then added back on to the difference time series (b) to form the adjusted bloom timing time series (c). This results in the sign of a fitted linear trend reflecting the actual direction of the shift in bloom timing.

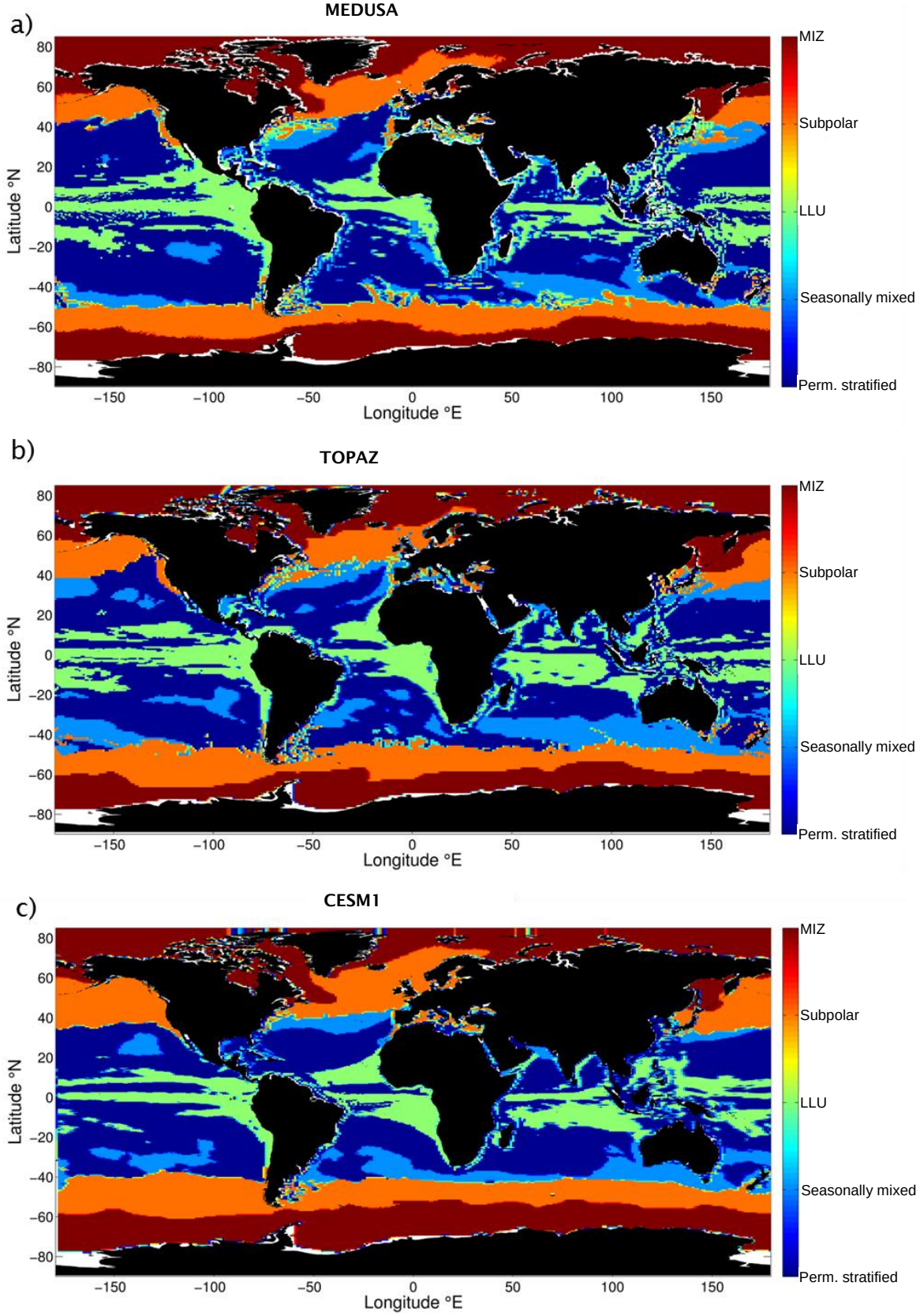

Figure 6.10: Geographical distribution of the oceanographic biomes in MEDUSA (a), TOPAZ (b) and CESM1 (c). The biomes are permanently stratified (dark blue), seasonally mixed (light blue), low latitude upwelling (LLU, green), subpolar (orange) and the marginal ice zone (MIZ, red).

annual mean surface irradiance of 120 W m^{-2} was chosen to separate light-limited regions from subtropical and equatorial regions. This value was chosen because its latitudinal location matched that of the switch from positive to negative correlations between chlorophyll and MLD. Positive correlations between the annual cycle of chlorophyll and MLD are seen in subtropical regions (deeper MLD = higher chlorophyll) whereas negative correlations occur in subpolar regions (deeper MLD = lower chlorophyll). The correlation of annual cycles in chlorophyll and MLD was used in Chapter 5 to separate subpolar and subtropical regions. However, the annual surface irradiance is used here instead to save a significant amount of computational time.

The results were also split by ocean basin (North Atlantic South Atlantic, North Pacific, South Pacific, Indian, Arctic and Southern Ocean). These biomes are expected to vary in extent each year and to change over the analysis period. Thus, the mean area and mean latitude of the biomes were calculated each year to identify strong trends over the century in the biomes. These averages were calculated as the mean total area of a biome across the three models. The multimodel mean latitudes were split into northern and southern hemisphere changes rather than calculating a global mean since northerly and southerly movements might cancel each other out.

The monthly temporal resolution used means it is difficult to properly capture the trends in phenological metrics. This makes fitting regression lines unreliable (Henson *et al.*, 2013). Instead it is better to find the difference in dates between the beginning and end of the century. This was calculated as the difference between the mean date in the last 20 years and the mean of the first 20 years. Since the differences in the biome area and latitude means were quite pronounced in some regions between the beginning and end of the century, a biome classification calculated as a mean over the whole run was not used. Rather, the biome distribution at the beginning and end of the century was used to calculate the median dates at the beginning and end of the century. This was done for the annual mean MLD, NHF, DIN and for the physical metric timings as well. A one way ANOVA (Analysis of Variance) test was used on a pixel-by-pixel basis to see if the distribution of bloom dates in the first 20 years was statistically different to the distribution of dates in the last 20 years. If a p-value of less than 0.05 was returned then the null hypothesis (that the two distributions had the same mean) was rejected at the 95% confidence interval. Those pixels that did not show a difference were excluded from analysis. The results from each model were grouped together and averaged to find a mean across the models for each basin and biome. In addition, the range (maximum – minimum) across the models for each biome and

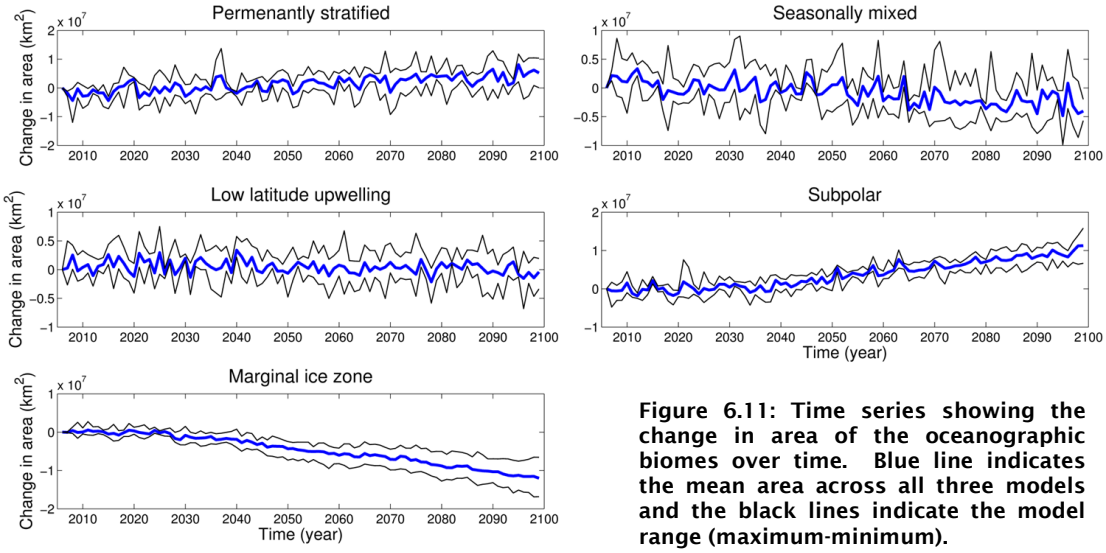

Figure 6.11: Time series showing the change in area of the oceanographic biomes over time. Blue line indicates the mean area across all three models and the black lines indicate the model range (maximum-minimum).

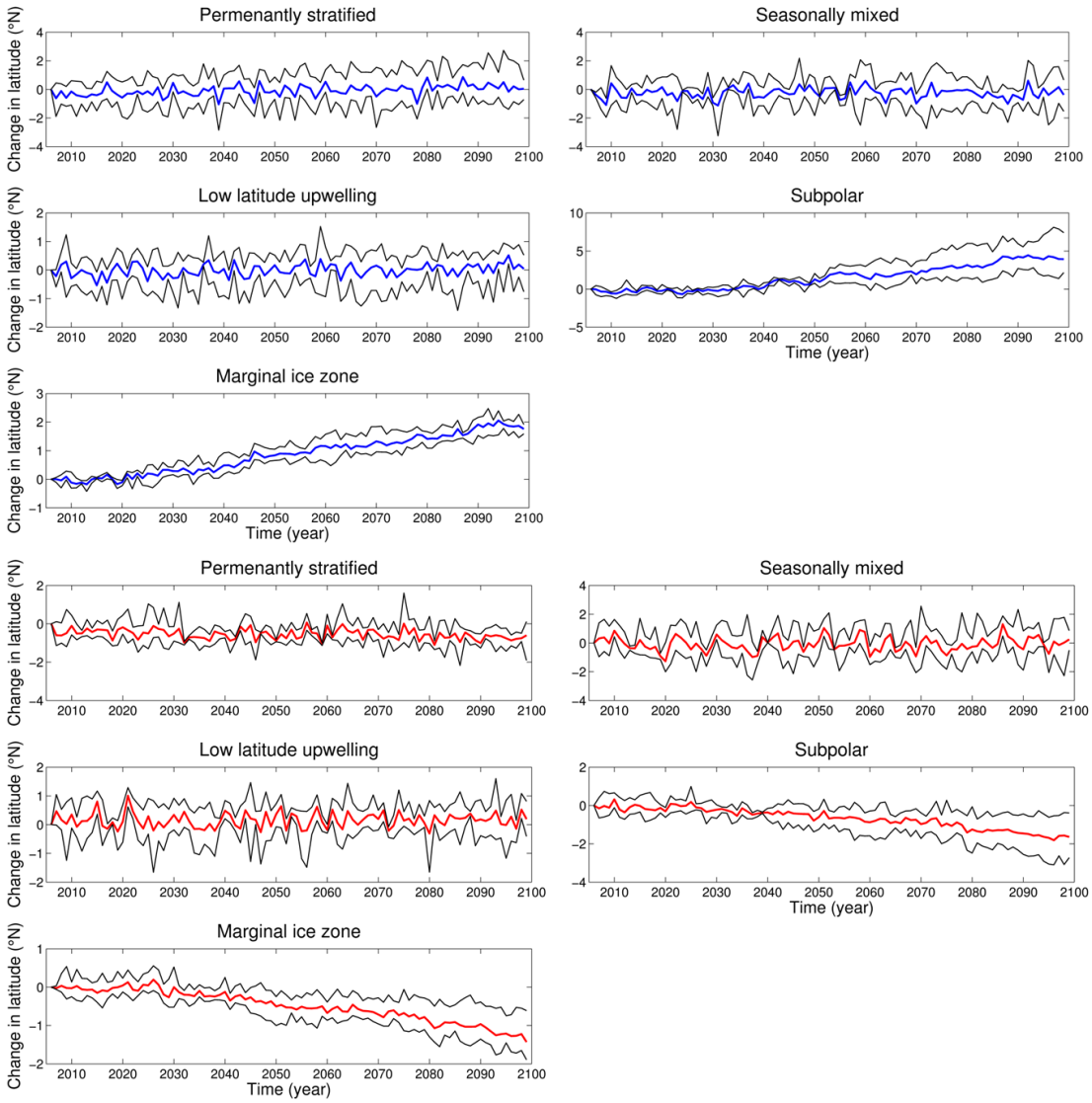

Figure 6.12: Time series showing the change in mean latitude of the oceanographic biomes over time in the northern hemisphere (blue) and southern hemisphere (red). Blue and red lines indicate the mean latitude across all three models and the black lines indicate the model range (maximum-minimum).

basin was found. Regions of low seasonality were removed using the threshold CV values detailed in section 6.2.1. To see how sensitive the changes were to the choice of CV value, the analysis was repeated but with higher and lower CV values. The results of this showed that for most biome-basin-metric combinations the difference in median values between the beginning and end of the century varied little with the choice of CV value (Appendix E).

Table 6.2: Oceanographic biome definitions[a]

Biome	Definition
Marginal ice zone	Annual total ice concentration >0
Subpolar	Vertical velocity at 50m >0 ms^{-1}, latitude >30˚N or latitude <-30˚N, or surface irradiance <120 W m^{-2}
Low latitude upwelling	Vertical velocity at 50m depth >0 m s^{-1}, surface irradiance >=120 W m^{-2}, latitude <30˚N and >-30˚N
Seasonally mixed	Surface irradiance >120 W m^{-2}, maximum MLD >=150m
Permanently stratified	Vertical velocity at 50m depth <0 m s^{-1}, surface irradiance >=120 W m^{-2}, maximum MLD <150m

[a] All criteria were based on using annual mean values for total ice concentration, surface irradiance, mixed layer depth (MLD) and vertical velocity at 50m depth.

6.3.2 Biome Changes

The spatial distribution of the biomes was very similar in all the models (Figure 6.10). However, the distribution of biomes changed during the century with changes in both total area and mean latitude. The model mean total area of the permanently stratified biome and subpolar biome both increased over time by ~3% ($0.5x10^7$ km^2) and ~18% ($1x10^7$ km^2) respectively. Both the seasonally mixed and marginal ice zone decreased in total area by ~12% ($0.5x10^7$ km^2) and ~ 29% ($1x10^7$ km^2) respectively. However, the low latitude upwelling biome remained approximately the same although showed great interannual variability. These changes in area were consistent across the models and across ocean basins.

Some changes were also seen in the mean latitude of the biomes (Figure 6.11 and 6.12). The mean latitude of the subpolar biomes in the northern hemisphere and MIZ biomes moved northwards by ~4˚ of latitude and ~2˚ of latitude respectively. This is also true of the subpolar and MIZ biomes in the southern hemisphere which moved towards the South Pole by ~2˚ degrees of latitude and ~1.5˚ of latitude respectively. Interestingly, little change was seen in the latitude of the permanently stratified, seasonally mixed and low latitude upwelling biomes in both hemispheres. This may be because the biome expansion and reduction

happens more in an east-west direction or alternatively because of differences in the latitudinal change between the models.

Overall, this indicates that the greatest changes will be near the poles with a reduction in the marginal ice zone biome as it is replaced by the subpolar biome. Though the permanently stratified biome expands by the same amount that the seasonally mixed biome shrinks a net change in mean latitude was not seen. The low latitude upwelling biome did not change in area or mean latitude over the period.

6.3.3 Trends in Bloom Timing

The trends in bloom timing were quite variable between the models and in some cases in opposite directions (Figure 6.13-6.15). Globally, changes in the bloom initiation date of ~21 for bloom initiation timing and ~25 days for bloom termination were observed (Figure 6.13 and 6.15). Similarly, differences in the peak timing between the beginning and end of the century were ~25 days (Figure 6.14). However, the largest changes in bloom timing were up to up to ±150 days in regions where there is a change from mid-summer to mid-winter blooms or vice versa. The difference in bloom timing between the start and end of the century was not statistically significant over much of the subtropical regions, across all three models and all bloom metrics.

Changes in bloom timing in subpolar regions were consistent in direction across the models (Figure 6.13-6.15). For bloom initiation, much of the Arctic and subpolar North Atlantic, North Pacific and Southern Ocean had earlier dates by the end of the century (Figure 6.13). The peak date changed in a similar fashion with much of the Arctic and Southern Ocean moving towards earlier dates (Figure 6.14). The termination date also became earlier over the majority of subpolar regions (Figure 6.15). The changes in duration in the Southern Ocean are associated with ocean fronts and generally become shorter. The largest duration changes are observed in the Arctic with bloom durations becoming, on average, ~25 days shorter.

In the subtropics there was generally a mix of areas of both later and earlier timing in initiation, peak and termination in all three models. Additionally, the direction and magnitude of the trends were inconsistent across the models. For example, in MEDUSA much of the subtropical North Atlantic moved towards slightly later bloom initiation, peak and termination dates (Figures 6.14 - 6.16). However, in TOPAZ and CESM1 the changes in bloom timing were either towards earlier dates or did not change. Interestingly, the boundary between the subpolar and subtropical gyres was visible in many of the maps with bloom initiation and

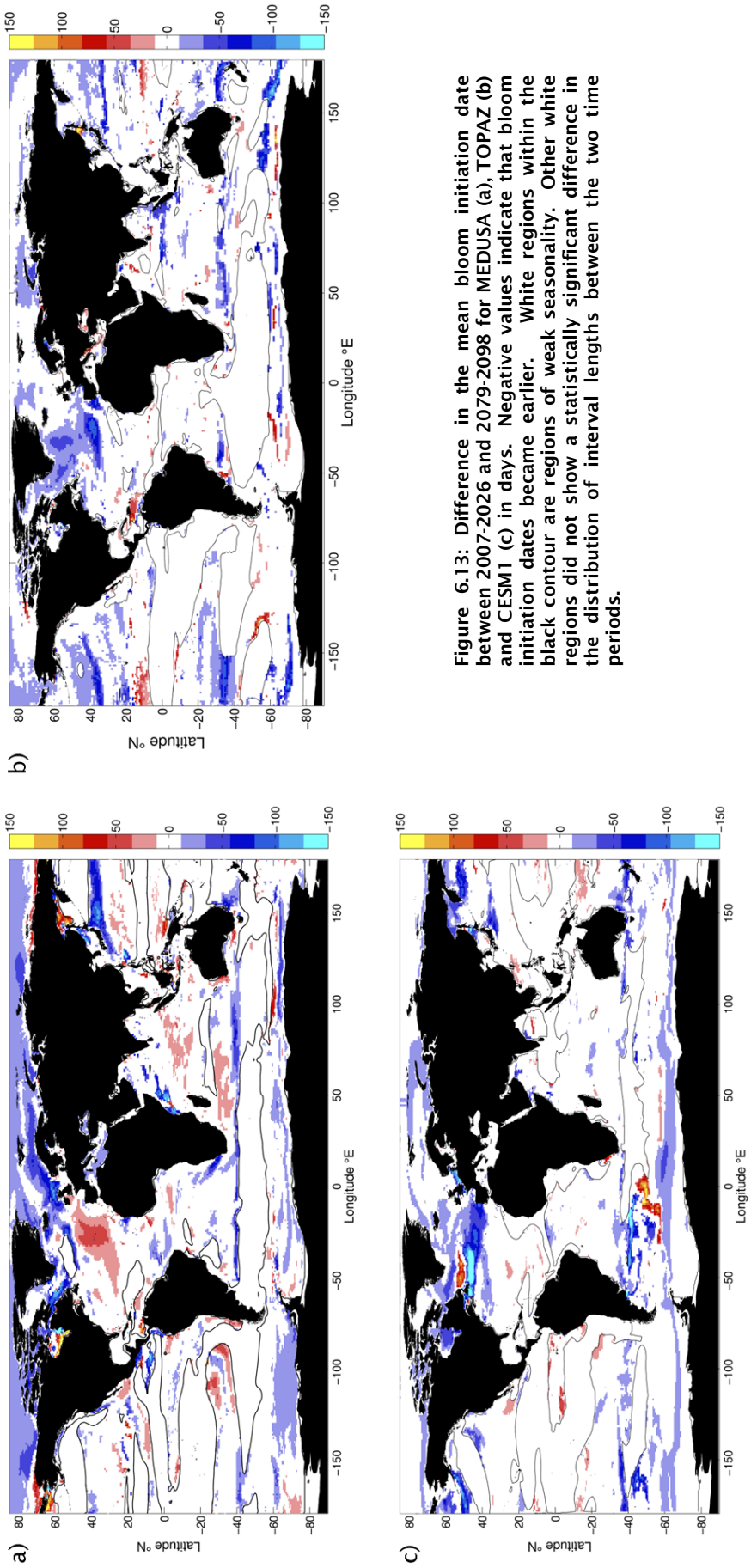

Figure 6.13: Difference in the mean bloom initiation date between 2007-2026 and 2079-2098 for MEDUSA (a), TOPAZ (b) and CESM1 (c) in days. Negative values indicate that bloom initiation dates became earlier. White regions within the black contour are regions of weak seasonality. Other white regions did not show a statistically significant difference in the distribution of interval lengths between the two time periods.

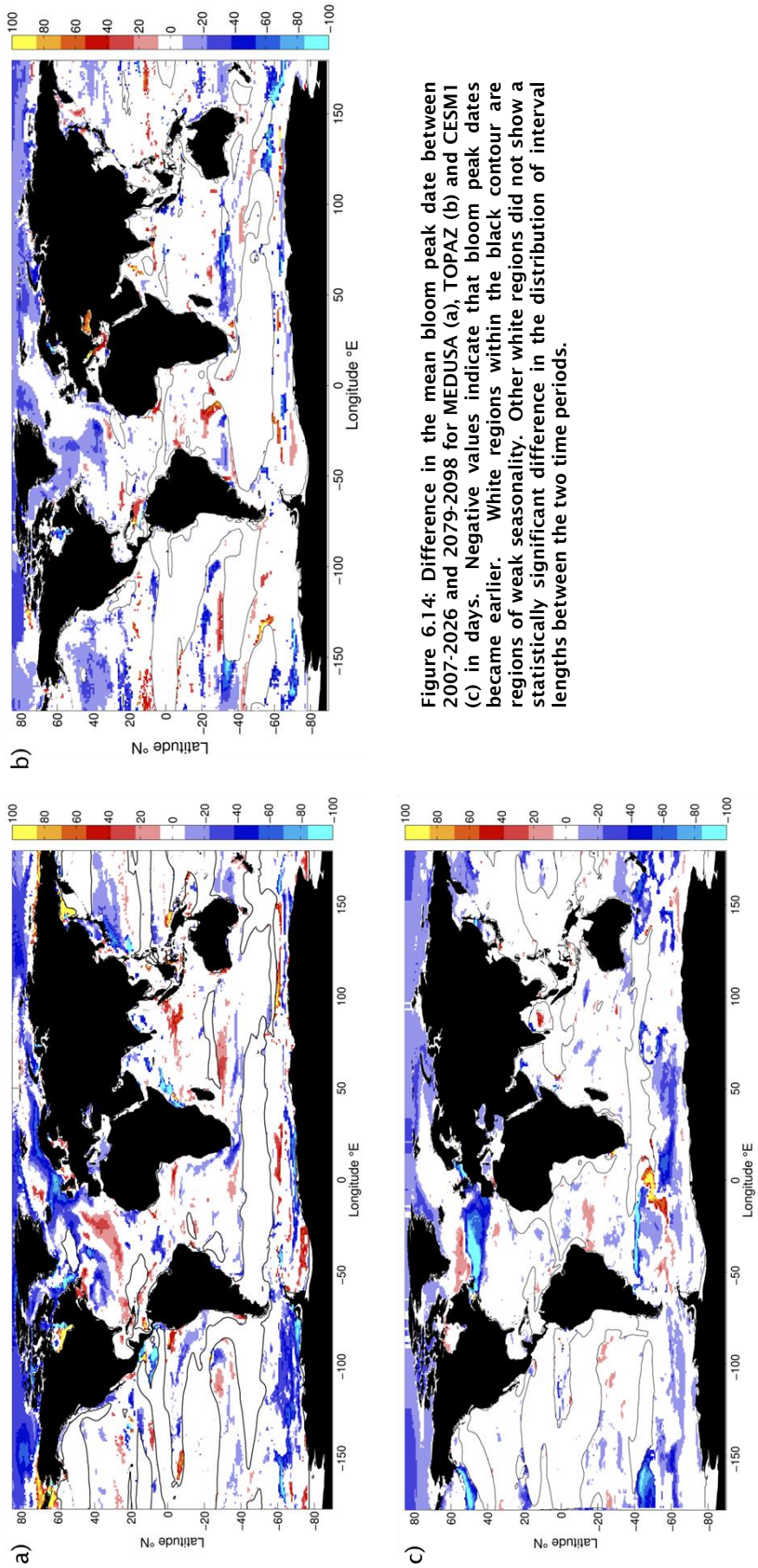

Figure 6.14: Difference in the mean bloom peak date between 2007-2026 and 2079-2098 for MEDUSA (a), TOPAZ (b) and CESM1 (c) in days. Negative values indicate that bloom peak dates became earlier. White regions within the black contour are regions of weak seasonality. Other white regions did not show a statistically significant difference in the distribution of interval lengths between the two time periods.

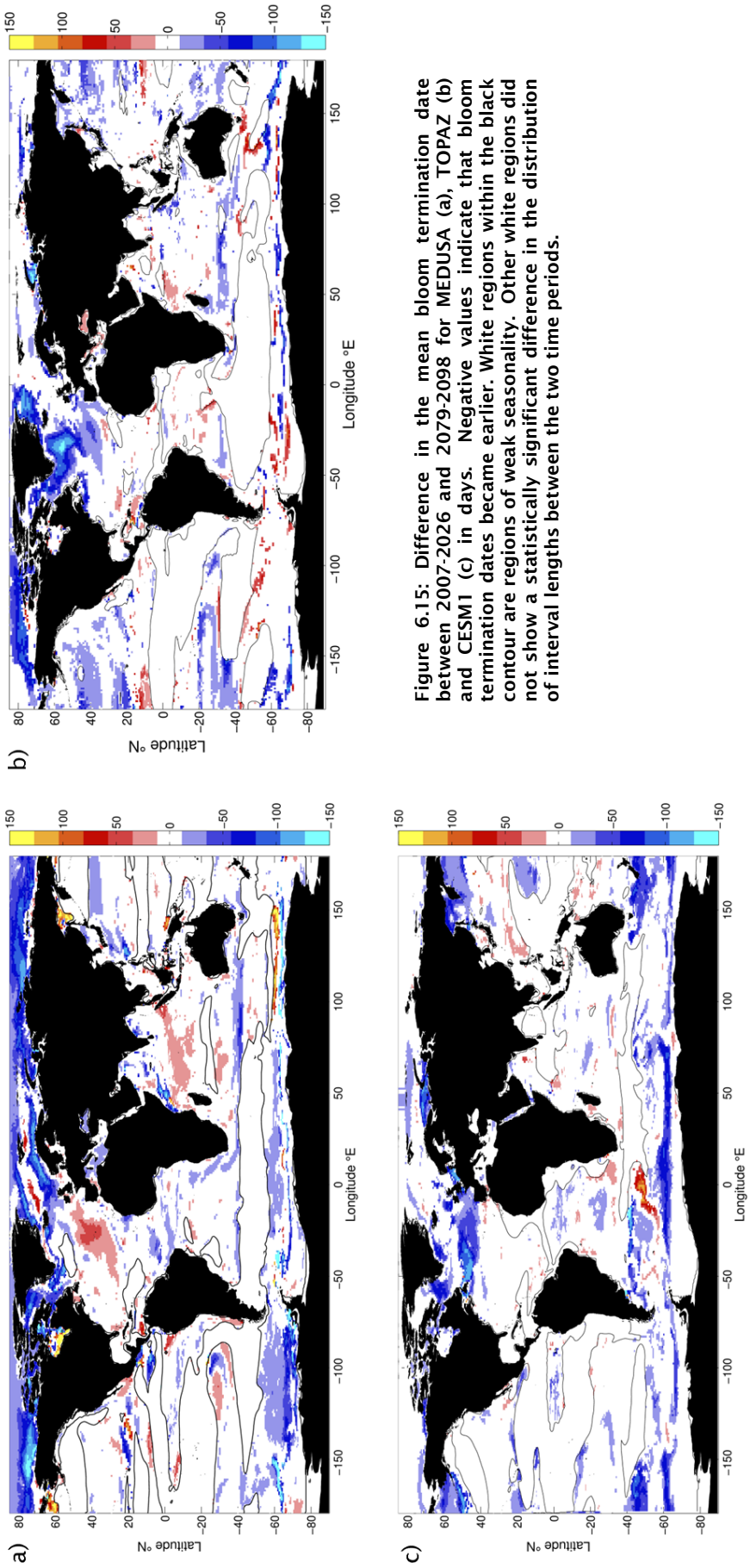

Figure 6.15: Difference in the mean bloom termination date between 2007-2026 and 2079-2098 for MEDUSA (a), TOPAZ (b) and CESM1 (c) in days. Negative values indicate that bloom termination dates became earlier. White regions within the black contour are regions of weak seasonality. Other white regions did not show a statistically significant difference in the distribution of interval lengths between the two time periods.

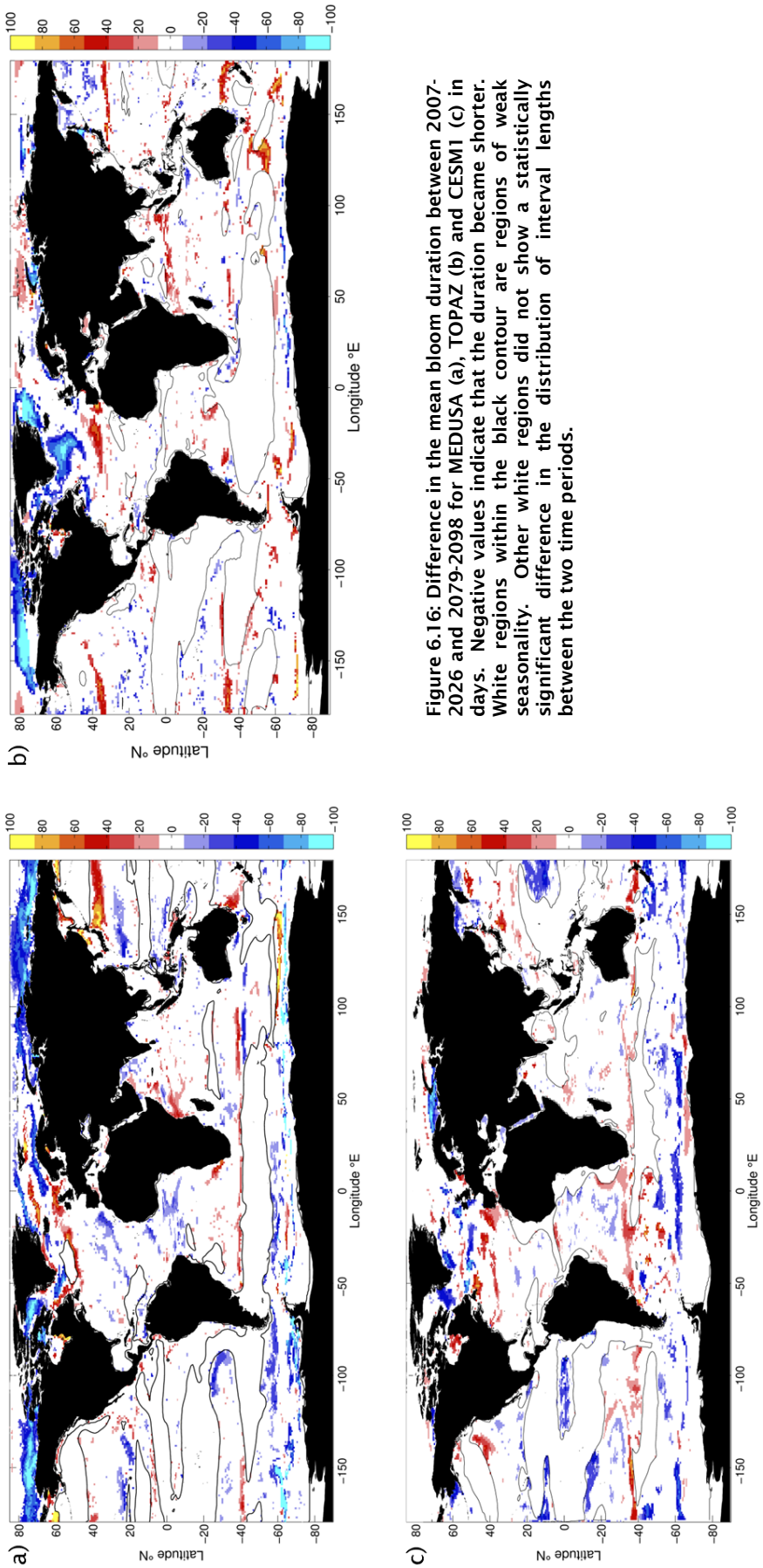

Figure 6.16: Difference in the mean bloom duration between 2007-2026 and 2079-2098 for MEDUSA (a), TOPAZ (b) and CESM1 (c) in days. Negative values indicate that the duration became shorter. White regions within the black contour are regions of weak seasonality. Other white regions did not show a statistically significant difference in the distribution of interval lengths between the two time periods.

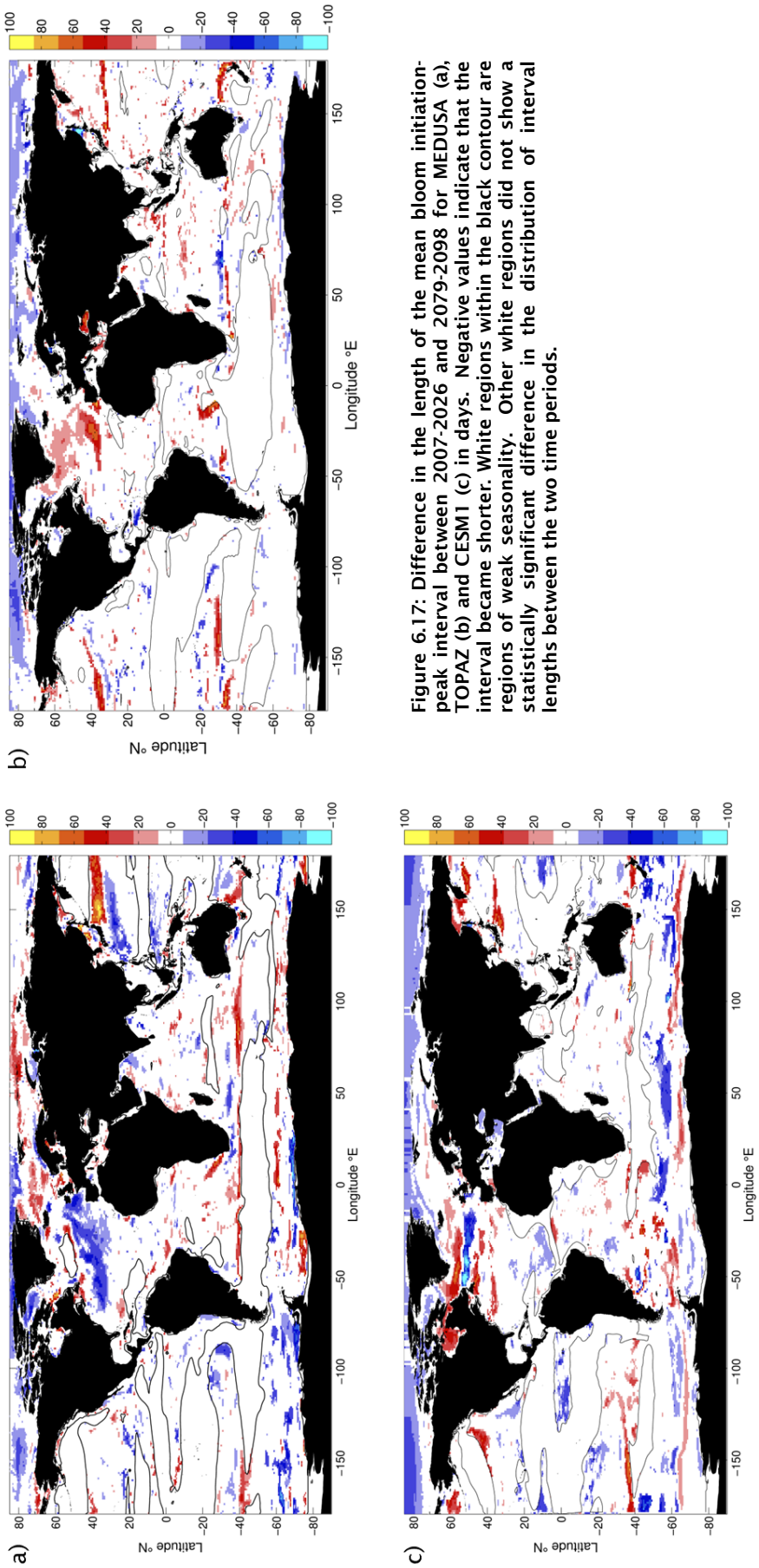

Figure 6.17: Difference in the length of the mean bloom initiation-peak interval between 2007-2026 and 2079-2098 for MEDUSA (a), TOPAZ (b) and CESM1 (c) in days. Negative values indicate that the interval became shorter. White regions within the black contour are regions of weak seasonality. Other white regions did not show a statistically significant difference in the distribution of interval lengths between the two time periods.

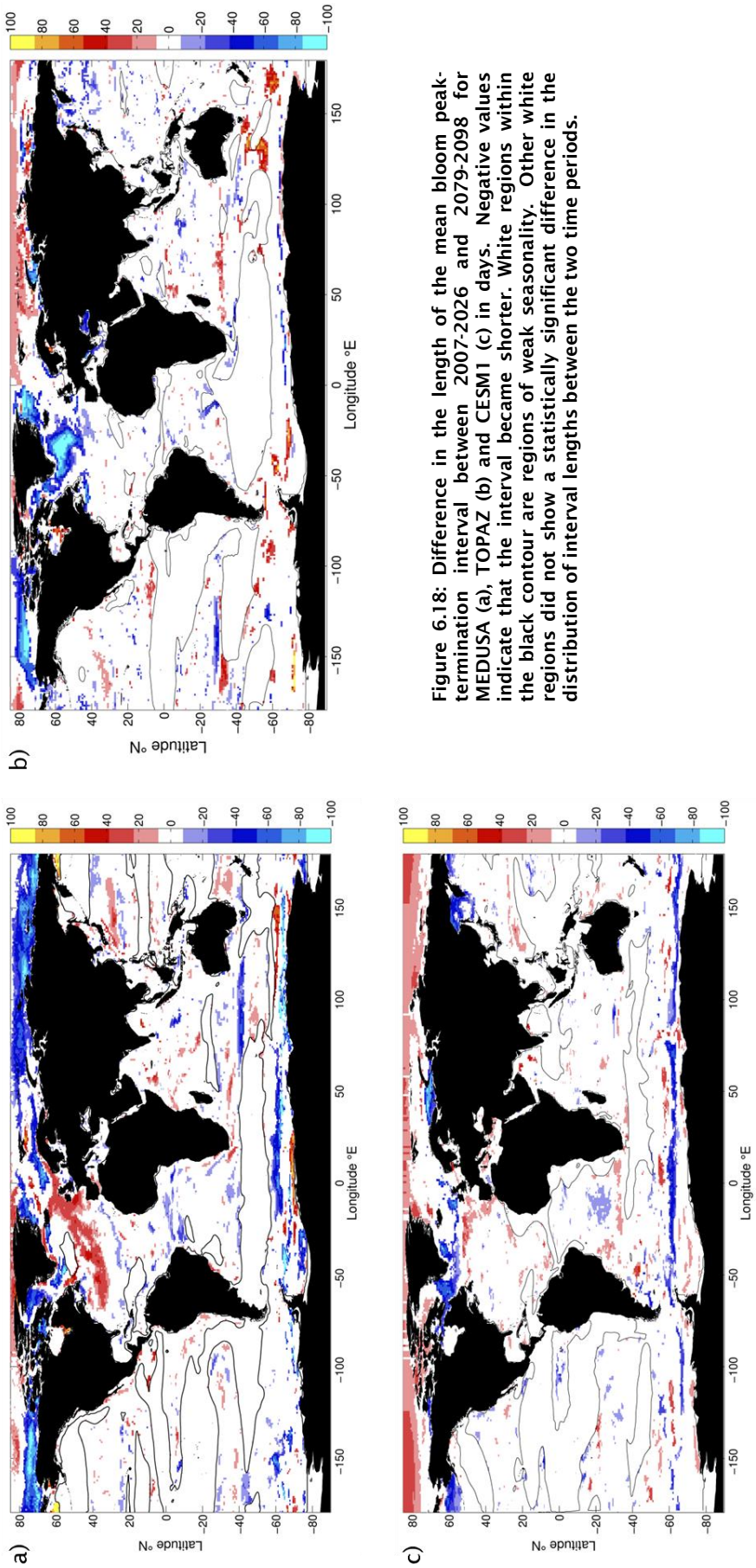

Figure 6.18: Difference in the length of the mean bloom peak-termination interval between 2007-2026 and 2079-2098 for MEDUSA (a), TOPAZ (b) and CESM1 (c) in days. Negative values indicate that the interval became shorter. White regions within the black contour are regions of weak seasonality. Other white regions did not show a statistically significant difference in the distribution of interval lengths between the two time periods.

termination dates tending to be earlier at the end of the century compared to the beginning. The subpolar-subtropical gyre boundaries are also visible in the changes in bloom duration, becoming longer over the century (Figure 6.16). As both bloom initiation and termination dates become earlier but the duration becomes longer this indicates that the bloom initiation dates are moving earlier by a greater number of days than the termination date at the boundaries. This indicates an expansion of the subtropical gyres polewards and a switch from subpolar-like to subtropical-like cycles, which are characteristic of longer but smaller amplitude blooms (see Figure 1.5 in Chapter 1 for example seasonal cycles). The transition zones are located at ~40˚S and 30-40˚N in the North Pacific in all models. The transition zone in the North Atlantic is located further north (50-60˚N) in MEDUSA than in TOPAZ and CESM1 (~40˚N). Other changes in duration across much of the subtropics are mostly insignificant and inconsistent between models.

The size of the interval between initiation and peak, and peak and termination, gives an indication of the shape of the seasonal cycle. Subpolar-like blooms tend to have a shorter time between the start and peak of the bloom than the peak and the end whereas subtropical-like blooms are the opposite (see Figures 5.5, 5.6 and 5.7 in Chapter 5 to compare bloom timing dates in subpolar and subtropical regions). In accordance with the changes in duration between subpolar and subtropical gyres the initiation-peak interval becomes longer over the century (Figure 6.17) as the seasonal cycle becomes more subtropical-like. This trend is consistent across the three models. Changes in the Arctic are mostly towards shorter intervals indicating that though the peak and initiation both become earlier in this region the peak is shifting faster.

The peak-termination interval shows quite a mixed response between the models. In the Southern Ocean there is a band of shorter intervals at the approximate location of the ice edge (Figure 6.18). Ocean fronts also seem to be areas of great change in the length of the interval corresponding to changes in peak and termination dates. For example, in MEDUSA at 60˚S between 0 and 50˚E, the peak date shifts later by ~39 days, the termination date shifts earlier by ~23 days and the peak-terminal interval shortens by ~ 62 days. The interval gets longer across much of the North Atlantic in the MEDUSA model but shorter in the TOPAZ model. Changes at the gyre boundaries are indistinct compared to previous metrics and were sometimes in opposite directions between models.

The trends in bloom timing can be broken down further by oceanographic biome (Figure 6.19 and Figure 6.20). The marginal ice zone (MIZ) has earlier initiation dates by up to ~30-75 days in the Arctic, North Atlantic, North Pacific and

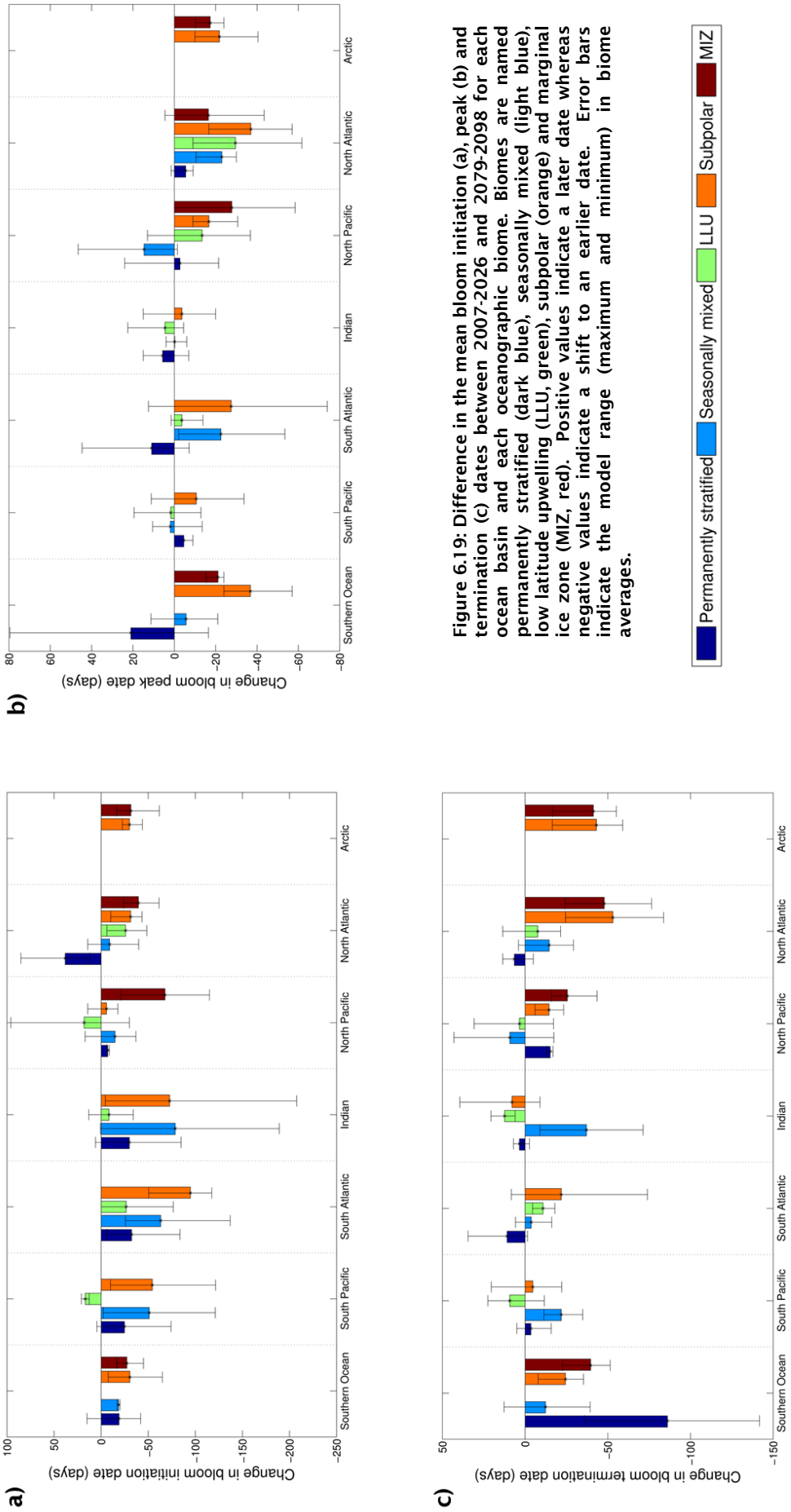

Figure 6.19: Difference in the mean bloom initiation (a), peak (b) and termination (c) dates between 2007-2026 and 2079-2098 for each ocean basin and each oceanographic biome. Biomes are named permanently stratified (dark blue), seasonally mixed (light blue), low latitude upwelling (LLU, green), subpolar (orange) and marginal ice zone (MIZ, red). Positive values indicate a later date whereas negative values indicate a shift to an earlier date. Error bars indicate the model range (maximum and minimum) in biome averages.

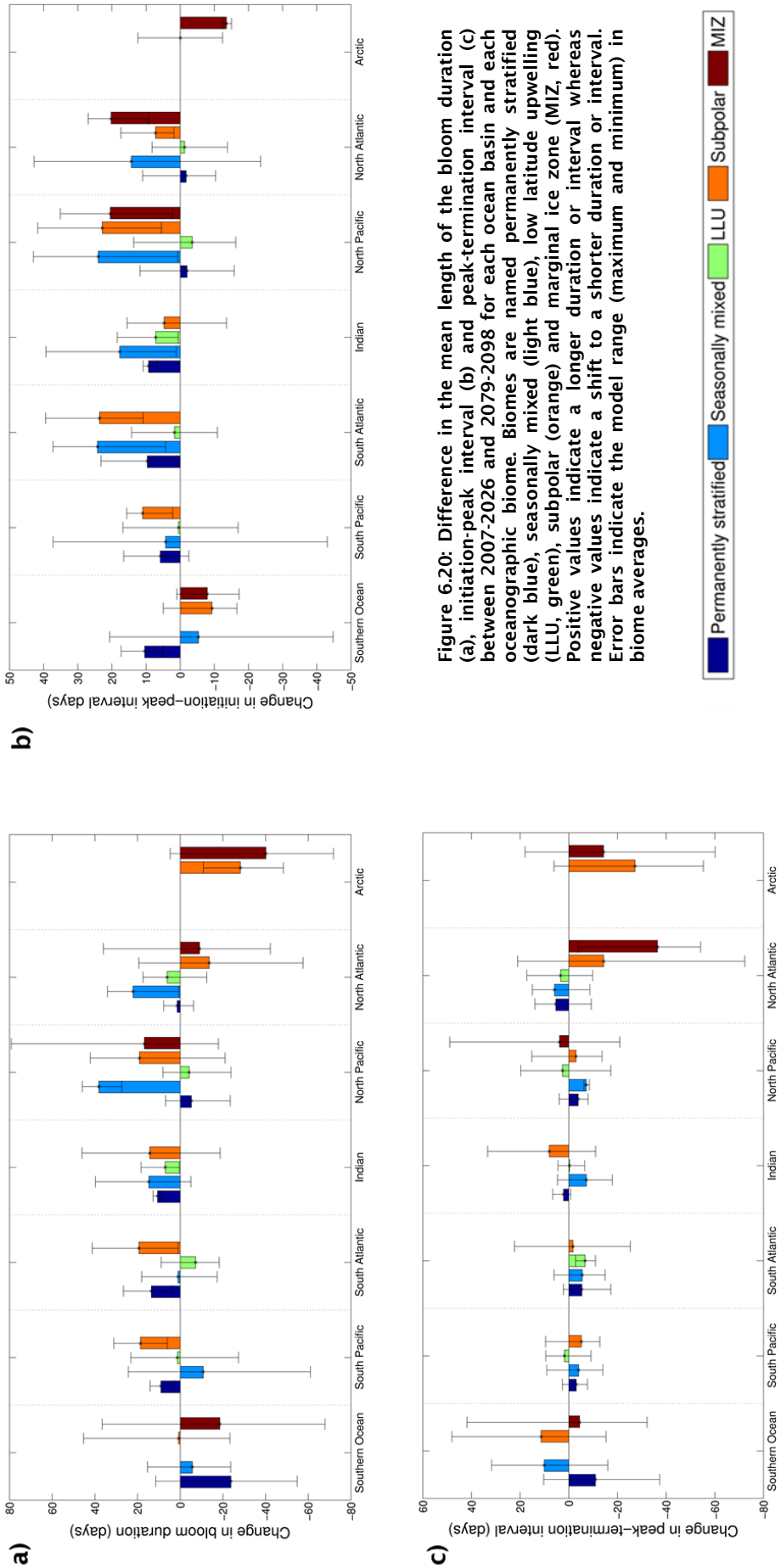

Figure 6.20: Difference in the mean length of the bloom duration (a), initiation-peak interval (b) and peak-termination interval (c) between 2007-2026 and 2079-2098 for each ocean basin and each oceanographic biome. Biomes are named permanently stratified (dark blue), seasonally mixed (light blue), low latitude upwelling (LLU, green), subpolar (orange) and marginal ice zone (MIZ, red). Positive values indicate a longer duration or interval whereas negative values indicate a shift to a shorter duration or interval. Error bars indicate the model range (maximum and minimum) in biome averages.

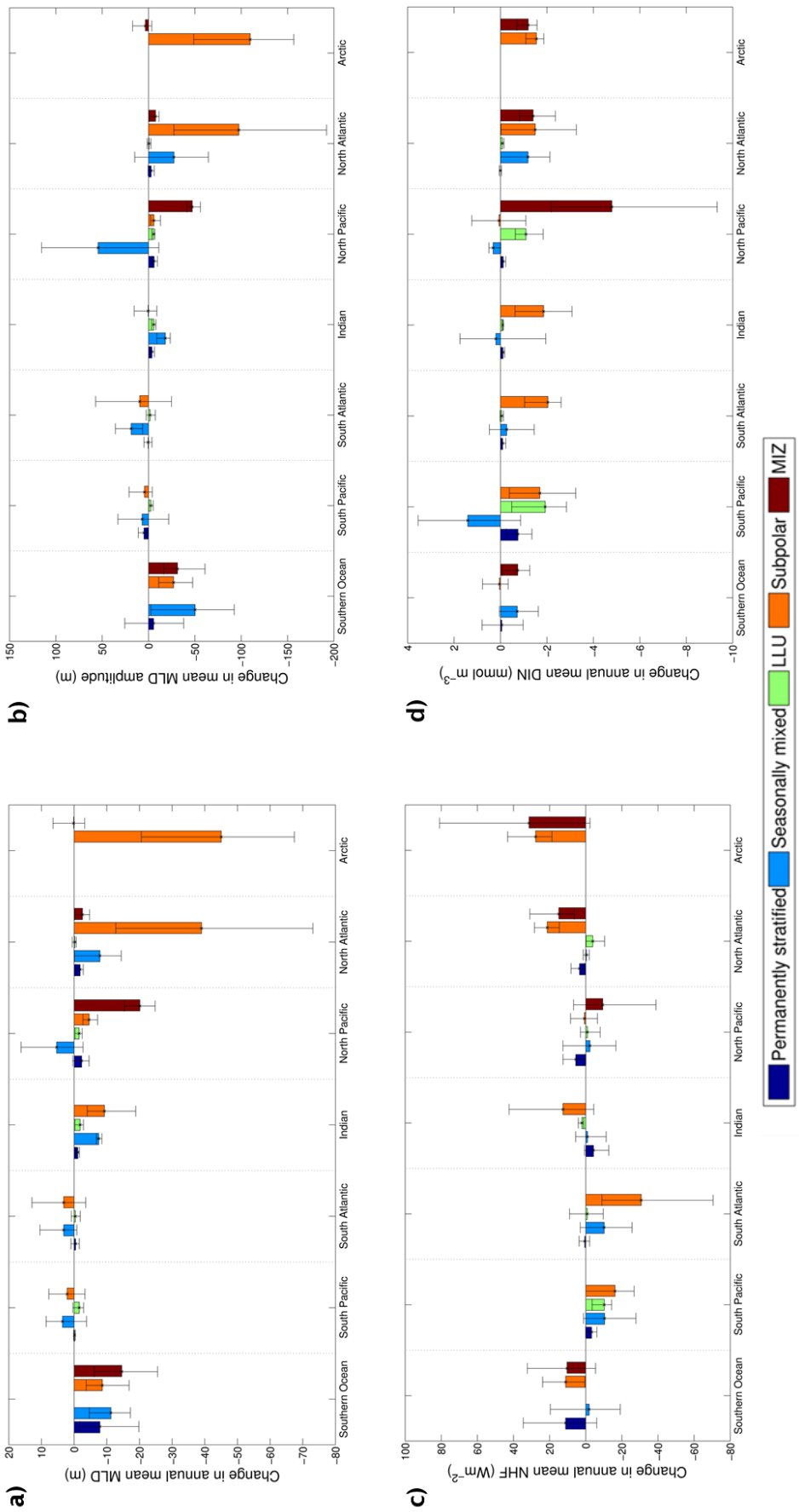

Figure 6.21: Difference in the annual mean mixed layer depth (MLD) (a), MLD amplitude (b) net heat flux (c) and dissolved inorganic nitrogen (d) between 2007-2026 and 2079-2098 for each ocean basin and each oceanographic biome. Biomes are named permanently stratified (dark blue), seasonally mixed (light blue), low latitude upwelling (LLU, green), subpolar (orange) and marginal ice zone (MIZ, red). For the annual mean MLD and MLD amplitude negative value indicate a shallower MLD or smaller amplitude. Negative values of annual mean NHF indicate a reduction in NHF but this may not necessarily mean it has become negative. Error bars indicate the model range (maximum and minimum) in biome averages.

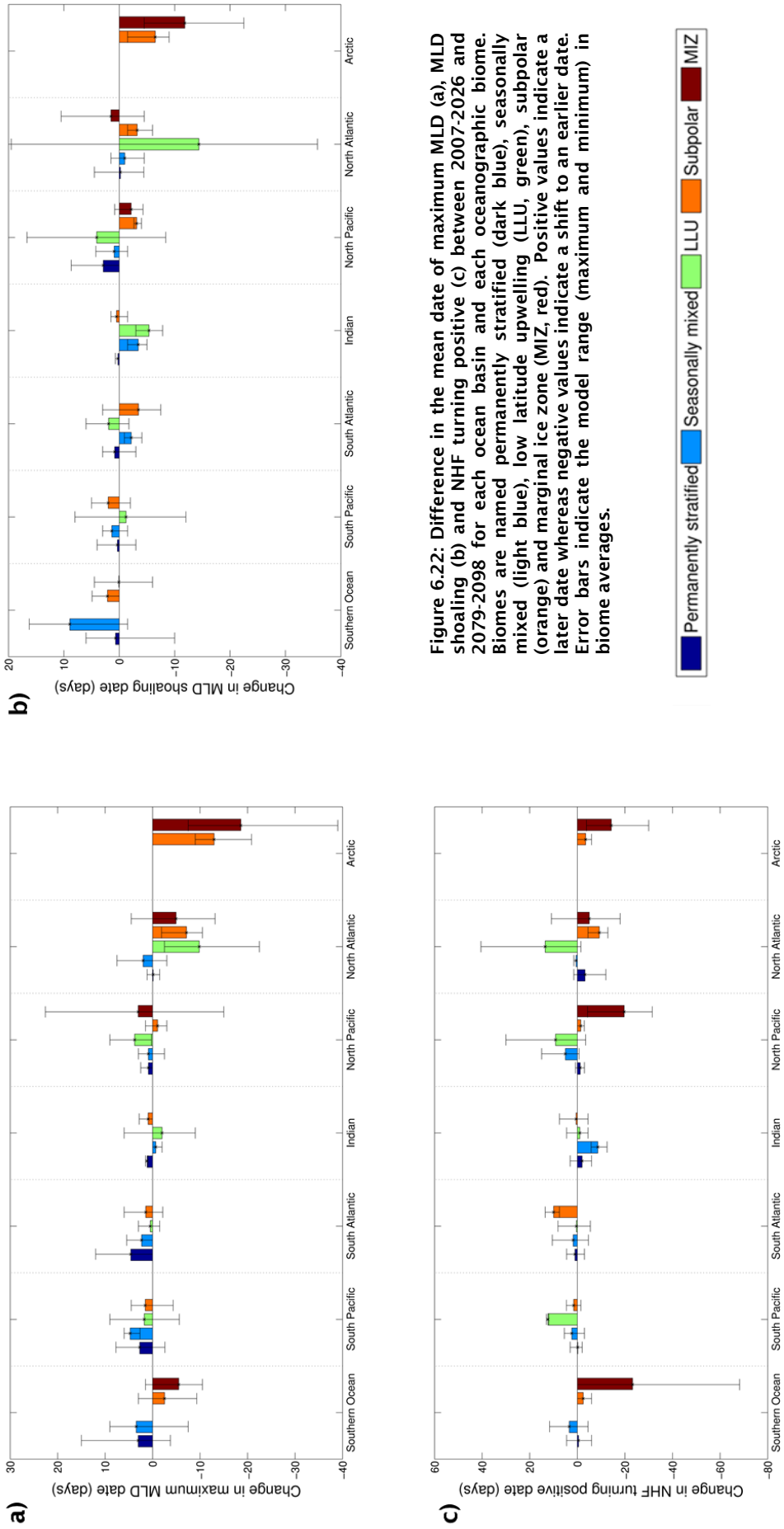

Figure 6.22: Difference in the mean date of maximum MLD (a), MLD shoaling (b) and NHF turning positive (c) between 2007-2026 and 2079-2098 for each ocean basin and each oceanographic biome. Biomes are named permanently stratified (dark blue), seasonally mixed (light blue), low latitude upwelling (LLU, green), subpolar (orange) and marginal ice zone (MIZ, red). Positive values indicate a later date whereas negative values indicate a shift to an earlier date. Error bars indicate the model range (maximum and minimum) in biome averages.

Southern Ocean. The peak also moves earlier in all basins for this biome (~10-30 days) as do the bloom termination dates (~20-50 days). Overall, the duration of the bloom becomes shorter over the century in the Arctic (~40 days), North Atlantic (~10 days) and Southern Oceans (~20 days) however, the mean duration becomes longer in the North Pacific (~20 days). The change in the length of the initiation-peak and peak-termination interval was mixed. Both become shorter in the Arctic and Southern Ocean. The initiation-peak interval becomes longer in the both the North Atlantic and North Pacific whereas the mean peak-termination interval becomes shorter in the North Atlantic and slightly longer in the North Pacific. However, not all of these changes are consistent across the models.

The mean initiation, peak and termination date becomes earlier in most basins for the subpolar biome (Figure 6.19). The bloom initiation dates are mostly earlier across the models by ~10-75 days. The peak dates move earlier in all basins (~5-35 days). Bloom termination dates become earlier in all basins (~10-50 days) except the Indian Ocean, which becomes ~10 days later. The duration becomes shorter in the North Atlantic and Arctic (~30 days) and longer in the other basins (<20 days) (Figure 6.20). However, on average the duration becomes shorter in the Arctic and North Atlantic and longer in the other basins. The initiation-peak interval becomes longer in all basins except for the Arctic where there is no change and the Southern Ocean, which becomes shorter. The changes in peak-termination interval are mostly small and are model dependent though large changes towards shorter intervals are seen in the Arctic and North Atlantic.

The low latitude biome generally showed a mixed response in the direction of bloom timing change. Changes in bloom initiation and peak date are relatively small (<40 days) and mostly towards earlier dates. The termination dates change less than 20 days and the direction is seen to vary between models. This is also reflected in the changes in duration, the initiation-peak and peak-termination intervals (change <10 days).

The date of bloom initiation becomes earlier (~10-80 days) in all basins for the seasonally mixed biome. Peak timing changes are also mostly earlier with the exception of the Pacific basins, which both move later by up to 15 days. The termination dates become earlier in most basins (<40 days) except the North Pacific where it becomes later (<10 days). The bloom duration becomes longer by up to 40 days in all of the basins except for the South Pacific and Southern Ocean. Similarly, the initiation-peak interval becomes longer by up to 25 days in all basins except the Southern Ocean whereas, changes in the peak-termination interval are relatively small and model dependent.

The smallest changes in bloom initiation date occur in the permanently stratified biome (Figure 6.19). In most basins, the bloom initiation becomes earlier by up to 25 days but becomes later by up to 30 days in the North Atlantic. The changes in peak timing are again relatively small (<25 days) and are model dependent in direction. However, large changes (<80 days) are seen in the timing of bloom termination though this is towards earlier dates in the Southern Ocean and Pacific basins and towards later dates everywhere else. This mixed and generally small response in initiation and termination dates is reflected in the small changes in bloom duration (<25 days) (Figure 6.20). The changes in the initiation-peak interval are towards a longer interval in most basins but only by up to ~10 days. Similarly, relatively small changes (<15 days) are seen in the peak-termination interval length.

6.3.4 Trends in Bloom Timing Drivers

Next, trends in the drivers of bloom timing identified in Chapter 5 in addition to trends in annual mean values will be examined. Again, the changes in the physical forcing can be summarized by oceanographic biome (Figure 6.21 and Figure 6.22). In the MIZ, over the century, decreases in the annual mean MLD and annual amplitude of the MLD were seen in all basins except the Arctic with the largest change seen in the North Pacific of approximately -20 m (annual mean MLD) and -45 m (MLD amplitude). Over the same period the annual mean NHF increased by ~15-30 W m^{-2} in the Arctic, North Atlantic and Southern Oceans whereas it decreased by ~10 W m^{-2} in the North Pacific. Decreases in dissolved inorganic nitrogen (DIN) were seen in all the basins with the largest decrease of ~5 mmol m^{-3} occurring in the North Pacific. In this biome the date of maximum MLD shifted earlier in all basins except the North Pacific by up to 20 days (Figure 6.22). The changes in the timing of MLD shoaling were slightly different becoming earlier in the North Pacific and Arctic (<12 days). The response in the Southern Ocean and North Atlantic were very model dependent. The response of the date that the NHF turns positive was more consistent, becoming earlier in all basins (<20 days).

The subpolar regions showed the largest changes in annual mean MLD reducing by up to 45 metres in the Arctic, North Atlantic, North Pacific and Southern Oceans (Figure 6.21). The amplitude of the MLD followed a similar pattern. However, there were slight increases in both the annual mean MLD and MLD amplitude in the South Pacific and South Atlantic. In accordance with these changes, the annual mean NHF increased (more warming) in the Arctic, North Atlantic, North Pacific, Indian and Southern Oceans (<25 W m^{-2}) and decreased (more cooling) in the South Pacific, and South Atlantic (<30 W m^{-2}). Interestingly, the annual mean DIN decreased slightly in all basins by up to ~2 mmol m^{-3}. The

date of maximum MLD became earlier (~1-15 days) in the Arctic, North Atlantic, North Pacific and Southern Ocean but later in the South Pacific, South Atlantic and Indian Oceans (Figure 6.22). The changes in the date of MLD shoaling were slightly different with the timing becoming earlier only in the Arctic, North Atlantic and North Pacific. On average, the timing of the NHF turning positive became earlier in the Arctic, North Atlantic, North Pacific and Southern Ocean (~2-10 days) and later in the South Pacific and South Atlantic (~2-10 days)

The Low Latitude Upwelling (LLU) biome showed mixed responses in the physical drivers across the basins (Figures 6.21 and 6.22). Only trivial changes were seen in the annual mean MLD, MLD amplitude and annual mean NHF. A reduction in DIN was only seen in the North and South Pacific (~2 mmol m^{-3}). The direction of the changes in the MLD maximum date varied between the models but was towards an earlier date in the North Atlantic (~10 days). A similar result was seen for the date the MLD shoals where it became earlier in only the Indian Ocean in all three models. Differences in the timing of NHF turning positive were more consistent between the models becoming later everywhere (<15 days).

The direction of changes in the seasonally mixed biome varied between both basin and models. Changes in the annual mean MLD and MLD amplitude were towards shallower MLD and smaller amplitude in the North Atlantic, Indian and Southern Ocean and towards deeper and larger amplitude MLD everywhere else. Similarly, the reduction (more cooling) in the annual mean NHF were small with the largest change occurring in the South Pacific and South Atlantic (-10 W m^{-2}). DIN reduced in most basins (~1 mmol m^{-3}) but increased in most models in the North and South Pacific (<1.5 mmol m^{-3}). The date of maximum MLD became later by up to 5 days in all basins except the Indian Ocean whereas the date of MLD shoaling became later in the Indian, North Pacific, South Pacific and Southern Ocean and had relatively small changes in the other basins. Similarly, the changes in the date of NHF turning positive were small (<5 days) and became later in most basins.

In the permanently stratified biome the annual mean MLD and MLD amplitude became shallower and smaller but overall the changes were small (<10m) (Figure 6.21). Similarly, changes in the mean NHF were small (<10 W m^{-2}) and there were increases in NHF in most basins (more warming) except the South Pacific and Indian Oceans. The annual mean DIN changed little but decreased in all basins the largest of which was ~1 mmol m^{-3} in the South Pacific. The date of maximum MLD became later in all basins though by a small amount (<5 days) (Figure 6.22). The changes in the date of MLD shoaling varied between the basins but overall were mostly towards later dates. Likewise, there was little change in the date the NHF turns positive and the response in most basins varied between models.

6.3.5 Drivers of Change

The trends described above are predictions of the changes in bloom timing and the drivers over the next century. For each metric, basin and biome there was generally a large range in the magnitude of these trends but a model mean value gives the most likely change. If all three models agree on the direction of the trend greater confidence can be assigned to the prediction.

With future warming the expected response is for longer periods of stronger stratification. This is expected to result in shallower MLD, increased ocean warming (net heat flux) and reduced DIN as nutrient entrainment through mixing is inhibited. Furthermore, the timing of maximum MLD, MLD shoaling and the NHF becoming positive are expected to shift earlier than current timing. The bloom timing response is anticipated to be earlier bloom initiation and later termination in subpolar regions as the alleviation of light limitation extends over a longer period. Conversely, subtropical blooms are expected to initiate later and terminate earlier as the period of nutrient limitation is prolonged.

The largest changes in bloom timing were seen in subpolar regions suggesting that bloom timing is particularly sensitive to climate change. In the subpolar biomes the annual mean MLD and MLD amplitude are, as expected, reduced and the annual mean NHF increases indicating that the ocean is warming more. Correspondingly, the annual mean DIN also reduced (~33% reduction in the North Atlantic) reflecting the shallower MLD and reduction in mixing. However, the response in the physical timing metrics was mixed across the basins. The largest changes occurred in the Arctic, North Atlantic and Southern Oceans with the date of maximum MLD and NHF turning positive becoming earlier though generally by less than 30 days. Though the timing of MLD shoaling shifts towards earlier dates in the Arctic and North Atlantic it becomes later in the Southern Ocean. Overall, the NHF turning positive is the only timing metric that consistently becomes earlier in the primary subpolar basins (North Atlantic, North Pacific, Arctic and Southern Oceans). As would be expected from the changes in the environmental factors the date of bloom initiation and peak become earlier. This is consistent with the prediction of earlier stratification onset. However, the timing of MLD shoaling did not become earlier in Southern Ocean; only the date of NHF turning positive consistently shifted towards earlier dates in the Arctic, North Atlantic, North Pacific and Southern Oceans. This agrees with the results in Chapter 5 which found that the date of NHF turning positive was a strong driver for initiating the subpolar spring bloom. However, the timing of bloom termination also became earlier across the basins though later dates were expected. This suggests that any potential for a longer growing season from the later onset of light limitation in the

autumn is overcome by seasonal nutrient limitation by the end of the century. This is supported by the reduction in duration in the North Atlantic and Arctic and is likely accompanied by a reduction in the bloom magnitude as nutrient limitation limits the size of the bloom.

The climate change response in the MIZ biome was similar to the subpolar regions with the timing of bloom initiation, peak and termination all becoming earlier. The expected climate change response is earlier bloom initiation and later bloom termination as earlier sea ice retreat and later formation extends the growing season. Though the bloom initiation does become earlier the timing of termination also shifts earlier. However, the exact response of MIZ regions still has some uncertainty. The bloom starts in these regions when light limitation is alleviated as sea ice melts and stratifies the water column, but overall primary production is controlled by the nutrient supply (Popova *et al.*, 2010). In the Arctic, earlier ice break up would lead to increased exposure to buoyancy forcing resulting in increases in nutrient concentrations providing there is not a change in riverine output which would increase haline stratification (Popova *et al.*, 2010).

The change in the physical parameters gives an indication to the drivers of the change in bloom timing. The annual mean NHF flux became much larger indicating more warming over the year resulting in a shallower annual mean MLD. The implications of this change are evident in the reduction in DIN. This is consistent with a warmer future with stronger stratification. In addition, the timing of maximum MLD, MLD shoaling and NHF turning positive all became earlier, consistent with the earlier bloom onset. The initiation-peak and peak-termination intervals became shorter suggesting that the growing season contracted and shifted earlier. Given that total primary production is governed by nutrient availability this would suggest that it is nutrient limitation that causes the bloom to terminate which here is predicted to occur earlier.

The smallest changes in the bloom timing and environmental factors were seen in the subtropics. This region can be split into 2 primary biomes the permanently stratified and seasonally mixed biome. The primary difference is the deeper winter MLD found in the seasonally mixed biome. The expected climate change response is stronger and longer stratification resulting in a later bloom initiation and earlier bloom termination. This results from greater nutrient limitation as the entrainment of nutrients into the mixed layer is reduced.

However, the trends in bloom timing were seen to have different directions in different models. This makes it difficult to say with any certainty what the basin wide phenological response would be in these regions. The North Atlantic permanently stratified biome responds in the expected way with later bloom

initiation though the bloom termination date does not become earlier. On average, the bloom initiation became earlier in all other subtropical regions contrary to the expected response. Conversely, the bloom termination became earlier in most regions as expected. The change in bloom peak timing was seen to be very variable between the models.

The changes in the annual mean MLD, NHF and DIN were more consistent with the expected climate change response in subtropical regions. In most regions the changes in annual mean NHF were small, the largest changes in MLD were towards shallower mixed layers and the largest changes in DIN were most often a reduction (albeit a very small change of <1 mmol m^{-3}). Previously, in Chapter 5, the date of maximum MLD, MLD shoaling and NHF turning positive were seen to be drivers of bloom peak timing. However, it is difficult to see a similar relationship between the change in the physical timing metrics and changes in bloom peak timing. In fact, the responses vary between the models and the model means in peak timing are not always in the same direction as the model mean changes in the physical timing metrics. Furthermore, the changes in the physical timing metrics were relatively very small (less than ~5 days) compared to the changes in peak timing for these biomes (10-25 days). Though the phenological changes seem to be weakly in accordance with the expected climate change response it is difficult to attribute the response to a change in environmental conditions. Additionally, the results in these biomes are based on chlorophyll time series which may not be representative of biomass changes in oligotrophic regions which may be responding to the changes in environmental factors (Behrenfeld *et al.*, 2005). Previously, a coincident increase in chlorophyll and reduction in biomass was reported for the Pacific Ocean in MEDUSA over the 21st century (Yool *et al.*, 2013).

However, this lack of consistency in phenological response is in agreement with several recent studies which found little response in contemporary primary production variability to environmental forcing (Dave and Lozier, 2010, Lozier *et al.*, 2011, Dave and Lozier, 2013). These studies conclude that environmental changes in the subtropics may be too small to provoke a detectable response in the phytoplankton community. This is particularly relevant given the monthly temporal resolution of these models. Moreover, phytoplankton responses tend to be one-sided in the subtropics with biomass changes occurring when nutrient availability increases being much larger than if nutrient availability becomes more limiting (Williams and Follows, 2011). This contradicts the results of Behrenfeld *et al.* (2006) which found a strong, coupling between stratification and primary production was found in subtropical regions.

As well as these trends within ocean biomes the biomes themselves are expected to change their extent with future warming. The permanently stratified and subpolar regions were seen to expand at the expense of the seasonally mixed and MIZ biomes with corresponding poleward movement (Figures 6.11 and 6.12). The boundary regions where these changes occurred experienced the largest changes in all three bloom timing metrics which were consistent with a shift in forcing. This was most evident at the subpolar-subtropical boundary where the change in bloom timing was consistent with a shift from subtropical-like to subpolar-like forcing (Figure 6.17). A similar mechanism is seen in the Southern Ocean where ocean fronts also seem to be areas of great change in bloom timing as the mean position of the fronts change over time.

Overall, the modelled climate change response in bloom timing is not wholly what is expected from observations of contemporary variability. The changes in annual mean MLD, NHF, MLD amplitude and DIN are as expected in the majority of regions and indicate increased ocean warming, shallower MLD and lower DIN concentrations. However, the climate change response in the physical timing metrics is more complex with little agreement between models in some regions and very small changes in subtropical regions. The most consistent changes were seen in the subpolar and MIZ biomes of the Arctic, North Atlantic, North Pacific and Southern Oceans and were in accordance with the expected climate change response.

Similarly, the phenological changes were not wholly as expected. Though subpolar bloom initiation became earlier in response to the earlier reduction in turbulence and onset of stratification as expected, the bloom termination also shifted towards earlier dates. Overall, this results in shorter bloom duration. This suggests that by the end of the century, any potential for longer growing seasons through delayed light limitation is offset by increased nutrient limitation.

The phenological changes in subtropical regions were very small especially in the physical timing metrics. This could reflect the inability of small changes in the physical timing metrics to be captured at the monthly temporal resolution used here, in these regions. Thus, it is difficult to attribute subtropical changes in bloom timing to the physical drivers since the physical phenological changes are relatively small. However, using a finer temporal resolution may allow relatively small phenological changes to become apparent (this is investigated in the next section).

Overall, it would seem that subpolar blooms will initiate earlier due to the earlier onset of ocean warming, and by then end of the century, terminate earlier due to nutrient limitation. This has implications for the survival of larvae at higher trophic levels. The shift in the timing of maximum food abundance by up to 40

days may result in a timing mismatch with species that match their timing of egg hatching to that of the bloom (Cushing, 1990). This is particularly relevant for long-lived organisms such as fish which have evolved to target the mean bloom date as a shift in the average date will mean their larvae miss the bloom (Mackas *et al.*, 2012). Alternatively, many types of zooplankton display an "earlier when warmer" response to temperature and so zooplankton seasonal cycles may respond by shifting earlier as well. However, overall the growing season will be shorter reducing the amount of time food is available for grazers. Potentially, this could propagate up the food chain and affect global fisheries. Furthermore, the changes in duration may have impacts on the quantity and efficiency of carbon export. The quantity of carbon export is linked to overall productivity with highly productive regions exporting higher amounts of carbon (Eppley and Peterson, 1979). Shorter productive seasons may translate into lower amounts of carbon export. Additionally, the expansion of low productivity biomes and reduction of high productivity biomes may also reduce global export production. Despite this, low productivity regions are associated with higher export efficiency (Francois *et al.*, 2002) meaning the exported carbon reaches deeper waters before being fully remineralised. Thus, an expansion of low productivity biomes may result in deeper remineralisation depths which, has further implications for the air-sea partitioning of CO_2.

6.4 Temporal Resolution and Detectability

In the previous analysis the differences in bloom timing between the beginning and end of the century were relatively small in some regions indicating that the climate change response was smaller than the temporal resolution of 30 days. The utilisation of higher temporal resolution was suggested by Henson *et al.* (2013) to increase the sensitivity of phenological metrics to climate change forcing. This would increase the confidence in the model predictions since the small phenological changes would be properly captured. Furthermore, using a finer temporal resolution may lead to trends being detected earlier because the magnitude of change would become larger than the model temporal resolution at an earlier point in time. This is particularly pertinent since phytoplankton phenology is highly responsive to environmental changes (Ji *et al.*, 2010). Furthermore, global satellite-derived observations are available at ~daily frequency and by using a similarly high temporal resolution may reveal how quickly climate change-driven trends in phenology may be detected. The aim of this section is to test this hypothesis.

6.4.1 Methods

MEDUSA was the only model used for this analysis since it was available at the finer temporal resolution of 5 days. These runs were exactly the same as those used in section 6.3 but at a finer temporal resolution. However, upon inspection the MEDUSA output was seen to be slightly different to the monthly resolution chlorophyll output used in the previous section. Though winter values of chlorophyll were exactly the same the chlorophyll values diverged in the summer months with the greatest differences observed in the North Pacific and high-latitude North Atlantic. This divergence was seen in other regions though the deviations were very small (globally, 90% of deviations were <0.05 mg m^{-3}). This affects the estimation of bloom timing dates as higher summer values raises the annual median resulting in later initiation and earlier termination dates compared to the monthly MEDUSA run. Though this brings uncertainty to a direct comparison with the results of the last section it does not affect the validity of the results presented here on trend detectability.

For each pixel the 5 day mean chlorophyll time series were averaged down to 10, 15, 20 and 30 day resolutions. This was done simply by averaging together consecutive time steps. The difference between bloom timing dates using 5 and 30 day temporal resolution is relatively high in some regions (Figure 6.23). In most regions, the differences were smallest for bloom initiation (~10 days), 20-30 days for bloom peak date, 30 days for bloom termination and ~30 days for bloom duration. The largest values were seen at high latitudes in the Arctic and Southern Oceans.

The option of a 25 day temporal resolution was not used because the averaging scheme caused inconsistencies in the estimation of the trend. The MEDUSA model was based on a 360 day calendar which was split into 72 time steps for the 5 day mean output. When this is averaged down to 25 days, two time steps are left over at the end of the year. Averaging down to 25 days would mean using, and correcting for, a moving averaging window which would have arisen from there being a partial number of time steps per year (14.4 in the case of 25 day means). This resulted in an underlying trend in the bloom timing time series and an overestimation of the trend magnitude. Since this was not consistent with the other temporal resolution options it was not included.

The initiation, peak and termination dates were calculated as described in Chapter 3 with the same alterations detailed in section 6.3.1 to adjust for trending seasonality and calendar effects (Figure 6.8). The rest of the analysis follow the methodology of Henson *et al.* (2010) and Henson *et al.* (2013). Once the bloom

timing time series had been corrected a linear trend was fitted using the simple model:

$$Y_t = \mu + \omega X_t + N_t \tag{6.1}$$

where Y_t is the bloom timing time series, μ is the intercept, ω is the trend magnitude and N_t is the noise (residuals). N_t is assumed to follow a first order autoregressive process (AR1) stated as:

$$N_t = \varphi N_{t-1} + \varepsilon_t \tag{6.2}$$

where φ is the first order autocorrelation (i.e. successive measurements are correlated, $\varphi = corr(N_t, N_{t-1})$) and ε_t are normally distributed random errors with mean of zero and a constant variance.

An exponential curve was also fitted but was not seen to give a better fit. The standard deviation of the residuals and coefficient of determination were compared for the two fitted models. As the results were similar, in the interest of parsimony, the linear trend model was used. It should be noted that at the subpolar-subtropical gyre boundaries, where bloom timing trends are linked to biome changes, a step change model would have been more suitable. However, this was only valid for a relatively small number of grid cells.

Equation 6.1 includes an autoregressive process term because autocorrelation is common in geophysical time series. However, the results of the Durbin-Watson test (Chatfield, 2005) indicated that for all bloom timing metrics and all temporal resolution in both models autocorrelation was only present at very high latitudes and over relatively small areas. Additionally, using a subset of bloom metric-temporal resolution combinations, the trend magnitude estimated from trend fitting that accounted for autocorrelation was not statistically different from trend fitting that ignored autocorrelation. Thus, to save a substantial amount of computation time, autocorrelation was assumed to be zero for the trend magnitude estimation. Additionally, grid cells where the probability of the trend magnitude being statistically different from zero was low (95th confidence interval) were removed from further analysis as were regions of low seasonality using the coefficient of variation (same method as described in section 6.3.1).

The parameter n* gives the number of years of continuous data required to detect a trend of a specified magnitude with 90% probability of detection and a 5% significance level (Weatherhead *et al.*, 1998):

$$n^* = \left[\frac{3.3\sigma_{N_t}}{|\omega|}\sqrt{\frac{1+\varphi}{1-\varphi}}\right]^{2/3} \tag{6.3}$$

where σ_{Nt} is the standard deviation of the residuals (noise), |ω| is the magnitude of the trend and φ is the autocorrelation of the residuals. The factor of 3.3 corresponds to the 90% probability of detection and the 5% significance level as derived by (Tiao *et al.*, 1990). The significance level is the probability of rejecting the null hypothesis (no trend present) when a trend is present (Beaulieu *et al.*, 2013). The probability of detection indicates that in 90% of cases, if a trend exists then it will be detected (Weatherhead *et al.*, 1998). Larger values of n* are obtained if the variance of the residuals is large (signal to noise issue) or if the autocorrelation is high. High autocorrelation leads to longer trend-like portions of the time series and thus makes it difficult to estimate the actual trend magnitude. An example detailed by Weatherhead *et al.* (1998) indicated that for a trend of 0.5% per year and a residual standard deviation of 10% that the number of years needed to detect the trend would be increased by 7 years when autocorrelation was raised from 0 to 0.5. Because of the importance of autocorrelation in the estimation of n* it is included in the analysis though it was excluded from the linear trend fitting.

The change in n* with temporal resolution for each bloom timing metric was summarised over each ocean basin. This was done by calculating the weighted median value and the median absolute deviation (MAD) which were the most appropriate parameters to use as these datasets were highly skewed. The final step was to transform the median values into a percentage change from the 5 day mean n* values.

6.4.2 Changes in Detectability

At a temporal resolution of 5 days the number of years needed to detect a trend in the bloom metrics is ~40 years for all metrics globally (Table 6.3) though variability in n* across the basins is large (Figure 6.24). The majority of the subtropics and large regions of the Southern Ocean do not experience a significant trend in any bloom timing metric. Large regions of the Arctic, North Atlantic and North Pacific do however, with some n* values being as low as ~15-20 years. The smallest basin mean n* value was seen in the Arctic (28-37 years) and the largest in

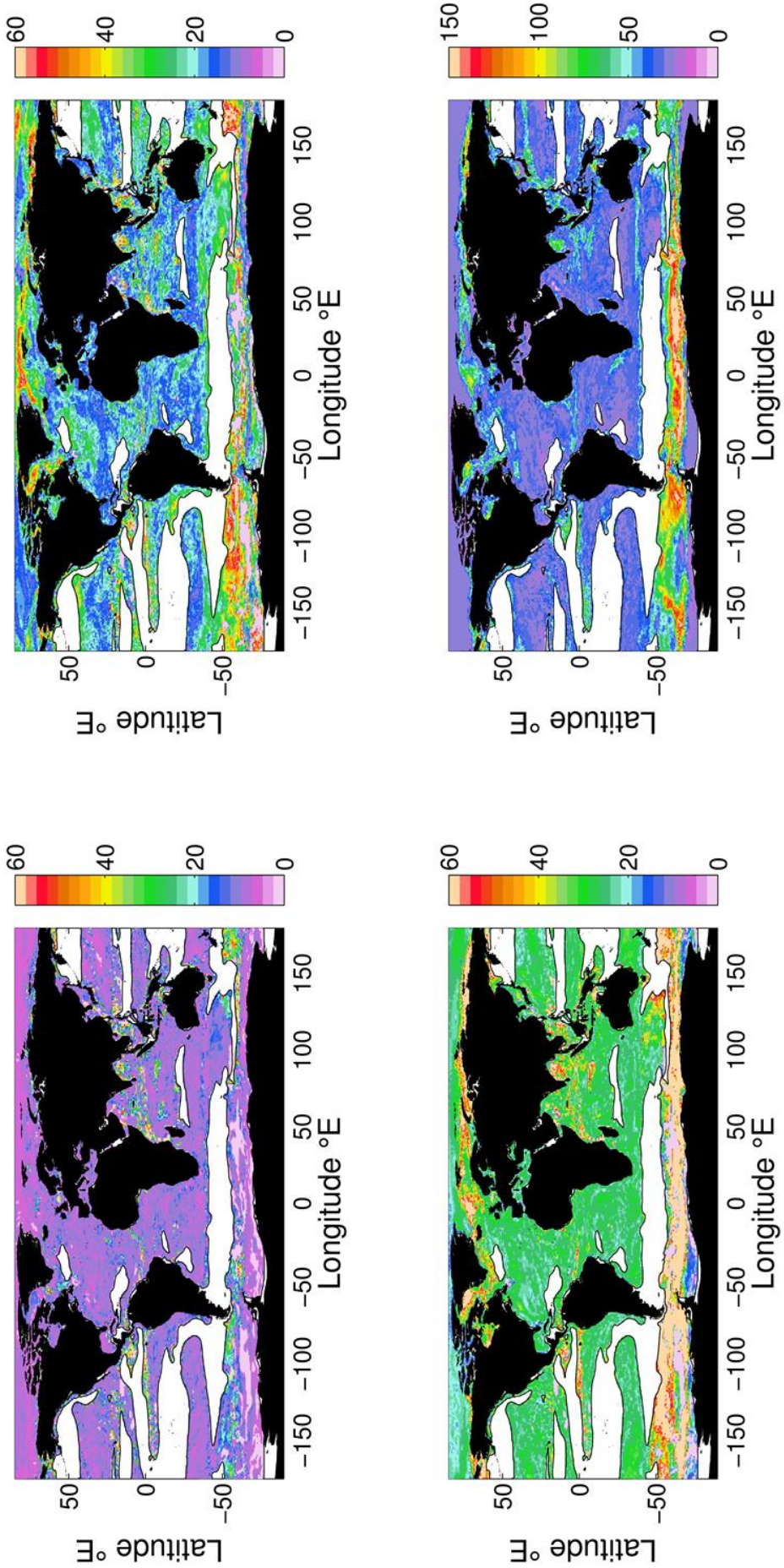

Figure 6.22: The difference in (a) bloom initiation, (b) bloom peak (c) bloom termination and (d) bloom duration when using 5 day and 30 day temporal resolution over the period 2007-2026. On average, dates at 30 day temporal resolution are always later than at 5 day resolution. White regions within the black contour are regions of weak seasonality.

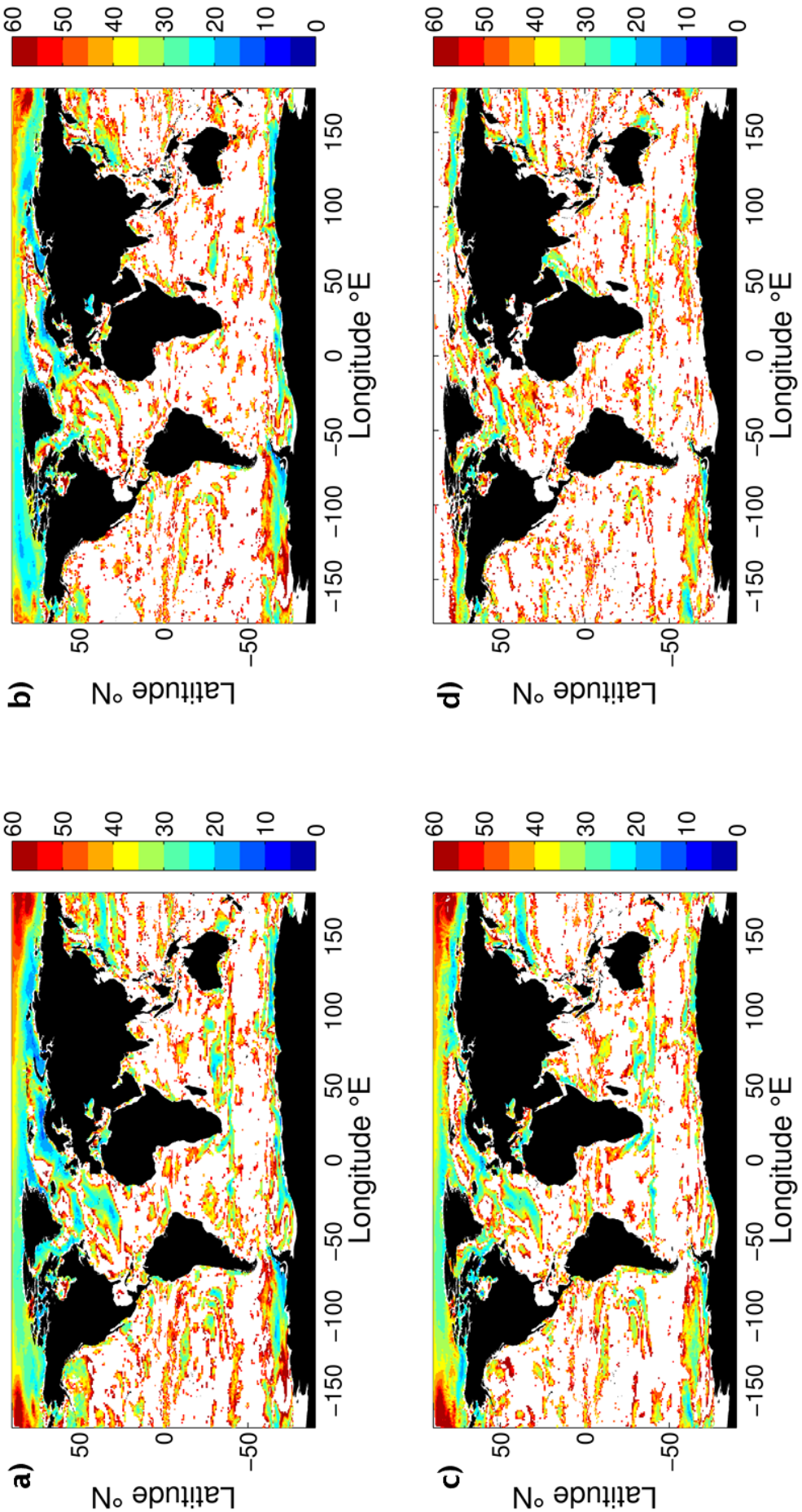

Figure 6.24: Maps showing the value of n* (the number of years required to detect a trend) in bloom initiation (a), bloom peak (b), bloom termination (c) and bloom duration (d) calculated from MEDUSA chlorophyll time series (2006-2099) at 5 day temporal resolution. White regions are regions were the trend in bloom timing was not statistically different from zero.

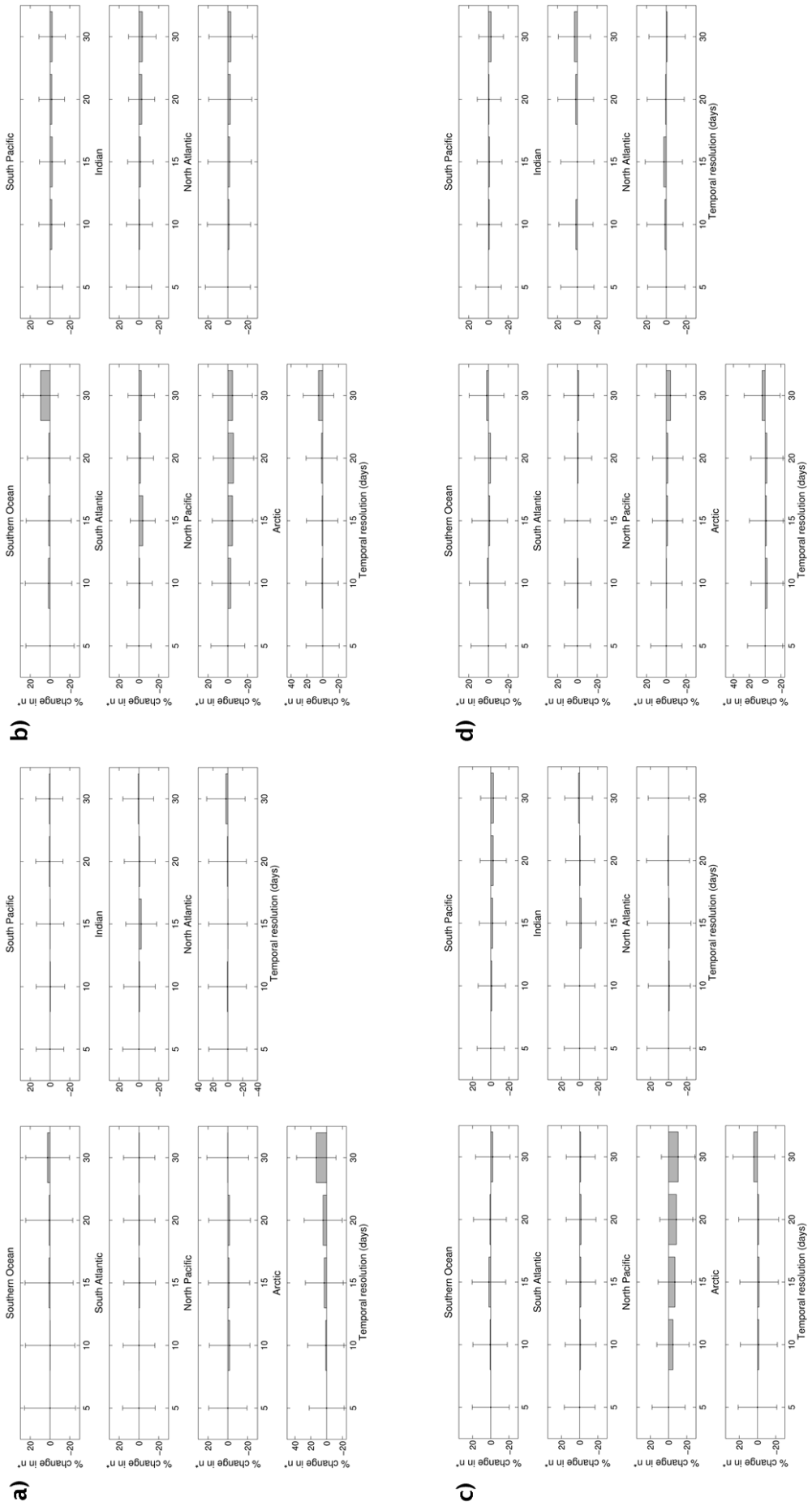

Figure 6.25: Median percentage change in n* with temporal resolution for bloom initiation (a), bloom peak (b), bloom termination (c) and bloom duration (d) for different ocean basins. Error bars indicate the median absolute deviation in n*.

the North and South Pacific and Indian Oceans in all metrics. The median absolute deviations of the n* values between the models were typically small (~5-10 years).

The majority of basins, for all 4 metrics, show little change in n* with coarser temporal resolution (Figure 6.25). For bloom initiation the largest change is seen in the Arctic with n* at 30 day mean resolution being ~15% larger. Slight increases (<5%) were seen in the Southern Ocean. Conversely, the changes in n* for the peak timing are largest in the Southern Ocean with the n* increasing by ~10% at 30 day mean resolution. Small increases (~5%) were seen in the North Atlantic with coarser resolution for peak timing. All basins showed little change in n* for the bloom termination timing except for the North Pacific which saw a decrease of ~10% in n* with coarser resolution. Similarly, little change was seen in n* for all basins in the bloom duration.

Table 6.3: Mean number of years required to detect a trend (n*) per ocean basin and globally for each of the bloom timing metrics[a]

	Southern Ocean	South Pacific	South Atlantic	Indian	North Pacific	North Atlantic	Arctic	Global
Initiation	41 (10)	44 (6)	41 (7)	42 (7)	40 (8)	36 (9)	28 (6)	40 (9)
Peak	41 (10)	45 (6)	45 (6)	46 (6)	43 (7)	39 (9)	28 (9)	42 (9)
Termination	41 (8)	43 (6)	42 (7)	41 (7)	42 (8)	37 (9)	33 (7)	40 (8)
Duration	42 (8)	46 (6)	45 (6)	42 (7)	44 (7)	42 (8)	37 (8)	43 (7)

[a] Values are rounded to the nearest whole year. Numbers in brackets are the median absolute deviation which is also rounded to the nearest year. Note that each basin shows high amounts of variability (Figure 6.24)

6.4.3 Discussion

The reason for the lack of change in n* with increasing temporal resolution lies in the response of the variables in the n* equation. The n* parameter is primarily affected by the size of the variability of the residuals from the trend fitting and by the magnitude of the trend. Thus, it may be there is no relationship in n* with temporal resolution because changes in the magnitude of the bloom timing trend may be compensated for by changes in the residual variability as the temporal resolution becomes coarser. Additionally, changes in autocorrelation can alter n* with larger autocorrelation raising the value of n*. If the bloom timing trend fitting becomes poorer with coarser resolution then the residual variability will increase relative to changes in the trend magnitude resulting in a larger n* value. Though the trend magnitude may change with coarser resolution this does not indicate that the precision of the trend estimate is improved. It is the precision of the trend

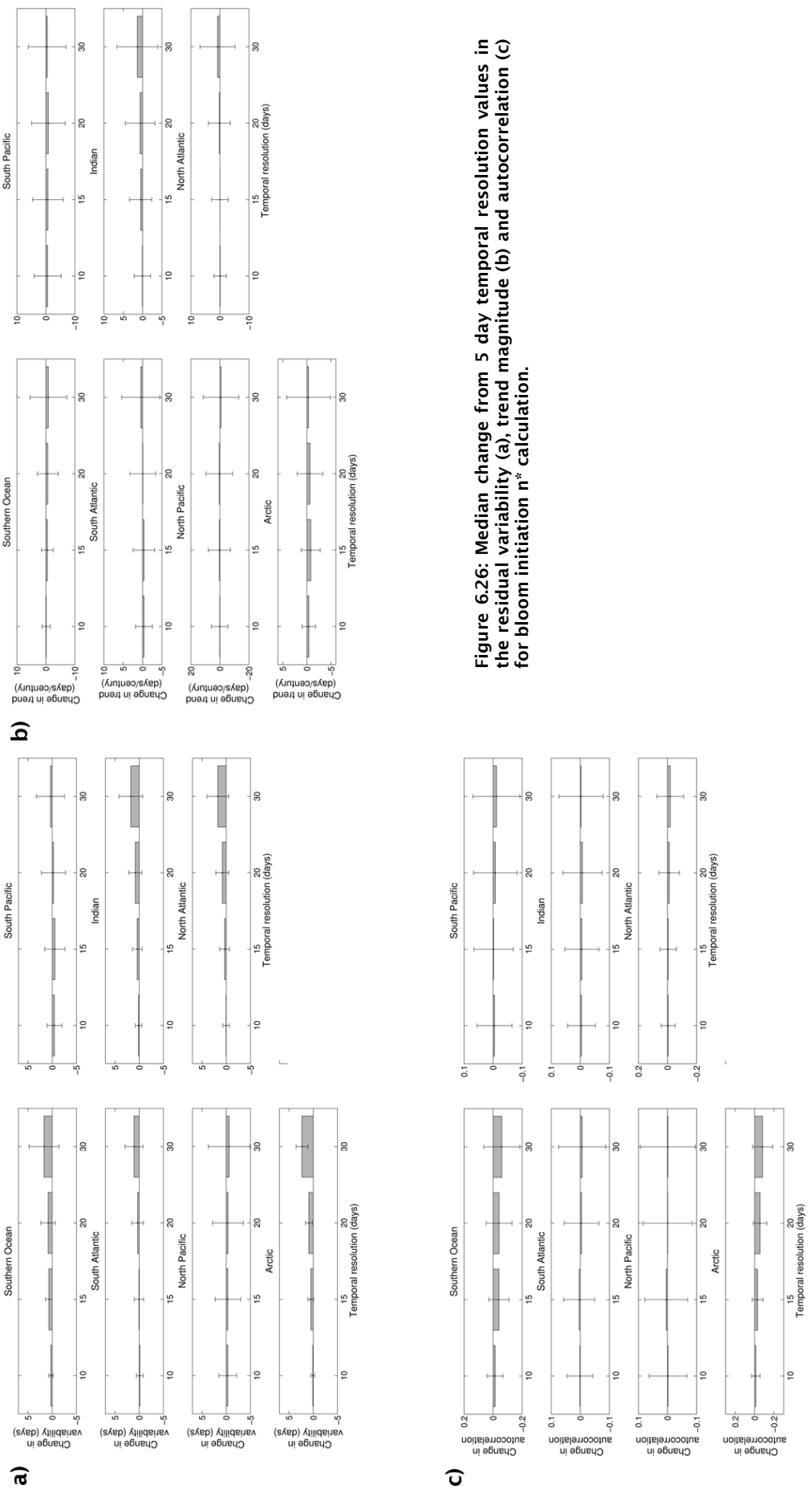

Figure 6.26: Median change from 5 day temporal resolution values in the residual variability (a), trend magnitude (b) and autocorrelation (c) for bloom initiation n* calculation.

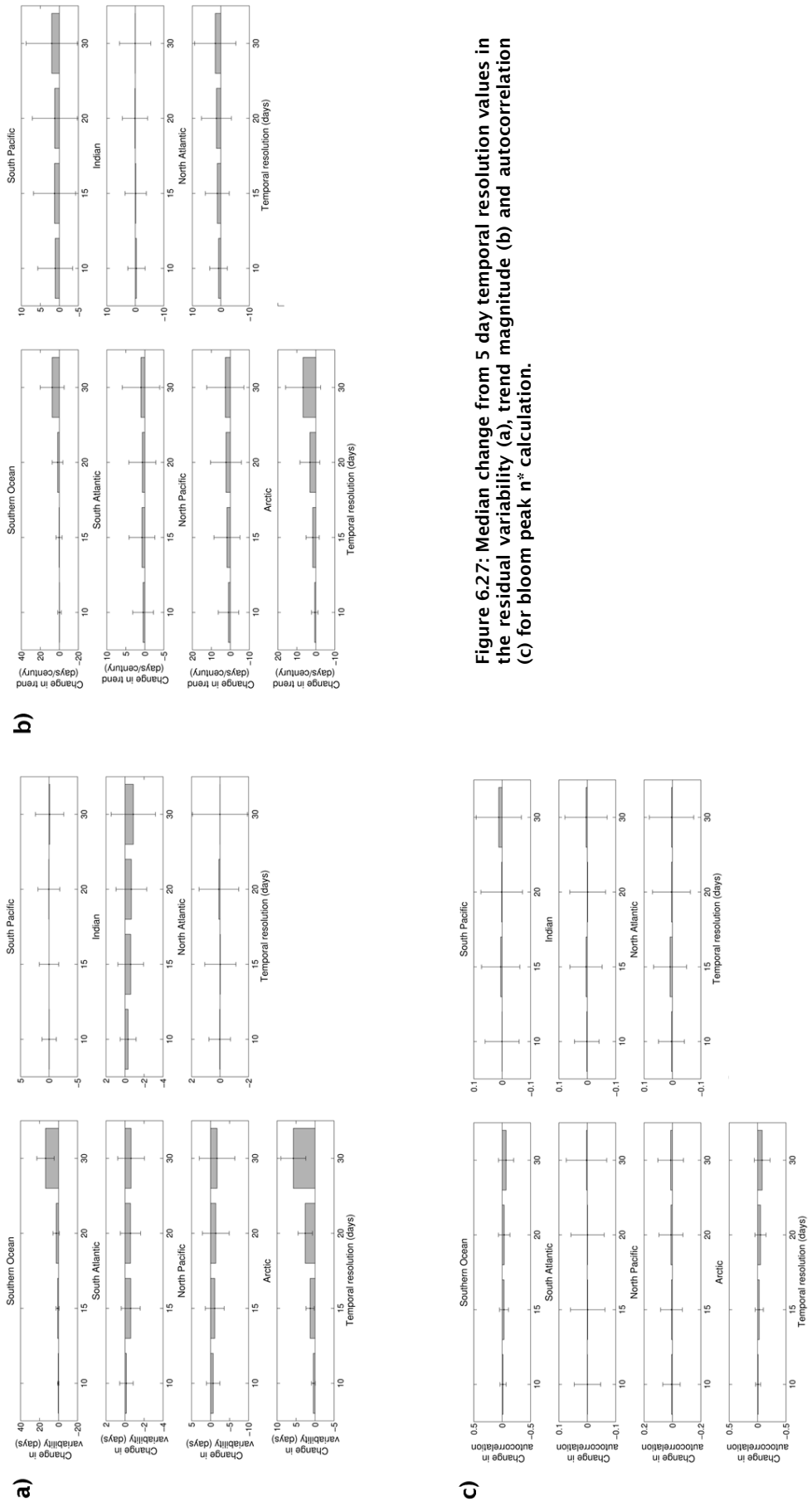

Figure 6.27: Median change from 5 day temporal resolution values in the residual variability (a), trend magnitude (b) and autocorrelation (c) for bloom peak n* calculation.

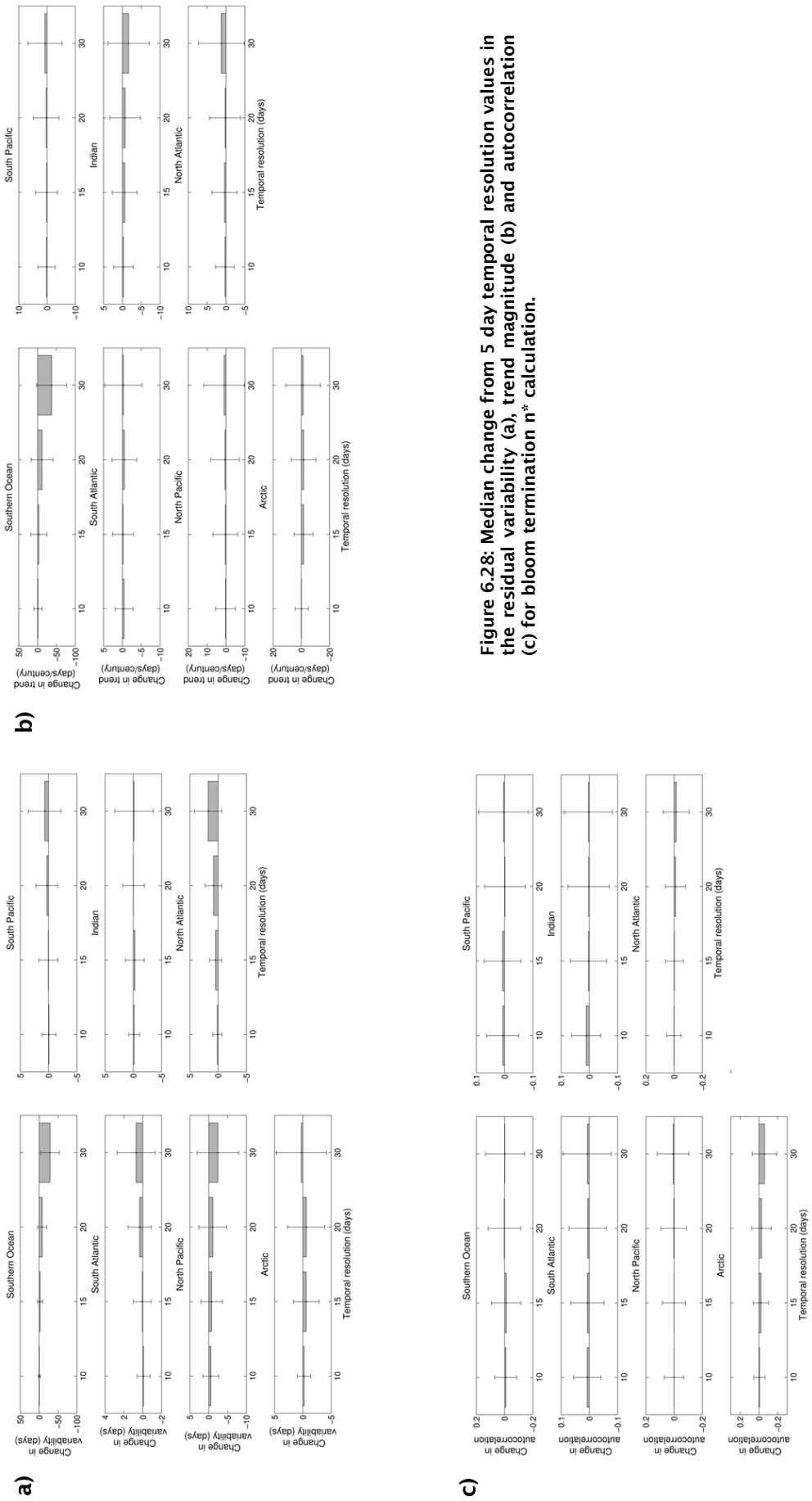

Figure 6.28: Median change from 5 day temporal resolution values in the residual variability (a), trend magnitude (b) and autocorrelation (c) for bloom termination n* calculation.

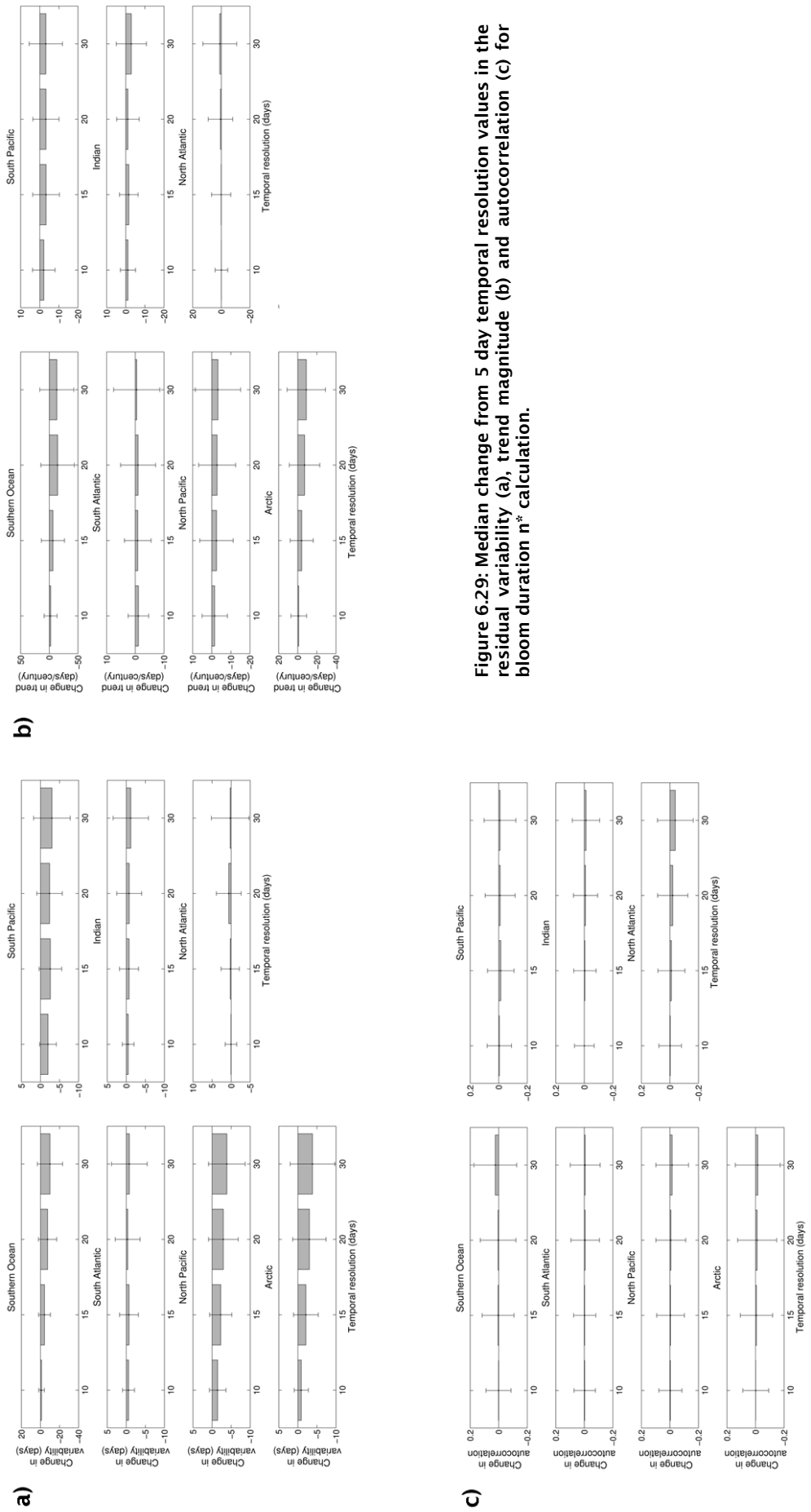

Figure 6.29: Median change from 5 day temporal resolution values in the residual variability (a), trend magnitude (b) and autocorrelation (c) for bloom duration n* calculation.

magnitude estimation that is related to the variability and autocorrelation in the residuals (Weatherhead *et al.*, 1998). A higher precision (i.e. lower variability) in the trend magnitude estimation will lower the value of n*. Ultimately, small trends will be more detectable if residual variability is low and only large trends will be detected if residual variability is relatively high.

The relationship between these three terms (trend magnitude, residual variability and autocorrelation) and coarser temporal resolution is shown for each bloom timing metric in Figures 6.26 – 6.29. For bloom initiation in most basins the residual variability, trend magnitude and autocorrelation were unchanged with coarser resolution (Figure 6.26). The larger trend in n* in the Arctic corresponds to an increase in the residual variability (~3 days) whereas the magnitude of the trend remained similar. The autocorrelation decreased slightly (<0.1), though as this change was very small the overall effect was an increase in n*.

Similarly, for the peak timing metric there was not much change in many of the basins for these terms (Figure 6.26). The peak n* value increased in the Southern Ocean and the Arctic. Additionally, there was a reduction in the North Pacific n* values. In the Southern Ocean there was a large increase in the variability of the residuals (~15 days), an increase in the trend magnitude (<10 days/century) and a slight reduction in autocorrelation (<0.1). Overall, the large increase in residual variability is responsible for the increase in n*. In the Arctic there was also an increase in the residual variability (~6 days) though smaller in magnitude compared to the Southern Ocean which again accounts for the increase in n*. In the North Pacific the reduction in n* seems to be driven by the small reduction in the residual variability. This indicated that for this basin the coarser resolution improved the trend fitting. This may be because short-term processes that increase bloom timing variability are not resolved at 30 day mean resolution.

The n* values for the bloom termination changed little in all basins (Figure 6.28). However there was a large reduction in n* in the North Pacific probably driven by a slight reduction in the residual variability (~3 days). Though overall there was not much change in n* there were large reductions in the residual variability in the Southern Ocean (~30 days) which is compensated for by a large reduction in the trend magnitude (~30 days/century) resulting in little change in n*. A similar situation was seen in residual variability and trend magnitude changes in the North Atlantic.

The n* values for the bloom duration did not change much in any basin (Figure 6.29). This was again seen to be because of an offset in changes in the trend magnitude by changes in the residual variability.

Overall, the seemingly simplistic view of detecting a trend earlier with higher resolution is actually more complicated. This is because of the way the temporal resolution affects the character of the residuals. Interestingly, the magnitude of the trend changes by becoming both larger and smaller with coarser resolution. However, this does not mean it is a better estimate as its precision is affected by the variability and the autocorrelation of the noise in the time series (Weatherhead *et al.*, 1998). A larger variance in the residuals and a higher autocorrelation increase the standard deviation of the trend magnitude estimate resulting in larger n* values (Weatherhead *et al.*, 1998). An increase in residual variability indicates that the trend fitting is poor and thus the trend magnitude estimation is less certain.

The largest changes in n* were typically seen in the Arctic and Southern Oceans where trends in bloom timing are likely to be of a magnitude similar to the temporal resolutions tested (5-30 days). Correspondingly, it is these regions that show the largest difference in bloom metric dates at 5 and 30 day temporal resolution (Figure 6.23). Conversely, many of the subtropical dominated basins showed little sensitivity to the resolution suggesting that any trend is likely to be smaller than 5 days per century. This is supported by the lack of statistically significant trends in the analysis in both this section and section 6.3. Ultimately, this indicates that a better model to fit to time series of bloom timing metrics is needed to reduce the residual variability. One possibility would be to include a term to account for interannual variability such as a term for the El Niño-Southern Oscillation as suggested by Henson *et al.* (2010). Another would be using a step change function especially in regions near gyre boundaries.

Another outcome from this analysis is that though the finer resolution has the smallest n* in the high latitudes the variability in the n* values is still large across these basins. Additionally, the n* value tended to be very similar in the 5 to 20 day mean resolution interval with only small changes in the median n* value. This indicates that using a temporal resolution smaller than a 20 day mean would not improve the detectability of the climate change-driven trends. Thus, this gives an indication for a suitable compromise between trend detectability and computational constraints.

Additionally, the results have implications for satellite oceanography as remote sensing is the primary method for studying global changes in chlorophyll and primary production. Satellite data is available at daily frequency over much of the globe. However, MODIS is the only ocean colour satellite current operational and it is already well past its planned life span. The next ocean colour satellite to be launched will be ESA's Sentinel 3 but this mission is not planned to launch until

late 2014. Thus a gap in the ocean colour record may well occur which would substantially increase the number of years needed to detect a trend as shown by Henson *et al.* (2010) and Beaulieu *et al.* (2013). To minimize the impact of this a successful launch with a long enough overlap with current sensors to enable cross calibration will be needed. In the context of satellite ocean colour a gap in the record would also constitute a discontinuity because of the change of instrument and lack of cross calibration. Thus, as demonstrated by Beaulieu *et al.* (2013) this would increase n* by ~13 years globally for trends in surface chlorophyll.

The results of this analysis indicate that ~40 years of data, with a minimum of 30 years in the Arctic would be needed to detect a climate change-driven trend in bloom timing across much of the world's oceans. However, it is worth noting the variability over the basins as some regions, especially high latitudes, show that as little as 15 years of data would be needed to detect a trend in phenology. In comparison to this Henson *et al.* (2010) and Henson *et al.* (2013) found that ~40 years and ~36 years of data are needed to detect a trend in the total annual and seasonal amplitude of primary production, whereas only 27 years are needed for surface chlorophyll (Beaulieu *et al.*, 2013). It would seem that changes in primary production and bloom timing may occur at similar rates.

6.5 Summary

- Mean bloom timing metrics from a suite of ocean biogeochemical models agree well with metrics derived from satellite chlorophyll data. Comparisons with interannual variability in bloom timing were slightly less favourable.
- The climate change response in phenology was seen to be largest at higher latitudes and was consistent across the three biogeochemical models.
- Changes at higher latitudes in physical forcing were consistent with a climate change response of longer and stronger periods of stratification and agreed with trends in the bloom timing metrics.
- Changes in both bloom timing and physical forcing were relatively small in the subtropics and varied in direction between the models. This observation agrees with recent studies that found weak interannual relationships between stratification and primary production.

- The number of years required to detect a trend in bloom initiation and peak dates was only seen to increase with coarser temporal resolution at high latitudes. The increase in temporal resolution resulted in larger variability in the residuals from fitting a linear trend which increased the number of years needed to detect the trend.
- In other regions the variability in the residuals was seen to vary little with temporal resolution indicating that finer resolution did not result in climate change-driven trends being detected earlier.

7 Summary

7.1 Summary of Conclusions

This thesis has aimed to characterise contemporary seasonal variability, the factors driving that variability and to assess the potential climate change-driven trends in bloom timing. By combining multiple datasets, including satellite-derived data, *in situ* observations and output from global biogeochemical models, a global view of the natural variability and climate change response in phytoplankton phenology has been formed. Both natural variability and climate change-driven trends in phytoplankton phenology have wide reaching implications, from determining when the greatest abundance of food is available for higher tropic levels, to the quantity and efficiency of carbon export.

7.1.1 Characterising Phenological Variability

Satellite-derived chlorophyll concentrations have proved to be a key dataset with which to study bloom timing at global scales. The relatively high temporal resolution of 8 days was found to be sufficient to quantify interannual variability in phenology. Several approaches have been used in the literature to objectively measure the date of bloom initiation, peak and termination and four methods were compared here. These methods all defined the onset and decline of the bloom as a relative change in chlorophyll (i.e. crossing a threshold value), though the different approaches give different dates, they co-vary with each other strongly. Ultimately the "best" approach to use is the method best suited to the research questions being investigated.

For this study the metric had to be applicable to a wide range of seasonal cycle shapes, to capture interannual variability and to be relatively insensitive to noise and missing data. Thus, in Chapter 3 the definition for bloom initiation and termination based on a threshold value of 105% of the annual median was chosen because it satisfied these criteria. Additionally, the requirement to exclude weakly seasonal regions from further analysis was realised during the development of the bloom timing metrics. Subseasonal processes dominate the chlorophyll variability in these regions and a robust method to isolate regions with strong seasonality was identified. The method decided upon was the coefficient of variation (standard deviation/mean) and a value of <0.35 was used to classify non-seasonal regions. Overall, the results from each chapter were influenced little by the choice of coefficient of variation value.

The largest limitation of using satellite chlorophyll data in phenology studies is the prevalence of missing data. The results of Chapter 4 show that missing data has specific implications for the thesis aim of characterising contemporary seasonality. The increased uncertainty in the metric dates from missing data must be carefully considered when quantifying interannual variability. By using the output from a global biogeochemical model that assimilates SeaWiFS chlorophyll data as a gap free dataset, empirical relationships were found between the quantity of missing data and the error in the bloom timing metrics. This quantifies the uncertainty due to missing data on phenological characteristics calculated from satellite datasets and is ~30 days for bloom initiation, ~15 days for the peak and ~50 days for bloom termination over the majority of the world's oceans. These findings have implications beyond phytoplankton phenology and can be applied to any phenological study using incomplete datasets. For the metric definition used here, the missing data causes incorrect quantification of the annual median and thus causes errors in the threshold value. Secondly, when data are missing on the real date on which the bloom initiated or terminated, errors are unavoidable.

Having defined a method to quantify phenology and determined how to account for the uncertainty introduced by missing data, Chapter 5 moved on to quantify interannual variability in bloom timing and to identify drivers of spatial and interannual variability. Interannual variability was lowest in the subpolar and subtropical gyres, varying by 16-48 days for all metrics. Higher interannual variability was seen in the boundary regions between the gyres, in association with ocean fronts and upwelling regions (~60-140 days). These regions experience interannual changes in the conditions that affect bloom timing as the mean position of the gyre boundaries or ocean fronts vary each year.

To further characterise seasonal variability, the major drivers of bloom timing were examined. In subpolar regions the relationship between physical drivers and bloom timing were strongest for bloom initiation both spatially and interannually. On interannual timescales the variability in bloom peak and termination was weakly related to environmental changes in subpolar regions. Conversely, in subtropical regions spatial relationships were strong though weak relationships were again seen on interannual timescales. However, some basins did show strong correlations and indicated that a decrease in turbulence is a key player in driving interannual variability in peak timing through a reduction in entrainment of nutrients from below the thermocline. This indicates that other drivers, either biogeochemical or ecological may be important for controlling variability in the other bloom timing metrics or that the described variability is driven by a complex combination of factors.

Furthermore, the characterisation of interannual variability in bloom initiation allows us to examine the mechanisms that initiate the subpolar spring bloom. More specifically it allows the evaluation of the critical depth hypothesis versus the critical turbulence hypothesis. The results here support the critical turbulence hypothesis as a valid mechanism for bloom initiation. This is based on the strong correlations between interannual variability in bloom initiation and interannual variability in the date the net heat flux becomes positive signifying a reduction in turbulent mixing. A bloom is initiated, even in deep mixed layers, as the reduction in turbulence means that phytoplankton are no longer rapidly mixed out of the euphotic zone and can increase in abundance near the surface. This relationship was seen to be strongest in the North Atlantic but was also seen in large areas of the North Pacific and Southern Ocean. Variability in bloom initiation was less strongly related to MLD shoaling in the North Atlantic and even more weakly in other basins.

Overall, we can characterise contemporary phytoplankton phenology on basin scales as:

- Adequately captured in satellite-derived chlorophyll datasets of 8 day composites.
- Influenced by the limitations in the method used to quantify the date of phenological events (i.e. sensitivity to missing data).
- Strongly variable both spatially and on interannual timescales with the highest variability associated with regions of dynamic physical forcing.
- Having strong spatial co-variance with physical drivers in subpolar bloom initiation dates and subtropical initiation, peak and termination dates.
- Having strong relationships between subpolar bloom initiation and subtropical peak timing with some physical drivers on interannual timescales, particularly in the North Atlantic.
- Needing further investigation into other, non-physical drivers (i.e. grazing) of phytoplankton phenology.

7.1.2 Assessing Climate Change Response

The findings in Chapter 4 of the sensitivity of bloom timing quantification to missing data is an important consideration for detecting climate change-driven trends in phenology. The uncertainty that missing data adds to the estimation of bloom timing makes the detection of trends more difficult as it increases the noise to signal ratio. This is particularly pertinent since satellite data will be the primary source for future monitoring of phenology in the oceans. This is also relevant to

other phenological studies that use incomplete datasets to look for trends in other geophysical and biological datasets. Such examples include studying the timing of sea ice melting and formation and zooplankton phenology. Furthermore, it encourages the expansion of methods to compensate for missing data such as assimilating the dataset into a global biogeochemical model such as NOBM to compensate for gaps in satellite data.

Variability in phytoplankton phenology was observed to be strongly related to environmental change and various drivers were identified. Since climate change is expected to alter the dynamics of these drivers it follows that bloom phenology may also change. This implies that current variability may allow us to predict the magnitude and direction of the climate change response.

Global biogeochemical models are a comprehensive tool for studying responses to climate change. The suite of models tested in Chapter 6 indicates that these types of models already adequately simulate phenological variability (though whether this occurs for the correct reasons is beyond this study). However, though mean dates were highly correlated with satellite observations the models overestimated spatial variability and underestimated interannual variability. Despite this, the adequate simulation of mean bloom timing improves the confidence in the climate change-driven trends in bloom timing observed in the models. Moreover, many of the trends in bloom timing were seen to be consistent across the models used here, further improving confidence in the predicted response to climate change. Of these changes the most consistent were seen at high latitudes. Bloom timing in these regions is predicted to shift earlier than current timing. Correspondingly, the environmental drivers were consistent with the expected shift towards earlier onset of conditions suitable for bloom initiation. In the subpolar regions the earlier peak and termination dates along with stronger stratification and lower nutrient concentrations indicate that nutrient limitation may be an important future driver of phenology. Trends in the subtropics in both phenology and environmental drivers were smaller and less consistent between models. This suggests that the changes are too small to be properly resolved or may reflect the one sided nature of biological responses to local changes in stratification. For example, phytoplankton biomass may rise in response to an increase in nutrient concentrations though a reduction in biomass of a similar magnitude may not be seen if conditions become more nutrient-limited.

This leads onto the detectability of climate change-driven trends. Detectability is enhanced if the magnitude of the trend is large relative to the natural variability. Thus, by using a finer temporal resolution to increase sensitivity to interannual changes in bloom timing, the number of years of data required to

detect the trend may be reduced. This was seen to be true for phenological changes in the high latitudes where the largest changes in bloom timing occurred. Finer resolution resulted in smaller residual variability and therefore a reduced number of years needed to detect the trend. However, much of the subtropical regions did not show a change in the number of years needed to detect a trend. This was probably because the trend magnitude was very small in these regions and finer temporal resolution did not substantially improve the detectability.

From these results the assessment of the climate change response showed that:

- The missing data must be accounted for in future satellite data used for monitoring phenological changes to improve the estimation of climate change-driven trends from satellite-derived chlorophyll data.
- The biogeochemical models used here adequately simulate contemporary seasonality and thus, are a suitable tool for predicting phenological changes.
- The phenological response to climate change is predicted here to be most evident at higher latitudes and smaller than the monthly temporal resolution used here in subtropical regions.
- In mid to high latitudes the earlier onset of conditions suitable for bloom initiation drives the trend towards earlier bloom initiation. Furthermore, nutrient limitation is expected to be an important control on future bloom peak and termination timing.
- Using finer temporal resolution may slightly reduce the number of years of data needed to detect climate change-driven trends at high latitudes but would not improve detectability in subtropical regions.

7.2 Evaluation of Data and Methods

Satellite-derived chlorophyll data enables the study of phenology on a global scale and with a temporal resolution adequate for resolving interannual variability. However, satellite data does have its limitations. Firstly, it is subject to missing data especially at higher latitudes and so careful consideration is needed when trading off temporal resolution for data coverage. This is countered here by using the biogeochemical model NOBM which assimilates SeaWiFS chlorophyll data giving complete data coverage and maintaining fidelity to seasonal characteristics. Alternatively, the uncertainty in bloom timing due to missing data calculated here could be used in conjunction with satellite datasets to account for errors in bloom timing estimation. Secondly, satellites are restricted to a surface view and so

subsurface variability in chlorophyll (i.e. the deep chlorophyll maximum) is not included in the analysis. Lastly, chlorophyll is not a measure of biomass and so careful interpretation is needed in oligotrophic regions where chlorophyll changes are driven by photoacclimation.

The use of chlorophyll output from NOBM was used to quantify the impact missing data had on the accuracy of the bloom timing metrics and was used in place of GlobColour to investigate the drivers of interannual variability. Though NOBM performed well in reproducing seasonal characteristics the deviations in absolute chlorophyll concentrations were large in some regions. Furthermore, subsurface chlorophyll is not updated by the assimilation. However, improved assimilation techniques may give more reliable chlorophyll concentrations. This could be done by reducing errors in both the assimilated chlorophyll data and the model estimation. Additionally, subsurface chlorophyll could be updated if the correlations with surface chlorophyll concentrations and the seasonal variability in the correlations were known globally. Another drawback of using NOBM output is that it only spans 6 years of data whereas the satellite data era covers 16 years. A longer dataset would provide more precise estimates of interannual variability in bloom timing by capturing the variability over decadal timescales.

The physical datasets used in this study were able to resolve interannual variability in the physical drivers and give meaningful correlations with bloom timing. However, there are again some limitations of the datasets. One consideration is that the net heat flux is measured synoptically from satellite and reanalysis products much like the chlorophyll data with each pixel being an areal average. Conversely, the MLD was calculated from sporadic point samples of temperature and salinity. This means there is uncertainty in the representivity of the point sample to the whole of the grid cell. However, this is tempered by aggregating multiple temperature and salinity profiles within a radius of influence in both space and time, which increases the number of temperature and salinity samples per pixel. Given the large pixel size (1°x1°), a larger number of profiles would benefit the representivity of the pixel average in regions where temperature and salinity are highly variable on smaller scales. Furthermore, the temperature and salinity coverage is not equal everywhere in the ocean or every year and so the amount of spatial and temporal variability in MLD may be reduced in some regions and years. Furthermore, these considerations also apply to the mean mixed layer PAR (PAR_{ML}) dataset. This is calculated from satellite PAR and attenuation coefficient datasets and the MLD dataset. Thus, the MLD uncertainties are introduced when calculating the average irradiance in the mixed layer. Though estimation of variability in the surface PAR and attenuation coefficient will be similar to that of satellite-derived chlorophyll, the variability in the PAR_{ML} may be reduced by the use

of the MLD dataset. This means that these datasets cannot be treated equally when comparing the strength of correlation with bloom timing since the spatial and temporal variability captured varies between the datasets. Allowances need to be made for the uncertainties in the estimation of the MLD, such as allowing for lower correlation coefficients relative to the other physical datasets.

In all of the datasets a further consideration is that spatial changes, in terms of a spatial signal appearing as a temporal one, are ignored. For instance the bloom timing may not be a local increase in chlorophyll based on increased phytoplankton abundance but rather an advection of high chlorophyll water into previously low chlorophyll water. The effect of this should be countered by the large spatial resolution (1˚x1˚) used for most analyses and by calculating basin wide averages. Thus, the changes here are assumed to be local but may in fact be a combination of spatial and temporal changes.

One key question when estimating phenology is what constitutes a bloom? Bloom initiation and termination can only be defined once the definition of a bloom has been decided. In this study a bloom is defined as a significant rise in chlorophyll above a background level and the metric choice reflects this definition. Increases in chlorophyll signify a source of food for zooplankton plus the potential for carbon export events. Thus it is an ecologically and biogeochemically relevant definition. However, other ways to define a bloom could be used such as by measuring phytoplankton growth rates. However, this method applies to the timing of bloom initiation only since a peak in biomass (bloom peak timing) cannot be derived from growth rates alone. Furthermore, for cases where both phytoplankton growth and zooplankton grazing rates are high, biomass accumulation might not occur and thus it is questionable whether a bloom has actually occurred since there is no peak in abundance. This situation is still ecologically interesting though, as it indicates tight coupling between phytoplankton and grazers, potentially high secondary production and the potential for high carbon export, for example, through sinking faecal pellets. However, this requires *in situ* measurements of phytoplankton and zooplankton biomass, growth rates and grazing rates for proper study. To study phenology on a global scale as done here a measureable change is needed, such as seasonally elevated chlorophyll concentrations, which can be detected *in situ* as well as remotely.

A coefficient of variation value of 0.35 was chosen, rather subjectively, to define non-seasonal regions. This was based on a visual estimation of seasonality. In the biogeochemical models lower values were used. These were based on matching the total area excluded in the model to the total area excluded in the satellite data. This was seen to have a similar spatial pattern to the satellite data.

However, to compensate for the lack of objectivity in choosing this value, results were also calculated for slightly higher and lower coefficient of variation values. The main findings in this thesis were observed to be insensitive to the choice of coefficient of variation value.

The trends fitted to future changes in bloom timing were assumed to be linear. For the majority of regions this gave similar statistics as fitting an exponential model. However, a visual estimation of the suitability of a linear model revealed that some regions experienced a step change in bloom timing. This occurred in regions which shifted from one biome to another resulting in an abrupt shift in the dates. Thus, in some cases, fitting a step change model would have been more suitable.

7.3 Future Directions

The techniques used in this thesis could be extended and used in a variety of future studies. Firstly, bloom timing metrics have been used here to study variability and trends in phytoplankton phenology. However, estimates of bloom timing can be used to expand population studies of organisms at higher trophic levels and evaluate the match-mismatch hypothesis. This has already been done for some commercially important species including haddock, cod and a species of North Atlantic shrimp (Platt *et al.*, 2003, Koeller *et al.*, 2009, Kristiansen *et al.*, 2011). Additionally, the bloom timing metrics could be used to investigate relationships between phenology and the biological carbon pump. Examples include linking interannual variability in annual carbon export to that of bloom duration or relating seasonal characteristics to carbon export efficiency.

Furthermore, studies investigating the triggers for the onset of the subpolar North Atlantic spring bloom have become a “hot topic” recently and objective measures of bloom timing could expand this research into other regions of the world’s oceans as is done here. *In situ* measurements have found that blooms can initiate before the MLD has shoaled contrary to Sverdrup’s critical depth theory. Satellite-derived or *in situ* bloom timing estimates could be combined with *in situ* measurements of turbulence and subsurface irradiance to fully investigate the mechanisms that lead to the initiation of the subpolar spring bloom. This may provide further results that corroborate the validity of the critical turbulence hypothesis and allow the re-evaluation of the critical depth theory.

The list of physical drivers of bloom timing used here is not exhaustive. One obvious missing physical driver in this study is wind. Variability in wind mixing drives MLD and turbulence changes, which influences the availability of light and

nutrients to phytoplankton. Thus, the work here could be expanded to look at interannual variability in wind speed and wind stress. Furthermore, climate indices, such as the North Atlantic Oscillation, encapsulate variability in many physical drivers (i.e. wind speed and sea surface temperature) and provide a useful way to bring together multiple drivers of bloom timing. Climate indices could be used to quantify interannual and decadal changes in bloom timing over large areas and provide more information on the environmental conditions that drive variability. Additionally, physical drivers were not seen to be important drivers of variability in the subtropics or for subpolar peak and termination timing. Thus, future work investigating other drivers could deepen our knowledge of bloom dynamics. In particular, the role of grazing on phenological variability needs to be investigated. This could be done either through *in situ* observations of grazing rates and zooplankton biomass or by using biogeochemical model output. Furthermore, the bloom timing metrics could be used to investigate variability in the seasonal progression of different species of phytoplankton. This has implications for carbon export since some phytoplankton groups such as diatoms form large blooms in early spring and have silica frustules, which provide ballast and increase sinking speeds. In addition, coccolithophores bloom when the water column is strongly stratified and produce calcium carbonate coccoliths, which also provide ballast. Thus, investigating changes in the seasonal succession may reveal the potential drivers for efficient carbon export.

The consideration of spatial scales is an important one since different processes can dominate as different spatial scales. Here the focus has been on basin scales but variability on smaller scales is also of interest as it may reveal further controls on bloom timing. Firstly the basins could be broken down into smaller biological provinces to investigate if the signal is stronger in some than others. This could tell us if certain physical processes (such as the a reduction in turbulence) dominate across an area when more complex regions such as boundary current, marginal sea ice and upwelling regions are excluded. Additionally, smaller scale physical processes such as mesoscale eddies, submesoscale fronts and filaments may reveal that the drivers on basin scales are not significant drivers of smaller scale variability (Mahadevan *et al.*, 2012). For example, the reduction in turbulence associated with the onset of ocean warming (net heat flux turns positive) may dominate at basins scales. However, the role of eddies and fronts in stratifying the water column through the advection of water with different densities may dominate bloom timing variability at mesoscale and submesoscales. Indeed small scale, feature-driven stratification (e.g. from eddies and fronts) may be a viable process for phytoplankton survival over the winter months when large scale ocean cooling is occurring.

As noted above, the analysis here has focussed on broad basin scale patterns and the comparison between subpolar and subtropical regimes. However, the bloom timing metric techniques developed here could be used to study regions where variability is more complex. One such example would be investigating the impact of monsoonal variability in physical drivers on bloom timing in the Indian Ocean or focussing on the timing and frequency of harmful algal blooms. Furthermore, because of the limitations of satellite data, phenology at very high latitudes has been ignored. However, another region where variability is more complex is the Arctic where the melting of sea ice is an important driver of bloom timing variability. Given that the Arctic is expected to undergo drastic changes due to climate change, establishing a baseline of current variability in phenology and identifying the specific drivers in this region is of extreme importance.

The model output variable primarily used here was chlorophyll as it is easily compared to satellite data. However, phenology of primary production would be more significant to life on Earth and avoids the complication of photoacclimation at low latitudes. Thus repeating the analysis of future climate trends in primary production would be an obvious extension to this work. This would be relatively easy to implement in global biogeochemical models, though investigating phenology using chlorophyll allows for straightforward comparison with satellite data.

Although the drivers of variability in bloom timing across the world's oceans still need further investigation, the results presented in this thesis give greater insight into the role of environmental change on bloom development. This is particularly pertinent to current research into the mechanisms that initiate the subpolar spring bloom and the evaluation of the critical turbulence hypothesis. Though both remotely sensed data and modelling results have addressed this previously in the North Atlantic, the results in this thesis represent the first global assessment of this hypothesis and its role in driving interannual variability. Moreover, the results here reveal that the phenological response to climate change remains uncertain over much of the world's oceans, especially in subtropical regions. Thus, additional examination of the controls on bloom timing will further constrain the predicted climate change response in phytoplankton phenology.

8 Appendix A

COLE, H., HENSON, S., MARTIN, A. & YOOL, A. 2012. Mind the gap: The impact of missing data on the calculation of phytoplankton phenology metrics. *Journal of Geophysical Research,* 117**,** C08030. doi:10.1029/2012jc008249

JOURNAL OF GEOPHYSICAL RESEARCH, VOL. 117, C08030, doi:10.1029/2012JC008249, 2012

Mind the gap: The impact of missing data on the calculation of phytoplankton phenology metrics

Harriet Cole,[1] Stephanie Henson,[2] Adrian Martin,[2] and Andrew Yool[2]

Received 1 June 2012; revised 11 July 2012; accepted 11 July 2012; published 24 August 2012.

[1] Annual phytoplankton blooms are key events in marine ecosystems and interannual variability in bloom timing has important implications for carbon export and the marine food web. The degree of match or mismatch between the timing of phytoplankton and zooplankton annual cycles may impact larval survival with knock-on effects at higher trophic levels. Interannual variability in phytoplankton bloom timing may also be used to monitor changes in the pelagic ecosystem that are either naturally or anthropogenically forced. Seasonality metrics that use satellite ocean color data have been developed to quantify the timing of phenological events which allow for objective comparisons between different regions and over long periods of time. However, satellite data sets are subject to frequent gaps due to clouds and atmospheric aerosols, or persistent data gaps in winter due to low sun angle. Here we quantify the impact of these gaps on determining the start and peak timing of phytoplankton blooms. We use the NASA Ocean Biogeochemical Model that assimilates SeaWiFS data as a gap-free time series and derive an empirical relationship between the percentage of missing data and error in the phenology metric. Applied globally, we find that the majority of subpolar regions have typical errors of 30 days for the bloom initiation date and 15 days for the peak date. The errors introduced by intermittent data must be taken into account in phenological studies.

Citation: Cole, H., S. Henson, A. Martin, and A. Yool (2012), Mind the gap: The impact of missing data on the calculation of phytoplankton phenology metrics, *J. Geophys. Res.*, *117*, C08030, doi:10.1029/2012JC008249.

1. Introduction

[2] Phenology is the study of the timing of annually occurring biological events. The timing of the annual phytoplankton bloom is a key event for marine ecosystems and provides a food source for zooplankton and higher trophic levels [*Cushing*, 1990]. Interannual variability in bloom timing may directly affect larval survival through the match-mismatch hypothesis [*Cushing*, 1990]. Lower larval survival is expected if a mismatch in the timing of phytoplankton growth and larval spawning occurs. North Atlantic studies have concluded that haddock larval survival is related to anomalies in bloom timing and that the timing of shrimp (*Pandalus borealis*) hatching has evolved to coincide with the mean bloom initiation date [*Platt et al.*, 2003; *Koeller et al.*, 2009]. This has direct implications for resource species and thus fisheries yield [*Fuentes-Yaco et al.*, 2007; *Koeller et al.*, 2009]. As it is a time of high productivity the phytoplankton bloom is also a period of potentially high carbon export [*Deuser*, 1986; *Lutz et al.*, 2007]. In addition, variability in the duration of the bloom may lead to variability in carbon export and the depth of remineralization [*Lutz et al.*, 2007]. The main phenological events of interest associated with the bloom include the timing of initiation, peak and decline and its duration [*Platt and Sathyendranath*, 2008].

[3] Seasonality metrics can be used to quantify spatial and interannual variability in phenology. These metrics have been developed as ecological indicators for monitoring pelagic ecosystems, and in particular, for detecting consequences of change from natural and anthropogenically driven forcing [*Platt and Sathyendranath*, 2008]. In addition, they allow for quantitative comparison of seasonal characteristics between regions and years [*Racault et al.*, 2012]. In a warmer world seasonal stratification is expected to occur earlier and last longer [*Sarmiento et al.*, 2004]. The canonical response of phytoplankton to increased stratification varies regionally, so that in light-limited high-latitude regions, mixed-layer irradiance would increase to levels sufficient to initiate a bloom earlier, extending the growing season and potentially boost primary production [*Bopp et al.*, 2001; *Steinacher et al.*, 2010]. In mid and low latitudes, increased stratification is postulated to result in a longer period of nutrient limitation as the entrainment of nutrients from below the thermocline is inhibited, leading to reduced phytoplankton growth [*Behrenfeld et al.*, 2006]. Although warming in the ocean is slower than on land, climate change driven trends in phenological events are expected to occur earlier in the ocean than in

[1]Ocean and Earth Science, National Oceanography Centre Southampton, University of Southampton, Southampton, UK.
[2]National Oceanography Centre, Southampton, UK.

Corresponding author: H. Cole, Ocean and Earth Science, National Oceanography Centre Southampton, University of Southampton, Southampton SO14 3ZH, UK. (harriet.cole@noc.soton.ac.uk)

©2012. American Geophysical Union. All Rights Reserved.
0148-0227/12/2012JC008249

terrestrial environments as marine seasonal temperature variations are smaller [*Burrows et al.*, 2011]. To assess interannual variability and climate change-driven trends in phytoplankton blooms, the timing of phenological events must be accurately estimated.

[4] Remote sensing of ocean color is an invaluable tool for studying phytoplankton phenology at large spatial scales and at high temporal resolution over annual cycles [*Platt et al.*, 2010]. However, many regions that display a strong seasonal cycle, such as high latitudes, also experience frequent cloud cover which may persist for long periods. Long gaps in satellite ocean color data also occur due to low sun angle in winter, sea-ice and atmospheric aerosols. The loss of data coverage in the North Pacific was recognized as a potential problem in bloom timing studies by *Sasaoka et al.* [2011]. They found that ocean color data was present between 3 and 15 days per month at individual pixels over their spring and summer study period. Missing data may affect the accuracy of seasonality metrics in two ways. The date of interest might occur during a period of missing data or the calculation method of the metric may be biased by missing data.

[5] Several methods have been employed to reduce the impact of gaps in satellite data time series. Although, averaging over time and space reduces the number of gaps it also smoothes out high-frequency variability [*Winder and Cloern*, 2010]. This means that higher frequency processes cannot be resolved and so tradeoffs often need to be made between resolution and data coverage (i.e., data sets with monthly resolution have better data coverage but daily and weekly processes cannot be resolved). Interpolation is also an unsatisfactory method for filling the long persistent gaps in winter. Interpolation can work well over small gaps but is inaccurate and often underestimates variability when filling long gaps in the data when trends may not be linear. Other studies exclude high-latitude regions from the analysis in order to remove the most gap affected regions [*Dandonneau et al.*, 2004]. However, high-latitude areas are very productive and display some of the strongest and most seasonally variable cycles and furthermore, can be relatively cloud-free in the summer months. This study aims to quantify the impact missing data has on the accuracy of seasonality metrics and to present a method for estimating the likely uncertainty in the metric based on the proportion of missing data.

2. Data, Model and Methods

2.1. Satellite Data and Model Output

[6] To estimate errors in the metrics a completely gap-free data set was needed to calculate the true metric date for comparison to those estimated from intermittent time series. The NASA Ocean Biogeochemical Model (NOBM) is a fully coupled radiative, general circulation and biogeochemical model that assimilates Sea-viewing Wide Field-of-view Sensor (SeaWiFS) chlorophyll data on a daily basis [*Nerger and Gregg*, 2008]. As a result the phases of the annual cycles in NOBM and satellite observations from the GlobColor data set are very similar. For this phenological study it is important that the start, peak and end of the bloom occur at the same point in time in NOBM and satellite observations. The NOBM output was obtained from the Giovanni application developed by the NASA Goddard Earth Sciences Data and Information Services Center (GES DISC) available from http://giovanni.gsfc.nasa.gov. Daily fields of 2/3° latitude and 5/4° longitude resolution were averaged to 8 day composites to match the satellite data set.

[7] For satellite ocean color data, we use GlobColor, a level 4 merged product that incorporates data from the SeaWiFS, MODIS and MERIS instruments and uses a weighted average to generate a global chlorophyll data set. Further details on the GlobColor data set can be found at: http://www.globcolour.info/CDR_Docs/GlobCOLOUR_PUG.pdf. Combining the 3 sensors increases the data coverage in both time and space. Eight day composites with a spatial resolution of 0.25° were obtained from the GlobColor website http://www.globcolour.info. The satellite data set was regridded onto the coarser resolution grid of the NOBM. GlobColor and NOBM overlap for the years 2002 to 2006.

[8] Regions that did not display a seasonal cycle in chlorophyll were removed before further analysis. The coefficient of variation (standard deviation/mean, also known as the seasonal variation index [*Lutz et al.*, 2007]) was calculated from the climatological year. Low coefficient of variation values characterize oligotrophic regions where production is relatively constant all year-round with no pronounced annual cycle [*Doney et al.*, 2003; *Lutz et al.*, 2007]. Any pixel with a coefficient of variation value below 0.35 was classified as having a weak indistinct seasonal cycle. This value was chosen based on the spatial pattern of the coefficient of variation and a visual inspection of individual time series. These regions are masked out in the figures presented here (see auxiliary material for details).[1]

2.2. Metrics

[9] Two metrics, the dates of the bloom initiation and the peak, were chosen for this study. Many phenological metrics have been defined in previous studies and several different methods to calculate the same metric have been described [*Siegel et al.*, 2002; *Platt and Sathyendranath*, 2008; *Henson et al.*, 2009; *Kahru et al.*, 2011]. As the timing of bloom events varies with location using 1st January as the starting point for each annual cycle of chlorophyll was not appropriate. Instead the timing of the bloom peak (maximum chlorophyll concentration) was used to define the center point of the annual cycle for each grid location. To do this the bloom peak in each year of the GlobColor data set was found; then the 6 months of data before and after this date were used to form the "year" around the peak of the bloom.

[10] The bloom initiation was defined as the date in each year on which the chlorophyll concentration first rises 5% above the annual median value. This condition had to be met for two consecutive time points (i.e., 16 days) to be valid. Using a fixed chlorophyll concentration to define a bloom would only be valid for short-term regional applications since the seasonal amplitude of phytoplankton blooms is highly variable both spatially and interannually. Therefore, a relative threshold was used to define the start of a bloom. *Siegel et al.* [2002] tested threshold values ranging from 1% to 30% above the annual median and found little difference in the resultant bloom initiation date. We use 5% here to remain consistent with *Siegel et al.* [2002]. This metric definition was chosen as it has been used extensively in other studies and is suitable to apply on a global scale encompassing areas

[1]Auxiliary materials are available in the HTML. doi:10.1029/2012JC008249.

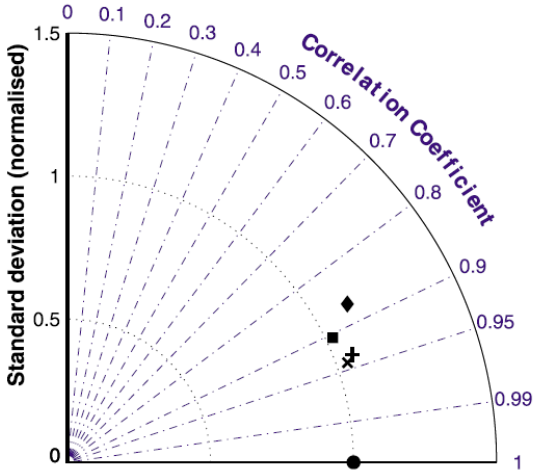

Figure 1. Taylor diagram comparing the bloom initiation (diamond) and bloom peak (plus) metric results from NOBM to those from satellite observations (circle). Sub-sampling NOBM where GlobColor data is present improves the agreement between NOBM and satellite observations for both metrics, bloom initiation (square) and peak (cross).

that incorporate many different types of annual cycle [*Siegel et al.*, 2002; *Henson et al.*, 2006, 2009; *Platt et al.*, 2009; *Thomalla et al.*, 2011; *Racault et al.*, 2012]. The peak was defined as the date on which the chlorophyll concentration reached its maximum value in each year.

2.3. Error Estimation

[11] The NOBM provides a gap-free chlorophyll time series with high fidelity to the seasonal characteristics of the satellite data (see Figure S2 in Text S1 of auxiliary material) while the satellite observations supply a record of when missing data occurred. The seasonality metrics were calculated using the NOBM output twice: once with the complete chlorophyll time series and again when NOBM was sub-sampled only on the dates when GlobColor data were present. The error in bloom timing at each location was found by calculating the difference between the two metric estimates. The satellite observations and NOBM output overlapped in time by 5 years and so only 5 error estimates could be calculated initially at each pixel. To increase the number of error estimates at each pixel, each of the 5 years in NOBM was sub-sampled 5 times. This was done by shuffling around the 5 years in the GlobColor gap data set so that every year in NOBM was sub-sampled using every year in GlobColor (i.e., each year in NOBM was sub-sampled using dates when GlobColor data are present in 2002, then the dates when data are present in 2003, then the dates when data are present in 2004 etc.). This gives a total of 25 error estimates at each pixel. While this creates a larger pool to draw estimates from, it does assume that the temporal distribution of missing data is broadly similar each year and that it does not strongly regulate underlying chlorophyll concentrations. The mean error magnitude and percentage of missing data at each pixel was calculated and ln(y + 1) transformation applied to make the data more Gaussian for linear regression. The regression analysis was performed on the global data set.

3. Results

3.1. Comparison of NOBM and GlobColor

[12] To use NOBM as a gap-free data set to estimate bloom timing we must first ensure that bloom timing in NOBM matches that in GlobColor for the error estimates to have any meaning. Co-located time series from NOBM and GlobColor (see auxiliary material) show that the timing of bloom characteristics match well. This is summarized globally in a Taylor diagram (Figure 1). There is high agreement between satellite observations and NOBM output for both bloom initiation (0.87) and for the bloom peak (0.94). In addition the metrics both have a normalized standard deviation close to 1 (indicating that the metric spatial variability is approximately equal in both the satellite observations and NOBM output). The correlation may be reduced due to gaps present in the GlobColor data set which may change the bloom timing dates. This means that NOBM bloom timing dates will not agree with GlobColor dates even if their seasonal cycle matches perfectly. When NOBM is sub-sampled on dates when GlobColor data is present the agreement between NOBM and GlobColor for both metrics improves with the standard deviation moving closer to 1 and the correlation coefficient rising to 0.92 for bloom initiation.

3.2. Empirical Relationship Between Error and Missing Data

[13] The spatial variability of missing data from satellite ocean color data is shown in Figure 2 where the highest proportion of missing data is found at high latitudes and in equatorial regions. This pattern varies seasonally with the majority of gaps occurring during the winter and persisting for months at high to midlatitudes. Though a relatively large proportion of gaps occur in equatorial regions these gaps are smaller lasting for days to weeks.

[14] Figure 3 shows the relationship between the percentage of missing data and the ln(y + 1) transform of the absolute magnitudes of both the bloom initiation and peak metric errors. Every pixel was included in the regression though data has been binned for plotting purposes in Figure 3. A cubic polynomial was fitted to both metrics giving the relationship with the percentage of missing data,

$$Err_{BI} = \exp\left[2.27(\pm 0.03) \times 10^{-5}x^3 - 3.72(\pm 0.04) \times 10^{-3}x^2 + 0.20(\pm 1.34 \times 10^{-3})x\right] - 1 \quad (R^2 = 0.515, \text{p-value} < 0.05) \tag{1}$$

$$Err_{P} = \exp\left[1.10(\pm 0.04) \times 10^{-5}x^3 - 1.94(\pm 0.05) \times 10^{-3}x^2 + 0.12(\pm 1.62 \times 10^{-3})x\right] - 1 \quad (R^2 = 0.428, \text{p-value} < 0.05) \tag{2}$$

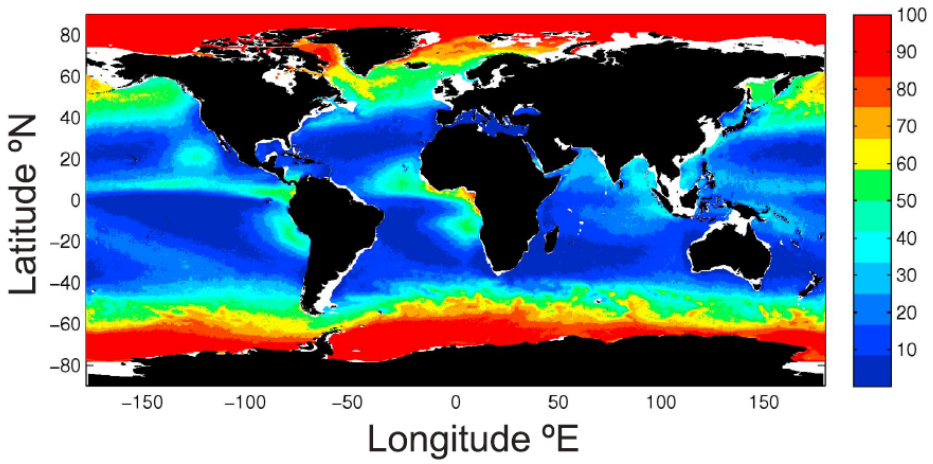

Figure 2. Map of the percentage of missing data at each pixel in the GlobColor data set using 8 day composites over the time span 2002–2006.

where Err_{BI} is the error in bloom initiation date and Err_P is the error in bloom peak date. As the error should be zero when all data are present the regressions were forced to go through zero. The values in brackets indicate the 95% confidence intervals on the regression coefficients and were obtained through bootstrapping the regression by repeatedly sub-sampling the data. Several other regression models were tried (see auxiliary material for details), however the cubic polynomial was found to provide the best fit while minimizing overfitting.

3.3. Application to Determining Uncertainty in Metric Dates

[15] Error maps for the bloom initiation and peak metrics using equations (1) and (2) respectively, are displayed alongside the seasonality metrics calculated from the satellite observations in Figures 4 and 5. In the northern hemisphere there is a clear gradient in bloom initiation date from subtropical regions where it starts in November/December through to June/July at high latitudes (Figure 4a). A similar pattern is seen in the southern hemisphere with blooms starting during May/June in subtropical regions through to October/January at higher latitudes. The error uncertainty on the bloom initiation date varies spatially, but the majority of mid to high-latitude regions (excluding the Southern Ocean) have a predicted error of approximately 30 days, decreasing to close to zero toward subtropical regions (Figure 4b).

[16] A clear latitudinal gradient is also seen in the peak metric date (Figure 5a). In the Northern Hemisphere the bloom peak transitions from February in subtropical regions through to August at high latitudes. These timings are 6 months out of phase in the Southern Hemisphere with the peak occurring in August/September in subtropical regions and in December/January at high latitudes. The uncertainty in peak date shows more spatial variability than the bloom initiation metric (Figure 5b). The largest uncertainty is approximately 30 days and is again seen in the high-latitude Southern Ocean. Outside of the Southern Ocean the predicted error is typically less than 15 days, again highest at high latitudes and decreasing toward the subtropical gyres.

[17] Broadly speaking, the largest errors in both bloom initiation and peak timing metrics are seen in the subpolar regions, while the smallest errors occur at lower latitudes. The regions with large errors unsurprisingly coincide with regions that have a high percentage of missing data. More specifically, large errors in the bloom initiation date (~50–60 days) are seen in the North Pacific (between 35°N and 50°N) and the western North Atlantic (north of 40°N). Substantial errors in the peak date (~35–49 days) occur in the North Pacific, Congo outflow region and central North Atlantic. The largest errors occur in the Southern Ocean, south of 60°S where the error in bloom initiation date is 3–4 months. Overall, the peak metric has smaller errors (~15 days) than the bloom initiation metric (~30 days).

[18] Errors are either a number of days earlier (too early) or later (too late) than the true metric date. Given that an error has occurred the probability that an error is a "too late" error is plotted in Figure 6. The direction of the error in bloom initiation date depends on latitude. Missing data in the subpolar regions (north of 50°N and south of 50°S) are more likely to result in the bloom start date identified from intermittent data being later than the true start date. At subtropical latitudes, this is reversed with the bloom initiation identified from intermittent data likely to be earlier than the true date. Only the Southern Ocean stands out as a region where the peak date identified from intermittent data is consistently later than the actual date (Figure 6). The majority of ocean regions display a random pattern with no coherent patches where the errors in peak date are consistently earlier or later than the true date.

4. Discussion

4.1. Impact on Seasonality Metrics

[19] The mean dates of bloom initiation and peak (Figures 4a and 5a) are consistent with those reported by *Racault et al.*

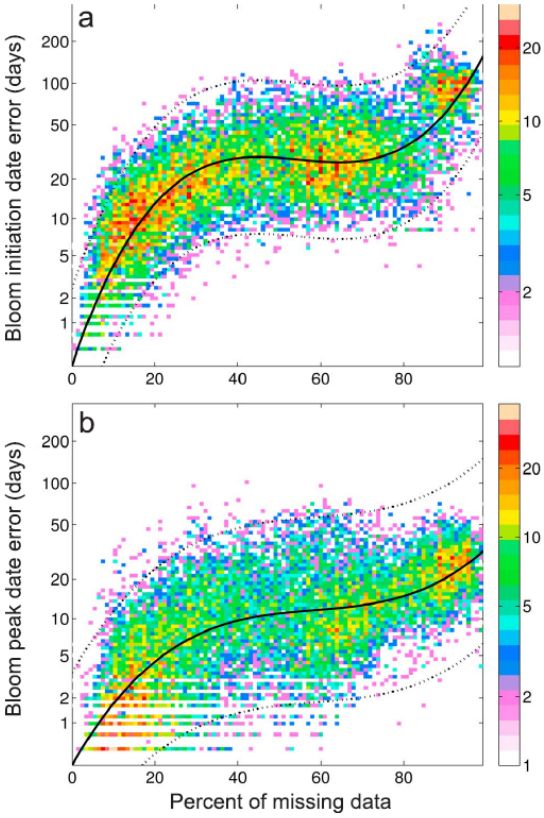

Figure 3. Relationship between percentage of missing data and the error in (a) bloom initiation date and (b) peak date. Regression lines for both metrics are cubic polynomial fits. Dotted lines represent the 95% confidence intervals. Data has been binned for plotting purposes and the color bar denotes the number of data points in a particular bin.

[2012] and exhibit a similar global spatial pattern, adding validity to our bloom timing estimates. However, missing data in chlorophyll time series are shown here to have a significant impact on the accuracy of seasonality metrics. The majority of affected regions display uncertainty of approximately 30 days for the bloom initiation date and up to 15 days for the peak date. The reason for this difference lies in how the metrics are calculated. As the peak date is defined as the date of maximum chlorophyll concentration, its accuracy depends on the presence of a data point on the date in question. If data are missing on that particular date then the next highest concentration is likely to occur on a date very near the actual date. Conversely, the accuracy of the bloom initiation metric depends both on the presence of data on the date in question and on the accuracy of the estimate for the threshold value used to define bloom initiation. The threshold value used here is 105% of the annual median and a bias in the metric error indicates that the annual median is incorrectly estimated. If data are missing during the winter then the median-based threshold value is biased toward the higher summer values, so that the chlorophyll concentration exceeds the threshold later in the growing season. This is highlighted in Figure 6 which shows that the errors in subpolar regions are more likely to be later than the true date. In contrast, the errors in the peak date have almost an equal chance of being either earlier or later than the true date.

[20] Subtropical regions characterized as displaying a seasonal cycle are subject to either very small or zero errors for both metrics. Unlike subpolar regions these regions do not experience long gaps in the time series from low sun angle and persistent cloud cover though intermittent gaps do occur through short-term cloud cover and atmospheric aerosols. Consequently errors are small as the small amount of missing data has a minor impact on the calculation of the seasonality metrics. As shown in Figure 6, errors in the bloom initiation date in subtropical regions are more likely to be toward an earlier date whereas the bloom peak date is equally likely to be either earlier or later. Just like subpolar regions missing data are most common during the local winter months however, in subtropical regions this is when chlorophyll values are highest. This results in the threshold value being biased toward lower values, in which case an earlier date is identified as the start of the bloom. For this particular method of calculating the bloom initiation date, the timing of missing data has a significant effect on the accuracy of the metric.

4.2. Implications

[21] These results have implications for any studies relying on intermittent data to determine the timing of seasonal events. In the case of phytoplankton phenology, the missing data adds uncertainty to the estimation of seasonality metrics that may be mistaken for real interannual variability in bloom timing. Current research uses seasonality metrics as ecological indicators for assessing interannual variability and detecting trends through either natural or anthropogenic influences [*Chiba et al.*, 2008; *Martinez et al.*, 2011; *Thomalla et al.*, 2011; *Racault et al.*, 2012]. However, trends may go undetected due to the noise that missing data add to the interannual variability of bloom timing. The metrics are designed to enable quantitative comparison between different bloom regimes, but the uncertainty in the metrics varies spatially, making intercomparison of different regions difficult. Our results are particularly relevant to ongoing research into the relationship between bloom timing and the survival and recruitment of fish and invertebrates, specifically with regards to the match-mismatch hypothesis [*Cushing*, 1990; *Platt et al.*, 2003; *Fuentes-Yaco et al.*, 2007].

[22] The uncertainty in bloom timing estimates must be smaller than the interannual variability for the interannual variability to be calculated with any certainty. Bloom timing studies so far have found that the bloom initiation and peak date are highly variable interannually. For example, in the California Current region the range in bloom initiation date varied from 1 to 3 months interannually [*Henson and Thomas*, 2007] with a mean uncertainty of ~21 days due to missing data. In the North Atlantic the range in bloom initiation date varied from 2 to 3 weeks up to 10 weeks in most subpolar regions (mean uncertainty of ~26 days), 5–6 weeks in the Irminger basin (mean uncertainty of ~27 days) and up to 20 weeks in the subpolar-subtropical boundary region (mean uncertainty of ~24 days) [*Henson et al.*, 2006, 2009]. Similar spatial patterns have been described in the Southern Ocean with typical bloom initiation timing standard deviations of

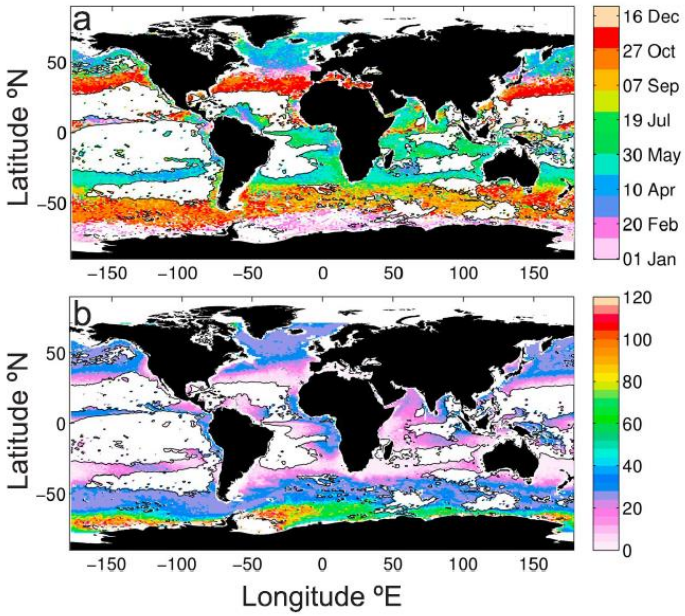

Figure 4. Maps of (a) mean bloom initiation date (2002–2006), (b) uncertainty in bloom initiation date calculated from equation (1) (days). Areas within the white contour do not display a distinct seasonal cycle or are areas of permanent ice cover.

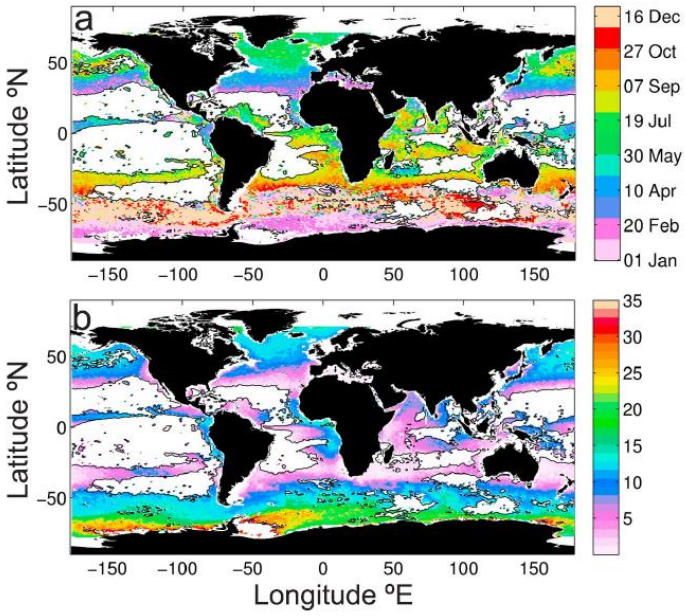

Figure 5. Maps of (a) mean bloom peak date (2002–2006) and (b) uncertainty in bloom peak date calculated from equation (2) (days). Areas within the white contour do not display a distinct seasonal cycle or are areas of permanent ice cover.

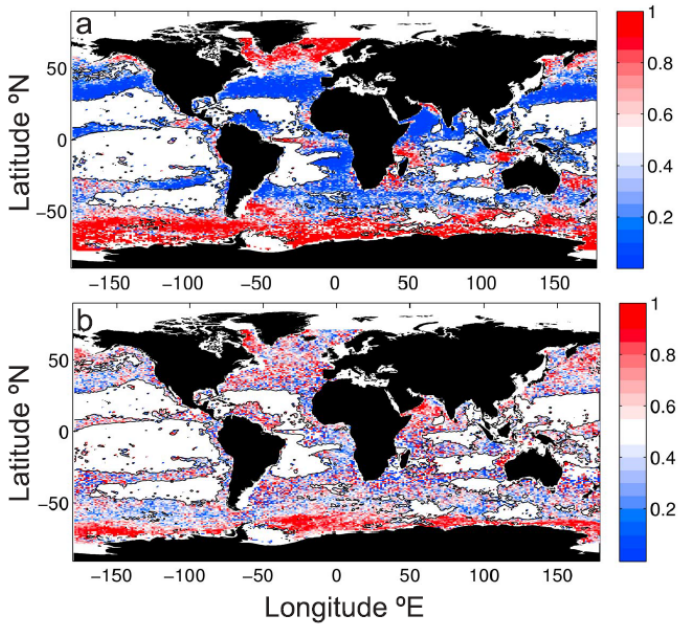

Figure 6. Maps of the probability that an error resulting from missing data in (a) bloom initiation and (b) bloom peak is toward a date later than the true date. If probability is greater than 0.5 then the error is more likely to be toward a date later than the true date. If probability is less than 0.5 then the error is more likely to be toward a date earlier than the true date. Areas within the white contour do not display a distinct seasonal cycle or are areas of permanent ice cover.

24 days in subpolar regions (mean uncertainty of ~51 days) and 64–80 days in the subpolar-subtropical boundary region (mean uncertainty of ~19 days) [*Thomalla et al.*, 2011]. The date of peak timing varied by 40 days in the Japan Sea (mean uncertainty of 7 days) [*Yamada and Ishizaka*, 2006] and an advancement of 50 days in peak timing over 1997–2009 was reported in some regions of the Arctic Ocean (mean uncertainty of 16 days in Baffin Bay, the only region that overlapped spatially with this study where an advancement was reported) [*Kahru et al.*, 2011]. Many studies have looked at links between interannual variability in physical ocean processes and bloom timing to deepen our understanding of bloom dynamics [*Edwards and Richardson*, 2004; *Chiba et al.*, 2008; *Sasaoka et al.*, 2011; *Racault et al.*, 2012]. This may not be possible in regions where the uncertainty in bloom timing is too great.

[23] Satellite observations are an ideal tool to expand these studies over larger areas and the results shown here will enable researchers to calculate the uncertainty in their bloom timing metrics. It also provides a useful tool for making objective decisions about the accuracy of interannual variability estimates. Furthermore, there is the potential to apply these results to in situ time series, where regular sampling is interrupted through bad weather or equipment failure. This is pertinent to any seasonal study that uses satellite or in situ data of any variable with gaps in the time series where the timing of an event is important. There are several other seasonality metrics that define the onset of the bloom differently in addition to metrics that quantify other phenological characteristics of phytoplankton blooms. The methodology used here provides a useful way to identify those metrics which are most insensitive to gaps thus reducing the uncertainty in bloom timing.

[24] This study provides a method to quantify the uncertainty in seasonality metrics from the percentage of data missing in a year. An indication of the direction of this error is also given. Only two metrics have been analyzed here but the overall concept is valid for other seasonality metrics calculated from incomplete data sets. Fundamentally, the method of metric calculation must be considered carefully to understand the influence that missing data may have on the accuracy of the results.

[25] **Acknowledgments.** GlobColor data were provided by ACRI-ST GlobColor service, supported by EU FP7 MyOcean & ESA GlobColor projects, using ESA ENVISAT MERIS data, NASA MODIS and SeaWiFS data. The NASA Ocean Biogeochemical Model output was obtained using the Giovanni online data system, developed and maintained by the NASA GES DISC. This work was funded by the UK Natural Environment Research Council (NERC) as part of an Ocean and Earth Science postgraduate research program at the University of Southampton. In addition, this work was supported by NERC grant NE/G013055/1 to S.A.H. and by NERC NA funding for A.P.M. and A.Y.

References

Behrenfeld, M. J., R. T. O'Malley, D. A. Siegel, C. R. McClain, J. L. Sarmiento, G. C. Feldman, A. J. Milligan, P. G. Falkowski, R. M. Letelier, and E. S. Boss (2006), Climate-driven trends in contemporary ocean productivity, *Nature*, *444*(7120), 752–755, doi:10.1038/nature05317.

Bopp, L., P. Monfray, O. Aumont, J. L. Dufresne, H. Le Treut, G. Madec, L. Terray, and J. C. Orr (2001), Potential impact of climate change on marine export production, *Global Biogeochem. Cycles*, *15*(1), 81–99, doi:10.1029/1999GB001256.

Burrows, M. T., et al. (2011), The pace of shifting climate in marine and terrestrial ecosystems, *Science*, *334*(6056), 652–655, doi:10.1126/science.1210288.

Chiba, S., M. N. Aita, K. Tadokoro, T. Saino, H. Sugisaki, and K. Nakata (2008), From climate regime shifts to lower-trophic level phenology: Synthesis of recent progress in retrospective studies of the western North Pacific, *Prog. Oceanogr.*, *77*(2–3), 112–126, doi:10.1016/j.pocean.2008.03.004.

Cushing, D. H. (1990), Plankton production and year-class strength in fish populations: An update of the match mismatch hypothesis, *Adv. Mar. Biol.*, *26*, 249–293, doi:10.1016/S0065-2881(08)60202-3.

Dandonneau, Y., P. Y. Deschamps, J. M. Nicolas, H. Loisel, J. Blanchot, Y. Montel, F. Thieuleux, and G. Bécu (2004), Seasonal and interannual variability of ocean color and composition of phytoplankton communities in the North Atlantic, equatorial Pacific and South Pacific, *Deep Sea Res., Part II*, *51*(1–3), 303–318, doi:10.1016/j.dsr2.2003.07.018.

Deuser, W. G. (1986), Seasonal and interannual variations in deep-water particle fluxes in the Sargasso Sea and their relation to surface hydrography, *Deep Sea Res., Part A*, *33*(2), 225–246, doi:10.1016/0198-0149(86)90120-2.

Doney, S. C., D. M. Glover, S. J. McCue, and M. Fuentes (2003), Mesoscale variability of Sea-viewing Wide Field-of-view Sensor(SeaWiFS) satellite ocean color: Global patterns and spatial scales, *J. Geophys. Res.*, *108*(C2), 3024, doi:10.1029/2001JC000843.

Edwards, M., and A. J. Richardson (2004), Impact of climate change on marine pelagic phenology and trophic mismatch, *Nature*, *430*(7002), 881–884, doi:10.1038/nature02808.

Fuentes-Yaco, C., P. A. Koeller, S. Sathyendranath, and T. Platt (2007), Shrimp (Pandalus borealis) growth and timing of the spring phytoplankton bloom on the Newfoundland-Labrador Shelf, *Fish. Oceanogr.*, *16*(2), 116–129, doi:10.1111/j.1365-2419.2006.00402.x.

Henson, S. A., and A. C. Thomas (2007), Interannual variability in timing of bloom initiation in the California Current System, *J. Geophys. Res.*, *112*, C08007, doi:10.1029/2006JC003960.

Henson, S. A., I. Robinson, J. T. Allen, and J. J. Waniek (2006), Effect of meteorological conditions on interannual variability in timing and magnitude of the spring bloom in the Irminger Basin, North Atlantic, *Deep Sea Res., Part I*, *53*(10), 1601–1615, doi:10.1016/j.dsr.2006.07.009.

Henson, S. A., J. P. Dunne, and J. L. Sarmiento (2009), Decadal variability in North Atlantic phytoplankton blooms, *J. Geophys. Res.*, *114*, C04013, doi:10.1029/2008JC005139.

Kahru, M., V. Brotas, M. Manzano-Sarabia, and B. G. Mitchell (2011), Are phytoplankton blooms occurring earlier in the Arctic?, *Global Change Biol.*, *17*, 1733–1739, doi:10.1111/j.1365-2486.2010.02312.x.

Koeller, P., et al. (2009), Basin-scale coherence in phenology of shrimps and phytoplankton in the North Atlantic Ocean, *Science*, *324*(5928), 791–793, doi:10.1126/science.1170987.

Lutz, M. J., K. Caldeira, R. B. Dunbar, and M. J. Behrenfeld (2007), Seasonal rhythms of net primary production and particulate organic carbon flux to depth describe the efficiency of biological pump in the global ocean, *J. Geophys. Res.*, *112*, C10011, doi:10.1029/2006JC003706.

Martinez, E., D. Antoine, F. D'Ortenzio, and C. de Boyer Montégut (2011), Phytoplankton spring and fall blooms in the North Atlantic in the 1980s and 2000s, *J. Geophys. Res.*, *116*, C11029, doi:10.1029/2010JC006836.

Nerger, L., and W. W. Gregg (2008), Improving assimilation of SeaWiFS data by the application of bias correction with a local SEIK filter, *J. Mar. Syst.*, *73*(1–2), 87–102, doi:10.1016/j.jmarsys.2007.09.007.

Platt, T., and S. Sathyendranath (2008), Ecological indicators for the pelagic zone of the ocean from remote sensing, *Remote Sens. Environ.*, *112*(8), 3426–3436, doi:10.1016/j.rse.2007.10.016.

Platt, T., C. Fuentes-Yaco, and K. T. Frank (2003), Marine ecology: Spring algal bloom and larval fish survival, *Nature*, *423*(6938), 398–399, doi:10.1038/423398b.

Platt, T., G. N. White, L. Zhai, S. Sathyendranath, and S. Roy (2009), The phenology of phytoplankton blooms: Ecosystem indicators from remote sensing, *Ecol. Modell.*, *220*(21), 3057–3069, doi:10.1016/j.ecolmodel.2008.11.022.

Platt, T., S. Sathyendranath, G. N. White III, C. Fuentes-Yaco, L. Zhai, E. Devred, and C. Tang (2010), Diagnostic properties of phytoplankton time series from remote sensing, *Estuaries Coasts*, *33*, 428–439, doi:10.1007/s12237-009-9161-0.

Racault, M.-F., C. Le Quéré, E. Buitenhuis, S. Sathyendranath, and T. Platt (2012), Phytoplankton phenology in the global ocean, *Ecol. Indic.*, *14*(1), 152–163, doi:10.1016/j.ecolind.2011.07.010.

Sarmiento, J. L., et al. (2004), Response of ocean ecosystems to climate warming, *Global Biogeochem. Cycles*, *18*(3), GB3003, doi:10.1029/2003GB002134.

Sasaoka, K., S. Chiba, and T. Saino (2011), Climatic forcing and phytoplankton phenology over the subarctic North Pacific from 1998 to 2006, as observed from ocean color data, *Geophys. Res. Lett.*, *38*, L15609, doi:10.1029/2011GL048299.

Siegel, D. A., S. C. Doney, and J. A. Yoder (2002), The North Atlantic spring phytoplankton bloom and Sverdrup's critical depth hypothesis, *Science*, *296*(5568), 730–733, doi:10.1126/science.1069174.

Steinacher, M., et al. (2010), Projected 21st century decrease in marine productivity: A multi-model analysis, *Biogeosciences*, *7*(3), 979–1005, doi:10.5194/bg-7-979-2010.

Thomalla, S. J., N. Fauchereau, S. Swart, and P. M. S. Monteiro (2011), Regional scale characteristics of the seasonal cycle of chlorophyll in the Southern Ocean, *Biogeosciences*, *8*(10), 2849–2866, doi:10.5194/bg-8-2849-2011.

Winder, M., and J. E. Cloern (2010), The annual cycles of phytoplankton biomass, *Philos. Trans. R. Soc. B*, *365*(1555), 3215–3226, doi:10.1098/rstb.2010.0125.

Yamada, K., and J. Ishizaka (2006), Estimation of interdecadal change of spring bloom timing, in the case of the Japan Sea, *Geophys. Res. Lett.*, *33*, L02608, doi:10.1029/2005GL024792.

9 Appendix B

Objective Analysis

Objective analysis is based on the Gauss-Markov theorem from statistical estimation theory (Liebelt, 1967) and was described for application to the ocean by Bretherton *et al.* (1976). Objective analysis uses estimation theory to map sparse and irregularly spaced data onto a regular grid (Bretherton *et al.*, 1976). The estimate at each grid point is derived linearly from the available observational data. Objective analysis is based on minimizing the mean square error (Bretherton *et al.*, 1976). The minimum error can be calculated *a priori* from the design of the sampling grid. This also indicates that the grid design can be adjusted to reduce the error to within an acceptable range. Thus, the sampling grid design gives a limit on the scale of processes that are able to be studied (Bretherton *et al.*, 1976).

MLD Data Error Estimation

In the objective analysis of the temperature and salinity data used to calculate mixed layer depths in Chapter 2, the interpolated field was constructed as a departure from a reference field (i.e. a climatology). The climatology used was the NODC World Ocean Atlas (Gaillard *et al.*, 2009). The results of the objective analysis also give information on the errors associated with the interpolated field. This is simply calculated as the difference between the variance of the reference field (climatology) and the variance of the information provided by the observations used in the analysis.

The variance of the climatology is the total variance (σ_{tot}^2) (Gaillard, 2010), and is calculated at each grid point using all data within a 10x10 grid point square. The variance of the information given in the observation is calculated from 4 covariance terms based on the ARGO array:

$$\sigma_{tot}^2 = \sigma_{LS}^2 + \sigma_{MS}^2 + \sigma_{UR}^2 + \sigma_{ME}^2$$

The first two terms ($\sigma_{LS}^2, \sigma_{MS}^2$) are the total field variance and represent the covariance on the analysed field and is specified by the sum of two Gaussian functions covering different time and space scales (Gaillard, 2010). The first

Gaussian function has a length scale set at the target resolution of the ARGO array of 300km and a corresponding time scale of 3 weeks. The second Gaussian function has a length scale set to the Rossby radius and an associated time scale of 1 week. These two scales represents a compromise between important ocean time and space scales and the scales that the ARGO array can resolve (Gaillard *et al.*, 2009).

The last two terms ($\sigma_{UR}^2, \sigma_{ME}^2$) represent the total error variance arising from variance on scales too small to be resolved and measurement error from the instruments used to record temperature and salinity (Gaillard *et al.*, 2009). Thus, the total variance is wholly represented when the observational dataset is vast enough to fully capture these four terms. Thus, the error statistics associated with the temperature and salinity objective analysis datasets are expressed as a percentage of the total variance (i.e. the total variance that is expected). Thus, errors of 0% indicate that all expected variance is accounted for and variances of 100% indicate that no data has been added. However, given the coarse resolution of the ARGO array errors less than 50% are not expected as mesoscale processes are excluded (Gaillard, 2007).

10 Appendix C

Coefficient of Variation and Percentage of Missing Data

In Chapter 4, results are derived from bloom timing datasets that have had regions which do not display a strong seasonal cycle removed. The criterion for a strong seasonal cycle is for the chlorophyll time series to have a coefficient of variation above 0.35 (see Chapter 3 for more details). Results should not be dependent on this choice of value. To investigate the impact of the correlation of coefficient value on the results obtained in this thesis, the results are repeated using a coefficient of variation value of 0.3 and 0.4 to identify regions with a weak seasonal cycle. The results from using these other values are reported here alongside the 0.35 results.

Table 10.1: Coefficients for the equations obtained from the regression of bloom timing metric errors and percentage of missing data[a]

Equation	Equation term	CV 0.3	CV 0.35	CV 0.4
4.1 - Initiation	X^3	2.27[b] (0.03[b])	2.27[b] (0.03[b])	2.30[b] (0.04[b])
	X^2	-3.74[c] (0.04[c])	-3.72[c] (0.04[c])	-3.77[c] (0.05[c])
	X	0.20 ($1.22*10^{-3}$)	0.20 ($1.34*10^{-3}$)	0.20 ($1.49*10^{-3}$)
4.2 - Peak	X^3	1.17[b] (0.04[b])	1.10[b] (0.04[b])	1.09[b] (0.04[b])
	X^2	-2.07[c] (0.05[c])	-1.94[c] (0.05[c])	-1.89 (0.06[c])
	X	0.13 ($1.43*10^{-3}$)	0.12 ($1.62*10^{-3}$)	0.12 ($1.79*10^{-3}$)
4.3 - Termination	X^3	1.60[b] (0.03[b])	1.45[b] (0.04[b])	1.34 (0.04[b])
	X^2	-2.83[c] (0.04[c])	-2.62[c] (0.05[c])	-2.47[c] (0.05[c])
	X	0.18 ($1.29*10^{-3}$)	0.17 ($1.40*10^{-3}$)	0.16 ($1.51*10^{-3}$)

[a] Equations 4.1, 4.2 and 4.3 are found in Chapter 4 and describe the relationship between the percentage of missing data and the error in bloom timing metric date. Each equation has a x^3, x^2 and x term. The coefficients of these terms are reported here for three cases: when a coefficient of variation (CV) value of 0.3, 0.35 and 0.4 were used to remove regions without a strong seasonal cycle. The values in brackets indicate the 95% confidence intervals on the regression coefficients and were obtained through bootstrapping the regression by repeatedly sub-sampling the data.

[b] These values are of the order 10^{-5}.

[c] These values are of the order 10^{-3}.

Table 10.2: Correlation coefficients and normalised standard deviations for the comparison of metric dates from GlobColour to the full NOBM dataset and to the subsampled NOBM dataset[a]

		CV 0.3		CV 0.35		CV 0.4	
	Datasets compared	Standard deviation	Correlation coefficient	Standard deviation	Correlation coefficient	Standard deviation	Correlation coefficient
Initiation	NOBM vs. GC	1.12	0.86	1.12	0.87	1.14	0.88
	Subsampled NOBM vs. GC	1.03	0.90	1.02	0.91	1.02	0.91
Peak	NOBM vs. GC	1.06	0.93	1.06	0.94	1.07	0.94
	Subsampled NOBM vs. GC	1.04	0.93	1.04	0.94	1.04	0.95
Termination	NOBM vs. GC	0.95	0.84	0.95	0.85	094	0.84
	Subsampled NOBM vs. GC	1.04	0.92	1.04	0.93	1.04	0.93

[a] The bloom metric dates calculated from GlobColour (GC) are compared to the dates from the full NOBM dataset and from the subsampled NOBM dataset in Chapter 4. The comparisons are summarised by correlation coefficients and normalised standard deviations. These values are reported here for three cases: when a coefficient of variation (CV) value of 0.3, 0.35 and 0.4 were used to remove regions without a strong seasonal cycle.

11 Appendix D

Coefficient of Variation and Bloom Timing Variability

In Chapter 5 results are calculated from satellite-derived bloom timing that have had regions which do not display a strong seasonal cycle removed. The criterion for a strong seasonal cycle is for the chlorophyll time series to have a coefficient of variation above 0.35 for the GlobColour and NOBM chlorophyll datasets (see Chapter 3 for more details). Results should not be dependent on this choice of value. To investigate the impact of the coefficient of variation value on the results obtained in this thesis, the results are repeated using the original coefficient of variation value as well as a value of 0.3 and 0.4 to identify regions with a weak seasonal cycle. The results from using these other values are reported here alongside the original coefficient of variation value results.

Table 11.1: Correlation coefficients and latitudinal speeds for bloom initiation and associated physical timing metrics in the subpolar basins for both GlobColour and NOBM chlorophyll datasets

			Bloom initiation			NHF positive			MLD max			MLD shoaling			MLD<Zeu[a]			Fastest rise in PAR_{ML}			PAR_{ML} starts to increase		
		CV value	**0.30**	**0.35**	**0.40**	**0.30**	**0.35**	**0.40**	**0.30**	**0.35**	**0.40**	**0.30**	**0.35**	**0.40**	**0.30**	**0.35**	**0.40**	**0.30**	**0.35**	**0.40**	**0.30**	**0.35**	**0.40**
North Atlantic	GlobColour	Correlation coefficient[b]				0.77*	0.77*	0.77*	0.52*	0.52*	0.52*	0.72*	0.72*	0.72*	0.65*	0.65*	0.65*	-0.18	-0.18	-0.18	0.92*	0.92*	0.92*
		Latitudinal speed (km day^{-1})[c]	6.91	6.91	6.91	9.74	9.74	9.74	10.55	10.55	10.55	9.55	9.55	9.55	3.69	3.69	3.69	-5.49	-5.49	-5.49	7.12	7.12	7.12
	NOBM	Correlation coefficient[b]				0.51*	0.51*	0.51*	0.19	0.19	0.19	0.44*	0.44*	0.44*	0.73*	0.73*	0.73*	-0.45*	-0.45*	-0.45*	0.65*	0.65*	0.65*
		Latitudinal speed (km day^{-1})[c]	7.54	7.54	7.54	7.87	8.03	8.03	13.22	13.24	13.24	12.05	11.97	11.97	3.96	3.96	3.96	4.38	4.37	4.37	6.89	6.89	6.89
North Pacific	GlobColour	Correlation coefficient[b]				0.90*	0.90*	0.92*	0.93*	0.93*	0.94*	0.70*	0.69*	0.71*	0.88*	0.88*	0.90*	0.90*	0.89*	0.93*	0.83*	0.83*	0.88*
		Latitudinal speed (km day^{-1})[c]	2.75	2.76	2.68	2.28	2.29	2.28	4.69	4.67	4.65	3.02	2.95	3.04	2.06	2.07	2.10	4.11	4.24	4.04	3.68	3.63	3.20
	NOBM	Correlation coefficient[b]				-0.76*	-0.76*	-0.77*	0.65*	0.65*	0.64*	0.80*	0.80*	0.80*	0.97*	0.97*	0.97*	-0.88*	-0.88*	-0.87*	-0.94*	-0.94*	-0.93*
		Latitudinal speed (km day^{-1})[c]	-2.30	-2.30	-2.47	2.26	2.26	2.25	4.95	4.93	4.90	3.08	3.01	3.10	1.87	1.87	1.89	3.73	3.93	3.69	3.38	3.26	3.14
Southern Ocean	GlobColour	Correlation coefficient[b]				0.99*	0.99*	0.99*	0.89*	0.89*	0.89*	0.70*	0.72*	0.74*	0.90*	0.90*	0.90*	0.97*	0.97*	0.97*	0.97*	0.97*	0.97*
		Latitudinal speed (km day^{-1})[c]	-2.82	-2.83	-2.85	-2.58	-2.58	-2.58	-2.45	-2.45	-2.47	-7.92	-8.02	-8.12	-4.12	-4.16	-4.20	-5.85	-5.92	-6.04	-2.91	-2.93	-2.94
	NOBM	Correlation coefficient[b]				0.74*	0.73*	0.72*	0.50*	0.48*	0.48*	0.54*	0.55*	0.55*	0.44*	0.42*	0.40*	0.79*	0.77*	0.76*	0.67*	0.66*	0.65*
		Latitudinal speed (km day^{-1})[c]	-6.89	-6.92	-7.07	-2.61	-2.60	-2.61	-2.45	-2.46	-2.47	-8.31	-8.41	-8.35	-3.73	-3.77	-3.80	-5.67	-5.75	-5.81	-2.79	-2.81	-2.82

[a] MLD<Zeu stands for the date the MLD becomes shallower than the euphotic depth.

[b] A * indicates correlation coefficients which are statistically significant at the 95% confidence interval. Correlations were calculated between the bloom initiation latitudinal mean date and the physical metric latitudinal mean date. Mean dates were calculated over the years 2002-2009 for GlobColour data and 2002-2007 for NOBM data.

[c] Latitudinal speeds were calculated by regressing the metric dates on latitude (latitude = a+ b*date) and then multiplying the linear coefficient (b) by 111.19493 km/°latitude.

Table 11.2: Correlation coefficients and latitudinal speeds for bloom peak and associated physical timing metrics in the subpolar basins for both GlobColour and NOBM chlorophyll datasets

			Bloom peak			NHF positive			MLD min			NHF max		
		CV value	**0.30**	**0.35**	**0.40**	**0.30**	**0.35**	**0.40**	**0.30**	**0.35**	**0.40**	**0.30**	**0.35**	**0.40**
North Atlantic	GlobColour	Correlation coefficient[a]				0.51*	0.51*	0.51*	0.10	0.10	0.10	-0.49*	-0.49*	-0.49*
		Latitudinal speed (km day^{-1})[b]	5.46	5.46	5.46	9.74	9.74	9.74	-3.78	-3.78	-3.78	4.90	4.90	4.90
	NOBM	Correlation coefficient[a]				0.26	0.26	0.26	-0.11	-0.11	-0.11	-0.59*	-0.59*	-0.59*
		Latitudinal speed (km day^{-1})[b]	3.99	3.99	3.99	7.87	8.03	8.03	-12.03	-12.17	-12.17	8.93	8.98	8.98
North Pacific	GlobColour	Correlation coefficient[a]				0.10	0.10	0.15	0.33	0.33	0.33	0.25	0.25	0.29
		Latitudinal speed (km day^{-1})[b]	-0.67	-0.65	-0.32	2.28	2.29	2.28	-12.64	-12.11	-12.04	6.44	6.46	6.40
	NOBM	Correlation coefficient[a]				-0.81*	-0.81*	-0.81*	0.90*	0.90*	0.89*	-0.25	-0.25	-0.30
		Latitudinal speed (km day^{-1})[b]	-2.16	-2.16	-2.17	2.26	2.26	2.25	-11.40	-11.06	-10.91	6.03	6.09	6.04
Southern Ocean	GlobColour	Correlation coefficient[a]				0.95*	0.95*	0.95*	0.48*	0.46*	0.39*	0.90*	0.90*	0.90*
		Latitudinal speed (km day^{-1})[b]	-4.07	-4.08	-4.01	-2.58	-2.58	-2.58	-10.20	-9.81	-8.13	-10.31	-10.28	-10.29
	NOBM	Correlation coefficient[a]				0.82*	0.81*	0.81*	0.60*	0.59*	0.55*	0.92*	0.91*	0.91*
		Latitudinal speed (km day^{-1})[b]	-6.45	-6.42	-6.35	-2.61	-2.60	-2.61	-10.63	-10.30	-8.92	-10.66	-10.62	-10.61

[a] A * indicates correlation coefficients which are statistically significant at the 95% confidence interval. Correlations were calculated between the bloom peak latitudinal mean date and the physical metric latitudinal mean date. Mean dates were calculated over the years 2002-2009 for GlobColour data and 2002-2007 for NOBM data.

[b] Latitudinal speeds were calculated by regressing the metric dates on latitude (latitude = a+ b*date) and then multiplying the linear coefficient (b) by 111.19493 km/°latitude.

Table 11.3: Correlation coefficients and latitudinal speeds for bloom termination and associated physical timing metrics in the subpolar basins for both GlobColour and NOBM chlorophyll datasets

			Bloom termination			NHF negative			MLD min			MLD deepening			NHF max			MLD>Zeu[a]			Fastest fall in PAR_{ML}		
		CV value	0.30	0.35	0.40	0.30	0.35	0.40	0.30	0.35	0.40	0.30	0.35	0.40	0.30	0.35	0.40	0.30	0.35	0.40	0.30	0.35	0.40
North Atlantic	GlobColour	Corr. coef[b]				0.66*	0.66*	0.66*	0.15	0.15	0.15	0.29	0.29	0.29	-0.52*	-0.52*	-0.52*	0.13	0.13	0.13	-0.07	-0.07	-0.07
		Lat speed (km day^{-1})[c]	-3.86	-3.86	-3.86	-19.31	-19.31	-19.31	-3.78	-3.78	-3.78	-8.83	-8.83	-8.83	4.90	4.90	4.90	-6.13	-6.13	-6.13	-12.02	-12.02	-12.02
	NOBM	Corr. coef[b]				-0.69*	-0.69*	-0.69*	-0.59*	-0.59*	-0.59*	-0.71*	-0.71*	-0.71*	-0.03	-0.03	-0.03	-0.89*	-0.89*	-0.89*	-0.73*	-0.73*	-0.73*
		Lat speed (km day^{-1})[c]	7.88	7.88	7.88	-18.24	-18.27	-18.27	-12.03	-12.17	-12.17	-8.08	-7.88	-7.88	8.93	8.98	8.98	-5.86	-5.86	-5.86	-12.94	-12.94	-12.94
North Pacific	GlobColour	Corr. coef[b]				0.85*	0.83*	0.86*	0.72*	0.71*	0.74*	0.48*	0.42*	0.41	-0.44*	-0.42*	-0.35	0.69*	0.67*	0.66*	0.91*	0.90*	0.90*
		Lat speed (km day^{-1})[c]	-4.73	-4.65	-2.95	-13.29	-13.25	-13.33	-12.64	-12.11	-12.04	-6.79	-5.96	-5.92	6.44	6.46	6.40	-5.65	-5.69	-5.73	-5.26	-5.26	-5.25
	NOBM	Corr. coef[b]				-0.51	-0.51	-0.51	-0.47	-0.47	-0.48	-0.49	-0.49	-0.49	0.54	0.54	0.54	-0.39	-0.39	-0.40	-0.47	-0.47	-0.49
		Lat speed (km day^{-1})[c]	6.50	6.50	8.13	-13.99	-13.97	-14.08	-11.40	-11.06	-10.91	-6.28	-5.49	-5.52	6.03	6.09	6.04	-5.70	-5.76	-5.75	-4.98	-4.98	-4.99
Southern Ocean	GlobColour	Corr. coef[b]				0.36*	0.36*	0.35*	0.05	0.06	0.12	0.03	0.07	0.13	-0.08	-0.11	-0.12	0.72*	0.74*	0.75*	0.37*	0.35*	0.35*
		Lat speed (km day^{-1})[c]	7.54	7.35	6.96	6.12	6.11	6.13	-10.20	-9.81	-8.13	3.28	4.98	7.70	-10.31	-10.28	-10.29	7.75	7.80	7.71	9.64	9.89	10.21
	NOBM	Corr. coef[b]				-0.73*	-0.73*	-0.72*	0.21	0.19	0.11	0.10	0.03	-0.13	0.85*	0.86*	0.85*	-0.62*	-0.61*	-0.60*	0.04	0.01	-0.02
		Lat speed (km day^{-1})[c]	-6.02	-6.12	-6.16	5.98	5.96	6.01	-10.63	-10.30	-8.92	4.00	5.69	8.23	-10.66	-10.62	-10.61	6.27	6.30	6.22	8.62	9.05	9.55

[a] MLD>Zeu stands for the date the MLD becomes deeper than the euphotic depth.

[b] A * indicates correlation coefficients which are statistically significant at the 95% confidence interval. Correlations were calculated between the bloom termination latitudinal mean date and the physical metric latitudinal mean date. Mean dates were calculated over the years 2002-2009 for GlobColour data and 2002-2007 for NOBM data.

[c] Latitudinal speeds were calculated by regressing the metric dates on latitude (latitude = a+ b*date) and then multiplying the linear coefficient (b) by 111.19493 km/°latitude.

Table 11.4: Correlation coefficients between interannual variability in bloom initiation and physical timing metrics in the subpolar basin[a]

	NHF positive			MLD max			MLD shoaling			Mean winter MLD			Mean winter NHF			Fastest rise in PAR_{ML}			MLD<Zeu[b]			PAR_{ML} starts to increase		
CV value	0.30	0.35	0.40	0.30	0.35	0.40	0.30	0.35	0.40	0.30	0.35	0.40	0.30	0.35	0.40	0.30	0.35	0.40	0.30	0.35	0.40	0.30	0.35	0.40
North Atlantic	0.73*	0.73*	0.73*	0.38*	0.38*	0.38*	0.45*	0.45*	0.45*	0.19	0.19	0.19	-0.20	-0.20	-0.20	-0.12	-0.12	-0.12	0.36*	0.36*	0.36*	-0.01	-0.01	-0.01
North Pacific	0.32*	0.32*	0.32*	0.03	0.03	0.02	-0.11	-0.11	-0.10	-0.14	-0.14	-0.14	-0.03	-0.04	-0.04	0.06	0.06	0.06	-0.04	-0.04	-0.04	-0.07	-0.07	-0.06
Southern Ocean	0.01	0.02	0.02	-0.08	-0.11	-0.15*	-0.06	-0.08	-0.09	0.01	0.03	0.03	-0.04	-0.06	-0.08	0.09	0.09	0.09	-0.03	-0.03	-0.02	0.21*	0.23*	0.22*

[a] A * indicates correlation coefficients which are statistically significant at the 95% confidence interval.

[b] MLD<Zeu stands for the date the MLD becomes shallower than the euphotic depth.

Table 11.5: Correlation coefficients between interannual variability in bloom peak and physical timing metrics in the subpolar basin[a]

	NHF positive			MLD min			NHF max		
CV value	**0.30**	**0.35**	**0.40**	**0.30**	**0.35**	**0.40**	**0.30**	**0.35**	**0.40**
North Atlantic	0.46*	0.46*	0.46*	-0.21	-0.21	-0.21	-0.13	-0.13	-0.13
North Pacific	0.12*	0.12*	0.13*	0.28*	0.28*	0.29*	0.32*	0.32*	0.32*
Southern Ocean	-0.18*	-0.17*	-0.16*	0.09	0.08	0.08	-0.11	-0.10	-0.10

[a] A * indicates correlation coefficients which are statistically significant at the 95% confidence interval.

Table 11.6: Correlation coefficients between interannual variability in bloom termination and physical timing metrics in the subpolar basin[a]

	MLD min			NHF max			NHF negative			MLD deepening			MLD>Zeu[b]			Fastest fall in PAR		
CV value	**0.30**	**0.35**	**0.40**	**0.30**	**0.35**	**0.40**	**0.30**	**0.35**	**0.40**	**0.30**	**0.35**	**0.40**	**0.30**	**0.35**	**0.40**	**0.30**	**0.35**	**0.40**
North Atlantic	0.24	0.24	0.24	0.31*	0.31*	0.31*	-0.20	-0.20	-0.20	0.07	0.07	0.07	0.13	0.13	0.13	0.17	0.17	0.17
North Pacific	0.18	0.18	0.18	0.08	0.08	0.09	0.04	0.04	0.04	0.34*	0.34*	0.34*	-0.14	-0.14	-0.14	0.06	0.06	0.06
Southern Ocean	0.13*	0.14*	0.16*	0.00	-0.06	-0.04	0.02	-0.01	0.01	0.05	0.05	0.01	-0.22*	-0.25*	-0.22*	-0.02	-0.02	0.02

[a] A * indicates correlation coefficients which are statistically significant at the 95% confidence interval.

[b] MLD>Zeu stands for the date the MLD becomes deeper than the euphotic depth

Table 11.7: Correlations coefficients and latitudinal speeds for bloom initiation and associated physical timing metrics in the subtropical basins for both GlobColour and NOBM chlorophyll datasets

			Bloom Initiation			NHF negative			MLD min			MLD deepening			NHF max			MLD>Zeu[a]			Fastest fall in PAR_{ML}		
		CV value	**0.30**	**0.35**	**0.40**	**0.30**	**0.35**	**0.40**	**0.30**	**0.35**	**0.40**	**0.30**	**0.35**	**0.40**	**0.30**	**0.35**	**0.40**	**0.30**	**0.35**	**0.40**	**0.30**	**0.35**	**0.40**
North Atlantic	GlobColour	Corr. coef[b]				-0.13	-0.11	-0.11	-0.39*	-0.32	-0.30	0.00	0.01	0.03	-0.11	-0.07	-0.01	0.60*	0.54*	0.50*	-0.13	-0.12	-0.14
		Lat speed (km day^{-1})[c]	-0.08	-0.03	0.05	-5.07	-5.07	-4.93	-5.27	-5.88	-6.20	9.46	6.95	5.87	3.85	2.50	2.05	-9.25	-9.25	-9.14	-6.25	-5.83	-5.58
	NOBM	Corr. coef[b]				0.38*	0.40*	0.39*	-0.04	-0.01	0.00	-0.20	-0.18	-0.16	-0.21	-0.17	-0.15	0.69*	0.66*	0.60*	0.32	0.33*	0.28
		Lat speed (km day^{-1})[c]	-0.78	-0.76	-0.71	-5.31	-5.30	-5.18	-6.00	-6.53	-6.76	10.86	6.63	5.14	4.97	3.71	3.34	-8.69	-6.78	-6.27	-5.50	-5.29	-5.01
South Atlantic	GlobColour	Corr. coef[b]				-0.50*	-0.49*	-0.41*	-0.42*	-0.48*	-0.37*	0.13	0.20	0.17	-0.15	-0.09	-0.19	-0.87*	-0.81*	-0.71*	-0.09	-0.03	-0.01
		Lat speed (km day^{-1})[c]	-2.44	-2.44	-2.36	5.37	5.01	4.60	1.42	0.82	0.38	-0.22	-1.99	-1.09	-0.64	-0.70	-0.71	11.05	10.79	10.32	5.32	5.48	6.50
	NOBM	Corr. coef[b]				-0.27	-0.24	-0.21	-0.43*	-0.51*	-0.50*	0.22	0.22	0.20	-0.46*	-0.38*	-0.42*	-0.75*	-0.69*	-0.61*	-0.08	-0.05	0.01
		Lat speed (km day^{-1})[c]	-1.65	-1.47	-1.42	5.29	4.88	4.52	1.47	0.68	0.36	0.87	-1.87	-1.13	-0.20	-0.13	0.01	10.67	10.40	9.73	5.42	5.83	6.78
North Pacific	GlobColour	Corr. coef[b]				-0.37*	-0.37*	-0.34*	-0.70*	-0.72*	-0.58*	-0.14	-0.13	0.04*	-0.39*	-0.45*	0.11	0.54*	0.53*	0.43*	-0.41*	-0.36*	-0.11
		Lat speed (km day^{-1})[c]	-0.75	-0.88	-0.60	-5.27	-4.93	-4.36	-0.29	-0.86	-0.97	10.60	9.73	6.13	1.83	1.22	-0.22	-9.81	-9.24	-8.98	-7.70	-8.35	-8.99
	NOBM	Corr. coef[b]				0.03	0.02	-0.01	-0.63*	-0.61*	-0.53*	-0.55*	-0.54*	-0.46*	0.07	0.07	0.19	0.85*	0.82*	0.78*	-0.18	-0.07	0.02
		Lat speed (km day^{-1})[c]	-1.58	-1.48	-1.44	-5.12	-4.76	-4.25	0.06	-0.55	-0.69	16.08	12.84	6.99	-0.23	-0.21	-0.29	-10.00	-9.21	-9.05	-7.18	-7.78	-8.89

			Bloom Initiation			NHF negative			MLD min			MLD deepening			NHF max			MLD>Zeu[a]			Fastest fall in PAR_{ML}		
South Pacific	GlobColour	Corr. coef[b]				0.28	0.09	0.00	-0.31	-0.54*	-0.43*	-0.05	0.00	0.01	-0.20	-0.07	0.06	-0.76*	-0.75*	-0.68*	-0.02	-0.24	-0.40*
		Lat speed (km day^{-1})[c]	-0.82	-1.64	-2.11	6.72	5.56	5.05	0.40	0.43	0.37	12.61	5.03	8.66	-0.82	-0.92	-1.05	15.39	12.39	6.09	4.82	4.78	4.82
	NOBM	Corr. coef[b]				0.10	0.17	0.21	-0.29	-0.42*	-0.43*	-0.23	-0.20	0.03	0.05	0.08	0.05	-0.86*	-0.84*	-0.80*	-0.30	-0.40*	-0.26
		Lat speed (km day^{-1})[c]	-2.21	-1.85	-1.02	7.10	5.76	5.17	0.15	0.46	0.34	13.82	8.07	10.57	-0.81	-0.92	-0.98	13.63	10.69	4.58	5.43	5.67	5.43
North Indian	GlobColour	Corr. coef[b]				-0.68*	-0.69*	-0.69*	-0.59*	-0.62*	-0.63*	0.10	0.10	0.09	0.06	0.04	0.03	0.28	0.23	0.24	0.31	0.34	0.34
		Lat speed (km day^{-1})[c]	0.81	0.84	0.85	-4.01	-4.03	-4.05	-1.96	-1.97	-1.99	3.54	3.03	3.17	-2.51	-2.54	-2.70	-18.01	-2.30	-0.50	2.97	3.00	3.01
	NOBM	Corr. coef[b]				0.25	0.22	0.22	0.28	0.26	0.25	-0.06	-0.06	-0.07	-0.52	-0.52	-0.56*	-0.40	-0.40	-0.40	0.09	0.10	0.10
		Lat speed (km day^{-1})[c]	0.96	0.95	0.96	-4.18	-4.24	-4.27	-1.99	-2.00	-2.02	2.12	2.21	2.29	-2.19	-2.19	-2.36	-15.11	-14.05	-13.86	3.02	3.03	3.12
South Indian	GlobColour	Corr. coef[b]				-0.04	-0.02	-0.01	-0.55*	-0.43*	-0.19	0.14	0.21	0.16	0.04	0.04	0.12	-0.88*	-0.90*	-0.90*	-0.34	-0.28	-0.14
		Lat speed (km day^{-1})[c]	-1.82	-1.94	-1.97	8.15	7.60	7.26	-0.32	-0.54	-0.42	6.13	4.96	-0.30	2.52	2.39	10.88	10.21	10.10	10.05	5.38	5.90	5.85
	NOBM	Corr. coef[b]				-0.03	-0.01	0.06	-0.53*	-0.24	-0.33	0.11	0.00	-0.04	0.13	0.10	0.18	-0.90*	-0.89*	-0.84*	-0.46*	-0.27	-0.16
		Lat speed (km day^{-1})[c]	-1.58	-1.51	-1.25	8.62	7.99	7.69	-0.55	-0.57	-0.54	5.11	4.61	0.06	2.11	2.03	9.87	9.32	9.22	9.20	6.20	6.37	5.81

[a] MLD>Zeu stands for the date the MLD becomes deeper than the euphotic depth.

[b] A * indicates correlation coefficients which are statistically significant at the 95% confidence interval. Correlations were calculated between the bloom initiation latitudinal mean date and the physical metric latitudinal mean date. Mean dates were calculated over the years 2002-2009 for GlobColour data and 2002-2007 for NOBM data. Correlations were calculated separately for the North (11˚N to 45˚N) and South (45˚S to 11˚S) basins using data shown in Figure 5.22.

[c] Latitudinal speeds were calculated by regressing the metric dates on latitude (latitude = a+ b*date) and then multiplying the linear coefficient (b) by 111.19493 km/˚latitude. Speeds were calculated separately for the North (11˚N to 45˚N) and South (45˚S to 11˚S) basins using data shown in Figure 5.22.

Table 11.8: Correlation coefficients and latitudinal speeds for bloom peak and associated physical timing metrics in the subtropical basins for both GlobColour and NOBM chlorophyll datasets

			Bloom Peak			NHF positive			MLD max			MLD shoaling			Fastest rise in PAR_{ML}			PAR_{ML} starts to rise		
		CV value	**0.30**	**0.35**	**0.40**	**0.30**	**0.35**	**0.40**	**0.30**	**0.35**	**0.40**	**0.30**	**0.35**	**0.40**	**0.30**	**0.35**	**0.40**	**0.30**	**0.35**	**0.40**
North Atlantic	GlobColour	Corr. coef[a]				-0.74*	-0.64*	-0.62*	0.38*	0.35*	0.32*	0.62*	0.61*	0.62*	-0.04	0.14	0.16	0.32*	0.38*	0.36*
		Lat speed (km day^{-1})[b]	-4.08	-3.33	-3.18	6.79	6.48	6.32	-2.81	-2.31	-1.66	-5.46	-5.78	-5.53	6.42	6.46	6.22	1.51	1.19	0.87
	NOBM	Corr. coef[a]				-0.09	-0.07	-0.12	0.41*	0.36*	0.39*	0.46*	0.42*	0.45*	0.40*	0.46*	0.45*	0.58*	0.56*	0.53*
		Lat speed (km day^{-1})[b]	0.06	0.19	-0.29	7.23	6.97	6.76	-1.48	-0.29	0.91	-5.58	-5.84	-5.31	6.31	6.39	6.01	4.67	4.31	4.47
South Atlantic	GlobColour	Corr. coef[a]				0.35	0.32*	0.35*	-0.16	-0.28	-0.31*	-0.09	-0.23	-0.23	-0.05	-0.11	-0.15	-0.04	-0.14	-0.37*
		Lat speed (km day^{-1})[b]	-1.93	-2.32	-2.61	-6.65	-5.89	-5.33	-0.34	6.78	7.82	-1.85	6.92	6.80	-4.10	-2.26	-1.81	-0.86	0.14	1.69
	NOBM	Corr. coef[a]				0.50*	0.53*	0.57*	0.44	0.32	0.25	0.26	0.15	0.12	0.12	0.08	0.05	0.30	0.19	-0.10
		Lat speed (km day^{-1})[b]	-2.69	-2.89	-3.17	-6.63	-5.84	-5.48	-2.04	1.95	3.16	-1.78	0.36	7.15	-3.12	-3.17	-1.81	-4.29	-2.20	0.98
North Pacific	GlobColour	Corr. coef[a]				-0.76*	-0.77*	-0.78*	0.52*	0.54*	0.74*	0.51*	0.51*	0.79*	-0.34*	-0.38*	-0.32*	-0.06	-0.17	-0.43*
		Lat speed (km day^{-1})[b]	-2.12	-1.65	-1.26	4.00	3.90	4.44	-2.87	-2.99	-2.45	-1.68	-1.97	-1.96	4.65	4.77	4.85	7.45	7.58	7.68
	NOBM	Corr. coef[a]				-0.81*	-0.75*	-0.56*	0.71*	0.63*	0.33*	0.73*	0.65*	0.30	0.01	0.16	0.37*	0.33	0.34*	0.38*
		Lat speed (km day^{-1})[b]	-0.58	-0.32	0.08	4.24	4.02	4.28	-2.91	-2.88	-2.20	-1.89	-2.08	-1.83	4.68	4.64	4.65	7.63	7.98	7.90

			Bloom Peak			NHF positive			MLD max			MLD shoaling			Fastest rise in PAR_{ML}			PAR_{ML} starts to rise		
South Pacific	GlobColour	Corr. coef[a]				0.65*	0.57*	0.60*	0.48*	0.38*	0.06	0.26	0.10	0.06	0.82*	0.64*	0.66*	-0.47*	-0.60*	-0.64*
		Lat speed (km day^{-1})[b]	-5.04	-4.82	-4.29	-9.96	-7.20	-5.87	-17.31	-9.18	0.44	-6.94	-5.24	0.52	-5.62	-5.21	-4.63	14.51	10.40	5.11
	NOBM	Corr. coef[a]				0.45*	0.38*	0.41*	0.43*	0.18	-0.07	0.38*	0.32	0.21	0.80*	0.69*	0.71*	-0.38*	-0.44*	-0.48*
		Lat speed (km day^{-1})[b]	-5.04	-4.85	-4.72	-10.11	-7.71	-6.31	-8.52	-0.24	8.38	-7.27	-5.25	-0.30	-5.46	-4.92	-4.21	17.85	13.77	6.11
North Indian	GlobColour	Corr. coef[a]				-0.63*	-0.63*	-0.64*	0.77*	0.78*	0.77*	0.76*	0.76*	0.76*	-0.81*	-0.81*	-0.81*	0.11	0.12	0.13
		Lat speed (km day^{-1})[b]	-1.14	-1.14	-1.14	4.35	4.30	4.30	-1.44	-1.37	-1.41	-1.23	-1.35	-1.36	5.52	5.67	5.71	10.48	10.28	10.49
	NOBM	Corr. coef[a]				-0.69*	-0.68*	-0.68*	0.86*	0.86*	0.86*	0.88*	0.87*	0.87*	-0.85*	-0.82*	-0.81*	-0.82*	-0.79*	-0.79*
		Lat speed (km day^{-1})[b]	-0.77	-0.75	-0.74	4.39	4.32	4.33	-1.37	-1.40	-1.39	-1.24	-1.33	-1.33	5.61	5.64	5.68	9.94	9.69	9.72
South Indian	GlobColour	Corr. coef[a]				-0.02	-0.06	-0.10	0.76*	0.77*	0.69*	0.64*	0.54*	0.56*	0.36*	0.33*	0.45*	0.37*	0.44*	0.45*
		Lat speed (km day^{-1})[b]	-2.02	-1.73	-1.67	-3.37	-3.76	-3.53	1.16	0.86	-0.64	5.93	7.18	6.24	-5.15	-4.96	-4.94	7.05	6.02	5.58
	NOBM	Corr. coef[a]				-0.69*	-0.68*	-0.68*	0.86*	0.86*	0.86*	0.88*	0.87*	0.87*	-0.85*	-0.82*	-0.81*	-0.82*	-0.79*	-0.79*
		Lat speed (km day^{-1})[b]	-2.27	-2.11	-1.98	-3.07	-3.25	-3.24	0.59	0.59	-0.78	5.57	7.18	5.02	-5.20	-4.91	-4.64	8.77	6.89	6.02

[a] A * indicates correlation coefficients which are statistically significant at the 95% confidence interval. Correlations were calculated between the bloom peak latitudinal mean date and the physical metric latitudinal mean date. Mean dates were calculated over the years 2002-2009 for GlobColour data and 2002-2007 for NOBM data. Correlations were calculated separately for the North (11˚N to 45˚N) and South (45˚S to 11˚S) basins using data shown in Figure 5.23.

[b] Latitudinal speeds were calculated by regressing the metric dates on latitude (latitude = a+ b*date) and then multiplying the linear coefficient (b) by 111.19493 km/˚latitude. Speeds were calculated separately for the North (11˚N to 45˚N) and South (45˚S to 11˚S) basins using data shown in Figure 5.23.

Table 11.9: Correlation coefficients and latitudinal speeds for bloom termination and associated physical timing metrics in the subtropical basins for both GlobColour and NOBM chlorophyll datasets

			Bloom termination			NHF positive			MLD max			MLD shoaling			Fastest rise in PAR_{ML}			MLD<Zeu[a]			PAR_{ML} starts to increase		
		CV value	**0.30**	**0.35**	**0.40**	**0.30**	**0.35**	**0.40**	**0.30**	**0.35**	**0.40**	**0.30**	**0.35**	**0.40**	**0.30**	**0.35**	**0.40**	**0.30**	**0.35**	**0.40**	**0.30**	**0.35**	**0.40**
North Atlantic	GlobColour	Corr. coef[b]				0.12	0.14	0.13	0.36*	0.27	0.29	0.35*	0.28	0.30	0.64*	0.62*	0.56*	0.37*	0.22	0.05	0.71*	0.58*	0.48*
		Lat speed (km day^{-1})[c]	1.78	2.13	1.83	6.79	6.48	6.32	-2.81	-2.31	-1.66	-5.46	-5.78	-5.53	6.42	6.46	6.22	6.63	6.16	5.91	1.51	1.19	0.87
	NOBM	Corr. coef[b]				0.23	0.16	0.13	0.49*	0.44*	0.42*	0.40*	0.40*	0.36*	0.69*	0.65*	0.60*	0.40*	0.30*	0.20*	0.58*	0.64*	0.59*
		Lat speed (km day^{-1})[c]	3.00	2.72	2.55	7.23	6.97	6.76	-1.48	-0.29	0.91	-5.58	-5.84	-5.31	6.31	6.39	6.01	6.21	5.73	5.37	4.67	4.31	4.47
South Atlantic	GlobColour	Corr. coef[b]				-0.20	-0.17	-0.06	-0.61*	-0.53*	-0.44*	-0.62*	-0.61*	-0.61*	-0.36*	-0.18	-0.05	-0.30	-0.19	-0.17	-0.57*	-0.44*	-0.18
		Lat speed (km day^{-1})[c]	1.07	0.88	0.57	-6.65	-5.89	-5.33	-0.34	6.78	7.82	-1.85	6.92	6.80	-4.10	-2.26	-1.81	-6.13	-2.51	0.71	-0.86	0.14	1.69
	NOBM	Corr. coef[b]				-0.34*	-0.37*	-0.24	-0.64*	-0.54*	-0.37*	-0.63*	-0.56*	-0.52*	-0.38*	-0.25	-0.07	-0.04	0.16	0.16	-0.67*	-0.51*	-0.06
		Lat speed (km day^{-1})[c]	0.86	0.85	0.69	-6.63	-5.84	-5.48	-2.04	1.95	3.16	-1.78	0.36	7.15	-3.12	-3.17	-1.81	-2.79	1.95	3.04	-4.29	-2.20	0.98
North Pacific	GlobColour	Corr. coef[b]				-0.42*	-0.32*	-0.15	0.35*	0.21	-0.09	0.49*	0.36*	-0.03	0.70*	0.72*	0.57*	0.73*	0.73*	0.62*	0.73*	0.69*	0.58*
		Lat speed (km day^{-1})[c]	4.79	4.71	4.39	4.00	3.90	4.44	-2.87	-2.99	-2.45	-1.68	-1.97	-1.96	4.65	4.77	4.85	3.04	3.05	3.01	7.45	7.58	7.68

			Bloom termination			NHF positive			MLD max			MLD shoaling			Fastest rise in PAR_{ML}			MLD<Zeu[a]			PAR_{ML} starts to increase		
South Pacific	NOBM	Corr. coef[b]				-0.10	-0.04	0.07	0.13	0.03	-0.22	0.25	0.15	-0.21	0.77*	0.76*	0.66*	0.81*	0.81*	0.70*	0.81*	0.81*	0.69*
		Lat speed (km day^{-1})[c]	5.51	5.45	5.31	4.24	4.02	4.28	-2.91	-2.88	-2.20	-1.89	-2.08	-1.83	4.68	4.64	4.65	3.10	3.09	3.08	7.63	7.98	7.90
	GlobColour	Corr. coef[b]				0.85*	0.73*	0.74*	0.16	0.09	-0.21	0.11	-0.15	0.12	0.74*	0.39*	0.36*	0.41*	0.08	-0.21	-0.74*	-0.77*	-0.75*
		Lat speed (km day^{-1})[c]	-3.10	-3.41	-2.64	-9.96	-7.20	-5.87	-17.31	-9.18	0.44	-6.94	-5.24	0.52	-5.62	-5.21	-4.63	-4.21	-3.72	-2.62	14.51	10.40	5.11
	NOBM	Corr. coef[b]				0.83*	0.64*	0.68*	0.00	0.06	-0.26	0.10	-0.12	0.30*	0.64*	0.16	0.20	0.23	-0.10	-0.31	-0.56*	-0.46*	-0.49*
		Lat speed (km day^{-1})[c]	-3.29	-2.89	-2.18	-10.11	-7.71	-6.31	-8.52	-0.24	8.38	-7.27	-5.25	-0.30	-5.46	-4.92	-4.21	-4.34	-3.63	-2.36	17.85	13.77	6.11
North Indian	GlobColour	Corr. coef[b]				-0.53*	-0.53*	-0.52*	0.77*	0.77*	0.75*	0.74*	0.75*	0.74*	-0.75*	-0.75*	-0.75*	-0.25	-0.21	-0.17	0.08	0.09	0.11
		Lat speed (km day^{-1})[c]	-2.40	-2.20	-2.16	4.35	4.30	4.30	-1.44	-1.37	-1.41	-1.23	-1.35	-1.36	5.52	5.67	5.71	7.57	7.64	7.93	10.48	10.28	10.49
	NOBM	Corr. coef[b]				-0.48*	-0.48*	-0.48*	0.70*	0.70*	0.70*	0.72*	0.70*	0.70*	-0.63*	-0.62*	-0.61*	-0.43	-0.39	-0.38	-0.72*	-0.70*	-0.70*
		Lat speed (km day^{-1})[c]	-0.73	-0.72	-0.71	4.39	4.32	4.33	-1.37	-1.40	-1.39	-1.24	-1.33	-1.33	5.61	5.64	5.68	7.39	7.46	1.24	9.94	9.69	9.72
South Indian	GlobColour	Corr. coef[b]				0.12	0.10	0.09	0.52*	0.52*	0.32*	0.53*	0.46*	0.40*	0.01	0.03	0.18	0.30	0.30	0.29	0.42*	0.46*	0.35*
		Lat speed (km day^{-1})[c]	1.02	0.93	0.77	-3.37	-3.76	-3.53	1.16	0.86	-0.64	5.93	7.18	6.24	-5.15	-4.96	-4.94	-4.40	-4.27	-4.30	7.05	6.02	5.58
	NOBM	Corr. coef[b]				0.12	0.09	-0.01	0.49*	0.56*	0.50*	0.43*	0.30	0.41*	-0.21	-0.18	0.07	0.04	0.09	0.16	0.49*	0.56*	0.45*
		Lat speed (km day^{-1})[c]	0.91	0.82	0.77	-3.07	-3.25	-3.53	0.59	0.59	-0.64	5.57	7.18	6.24	-5.20	-4.91	-4.94	-4.30	-4.13	-4.30	8.77	6.89	5.58

[a] MLD<Zeu stands for the date the MLD becomes shallower than the euphotic depth.

[b] A * indicates correlation coefficients which are statistically significant at the 95% confidence interval. Correlations were calculated between the bloom termination latitudinal mean date and the physical metric latitudinal mean date. Mean dates were calculated over the years 2002-2009 for GlobColour data and 2002-2007 for NOBM data. Correlations were calculated separately for the North (11˚N to 45˚N) and South (45˚S to 11˚S) basins using data shown in Figure 5.24.

[c] Latitudinal speeds were calculated by regressing the metric dates on latitude (latitude = a+ b*date) and then multiplying the linear coefficient (b) by 111.19493 km/˚latitude. Speeds were calculated separately for the North (11˚N to 45˚N) and South (45˚S to 11˚S) basins using data shown in Figure 5.24.

Table 11.10: Correlation coefficients between interannual variability in bloom initiation and physical timing metrics in the subtropical basin[a]

	NHF negative			MLD min			MLD deepening			NHF max			MLD>Zeu[b]			Fastest fall in PAR_{ML}		
CV value	**0.30**	**0.35**	**0.40**	**0.30**	**0.35**	**0.40**	**0.30**	**0.35**	**0.40**	**0.30**	**0.35**	**0.40**	**0.30**	**0.35**	**0.40**	**0.30**	**0.35**	**0.40**
North Atlantic	0.44*	0.30	0.27	-0.09	0.23	0.06	0.26	0.26	0.25	0.06	0.35	0.37	-0.14	-0.10	-0.12	-0.04	-0.10	0.01
South Atlantic	0.02	0.12	-0.07	-0.39	-0.36	-0.22	0.07	-0.19	-0.51	-0.15	-0.01	0.00	0.29	0.40	0.18	0.18	0.05	0.60*
North Pacific	0.03	-0.07	0.14	0.05	0.14	-0.02	0.14	-0.40*	-0.48*	-0.07	0.08	-0.15	0.05	0.02	-0.02	0.13	-0.07	-0.47*
South Pacific	-0.25	-0.27	-0.24	-0.29	-0.30	-0.10	-0.37*	-0.43*	-0.47*	-0.24	-0.16	-0.15	0.18	0.28*	0.26*	-0.31*	-0.20	-0.03
Indian	0.07	0.12	0.15	-0.10	-0.06	-0.07	-0.15	0.00	-0.13	-0.20	-0.27	-0.26*	0.10	0.12	0.07	-0.24	-0.28*	-0.22

[a] A* indicates correlation coefficients which are statistically significant at the 95% confidence interval.

[b] MLD>Zeu stands for the date the MLD becomes deeper than the euphotic depth.

Table 11.11: Correlation coefficients between interannual variability in bloom peak and physical timing metrics in the subtropical basin[a]

	NHF positive			MLD max			MLD shoaling			Fastest rise in PAR_{ML}			PAR_{ML} starts to rise		
CV value	**0.30**	**0.35**	**0.40**	**0.30**	**0.35**	**0.40**	**0.30**	**0.35**	**0.40**	**0.30**	**0.35**	**0.40**	**0.30**	**0.35**	**0.40**
North Atlantic	0.52*	0.44*	0.35	0.76*	0.56*	0.52*	0.59*	0.35*	0.55*	0.50*	-0.05	0.38	0.01	0.21	-0.04
South Atlantic	-0.09	-0.12	0.03	0.07	0.35	0.01	0.05	-0.02	-0.34	0.08	-0.19	0.08	-0.71*	-0.64*	-0.31
North Pacific	-0.22*	-0.40*	-0.40*	-0.23	0.35	0.19	-0.59*	-0.16	-0.22	-0.32	-0.02	-0.01	0.09	0.03	-0.11
South Pacific	0.48*	0.45*	0.43*	0.23	0.24	0.24	0.08	0.00	-0.03	0.14	0.22	0.07	-0.41	-0.35	-0.04
Indian	0.37*	0.33*	0.29*	0.08	0.08	-0.03	-0.06	-0.07	-0.21	-0.20	-0.15	0.05	-0.02	0.03	0.13

[a] A * indicates correlation coefficients which are statistically significant at the 95% confidence interval.

Table 11.12: Correlation coefficients between interannual variability in bloom termination and physical timing metrics in the subtropical basin[a]

	NHF positive			MLD max			MLD shoaling			MLD winter mean			NHF winter mean			Fastest rise in PAR_{ML}			MLD<Zeu[b]			PAR_{ML} starts to increase		
CV value	**0.30**	**0.35**	**0.40**	**0.30**	**0.35**	**0.40**	**0.30**	**0.35**	**0.40**	**0.30**	**0.35**	**0.40**	**0.30**	**0.35**	**0.40**	**0.30**	**0.35**	**0.40**	**0.30**	**0.35**	**0.40**	**0.30**	**0.35**	**0.40**
North Atlantic	0.45*	0.25	0.25	0.44*	0.32	0.27	0.35	0.04	0.05	0.29	0.24	0.18	-0.52*	-0.44*	-0.37	0.01	-0.10	0.22	-0.17	-0.24	-0.26	0.43	0.37	0.19
South Atlantic	-0.53*	-0.59*	-0.63*	-0.28	-0.25	0.00	-0.36	-0.22	-0.05	-0.25	-0.32	-0.25	0.40*	0.36	0.29	-0.07	-0.12	-0.14	-0.41	-0.44	-0.39	0.31	0.34	0.13
North Pacific	0.08	-0.25	-0.35*	0.05	-0.02	0.34*	0.35*	0.09	0.18	0.01	-0.08	-0.11	-0.26	-0.04	-0.01	0.44*	0.43*	0.27*	0.08	-0.25	-0.47*	-0.19	-0.30	-0.16
South Pacific	0.12	0.09	0.28*	0.08	0.04	0.02	0.03	-0.05	-0.11	0.25	0.14	0.25	-0.30*	-0.29*	-0.34*	0.07	0.06	0.12	0.17	0.06	0.20	-0.40*	-0.25	-0.06
Indian	0.04	0.00	-0.02	-0.11	-0.08	-0.05	0.05	0.09	0.00	-0.07	-0.09	-0.06	-0.17	-0.13	-0.02	0.11	0.02	-0.01	0.03	-0.01	0.00	0.21	0.12	-0.09

[a] A * indicates correlation coefficients which are statistically significant at the 95% confidence interval.

[b] MLD<Zeu stands for the date the MLD becomes shallower than the euphotic depth.

12 Appendix E

Coefficient of Variation and Trends in Bloom Timing

In Chapter 6 results are calculated from model-derived bloom timing model output that have had regions which do not display a strong seasonal cycle removed. The criterion for a strong seasonal cycle is for the chlorophyll time series to have a coefficient of variation above 0.23 in MEDUSA, 0.25 in TOPAZ, 0.20 in CCSM3 and 0.47 in PlankTOM5. These values are chosen to cover the same spatial areas as the observations. Results should not be dependent on this choice of value. To investigate the impact of the coefficient of variation value on the results obtained in this thesis, the results are repeated using a coefficient of variation value subtracting and adding 0.1 to identify regions with a weak seasonal cycle. The results from using these other values are reported here alongside the original coefficient of variation value results. Overall, the differences were small though larger changes were seen when a particular biome-metric combination did not include many pixels, such as the permanently stratified and seasonally mixed biomes in the Southern Ocean and subpolar biome in the Indian Ocean.

Table 12.1: Correlation coefficients, root mean square difference (RMSD) and normalised standard deviations for the comparison of mean metric dates from GlobColour to the dates from 4 biogeochemical models[a]

		MEDUSA			TOPAZ			CCSM3			PlankTOM5		
		CV-0.1	CV	CV+0.1	CV-0.1	CV	CV+0.1	CV-0.1	CV	CV+0.1	CV-0.1	CV	CV+0.1
Initiation mean date	Standard deviation	1.36	1.37	1.38	1.36	1.36	1.37	1.35	1.31	1.29	1.30	1.29	1.29
	RMSD	0.95	0.96	0.95	0.88	0.82	0.75	0.90	0.76	0.69	1.09	1.05	1.02
	Correlation	0.71	0.72	0.73	0.77	0.80	0.84	0.74	0.82	0.85	0.58	0.61	0.63
Peak mean date	Standard deviation	1.38	1.37	1.34	1.27	1.28	1.30	1.37	1.33	1.33	1.34	1.35	1.38
	RMSD	0.97	0.92	0.85	0.93	0.88	0.84	1.01	0.91	0.90	0.99	0.99	1.00
	Correlation	0.71	0.74	0.78	0.69	0.73	0.76	0.68	0.73	0.74	0.68	0.68	0.70
Termination mean date	Standard deviation	1.15	1.15	1.15	1.22	1.21	1.20	0.89	0.84	1.33	1.05	1.04	0.99
	RMSD	0.99	0.98	0.94	1.01	0.99	0.98	0.86	0.75	0.75	0.89	0.87	0.83
	Correlation	0.58	0.60	0.63	0.60	0.61	0.62	0.59	0.68	0.69	0.62	0.63	0.65

[a] The bloom metric dates calculated from GlobColour (GC) were compared to the dates from MEDUSA, TOPAZ, CCSM3 and PlankTOM5. The comparisons are summarised by correlation coefficients, root mean square difference (RMSD) and normalised standard deviations. Each model has a corresponding coefficient of variation value which is used to remove regions without a strong seasonal cycle before the comparison is made. The values reported here are for three cases: when the original coefficient of variation (CV) value is used (MEDUSA – 0.23, TOPAZ = 0.25, CCSM3 = 0.2 and PlankTOM5 = 0.47), the CV-0.1 values and CV+0.1 values were used to remove regions without a strong seasonal cycle.

Table 12.2: Correlation coefficients, root mean square difference (RMSD) and normalised standard deviations for the comparison of interannual variation in metric dates from GlobColour to the interannual variability from 4 biogeochemical models[a]

		MEDUSA			TOPAZ			CCSM3			PlankTOM5		
		CV-0.1	CV	CV+0.1	CV-0.1	CV	CV+0.1	CV-0.1	CV	CV+0.1	CV-0.1	CV	CV+0.1
Initiation interannual variability	Standard deviation	0.95	0.93	0.83	1.12	1.06	0.96	0.90	0.79	0.73	1.26	1.28	1.24
	RMSD	1.08	1.04	1.03	1.35	1.30	1.21	1.05	1.02	1.03	1.20	1.28	1.26
	Correlation	0.39	0.42	0.38	0.19	0.21	0.24	0.39	0.37	0.33	0.45	0.39	0.36
Peak interannual variability	Standard deviation	0.86	0.80	0.70	1.13	1.07	0.95	0.66	0.54	0.48	1.05	1.00	0.91
	RMSD	1.07	1.01	0.99	1.35	1.28	1.18	0.93	0.92	0.93	1.11	1.14	1.09
	Correlation	0.35	0.39	0.37	0.20	0.24	0.27	0.43	0.42	0.38	0.41	0.35	0.36
Termination interannual variability	Standard deviation	1.08	1.04	1.02	1.19	1.16	1.10	1.06	1.10	1.21	1.25	1.25	1.23
	RMSD	1.37	1.39	1.42	1.42	1.39	1.33	1.20	1.21	1.28	1.28	1.32	1.29
	Correlation	0.13	0.08	0.01	0.16	0.18	0.19	0.33	0.33	0.35	0.37	0.33	0.34

[a] The interannual variability (standard deviation) bloom metric dates calculated from GlobColour (GC) were compared to the dates from MEDUSA, TOPAZ, CCSM3 and PlankTOM5. The comparisons are summarised by correlation coefficients, root mean square difference (RMSD) and normalised standard deviations. Each model has a corresponding coefficient of variation value which is used to remove regions without a strong seasonal cycle before the comparison is made. The values reported here are for three cases: when the original coefficient of variation (CV) value is used (MEDUSA – 0.23, TOPAZ = 0.25, CCSM3 = 0.2 and PlankTOM5 = 0.47), the CV-0.1 values and CV+0.1 values were used to remove regions without a strong seasonal cycle.

Table 12.3: Median difference (in days) in bloom initiation date between 2007-2026 and 2079-2098 per basin and biome using different coefficient of variation values[a]

	Permanently stratified			Seasonally mixed			LLU			Subpolar			MIZ		
	CV-0.1	CV	CV+0.1	CV-0.1	CV	CV+0.1	CV-0.1	CV	CV+0.1	CV-0.1	CV	CV+0.1	CV-0.1	CV	CV+0.1
Southern Ocean[b]	-16.03	-19.00	64.50	-16.99	-18.57	-24.00	-	-	-	-56.75	-33.96	-1.50	-39.33	-39.30	22.02
South Pacific	-24.26	-24.76	-24.91	-23.68	-27.63	-33.56	17.80	11.63	9.56	-51.28	-51.29	-51.87	-	-	-
South Atlantic	-35.72	-32.87	-29.38	-55.38	-58.86	-56.34	-25.94	-26.52	-23.33	-63.23	-77.58	-67.86	-	-	-
Indian	-26.49	-27.42	-26.97	-79.42	-80.94	-75.82	-26.52	-36.85	-15.23	-81.65	-73.20	-66.43	-	-	-
North Pacific	20.29	20.54	18.91	-11.09	-14.75	-5.88	18.40	18.12	21.13	-19.46	-5.69	-28.79	-76.50	-67.83	-73.50
North Atlantic	33.89	33.70	35.53	-8.15	-9.00	-9.26	-15.11	-15.65	5.86	-31.53	-31.32	-27.83	-26.66	-26.10	-33.98
Arctic	-	-	-	-	-	-	-	-	-	-30.45	-30.10	-28.67	-29.25	-31.58	-24.07

[a] Median differences were calculated using the models MEDUSA, TOPAZ and CCSM4/CESM1. The coefficient of variation (CV) values used for MEDUSA was 0.23, for TOPAZ 0.25 and 0.20 for CCSM4/CESM1. The median differences reported were calculated by first removing grid cells with a CV value less than those stated. To test sensitivity to the choice of CV value the median differences calculated using CV-0.1 values and CV+0.1 values are reported for comparison. A dash means that no pixels were present for that biome and basin combination.

[b] Total number of grid cells in some biome/basin combinations were small (Southern Ocean and permanently stratified, Southern Ocean seasonally mixed).

Table 12.4: Median difference (in days) in bloom peak date between 2007-2026 and 2079-2098 per basin and biome using different coefficient of variation values[a]

	Permanently stratified			Seasonally mixed			LLU			Subpolar			MIZ		
	CV-0.1	CV	CV+0.1	CV-0.1	CV	CV+0.1	CV-0.1	CV	CV+0.1	CV-0.1	CV	CV+0.1	CV-0.1	CV	CV+0.1
Southern Ocean[b]	15.87	21.50	-22.39	-7.65	-8.78	-10.77	-	-	-	-15.00	-17.98	73.35	-12.50	-12.22	-13.50
South Pacific	-3.68	-4.61	-2.50	5.93	1.94	-6.77	-0.65	-0.97	-2.89	-3.00	-3.41	-3.33	-	-	-
South Atlantic	10.50	10.98	12.37	-11.50	-16.71	-15.50	-5.00	-3.63	-4.00	-20.00	-11.83	-16.00	-	-	-
Indian	7.72	6.86	1.36	-2.51	-0.17	3.33	11.50	15.00	18.12	-3.50	6.05	-19.00	-	-	-
North Pacific	-14.58	-9.58	-15.50	16.50	14.63	16.75	-12.00	-13.46	-16.76	-47.17	-16.72	-14.18	-29.67	-27.83	-29.00
North Atlantic	-4.50	-4.53	-3.35	-20.16	-20.13	-22.50	-29.94	-31.07	-31.50	-37.63	-37.06	-37.00	-16.00	-16.50	-22.83
Arctic	-	-	-	-	-	-	-	-	-	-22.00	-21.83	-20.66	-18.85	-17.37	-16.18

[a] Median differences were calculated using the models MEDUSA, TOPAZ and CCSM4/CESM1. The coefficient of variation (CV) values used for MEDUSA was 0.23, for TOPAZ 0.25 and 0.20 for CCSM4/CESM1. The median differences reported were calculated by first removing grid cells with a CV value less than those stated. To test sensitivity to the choice of CV value the median differences calculated using CV-0.1 values and CV+0.1 values are reported for comparison. A dash means that no pixels were present for that biome and basin combination.

[b] Total number of grid cells in some biome/basin combinations were small (Southern Ocean and permanently stratified, Southern Ocean seasonally mixed).

Table 12.5: Median difference (in days) in bloom termination date between 2007-2026 and 2079-2098 per basin and biome using different coefficient of variation values[a]

	Permanently stratified			Seasonally mixed			LLU			Subpolar			MIZ		
	CV-0.1	CV	CV+0.1	CV-0.1	CV	CV+0.1	CV-0.1	CV	CV+0.1	CV-0.1	CV	CV+0.1	CV-0.1	CV	CV+0.1
Southern Ocean[b]	-90.75	-86.08	-67.25	10.83	14.08	0.14	-	-	-	-24.56	-26.44	-23.86	-20.97	-19.50	-21.54
South Pacific	-8.23	-72.19	-23.14	16.61	19.52	-5.00	-7.62	-8.87	-7.89	-1.85	-9.81	-56.54	-	-	-
South Atlantic	4.36	6.34	7.45	10.17	9.16	16.38	-8.61	-6.81	-4.71	-49.01	-40.40	-106.85	-	-	-
Indian	14.78	15.44	8.50	-25.97	-30.13	-110.57	-7.58	-10.00	-10.28	-1.47	84.52	138.86	-	-	-
North Pacific	-15.10	-15.24	-10.15	9.12	9.20	9.88	4.53	3.41	-1.17	-41.54	-14.50	-13.55	-31.50	-25.57	-31.33
North Atlantic	6.63	6.33	6.71	-14.68	-14.58	-14.44	-11.24	-9.17	-10.57	-53.36	-53.07	-45.85	-45.43	-47.90	-46.27
Arctic	-	-	-	-	-	-	-	-	-	-43.18	-43.18	-41.80	-41.63	-41.33	-42.04

[a] Median differences were calculated using the models MEDUSA, TOPAZ and CCSM4/CESM1. The coefficient of variation (CV) values used for MEDUSA was 0.23, for TOPAZ 0.25 and 0.20 for CCSM4/CESM1. The median differences reported were calculated by first removing grid cells with a CV value less than those stated. To test sensitivity to the choice of CV value the median differences calculated using CV-0.1 values and CV+0.1 values are reported for comparison. A dash means that no pixels were present for that biome and basin combination.

[b]Total number of grid cells in some biome/basin combinations were small (Southern Ocean and permanently stratified, Southern Ocean seasonally mixed).

Table 12.6: Median difference (in days) in bloom duration between 2007-2026 and 2079-2098 per basin and biome using different coefficient of variation values[a]

	Permanently stratified			Seasonally mixed			LLU			Subpolar			MIZ		
	CV-0.1	CV	CV+0.1	CV-0.1	CV	CV+0.1	CV-0.1	CV	CV+0.1	CV-0.1	CV	CV+0.1	CV-0.1	CV	CV+0.1
Southern Ocean[b]	-14.94	-23.76	-21.80	-1.07	-5.70	-7.34	-	-	-	0.34	0.77	-1.64	-19.74	-18.58	-28.44
South Pacific	9.76	9.07	7.12	-6.04	-10.80	-8.68	0.61	1.30	-4.19	16.21	18.62	19.25	-	-	-
South Atlantic	15.05	13.53	17.67	0.94	1.03	-1.33	-8.13	-7.21	-4.27	19.06	19.35	16.73	-	-	-
Indian	12.90	10.63	12.57	12.40	14.69	16.83	4.58	7.03	6.02	19.08	14.28	-1.05	-	-	-
North Pacific	-5.20	-5.25	-5.27	35.66	38.15	36.82	-2.75	-4.18	-5.34	14.99	19.10	22.91	15.88	16.82	16.14
North Atlantic	1.26	1.44	1.18	22.42	22.12	21.05	5.11	6.15	2.28	-12.04	-13.59	-12.60	-6.49	-9.09	-1.80
Arctic	-	-	-	-	-	-	-	-	-	-27.52	-28.23	-27.13	-40.10	-40.19	-38.82

[a] Median differences were calculated using the models MEDUSA, TOPAZ and CCSM4/CESM1. The coefficient of variation (CV) values used for MEDUSA was 0.23, for TOPAZ 0.25 and 0.20 for CCSM4/CESM1. The median differences reported were calculated by first removing grid cells with a CV value less than those stated. To test sensitivity to the choice of CV value the median differences calculated using CV-0.1 values and CV+0.1 values are reported for comparison. A dash means that no pixels were present for that biome and basin combination.

[b] Total number of grid cells in some biome/basin combinations were small (Southern Ocean and permanently stratified, Southern Ocean seasonally mixed).

Table 12.7: Median difference (in days) in initiation-peak interval between 2007-2026 and 2079-2098 per basin and biome using different coefficient of variation values[a]

	Permanently stratified			Seasonally mixed			LLU			Subpolar			MIZ		
	CV-0.1	CV	CV+0.1	CV-0.1	CV	CV+0.1	CV-0.1	CV	CV+0.1	CV-0.1	CV	CV+0.1	CV-0.1	CV	CV+0.1
Southern Ocean[b]	7.16	10.40	15.22	-11.15	-5.38	-5.25	-	-	-	-9.77	-9.33	-9.18	-8.02	-7.95	-8.47
South Pacific	7.14	5.82	5.19	6.46	4.28	6.27	1.12	0.50	-3.75	11.42	11.02	11.18	-	-	-
South Atlantic	12.61	9.65	10.09	24.59	24.23	22.53	1.98	1.67	-1.30	29.96	23.63	7.85	-	-	-
Indian	8.97	9.30	11.07	15.52	17.72	14.56	7.96	7.18	6.62	22.27	4.72	1.08	-	-	-
North Pacific	-2.03	-2.00	-3.40	25.65	24.01	25.62	-2.83	-3.51	-8.08	15.13	22.85	26.03	19.31	20.50	24.42
North Atlantic	-1.46	-1.75	-1.15	14.19	14.34	17.47	-1.48	-1.28	-2.42	7.82	7.22	3.78	20.75	20.24	22.50
Arctic	-	-	-	-	-	-	-	-	-	-0.55	-0.03	4.37	-13.70	-13.55	-12.72

[a] Median differences were calculated using the models MEDUSA, TOPAZ and CCSM4/CESM1. The coefficient of variation (CV) values used for MEDUSA was 0.23, for TOPAZ 0.25 and 0.20 for CCSM4/CESM1. The median differences reported were calculated by first removing grid cells with a CV value less than those stated. To test sensitivity to the choice of CV value the median differences calculated using CV-0.1 values and CV+0.1 values are reported for comparison. A dash means that no pixels were present for that biome and basin combination.

[b] Total number of grid cells in some biome/basin combinations were small (Southern Ocean and permanently stratified, Southern Ocean seasonally mixed).

Table 12.8: Median difference (in days) in peak-termination interval between 2007-2026 and 2079-2098 per basin and biome using different coefficient of variation values[a]

	Permanently stratified			Seasonally mixed			LLU			Subpolar			MIZ		
	CV-0.1	CV	CV+0.1	CV-0.1	CV	CV+0.1	CV-0.1	CV	CV+0.1	CV-0.1	CV	CV+0.1	CV-0.1	CV	CV+0.1
Southern Ocean[b]	-19.00	-10.96	-19.02	13.43	10.08	-9.75	-	-	-	13.55	11.38	3.08	-4.75	-4.46	-9.13
South Pacific	-3.45	-3.08	-4.41	-3.27	-4.05	-3.49	4.49	1.79	-0.58	-2.28	-5.18	-13.05	-	-	-
South Atlantic	-5.26	-5.37	-5.29	-6.14	-5.56	-6.10	-6.26	-6.72	-4.25	1.43	-1.72	5.57	-	-	-
Indian	3.30	2.18	4.41	-6.60	-7.26	-7.49	-0.21	-0.29	-5.10	4.58	8.06	-18.39	-	-	-
North Pacific	-5.11	-3.89	-2.84	-7.00	-7.18	-9.04	3.31	2.61	2.78	4.68	-2.97	0.82	4.34	3.84	2.65
North Atlantic	4.83	5.36	4.10	5.99	5.90	2.50	2.54	3.36	3.90	-14.57	-14.34	-10.41	-33.43	-36.47	-30.68
Arctic	-	-	-	-	-	-	-	-	-	-26.77	-27.22	-30.03	-13.42	-14.32	-17.99

[a] Median differences were calculated using the models MEDUSA, TOPAZ and CCSM4/CESM1. The coefficient of variation (CV) values used for MEDUSA was 0.23, for TOPAZ 0.25 and 0.20 for CCSM4/CESM1. The median differences reported were calculated by first removing grid cells with a CV value less than those stated. To test sensitivity to the choice of CV value the median differences calculated using CV-0.1 values and CV+0.1 values are reported for comparison. A dash means that no pixels were present for that biome and basin combination.

[b] Total number of grid cells in some biome/basin combinations were small (Southern Ocean and permanently stratified, Southern Ocean seasonally mixed).

Table 12.9: Median difference (in metres) in annual mean MLD between 2007-2026 and 2079-2098 per basin and biome using different coefficient of variation values[a]

	Permanently stratified			Seasonally mixed			LLU			Subpolar			MIZ		
	CV-0.1	CV	CV+0.1	CV-0.1	CV	CV+0.1	CV-0.1	CV	CV+0.1	CV-0.1	CV	CV+0.1	CV-0.1	CV	CV+0.1
Southern Ocean[b]	-2.18	-7.90	-26.18	-8.78	-11.28	-13.55	-	-	-	-8.39	-8.65	-12.32	-14.28	-14.60	-15.36
South Pacific	-0.22	-0.13	-0.86	3.38	3.55	2.21	-1.19	-1.59	-2.04	1.92	2.16	2.10	-	-	-
South Atlantic	-0.47	-0.47	-1.32	2.83	3.20	4.68	-0.48	-0.40	-0.42	3.55	3.20	5.26	-	-	-
Indian	-1.13	-1.14	-1.42	-5.38	-7.55	-8.47	-1.77	-1.86	-1.36	2.01	-9.29	-17.85	-	-	-
North Pacific	-2.38	-2.30	-1.92	4.82	5.36	4.63	-1.68	-1.52	-1.19	-6.13	-4.59	-4.90	-20.08	-20.13	-19.41
North Atlantic	-1.88	-1.85	-2.15	-8.49	-7.90	-8.76	-0.45	-0.23	0.31	-38.54	-39.01	-34.79	-2.60	-2.56	-2.76
Arctic	-	-	-	-	-	-	-	-	-	-45.73	-45.06	-40.32	0.54	0.15	0.22

[a] Median differences were calculated using the models MEDUSA, TOPAZ and CCSM4/CESM1. The coefficient of variation (CV) values used for MEDUSA was 0.23, for TOPAZ 0.25 and 0.20 for CCSM4/CESM1. The median differences reported were calculated by first removing grid cells with a CV value less than those stated. To test sensitivity to the choice of CV value the median differences calculated using CV-0.1 values and CV+0.1 values are reported for comparison. A dash means that no pixels were present for that biome and basin combination.

[b] Total number of grid cells in some biome/basin combinations were small (Southern Ocean and permanently stratified, Southern Ocean seasonally mixed).

Table 12.10: Median difference (in metres) in annual mean MLD amplitude between 2007-2026 and 2079-2098 per basin and biome using different coefficient of variation values[a]

	Permanently stratified			Seasonally mixed			LLU			Subpolar			MIZ		
	CV-0.1	CV	CV+0.1	CV-0.1	CV	CV+0.1	CV-0.1	CV	CV+0.1	CV-0.1	CV	CV+0.1	CV-0.1	CV	CV+0.1
Southern Ocean[b]	5.70	-5.44	-69.32	-39.08	-50.24	-72.96	-	-	-	-23.13	-27.01	-35.96	-29.90	-31.22	-34.91
South Pacific	5.00	4.94	3.40	7.32	6.95	7.52	-2.83	-2.56	-3.86	4.61	4.41	4.28	-	-	-
South Atlantic	0.76	0.46	0.29	20.69	18.72	20.68	-1.67	-1.72	-0.99	12.70	9.54	19.25	-	-	-
Indian	-4.52	-3.66	-4.11	-14.87	-18.12	-12.63	-5.51	-5.67	-5.41	31.63	0.41	-32.74	-	-	-
North Pacific	-5.89	-6.03	-5.14	55.08	54.46	49.16	-5.56	-5.60	-5.20	-9.75	-5.75	-6.69	-47.67	-47.23	-45.70
North Atlantic	-2.65	-2.77	-3.68	-27.88	-27.44	-26.13	-0.79	-0.49	0.87	-96.03	-97.44	-90.65	-7.23	-7.54	-8.19
Arctic	-	-	-	-	-	-	-	-	-	-117.93	-109.73	-97.26	4.45	3.51	3.91

[a] Median differences were calculated using the models MEDUSA, TOPAZ and CCSM4/CESM1. The coefficient of variation (CV) values used for MEDUSA was 0.23, for TOPAZ 0.25 and 0.20 for CCSM4/CESM1. The median differences reported were calculated by first removing grid cells with a CV value less than those stated. To test sensitivity to the choice of CV value the median differences calculated using CV-0.1 values and CV+0.1 values are reported for comparison. A dash means that no pixels were present for that biome and basin combination.

[b] Total number of grid cells in some biome/basin combinations were small (Southern Ocean and permanently stratified, Southern Ocean seasonally mixed).

Table 12.11: Median difference (in Wm^{-2}) in annual mean net heat flux between 2007-2026 and 2079-2098 per basin and biome using different coefficient of variation values[a]

	Permanently stratified			Seasonally mixed			LLU			Subpolar			MIZ		
	CV-0.1	CV	CV+0.1	CV-0.1	CV	CV+0.1	CV-0.1	CV	CV+0.1	CV-0.1	CV	CV+0.1	CV-0.1	CV	CV+0.1
Southern Ocean[b]	-1.44	11.16	2.85	-6.77	-1.88	4.14	-	-	-	9.00	11.12	16.03	10.27	10.39	8.43
South Pacific	-3.46	-3.24	-3.09	-10.74	-10.45	-13.73	-8.28	-10.26	-6.34	-14.92	-16.25	-17.83	-	-	-
South Atlantic	0.97	0.54	0.39	-10.56	-10.24	-9.48	-0.91	-0.84	1.81	-32.82	-30.72	-28.92	-	-	-
Indian	-4.46	-4.31	-3.36	-1.31	-0.97	-1.60	2.41	2.19	1.54	1.78	12.63	5.31	-	-	-
North Pacific	5.68	5.55	5.12	-2.44	-2.35	-3.30	-0.98	-0.95	-0.99	4.31	0.77	4.79	-9.56	-9.44	-5.85
North Atlantic	3.25	3.45	2.70	-0.37	-0.36	-0.31	-3.68	-3.91	-3.07	21.00	21.34	19.03	14.21	14.94	12.54
Arctic	-	-	-	-	-	-	-	-	-	27.62	27.75	28.87	31.76	31.40	30.78

[a] Median differences were calculated using the models MEDUSA, TOPAZ and CCSM4/CESM1. The coefficient of variation (CV) values used for MEDUSA was 0.23, for TOPAZ 0.25 and 0.20 for CCSM4/CESM1. The median differences reported were calculated by first removing grid cells with a CV value less than those stated. To test sensitivity to the choice of CV value the median differences calculated using CV-0.1 values and CV+0.1 values are reported for comparison. A dash means that no pixels were present for that biome and basin combination.

[b] Total number of grid cells in some biome/basin combinations were small (Southern Ocean and permanently stratified, Southern Ocean seasonally mixed).

Table 12.12: Median difference (in mmol m^{-3}) in annual mean dissolved inorganic nitrogen between 2007-2026 and 2079-2098 per basin and biome using different coefficient of variation values[a]

	Permanently stratified			Seasonally mixed			LLU			Subpolar			MIZ		
	CV-0.1	CV	CV+0.1	CV-0.1	CV	CV+0.1	CV-0.1	CV	CV+0.1	CV-0.1	CV	CV+0.1	CV-0.1	CV	CV+0.1
Southern Ocean[b]	-0.57	0.26	-2.93	-0.73	-0.54	-0.86	-	-	-	-0.01	-0.11	-0.04	-0.41	-0.42	-0.44
South Pacific	-0.33	-0.22	-0.21	0.98	1.18	0.77	-0.65	-0.82	-1.26	-0.31	-0.13	-0.06	-	-	-
South Atlantic	-0.02	-0.01	-0.01	-0.52	-0.48	-0.41	-0.02	-0.02	-0.02	-1.39	-0.35	-0.05	-	-	-
Indian	-0.01	-0.01	-0.01	0.52	0.58	0.59	-0.02	-0.02	-0.02	-1.60	-0.21	-0.13	-	-	-
North Pacific	-0.02	-0.01	0.00	0.00	0.00	0.00	-0.68	-0.61	-0.56	-0.61	0.02	-0.01	-3.25	-3.11	-2.99
North Atlantic	0.00	0.00	0.00	0.00	0.00	0.00	0.00	0.00	0.00	-0.01	-0.01	-0.01	-0.33	-0.35	-0.52
Arctic	-	-	-	-	-	-	-	-	-	-0.36	-0.36	-0.36	-0.23	-0.23	-0.23

[a] Median differences were calculated using the models MEDUSA, TOPAZ and CCSM4/CESM1. The coefficient of variation (CV) values used for MEDUSA was 0.23, for TOPAZ 0.25 and 0.20 for CCSM4/CESM1. The median differences reported were calculated by first removing grid cells with a CV value less than those stated. To test sensitivity to the choice of CV value the median differences calculated using CV-0.1 values and CV+0.1 values are reported for comparison. A dash means that no pixels were present for that biome and basin combination.

[b] Total number of grid cells in some biome/basin combinations were small (Southern Ocean and permanently stratified, Southern Ocean seasonally mixed).

Table 12.13: Median difference (in days) in the date of maximum MLD between 2007-2026 and 2079-2098 per basin and biome using different coefficient of variation values[a]

	Permanently stratified			Seasonally mixed			LLU			Subpolar			MIZ		
	CV-0.1	CV	CV+0.1	CV-0.1	CV	CV+0.1	CV-0.1	CV	CV+0.1	CV-0.1	CV	CV+0.1	CV-0.1	CV	CV+0.1
Southern Ocean[b]	4.18	3.04	-9.86	5.32	3.45	5.75	-	-	-	-2.50	-2.52	-1.00	-5.50	-5.50	-6.44
South Pacific	2.50	2.30	2.79	5.38	4.72	1.86	1.86	1.33	2.58	3.26	1.56	1.93	-	-	-
South Atlantic	5.00	4.58	5.25	2.50	2.32	1.50	-1.50	-1.25	-1.14	0.89	0.79	5.00	-	-	-
Indian	2.00	1.96	2.78	2.29	2.50	2.77	-2.42	-2.00	-1.16	3.00	0.88	0.74	-	-	-
North Pacific	1.14	0.89	2.03	0.00	0.88	-0.50	2.64	3.79	3.27	-1.94	-1.06	-0.89	2.00	3.03	-0.67
North Atlantic	0.00	-0.12	-0.88	2.00	2.00	1.93	-6.81	-9.83	-4.31	-7.28	-7.13	-7.11	-5.00	-4.94	-3.93
Arctic	-	-	-	-	-	-	-	-	-	-12.36	-12.95	-12.07	-19.78	-18.59	-15.50

[a] Median differences were calculated using the models MEDUSA, TOPAZ and CCSM4/CESM1. The coefficient of variation (CV) values used for MEDUSA was 0.23, for TOPAZ 0.25 and 0.20 for CCSM4/CESM1. The median differences reported were calculated by first removing grid cells with a CV value less than those stated. To test sensitivity to the choice of CV value the median differences calculated using CV-0.1 values and CV+0.1 values are reported for comparison. A dash means that no pixels were present for that biome and basin combination.

[b] Total number of grid cells in some biome/basin combinations were small (Southern Ocean and permanently stratified, Southern Ocean seasonally mixed).

Table 12.14: Median difference (in days) in the date of MLD shoaling between 2007-2026 and 2079-2098 per basin and biome using different coefficient of variation values[a]

	Permanently stratified			Seasonally mixed			LLU			Subpolar			MIZ		
	CV-0.1	CV	CV+0.1	CV-0.1	CV	CV+0.1	CV-0.1	CV	CV+0.1	CV-0.1	CV	CV+0.1	CV-0.1	CV	CV+0.1
Southern Ocean[b]	3.00	0.67	-2.00	9.00	8.92	4.72	-	-	-	1.50	1.68	3.06	-0.95	-0.50	-1.00
South Pacific	-0.87	-1.50	-0.50	5.26	3.11	1.79	-0.40	0.32	-2.79	3.22	2.00	1.00	-	-	-
South Atlantic	0.05	0.50	-0.50	-1.50	-2.17	-1.34	0.50	0.00	0.50	0.50	0.64	-2.00	-	-	-
Indian	0.00	0.50	0.42	4.00	4.37	2.77	-8.50	-5.36	-1.41	3.69	0.50	-0.50	-	-	-
North Pacific	2.76	2.89	3.22	-0.50	0.91	-1.00	2.76	4.07	6.79	-2.63	-3.14	-2.50	-3.00	-2.15	-4.62
North Atlantic	0.17	-0.21	-1.33	-1.63	-1.00	-1.50	-14.00	-14.37	-5.13	-2.50	-3.24	-3.05	1.00	1.50	-2.89
Arctic	-	-	-	-	-	-	-	-	-	-6.00	-6.50	-6.34	-11.50	-11.83	-10.33

[a] Median differences were calculated using the models MEDUSA, TOPAZ and CCSM4/CESM1. The coefficient of variation (CV) values used for MEDUSA was 0.23, for TOPAZ 0.25 and 0.20 for CCSM4/CESM1. The median differences reported were calculated by first removing grid cells with a CV value less than those stated. To test sensitivity to the choice of CV value the median differences calculated using CV-0.1 values and CV+0.1 values are reported for comparison. A dash means that no pixels were present for that biome and basin combination.

[b] Total number of grid cells in some biome/basin combinations were small (Southern Ocean and permanently stratified, Southern Ocean seasonally mixed).

Table 12.15: Median difference (in days) in the date the net heat flux turns positive between 2007-2026 and 2079-2098 per basin and biome using different coefficient of variation values[a]

	Permanently stratified			Seasonally mixed			LLU			Subpolar			MIZ		
	CV-0.1	CV	CV+0.1	CV-0.1	CV	CV+0.1	CV-0.1	CV	CV+0.1	CV-0.1	CV	CV+0.1	CV-0.1	CV	CV+0.1
Southern Ocean[b]	-0.74	-0.50	-6.15	2.96	3.36	3.00	-	-	-	-3.00	-3.00	-4.00	-4.50	-2.95	-4.00
South Pacific	0.50	-0.03	0.24	4.77	2.87	3.00	11.33	10.50	8.90	3.17	1.53	0.50	-	-	-
South Atlantic	0.50	1.00	1.00	1.50	1.75	1.68	1.50	0.38	-1.98	10.64	9.94	10.88	-	-	-
Indian	0.22	0.00	-0.50	1.50	1.18	1.89	-7.82	-8.29	-7.83	1.82	0.50	5.67	-	-	-
North Pacific	-1.68	-1.24	-3.00	3.00	5.00	6.13	8.61	9.15	6.17	-0.88	-1.47	-2.11	-17.08	-19.71	-22.50
North Atlantic	-3.39	-3.22	-1.14	0.42	0.50	0.50	12.17	13.50	7.97	-9.50	-9.28	-9.00	-4.51	-5.04	-4.35
Arctic	-	-	-	-	-	-	-	-	-	-3.50	-3.50	-3.67	-12.44	-14.28	-13.94

[a] Median differences were calculated using the models MEDUSA, TOPAZ and CCSM4/CESM1. The coefficient of variation (CV) values used for MEDUSA was 0.23, for TOPAZ 0.25 and 0.20 for CCSM4/CESM1. The median differences reported were calculated by first removing grid cells with a CV value less than those stated. To test sensitivity to the choice of CV value the median differences calculated using CV-0.1 values and CV+0.1 values are reported for comparison. A dash means that no pixels were present for that biome and basin combination.

[b] Total number of grid cells in some biome/basin combinations were small (Southern Ocean and permanently stratified, Southern Ocean seasonally mixed).

13 References

ANDERSON, T. R. 2005. Plankton functional type modelling: running before we can walk? Journal of Plankton Research, 27, 1073-1081. doi:10.1093/plankt/fbi076

ANTOINE, D., MOREL, A., GORDON, H. R., BANZON, V. F. & EVANS, R. H. 2005. Bridging ocean color observations of the 1980s and 2000s in search of long-term trends. Journal of Geophysical Research-Oceans, 110, C06009. doi:10.1029/2004jc002620

BACKHAUS, J. O., HEGSETH, E. N. S., WEHDE, H., IRIGOIEN, X., HATTEN, K. & LOGEMANN, K. 2003. Convection and primary production in winter. Marine Ecology Progress Series, 251, 1-14.

BACKHAUS, J. O., WEHDE, H., HEGSETH, E. N. & KÄMPF, J. 1999. 'Phyto-convection': the role of oceanic convection in primary production. Marine ecology. Progress series, 189, 77-92.

BANSE, K. & ENGLISH, D. C. 1999. Comparing phytoplankton seasonality in the eastern and western subarctic Pacific and the western Bering Sea. Progress in Oceanography, 43, 235-287.

BARNETT, T. P., PIERCE, D. W. & SCHNUR, R. 2001. Detection of Anthropogenic Climate Change in the World's Oceans. Science, 292, 270-274. doi:10.1126/science.1058304

BARROT, G. 2010. Product User Guide. GlobCOLOUR: An EO based service supporting global ocean carbon cycle research. GC-UM-ACR-PUG-01. European Space Agency

BEAUGRAND, G. 2004. The North Sea regime shift: evidence, causes, mechanisms and consequences. Progress in Oceanography, 60, 245-262. doi:10.1016/j.pocean.2004.02.018

BEAUGRAND, G., LUCZAK, C. & EDWARDS, M. 2009. Rapid biogeographical plankton shifts in the North Atlantic Ocean. Global Change Biology, 15, 1790-1803. doi:10.1111/j.1365-2486.2009.01848.x

BEAULIEU, C., HENSON, S., SARMIENTO, J. L., DUNNE, J., DONEY, S., RYKACZEWSKI, R. & BOPP, L. 2013. Factors challenging our ability to detect long-term trends in ocean chlorophyll. Biogeosciences, 10, 2711-2724. doi:10.5194/bg-10-2711-2013

BEHRENFELD, M. J. 2010. Abandoning Sverdrup's Critical Depth Hypothesis on phytoplankton blooms. Ecology, 91, 977-989. doi:10.1890/09-1207.1

BEHRENFELD, M. J., EMMANUEL, B., DAVID, A. S. & DONALD, M. S. 2005. Carbon-based ocean productivity and phytoplankton physiology from space. Global Biogeochemical Cycles, 19. doi:10.1029/2004gb002299

BEHRENFELD, M. J., O'MALLEY, R. T., SIEGEL, D. A., MCCLAIN, C. R., SARMIENTO, J. L., FELDMAN, G. C., MILLIGAN, A. J., FALKOWSKI, P. G., LETELIER, R. M. & BOSS, E. S. 2006. Climate-driven trends in contemporary ocean productivity. Nature, 444, 752-755. doi:10.1038/nature05317

BLACKBURN, M., LAURS, R. M., OWEN, R. W. & ZEITZSCH.B 1970. Seasonal and areal changes in standing stocks of phytoplankton, zooplankton and micronekton in eastern tropical Pacific. Marine Biology, 7, 14-31.

BLAIN, S., TRÉGUER, P., BELVISO, S., BUCCIARELLI, E., DENIS, M., DESABRE, S., FIALA, M., MARTIN JÉZÉQUEL, V., LE FÈVRE, J., MAYZAUD, P., MARTY, J.-C. & RAZOULS, S. 2001. A biogeochemical study of the island mass effect in the context of the iron hypothesis: Kerguelen Islands, Southern Ocean. Deep Sea Research Part I: Oceanographic Research Papers, 48, 163-187. doi:10.1016/S0967-0637(00)00047-9

BOPP, L., MONFRAY, P., AUMONT, O., DUFRESNE, J. L., LE TREUT, H., MADEC, G., TERRAY, L. & ORR, J. C. 2001. Potential impact of climate change on marine export production. *Global Biogeochemical Cycles,* 15**,** 81-99.

BORKMAN, D. G. & SMAYDA, T. J. 2009. Gulf Stream position and winter NAO as drivers of long-term variations in the bloom phenology of the diatom Skeletonema costatum "species-complex" in Narragansett Bay, RI, USA. *Journal of Plankton Research,* 31**,** 1407-1425. doi:10.1093/plankt/fbp072

BOSS, E. & BEHRENFELD, M. 2010. In situ evaluation of the initiation of the North Atlantic phytoplankton bloom. *Geophysical Research Letters,* 37**,** L18603. doi:10.1029/2010gl044174

BOYCE, D. G., LEWIS, M. R. & WORM, B. 2010. Global phytoplankton decline over the past century. *Nature,* 466**,** 591-596. doi:10.1038/nature09268

BOYD, P. & HARRISON, P. J. 1999. Phytoplankton dynamics in the NE subarctic Pacific. *Deep Sea Research Part II: Topical Studies in Oceanography,* 46**,** 2405-2432.

BRAINERD, K. E. & GREGG, M. C. 1995. SURFACE MIXED AND MIXING LAYER DEPTHS. *Deep-Sea Research Part I-Oceanographic Research Papers,* 42**,** 1521-1543. doi:10.1016/0967-0637(95)00068-h

BRETHERTON, F. P., DAVIS, R. E. & FANDRY, C. B. 1976. A technique for objective analysis and design of oceanographic experiments applied to MODE-73. *Deep Sea Research and Oceanographic Abstracts,* 23**,** 559-582.

BROCK, T. D. 1981. Calculating solar radiation for ecological studies. *Ecological Modelling,* 14**,** 1-19.

BRODY, S. R., LOZIER, M. S. & JOHN, P. D. 2013. A comparison of methods to determine phytoplankton bloom initiation. *Journal of Geophysical Research: Oceans.* doi:10.1002/jgrc.20167

BUESSELER, K. O. 1998. The decoupling of production and particulate export in the surface ocean. *Global Biogeochemical Cycles,* 12**,** 297-310.

BUITENHUIS, E. T., RIVKIN, R. B., SAILLEY, S. & LE QUÉRÉ, C. 2010. Biogeochemical fluxes through microzooplankton. *Global Biogeochemical Cycles,* 24**,** GB4015. doi:10.1029/2009GB003601

CARMACK, E., BARBER, D., CHRISTENSEN, J., MACDONALD, R., RUDELS, B. & SAKSHAUG, E. 2006. Climate variability and physical forcing of the food webs and the carbon budget on panarctic shelves. *Progress in Oceanography,* 71**,** 145-181. doi:10.1016/j.pocean.2006.10.005

CHATFIELD, C. 2005. Durbin–Watson Test. *Encyclopedia of Biostatistics.* John Wiley & Sons, Ltd.

CHAVEZ, F. P. 1989. Size distribution of phytoplankton in the central and eastern tropical Pacific. *Global Biogeochemical Cycles,* 3**,** 27-35.

CHENILLAT, F., RIVIÈRE, P., CAPET, X., DI LORENZO, E. & BLANKE, B. 2012. North Pacific Gyre Oscillation modulates seasonal timing and ecosystem functioning in the California Current upwelling system. *Geophysical Research Letters,* 39**,** L01606. doi:10.1029/2011gl049966

CHIBA, S., AITA, M. N., TADOKORO, K., SAINO, T., SUGISAKI, H. & NAKATA, K. 2008. From climate regime shifts to lower-trophic level phenology: Synthesis of

recent progress in retrospective studies of the western North Pacific. *Progress in Oceanography,* 77**,** 112-126. doi:10.1016/j.pocean.2008.03.004

CHIBA, S., BATTEN, S., SASAOKA, K., SASAI, Y. & SUGISAKI, H. 2012. Influence of the Pacific Decadal Oscillation on phytoplankton phenology and community structure in the western North Pacific. *Geophysical Research Letters,* 39**,** L15603. doi:10.1029/2012gl052912

CHIBA, S., TADOKORO, K., SUGISAKI, H. & SAINO, T. 2006. Effects of decadal climate change on zooplankton over the last 50 years in the western subarctic North Pacific. *Global Change Biology,* 12**,** 907-920. doi:10.1111/j.1365-2486.2006.01136.x

COLE, H., HENSON, S., MARTIN, A. & YOOL, A. 2012. Mind the gap: The impact of missing data on the calculation of phytoplankton phenology metrics. *Journal of Geophysical Research,* 117**,** C08030. doi:10.1029/2012jc008249

COLEBROOK, J. M. 1979. Continuous Plankton Records: Seasonal cycles of phytoplankton and copepods in the North Atlantic Ocean and the North Sea. *Marine Biology,* 51**,** 23-32. doi:10.1007/bf00389027

COLLINS, A. K., ALLEN, S. E. & PAWLOWICZ, R. 2009. The role of wind in determining the timing of the spring bloom in the Strait of Georgia. *Canadian Journal of Fisheries and Aquatic Sciences,* 66**,** 1597-1616. doi:10.1139/f09-071

CONVERSI, A., PELUSO, T. & FONDA-UMANI, S. 2009. Gulf of Trieste: A changing ecosystem. *Journal of Geophysical Research,* 114**,** C03S90. doi:10.1029/2008jc004763

CRONIN, M. F. & SPRINTALL, J. 2001. Wind And Buoyancy-forced Upper Ocean. *In:* EDITOR-IN-CHIEF: JOHN, H. S. (ed.) *Encyclopedia of Ocean Sciences.* Oxford: Academic Press.

CUSHING, D. H. 1990. Plankton production and year-class strength in fish populations - an update of the match mismatch hypothesis. *Advances in Marine Biology,* 26**,** 249-293.

D'ORTENZIO, F., ANTOINE, D., MARTINEZ, E. & RIBERA D'ALCALÀ, M. 2012. Phenological changes of oceanic phytoplankton in the 1980s and 2000s as revealed by remotely sensed ocean-color observations. *Global Biogeochemical Cycles,* 26**,** GB4003. doi:10.1029/2011gb004269

DAGG, M. J. & TURNER, J. T. 1982. THE IMPACT OF COPEPOD GRAZING ON THE PHYTOPLANKTON OF GEORGES BANK AND THE NEW YORK BIGHT. *Canadian Journal of Fisheries and Aquatic Sciences,* 39**,** 979-990. doi:10.1139/f82-133

DANABASOGLU, G., BATES, S. C., BRIEGLEB, B. P., JAYNE, S. R., JOCHUM, M., LARGE, W. G., PEACOCK, S. & YEAGER, S. G. 2011. The CCSM4 Ocean Component. *Journal of Climate,* 25**,** 1361-1389. doi:10.1175/JCLI-D-11-00091.1

DANDONNEAU, Y., DESCHAMPS, P. Y., NICOLAS, J. M., LOISEL, H., BLANCHOT, J., MONTEL, Y., THIEULEUX, F. & BÉCU, G. 2004. Seasonal and interannual variability of ocean color and composition of phytoplankton communities in the North Atlantic, equatorial Pacific and South Pacific. *Deep-Sea Research Part II-Topical Studies in Oceanography,* 51**,** 303-318. doi:10.1016/j.dsr2.2003.07.018

DAVE, A. C. & LOZIER, M. S. 2010. Local stratification control of marine productivity in the subtropical North Pacific. *Journal of Geophysical Research,* 115. doi:10.1029/2010jc006507

DAVE, A. C. & LOZIER, M. S. 2013. Examining the global record of interannual variability in stratification and marine productivity in the low-latitude and mid-latitude ocean. *Journal of Geophysical Research: Oceans***,** 3114–3127. doi:10.1002/jgrc.20224

DEMIDOV, A. B., GAGARIN, V. I. & GRIGORIEV, A. V. 2010. Seasonal variability of the surface chlorophyll "a" in the Drake Passage. *Oceanology,* 50**,** 327-341. doi:10.1134/S0001437010030045

DONEY, S. 2006. Oceanography: Plankton in a warmer world. *Nature,* 444**,** 695-696. doi:10.1038/444695a

DONEY, S. C., GLOVER, D. M., MCCUE, S. J. & FUENTES, M. 2003. Mesoscale variability of Sea-viewing Wide Field-of-view Sensor(SeaWiFS) satellite ocean color: Global patterns and spatial scales. *Journal of Geophysical Research-Oceans,* 108. doi:10.1029/2001jc000843

DORE, J. E., LETELIER, R. M., CHURCH, M. J., LUKAS, R. & KARL, D. M. 2008. Summer phytoplankton blooms in the oligotrophic North Pacific Subtropical Gyre: Historical perspective and recent observations. *Progress in Oceanography,* 76**,** 2-38. doi:10.1016/j.pocean.2007.10.002

DORON, M., BABIN, M., MANGIN, A. & HEMBISE, O. 2007. Estimation of light penetration, and horizontal and vertical visibility in oceanic and coastal waters from surface reflectance. *Journal of Geophysical Research: Oceans,* 112**,** C06003. doi:10.1029/2006JC004007

DUNNE, J. P., GNANADESIKAN, A., SARMIENTO, J. L. & SLATER, R. D. 2010. Technical description of the prototype version (v0) of Tracers of Phytoplankton with Allometric Zooplankton (TOPAZ) ocean biogeochemical model as used in the Princeton IFMIP model. . *Biogeosciences,* 7 (Suppl.). doi:10.5194/bg-7-3593-2010

DUNNE, J. P., JOHN, J. G., SHEVLIAKOVA, E., STOUFFER, R. J., KRASTING, J. P., MALYSHEV, S. L., MILLY, P. C. D., SENTMAN, L. T., ADCROFT, A. J., COOKE, W., DUNNE, K. A., GRIFFIES, S. M., HALLBERG, R. W., HARRISON, M. J., LEVY, H., WITTENBERG, A. T., PHILLIPS, P. J. & ZADEH, N. 2013. GFDL's ESM2 Global Coupled Climate–Carbon Earth System Models. Part II: Carbon System Formulation and Baseline Simulation Characteristics*. *Journal of Climate,* 26**,** 2247-2267. doi:10.1175/JCLI-D-12-00150.1

DURAND, D. 2007. Full Validation Report. *GlobCOLOUR: An EO based service supporting global ocean carbon cycle research*. GC-PL-NIVA-FVR-01. European Space Agency

DUTKIEWICZ, S., FOLLOWS, M., MARSHALL, J. & GREGG, W. W. 2001. Interannual variability of phytoplankton abundances in the North Atlantic. *Deep-Sea Research Part II-Topical Studies in Oceanography,* 48**,** 2323-2344.

DUTKIEWICZ, S., FOLLOWS, M. J. & PAREKH, P. 2005. Interactions of the iron and phosphorus cycles: A three-dimensional model study. *Global Biogeochemical Cycles,* 19**,** GB1021. doi:10.1029/2004GB002342

EDWARDS, M., REID, P. & PLANQUE, B. 2001. Long-term and regional variability of phytoplankton biomass in the Northeast Atlantic (1960-1995). *ICES Journal of Marine Science,* 58**,** 39-49. doi:10.1006/jmsc.2000.0987

EDWARDS, M. & RICHARDSON, A. J. 2004. Impact of climate change on marine pelagic phenology and trophic mismatch. *Nature,* 430**,** 881-884. doi:10.1038/nature02808

ENRIGHT, C., BUITENHUIS, E., VOGT, M. & QUÉRÉ, C. L. 2009. PlankTOM10 User Manual v.1.02. Dynamic Green Ocean Project

EPPLEY, R. W. 1972. Temperature and phytoplankton growth in the sea. *Fishery Bulletin,* 70**,** 1063-1085.

EPPLEY, R. W. & PETERSON, B. J. 1979. Particulate organic matter flux and planktonic new production in the deep ocean. *Nature,* 282**,** 677-680.

EVANS, G. T. & PARSLOW, J. S. 1985. A model of annual plankton cycles. *Biological Oceanography,* 3**,** 327-347.

FASHAM, M. J. R. 1995. Variations in the seasonal cycle of biological production in subarctic oceans: A model sensitivity analysis. *Deep Sea Research Part I: Oceanographic Research Papers,* 42**,** 1111-1149. doi:10.1016/0967-0637(95)00054-A

FIEDLER, P. C. 2010. Comparison of objective descriptions of the thermocline. *Limnology and Oceanography-Methods,* 8**,** 313-325. doi:10.4319/lom.2010.8.313

FIELD, C. B., BEHRENFELD, M. J., RANDERSON, J. T. & FALKOWSKI, P. 1998. Primary Production of the Biosphere: Integrating Terrestrial and Oceanic Components. *Science,* 281**,** 237-240. doi:10.1126/science.281.5374.237

FINDLAY, H. S., YOOL, A., NODALE, M. & PITCHFORD, J. W. 2006. Modelling of autumn plankton bloom dynamics. *Journal of Plankton Research,* 28**,** 209-220. doi:10.1093/plankt/fbi114

FOLLOWS, M. & DUTKIEWICZ, S. 2002. Meteorological modulation of the North Atlantic spring bloom. *Deep-Sea Research Part Ii-Topical Studies in Oceanography,* 49**,** 321-344.

FRAJKA-WILLIAMS, E., RHINES, P. B. & ERIKSEN, C. C. 2009. Physical controls and mesoscale variability in the Labrador Sea spring phytoplankton bloom observed by Seaglider. *Deep Sea Research Part I: Oceanographic Research Papers,* 56**,** 2144-2161.

FRANCOIS, R., HONJO, S., KRISHFIELD, R. & MANGANINI, S. 2002. Factors controlling the flux of organic carbon to the bathypelagic zone of the ocean. *Global Biogeochemical Cycles,* 16**,** 1087. doi:10.1029/2001GB001722

FROST, B. W. 1991. THE ROLE OF GRAZING IN NUTRIENT-RICH AREAS OF THE OPEN SEA. *Limnology and Oceanography,* 36**,** 1616-1630.

FROUIN, R., FRANZ, B. & WANG, M. 2001. Algorithm to estimate PAR from SeaWiFS data Version 1.2-Documentation. *Ocean Colour Products*. NASA

FUENTES-YACO, C., KOELLER, P. A., SATHYENDRANATH, S. & PLATT, T. 2007. Shrimp (Pandalus borealis) growth and timing of the spring phytoplankton bloom on the Newfoundland-Labrador Shelf. *Fisheries Oceanography,* 16**,** 116-129. doi:10.1111/j.1365-2419.2006.00402.x

GAILLARD, F. 2007. Collection of new climatologies and statistics over the Atlantic, identification of key data for the physical parameters. *MERSEA Del 5.4.2*.

GAILLARD, F. 2010. ISAS tool version 5.3: method and configuration. *SO-Argo report*. Coriolis Project

GAILLARD, F., AUTRET, E., THIERRY, V., GALAUP, P., COATANOAN, C. & LOUBRIEU, T. 2009. Quality Control of Large Argo Datasets. *Journal of Atmospheric and Oceanic Technology,* 26**,** 337-351. doi:10.1175/2008jtecho552.1

GEIDER, R. J., MACINTYRE, H. L. & KANA, T. M. 1998. A dynaic regulatory model of phytoplanktonic acclimation to light, nutrients, and temperature. *Limnology and Oceanography,* 43**,** 679-694.

GENT, P. R., DANABASOGLU, G., DONNER, L. J., HOLLAND, M. M., HUNKE, E. C., JAYNE, S. R., LAWRENCE, D. M., NEALE, R. B., RASCH, P. J., VERTENSTEIN, M., WORLEY, P. H., YANG, Z.-L. & ZHANG, M. 2011. The Community Climate System Model Version 4. *Journal of Climate,* 24**,** 4973-4991. doi:10.1175/2011jcli4083.1

GIFFORD, D. J., FESSENDEN, L. M., GARRAHAN, P. R. & MARTIN, E. 1995. Grazing by microzooplankton and mesozooplankton in the high-latitude North Atlantic

Ocean: Spring versus summer dynamics. *Journal of Geophysical Research: Oceans,* 100**,** 6665-6675. doi:10.1029/94jc00983

GLADAN, Z. N., MARASOVIC, I., GRBEC, B., SKEJIC, S., BUZANCIC, M., KUSPILIC, G., MATIJEVIC, S. & MATIC, F. 2010. Inter-decadal variability in phytoplankton community in the Middle Adriatic (Katela Bay) in relation to the North Atlantic Oscillation. *Estuaries and Coasts,* 33**,** 376-383. doi:10.1007/s12237-009-9223-3

GOES, J. I., SASAOKA, K., GOMES, H. D. R., SAITOH, S. & SAINO, T. 2004. A comparison of the seasonality and interannual variability of phytoplankton biomass and production in the western and eastern gyres of the subarctic Pacific using multi-sensor satellite data. *Journal of Oceanography,* 60**,** 75-91. doi:10.1023/B:JOCE.0000038320.94273.25

GORDON, H. & MCCLUNEY, W. 1975. Estimation of the depth of sunlight penetration in the sea for remote sensing. *Applied Optics,* 14**,** 413-416.

GRAN, H. H. & BRAARUD, T. 1935. A Quantitative Study of the Phytoplankton in the Bay of Fundy and the Gulf of Maine (including Observations on Hydrography, Chemistry and Turbidity). *Journal of the Biological Board of Canada,* 1**,** 279-467. doi:10.1139/f35-012

GREGG, W. W. 2002. A coupled ocean-atmosphere radiative model for global ocean biogeochemical models*. NASA Global Modelling and Assimilation Series*.

GREGG, W. W. & CASEY, N. W. 2004. Global and regional evaluation of the SeaWiFS chlorophyll data set. *Remote Sensing of Environment,* 93**,** 463-479.

GREGG, W. W. & CONKRIGHT, M. E. 2002. Decadal changes in global ocean chlorophyll. *Geophysical Research Letters,* 29. doi:10.1029/2002gl014689

GREGG, W. W., CONKRIGHT, M. E., GINOUX, P., O'REILLY, J. E. & CASEY, N. W. 2003a. Ocean primary production and climate: Global decadal changes. *Geophysical Research Letters,* 30. doi:10.1029/2003gl016889

GREGG, W. W., GINOUX, P., SCHOPF, P. S. & CASEY, N. W. 2003b. Phytoplankton and iron: validation of a global three-dimensional ocean biogeochemical model. *Deep-Sea Research Part Ii-Topical Studies in Oceanography,* 50**,** 3143-3169. doi:10.1016/j.dsr2.2003.07.013

GREVE, W., PRINAGE, S., ZIDOWITZ, H., NAST, J. & REINERS, F. 2005. On the phenology of north sea ichthyoplankton. *ICES Journal of Marine Science,* 62**,** 1216-1223. doi:10.1016/j.iccsjms.2005.03.011

GRIFFIES, S. M., M. J., H., PACANOWSKI, R. C. & ROSATI, A. 2004. A technical guide to MOM4*. GFDL Ocean Group Technical Report*.

GRODSKY, S. A., CARTON, J. A. & MCCLAIN, C. R. 2008. Variability of upwelling and chlorophyll in the equatorial Atlantic. *Geophysical Research Letters,* 35. doi:10.1029/2007gl032466

HAMME, R. C., WEBLEY, P. W., CRAWFORD, W. R., WHITNEY, F. A., DEGRANDPRE, M. D., EMERSON, S. R., ERIKSEN, C. C., GIESBRECHT, K. E., GOWER, J. F. R., KAVANAUGH, M. T., PEÑA, M. A., SABINE, C. L., BATTEN, S. D., COOGAN, L. A., GRUNDLE, D. S. & LOCKWOOD, D. 2010. Volcanic ash fuels anomalous plankton bloom in subarctic northeast Pacific. *Geophysical Research Letters,* 37**,** L19604. doi:10.1029/2010gl044629

HAYS, G. C., RICHARDSON, A. J. & ROBINSON, C. 2005. Climate change and marine plankton. *Trends in Ecology & Evolution,* 20**,** 337-344. doi:10.1016/j.tree.2005.03.004

HEGSETH, E. N. & SUNDFJORD, A. 2008. Intrusion and blooming of Atlantic phytoplankton species in the high Arctic. *Journal of Marine Systems,* 74**,** 108-119. doi:10.1016/j.jmarsys.2007.11.011

HEINRICH, A. K. 1962. The life histories of plankton animals and seasonal cycles of plankton communities in the oceans. *Journal du Conseil Internationale pour Exploration de la Mer,* 27**,** 15-25.

HENSON, S., COLE, H., BEAULIEU, C. & YOOL, A. 2013. The impact of global warming on seasonality of ocean primary production. *Biogeosciences Discuss,* 10**,** 1421-1450.

HENSON, S. A. 2007. Water column stability and spring bloom dynamics in the Gulf of Alaska. *Journal of Marine Research,* 65**,** 715-736. doi:10.1357/002224007784219002

HENSON, S. A., DUNNE, J. P. & SARMIENTO, J. L. 2009. Decadal variability in North Atlantic phytoplankton blooms. *Journal of Geophysical Research,* 114**,** C04013. doi:01.1029/2008jC005139

HENSON, S. A., ROBINSON, I., ALLEN, J. T. & WANIEK, J. J. 2006. Effect of meteorological conditions on interannual variability in timing and magnitude of the spring bloom in the Irminger Basin, North Atlantic. *Deep-Sea Research Part I-Oceanographic Research Papers,* 53**,** 1601-1615. doi:10.1016/j.dsr.2006.07.009

HENSON, S. A., SARMIENTO, J. L., DUNNE, J. P., BOPP, L., LIMA, I., DONEY, S. C., JOHN, J. & BEAULIEU, C. 2010. Detection of anthropogenic climate change in satellite records of ocean chlorophyll and productivity. *Biogeosciences,* 7**,** 621-640. doi:10.5194/bg-7-621-2010

HENSON, S. A. & THOMAS, A. C. 2007. Interannual variability in timing of bloom initiation in the California Current System. *Journal of Geophysical Research-Part C-Oceans,* 112**,** C08007. doi:10.1029/2006jc003960

HOLMES, R. W. 1956. The annual cycle of phytoplankton in the Labrador Sea, 1950-51. *Bull Bingham Oceanogr Coll,* 16**,** 3-74.

HOLTE, J. & TALLEY, L. 2009. A New Algorithm for Finding Mixed Layer Depths with Applications to Argo Data and Subantarctic Mode Water Formation. *Journal of Atmospheric and Oceanic Technology,* 26**,** 1920-1939. doi:10.1175/2009jtecho543.1

HUDSON, R. J. M. & MOREL, F. M. M. 1990. Iron transport in marine phytoplankton - kinetics of cellular and medium coordination reactions. *Limnology and Oceanography,* 35**,** 1002-1020.

HUISMAN, J., OOSTVEEN, P. V. & WEISSING, F. J. 1999. Critical Depth and Critical Turbulence: Two Different Mechanisms for the Development of Phytoplankton Blooms. *Limnology and Oceanography,* 44**,** 1781-1787.

HULBURT, E. M., RYTHER, J. H. & GUILLARD, R. R. L. 1960. The phytoplankton of the Sargasso Sea off Bermuda. *Jour Conseil Perm Internatl Explor Mer,* 25**,** 115-128.

HURRELL, J. W. 1995. Decadal trends in the North Atlantic Oscillation - regional temperatures and precipitation. *Science,* 269**,** 676-679. doi:10.1126/science.269.5224.676

HUTCHINS, D. A., WITTER, A. E., BUTLER, A. & LUTHER, G. W. 1999. Competition among marine phytoplankton for different chelated iron species. *Nature,* 400**,** 858-861.

IRIGOIEN, X., HARRIS, R. P., HEAD, R. N. & HARBOUR, D. 2000. North Atlantic Oscillation and spring bloom phytoplankton composition in the English Channel. *Journal of Plankton Research,* 22**,** 2367-2371.

IRWIN, A. J. & FINKEL, Z. V. 2008. Mining a sea of data: deducing the environmental controls of ocean chlorophyll. *PLoS One,* 3**,** e3836. doi:10.1371/journal.pone.0003836

IRWIN, A. J. & OLIVER, M. J. 2009. Are ocean deserts getting larger? *Geophysical Research Letters,* 36**,** L18609. doi:10.1029/2009gl039883

JANG, C. J., PARK, J., PARK, T. & YOO, S. 2011. Response of the ocean mixed layer depth to global warming and its impact on primary production: a case for the North Pacific Ocean. *ICES Journal of Marine Science: Journal du Conseil,* 68**,** 996-1007. doi:10.1093/icesjms/fsr064

JI, R., EDWARDS, M., MACKAS, D. L., RUNGE, J. A. & THOMAS, A. C. 2010. Marine plankton phenology and life history in a changing climate: current research and future directions. *Journal of Plankton Research,* 32**,** 1355-1368. doi:10.1093/plankt/fbq062

JI, R., JIN, M. & VARPE, Ø. 2012. Sea ice phenology and timing of primary production pulses in the Arctic Ocean. *Global Change Biology,* 19**,** 734-741. doi:10.1111/gcb.12074

KAHRU, M., BROTAS, V., MANZANO-SARABIA, M. & MITCHELL, B. G. 2011. Are phytoplankton blooms occurring earlier in the Arctic? *Global Change Biology,* 17**,** 1733-1739. doi:10.1111/j.1365-2486.2010.02312.x

KAHRU, M., GILLE, S. T., MURTUGUDDE, R., STRUTTON, P. G., MANZANO-SARABIA, M., WANG, H. & MITCHELL, B. G. 2010. Global correlations between winds and ocean chlorophyll. *Journal of Geophysical Research,* 115**,** C12040. doi:10.1029/2010jc006500

KARA, A. B., ROCHFORD, P. A. & HURLBURT, H. E. 2000. An optimal definition for ocean mixed layer depth. *Journal of Geophysical Research-Oceans,* 105**,** 16803-16821. doi:10.1029/2000jc900072

KOELLER, P., FUENTES-YACO, C., PLATT, T., SATHYENDRANATH, S., RICHARDS, A., OUELLET, P., ORR, D., SKÚLADÓTTIR, U., WIELAND, K., SAVARD, L. & ASCHAN, M. 2009. Basin-scale coherence in phenology of shrimps and phytoplankton in the North Atlantic Ocean. *Science,* 324**,** 791-793. doi:10.1126/science.1170987

KRISTIANSEN, T., DRINKWATER, K. F., LOUGH, R. G. & SUNDBY, S. 2011. Recruitment Variability in North Atlantic Cod and Match-Mismatch Dynamics. *PLoS One,* 6**,** e17456. doi:10.1371/journal.pone.0017456

KWON, E. Y., PRIMEAU, F. & SARMIENTO, J. L. 2009. The impact of remineralization depth on the air-sea carbon balance. *Nature Geoscience,* 2**,** 630-635. doi:10.1038/ngeo612

LANDRY, M. R., BARBER, R. T., BIDIGARE, R. R., CHAI, F., COALE, K. H., DAM, H. G., LEWIS, M. R., LINDLEY, S. T., MCCARTHY, J. J., ROMAN, M. R., STOECKER, D. K., VERITY, P. G. & WHITE, J. R. 1997. Iron and grazing constraints on primary production in the central equatorial Pacific: An EqPac synthesis. *Limnology and Oceanography,* 42**,** 405-418.

LANDRY, M. R., MONGER, B. C. & SELPH, K. E. 1993. Time-dependency of microzooplankton grazing and phytoplankton growth in the subarctic Pacific. *Progress in Oceanography,* 32**,** 205-222.

LANGDON, C. 1988. On the causes of interspecific differences in the growth-irradiance relationship for phytoplankton. II. A general review. *Journal of Plankton Research,* 10. doi:10.1093/plankt/10.6.1291

LETELIER, R. M., KARL, D. M., ABBOTT, M. R. & BIDIGARE, R. R. 2004. Light driven seasonal patterns of chlorophyll and nitrate in the lower euphotic zone of the North Pacific Subtropical Gyre. *Limnology and Oceanography,* 49**,** 508-519.

LEU, E., SØREIDE, J. E., HESSEN, D. O., FALK-PETERSEN, S. & BERGE, J. 2011. Consequences of changing sea-ice cover for primary and secondary

producers in the European Arctic shelf seas: Timing, quantity, and quality. *Progress in Oceanography,* 90**,** 18-32. doi:10.1016/j.pocean.2011.02.004

LEVITUS, S., ANTONOV, J. I., WANG, J., DELWORTH, T. L., DIXON, K. W. & BROCCOLI, A. J. 2001. Anthropogenic warming of Earth's climate system. *Science,* 292**,** 267-270.

LIEBELT, P. B. 1967. *An introduction to optimal estimation,* USA, Addison-Wesley Publishing Company.

LINDSAY, K. 2012. *The CESM Ocean Ecosystem Scientific Description* [Online]. Available: http://www.cesm.ucar.edu/models/cesm1.1/pop2/doc/sci/ecosys_placeholder.html [Accessed 05/09/2013 2013].

LOMB, N. R. 1976. Least-squares frequency analysis of unequally spaced data. *Astrophysics and Space Science,* 39. doi:10.1007/bf00648343

LONGHURST, A. 1995. Seasonal cycles of pelagic production and consumption. *Progress in Oceanography,* 36**,** 77-167.

LONGHURST, A. 2001. A major seasonal phytoplankton bloom in the Madagascar Basin. *Deep Sea Research Part I: Oceanographic Research Papers,* 48**,** 2413-2422.

LOZIER, M. S., DAVE, A. C., PALTER, J. B., GERBER, L. M. & BARBER, R. T. 2011. On the relationship between stratification and primary productivity in the North Atlantic. *Geophysical Research Letters,* 38**,** L18609. doi:10.1029/2011gl049414

LUTZ, M. J., CALDEIRA, K., DUNBAR, R. B. & BEHRENFELD, M. J. 2007. Seasonal rhythms of net primary production and particulate organic carbon flux to depth describe the efficiency of biological pump in the global ocean. *Journal of Geophysical Research-Oceans,* 112**,** C10011. doi:10.1029/2006JC003706

MACKAS, D. L., GREVE, W., EDWARDS, M., CHIBA, S., TADOKORO, K., ELOIRE, D., MAZZOCCHI, M. G., BATTEN, S., RICHARDSON, A. J., JOHNSON, C., HEAD, E., CONVERSI, A. & PELUSO, T. 2012. Changing zooplankton seasonality in a changing ocean: Comparing time series of zooplankton phenology. *Progress in Oceanography,* 97-100**,** 31-62.

MADEC, G. 2008. NEMO reference manual, ocean dynamic component: NEMO-OPA. *Note du ple de modelisation.* Institut Pierre Simmon Lapalce (IPSL)

MAHADEVAN, A., D'ASARO, E., LEE, C. & PERRY, M. J. 2012. Eddy-Driven Stratification Initiates North Atlantic Spring Phytoplankton Blooms. *Science,* 337**,** 54-58. doi:10.1126/science.1218740

MANTUA, N. J., HARE, S. R., ZHANG, Y., WALLACE, J. M. & FRANCIS, R. C. 1997. A Pacific interdecadal climate oscillation with impacts on salmon production. *Bulletin of the American Meteorological Society,* 78**,** 1069-1079.

MARINOV, I., DONEY, S. C. & LIMA, I. D. 2010. Response of ocean phytoplankton community structure to climate change over the 21st century: partitioning the effects of nutrients, temperature and light. *Biogeosciences,* 7**,** 3941-3959. doi:10.5194/bg-7-3941-2010

MARRA, J. 1997. Analysis of diel variability in chlorophyll fluorescence. *Journal of Marine Research,* 55**,** 767-784.

MARRA, J. 2004. The compensation irradiance for phytoplankton in nature. *Geophysical Research Letters,* 31. doi:10.1029/2003gl018881

MARSHALL, J. & SCHOTT, F. 1999. Open-ocean convection: Observations, theory, and models. *Reviews of Geophysics,* 37**,** 1-64.

MARTIN, J. H., GORDON, R. M. & FITZWATER, S. E. 1991. The case for iron. *Limnology and Oceanography,* 36**,** 1793-1802.

MARTINEZ, E., ANTOINE, D., D'ORTENZIO, F. & DE BOYER MONTÉGUT, C. 2011. Phytoplankton spring and fall blooms in the North Atlantic in the 1980s and 2000s. *Journal of Geophysical Research,* 116**,** C11029. doi:10.1029/2010JC006836

MARTINEZ, E., ANTOINE, D., D'ORTENZIO, F. & GENTILI, B. 2009. Climate-driven basin-scale decadal oscillations of oceanic phytoplankton. *Science,* 326**,** 1253-1256.

MCCLAIN, C. R., CLEAVE, M. L., FELDMAN, G. C., GREGG, W. W., HOOKER, S. B. & KURING, N. 1998. Science quality SeaWiFS data for global biosphere research. *Sea Technology,* 39**,** 10-16.

MCCLAIN, C. R., SIGNORINI, S. R. & CHRISTIAN, J. R. 2004. Subtropical gyre variability observed by ocean-color satellites. *Deep Sea Research Part II: Topical Studies in Oceanography,* 51**,** 281-301. doi:10.1016/j.dsr2.2003.08.002

MCQUATTERS-GOLLOP, A., REID, P. C., EDWARDS, M., BURKILL, P. H., CASTELLANI, C., BATTEN, S., GIESKES, W., BEARE, D., BIDIGARE, R. R., HEAD, E., JOHNSON, R., KAHRU, M., KOSLOW, J. A. & PENA, A. 2011. Is there a decline in marine phytoplankton? *Nature,* 472**,** E6-E7.

MENZEL, D. W. & RYTHER, J. H. 1961. Annual variation in primary production of the Sargasso Sea off Bermuda. *Deep Sea Research,* 7**,** 282-288.

MILLER, C. B. 1993. Pelagic production production in the Subacrtic Pacific. *Progress in Oceanography,* 32**,** 1-15.

MONTÉGUT, C. D., MADEC, G., FISCHER, A. S., LAZAR, A. & IUDICONE, D. 2004. Mixed layer depth over the global ocean: An examination of profile data and a profile-based climatology. *Journal of Geophysical Research-Oceans,* 109**,** C12003. doi:

10.1029/2004jc002378

MOORE, J. K., LINDSAY, K., DONEY, S. C., LONG, M. C. & MISUMI, K. 2013. Marine Ecosystem Dynamics and Biogeochemical Cycling in the Community Earth System Model [CESM1(BGC)]: Comparison of the 1990s with the 2090s under the RCP4.5 and RCP8.5 Scenarios. *Journal of Climate.* doi:10.1175/JCLI-D-12-00566.1

MORAN, X. A. G., LOPEZ-URRUTIA, A., CALVO-DIAZ, A. & LI, W. K. W. 2010. Increasing importance of small phytoplankton in a warmer ocean. *Global Change Biology,* 16**,** 1137-1144. doi:10.111/j.1365-2486.2009.01960.x

MOREL, A., YANNICK, H., BERNARD, G., WERDELL, P. J., STANFORD, B. H. & BRYAN, A. F. 2007. Examining the consistency of products derived from various ocean color sensors in open ocean (Case 1) waters in the perspective of a multi-sensor approach. *Remote Sensing of Environment,* 111. doi:10.1016/j.rse.2007.03.012

MOREL, F., RUETER, J. & PRICE, N. 1991. Iron nutrition of phytoplankton and its possible importance in the ecology of ocean regions with high nutrient and low biomass. *Oceanography,* 4**,** 56-61.

MULHOLLAND, M. R. & BERNHARDT, P. W. 2005. The effect of growth rate, phosphorus concentration, and temperature on N2 fixation, carbon fixation, and nitrogen release in continuous cultures of Trichodesmium IMS101. *Limnol. Oceanogr,* 50**,** 839-849. doi:10.4319/lo.2005.50.3.0839

MULHOLLAND, M. R., BERNHARDT, P. W., HEIL, C. A., BRONK, D. A. & O'NEIL, J. M. 2006. Nitrogen fixation and release of fixed nitrogen by Trichodesmium

spp. in the Gulf of Mexico. *Limnology and Oceanography,* 51, 1762-1776. doi:10.4319/lo.2006.51.4.1762

NERGER, L. & GREGG, W. W. 2007. Assimilation of SeaWiFS data into a global ocean-biogeochemical model using a local SEIK filter. *Journal of Marine Systems,* 68, 237-254.

NERGER, L. & GREGG, W. W. 2008. Improving assimilation of SeaWiFS data by the application of bias correction with a local SEIK filter. *Journal of Marine Systems,* 73, 87-102. doi:10.1016/j.jmarsys.2007.09.007

O'REILLY, J. E., MARITORENA, S., MITCHELL, B. G., SIEGEL, D. A., CARDER, K. L., GARVER, S. A., KAHRU, M. & MCCLAIN, C. 1998. Ocean color chlorophyll algorithms for SeaWiFS. *Journal of Geophysical Research-Oceans,* 103, 24937-24953. doi:10.1029/98jc02160

OBATA, A., ISHIZAKA, J. & ENDOH, M. 1996. Global verification of critical depth theory for phytoplankton bloom with climatological in situ temperature and satellite ocean color data. *Journal of Geophysical Research-Oceans,* 101, 20657-20667.

PAREKH, P., FOLLOWS, M. J. & BOYLE, E. A. 2005. Decoupling of iron and phosphate in the global ocean. *Global Biogeochemical Cycles,* 19, GB2020. doi:10.1029/2004GB002280

PARSONS, T. R. & LALLI, C. M. 1988. Comparative oceanic ecology of the plankton communities of the subarctic Atlantic and Pacific oceans. *Oceanography and Marine Biology: an Annual Review,* 26, 317-359.

PEREZ, V., FERNANDEZ, E., MARANON, E., MORAN, X. A. G. & ZUBKOVC, M. V. 2006. Vertical distribution of phytoplankton biomass, production and growth in the Atlantic subtropical gyres. *Deep-Sea Research Part I-Oceanographic Research Papers,* 53, 1616-1634. doi:10.1016/j.dsr.2006.07.008

PEZZULLI, S., STEPHENSON, D. B. & HANNACHI, A. 2005. The variability of seasonality. *Journal of Climate,* 18, 71-88. doi:10.1175/JCLI-3256.1

PINGREE, R. D., PUGH, P. R., HOLLIGAN, P. M. & FORSTER, G. R. 1975. SUMMER PHYTOPLANKTON BLOOMS AND RED TIDES ALONG TIDAL FRONTS IN APPROACHES TO ENGLISH-CHANNEL. *Nature,* 258, 672-677. doi:10.1038/258672a0

PLATT, T., FUENTES-YACO, C. & FRANK, K. T. 2003. Marine ecology: Spring algal bloom and larval fish survival. *Nature,* 423, 398-399. doi:10.1038/423398b

PLATT, T., HARRISON, W. G., BRIAN, I., EDWARD, P. H. & CHARLES, L. G. 1982. Photosynthesis and photoadaptation of marine phytoplankton in the arctic. *Deep Sea Research Part A. Oceanographic Research Papers,* 29. doi:10.1016/0198-0149(82)90087-5

PLATT, T. & SATHYENDRANATH, S. 1988. Oceanic primary production: estimation by remote sensing at local and regional scales. *Science (New York, N.Y.),* 241, 1613-1620. doi:10.1126/science.241.4873.1613

PLATT, T. & SATHYENDRANATH, S. 2008. Ecological indicators for the pelagic zone of the ocean from remote sensing. *Remote Sensing of Environment,* 112, 3426-3436. doi: 10.1016/j.rse.2007.10.016

PLATT, T., SATHYENDRANATH, S., WHITE, G. N., III, FUENTES-YACO, C., ZHAI, L., DEVRED, E. & TANG, C. 2010. Diagnostic Properties of Phytoplankton Time Series from Remote Sensing. *Estuaries and Coasts,* 33. doi:10.1007/s12237-009-9161-0

PLATT, T., WHITE, G. N., ZHAI, L., SATHYENDRANATH, S. & ROY, S. 2009. The phenology of phytoplankton blooms: Ecosystem indicators from remote

sensing. *Ecological Modelling,* 220**,** 3057-3069. doi:10.1016/j.ecolmodel.2008.11.022

POLOVINA, J. J., HOWELL, E. A. & ABECASSIS, M. 2008. Ocean's least productive waters are expanding. *Geophys. Res. Lett.,* 35**,** L03618. doi:10.1029/2007gl031745

POPOVA, E. E., YOOL, A., COWARD, A. C., AKSENOV, Y. K., ALDERSON, S. G., DE CUEVAS, B. A. & ANDERSON, T. R. 2010. Control of primary production in the Arctic by nutrients and light: insights from a high resolution ocean general circulation model. *Biogeosciences,* 7**,** 3569-3591. doi:10.5194/bg-7-3569-2010

PRICE, N. M., ANDERSEN, L. F. & MOREL, F. M. M. 1991. Iron and nitrogen nutrition of equatorial Pacific plankton. *Deep Sea Research Part A. Oceanographic Research Papers,* 38**,** 1361-1378.

QUÉRÉ, C. L., HARRISON, S. P., COLIN PRENTICE, I., BUITENHUIS, E. T., AUMONT, O., BOPP, L., CLAUSTRE, H., COTRIM DA CUNHA, L., GEIDER, R., GIRAUD, X., KLAAS, C., KOHFELD, K. E., LEGENDRE, L., MANIZZA, M., PLATT, T., RIVKIN, R. B., SATHYENDRANATH, S., UITZ, J., WATSON, A. J. & WOLF-GLADROW, D. 2005. Ecosystem dynamics based on plankton functional types for global ocean biogeochemistry models. *Global Change Biology,* 11**,** 2016-2040. doi:10.1111/j.1365-2486.2005.1004.x

RACAULT, M.-F., LE QUÉRÉ, C., BUITENHUIS, E., SATHYENDRANATH, S. & PLATT, T. 2012. Phytoplankton phenology in the global ocean. *Ecological Indicators,* 14**,** 152-163. doi:doi:10.1016/j.ecolind.2011.07.010

RASMUSSON, E. M. & WALLACE, J. M. 1983. Meteorological aspects of the El Nino/southern oscillation. *Science,* 222**,** 1195-1202.

RAYMONT, J. E. G. 1980. *Plankton and Productivity in the Oceans,* London, Pergamon Press.

RILEY, G. A. 1942. The relationship of vertical turbulence and spring diatom flowerings. *J. mar. Res,* 5**,** 67-87.

RILEY, G. A. 1957. Phytoplankton of the North Central Sargasso Sea. *Limnology and Oceanography,* 252-270.

ROSSOW, W. & ZHANG, Y. 1995. Calculation of surface and top of atmosphere radiative fluxes from physical quantities based on ISCCP data sets: 2. Validation and first results. *Journal of Geophysical Research.* doi:10.1029/94jd02746

SAPIANO, M. R. P., BROWN, C. W., SCHOLLAERT UZ, S. & VARGAS, M. 2012. Establishing a global climatology of marine phytoplankton phenological characteristics. *J. Geophys. Res.,* 117**,** C08026. doi:10.1029/2012jc007958

SARMIENTO, J. L., SLATER, R., BARBER, R., BOPP, L., DONEY, S. C., HIRST, A. C., KLEYPAS, J., MATEAR, R., MIKOLAJEWICZ, U., MONFRAY, P., SOLDATOV, V., SPALL, S. A. & STOUFFER, R. 2004. Response of ocean ecosystems to climate warming. *Global Biogeochemical Cycles,* 18**,** GB3003. doi:10.1029/2003gb002134

SASAOKA, K., CHIBA, S. & SAINO, T. 2011. Climatic forcing and phytoplankton phenology over the subarctic North Pacific from 1998 to 2006, as observed from ocean color data. *Geophysical Research Letters,* 38**,** L15609. doi:10.1029/2011gl048299

SCARGLE, J. D. 1982. Studies in astronomical time series analysis. II-Statistical aspects of spectral analysis of unevenly spaced data. *The Astrophysical Journal,* 263**,** 835-853.

SCHLÜTER, M. H., KRABERG, A. & WILTSHIRE, K. H. 2012. Long-term changes in the seasonality of selected diatoms related to grazers and environmental conditions. *Journal of Sea Research,* 67**,** 91-97. doi:10.1016/j.seares.2011.11.001

SCHMITTNER, A., LATIF, M. & SCHNEIDER, B. 2005. Model projections of the North Atlantic thermohaline circulation for the 21st century assessed by observations. *Geophysical Research Letters,* 32**,** L23710. doi:10.1029/2005GL024368

SCHOPF, P. & LOUGHE, A. 1995. A reduced-gravity isopycnal ocean model: Hindcasts of El Niño. *Monthly Weather Review*.

SHARPLES, J., ROSS, O. N., SCOTT, B. E., GREENSTREET, S. P. R. & FRASER, H. 2006. Inter-annual variability in the timing of stratification and the spring bloom in the North-western North Sea. *Continental Shelf Research,* 26**,** 733-751. doi:10.1016/j.csr.2006.01.011

SHEVYRNOGOV, A. & VYSOTSKAYA, G. 2006. Spatial distribution of chlorophyll concentration seasonal dynamics types in the ocean based on the autocorrelation analysis of SeaWiFS data. *In:* SHEA, M. A., GUPTA, R. K., MENENTI, M. & LOPEZ, R. A. (eds.) *Remote Sensing of Oceanographic Processes and Land Surfaces; Space Science Education and Outreach.* Oxford: Elsevier Science Ltd.

SIEGEL, D. A., DONEY, S. C. & YODER, J. A. 2002. The North Atlantic spring phytoplankton bloom and Sverdrup's critical depth hypothesis. *Science,* 296**,** 730-733. doi: 10.1126/science.1069174

SMITH, R., JONES, P., BRIEGLEB, B., BRYAN, F., DANABASOGLU, G., DENNIS, J., DUKOWICZ, J., EDEN, C., FOX-KEMPER, B., GENT, P., HECHT, M., JAYNE, S., JOCHUM, M., LARGE, W., LINDSAY, K., MALTRUD, M., NORTON, N., PEACOCK, S., VERTENSTEIN, M. & YEAGER, S. 2010. The Parallel Ocean Program (POP) Reference Manual: Ocean Component of the Communitty Climate System Model (CCSM) and Community Earth System Model (CESM). Technical Report LAUR-10-01853. Los Alamos National Laboratory

SOMMER, U. & LENGFELLNER, K. 2008. Climate change and the timing, magnitude, and composition of the phytoplankton spring bloom. *Global Change Biology,* 14**,** 1199-1208. doi:10.1111/j.1365-2486.2008.01571.x

SONG, H. J., JI, R. B., STOCK, C. & WANG, Z. L. 2010. Phenology of phytoplankton blooms in the Nova Scotian Shelf-Gulf of Maine region: remote sensing and modeling analysis. *Journal of Plankton Research,* 32**,** 1485-1499. doi:10.1093/plankt/fbq086

SOURNIA, A. 1969. Annual cycle of phytoplankton and of primary production in the tropical seas. *Marine Biology (Berlin),* 3**,** 287-303.

STONE, D. I. A., WEAVER, A. J. & STOUFFER, R. J. 2001. Projection of Climate Change onto Modes of Atmospheric Variability. *Journal of Climate,* 14**,** 3551-3565. doi:10.1175/1520-0442(2001)014<3551:poccom>2.0.co;2

STRUTTON, P. G., EVANS, W. & CHAVEZ, F. P. 2008. Equatorial Pacific chemical and biological variability, 1997-2003. *Global Biogeochemical Cycles,* 22. doi:10.1029/2007gb003045

STRUTTON, P. G., RYAN, J. P. & CHAVEZ, F. P. 2001. Enhanced chlorophyll associated with tropical instability waves in the equatorial Pacific. *Geophysical Research Letters,* 28**,** 2005-2008. doi:0.1029/2000GL012166

SVERDRUP, H. U. 1953. On conditions for the vernal blooming of phytoplankton

ICES Journal of Marine Science, 18**,** 287-295.

TAUCHER, J. & OSCHLIES, A. 2011. Can we predict the direction of marine primary production change under global warming? *Geophysical Research Letters,* 38. doi:10.1029/2010gl045934

TAYLOR, J. R. & FERRARI, R. 2011. Shutdown of turbulent convection as a new criterion for the onset of spring phytoplankton blooms. *Limnology and Oceanography,* 56**,** 2293-2307. doi:10.4319/lo.2011.56.6.2293

THOMALLA, S. J., FAUCHEREAU, N., SWART, S. & MONTEIRO, P. M. S. 2011. Regional scale characteristics of the seasonal cycle of chlorophyll in the Southern Ocean. *Biogeosciences,* 8**,** 2849-2866. doi:10.5194/bg-8-2849-2011

THOMSON, R. E. & FINE, I. V. 2003. Estimating Mixed Layer Depth from Oceanic Profile Data. *Journal of Atmospheric and Oceanic Technology,* 20**,** 319-329. doi:10.1175/1520-0426(2003)020<0319:emldfo>2.0.co;2

TIAO, G., REINSEL, G., XU, D., PEDRICK, J., ZHU, X., MILLER, A., DELUISI, J., MATEER, C. & WUEBBLES, D. 1990. Effects of autocorrelation and temporal sampling schemes on estimates of trend and spatial correlation. *Journal of Geophysical Research: Atmospheres (1984–2012),* 95**,** 20507-20517.

TIMMERMANS, K. R., STOLTE, W. & DEBAAR, H. J. W. 1994. Iron-mediated effects on nitrate reductase in marine phytoplankton. *Marine Biology,* 121**,** 389-396.

TOWNSEND, D. W., CAMMEN, L. M., HOLLIGAN, P. M., CAMPBELL, D. E. & PETTIGREW, N. R. 1994. Causes and consequences of variability in the timing of spring phytoplankton blooms. *Deep Sea Research Part I: Oceanographic Research Papers,* 41**,** 747-765.

TOWNSEND, D. W., KELLER, M. D., SIERACKI, M. E. & ACKLESON, S. G. 1992. Spring phytoplankton blooms in the absence of vertical water column stratification. *Nature,* 360**,** 59-62.

TRENBERTH, K. E. 2001. El Niño Southern Oscillation (ENSO). *In:* EDITORS-IN-CHIEF: JOHN, H. S., KARL, K. T. & STEVE, A. T. (eds.) *Encyclopedia of Ocean Sciences (Second Edition).* Oxford: Academic Press.

UEYAMA, R. & MONGER, B. C. 2005. Wind-induced modulation of seasonal phytoplankton blooms in the North Atlantic derived from satellite observations. *Limnology and Oceanography,* 50**,** 1820-1829.

UITZ, J., CLAUSTRE, H., GENTILI, B. & STRAMSKI, D. 2010. Phytoplankton class-specific primary production in the world's oceans: Seasonal and interannual variability from satellite observations. *Global Biogeochemical Cycles,* 24. doi:10.1029/2009gb003680

UZ, B. M. 2007. What causes the sporadic phytoplankton bloom southeast of Madagascar? *Journal of Geophysical Research-Oceans,* 112. doi:10.1029/2006jc003685

VANTREPOTTE, V. & MELIN, F. 2009. Temporal variability of 10-year global SeaWiFS time-series of phytoplankton chlorophyll a concentration. *ICES Journal of Marine Science,* 66**,** 1547-1556. doi:10.1093/icesjms/fsp107

VARGAS, M., BROWN, C. W. & SAPIANO, M. R. P. 2009. Phenology of marine phytoplankton from satellite ocean color measurements. *Geophysical Research Letters,* 36. doi:10.1029/2008gl036006

WANIEK, J. J. 2003. The role of physical forcing in initiation of spring blooms in the northeast Atlantic. *Journal of Marine Systems,* 39**,** 57-82.

WANIEK, J. J., HOLLIDAY, N. P., DAVIDSON, R., BROWN, L. & HENSON, S. A. 2005. Freshwater control of onset and species composition of Greenland shelf spring bloom. *Marine Ecology Progress Series,* 288**,** 45-57. doi:10.3354/meps288045

WEATHERHEAD, E. C., REINSEL, G. C., TIAO, G. C., MENG, X.-L., CHOI, D., CHEANG, W.-K., KELLER, T., DELUISI, J., WUEBBLES, D. J., KERR, J. B., MILLER, A. J., OLTMANS, S. J. & FREDERICK, J. E. 1998. Factors affecting the detection of trends: Statistical considerations and applications to environmental data. *Journal of Geophysical Research: Atmospheres,* 103**,** 17149-17161. doi:10.1029/98JD00995

WILLIAMS, R. G. & FOLLOWS, M. J. 2011. *Ocean dynamics and the carbon cycle,* New York, Cambridge University Press.

WILSON, C. & COLES, V. J. 2005. Global climatological relationships between satellite biological and physical observations and upper ocean properties. *J. Geophys. Res.,* 110**,** C10001. doi:10.1029/2004jc002724

WINDER, M. & CLOERN, J. E. 2010. The annual cycles of phytoplankton biomass. *Philosophical Transactions of the Royal Society B-Biological Sciences,* 365**,** 3215-3226. doi:10.1098/rstb.2010.0125

WOHLERS, J., ENGEL, A., ZOLLNER, E., BREITHAUPT, P., JURGENS, K., HOPPE, H. G., SOMMER, U. & RIEBESELL, U. 2009. Changes in biogenic carbon flow in response to sea surface warming. *Proceedings of the National Academy of Sciences of the United States of America,* 106**,** 7067-7072. doi:10.1073/pnas.0812743106

WOLTER, K. 1987. The Southern Oscillation in Surface Circulation and Climate over the Tropical Atlantic, Eastern Pacific, and Indian Oceans as Captured by Cluster Analysis. *Journal of Climate and Applied Meteorology,* 26**,** 540-558.

WU, Y. S., PETERSON, I. K., TANG, C. C. L., PLATT, T., SATHYENDRANATH, S. & FUENTES-YACO, C. 2007. The impact of sea ice on the initiation of the spring bloom on the Newfoundland and Labrador Shelves. *Journal of Plankton Research,* 29**,** 509-514. doi:10.1093/plankt/fbm035

WU, Y. S., PLATT, T., TANG, C. C. L. & SATHYENDRANATH, S. 2008. Regional differences in the timing of the spring bloom in the Labrador Sea. *Marine Ecology-Progress Series,* 355**,** 9-20. doi:10.3354/meps07233

YAMADA, K. & ISHIZAKA, J. 2006. Estimation of interdecadal change of spring bloom timing, in the case of the Japan Sea. *Geophys. Res. Lett.,* 33**,** L02608. doi:10.1029/2005gl024792

YEAGER, S. G., SHIELDS, C. A., LARGE, W. G. & HACK, J. J. 2006. The Low-Resolution CCSM3. *Journal of Climate,* 19**,** 2545-2566. doi:10.1175/JCLI3744.1

YOO, S., BATCHELDER, H. P., PETERSON, W. T. & SYDEMAN, W. J. 2008. Seasonal, interannual and event scale variation in North Pacific ecosystems. *Progress in Oceanography,* 77**,** 155-181. doi:10.1016/j.pocean.2008.03.013

YOOL, A., POPOVA, E. E. & ANDERSON, T. R. 2011. Medusa-1.0: a new intermediate complexity plankton ecosystem model for the global domain. *Geoscientific Model Development,* 4**,** 381-417. doi:10.5194/gmd-4-381-2011

YOOL, A., POPOVA, E. E., COWARD, A. C., BERNIE, D. & ANDERSON, T. R. 2013. Climate change and ocean acidification impacts on lower trophic levels and the export of organic carbon to the deep ocean. *Biogeosciences,* 10**,** 5831-5854. doi:10.5194/bg-10-5831-2013

YU, L., JIN, X. & WELLER, R. 2008. Multidecade Global Flux Datasets from the Objectively Analyzed Air-sea Fluxes (OAFlux) Project: Latent and Sensible Heat Fluxes, Ocean Evaporation, and Related Surface Meteorological Variables. *OAFlux Project Technical Report.* Woods Hole Oceanographic Institution

ZHAI, L., PLATT, T., TANG, C., SATHYENDRANATH, S. & HERNÃ¡NDEZ WALLS, R. 2011. Phytoplankton phenology on the Scotian Shelf. *ICES Journal of Marine Science: Journal du Conseil,* 68**,** 781-791. doi:10.1093/icesjms/fsq175

ZHAI, L., PLATT, T., TANG, C., SATHYENDRANATH, S. & WALNE, A. 2013. The response of phytoplankton to climate variability associated with the North Atlantic Oscillation. *Deep Sea Research Part II: Topical Studies in Oceanography*. doi:10.1016/j.dsr2.2013.04.009

ZHANG, Y., ROSSOW, W., LACIS, A., OINAS, V. & MISHCHENKO, M. 2004. Calculation of radiative fluxes from the surface to top of atmosphere based on ISCCP and other global data sets: Refinements of the radiative transfer model and the input data. *Journal of Geophysical Research,* 109. doi:10.1029/2003jd004457